32058

National Library of Canada
Bibliothèque nationale du Canada

CANADIAN THESES ON MICROFICHE

THÈSES CANADIENNES SUR MICROFICHE

NAME OF AUTHOR/*NOM DE L'AUTEUR* WILLIAM D. ROGGENSACK

TITLE OF THESIS/*TITRE DE LA THÈSE* GEOTECHNICAL PROPERTIES OF
FINE-GRAINED PERMAFROST SOILS

UNIVERSITY/*UNIVERSITÉ* UNIVERSITY OF ALBERTA

DEGREE FOR WHICH THESIS WAS PRESENTED/
GRADE POUR LEQUEL CETTE THÈSE FUT PRÉSENTÉE Ph. D.

YEAR THIS DEGREE CONFERRED/*ANNÉE D'OBTENTION DE CE GRADE* 1977

NAME OF SUPERVISOR/*NOM DU DIRECTEUR DE THÈSE* N. R. MORGENSTERN

Permission is hereby granted to the NATIONAL LIBRARY OF CANADA to microfilm this thesis and to lend or sell copies of the film.

The author reserves other publication rights, and neither the thesis nor extensive extracts from it may be printed or otherwise reproduced without the author's written permission.

L'autorisation est, par la présente, accordée à la BIBLIOTHÈQUE NATIONALE DU CANADA de microfilmer cette thèse et de prêter ou de vendre des exemplaires du film.

L'auteur se réserve les autres droits de publication; ni la thèse ni de longs extraits de celle-ci ne doivent être imprimés ou autrement reproduits sans l'autorisation écrite de l'auteur.

DATED/*DATÉ* APRIL 18, 1977 SIGNED/*SIGNÉ* WDRoggensack

PERMANENT ADDRESS/*RÉSIDENCE FIXÉ* 14411 - 87 AVENUE
EDMONTON, ALBERTA
CANADA T5R 4E1

NL-91 (3-74)

National Library of Canada

Cataloguing Branch
Canadian Theses Division

Ottawa, Canada
K1A 0N4

Bibliothèque nationale du Canada

Direction du catalogage
Division des thèses canadiennes

NOTICE

The quality of this microfiche is heavily dependent upon the quality of the original thesis submitted for microfilming. Every effort has been made to ensure the highest quality of reproduction possible.

If pages are missing, contact the university which granted the degree.

Some pages may have indistinct print especially if the original pages were typed with a poor typewriter ribbon or if the university sent us a poor photocopy.

Previously copyrighted materials (journal articles, published tests, etc.) are not filmed.

Reproduction in full or in part of this film is governed by the Canadian Copyright Act, R.S.C. 1970, c. C-30. Please read the authorization forms which accompany this thesis.

THIS DISSERTATION
HAS BEEN MICROFILMED
EXACTLY AS RECEIVED

AVIS

La qualité de cette microfiche dépend grandement de la qualité de la thèse soumise au microfilmage. Nous avons tout fait pour assurer une qualité supérieure de reproduction.

S'il manque des pages, veuillez communiquer avec l'université qui a conféré le grade.

La qualité d'impression de certaines pages peut laisser à désirer, surtout si les pages originales ont été dactylographiées à l'aide d'un ruban usé ou si l'université nous a fait parvenir une photocopie de mauvaise qualité.

Les documents qui font déjà l'objet d'un droit d'auteur (articles de revue, examens publiés, etc.) ne sont pas microfilmés.

La reproduction, même partielle, de ce microfilm est soumise à la Loi canadienne sur le droit d'auteur, SRC 1970, c. C-30. Veuillez prendre connaissance des formules d'autorisation qui accompagnent cette thèse.

LA THÈSE A ÉTÉ
MICROFILMÉE TELLE QUE
NOUS L'AVONS REÇUE

NL-339 (3/77)

THE UNIVERSITY OF ALBERTA

GEOTECHNICAL PROPERTIES OF FINE-GRAINED PERMAFROST SOILS

BY

Ⓒ WILLIAM D. ROGGENSACK

A THESIS
SUBMITTED TO THE FACULTY OF GRADUATE STUDIES
AND RESEARCH IN PARTIAL FULFILLMENT OF THE
REQUIREMENTS FOR THE DEGREE OF
DOCTOR OF PHILOSOPHY

DEPARTMENT OF CIVIL ENGINEERING
EDMONTON, ALBERTA
SPRING, 1977

THE UNIVERSITY OF ALBERTA

FACULTY OF GRADUATE STUDIES AND RESEARCH

The undersigned certify that they have read, and recommend to the Faculty of Graduate Studies and Research, for acceptance, a thesis entitled 'GEOTECHNICAL PROPERTIES OF FINE-GRAINED PERMAFROST SOILS' submitted by William D. Roggensack in partial fulfilment of the requirements for the degree of Doctor of Philosophy in Civil Engineering.

N. Morgenstern

N. Morgenstern, Supervisor

S Thomson

S. Thomson

D W Murray

D. Murray

B. Stimpson

B. Stimpson

B. Ladanyi

B. Ladanyi, External Examiner

Date April 12, 1977

ABSTRACT

This thesis describes a laboratory study conducted on samples of undisturbed, fine-grained permafrost soil. Specimens were obtained from sampling sites located near Fort Simpson, Norman Wells, and Inuvik, N.W.T., Canada. Both frozen and thawed soils were tested to explore fundamental behaviour and assess typical geotechnical properties.

Direct shear tests on frozen soil were conducted at slow rates, and obtained a friction angle identical to the value determined for the same soil when thawed. Moisture migration induced by shear was demonstrated by ice lenses which had formed along shear planes. Sustained displacement resulted in strengths which decreased with each shear box reversal. Transient and steady state deformation processes were identified in creep tests performed on the same soil, and analytical techniques used to assess and present the data have been described.

Residual stress tests on thawed soil indicated good correlations between log σ_o' and thawed, undrained void ratios. It was determined that post-thaw consolidation data could be used to estimate σ_o' values with accuracy sufficient for geotechnical purposes. Consolidation and triaxial shear tests demonstrated that fabric produced by segregated ice dominates behaviour at effective stresses below approximately 50 kN/m^2. Permeabilities decreased markedly as the secondary structure closed. The blocky macrostructure was also responsible for nonlinear failure envelopes which were caused by dilatant behaviour at low stress levels.

Site investigation techniques in permafrost terrain have been discussed and recommendations pertaining to improving existing practice are presented.

ACKNOWLEDGEMENTS

The experimental investigation reported in this thesis was conducted in the Soil Mechanics Laboratory, Department of Civil Engineering, University of Alberta, under the supervision of Professor N.R. Morgenstern. The author wishes to express his sincere appreciation for Professor Morgenstern's guidance, encouragement, and patience throughout the course of the research program. Professor S. Thomson also provided valuable advice and assisted in developing testing procedures and presenting the data.

The author is grateful to the University of Alberta and the National Research Council of Canada for his personal financial support between 1970 and 1976. Financial contributions to the research program were made by the National Research Council of Canada, Mackenzie Valley Pipeline Research Ltd., the Geological Survey of Canada, and the Department of Public Works (Canada). EBA Engineering Consultants Ltd., of Edmonton, have kindly provided personnel and facilities for typing and printing the thesis.

The work reported herein has benefitted greatly from discussions with the author's many colleagues at the University of Alberta. Special thanks are due to J. Krahn, D.E. Pufahl, and K.W. Savigny, who assisted with the field work. J.F. Nixon, D.C. Sego, and E.C. McRoberts have also contributed to various aspects of the research. M.B. Dusseault assisted the author greatly by consenting to edit the manuscript. His comments and suggestions were most helpful.

A. Muir participated in the design of field and laboratory equipment, and was also responsible for most of the fabrication and machining.

Assistance provided by O. Wood, R. Gitzel, and R. Howells with the experimental and computational work is also acknowledged. L. Staples, D. Hill, and G. Cyre performed some of the laboratory testing, and without their efforts, it would not have been possible to compile the quantity of data contained herein. The figures were prepared by the U. of A. Technical Services, Graphics Division under the supervision of W. Miller and N. Moroskat. The plates were prepared by C.G. Elias, and ~~he also~~ supervised the printing of the thesis.

Significant contributions were made by S. McAllister and L. Harris who typed the manuscript. Their evenings and weekends spent working on the text are sincerely appreciated.

In closing, the completion of this thesis would not have been possible without the assistance and encouragement of my wife, Muriel. Her patience, love, and understanding have made the past eight years much easier.

TABLE OF CONTENTS

Page

Release Form i

Title Page ii

Approval Sheet iii

Abstract iv

Acknowledgements v

Table of Contents vii

List of Tables xi

List of Figures xii

List of Photographic Plates xxii

CHAPTER I INTRODUCTION

1.1 General 1

1.2 Scope of Thesis 2

CHAPTER II REVIEW OF GEOTECHNICAL PROPERTIES OF FROZEN SOILS

2.1 Composition of Frozen Ground 7

2.2 Deformations in Ice 12

2.3 Deformations in Frozen Ground 35

2.4 Strength of Frozen Ground 44

2.5 Interaction Between Strength and Deformation 55

2.6 Application to Engineering Problems 61

CHAPTER III LABORATORY STUDIES OF FROZEN SOILS AT NEAR-THAWING TEMPERATURES

3.1 Stress-Strain Relationships for Frozen Soil 77

3.2 Direct Shear Tests on Frozen Soil 81

Page

3.3 Strength Behaviour from Laboratory Tests 87

3.4 Isothermal Confined Creep Tests on Frozen Soil 105

3.5 Creep Behaviour from Laboratory Tests 112

3.6 Discussion of Results 123

CHAPTER IV REVIEW OF GEOTECHNICAL PROPERTIES OF THAWING SOILS

4.1 Problems Associated with Thaw 148

4.2 Thawing of Frozen Soils 153

4.3 Consolidation of Thawing Soils 156

4.4 Shear Strength of Thawing Soils 166

4.5 Role of Macrostructure in Thawed Soil Behaviour 170

CHAPTER V LABORATORY STUDIES OF CONSOLIDATION IN THAWING SOILS

5.1 Basic Theory 187

5.2 Factors Affecting Consolidation and Settlement 187

5.3 Model for Closure of the Secondary Structure 191

5.4 Testing Equipment and Procedures 196

5.5 Description of Soils Tested 202

5.6 Residual Stress Measurements 208

5.7 Permeability Measurements 221

5.8 Coefficient of Consolidation Measurements 228

5.9 Thaw-Consolidation Tests 231

5.10 Interpretation of Laboratory Test Results 233

Page

CHAPTER VI LABORATORY STUDIES OF SHEAR STRENGTH IN THAWING SOILS

6.1 Introduction 265

6.2 Description of Soils Tested 267

6.3 Testing Equipment and Procedures 274

6.4 Role of Pore Water Pressures 282

6.5 Triaxial Shear Strength Tests on Undisturbed Permafrost 287

6.6 Undrained Shear Strength 291

6.7 Interpretation of Laboratory Results 295

CHAPTER VII CONCLUDING REMARKS

7.1 Site Investigation Practice 316

7.2 Geotechnical Behaviour of Permafrost Soils 319

7.3 Further Research 327

REFERENCES CITED 330

APPENDIX A FIELD WORK

A.1 Sampling Equipment and Procedures 348

A.2 Description of the Sampling Sites 353

A.3 Improving Site Investigation Techniques 359

APPENDIX B LABORATORY EQUIPMENT AND PROCEDURES

B.1 Sample Storage and Preparation 387

B.2 Laboratory Plant and Instrumentation 388

B.3 Scanning Electron Microscope Study of Microstructure 392

Page

APPENDIX C SUMMARY OF LABORATORY TEST DATA

C.1 Direct Shear Tests 401

C.2 Isothermal Confined Creep Tests 419

C.3 Residual Stress Tests 430

C.4 Thaw-Consolidation Tests 443

C.5 Triaxial Strength Tests 447

LIST OF TABLES

Table	Description	Page
2.1	Summary of Laboratory Creep Testing on Polycrystalline Ice	66
2.2	Summary of Field Observations of Ice Flow	67
3.1	Summary of Soil Index Properties	128
3.2	Comparison of Measured and Predicted Cohesion Intercepts	129
3.3	Summary of Laboratory Data from Constant Stress Confined, Isothermal Creep Tests	130
6.1	Frequency Analyses of w and γ_f for Zones 3 and 4	302
6.2	Comparison of Computed and Measured c_u/σ_o' Ratios	302
A.1	Summary of X-Ray Diffraction Analyses Conducted on Clay Fraction (< 2μ)	363
C.1	Summary of Data from Direct Shear Tests, Fort Simpson Landslide Headscarp Sampling Site (Zone 4)	402
C.2	Summary of Residual Stress and Consolidation Data Obtained in the Permode, Fort Simpson Landslide Headscarp Sampling Site	431
C.3	Summary of Residual Stress Data Obtained in the Permode, Norman Wells (MVPL) Sampling Site	432
C.4	Summary of Residual Stress Data Obtained in the Permode, Noell Lake Sampling Site	438
C.5	Summary of Residual Stress and Consolidation Data Obtained in the Triaxial Cell, Fort Simpson Landslide Headscarp Sampling Site	440
C.6	Summary of Residual Stress and Consolidation Data Obtained in the Triaxial Cell, Norman Wells (MVPL) Sampling Site	441
C.7	Summary of Results from Thaw-Consolidation Tests	444
C.8	Summary of Results from Consolidated Undrained Triaxial Tests, Fort Simpson Landslide Headscarp Sampling Site	448
C.9	Summary of Results from Consolidated Undrained Triaxial Tests, Norman Wells (MVPL) Sampling Site	449

LIST OF FIGURES

Figure	Description	Page
1.1	Map of the western part of the Canadian Arctic showing locations of sites where drilling and sampling operations were conducted	6
2.1	Flow relationship for polycrystalline ice based on laboratory and field behaviour (with effective shear strain rates and shear stresses as defined by Nye, 1953)	68
2.2	Schematic representation of creep of polycrystalline ice at various stress levels, temperature constant (from Barnes *et al.*, 1971)	69
2.3	Typical creep test data plotted to evaluate transient and steady state components	69
2.4	Constant stress creep of polycrystalline ice, first load stage (from Mellor and Testa, 1969b)	70
2.5	Constant stress relaxation and creep of polycrystalline ice, second load stage (from Mellor and Testa, 1969b)	70
2.6	Constant stress creep of polycrystalline ice, third load stage (from Mellor and Testa, 1969b)	71
2.7	Analysis of creep data from Mellor and Testa's first load stage	71
2.8	Analysis of creep data from Mellor and Testa's third load stage	72
2.9	Failure envelopes for medium and coarse-grained frozen sand (from Neuber and Wolters, 1970, with changes)	73
2.10	Failure envelopes for fine, silty frozen sand (from Neuber and Wolters, 1970, with changes)	73
2.11	Failure envelopes for frozen Ottawa sand (from Alkire and Andersland, 1973)	74
2.12	Failure envelopes for frozen Ottawa sand (from Sayles, 1973, with changes)	74
2.13	Rendulic plot for 'normally consolidated' frozen soil in compression (after Ladanyi, 1974)	75

Figure	Description	Page
2.14	Rendulic plot for 'normally consolidated' frozen soil stressed beyond its long term strength (after Ladanyi, 1974)	75
2.15	Rendulic plot for 'overconsolidated' frozen soil stressed beyond its long term strength (after Ladanyi, 1974)	76
2.16	Vertical deformation and ground temperature *versus* time for a room excavated in permafrost (from Thompson and Sayles, 1972)	76
3.1	Schematic layout of shear box and associated equipment used in direct shear tests on frozen soils	131
3.2	Typical results from a direct shear test conducted on frozen soil (TEST FS-01) $\sigma_n = 252$ kN/m^2, $\gamma_f = 1.95$ Mg/m^3, and sheared at 1.9 cm/day	132
3.3	Direct shear envelopes for reconstituted Mountain River clay, Series A (unfrozen)	133
3.4	Direct shear envelopes for reconstructed Mountain River clay, Series B (frozen)	133
3.5	Direct shear envelope for Fort Simpson silty clay (Rate 1)	134
3.6	Direct shear envelope for Fort Simpson silty clay (Rate 2)	134
3.7	Direct shear envelope for Fort Simpson silty clay (Rate 3)	135
3.8	Apparent cohesion intercept as a function of time to failure	135
3.9	Sketches of ice structure in sheared specimens of Fort Simpson silty clay	136
3.10	Water content profiles in sheared specimens of Fort Simpson silty clay	137
3.11	Sketch of possible shear-induced fabric observed in a core taken from the Fort Simpson landslide	138
3.12	Idealization of direct shear test to estimate strain rates from an assumed condition of simple shear	139
3.13	Elevation sectional view of apparatus used in isothermal, confined creep tests	140

Figure	Description	Page
3.14	Schematic layout of creep cell and associated equipment used in isothermal, confined creep tests on frozen soils	141
3.15	Detail of alternate methods of end-lubrication employed in creep tests	142
3.16	Results from a typical creep test illustrating the use of a five point moving average to smooth the ε - t curve (Test 3-B)	143
3.17	Complete results for a typical, multi-stage creep test (Tests 3-A and 3-B)	144
3.18	Logarithmic plots of strain rate versus time for first-stage loading	145
3.19	Relationship between primary creep exponent and applied deviatoric stress (includes some multi-stage data at higher stresses)	146
3.20	Tentative relationship between primary creep exponent and steady stage creep rate (includes data from some multi-stage tests obtained at higher stresses)	146
3.21	Tentative flow relationship established from creep tests conducted on fine-grained frozen soils	147
4.1	One-dimensional thaw-consolidation (after Morgenstern and Nixon, 1971)	180
4.2	Maximum base pore pressures and degree of consolidation: a comparison of theory and experiment (after Morgenstern and Smith, 1973)	180
4.3	Stress path for a soil during a closed system freeze-thaw cycle (after Nixon and Morgenstern, 1973b)	181
4.4	Different stress paths followed during the measurement of residual stress for reconstituted Athabasca clay (after Nixon and Morgenstern, 1973b)	182
4.5	Classification of underground ice (after Mackay, 1972a)	183
4.6	Structure of frozen soils and associated ground ice forms (after Tsytovich, 1973)	183
4.7	Permeability test results for low plasticity clays, Copper River Basin, Alaska (after Woodward-Clyde Associates, 1970)	184

Figure	Description	Page
4.8	Permeability as a function of stress for fissured boulder clay (after McGown and Radwan, 1975)	18[illegible]
4.9	Stress-strain curves for drained triaxial tests on 98 mm specimens of London clay (after Marsland, 1972)	185
4.10	Thawing in a soil with reticulate structure	186
5.1	Generalized thaw settlement curve	238
5.2	Model to investigate the effect of fissuring on permeability	238
5.3	Typical results from permeability tests on thawed soil	239
5.4	Comparison of predicted and observed permeabilities for thawed soil	239
5.5	10 cm diameter permode with sectional views of its major components	240
5.6	Schematic layout of permode and associated apparatus used in residual stress, thaw-consolidation and conventional consolidation tests	241
5.7	Textural summary of fine-grained permafrost soils tested	242
5.8	Typical residual stress test results, MVPL ice variability site, Norman Wells	243
5.9	Typical residual stress test results, Noell Lake site	244
5.10	Vertical thaw strain without drainage, samples from Norman Wells site	245
5.11	Summary of residual stress tests, Fort Simpson landslide headscarp site	245
5.12	Summary of residual stress tests, MVPL ice variability site, Norman Wells	246
5.13	Summary of residual stress tests, Noell Lake site	246
5.14	$e - \sigma'$ relationships on arithmetic and logarithmic scales showing δ'_o construction	247

Figure Page

5.15 e - log σ' curves for residual stress test specimens, Borehole NW2 248

5.16 e - log σ' curves for residual stress test specimens, Borehole NW3 248

5.17 e - log σ' curves for residual stress test specimens, Borehole NL2 249

5.18 Relationship between residual stress and thawed, undrained void ratio 250

5.19 Relationship between liquidity index and residual stress 251

5.20 Residual stress profile, Borehole NW2 252

5.21 Residual stress profile, Borehole NW3 252

5.22 Residual stress profile, Borehole NL2 253

5.23 Summary of permeability test results, Zone 2, Fort Simpson landslide headscarp 253

5.24 Summary of permeability test results, Zones 3 and 4, Fort Simpson landslide headscarp 254

5.25 Data from Figure 5.24 replotted to show low stress portion in more detail 254

5.26 Summary of permeability test results, MVPL ice variability site, Norman Wells 255

5.27 Summary of permeability test results, Noell Lake site 255

5.28 Profile of permeabilities at in situ effective overburden pressure, Norman Wells site 256

5.29 Profile of permeabilities at in situ effective overburden pressure, Noell Lake site 256

5.30 Void ratio - permeability relationship, stratified structure 257

5.31 Void ratio - permeability relationship, reticulate structure 257

5.32 Reproducibility of test results 258

5.33 Typical relationship between consolidation coefficient and permeability 258

Figure	Description	Page
5.34	c_v *versus* σ', stratified structure, Zone 2, Fort Simpson landslide headscarp	259
5.35	c_v *versus* σ' reticulate structure, Zone 3, Fort Simpson landslide headscarp	260
5.36	c_v *versus* σ', Norman Wells site	260
5.37	c_v *versus* σ', Noell Lake site	261
5.38	Profile of c_v at *in situ* effective overburden pressure, Norman Wells site	261
5.39	Profile of c_v at *in situ* effective overburden pressure, Noell Lake Site	262
5.40	Comparison of c_v determined in permode and triaxial cell	262
5.41	Thaw-consolidation test results for undisturbed permafrost samples	263
5.42	Thaw strains for undisturbed permafrost, Norman Wells site	263
5.43	Thaw strains for undisturbed permafrost, Noell Lake site	264
6.1	Frequency distributions of frozen bulk density and water content for samples from Zones 3 and 4, Fort Simpson landslide headscarp	303
6.2	Frozen bulk density - water content relationships for samples from Zones 3 and 4, Fort Simpson landslide headscarp	304
6.3	Schematic layout of triaxial cell and associated equipment used in strength tests	305
6.4	Pore pressure reaction test results for thawed soils, Norman Wells site	306
6.5	Pore pressure reaction test results for thawed soils, Noell Lake site	306
6.6	Pore pressure reaction test results related to stratigraphy, Norman Wells site	307
6.7	Pore pressure reaction parameter B measured with increasing consolidation stress	307

Figure	Description	Page
6.8	Pore pressure parameter A measured at failure in triaxial compression, Fort Simpson samples	308
6.9	Pore pressure parameter A measured at failure in triaxial compression, Norman Wells samples	308
6.10	Typical consolidated, undrained triaxial compression test results, Zones 3 and 4, Fort Simpson landslide headscarp	309
6.11	Stress paths during triaxial compression with σ_1'/σ_3' and $(\sigma_1 - \sigma_3)$ peaks indicated	310
6.12	Effects which secondary structure may have on stress path shape during shear	310
6.13	Shear strength envelope using a maximum deviatoric stress failure criterion	311
6.14	Shear strength envelope using a maximum obliquity failure criterion	311
6.15	Strength envelope for soils from Zones 3 and 4, Fort Simpson landslide headscarp	312
6.16	Strength envelope for soils from Norman Wells site	312
6.17	Nonlinearity of strength envelope over a wide stress range	313
6.18	Undrained strength test results in profile, Norman Wells site	313
6.19	Sensitivity of c_u/p ratio to A parameter for a typical range of friction angles	
6.20	Sensitivity of c_u/p ratio to friction angle for a typical range of A parameter values	314
6.21	Undrained strength as a function of residual stress, Fort Simpson site	315
6.22	Undrained strength as a function of residual stress, Norman Wells site	315

Figure	Description	Page
A.1	Sketch of modified CRREL auger core barrel used in sampling operations	364
A.2	Insulated core box used for field storage and transport of permafrost samples	364
A.3	Location plan for Fort Simpson landslide headscarp sampling site (Mile 226)	365
A.4	Location plan for Norman Wells sampling site	366
A.5	Location plan for Noell Lake sampling site	366
A.6	Log of typical headscarp section exposed at the Fort Simpson landslide (October, 1973)	367
A.7	Plasticity chart for soils from the Fort Simpson landslide headscarp sampling site	367
A.8	Moisture content and frozen bulk density data for soils from the Fort Simpson landslide headscarp sampling site	368
A.9	Grain size curves for soils from the Fort Simpson landslide headscarp sampling site (MIT scale)	369
A.10	Borehole log for Norman Wells sampling site	370
A.11	Plasticity chart for soils from the Norman Wells sampling site	371
A.12	Moisture content and frozen bulk density data for soils from the Norman Wells sampling site (this study)	372
A.13	Moisture content and frozen bulk density data for soils from the Norman Wells sampling site (data from MVPL)	373
A.14	Grain size curves for soils from the Norman Wells sampling site	374
A.15	Borehole log for Noell Lake sampling site	375
A.16	Plasticity chart for soils from the Noell Lake sampling site	376
A.17	Moisture content and frozen bulk density data for soils from the Noell Lake sampling site	376

Figure	Description	Page
A.18	Grain size curves (excluding pebbles) for soils from the Noell Lake sampling site	377
A.19	Comparison between density profiles obtained from laboratory measurements on core and downhole nuclear log (MVPL data)	378
A.20	Comparison between density profiles obtained from MVPL nuclear log and laboratory measurements on core from this study	378
A.21	Complete suite of logs for a borehole drilled in permafrost (courtesy of Well Reconnaissance Inc., Dallas, Texas)	379
B.1	Temperature record for an isothermal confined creep test	395
B.2	Circuit for linearizing output signal from thermistor	396
C.1	Direct shear test FS-01	403
C.2	Direct shear test FS-02	404
C.3	Direct shear test FS-03	405
C.4	Direct shear test FS-04	406
C.5	Direct shear test FS-05	407
C.6	Direct shear test FS-06	408
C.7	Direct shear test FS-07	409
C.8	Direct shear test FS-08	410
C.9	Direct shear test FS-09	411
C.10	Direct shear test FS-10	412
C.11	Direct shear test FS-11	413
C.12	Direct shear test FS-12	414
C.13	Direct shear test FS-13	415
C.14	Direct shear test FS-14	416
C.15	Direct shear test FS-15	417
C.16	Direct shear test FS-16	418

Figure	Description	Page
C.17	Creep tests 1-A,B,C (stage loaded)	420
C.18	Creep tests 2-A,B,C (stage loaded)	421
C.19	Creep tests 3-A,B (stage loaded)	422
C.20	Creep tests 4-A,B (stage loaded)	423
C.21	Creep tests 5-A,B,C, (stage loaded)	424
C.22	Creep tests 6-A,B,C, (stage loaded)	425
C.23	Creep tests 7-A,B (stage loaded)	426
C.24	Creep tests 8-A,B (stage loaded)	427
C.25	Creep tests 9-A,B (stage loaded)	428
C.26	Creep tests 10-A,B (stage loaded)	429
C.27a	Thaw-consolidation test data	445
C.27b	Thaw-consolidation test data (continued)	446

LIST OF PHOTOGRAPHIC PLATES

Plate	Description	Page
A.1	Aerial view of Fort Simpson landslide sampling site, Mile 226, Mackenzie River (May, 1973)	380
A.2	Headscarp sampling site, Fort Simpson landslide (October, 1973)	381
A.3	Headscarp sampling site showing contact between zones 2 and 3 (October, 1973)	381
A.4	Zone 3 structure exposed in vertical section, lens cap for scale (October, 1973)	382
A.5	Zone 2, horizontal core (10 cm diameter)	382
A.6	Zone 3, horizontal core (10 cm diameter)	382
A.7	Zone 4, horizontal core (10 cm diameter)	382
A.8	Borehole NW2, 1.03 to 1.34 m (10 cm diameter)	383
A.9	Borehole NW2, 1.83 to 2.07 m (10 cm diameter)	383
A.10	Borehole NW2, 3.66 to 3.90 m (10 cm diameter)	383
A.11	Borehole NW4, 5.82 to 6.00 m (10 cm diameter)	383
A.12	Borehole NW2, 7.92 to 8.12 m (10 cm diameter)	384
A.13	Borehole NW2, 8.17 to 8.38 m (10 cm diameter)	384
A.14	Borehole NW3, 10.45 to 10.67 m (10 cm diameter)	384
A.15	Borehole NW3, 11.89 to 12.13 m (10 cm diameter)	384
A.16	Borehole NL2, 0.64 to 0.92 m (10 cm diameter)	385
A.17	Borehole NL2, 4.26 to 4.39 m (10 cm diameter)	385
A.18	Borehole NL2, 6.55 to 6.71 m (10 cm diameter)	385
A.19	Borehole NL2, 7.50 to 7.62 m (10 cm diameter)	385
A.20	Borehole NL2, 9.45 to 9.69 m (10 cm diameter)	385
A.21	Borehole NL2, 10.97 to 11.21 m (10 cm diameter)	385

Plate	Description	Page
A.22	Modified CRREL core barrel driven by gasoline-powered post-augering unit	386
A.23	Heliportable 'Ranger' drill equipped with hydrostatic drive (Mobile Augers and Research Ltd., Edmonton, Alberta)	386
A.24	Closeup view of modified CRREL core barrel and cutting teeth	386
B.1	Soil lathe used to trim permafrost core	397
B.2	Overhead milling machine with carbide cutter, used to trim permafrost core	397
B.3	Direct shear apparatus	398
B.4	Isothermal confined creep apparatus	398
B.5	Residual stress test in progress showing permode and associated apparatus	399
B.6	Triaxial test in progress showing cell and associated apparatus	399
B.7	Vertical view of shear plane in frozen soil	400
B.8	Stratification and typical fabric, Zone 4, Fort Simpson sampling site	400
B.9	Aggregates of recognizable clay minerals making up silt-sized grains	400
B.10	Typical fabric in laminated silty clay, Norman Wells (MVPL) sampling site	400
B.11	Organic inclusion in silty clay, Norman Wells (MVPL) sampling site	400
B.12	Compact fabric in dense silty clay, Noell Lake sampling site	400

CHAPTER I

INTRODUCTION

1.1 GENERAL

In the Northern Hemisphere, approximately half of Alaska, Canada and the U.S.S.R. are underlain by permafrost or perennially frozen ground (Mackay, 1972a). The existence of permafrost conditions in the sea floor beneath shallow coastal waters on the Arctic continental margins has also been established (Mackay, 1972b). In his study of the distribution of frozen ground in Canada, Brown (1970) has described a number of surficial features unique to permafrost terrain and notes problems which have commonly been encountered with construction and other engineering activities in these regions.

Historically, the past decade has seen a gradual depletion of conventional reserves of oil and gas. This has brought about a dramatic increase in the demand for new sources of fossil fuel and other nonrenewable resources. Current and projected requirements have intensified exploration in frontier areas such as the Canadian Arctic. Furthermore, the imminent need to exploit petroleum, natural gas, and mineral deposits there will certainly enhance the eventual economic feasibility of developing and bringing these resources to market.

Resource exploration and development occurring in the Canadian Arctic since 1950 has been accompanied by engineering activities which range from work as crude as bulldozing seismic trails, to the construction of completely serviced communities. In addition to changing stress conditions at depth, these endeavours often produce disturbances that alter the prevailing ground thermal regime. The effects which these changes may have on the physical and mechanical properties of permafrost soils are of interest when it becomes necessary to either evaluate or predict the geotechnical behaviour of these materials.

Geotechnical concerns unique to permafrost terrain require that both strength and deformation properties be defined throughout the anticipated range of thermal conditions. Although engineering theories have been developed which ostensibly provide an adequate description of observed behaviour for both frozen (e.g. Ladanyi, 1972) and thawing soils (e.g. Morgenstern and Nixon, 1971), there is almost no data available which quantifies specific geotechnical properties for these materials. Specifically, difficulties experienced in dealing with fine-grained permafrost soils have lead to the development of considerable interest in their behaviour. From this, it was clear that, wherever possible, undisturbed samples should be used in laboratory testing programs. This study therefore made use of core which had been obtained from several different locations in the Mackenzie River Valley. To gain a more detailed description of geotechnical parameters and soil behaviour, the research described in this thesis has concentrated on defining certain strength and deformation properties for frozen and thawing, fine-grained permafrost soils.

1.2 SCOPE OF THESIS

Several facilities including an all-weather highway and oil and gas pipelines have been proposed to occupy a transportation corridor which generally follows the Mackenzie River Valley. To keep experimental data generated by this study relevant, permafrost cores tested were obtained from sites situated within or close to that same corridor. Figure 1.1 is a map of the western portion of the Canadian Arctic and illustrates locations for the three sampling sites used in this study. Although the main thrust of this research dealt with the strength and consolidation behaviour of thawing permafrost soils, additional experimental work also investigated selected properties of frozen soils.

Chapter II describes the composition and properties of frozen soil and documents the limited information available concerning their behaviour under typical loading conditions at temperatures within a few degrees of 0°C. The role which ice assumes in introducing rate dependence to strength and deformation behaviour has been given rather detailed attention. Efforts to develop a rational approach to deformation and limit equilibrium problems in frozen ground were commenced with a review of literature dealing with the creep and shear strength behaviour of ice and frozen soils. This revealed that most previous testing had been performed at relatively cold temperatures with applied stresses falling well beyond the usual range of geotechnical interest. Combining the results of these studies permitted construction of a flow relationship for ice which may be used to interpret certain aspects of frozen soil behaviour. It emerged that strength and deformation properties could be characterized with the aid of a descriptive model based upon certain concepts which had been described in the available literature.

Published data concerning frozen soil behaviour have been limited to that obtained from laboratory tests performed on reconstituted or artificially prepared specimens. Chapter III describes direct shear and creep tests which were conducted on undisturbed samples of a frozen silty clay. The results of these experiments have been analyzed, and for the most part, appear to substantiate the conceptual interrelationships established between strength and deformation processes in Chapter II. An attempt has also been made to identify those properties which will have the greatest effect on geotechnical designs involving frozen ground. Methods for evaluating these properties are suggested, and a discussion of those factors which should be considered in developing a design approach to deformation and limit equilibrium problems is given.

Of equal importance is an understanding of the mechanical properties and geotechnical behaviour of thawing soils. Chapter IV outlines thaw-related geotechnical concerns and reviews the development of a workable thaw-consolidation theory. The consolidation and shear strength characteristics of thawing permafrost soils are then discussed with reference to the unique stress history and macrostructure which result from soil freezing. Chapters V and VI describe the results of a comprehensive laboratory testing program conducted to investigate the behaviour of fine-grained permafrost soils during and after thaw. Specimens used in these tests were obtained by drilling and sampling at the three different sites indicated in Figure 1.1. The surficial geology of these sites, sampling equipment and procedures, core shipment, core storage, and sample preparation techniques are described in Appendices A and B.

Chapter V deals with the consolidation and related properties of permafrost soils upon thaw. The stress-sensitive secondary structure has been shown to dominate soil permeability, and hence, other facets of consolidation behaviour. Effective stresses following thaw in an undrained condition ('residual stresses') have been evaluated, and geological and geotechnical interpretations of these results are presented. The data obtained substantiate current theoretical concepts and provide some documentation of consolidation properties for undisturbed, fine-grained, permafrost soils.

Chapter VI contains the results of a triaxial testing program conducted on these same soils. Once again, the results show that macrostructure has an important influence on behaviour, particularly when shearing proceeds under conditions where low effective stresses prevail. Pore pressure response to changes in stress and the dependence of undrained strength on the magnitude of residual stress are also described. Results obtained were found to be in general agreement with behaviour observed for other similarly structured soils.

The final chapter contains a discussion of considerations which should be included in planning site investigations and commencing geotechnical design involving frozen or thawing soils. Definition of appropriate soil properties and obtaining a clear understanding of shear strength and deformation behaviour are essential to this process. Concluding remarks summarize the most important findings of the research described in this thesis. These are followed by suggestions regarding topics for related ongoing research which might help to resolve some of the more important questions which remain.

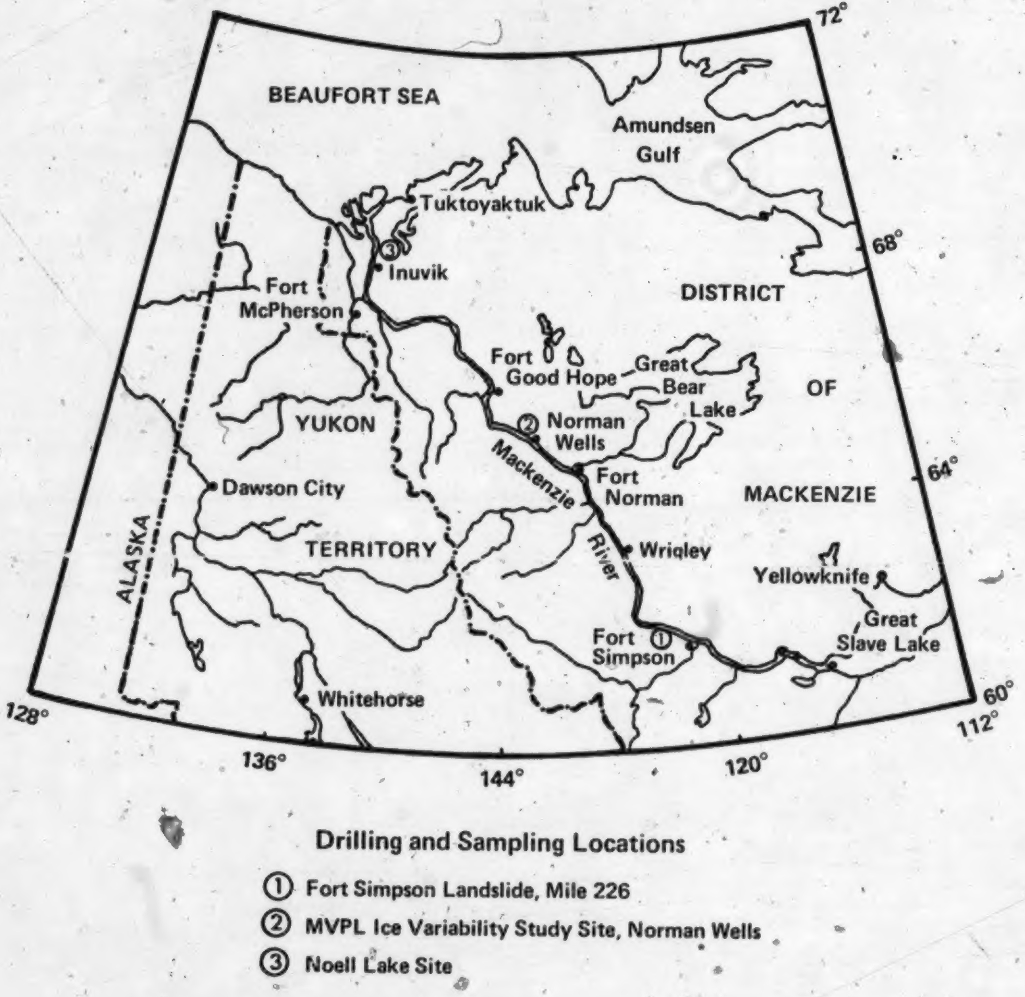
72°
BEAUFORT SEA
Amundsen Gulf
Tuktoyaktuk
③
Inuvik
68°
Fort McPherson
DISTRICT
Fort Good Hope
Great Bear Lake
OF
YUKON
② Norman Wells
Mackenzie River
Fort Norman
64°
Dawson City
MACKENZIE
ALASKA
TERRITORY
Wrigley
Yellowknife
Great Slave Lake
Fort Simpson ①
Whitehorse
60°
128°
112°
136°
144°
120°
Drilling and Sampling Locations
① Fort Simpson Landslide, Mile 226
② MVPL Ice Variability Study Site, Norman Wells
③ Noell Lake Site

Figure 1.1 Map of the western part of the Canadian Arctic showing locations of sites where drilling and sampling operations were conducted

CHAPTER II

REVIEW OF GEOTECHNICAL PROPERTIES OF FROZEN SOILS

2.1 COMPOSITION OF FROZEN GROUND

Frozen soils are a complex multiphase system which may consist of as many as four distinct phases, each possessing different properties. These phases are: mineral particles (silicates), liquid water, ice, and air or other gases. Also present are several interphases, the most important of these being ice-silicate, ice-water, water-silicate, air-water, and air-ice. The interrelationships of these soil constituents depend upon the properties of each phase as well as external influences such as temperature and stress.

Physical relationships between the silicates, water, and the water-silicate interphase are routinely described in most basic soil mechanics texts (e.g. Yong and Warkentin, 1966; Wu, 1966; Lambe and Whitman, 1969). These sources suggest that physico-chemical surface effects related to the size and composition of the mineral particles may have a considerable influence on the properties of frozen soil. Soils with large specific surface areas characteristically contain significant percentages of clay minerals. Experimental and theoretical aspects of the clay-water interaction have been reviewed by several authors (Rosenquist, 1959; Martin, 1962; Morgenstern, 1969). It is generally accepted that absorption of water onto silicate surfaces results in changes in the properties of the water in the interfacial region. Interaction effects may extend outward to include films many molecular layers thick but little is known about the effect this has on water held at the silicate surface (Anderson, 1967). Nuclear magnetic resonance studies (ibid.) have revealed a substantial reduction in the overall freedom of molecular movement, but the bound water apparently retains the mobility of a two-dimensional fluid. Theoretical considerations lead to the conclusion that the intensity of effects associated with the silicate-water interaction must diminish rapidly as the distance away from the surface is increased.

Many of the unique characteristics of frozen soil behaviour are closely related to the nature of these interfaces. For a complete summary of water-ice phase composition, interface characteristics, and applicable thermodynamic relationships, the reader is referred to a recent review paper by Anderson and Morgenstern (1973).

Experimental studies have shown that excluding the vapor phase, water in frozen ground exists in one or more of three possible states: ice, strongly bound water, and liquid water, the relative proportions of each being dependent upon temperature (Nersesova and Tsytovich, 1963). In any frozen soil, the unfrozen water content present is principally determined by temperature, and for all practical purposes, is independent of the soil's bulk water content. By specifying temperature, controlling variables are reduced to specific surface area, nature of the mineral surfaces, and pore water chemistry. Furthermore, it appears that the complex texture and matrix geometry characteristic of natural soils can be adequately approximated by determining total specific surface area (Anderson and Tice, 1972).

Several different experimental techniques have been used to determine the temperature dependence of the water phase composition in frozen soil. The results obtained have varied considerably. Although each approach involves its own inherent approximations, assumptions, and inaccuracies, the data obtained seem consistent when normalized with respect to the specific surface area. From the results of an isothermal calorimetric study conducted on several different soil types, Anderson and Tice (1972) have developed an empirical equation which relates unfrozen water content to specific surface area and temperature. This permits quantification of a soil's unfrozen water content when its specific surface area is known or can be estimated. Phase composition curves constructed on the basis of this relationship indicate that the most significant changes in unfrozen water content occur between the temperatures of 0°C and -5°C. The curves then assymptotically approach an unfrozen water content equivalent to an interfacial layer approximately two water molecules in thickness covering all silicate surfaces (Anderson and Tice, 1973).

Farrar and Coleman (1967) found a linear correlation between total specific surface area and liquid limit for nineteen different clayey soils; therefore, the liquid limit may also be used to predict unfrozen water contents. A relationship using the liquid limit has been obtained by Tice et al. (1973) who indicate that unfrozen water contents can be determined in this manner with an accuracy sufficient for use in geotechnical engineering. Phase composition correlations obtained appear to be consistent with our current understanding of the role of specific surface area in relationships between clay content, clay mineralogy, and soil plasticity.

As ice forms during soil freezing, soluble salts are excluded from its crystal structure, thus increasing the concentration of salts in the unfrozen water as the temperature decreases. This process enhances freezing point depression in the liquid phase and thereby affects the soil water phase relationship. Banin and Anderson (1974) have combined the equations describing salt concentration by the removal of water with those for freezing point depression in normal solutions to evaluate changes in freezing point depression during freezing. Effects which might be anticipated under various natural conditions have also been discussed.

Temperature hysteresis has been indicated in some unfrozen water content curves, Williams (1963, 1964) being the first to document this phenomenon. He observed differences in the apparent specific heat during cooling and warming of the same soil and suggested an analogy with the suction-moisture content hysteresis usually found when porous materials are wetted and dried. His experimental results indicate a lower unfrozen water content during warming than the soil had possessed at that same temperature while being cooled. Anderson and Morgenstern (1973) have described some of the inadequacies of adiabatic calorimetry (the method used by Williams) and conclude that the hysteresis was due to moisture content redistribution occurring during ice segregation.

As soils freeze, some ice in the soil is segregated into discrete lenses or veins, effectively removing that water from the influence of silicate surfaces. During soil warming, a longer time would then be required before ice melting could provide enough liquid water to establish an equilibrium film thickness on the mineral particle surfaces.

Even then, the process is not completely reversible during warming because the water, having been transformed to the solid state, cannot melt and be redistributed until the temperature is increased to about -5°C. A unique physical relationship that has been established between unfrozen water content, temperature and specific surface area, and it seems likely that the hysteresis observed by Williams (1963, 1964) at warmer temperatures was at least in part related to the rapidity with which his tests were performed. It follows that lower water contents would be interpreted from measurements made during warming, but by allowing longer times for water redistribution at each testing stage, the influence of sample thermal history would have probably been much less dramatic.

The equation defining unfrozen water content as a function of specific surface area and temperature has been incorporated into a second relationship which permits the evaluation of apparent specific heat as a temperature function for the same soil (Anderson et al., 1973).

Inspection of the phase diagram for water indicates that at pressures and temperatures encountered in engineering and geological situations, ice found in frozen ground will be normal hexagonal ice (Type Ih). The common occurrence of this ice form in frozen ground has been substantiated by Anderson and Hoekstra (1965). Ice crystals within lenses are usually elongated in the direction that heat flowed during freezing with the c-axes being oriented randomly in a plane orthogonal to the direction of growth (Penner, 1961; Osterkamp, 1975). The properties of ice are responsible for several aspects of unique behavior that characterize frozen soils. Their viscoplastic strength and deformation properties can be attributed largely to the presence of an ice matrix and ice cementation bonds. Changes in temperature alter the phase composition of water in frozen soils, and this in turn controls the degree of ice cementation and total ice content. The amount of unfrozen water therefore emerges as an important quantity in terms of its effects on mechanical and thermal properties. Furthermore, ice phase properties are also temperature dependent. Interaction between the soil mineral skeleton and ice in frozen soil will be discussed in subsequent sections.

2.2 DEFORMATIONS IN ICE

The rheological characteristics of frozen soils are a direct result of the presence of ice as a matrix or internal bonding agent. Grain-to-grain contact has an influence on soil behaviour, but in ice-rich materials, a significant portion of the particles are completely separated from each other by ice. With ice present as pore cement or discrete veins, ice phase behaviour will probably dominate any load-deformation relationships determined for frozen soil. Studies of creep in ice are therefore a useful starting point in the development of appropriate stress-strain relationships for frozen soils.

Measurements of ice deformation rates have been made under widely differing conditions and with various ice types. Early researchers assumed that ice would behave as a simple Newtonian viscous material, so that at any given temperature, strain rate would be linked to stress by a constant coefficient of viscosity (Hobbs, 1974). Attempts to determine this coefficient led to results which varied by as much as six orders of magnitude. From these data, it was apparent that ice was a non-Newtonian material; therefore an examination of deformation mechanisms was required. Before theoretical models could be developed for use in analyses, a meaningful constitutive relationship had to be obtained for ice.

Laboratory studies

Glen (1952, 1955) was one of the first to perform comprehensive, temperature-controlled laboratory creep tests by subjecting randomly oriented polycrystalline ice to uniaxial compression. He observed a rheological response with the ice undergoing a small instantaneous deformation (elastic strain) at the outset and continuing to deform at a rate that gradually decreased with time (transient or primary creep). With the sufficient passage of time, a steady creep rate was usually obtained (stationary or secondary creep). Under higher stresses, this eventually gave way to reacceleration and ultimately, failure. Since ice is a crystalline material, its deformation behaviour can probably be described with phenomenological models similar to those used in creep theories for metals. Typical developments using this approach can be found in any one of several basic textbooks dealing with the subject (e.g. Hult, 1966; Odquist, 1966).

Experimental studies on a wide variety of materials indicate that at a low to moderate stress level, a simple power law adequately describes the dependence of steady state creep rates upon the applied stress (Ladanyi, 1972). Within this framework, Glen (1952, 1955) developed a flow law for polycrystalline ice in simple compression that took the form:

$$\dot{\varepsilon}_s = A\,\sigma^n \qquad (2.1)$$

where $\dot{\varepsilon}_s$ denotes axial strain rate,

σ denotes axial stress,

A is constant for a given temperature and ice type, and

n is an exponent approximately equal to 4 (when the experimental results were corrected for transient effects).

Slight curvature of the log $\dot{\varepsilon}$ versus log σ curve suggested that the exponent, n, might actually increase slightly at higher stress levels.

Although true steady state conditions were established in few, if any of his tests, Glen's (1955) early work was a point of departure for the many studies that followed. His tests were conducted at stresses generally exceeding those of interest in both geotechnical engineering and field glaciology. Creep measurements at lower stresses were attempted by Butkovich and Landauer (1959, 1960). Their results suggested that linearly viscous behaviour was dominant for low stress conditions with temperatures near the melting point. Combining these data with his own field results, Meier (1960) suggested that a reduction in the power law exponent, n, would be appropriate with decreasing stress. At these lower stresses (i.e. those less than 50 kN/m^2), it was indicated that the relationship given in Equation 2.1 was not adequate to describe all of the data. An altern te flow law proposed to embrace the non-linear behaviour took the form:

$$\dot{\varepsilon}_s = A\sigma + B\sigma^n \qquad (2.2)$$

where A and B are constant for a given ice type and temperature, while,

n is constant at approximately 4.5.

Butkovich and Landauer (1960) found a similar flow law and suggested an exponent equal to 3 for the higher stress range. Mellor and Smith (1967) extrapolated results from their creep tests on snow ice to an ice density of 0.917 Mg/m^3 and obtained a two-term flow law that, in general terms, agreed with the results of previous workers.

A flow law of the form given by Equation 2.2 lends support to Meier's suggestion that two separate mechanisms could be responsible for deformations in ice. From the data available at that time, he concluded that at temperatures near the melting point, ice was linearly viscous at low stresses. Barnes and Tabor (1966) observed a rapid change in the indentation hardness of ice for temperatures warmer than -12°C. It would seem that at these temperatures, experimental methods suggested by Glen (1955) could not be reliably employed to obtain a satisfactory and comprehensive flow law for ice. Dillon and Andersland (1967) combined available data that encompassed a wide stress range and concluded that a transition from one mode of creep to another appears to separate regions of high and low stress. Their flow law was linearly viscous at low stresses and featured a transition region, eventually recovering an equation for higher stresses that was equivalent to Glen's power law. The two emergent terms were in general agreement with the flow law proposed by Meier (1960).

Studies by Mellor and Testa (1969a) investigated the effects which temperature has on creep rates. Their interpretation suggests that the apparent viscosity of ice decreases more rapidly with increasing temperature than might have been anticipated from Glen's earlier work (1955). A companion paper (Mellor and Testa, 1969b) has attracted considerable interest since the results of long term, low-stress tests suggest a power law relationship with an exponent of 1.8. These results were combined with data from Mellor and Smith (1967) and Mellor and Testa (1969a) to develop a composite curve which embraced a much wider range of stresses. The derived curve indicates an increase in the power law exponent as stress is increased.

Mellor and Testa (1969b) have qualified their conclusions by pointing out that their test data for the low stress range do not conclusively establish a flow law. Due to slower strain rates observed in their long-term tests, they criticize earlier laboratory studies on the basis of premature termination where steady state creep had been assumed to have been established within a few hours or days. Weertman (1969) in turn, refuted Mellor and Testa's claim that steady state creep rates had been established in their tests by arguing that true steady state creep rates should be obtained over a 10% interval of strain. The slowest rate that could then be reliably measured in a year-long laboratory test would be of order 10^{-8} $\sec^{-1}$. Weertman and Mellor and Testa were acutely aware of the experimental difficulties associated with obtaining secondary creep rates under conditions of low stress and near-melting temperatures. At the same time, Weertman's suggested standard of 10% strain appears to be somewhat arbitrary and a physical basis has not been presented. Mellor (1969) in reply, stated that the exact form of the dependence of creep rate on stress is of less interest than the importance of his finding that ice does not behave in a Newtonian manner at low stresses. Mellor and Testa's (1969b) reported strain rates may not necessarily be correct but they do represent an upper bound and therefore provide a better approximation of actual steady-state creep rates than those previously available. The conclusion to be derived from these studies is that classical laboratory creep tests are probably not practical if axial stresses of less than 50 to 100 kN/m^2 (7 to 15 psi) are to be used.

More recently, Colbeck and Evans (1973) have reported a flow law based on the results of polycrystalline ice tested in compression at the pressure melting point. Their equation takes the form:

$$\dot{\varepsilon}_s = A\sigma + B\sigma^3 + C\sigma^5 \tag{2.3}$$

and indicates strain rates which are at least a full order of magnitude faster than those observed by Meier (1960) or Mellor and Testa (1969b) under similar stresses. In view of the small total creep strains and relatively short test durations reported for this study (200 hr. maximum), Colbeck and Evans' (1973) results should probably be regarded with caution. Concern has been expressed that some of Glen's (1955) measurements were also inappropriate for secondary creep rate evaluation since reported values were often obtained from the brief creep interval separating the primary and tertiary stages. Budd (1969)[1] has indicated that at higher stresses, creep rates obtained in short duration tests do not differ significantly from those determined in longer tests at the same stress level. Voitkovski's (1960) experimental work suggests that for stresses below a certain limiting value, steady state creep can apparently continue over lengthy periods of time (e.g. at 100 kN/m^2, -1°C, a constant rate was observed over 5000 hr.).

---

[1] Referring to conclusions drawn by Voitkovski (1960)

Barnes et al. (1971) have conducted a comprehensive study of the creep behaviour of polycrystalline ice. Following the approach taken by Glen (1955) to distinguish transient effects, they have assumed that total deformation can be described by the superposition of the independent processes of elastic straining, transient, and steady state creep. The equation for creep strain is then given by:

$$\varepsilon = \varepsilon_o + \beta t^{1/3} + \dot{\varepsilon}_s t \qquad (2.4)$$

where ε_o denotes the instantaneous elastic strain,

β denotes an appropriate constant (with $\beta t^{1/3}$ giving the transient creep), and

$\dot{\varepsilon}_s$ denotes the steady state creep rate.

Using this equation, Barnes et al. (1971) then assumed that the steady state creep rate could be obtained from low stress tests even though creep strains throughout the test were dominated by transient processes. On this basis, secondary creep rates were obtained for a wide range of temperatures and applied stresses.

Glen (1955) was the first to suggest that an Arrhenius-type of equation could be used to describe ice creep over a limited range of stress. This equation differs from Equation 2.1 by including temperature effects and takes the form:

$$\dot{\varepsilon}_s = A'\sigma^n \exp\left(\frac{-Q}{RT}\right) \qquad (2.5)$$

where Q denotes the activation energy,
R denotes the gas constant, and
T denotes the absolute temperature.

The constant, A, in Equation 2.1 has been replaced here by $A' \exp(\frac{-Q}{RT})$. It is clear that if $\dot{\varepsilon}_s$ were proportional to σ^n, a plot of $\log \sigma$ against $\log \dot{\varepsilon}_s$ would produce a straight line with a slope of n. Barnes et al. (1971) found this to be the case for stresses of less than 1 MN/m^2 (150 psi) and obtained an exponent approximately equal to 3. At higher stresses, the exponent approached a value of 5 so they proposed a hyperbolic sine expression to describe the creep behaviour over a broad stress range. This new relationship is given by:

$$\dot{\varepsilon}_s = A'(\sinh\alpha'\sigma)^n \exp\left(\frac{-Q}{RT}\right) \qquad (2.6)$$

where A' and α' are new constants and the other symbols retain their meanings from above.

Most of the laboratory creep tests described above were conducted in the stress range of 10^2 kN/m^2 to 10^4 kN/m^2. These results generally fall outside the range of stresses and strain rates applicable to geotechnical engineering and studies of glacier flow. A summary of pertinent laboratory studies, including some not discussed above, appears in Table 2.1. This synthesis leads to the conclusion that for stresses in the 10^2 to 10^4 kN/m^2 (15 to 1500 psi) range, an exponent of approximately 3 is consistent with the reliable test data.

Field studies

The general applicability of a flow law derived from laboratory test results can be assessed by substituting that relationship into an appropriate model and comparing predicted results with field flow rates measured in glaciers and ice shelves. Some of the uncertainties associated with this approach are listed below:

1) The laboratory flow law is one-dimensional and experimental verification of its generalization to three dimensions has not yet been obtained.
2) Simplistic models of glacier and ice-shelf behaviour seldom incorporate appropriate non-uniformities of stress, longitudinal strain, or ice density.
3) Boundary conditions are difficult to establish with confidence when basal sliding, bed undulations, flow constriction, shelf grounding and edge effects are to be included in the analysis.

Ice bodies deforming naturally, in response to self-weight gravity stresses, have been the subject of numerous studies. Researchers have inferred relationships between stress and strain rate from the vertical gradient of horizontal velocity, borehole and tunnel closure rates, and ice surface velocities. A widely used technique has been the measurement of time changes in slope of boreholes initially drilled vertically into glacier ice. Nye (1957) reinterpreted an earlier analysis of data from the Jungfraufirn borehole experiment (Nye, 1953), the results of which were originally reported by Gerrard et al. (1952). The basic assumption of laminar flow was checked against field observations of ice movement. From this, it was concluded that deformation data gathered from the upper portion of these profiles were unreliable. Borehole inclination changes could not be uniquely attributed to shear strain and, as a result, it was not possible to deduce a flow law for ice directly from the field data. Substituting Glen's power law with an exponent of 4.2 did yield a velocity profile that compared well with the one obtained by including effects for estimated longitudinal strains. In the case of the Jungfraufirn results, accounting for the effects of longitudinal extension reduced the apparent power law coefficient from the value which had been calculated previously by using a simple laminar flow analysis.

Meier (1960) has assembled his observations of vertical and transverse velocity profiles from the Saskatchewan glacier with field and laboratory data from several other sources. By inferring stresses and relating them to strain rates deduced from borehole velocity profiles, he obtained a flow law for glacier ice, the form of which was given earlier as Equation 2.2. These data suggest that the flow law derived by Glen (1955) with Andrade's law used to separate transient effects is, in part, consistent with field behaviour (exponent equal to 4). A discrepancy was indicated at lower stresses, even after attempting to account for the effects of longitudinal strain using the approach described by Nye (1957). The form of Meier's flow law is more complex than the simple power law (Equation 2.1) and to explain this, he has suggested that two mechanisms of flow probably operate simultaneously in polycrystalline ice that sustain deformation:

1) Newtonian viscous flow due to grain boundary sliding.
2) Power law, steady state flow due to intracrystalline gliding by dislocation climb.

It would appear that Glen's equation for creep may not apply at low stresses; that is, for 'effective' stresses of less than approximately 70 to 100 kN/m^2 (10 to 15 psi). It should be noted, however, that at these same low stresses, the potential for error in analyzing Meier's field data is large. This shortcoming is confirmed both by the author's expression of uncertainty and by the considerable scatter evident in his field data. Budd (1969) has summarized results from several boreholes in colder, polar glaciers, including deformation measurements for the Tuto ice ramp[1] in Greenland, but these are all subject to the same interpretive difficulties.

Interpretation of borehole velocity measurements by using a simple laminar flow analyses becomes more complex when attempts are made to account for longitudinal stresses and strains. Data for the Athabasca Glacier given by Paterson and Savage (1963) are in general agreement with Meier's results, but similarly, exhibit significant scatter in the low-stress range.

Inclinometer surveys of several boreholes in the Blue Glacier have been conducted by Shreve and Sharp (1970) to investigate the flow law for ice at depth. Their study indicates reasonable correspondence between the field data and a flow law of the form suggested by Glen (1955). Raymond (1973) has developed methods to more accurately evaluate the three-dimensional distribution of velocity in a valley glacier. These techniques have been applied to measurements of internal deformation in the Athabasca Glacier which differed significantly from the theoretical distributions derived by Nye (1965). Raymond's interpretation of the field data supports the validity of extrapolating the flow law derived from Glen's (1955) experiments (i.e. $n \approx 4$ for temperatures near the melting point) to 'effective' stresses as low as 50 kN/m^2 (7.5 psi). Deformations obtained at lower stresses (i.e. near the glacier surface) were found to be completely anomalous. It was therefore not possible to establish the lower limit of applicability of the flow law described by Equation 2.1. Raymond's analysis demonstrates the necessity of correcting the results of creep experiments performed at low stresses to account for transient effects. His work has shown that measured rates of glacier flow were incompatible with Glen's relationship between minimum creep rate and stress.

---

[1] Data obtained from a report by Wilson (1959)

The difficulty and importance of distinguishing between true steady state creep and transient creep in laboratory tests conducted at low stress has been emphasized by various workers including Glen (1950), Mellor and Testa (1969b), Weertman (1969), and Barnes et al. (1971). Furthermore, it is apparent that attempts to evaluate flow rates corresponding to low stress conditions in natural ice masses have been hindered by the use of over-simplified theoretical models and an inability to obtain all of the relevant field data. Certain researchers have suggested that Newtonian or near-Newtonian viscous flow prevails at low stresses (e.g. Meier, 1960; Mellor and Testa, 1969b). However, the apparent inaccuracies associated with these studies are such that conclusions extracted directly from the data should be regarded with caution. Thomas (1971, 1973a, 1973b) has eliminated many of the uncertainties that accompany interpretation of movements in terrestrial glaciers by considering the deformation behaviour of floating ice shelves. These simplest of natural ice bodies rest upon a frictionless bed, have well defined boundary conditions at the upper and lower surfaces, and are distinguished by stress conditions that remain uniform over considerable distances. Equations derived to describe the creep of an ice-shelf (Thomas, 1973a) have been used to interpret available data on ice-shelf deformation (Thomas, 1973b). Good agreement was found between these field measurements and an extrapolation of the results of a previous laboratory study conducted at higher stress levels (Barnes et al., 1971).

Due to the extremely low strain rates involved, laboratory tests at stresses of less than about 100 kN/m^2 (15 psi) are very time consuming and have questionable reliability. With information derived from field glaciology, Thomas (1973b) has provided an important extension to our knowledge of the flow law for ice at low stresses. His interpretation of the data suggests that with an exponent of about 3, a generalized flow law of the form given by Equation 2.1 is applicable for the 40 to 1000 kN/m^2 (5 to 150 psi) stress range and may extend to stresses of less than 10 kN/m^2 (1 psi). The ice shelves studied had average temperatures of -6°C to -16°C so it remains to be determined whether this flow law generalization can be applied directly to ice deformations occurring at temperatures closer to the melting point.

Table 2.2 presents a summary of ice flow under field conditions. The field and laboratory observations described above have been assembled and plotted in Figure 2.1 as 'effective' shear stress against 'effective' shear strain rate (as defined by Nye, 1953). In summary, the following conclusions emerge from the data:

1) Difficulties in eliminating transient effects within reasonable periods of time render low stress laboratory creep tests impractical.
2) The necessity of including realistic field geometry and stress nonuniformities renders the interpretation of glacier flow from borehole velocity measurements a complex exercise in applied mechanics.
3) Adoption of a complex flow law does not seem justified since both field and laboratory data support Glen's simple relationships, with an exponent of 3 to 4 apparently being applicable for stresses as low as 20 to 50 kN/m^2 (3 to 7 psi),
4) Certain data describing creep under low stress suggest Newtonian viscous flow at temperatures near 0°C, but deformation mechanisms under these conditions have not been well defined.

The preceding should not be construed as an attempt to present a complete review of the literature dealing with the creep of ice. Rather, its intent has been to describe briefly the status of current knowledge pertaining to its flow behaviour. Emphasis has been placed on those features which bear on the development of a constitutive relationship for ice which could be applied to the solution of certain geotechnical problems. More detailed accounts can be found in recent papers by Budd (1969), Weertman (1972), and Langdon (1972). Extensive reviews of the literature are also given in Colbeck's thesis (1970) and a treatise authored by Hobbs (1974).

Analysis of data

Glen (1955) realized that the steady state creep rate ultimately obtained for a given stress might be considerably less than the minimum rate observed in a test of relatively short duration. To interpret his test results, the assumption was made that attenuating creep could be described by Andrade's one-third law. Transient and steady state components were then separated on this basis with the strain at any time being given by:

$$\varepsilon = \beta t^{1/3} + \dot{\varepsilon}_s t \qquad (2.7)$$

where β is a constant that depends on stress and temperature.

In a similar analysis, Barnes et al. (1971) employed the Cottrell-Aytekin equation with the implicit assumption that elastic strains and those resulting from the independent processes of transient and steady state creep could be superimposed to give the total strain. Equation 2.4 then describes strain with time and shows that transient creep will dominate at small times while steady state conditions are approached asymptotically as the test progresses. Creep curves typical of their laboratory data are illustrated in Figure 2.2. Curves I, II and III correspond respectively to constant temperature flow under high, moderate, and low stresses. Under favourable conditions, four distinct regions characterize each of the creep curves. Curve II for moderate stress shows these regions most clearly:

1) Instantaneous elastic strain (OA).
2) Creep dominated by transient processes (AB).
3) Creep in an essentially steady state mode (BC).
4) Acceleration to tertiary creep, continuing to failure (CD).

Secondary creep is suppressed at higher stresses (Curve I) while at low stresses, creep behaviour in this time interval is dominated almost entirely by transient processes (Curve III). For the tests which gave the type of results depicted by Curve III, steady state conditions were not established, even after test durations of up to 100 days. Similarly, for samples under low stress in Glen's (1955) experimental study, the transient creep still dominated deformations at the time the tests were terminated. Agreement with the Andrade law was not always perfect; nevertheless, its application apparently allowed a better estimate of steady state creep rates.

To obtain better agreement with experimental data, the transient term in Equation 2.4 can be generalized to parabolic form so the equation then becomes:

$$\varepsilon = \varepsilon_o + \beta t^m + \dot{\varepsilon}_s t \qquad (2.8)$$

where m is an experimentally determined exponent.

Differentiating Equation 2.8 with respect to time gives:

$$\frac{d\varepsilon}{dt} = \dot{\varepsilon} = At^{a} + B \tag{2.9}$$

where A is a constant equal to βm,

a is an exponent equal to $m-1$, and

B is a constant equal to $\dot{\varepsilon}_s$, the steady state creep rate.

By continuously determining strain rate throughout a creep test, the constants A, a and B can be determined from a plot of log $\dot{\varepsilon}$ against log t. With these terms known, Equation 2.9 can then describe both the transient and steady state creep processes. Furthermore, β, m and $\dot{\varepsilon}_s$ can be obtained for substitution into equation 2.8. Figure 2.3 shows data from an idealized creep test plotted in the format suggested by Equation 2.9

As steady state conditions are approached, the direct calculation of strain rate becomes increasingly sensitive to experimental error, temperature fluctuation, and the accuracy of the deformation measurements. The approach described above might also be used solely to determine the transient creep parameters. By subtracting transient and elastic strains from measured total strains, the remaining strain can be plotted against time to obtain an estimate of the steady state creep rate, $\dot{\varepsilon}_s$. This procedure makes the implicit assumption that transient and steady state creep commence at the time of stress application and occur simultaneously thereafter. Weertman (1969, 1972) has questioned the validity of superposition during the early stages of creep and suggests that it may be necessary to reach some finite strain (e.g. 10%) before the steady state deformation process has been fully established. His suggestion has not been supported by experimental data.

In the interest of obtaining a better estimate of steady state creep rates from laboratory tests, it seems reasonable to tentatively accept the assumption of superposition of strains until the whole matter is adequately resolved. It should be noted that transient creep constants can also be obtained from a plot of log ε against log t but the influence of initial elastic strain and choice of origin can interfere with linearity. For the sake of simplicity, use of the method employing a plot of log strain rate against log time is recommended. Even if data presented in this manner are not used to evaluate the transient component of creep, it does provide a convenient means of determining whether or not steady state conditions have been obtained in a particular test.

To obtain strain rate as a function of time, numerical differentiation can be performed on a smooth curve fitted through the experimental time-strain data. By now, it should be apparent that deformations measured in the early stages of a creep test are most important to the transient analysis since they will be least affected by other creep processes at that time. Similarly, it is of interest to re-examine the low stress creep data obtained by Mellor and Testa (1969b). Their published data is shown in Figures 2.4, 2.5 and 2.6. In each case, it would appear that a straight line could be fitted to the later stages of these curves to define an apparent steady state creep rate. Their time-displacement curves have been digitized and differentiated numerically to facilitate examination of the relative contributions of transient and steady state creep. Figure 2.7 summarizes the analysis of data from the first load stage. It was not possible to determine the early time-displacement data with much accuracy but the continued linearity of the log ε versus log t curve indicates that transient creep processes were still dominant in these tests at elapsed times of 15 days. There is remarkable agreement between results obtained from each of the three different tests.

An analysis of data from the second load stage was not performed since deformations occurring during more than half of that test period consisted of relaxation response. Data given are not sufficient to confirm that steady state creep conditions were established during this load stage.

To be completely rigorous, the relationships given previously to describe transient creep should only be applied to data from the first load stage in a multi-stage creep test. However, the results of the third load stage are still of interest when examined in this manner. Transient creep constants A and a (from Equation 2.9) which could be derived from the data in Figure 2.8 would obviously have no meaning. This form of presentation indicates that steady state creep may have been established in two of the tests by the time 20,000 to 30,000 minutes had elapsed. Although Mellor and Testa (1969b) have pointed out the necessity for long test durations under low stress conditions, their conclusion that true steady state strain rates would not be significantly less than their experimentally determined values is apparently without basis. Strain rates obtained in the third load stage are in reasonable agreement with the asympototic value indicated in Figure 2.8, but effects due to stage loading are not known. Primary creep constants obtained for the first load stage were similar for each of the three different tests. In addition to the simple methods discussed in the preceeding, a complete review of numerical methods for the analysis of creep data is given by Conway (1967). It should be noted that use of the procedures discussed above has been confined to conditions of uniform stress and temperature. Phenomenological description of the effects which changing stress and temperature have on material behaviour involves the use of equations which assume more complex and unwieldy forms.

Flow mechanisms

Langdon (1972) has reviewed various deformation processes which could possibly contribute to the creep of polycrystalline ice. Although a precise rate-controlling mechanism has not been identified, steady state creep rates are apparently proportional to stress raised to a power of 3 or more. He concludes that while the creep behaviour of ice compares well with that observed for hexagonal close-packed metals, existing creep theories are not sufficiently detailed to be reliable in a predictive capacity. Weertman (1972) has reviewed the same data sources with respect to dislocation mechanics and concludes that the Nabarro-Herring theory of diffusional creep is capable of accounting for the cubic power law that apparently describes steady state creep for both polycrystalline ice and single crystals in hard glide. Furthermore, he dismisses the idea of near-Newtonian creep at low stresses by pointing out that at the small total strains obtained in these tests, the dislocation density probably does not reach a steady state value compatible with the applied stress.

Creep deformations reflect changes in the dislocation structure over the course of time. In primary or transient creep, these substructures develop in response to the applied stress and remain essentially unchanged once steady state conditions have been established. Steady state creep behaviour may be somewhat temperature dependent. In many cases, creep deformations are thought to be a thermally activated process, and as such, can be described by an Arrhenius-type relationship like the one given in Equation 2.5. Both Glen (1955) and Steinemann (1958) have used this sort of relationship to describe steady state creep over a limited stress range. Barnes et al. (1971) found that the hyperbolic sine term in equation 2.6 provided a more effective description of their experimental results. Data from the low stress regions of these studies is of more interest in its application to problems being considered in this thesis, so it seems probable that equation 2.5 adequately expresses the temperature dependence of creep rates.

Values of creep activiation energies measured for ice have been summarized by Weertman (1972). Apparent activation energies determined from creep data range from 10 to 100 kcal/mole with a reasonably consistent value of 14 kcal/mole obtained at ice temperatures below -10°C. Higher values are reported at warmer temperatures where it seems possible that recrystallization and grain growth have accelerated the creep rate. Weertman (1972) indicates that anomalously high activation energies reported for ice at temperatures warmer than -10°C should be regarded as suspect until experiments have been conducted with single crystals at these same warmer temperatures. Studies conducted with monocrystals would eliminate any effects associated with movement along grain boundaries.

It could be anticipated that creep activation energy might be approximately equal to the self-diffusion activation energy, and for temperatures cooler than -8°C or -10°C, available data suggest that this is the case (Weertman, 1972). Barnes _et al_. (1971) have attributed agreement at colder temperatures to the dominance of intragranular creep processes (controlled by basal glide of dislocations) over dislocation climb.

At temperatures warmer than -10°C, indentation hardness tests indicate that for polycrystalline ice, softening is accompanied by a rise in the apparent activation energy. However, Mellor and Testa (1969a) do not feel that single crystals exhibit this same sort of behaviour. The basis for extending this conclusion to near-melting conditions is not clear since the warmest temperature they have plotted for tests on monocrystals is -11.9°C (their Figure 3). Measured creep rates for polycrystalline ice at these warmer temperatures are still slower than those observed for basal planes in single crystals, but the two rates converge rapidly as the melting point is approached. The softening mechanism is probably associated with processes occurring at the grain boundaries. In any case, arguments based upon increased activation energy as an explanation for anomalous behaviour are weak.

Liquid-like films are known to exist in ice, both on the surface and at crystal boundaries (Drost-Hansen, 1967; Jellinek, 1967). Furthermore, Hobbs (1974) has described fillets of water occupying the triple junctions of grain boundaries in warm ice and gives substantive physical arguments to account for their presence. Although these fillets have been observed at temperatures as cold as -10°C, their existence under colder conditions has not yet been satisfactorily explained. Impurities concentrated by selective exclusion during ice formation are one possible explanation for the presence of intergranular liquid. Barnes et al. (1971) have shown that these films are not usually thick enough to make a significant contribution to grain boundary sliding and conclude that even with these liquid-like layers, deformation will be primarily due to intragranular creep. Non-uniform stresses develop at the boundaries of intimately interlocked grains so that deformation would be accompanied by increased stresses at the triple junctions. If liquid is present at these junctions, ice deformation will occur more easily. Grain boundary sliding and the presence of liquid on the grain surfaces will then give rise to deformation. From this, it emerges that creep activation energies computed from the deformation of polycrystalline ice at warm temperatures will have no real significance since they cannot be attributed to a single creep process. It is well known that when two independent processes produce creep, the faster of these two will control the deformation rate. If each process has a different activation energy, the observed activation energy for creep will change with temperature, increasing as the temperature does.

At temperatures nearing the melting point, measured flow rates exceed those estimated from an extrapolation of creep data obtained at colder temperatures. At higher stress levels, pressure melting can occur at grain boundaries and further accelerate the deformation process. In addition to this, recrystallization can produce preferentially oriented crystals with their basal planes aligned parallel to the direction of shear. Such an arrangement would result in faster flow rates, the ice being oriented in easy glide.

All of the above leads to the conclusion that, at present, there exists no physical evidence suggesting an equation more complex than a simple power law to relate strain rate to stress. Convincing agreement has been obtained between ice-shelf flow rates and those extrapolated from an Arrhenius-type equation using an exponent of 3 to 4 with constants obtained from laboratory creep tests. Bilinear relationships such as Equation 2.2 lack credibility since they have been fitted, in part, to low stress data obtained from either misinterpreted laboratory results or grossly oversimplified englacial stress conditions.

2.3 DEFORMATIONS IN FROZEN GROUND

The preceding observations have important implications in the application of ice flow rate data to problems in geotechnical engineering. McRoberts (1975) has fitted a bilinear equation to a portion of the published secondary creep data for ice, and suggests that since ice forms a significant component of permafrost soils, its behaviour will serve as a reasonable guide to creep in frozen ground. He has made no comment concerning the reliability of secondary creep data synthesized in his flow law. A comparison of the ice flow law with laboratory and field data for frozen soils indicates that certain soils may creep faster than ice would at a similar temperature and stress level.

In the Tuto ice tunnel, Swinzow (1962) observed that closure rates for a band of silty ice were faster than for adjacent clear ice, while the opposite effect was noted for a dirty band containing pebbles and fragments of rock. A subsequent laboratory study by Hooke _et al_. (1972) determined that in some cases, creep rates in ice containing low concentrations of sand were actually higher than creep rates for clear ice. At higher concentrations, the creep rate decreased exponentially with an increasing volume fraction of sand. If creep rates can be increased by the presence of soil in the ice matrix, then a flow law for ice may well not constitute a limiting condition for deformation rates in frozen ground. Ice creep data used by McRoberts (1975) has been derived from tests conducted at temperatures ranging from -1 to -5°C. He has also suggested that since confining pressure would probably diminish observed strain rates, omission of its effect would leave the ice flow law as an upper bound for load-deformation behaviour.

Laboratory studies

In the first major published work dealing with deformations in frozen ground, Vialov (1959) hypothesized a relationship between the steady state strain rate and stress which takes the same general form as Equation 2.1. In his equation, the stress used has been redefined as the difference between the applied stress and the soil's long term strength. He has noted that if the applied shear stress is less than this strength, creep deformations will attenuate with time. The application of superposition principles to creep deformations in frozen soils has been advocated, it being a common practice in the mathematical treatment of creep in metals. Vialov also observed that his experimental data, obtained in a variety of test configurations, was dominated by transient creep processes.

His second major work (Vialov, 1962) has identified a specific threshold stress (equal to the long term strength) which must be exceeded for a process of steady state creep to be initiated and sustained. Deformations have been separated into three components, each associated with a different mechanism:

1) Elastic strain.
2) Transient creep.
3) Steady state creep.

He has described an empirical method that reduces to a generalized flow law in terms of stress and temperature. Cognizant that ice exhibits a long term strength of zero, Vialov (1962) has qualitatively explained behavioural differences observed for soils which possess dissimilar cryogenic structures. It was found that materials with massive structure (see Figure 4.6) exhibited greater long term strengths than those having a reticulate structure. The opposite was often observed in tests with shorter times to failure, which reflected the highly rate-dependent contribution which the ice matrix makes to soil strength. Experimental procedures and test equipment used in this study have been described in reasonable detail. Vialov's experimental studies (1959, 1962) were, however, limited to tests performed on artificially frozen soils deforming under relatively high stresses and at fast strain rates. The flow law exponents obtained in these tests were apparently insensitive to temperature and ranged from 3.5 to 3.7. Very few tests were reported for temperatures warmer than -5°C.

Sanger and Kaplar (1963) have summarized early laboratory studies carried out at CRREL. Although these were short duration, high stress tests, the authors developed a model for frozen soil behaviour that was based on the concept of an isothermal time-stress-strain surface. Strain rate dependence on ice content has been documented with a particular stress apparently producing the fastest strain rate at a volumetric ice to soil ratio of 1.5.

Recognizing stress, temperature, and soil structure as the chief variables affecting creep, Andersland and Akili (1967) employed a multiple stress reduction technique in an attempt to isolate the effect of stress on creep behaviour. Creep rates were obtained for very short test durations under high stresses and at relatively cold temperatures. Temperature dependence was analyzed in terms of rate process theory and the data apparently indicate that thermal activation energy is involved in the process of creep in a frozen soil. A constant activation energy of 93.6 kcal/mole was reported, suggesting that a single creep mechanism predominates at these stresses and temperatures. It seems unlikely that creep rates used in these activation energy calculations corresponded to steady state conditions. Andersland and Akili (1967) point out that for temperatures warmer than about -6°C, changes in unfrozen water content would handicap this method of creep analysis. The rate process aspects of this study have been discussed in more detail elsewhere by Akili (1966, 1970).

Hoekstra (1969) has noted that a creep activation energy for frozen soil evaluated with the method employed by Andersland and Akili (1967) may not be in complete agreement with its strict physical definition. Temperature differences, in addition to changing the energy of the moving molecules, also cause a gradual change of phase which constitutes a departure from equilibrium conditions. This may explain why the activation energies determined by Andersland and Akili (1967) were higher than those given for either polycrystalline ice (see Section 2.2) or unfrozen soils (Mitchell et al., 1968). In addition to this, Akili (1971) has suggested that temperature effects, as indicated by the amount of liquid water present in the soil, would influence the soil's ultimate load-deformation behaviour. Goughnour and Andersland (1968) have also used rate process theory to derive a general equation describing the creep behaviour of a sand-ice system. The role of soil particle contact was explored by observing changes in creep rate as the sand volume concentration was increased. Knowing that ice would creep perceptibly even at very low stresses, sand was selected for their testing program to minimize unfrozen water effects and reduce contamination alteration of the ice matrix. As in previous studies, high stresses were used, and once again, it seems unlikely that any of the creep rates reported were obtained under true steady state conditions.

In an extensive experimental study of the uniaxial deformation behaviour of two frozen sands, Sayles (1968) explored time dependent strength in terms of creep. His findings indicate that at stresses below the long-term strength, creep velocities will continue to decelerate with time. The early domination of creep deformations by transient processes was apparent from the linearity of plots of log strain rate against log time. The primary creep exponent obtained decreased from -1.0 to approximately -0.5 with increases in applied stress. Test durations were typically 40 to 50 days and some samples remained under load for more than 100 days without rupture. The time-strain curves allowed an approximation of secondary creep rates although no conclusive evidence was given to demonstrate that true steady state conditions had been obtained. Insufficient data were reported to permit construction of a flow law for the materials tested. Empirical relationships given to predict variations in deformation with stress, time and temperature were based upon curve-fitting transient creep and subsequent extrapolation to large times. Samples tested in this study contained no segregated ice and would be classified as structured or massive soils, which suggests that the effects of soil structure might be reflected in the creep response to load.

Andersland and AlNouri (1970) have concluded that increases in confining pressure produce an exponential decrease in strain rate. In view of the short test durations, it again seems probable that creep rates observed in this study were still attenuating. A complex method has been employed to interpret their data, but in the light of numerous ambiguities, their results must be regarded with skepticism.

Ladanyi (1972) has described a generalized creep theory which permits information required for problem solutions to be deduced from a set of constant stress creep tests. He has idealized time-deformation behaviour with a steady state creep line and a pseudo-instantaneous intercept at zero time that consists of the transient and elastic strains lumped. The creep law proposed is a simple power expression in the form of Norton's law with temperature effects on the creep rate embodied in a creep modulus as follows:

$$\frac{d\varepsilon}{dt} = \dot{\varepsilon} = \dot{\varepsilon}_c \, (\sigma/\sigma_c)^n \qquad (2.10)$$

where n is a constant which may depend on temperature,

σ_c is a temperature dependent creep modulus, and

$\dot{\varepsilon}_c$ is the secondary strain rate corresponding to an arbitrary stress of σ_c.

Ladanyi (1972) has discussed previous attempts to describe creep as a thermally activated process but expresses a personal preference for other methods of accounting for the effects of temperature. He has also suggested that changes in hydrostatic stress would have a definite effect on the stress-strain behaviour of frictional soils. After concluding that a clear understanding of the creep behaviour of frozen soils is still lacking, Ladanyi has suggested that a systematic and thorough investigation of both field and laboratory behaviour is a necessary prerequisite to meaningful progress.

A laboratory study of frozen remoulded soils has been described by Perkins and Ruedrich (1973), but once again, the work was performed using large stresses, fast strain rates, and relatively cold test temperatures. They found that strength could be estimated by using a flow relationship similar to the one given in Equation 2.1 with an exponent of 3.7 obtained under what were presumably steady state conditions. Data from constant strain rate compression and constant stress creep tests were found to be in reasonable agreement with each other. It was apparent that deformations in the early portions of constant stress tests were dominated by transient creep. Varying the soil texture from sand to silt to clay brought about a decrease in strength and an increase in strain rate, while for all three soil types, confining pressure increases were observed to diminish creep rates. Difficulty was encountered in determining the instantaneous elastic response at low strain rates, since this was apparently obscured by the more dominant flow behaviour.

Sayles (1973) explored the behaviour of Ottawa sand in constant stress triaxial compression at a test temperature of -3.85°C. These creep tests were conducted over periods as long as 3000 hours with deviator stresses of 260 to 6900 kN/M^2 (37 to 1000 psi) and confining pressures ranging from 0 to 5500 kN/m^2 (0 to 800 psi). Sayle's study showed that creep rates could be decreased by increasing the confining pressure. The linearity of log strain rate versus log time data once again indicated that creep strains were dominated by transient processes to elasped times exceeding 1000 hours. In some instances, axial strains of 20 percent were reached without clear indication that steady state conditions had been established.

Another study of the behaviour of frozen Ottawa sand was conducted by Alkire and Andersland (1973). They too report that the application of a confining pressure served to attenuate creep so that sample behaviour became increasingly dependent on the frictional nature of the sand. A comparison of results for different ice saturations emphasizes the dominant role of the ice matrix in the early portions of the creep tests, especially those performed at low confining pressures. Creep rates cited were minimum strain rates obtained within a specified time period and did not necessarily reflect a steady state condition. As a consequence, the data from these experiments are open to many of the same critisms which have been directed toward earlier studies.

Recently, Sayles and Haines (1974) have reported the creep behaviour of frozen silts and clays, presenting their work in a format similar to that adopted by Sayles (1968) for his earlier work on frozen sands. Apparent steady state strain rates obtained from tests of 50 to 120 days duration define a flow law with an exponent approximately equal to 3. Creep curves in this study characteristically displayed a continuous decrease in strain rate with time, a departure from the more classical curves previously obtained for the frozen sands. Analysis of the transient data gave a primary creep exponent that ranged from -0.6 to -1.0 as axial stress was increased.

Assessment of results

From the preceding, it may be concluded that a concise understanding of creep in frozen ground is lacking. Only the recent work of Sayles (1973) has been sufficiently detailed to quantify some of the factors which influence the rheology of frozen soils. Formulating constitutive relationships to obtain a realistic representation of soil behaviour requires that input data be derived from a systematic and thorough investigation of soil properties. As pointed out by Ladanyi (1972), even the verification of a simple uniaxial creep theory requires much further experimental study and should be complimented by an accumulation of detailed field performance data. Only then can the generalization of uniaxial stress data to more complex stress conditions be confirmed as an analytical method reliable for use in practice.

Theories drawn from studies of creep in metals provide a useful framework for describing frozen soil behaviour, but must be modified to include attenuation associated with interparticle friction as the mean stress is increased. Volume constancy during 'undrained' creep has been a common assumption in the studies described above. In support of this, Fukuo (1966) has measured lateral expansion during creep of a frozen soil and found that total volume changes were consistently less than 1% of the total sample volume. The importance of recognizing and analytically accounting for transient creep processes is also apparent. Derivation of a flow law for frozen soils at the stresses and temperatures of greatest interest remains an onerous task. Estimation of deformations in response to load is further complicated by the knowledge that, under certain conditions, frozen soils may undergo consolidation. This process has been shown to be in itself, capable of producing a significant volumetric strain (Brodskaia, 1962).

2.4 STRENGTH OF FROZEN GROUND

Laboratory studies

According to Vialov (1962), a group of failure envelopes can be derived from triaxial compression tests on frozen soil such that each separate envelope corresponds to a specific time to failure. He has also recognized the important role played by cryogenic structural features in determining the strength properties of frozen soils. Since strength is both time and temperature dependent, a modified Mohr-Coulomb failure theory has been proposed, taking the form:

$$\tau = c_T + \sigma_n \tan \phi_T \tag{2.11}$$

where τ denotes the shear strength,

σ_n denotes the normal stress on the shear plane, and

c_T and ϕ_T are functions of both temperature and time.

The results of tests on frozen sand indicated a relatively constant angle of friction obtained for times to failure ranging from 1 to 24 hours. Friction angles invariably fell just slightly below those obtained for the same soil in an unfrozen state.

In a subsequent contribution, Vialov and Shusherina (1964) have verified this approach for frozen soils by documenting the increase in shearing resistance in response to increased normal stress. They identify two components of shearing strength:

1) Resistance to 'smooth shear' (i.e. cohesion).

2) Frictional resistance to shear as a function of normal stress

It was recognized that creep and shear strength were intimately related since the strain required to mobilize friction was a direct function of the time required for the ice matrix to yield under the applied stress. On the basis of experimental data, they conclude that the shear strength of frozen sand can be described accurately by Equation 2.10. The variation of the cohesion intercept, C_T would be given by:

$$C_T = \beta/\log(t/B) \tag{2.12}$$

where β and B are constants obtained from a plot of c_T against log t.

This equation has the same form as the familiar expression proposed by Vialov (1962) to estimate long-term uniaxial compressive strengths from the results of several short-term creep tests.

In tests conducted at higher strain rates, large gains in shearing resistance were obtained as the soil's water content was increased. Since the short-term strength is mainly controlled by the ice matrix, it seems consistent that an increase in water (ice) content would be accompanied by a larger shear strength. This effect was also seen in the anomalously high apparent friction angles measured in the low normal stress range. Nonlinearity of the failure envelope reflects the dominance of the ice matrix in its contribution to strengths obtained at fast strain rates and cold (-10°C) temperatures.

Sayles (1968) and Sayles and Haines (1974) have interpreted their creep tests using Vialov's (1962) equation for long term strength. Expressions of this same form have been given to describe ultimate strength as a function of time and temperature for various soil types. Predictions appear to be in reasonable accord with experimental data.

Even in these two comprehensive studies, tests were seldom conducted beyond a 25 or 30 day duration, which means that evaluation of appropriate design strengths would still involve an extrapolation over several orders of magnitude of time.

Goughnour and Andersland (1968) studied the influence of sand concentration on the failure mode and strength of sand-ice mixtures at temperatures ranging from -4°C to -12°C. When sand concentration was increased beyond 42% by volume, the influence of interparticle friction and dilatancy became apparent, while at lower sand concentrations, strengths were relatively constant and approximately equal to those obtained for pure ice. Upon reaching the critical sand volume, particle contact produced a rapid increase in strength. An analogy was drawn between volumetric increases observed during shear of the frozen sand and the effective stress changes accompanying dilation in the undrained shear of a dense, unfrozen sand. It was thought that confining pressure, being largely carried by the ice matrix at the outset, was gradually transferred to the sand particle contacts as the ice crept under the influence of intrinsic shear stresses. The presence of unyielding sand particles apparently causes faster deformation rates in the ice matrix during the time that overall sample deformation is accommodated. This, in turn, results in higher shear strengths when sand concentrations are increased. Limited experimental evidence suggests that clays probably behave in a similar manner although larger strains might be required to mobilize peak shear strength.

Following Vialov's earlier work, Andersland and Al Nouri (1970) examined the time dependent strength behaviour of two frozen soils.

Sand behaved frictionally as might be expected, with a friction angle corresponding to that of the unfrozen soil. Failure envelopes were essentially parallel for the range of strain rates and stresses reported. It was concluded that the frictional component of strength was rate independent while the geometric cohesion intercept could be related to strain rate and test temperature. Confining pressure had little or no effect on the shear strength of clay when tested at these relatively fast strain rates and cold temperatures (-12°C).

Neuber and Wolters (1970) have summarized the results of numerous strength tests performed on artificially frozen soils. They determined that shear strength was a direct function of confining pressure, although friction angles obtained were slightly lower than those determined for the same soils in an unfrozen state. Figures 2.9 and 2.10 show typical strength envelopes taken from their study. The relatively large cohesive intercepts are associated with the fast strain rates and cold temperatures used in these tests. Probably because of the rather short test durations, no frictional response was detected for clay soils tested. Similar to the findings of Goughnour and Andersland (1968), Neuber and Wolters (1970) report that strains of 10% or more were required to fail the ice matrix and subsequently mobilize full frictional shear strength under triaxial conditions. It should be noted that due to the unusually large confining pressures used in this and some earlier research, the frictional component of shear strength was invariably a major part of the total strength, even at fast strain rates.

A brief study by Heiner (1972) concluded that short term strength in frozen soil was mainly dependent on the strength of its ice matrix, and hence, its moisture content. His strength envelopes indicate anomalously high values for the friction angle under normal stresses as high as 150 kN/m^2 (20 psi). Very fast strain rates were reported; therefore, this behaviour again reflects the overwhelming contribution to strength offered by the ice matrix.

By testing sand-ice specimens triaxially at -8°C, Perkins and Ruedrich (1973) were able to confirm an increase in strength that was proportional to confining pressure. Scatter in the data made the exact friction angle somewhat difficult to resolve but an average value appears to be in reasonable agreement with that obtained for the same sand in an unfrozen state. Some nonlinearity may be evidenced at higher confining pressures, and since the lowest cell pressure used was 4.3 MN/m^2 (625 psi), behaviour under sensible engineering stresses remains undefined. Ruedrich and Perkins (1973) have attempted to separate the shear strength of frozen soil into two components: the resistance of ice to deformation, and the frictional response of soil grain contacts. Their results show that these separate components can be well approximated by:

1) The time dependent strength of the ice matrix, taken as the unconfined compressive strength of the soil in question and obtained at an appropriate strain rate.
2) The essentially time-independent strength associated with the mobilization of frictional resistance at particle contacts under the applied boundary stresses.

If this is the case, then shear strength can be estimated by obtaining the uniaxial strength as a function of strain rate (or time to failure) and adding to this, the frictional response of the soil matrix for a particular mean stress or confining pressure. Computed and experimentally derived stress-strain curves have been given and appear to agree reasonably well with each other. Such close correspondence might not have been found for a finer-grained soil where the frictional response would also be time dependent. This approach to the rationalization of shear strength response is essentially identical to that described previously by Vialov and Shusherina (1964).

A recent study by Alkire and Andersland (1973) provides further information regarding the influence which confining pressure has on the shear strength of a sand-ice material. Varying the degree of ice-saturation in the soil pores has demonstrated the relative influences of the ice matrix and sand particles on overall mechanical behaviour. Volume increases were recorded at lower confining pressures, but under increased pressures, dilation was totally supressed. Considerable energy is required to overcome the strength of the ice matrix so that particle dilation can occur. This response produces a characteristic bilinear stress-strain curve. The ice first yields at a strain of about 1%. This is followed by the gradual development of frictional strength at larger strains. The contribution of dilatancy to the sand's frictional strength is inferred by a slight tendency for curvature of the failure envelope with increasing normal stress. These envelopes are still best approximated by a straight line and it seems unlikely that pronounced curvature would be apparent when testing in a narrower range of confining pressures appropriate for routine geotechnical engineering problems.

Full development of frictional strength may be inhibited as ice saturation is increased, but at fast strain rates, this will be accompanied by a higher cohesion intercept. Figure 2.11 shows two failure envelopes for a frozen sand that were obtained at different ice saturations. From these, it is clear that the Mohr-Coulomb equation adequately describes the shear strength behaviour of frozen soils. The observed friction angles of 29.5° and 33° are less than the 37° value given for the unfrozen sand, suggesting that ice does interfere with the development of full frictional resistance. Alkire (1972) has indicated that these lower values compare well with data reported elsewhere for dense sands tested at high confining pressures where dilatancy is suppressed. He suggests that at the temperatures and strain rates adopted in his study, ice effectively increases particle confinement, and hence, inhibits dilatancy. The analysis of all of these results has necessarily been based on total stresses.

Sayles (1973) has performed triaxial tests on frozen sands, shearing samples to more than 10% axial strain. The stress-strain curves obtained in his study typically exhibited two peaks: the first at approximately 1% strain, corresponding to failure of the ice matrix, and the second at strains as high as 10% where full interparticle friction was mobilized. Instances were noted where the first peak actually exceeded the second, since at lower confining pressures, the strength of the ice matrix exceeded the frictional strength of the sand. Results from the second resistance peak are summarized in Figure 2.12, from which it is clear that the friction angle obtained is approximately equal to the 37° value indicated for unfrozen sand. Compression data given for polycrystalline ice indicate a strength dependency on confining pressure consistent with the findings of others (Chamberlain, 1969; Roggensack, 1975). Friction is apparently mobilized between the ice crystals as failure planes form along grain boundaries, but slower testing rates and higher confining pressures subdue this response. A second test series is reported that determined the creep strength of frozen sand as a function of confining pressure: the results were similar to those obtained for the first series.

Chamberlain _et al_. (1972) have described an investigation of the effects of confining pressure on the shear strength of various soils at a temperature of -10°C. While the pressures and strain rates were intended to approximate those associated with shock waves, several of their observations are still applicable to behaviour under less unusual conditions. They indicate that pressure melting is the normal response to an application of hydrostatic or deviatoric stress to frozen soil. When stress concentrations are produced by a small deviatoric stress, melting occurs and the water moves to regions of lower stress where it refreezes. Once again, frozen sands exhibited dilation and a frictional response when sheared with confining pressures falling in a range that is relevant to normal geotechnical analyses.

Assessment of results

The laboratory studies described above permit several conclusions to be drawn regarding the behaviour of frozen soils in shear. A strong argument emerges in support of the adoption of frictional strength as the long term strength for massive soils. Best available data indicate that the appropriate friction angle can be approximated by the effective angle obtained for the same soil in its thawed state. There is some evidence that in icier materials, full mobilization of frictional strength may be hindered by the ice so that the observed friction angle is reduced. For dense and coarse-grained soils, dependence of shear strength on strain rate and temperature can be embodied in the cohesion intercept while the friction angle remains relatively unaffected. Limited data suggest that the geometric cohesion intercept can be described with an expression similar to the one given by Vialov (1962) for time-dependent strength.

To strain a frozen soil first requires that the strength of the ice matrix must be overcome. The stress necessary to accomplish this will depend on the imposed strain rate via some appropriate relationship describing a flow law for ice (several have been discussed in Section 2.2). As the soil and ice gradually deform, frictional strength can be mobilized at the mineral particle contacts. Ice has a long-term strength of zero, so the stresses transferred to these contacts must eventually equal the applied total stress. During shear, the ice restricts particle movement and supresses dilation. It is this impedance that leads to the unusually large cohesion intercepts obtained for frozen soils sheared at relatively fast strain rates. Data pertaining to fine-grained soils are inconclusive, but it seems probable that these soils will also behave frictionally at slower rates of strain.

Some researchers have indicated that unconfined compressive strengths (and possibly geometric cohesion intercepts) can be related to temperature by adopting a rate process theory approach. Activation energies determined in tests conducted at temperatures warmer than -10°C remain unreliable for reasons that were outlined in Section 2.3. Only limited data are available, and it seems unlikely that the rate process approach will meet with much success in the light of difficulties encountered in applying this theory to the warm-temperature, low-stress behaviour of polycrystalline ice.

It has not been possible to determine stresses carried by the ice phase and experimental measurement of pore pressures in the unfrozen water is similarly difficult and subject to ambiguity. As a consequence, the contributions of ice and unfrozen water in a frozen soil's response to the application of stress have not been clearly defined. The behaviour of frozen soils must therefore be interpreted in terms of total stresses.

At temperatures approaching 0°C, behaviour will likely be similar to that observed for unfrozen soil. However, at these same warm temperatures, segregated ice may exert a much greater influence on both strength and deformation behaviour. Under these circumstances, it will be important to recognize structural features such as high ice content or throughgoing and semi-continuous ice veins that could act as preferred planes of weakness under sustained load. Experiments have also shown that ice and water can be redistributed within a frozen soil by migrating in response to applied stresses. Experimental data of any sort is limited for fine-grained soils and completely lacking for natural permafrost soils, especially those containing segregated ice.

Evaluation of the behaviour of these soils at warm temperatures and under reasonable magnitudes of stress is an urgent research requirement.

2.5 INTERACTION BETWEEN STRENGTH AND DEFORMATION

Ladanyi (1974, 1975) has described a theoretical treatment that takes into consideration the processes of creep, consolidation and shear in frozen soils. An arbitrary boundary has been defined between 'hard frozen' and 'plastic frozen' soils on the basis of texture and temperature. Experimental limitations currently necessitate a quasi-single-phase approach to soil behaviour that lumps creep with those deformations which are actually due to consolidation volume change. Even so, it is still useful to analytically examine consolidation and creep as two separate but simultaneous processes. Since the relative amounts of each type of strain will depend upon the stress path and elapsed time, it is clear that the constitutive relationship chosen to represent this quasi-single-phase behaviour must be obtained by following a laboratory stress path coinciding with anticipated field conditions. Using an approach based upon the unique relationship between water content contours and effective stress paths (well known for saturated soils), Ladanyi (1974) has examined stress changes in frozen soils with the aid of the familiar Rendulic plot. This format permits the convenient separation of any stress into its normal and deviatoric components.

Frozen soil response to a stress increment

Following Ladanyi (1974), Figure 2.13 illustrates the diagonal plane of the principal stress space with different failure surfaces shown as a function of time. A 'normally consolidated' triaxial specimen (in equilibrium at point 0') is subjected to a stress increment that will be carried by the mineral particles and the pore-filling matrix. Some of the applied stress is immediately assumed by the soil skeleton and can be likened to an effective stress in unfrozen soils. In the case where the applied stress increment, $\Delta\sigma_1$ (0'A), does not exceed the long term strength, it can be separated into two components $\sqrt{3}\,\Delta\sigma_{OCT}$ and $\sqrt{3}\Delta\tau_{OCT}$ which are the octahedral normal and octahedral shear stress changes, respectively. As the soil deforms without drainage, unfrozen water in the soil will carry only the hydrostatic stress. Shear stresses can be temporarily supported by the ice matrix, and it will assume those not immediately taken up by the soil skeleton. A portion of the shear stress is initially supported by the ice, with the result that the soil skeleton will be less strained than it would be under the same stress in the unfrozen state. Effective shear strength is then mobilized initially to B' instead of B, and the hydrostatic pore pressure generated by this straining (assumed to be the same in the ice and unfrozen water) is given by:

$$\Delta u = \Delta\sigma_{OCT} - \Delta\sigma'_{OCT} \qquad (2.13)$$

This will be smaller than the pore pressure change that would be generated in the same soil if it were unfrozen. Shear stresses are shared by the ice matrix and soil skeleton; and, similarly, the following can be written:

$$\Delta\tau_{OCT,i} = \Delta\tau_{OCT} - \Delta\tau'_{OCT} \qquad (2.14)$$

where $\Delta\tau_{OCT,i}$ and $\Delta\tau_{OCT}$ are the shear stresses assumed by the ice and soil respectively.

Ladanyi suggests that the creep relaxation of the ice can be likened to the dissipation of the excess pore pressures during consolidation since it results in a gradual transfer of the applied stress to the soil skeleton. Eventually, under conditions of closed-system creep, $\Delta u_i \rightarrow \Delta u$ and $\Delta\tau_{OCT,i} \rightarrow 0$ (the long term strength of ice being zero) so that point B' will move toward B.

By opening the system when the effective stresses are at point B', consolidation will occur simultaneously with creep of the ice matrix and B' will move toward A. In this case, the long term conditions will have $\Delta u_i \rightarrow 0$, $\Delta u \rightarrow 0$, and $\Delta\tau_{OCT,i} \rightarrow 0$. With point A below the long term failure line, both creep and consolidation processes assume an attenuating character. Therefore, deformation rates will decrease continuously with time.

Two features distinguish frozen soil behaviour from that commonly associated with normally consolidated soils:

1) Although the soil appears to be very stiff at the outset and creep and consolidation attenuate with time, ultimate deformations can still be quite large.

2) By mobilizing the short term strength of the ice matrix, frozen soils can temporarily sustain stress increments which exceed the soil's long term strength.

This second characteristic is depicted in Figure 2.14. As before, the effective strength of the soil skeleton is initially mobilized to B' under closed system conditions. The ice matrix then creeps to mobilize full soil strength as B' moves toward B. Simultaneously, progressive straining brings the ice closer to failure. Loss of strength with time can be likened to a gradual shrinking of the delayed failure surface so that with point A lying outside the long-term strength envelope, failure will occur at some time, t_A. Permitting consolidation by opening the system at B', the stress path will move toward A'. The relative rates of consolidation and creep will determine whether A' is reached before failure occurs. In this case, straining consists of simultaneous consolidation and steady state creep, and would be characterized by parabolic time-deformation curves.

An approach similar to that shown in Figures 2.13 and 2.14 can be used for 'hard frozen' soils, with the difference being that these will behave as closed systems under all circumstances since the possibility of consolidation is eliminated by the virtual absence of mobile unfrozen water.

Figure 2.15 illustrates a similar consideration of the probable behaviour of an 'overconsolidated' frozen clay or dense granular soil by assuming a differently shaped effective stress path. Point B represents the peak undrained strength, and may lie slightly beyond the long-term strength envelope. Here, the application of stress produces a slight pore pressure decrease, causing the soil skeleton to carry a greater portion of the shear stress at the outset than in the previous cases. If point A lies beyond the long-term strength envelope, a steady-state creep response will be initiated with failure at some finite time being the inevitable result.

A precis of Ladanyi's (1974) excellent conceptual description of the response of frozen soil to a stress increment has been included here to clarify soil behaviour and demonstrate the interaction between strength and deformation properties. It is apparent that an estimate of the position of the applied stress with respect to the long-term strength is an essential first step in deciding the design approach to be adopted in either limit equilibrium or deformation analyses. Ladanyi's approach suggests that the long-term strength for ice-rich materials will be zero, while for massive soils, this strength can be approximated by the drained strength of the unfrozen soil. Between these extremes and the short-term strength, lie a number of delayed strength envelopes, each having a shape which may be different from the straight line Mohr-Coulomb failure envelope. These envelopes must be defined in terms of total stresses, so it seems entirely possible that the apparent friction angles obtained could be different from the drained friction angle found for the same soil in an unfrozen state. The extreme sensitivity of strength to strain rate or time to failure can be directly attributed to the extremely nonlinear behaviour of the ice matrix that is described by a flow law like Equation 2.1.

Experimental determination of the various strength and deformation components is an onerous task but Ladanyi's (1974) model is certainly a useful framework within which a better understanding of observed behaviour can be obtained.

Consolidation of frozen soils

It is essential that deformations associated with consolidation processes in frozen ground be recognized. Brodskaia (1962) has shown that frozen soils, hitherto considered incompressible, were capable of sustaining appreciable volume changes with the controlling factors being soil texture, temperature, structure and ice content. It was stated that complete consolidation had been obtained in the tests reported in her study, but a close examination of the time-settlement data indicates that this was not the case. Low permeabilities and the viscous nature of ice prolonged deformations so that even though the consolidation process did attenuate, equilibrium conditions were not reached in any of the tests. Based on this observation, there is good reason to suspect that compressibility coefficients for frozen ground reported by Brodskaia (1962) and given elsewhere in the Soviet literature may be nonconservative. Some experimental studies have reported finite soil permeabilities and confirmation of water flow in frozen soil (Williams and Burt, 1974; Burt and Williams, 1976).

Kent et al. (1975) have described a study that set out to verify the state variables required to describe deformation mechanisms in frozen soils. They proposed that two volume change processes would be produced by the application of an isotropic stress: firstly, steady state creep in the ice due to intrinsic shear stresses imposed at the micro scale; and secondly, attenuating consolidation. $(\sigma - u_w)$ was identified as a state variable and by plotting volume change against log time, a curve resembling the conventional consolidation relationship was obtained. This finding suggests that the rate of volume change in frozen soil is governed by the dissipation of excess pore water pressures. Similar results were obtained for volume changes produced by an incremental change in temperature. Volumetric strains resulting from a temperature increase exceeded the amount that could be explained by phase change alone. The authors attribute these volume changes to additional creep in the ice matrix as it yielded to conform to its new equilibrium ice porosity. Kent (1974) reports the possible diffusion of ethylene glycol into the test samples which complicates the interpretation of his experimental results. Behaviour observed in this study is in general agreement with the conceptual model for volume change in frozen soils proposed by Ladanyi (1974, 1975).

2.6 APPLICATION TO ENGINEERING PROBLEMS

The use of laboratory data to predict in situ behaviour requires the generalization of simple constitutive relationships to more complex conditions approximating field configurations. The usual practice in developing a flow law has been to express data in terms of 'effective' stresses and strain rates, for example, like those proposed by Nye (1953). Emery and Nguyen (1974) have reviewed the extension of uniaxial creep laws to the multiaxial case and concur with Ladanyi (1972) in recommending adoption of the 'effective' stress and strain rates defined by Odquist (1966):

$$\tau_{eff} = \sqrt{3}\ \sqrt{I}_2, \text{ and } = \sqrt{\frac{3}{2}}\ \sigma_{ij}'\ \sigma_{ij}'$$

where $\sigma'_{ij} = \sigma_{ij} - \bar{\sigma}\delta_{ij}$, with $\bar{\sigma}$ being the mean stress

$$\dot{\varepsilon}_{eff} = 2/\sqrt{3}\ \sqrt{J}_2 = \sqrt{\frac{2}{3}}\ \dot{\varepsilon}_{ij}\ \dot{\varepsilon}_{ij}$$

I_2 and J_2 denote the second invariants of deviatoric stress and strain rate, respectively. 'Effective' stresses and strain rates given by Odquist (1966) are preferred for generalization to multiaxial conditions since Norton's law is recovered when the multiaxial flow law is specialized to the uniaxial case. It should be cautioned that contained herein is the implicit assumption that hydrostatic stress will not influence behaviour, and although this may be approximately true for ice, available data suggests the contrary for massive soils. In synthesizing behaviour to develop a flow law, it is essential that the same stress and strain definitions be applied to all of the data. The practice of using these stresses and strain rates in multiaxial generalizations of uniaxial data has not yet been validated, either in the laboratory or the field. Further research is required to improve confidence in the application of these relationships in practice.

The only well-documented study of the in situ creep behaviour of frozen soil consists of measurements of the roof and wall displacements in an underground room in permafrost (Thompson and Sayles, 1972). The opening was located at a depth of approximately 20 m (65 ft) in ice-rich Fairbanks silt. Closure measurements were reported for a time interval exceeding one year. A relationship was derived between stress and strain rate from the results of short-term uniaxial creep tests performed on undisturbed samples in the laboratory. The finite element method was then employed to analyze measured deformations, and the authors have indicated close agreement between in situ and laboratory creep characteristics for the frozen silt. Their analysis was based upon the assumption that deformations were entirely dominated by steady state processes. By using a numerical analysis to generate closures corresponding to measured field behaviour, the back-calculated flow law thus determined indicated a strain rate some 3.3 times faster than had been obtained in the laboratory testing.

Examination of the vertical closure data, shown in Figure 2.16, suggests that assuming steady state conditions may have been an oversimplification. An early transition to steady state creep was reported from laboratory tests conducted on the frozen silt. This observation is difficult to resolve when compared with other creep data given for similar silts and clays at or about the same temperature (Sayles and Haines, 1974). In the more recent study, it was observed that strain rates were still attenuating after times exceeding 1000 hr. This writer has not conducted a detailed examination of the finite element analysis employed by Thompson and Sayles (1972), but in light of the complexities inherent with the creep formulation, it seems reasonable to suggest that several of their conclusions require more detailed substantiation before gaining acceptance. Some test of the accuracy of their program against a closed form creep solution would be appropriate before going on to suggest that transient creep deformations have made a negligible contribution to the closure of the room.

Records of ice tunnel closure over periods extending to 8 years have been reported by Bender (1967). These openings were advanced in snow ice, and although its lower density (0.8 Mg/m^3) may have influenced behaviour, the closure curves clearly illustrate sustained rate attenuation. Bender's (1967) observations suggest that transient processes may have a significant influence on creep under field conditions.

Nixon and McRoberts (1976) have used a secondary creep law for ice to relate the steady state settlement of a pile in ice or an ice-rich soil to the applied shaft stress. In part, their flow law has been based upon the same low stress creep data that was criticized in Section 2.2. They point out that their analysis will tend toward conservatism, but the issue of primary or transient creep has been completely omitted and deserves attention. There is a paucity of creep data in the range of stresses and deformation rates of greatest interest in pile design. If the creep rates reported by researchers like Mellor and Testa (1969b) or Colbeck and Evans (1973) are actually much faster than true steady state rates, then over long times, the flow law assumed by Nixon and McRoberts (1976) will grossly overpredict settlements. Their figures indicate that pile shaft stresses will have to be kept small to satisfy design requirements which limit deformations. On the other hand, if early settlements are dominated by transient processes, creep attenuation will occur and with slower long-term settlement rates, increased shaft stresses might then be permissible. Experimental results discussed previously have shown that the creep behaviour of ice at near-thawing temperatures is, at best, erratic. Without the benefit of satisfactory laboratory data or careful observations of field performance, it is extremely difficult to make estimates of deformation behaviour for structures founded in permafrost.

In summarizing the useful strength and creep rate testing reported for frozen soils, Anderson and Morgenstern (1973) have suggested that the bulk of existent data can be criticized for one or more of the following reasons:

1) Stresses employed were beyond the range of engineering interest.

2) Strain rates obtained were considerably faster than those anticipated for usual field conditions.

3) Test temperatures were considerably colder than normal ground temperatures.

4) Creep test durations at lower stresses were too short.

Little or no data are available defining the behaviour of natural permafrost materials. With respect to shear strength, an analysis of a landslide on the Mountain River, N.W.T. by McRoberts and Morgenstern (1974b) contains field evidence that the long-term strength of ice-poor permafrost is entirely frictional. Limitations to be placed upon this approach when ground ice is present as either continuous layers or a reticulate structure have yet to be determined.

TABLE 2.1 SUMMARY OF LABORATORY CREEP TESTING ON POLYCRYSTALLINE ICE

SOURCE	'EFFECTIVE' SHEAR* STRESS RANGE (kN/m^2)	TEMPERATURE (°C)	TEST DURATION (hr)	ICE TYPE	REMARKS
Glen (1955)	40 to 540	-13 to 0	150 max.	random	- no low stress tests - transient effects accounted for
Steinmann (1958)	50 to 580	-12 to -1.9	180 max.	random	- transient effects not accounted for - questionable testing techniques
Butkovich and Landauer (1959)	50 to 300 680 to 2700	-6.5 to -4 -5	170 max. 1 max.	random (also some elongated crystals)	- report only minimum strain rate - small samples used in pure shear
Butkovich and Landauer (1960)	1 to 12	-11 to -5.9	300 (?)	as above	- report only minimum strain rate - probably dominated by transient creep - very small strains
Voitkovski (1960) (in Budd, 1969)	25 to 240	-4 to -1.2	5000 max.	random	- original text not available to the writer
Dillon and Andersland (1967)	590 to 1600	-14 to -10	1 to 2 (?)	random	- small strains - steady state difficult to distinguish
Mellor and Smith (1967)	40 to 1000	-10 to -4	2700 max.	snow ice, random ($0.83\ Mg/m^3$)	- steady state not established in low stress tests
Mellor and Testa (1969a)	20 to 1200	-6.1 to 0 (mostly -10 to 0)	120 max. (approx.)	random	- some tests stage-loaded - recrystallization thought possible
Mellor and Testa (1969b)	5 to 25	-2	340 and 870	random	- steady state rates given are questionable - transient effects not accounted for - small strains
Tabor and Walker (1970) Barnes *et al.* (1971)	50 to 5800	-48 to -2	2400 max.	random	- transient effects accounted for
Colbeck and Evans (1973)	5 to 125	0	210 max.	random (glacier)	- small strains - crude testing apparatus - steady state questionable - recrystallization may complicate interpretation

* 'Effective' Shear Stress $\tau_{eff} = \frac{1}{\sqrt{3}} \sigma_{axial}$ (uniaxial compression)

'Effective' Strain Rate $\dot{\varepsilon}_{eff} = \frac{\sqrt{3}}{2} \dot{\varepsilon}_{axial}$

(definitions from Nye (1953), p. 486)

TABLE 2.2 SUMMARY OF FIELD OBSERVATIONS OF ICE FLOW

SOURCE	'EFFECTIVE' SHEAR STRESS RANGE (kN/m^2)	TEMPERATURE (°C)	TYPE OF MEASUREMENT REPORTED	LOCATION	REMARKS
Gerrard *et al.* (1952)	10 to 100	near 0	horizontal velocity from borehole inclinations	Jungfraufirn	- measurements in upper profile unreliable - no longitudinal strain measured
Nye (1953)	~10 to 100 and 100 to 400	-0.8 to 0	reanalysis of above and tunnel closure rates	Jungfraufirn, Skautizoe, Z'Matt and Arolla glaciers	- laminar flow analysis - longitudinal strain not accounted for - simplified stress conditions around tunnels
Nye (1957)	~10 to 100	near 0	reanalysis of above	Jungfraufirn	- renalaysis accounting for longitudinal strain - data from low stress regions questioned
Wilson (1959) (in Budd, 1969)	~ 5 to 40	-11	borehole inclinometer results	Tuto ice ramp Greenland	- laminar flow analyses neglecting longitudinal strain
Meier (1960)	~ 1 to 100	near 0	horizontal velocity from borehole inclinations	Saskatchewan and Maspina glaciers	- laminar flow analysis - some doubts about near-surface data
Paterson and Savage (1963)	~50 to 110 (estimated)	near 0	horizontal velocity from borehole inclinations	Athabasca glacier	- encountered large errors at low stress levels - discuss difficulties in laminar flow analysis accounting for longitudinal strains
Shreve and Sharp (1970)	~20 to 120 (estimated)	near 0	borehole inclinometer results	Blue glacier	- large deformations in basal ice and on glacier bed
Raymond (1973)	~50 to 150 (estimated)	near 0	borehole inclinometer results	Athabasca glacier	- analyzed for unique stress distributions - anomalous behaviour in upper half of profile
Thomas (1973)	~12 to 100	-16 to -6 (average values for each shelf)	surface velocities	Brunt, Maudheim, Amery, Ward Hunt, and Ross ice shelves	- model developed to account for lateral restraint, grounding restraint, and density variations with depth

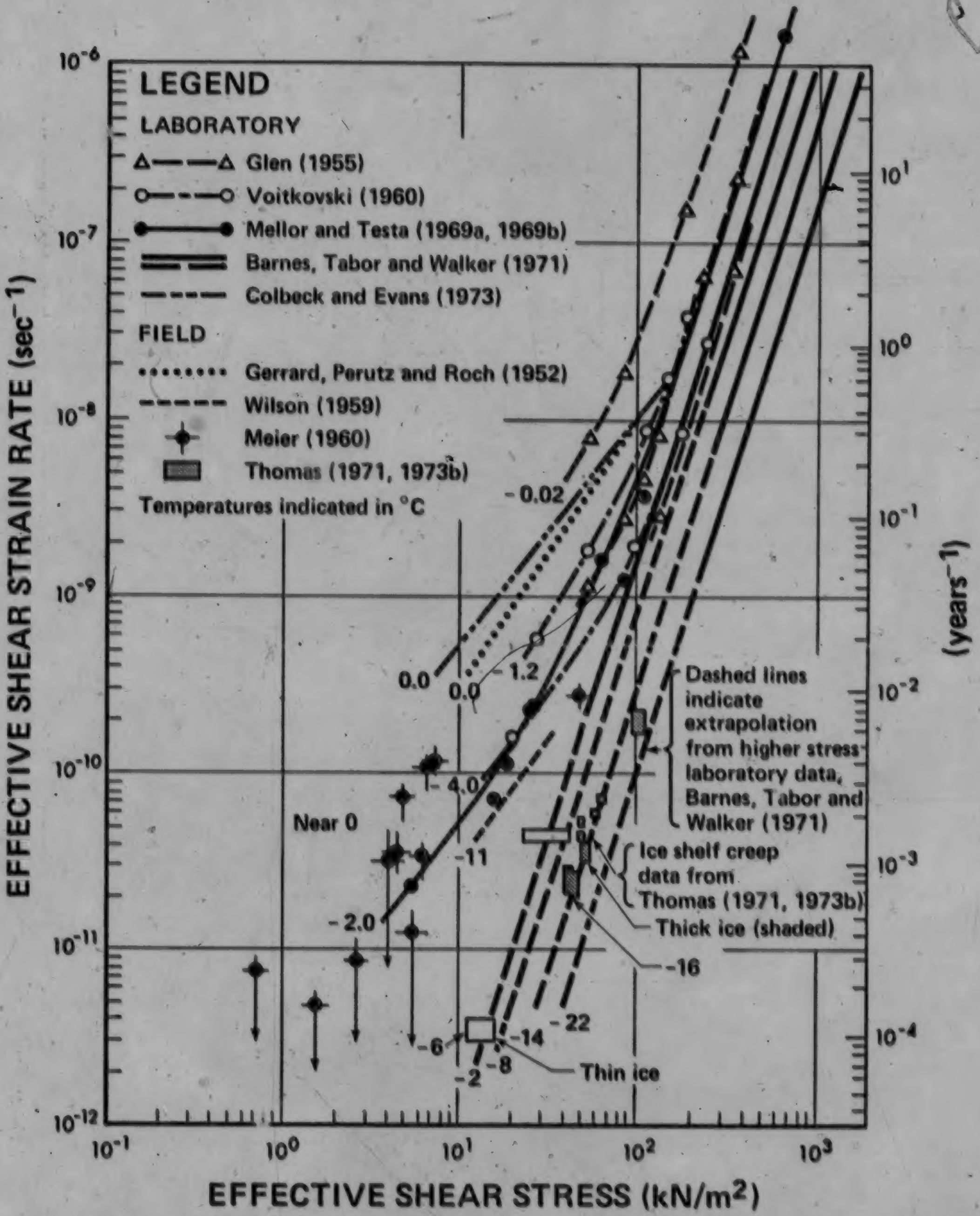

Figure 2.1 Flow relationship for polycrystalline ice based on laboratory and field behaviour (with effective shear strain rates and shear stresses as defined by Nye, 1953)

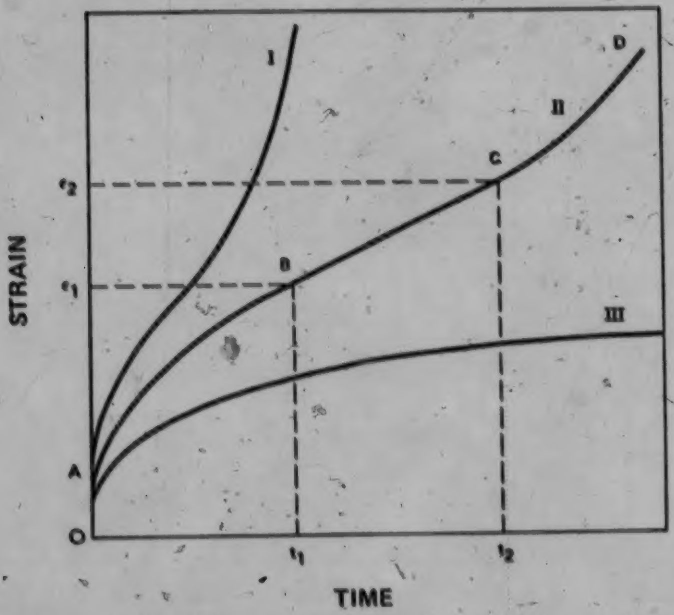

At any stage, creep rate $\dot{\epsilon} = (\epsilon_2 - \epsilon_1)/(t_2 - t_1)$

Figure 2.2 Schematic representation of creep of polycrystalline ice at various stress levels, temperature constant (from Barnes et al., 1971)

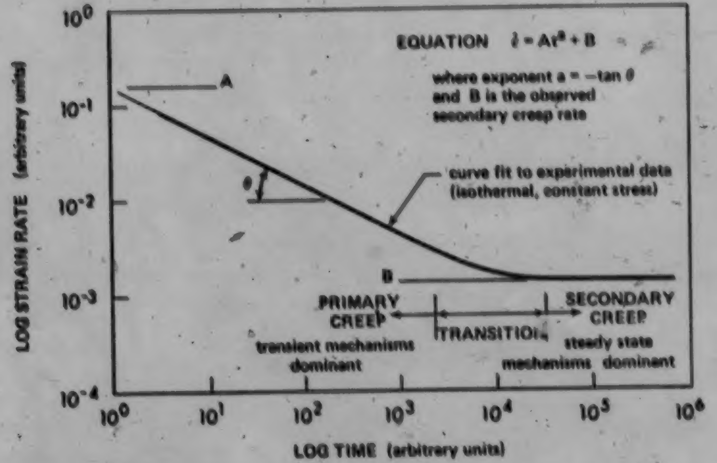

Figure 2.3 Typical creep test data plotted to evaluate transient and steady state components

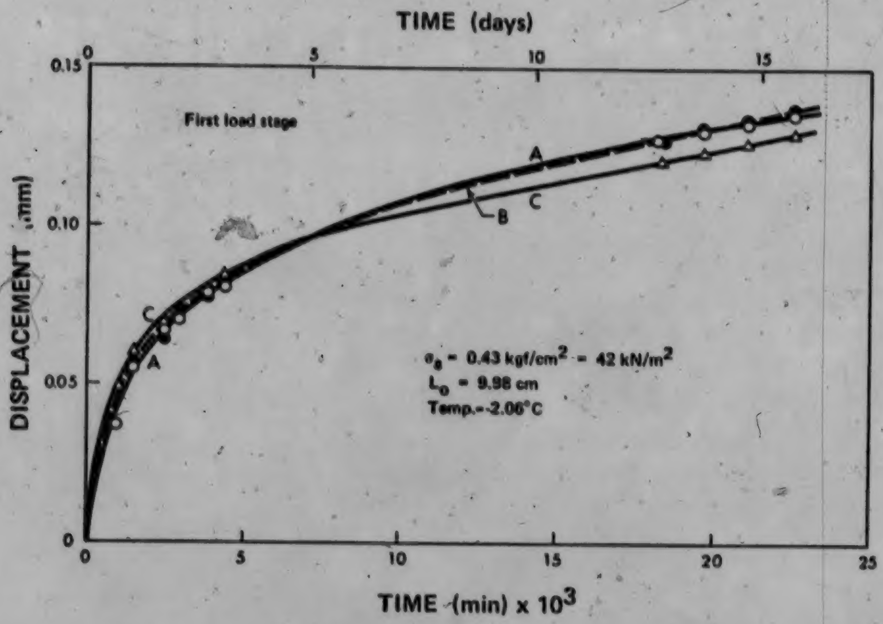

Figure 2.4 Constant stress creep of polycrystalline ice, first load stage (from Mellor and Testa, 1969b)

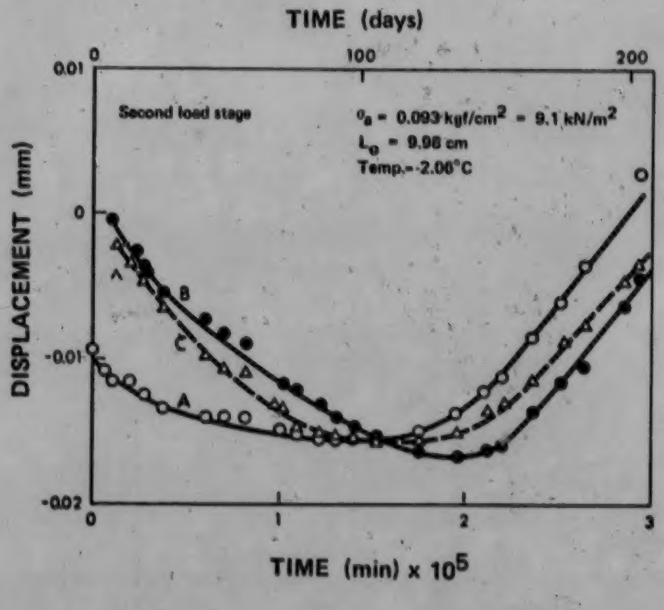

Figure 2.5 Constant stress relaxation and creep of polycrystalline ice, second load stage (From Mellor and Testa, 1969b)

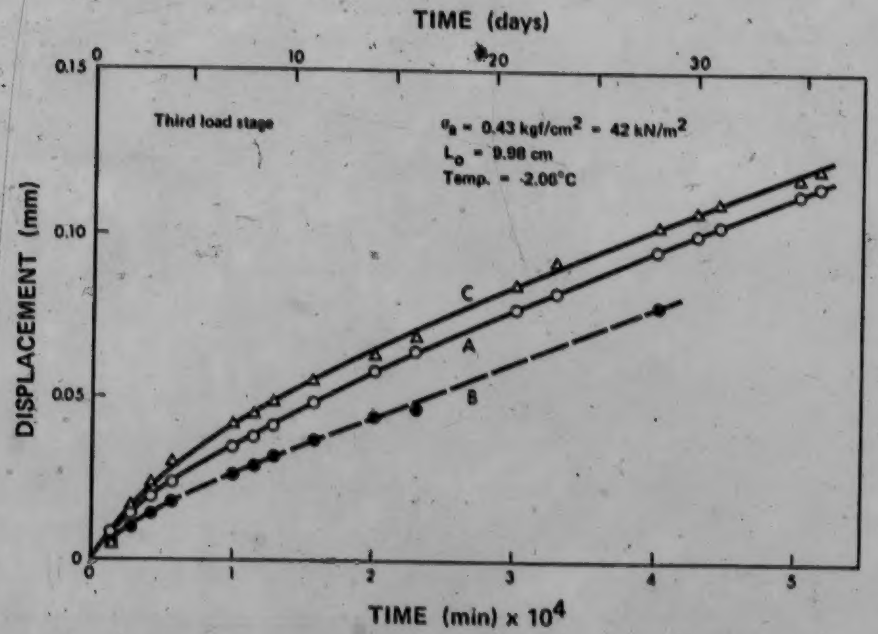

Figure 2.6 Constant stress creep of polycrystalline ice, third load stage (from Mellor and Testa, 1969b)

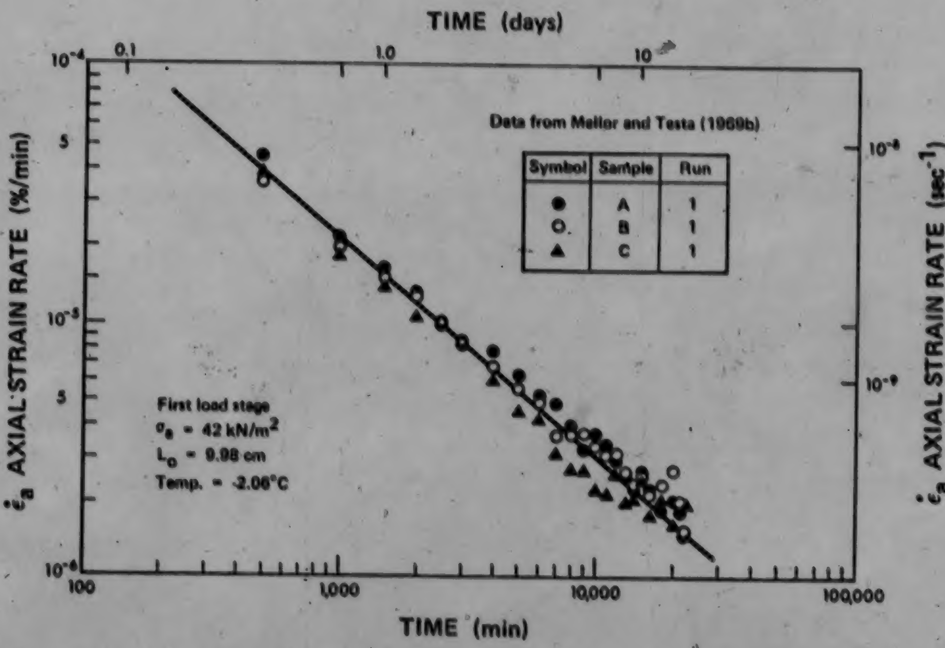

Figure 2.7 Analysis of creep data from Mellor and Testa's first load stage

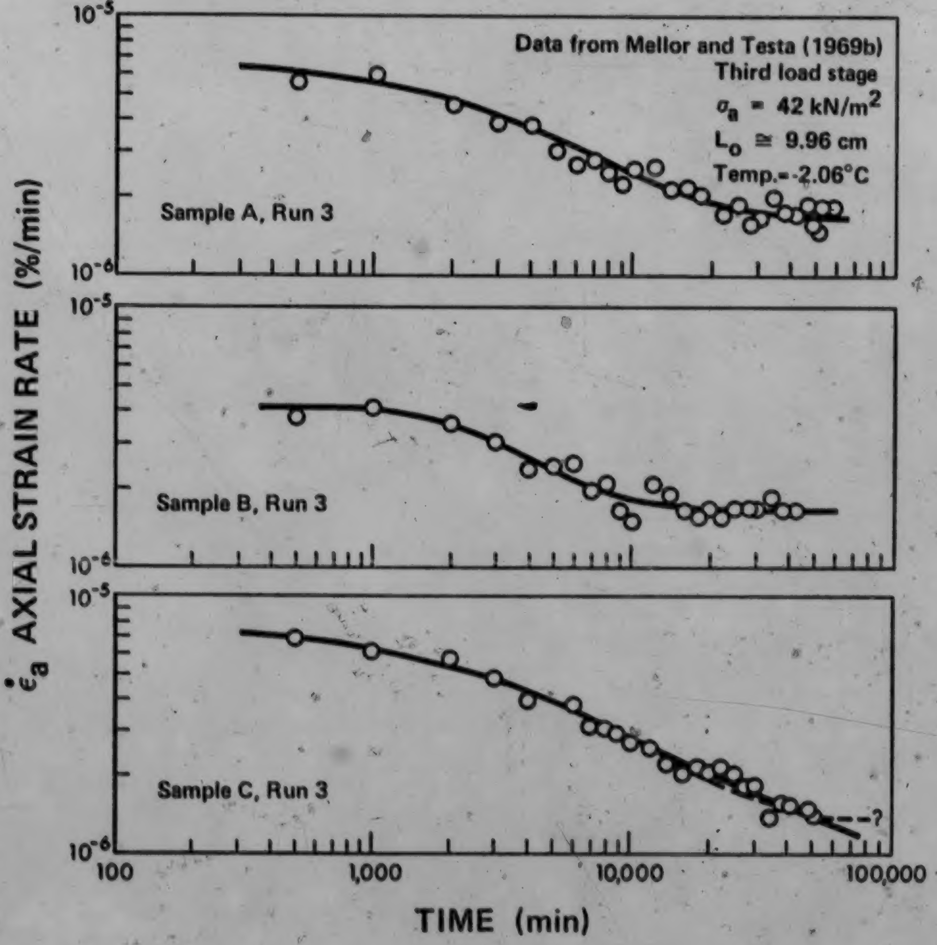

Figure 2.8 Analysis of creep data from Mellor and Testa's third load stage

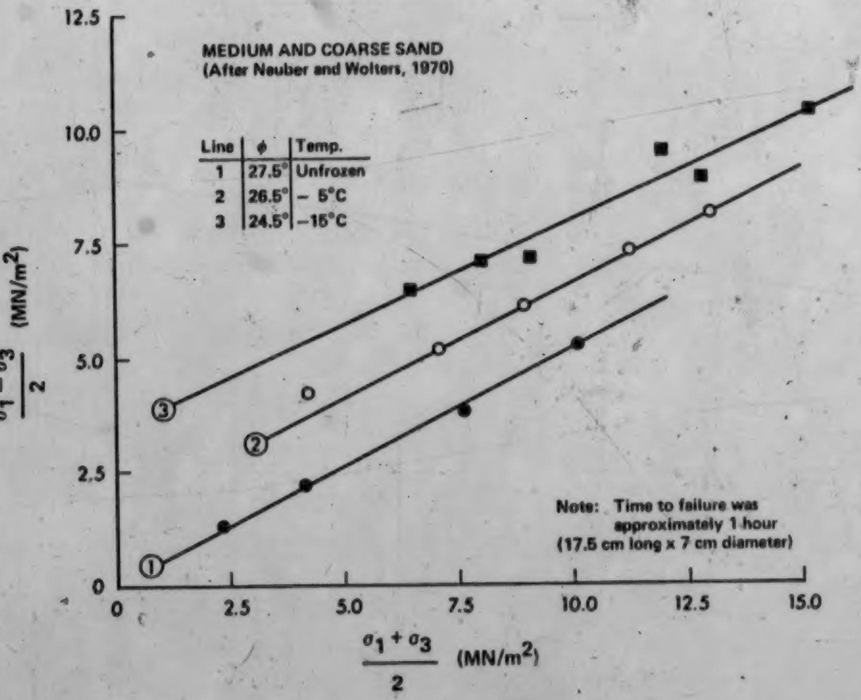

Figure 2.9 Failure envelopes for medium and coarse-grained frozen sand (from Neuber and Wolters, 1970, with changes)

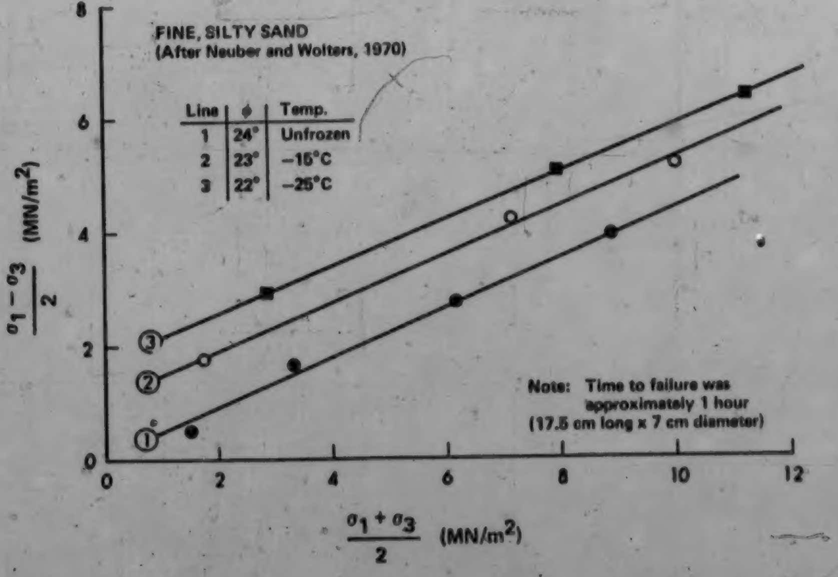

Figure 2.10 Failure envelopes for fine, silty frozen sand (from Neuber and Wolters, 1970, with changes)

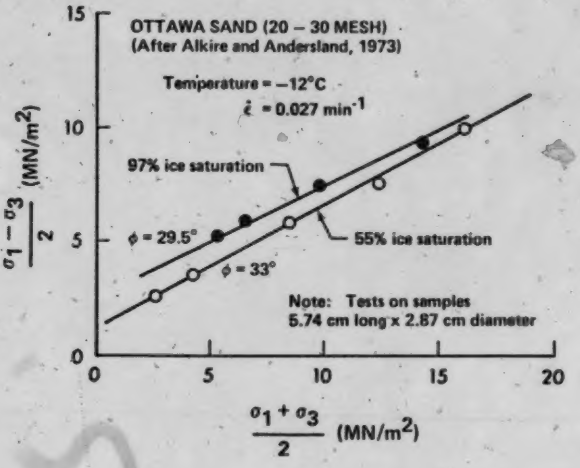

Figure 2.11 Failure envelopes for frozen Ottawa sand (from Alkire and Andersland, 1973)

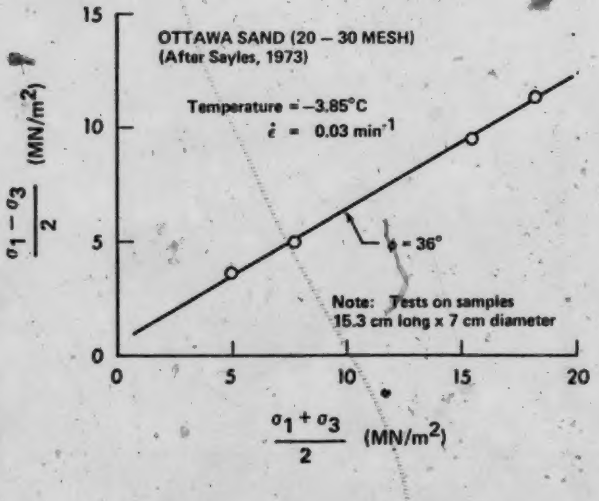

Figure 2.12 Failure envelope for frozen Ottawa sand (from Sayles, 1973, with changes)

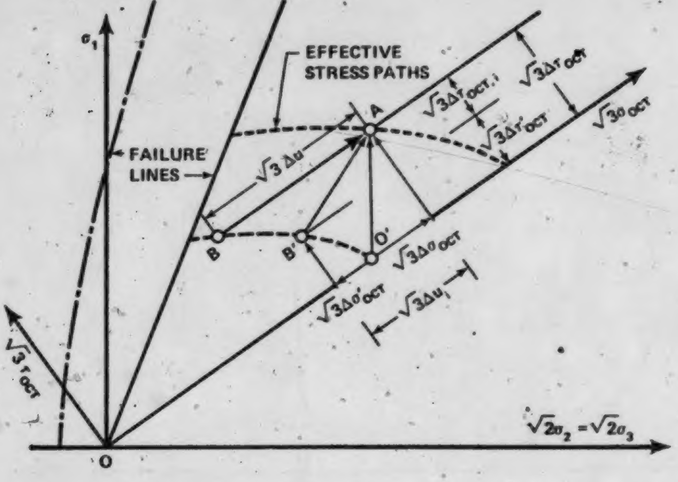
t = 0
t = ∞
σ_1
EFFECTIVE STRESS PATHS
FAILURE LINES
A
B
B'
O'
$\sqrt{3}\,\Delta u$
$\sqrt{3}\Delta\tau_{OCT,i}$
$\sqrt{3}\Delta\tau_{OCT}$
$\sqrt{3}\Delta\tau'_{OCT}$
$\sqrt{3}\sigma_{OCT}$
$\sqrt{3}\Delta\sigma_{OCT}$
$\sqrt{3}\Delta\sigma'_{OCT}$
$\sqrt{3}\Delta u_i$
$\sqrt{3}\tau_{OCT}$
$\sqrt{2}\sigma_2 = \sqrt{2}\sigma_3$
O

Figure 2.13 Rendulic plot for 'normally consolidated' frozen soil in compression (after Ladanyi, 1974)

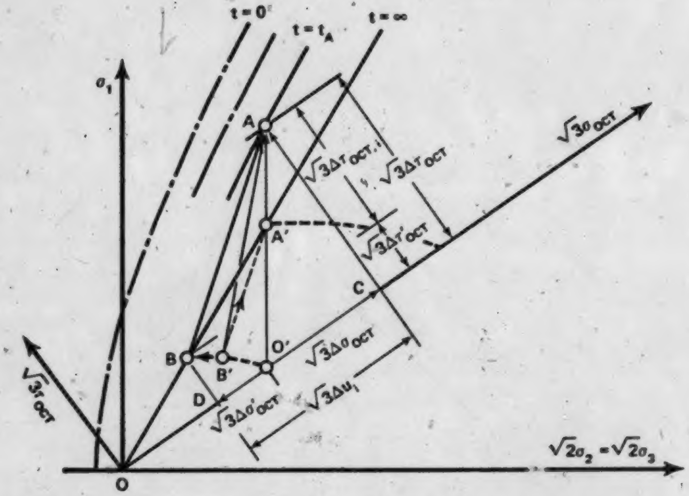
t = 0
t = t_A
t = ∞
σ_1
A
A'
B
B'
O'
C
D
$\sqrt{3}\Delta\tau_{OCT,i}$
$\sqrt{3}\Delta\tau_{OCT}$
$\sqrt{3}\Delta\tau'_{OCT}$
$\sqrt{3}\sigma_{OCT}$
$\sqrt{3}\Delta\sigma_{OCT}$
$\sqrt{3}\Delta\sigma'_{OCT}$
$\sqrt{3}\Delta u_i$
$\sqrt{3}\tau_{OCT}$
$\sqrt{2}\sigma_2 = \sqrt{2}\sigma_3$
O

Figure 2.14 Rendulic plot for 'normally consolidated' frozen soil stressed beyond its long term strength (after Ladanyi, 1974)

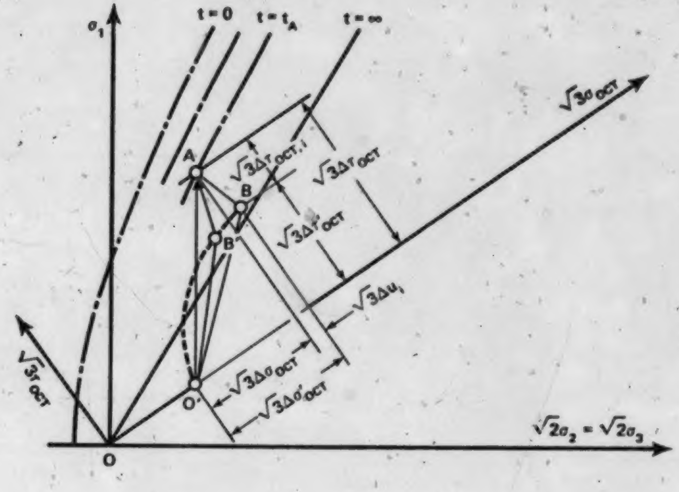
σ_1
t = 0
t = t_A
t = ∞
$\sqrt{3}\sigma_{OCT}$
A
B
B'
$\sqrt{3}\Delta\tau_{OCT,1}$
$\sqrt{3}\Delta\tau_{OCT}$
$\sqrt{3}\Delta\tau'_{OCT}$
$\sqrt{3}\Delta u_1$
$\sqrt{3}\Delta\sigma_{OCT}$
$\sqrt{3}\Delta\sigma'_{OCT}$
O'
$\sqrt{3}\tau_{OCT}$
O
$\sqrt{2}\sigma_2 = \sqrt{2}\sigma_3$

Figure 2.15 Rendulic plot for 'overconsolidated' frozen soil stressed beyond its long term strength (after Ladanyi, 1974)

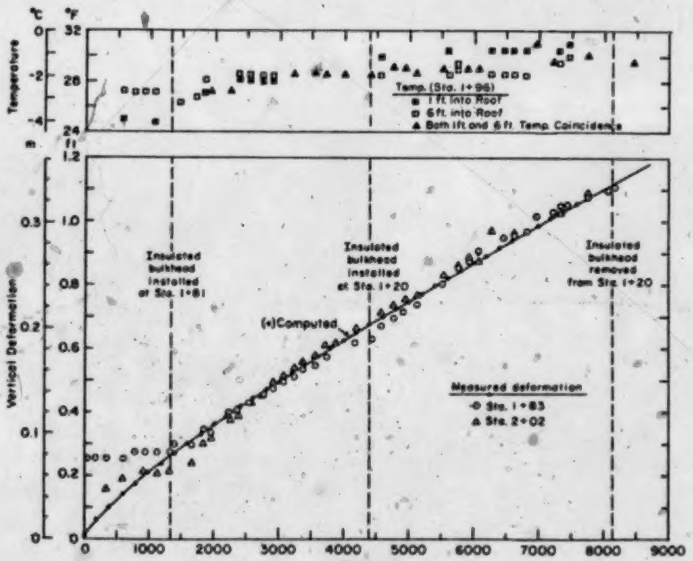

Figure 2.16 Vertical deformation and ground temperature *versus* time for a room excavated in permafrost (from Thompson and Sayles, 1972)

CHAPTER III

LABORATORY STUDIES OF FROZEN SOILS AT NEAR-THAWING TEMPERATURES

3.1 STRESS-STRAIN RELATIONSHIPS FOR FROZEN SOIL

The strength and deformation properties of ice and frozen soil and their response to the application of stress have been discussed at length in Chapter II. Features distinguishing the behaviour of permafrost from that of similar unfrozen soil are associated mainly with the amount of ice present in the soil. Unique properties, such as creep under sustained load and the marked dependence of strength on strain rate, can be attributed directly to the manner in which ice responds to the application of load. Research reported by others and described in the previous chapter has shown that ice behaves as a non-Newtonian, temperature dependent, viscous material. It appears that a constitutive relationship for ice can be described adequately by an experimentally-derived flow law.

The phenomenon of unfrozen water content has been discussed in connection with consolidation volume changes, water flow in frozen soils, and variations in matrix ice content produced by temperature changes. Ice is a causative factor in the well-documented rate-, time-, and temperature-dependent properties which characterize the behaviour of frozen soils. This emphasizes the need to recognize discrete forms of ground ice and to treat them as geological discontinuities which may exert a significant influence on overall geotechnical behaviour. It is therefore essential that the role assumed by ground ice should be recognized and accounted for in analyses or design work involving frozen soils.

In much of the literature dealing with frozen soils, the methods described for predicting movements and determining conditions of failure have been borrowed from classical soil mechanics. In unconfined compression, the ice matrix invariably makes a primary contribution to a soil's strength and to its resistance to deformation. However, it has been shown that the strength and deformation behaviour of ice-poor frozen soils depends to some extent upon the magnitude of normal or confining pressures. In soils which possess either massive or reticulate ground ice structure, frictional contact between mineral particles enables confining pressure to effect both shear strength and creep behaviour. Ladanyi (1974) has described the manner by which internal stresses in a frozen soil can be distributed between the ice, unfrozen water, and soil skeleton at various points in time. Similar concepts have been applied to the analytical solution of specific problems such as the bearing capacity and settlement of both strip and circular footings (Ladanyi, 1974; Ladanyi and Johnston, 1974; Ladanyi, 1975). These theoretical developments suggest that accounting for a soil's non-linear creep behaviour changes bearing capacity factors from conventional values and affects the rate and magnitude of settlement produced by any given load. Here and elsewhere, emphasis has been placed on the need to identify the components of both strength and deformation. This will enable the subsequent interpretation of field or laboratory data by separate consideration of the various phenomena involved.

Specific mathematical models formulated to describe stress-strain-time relationships for ice and frozen soil have been discussed in the previous chapter. Existing experimental data could be used to verify the adoption of these models for routine use, but it should be noted that virtually none of the documented research has involved either quantification of field behaviour or testing undisturbed permafrost at stress levels or temperatures which are pertinent to geotechnical engineering in the Arctic. More basic experimental (and probably field) information must be accumulated before designs involving frozen soil can be undertaken with confidence.

Much of the published data that was discussed in Chapter II has limited value, as interpretations and conclusions offered by the majority of authors cited have been hindered by failure to account for fundamental aspects of strength or creep behaviour in frozen soils. A typical example of this sort of omission appears in Mellor and Testa's (1969b) study where, after ignoring the process of transient creep, the authors have assumed that steady state conditions were established long before deformations came to be dominated by a stationary creep process. Errors like these can have serious consequences when others adopt published data blindly, and use it for their own purposes without first conducting a careful examination of its inherent quality. In this particular instance, Mellor and Testa's (1969b) results suggest that ice subjected to relatively low stresses will reach steady state creep rates which are much faster than those derived from more reliable data which has been published in the interim (Barnes et al., 1971). Relatively simple techniques exist which enable one to separate the transient from the steady state components of creep deformation. Flow laws can thus be developed with considerably greater accuracy. Similar criticisms could be directed toward descriptions of shear strength research on frozen soils. In this regard, experimental work has been largely restricted to cohesionless soils, with tests conducted at relatively cold temperatures, fast strain rates and stress levels considerably higher than those encountered in routine practice. Although this sort of data is easier to obtain experimentally, it has only limited applicability in the solution of geotechnical design problems. Purposefully designing research programs to expediate laboratory testing and avoid difficulty, while at the same time failing to obtain data pertinent to design, is a practice that has yielded only small returns.

To improve our ability to describe and predict the behaviour of frozen soils subjected to load, those soil properties used in the various phenomenological and mechanical models must first be quantified. It follows that experimental studies undertaken to accomplish this should include an assessment of the behaviour of naturally occurring permafrost soils. These comments apply equally well to data collected in the laboratory or the field. The subsequent sections of this chapter describe laboratory tests performed on samples of undisturbed, fine-grained permafrost soil obtained from the Fort Simpson landslide sampling site. Discussions concentrate on the shear strength and creep behaviour exhibited by this material in a temperature and stress environment intended to simulate conditions which would probably be found in a natural slope or beneath a loaded foundation.

3.2 DIRECT SHEAR TESTS ON FROZEN SOIL

Laboratory equipment

To facilitate performing direct shear tests on frozen soils, several changes were made on two Wykeham Farrance SBI machines. The testing was conducted inside a refrigerated laboratory in which ambient temperatures were maintained below 0°C. Controlling the room's air temperature proved insufficient to keep specimen temperature fluctuations within acceptable limits. Therefore, provision was made to circulate fluid from a constant temperature bath through the base and load cap of each of the shear boxes. To minimize side friction on the specimens, the boxes were lined with a thin sheet of Teflon, which reduced the final inside dimensions to 6.00 cm by 6.00 cm (2.35 in. x 2.35 in.).

Figure 3.1 is a schematic layout of the apparatus which was used to conduct the shear tests described below. Lead weights placed on the load hanger assembly acted via the plunger to apply normal stress. A system of microswitches and relays was attached to the motor drive unit to atuomatically reverse the shear box's direction of travel once it had reached a particular displacement from the midpoint position. The first reversal occurred after approximately 1.0 cm (0.4 in) of movement. Subsequent reversals were separated by approximately 2.0 cm (0.8 in) of horizontal displacement. With the system of gears, 25 different speed settings were available, so displacement rates could be selected over more than three orders of magnitude. As a safety precaution, shutoff switches were installed to disconnect the power supply and stop the drive motor in the event that reversal failed to occur at the end of a particular shear cycle.

A load ram connected the upper half of the shear box to a load cell and reaction frame. The bracket supporting this ram was fitted with a Thompson linear bushing to minimize friction in the shear force measurement system. The lower portion of the box was located in a bronze carriage trough running on ball tracks that were guided in ground and hardened vees. The samples were flooded with light paraffin oil instead of water. This minimized desiccation and avoided problems that would have arisen if samples had been degraded by the chemical action of aqueous solutions of antifreeze compounds like ethylene glycol. It was determined that surface tension forces would prevent the oil from intruding into the pores of fine-grained frozen soils. A detailed discussion of the use of oil in these tests is given in Section 3.4. Sintered stainless steel porous stones used in these tests were separated from the specimen by a single thickness of Whatman 54 filter paper.

Horizontal and vertical movements were measured with linearly variable displacement transducers (LVDT's) to an accuracy of approximately 0.0008 cm (0.0004 in). Shear loads were measured with temperature-compensated electrical resistance strain-gauged load cells with a capacity of 10 kN (1000 lb) and a resolution of approximately 2N (5 lb). Atkins type #3 thermistors were used to monitor temperatures. Thermistor beads were submerged in the oil surrounding the soil specimen, and it was assumed that temperatures measured there would not be significantly different from actual sample temperatures. It was also assumed that temperature fluctuations measured in the oil would exceed those actually experienced by the test specimen which was situated between two heat exchangers. Therefore, temperature control achieved was probably better than the data indicate. Temperature records were checked regularly, and, when necessary, the circulator bath controls were adjusted to minimize departures from thermal conditions established at the outset. LVDT, load cell and thermistor output signals were conveyed to a data acquisition system which recorded displacements, shear loads and temperatures at regular time intervals.

Several other equipment modifications were required before adequate control of test temperature was finally obtained. An insulated cabinet constructed around the direct shear apparatus diminished the effects of fluctuations in room temperature but was still not sufficient to obtain the degree of sample temperature control required. After trying several other arrangements, the best temperature control was finally achieved by increasing the volume of fluid circulated from the temperature controlled bath to the shear box heat exchangers.

Materials and sample preparation

At the time this research was initiated, undisturbed samples of permafrost were not available. A preliminary laboratory study was carried out to compare shear strengths determined for a reconstituted clay when frozen and unfrozen. The material used in this program had been excavated from a river bank exposure of dark grey, fissured clay near the mouth of the Mountain River, District of Mackenzie, N.W.T. (McRoberts, 1973). Its basic geotechnical index properties are summarized in Table 3.1. To obtain a uniform structure, the soil was air-dried, pulverized, and slurried at a water content corresponding to a liquidity index of two. A vibrating table and the application of vacuum were used to remove air from the slurry before placing it in a 25 cm (10 in) diameter oedometer. The soil was then consolidated in stages to an effective stress of about 25 kN/m^2 (3.5 psi) at which point the undrained strength was sufficient to permit handling the extruded soil as a block. By remoulding and reconsolidating the soil from a high liquidity index, it was felt that fabric differences existing prior to shear testing could be virtually eliminated.

To prepare the soil for direct shear testing, specimens were trimmed from the block and transferred directly to the shear box. Freezing was prevented by circulating fluid at temperatures of 2 to 4°C through the heat exchangers. Normal load was applied to consolidate the clay to an effective stress of 50 kN/m^2 (7 psi), which exceeded the maximum pressure previously experienced by the soil. When consolidation was complete, the water surrounding the specimen was removed from the shear box. The sample was then flooded with light paraffin oil, then cold fluid (-10°C or less) was circulated through the base and load cap to initiate freezing. It was hoped that redistribution of moisture within the sample could be kept to a minimum by freezing the soil rapidly. Vertical deformations were monitored during this part of the test. Once the sample had been frozen, circulator bath temperatures were adjusted to achieve the thermal conditions selected for the test. The specimen was left at this temperature for two or three days to ensure that thermal equilibrium had been established throughout. The artificial 'permafrost' specimens were then ready to be sheared.

A second group of tests was performed on natural permafrost cored from Zone 4 at the Fort Simpson landslide headscarp sampling site[1]. Geotechnical index properties characterizing this soil are given in Table 3.1. Direct shear specimens were prepared from 10 cm (4 in) diameter samples which had been cored with their long-axes oriented in the horizontal plane. Individual blocks were cut from the core with a power band saw, and an overhead milling machine fitted with a carbide insert rotary cutter was then used to trim them to the precise dimensions. Prior to testing, the sides of each sample were inspected and sketches were made to record any ice structure that was present prior to shear. External dimensions and specimen weights were also noted. After seating each sample, normal stresses were applied and refrigerated fluid was circulated through the shear boxes to maintain constant test temperatures.

Shear testing procedure

Prior to shear, the normal stress acting on the sample was increased to some predetermined value by placing additional lead weights on the direct loading frame. If the normal stress selected for a test was quite large, incremental load increases from the initial seating value were employed. Settlements were recorded for each increment of normal stress.

---

[1] This sampling site and its geology are described in Chapter 5 and Appendix A.

After the sample had reached a stable condition with prevailing temperatures and normal loads, the upper half of the shear box was raised slightly to leave a gap about 0.05 cm (0.02 in) wide. This gap determined the position of the shear plane that would form during the test. The gear train and driving motor were engaged to commence shear by driving the lower half of the shear box back and forth at a constant displacement rate. The load cell and reaction frame held the upper half immobile and shear loads produced by the differential movement were measured and recorded. During shear, horizontal and vertical movements were monitored with LVDT's. By plotting horizontal movements as a function of time, it was a simple matter to determine actual displacement rates occurring during the test. It was observed that these rates remained constant throughout the tests for each of the different gear combinations used in this study.

Every specimen was subjected to a minimum of one complete shear reversal before it was removed from the apparatus. Following the first reversal, two of the tests were interrupted at the midpoint and subjected to an increment in normal stress. When settlement had ceased, shear was resumed under this increased normal load. Sample temperatures were checked regularly during each test and minor adjustments to the bath controls were made on an as-required basis to limit undesireable temperature fluctuations.

When the shear test was complete, samples were extracted from the box and wiped clean to remove the film of paraffin oil left adhering to the external surfaces. The specimens were then cut longitudinally down the middle with a band saw to expose any ice structure which might have been generated by shear. Each of the cross-sections was sketched, and most of the soil slices were also photographed. Water content determinations completed the process of data accumulation for these direct shear tests.

3.3 STRENGTH BEHAVIOUR FROM LABORATORY TESTS

Typical test results

To permit comparison of the strength of frozen and unfrozen clays, shearing characteristics were determined for each state by employing identical testing conditions, with the obvious exception of differences in temperature. During each test, a data acquisition system recorded shear load, horizontal deformations, vertical deformation, and temperature. The data records were reduced with a simple Fortran program which tabulated the various quantities measured in the test. Figure 3.2 shows a computer-drawn summary of results from one of the direct shear tests conducted on frozen soil. These curves are typical of data obtained from tests performed on either 'artificial' or undisturbed permafrost soils.

Figure 3.2 indicates that shear stresses increased quickly and reached maximum values at relatively small shear displacements. This rapid shear stress build-up was usually accompanied by a slight increase in sample thickness (i.e. dilation). Vertical deformation recorded during shear was probably the result of volume changes occurring in the failure zone, but could have also been affected by temperature fluctuations and load cap tilt. After reversing the direction of travel, sample thickness decreased to less than the pre-shear value, but indications of dilation were usually observed as stresses built up during the second cycle of shear. Similar behaviour was observed with other tests on undisturbed Fort Simpson silty clay.

Generally, vertical deformations occurring during shear were quite small and rarely exceeded 0.1 mm. Not all of the samples displayed dilatant behaviour during shear. Tests performed under higher normal stresses were usually characterized by volume decreases or settlement from the outset. Maximum temperature fluctuations recorded were typically less than ± 0.2 °C over test durations of up to three weeks. Kent et al. (1975) have shown that small changes in sample temperature can result in consolidation, so it is conceivable that some portion of the vertical deformations recorded during shear were associated with phase change alone. However, settlements recorded in these shear tests were sufficiently small to justify dismissing any effect which temperature fluctuations might have had on the results.

A feature of almost every stress-strain curve was the reduction in peak shear strength mobilized for each successive reversal. The trend is clearly demonstrated by data from those few tests which ran to five or more reversals. Possible causes for this characteristic behaviour are discussed in a subsequent section of this chapter.

Accumulation of shear stress during the second and subsequent cycles of shear often faltered or lagged at a horizontal displacement corresponding roughly to the midpoint or starting position of the shear box. Following a brief plateau, the stress buildup resumed until a peak was reached in that particular cycle. This peculiar shape is apparent with the shear stress-deformation curve shown in Figure 3.2. More striking examples of this behaviour can be found among other test results which appear in Appendix C. These flat spots developed on the stress-strain curve are caused by two shear mechanisms which operate separately but simultaneously, and reach their individual peaks at different strains. Displacement rates indicated for each test were determined from actual rigid displacements measured during shear.

After removing the samples from the shear boxes, it could be seen that most had experienced some extrusion. Ice and varying amounts of soil had been displaced into the gap separating the upper and lower portions of the shear box. Ice had also accumulated in the porous stones which, in the tests on undisturbed samples, had been completely dry at the outset. These observations confirmed the mobility of water in frozen soils by providing clear evidence that it had made its way out of the specimens under the combined influences of compression, shear and changes in temperature. Relatively warm testing temperatures were employed in these experiments. With some unfrozen water still present, it may be that some of the vertical movement recorded during shear can be attributed to consolidation processes in the frozen soil. Ladanyi (1975), Kent et al. (1975) and Brodskaia (1962) each have indicated that time-dependent volumetric strain accompanying a change in stress may be the result of hydrodynamic time lag during consolidation. Attempts to define consolidation properties from settlement curves recorded in this study proved unsuccessful.

Summary of strength data

The first group of direct shear tests reported in this section was performed on samples of 'artificially-prepared' permafrost. Considerable care was taken to obtain uniform soil fabric, stress, and thermal histories for these specimens. Figure 3.3 shows the strength envelope obtained from Series A, which involved testing unfrozen, reconstituted samples of Mountain River clay. A peak effective friction angle of 26.5° and a small cohesive intercept equalling approximately 7 kN/m^2 (1 psi) were indicated. Multiple shear reversals on both natural and precut shear planes defined a residual friction angle of 23° that is consistent with predominantly illitic mineralogy and published relationships between residual strength and plasticity (Mitchell, 1976).

Series B consisted of five direct shear tests performed on samples identical to those used in Series A, except that they were frozen. Figure 3.4 shows the strength envelope obtained from these tests. Stress-strain curves from the different tests exhibited remarkable uniformity. This similarity was probably due to the virtually identical soil and ice structure which these specimens possessed. It should be noted that sudden commencement of cold fluid circulation through the heat exchangers was very effective in producing rapid soil freezing. This procedure ensured that similar ice structures were developed in each sample prior to shear. Inspection of longitudinal sections revealed that during the early portion of freezing, small lenses formed parallel to the top, bottom and sides of the shear box. Because the freezing plane advanced inward from the heat exchangers, ice lensing assumed a predominantly horizontal attitude. The internal ice structure present prior to shear could not be observed directly: it was therefore impossible to determine with any certainty, which of the post-shear lenses had formed solely as the result of shear.

The strength envelope shown in Figure 3.4 exhibits slight nonlinearity. Nevertheless, the average friction angle indicated was essentially identical to that determined for the same soil in an unfrozen state. Higher normal stresses were used in the tests on frozen soils to improve the definition of the frictional and cohesive components. Fitting a straight line to the Series B envelope for normal stresses between 100 and 300 kN/m^2 indicates a friction angle of 26 to 27°. This value agrees with the peak angle shown in Figure 3.3. Dissecting these samples after shear revealed a distinct horizontal, and apparently continuous ice lens occupying what appeared to be the principal shear plane. However, there was no way of determining whether this ice lens was a result of shear distortion in the soil. The samples could all be cleaved with relative ease along this ice lens, and although some slickensides were observed, it appeared that few secondary shear structures had developed.

In all of the Series B tests, strength continued to decrease with each reversal. None were continued beyond one or two reversals, so a 'residual strength' envelope could not be constructed. The failure envelope shown in Figure 3.4 indicates that a geometric cohesive intercept of 130 kN/m^2 (18.9 psi) was obtained with a rigid displacement rate of 6.9 x 10^{-2} cm/day (2.7 x 10^{-2} in/day).

Specific surface area measurements performed on the Mountain River clay gave a total surface area of approximately 300 m^2/gm.[1] This value seemed abnormally large for a material with clay-sized component of 55%, a liquid limit of 50% and composed predominantly of non-expanding clay minerals. A comprehensive x-ray diffraction analysis of the clay fraction revealed that although discrete montmorillonite was only present in trace amounts, a significant portion of the minerals previously identified as illite were actually interstratified montmorillonite-hydrous mica.[2] The clay sizes thus contained a total expansible component of approximately 30%. The anomalously low liquid limit obtained for Mountain River clay may be consistent with behaviour observed with mixtures of pure Mg-illite and Na-montmorillonite[3]. However, strength data for this same mixture of minerals indicates that residual friction angles measured for these soils would normally be considerably lower than 23° as the montmorillonite fraction dominates strength behaviour when present in amounts exceeding 10%. The 20° residual angle measured in this study remains as an unexplained peculiarity of the geotechnical behaviour of Mountain River clay. The higher friction angle is probably the result of illite and montmorillonite occurring as mixed-layer clays and accounting for only 40% of the soil solids in Mountain River clay.

With specific surface areas as high as 300 m^2/gm, there is little doubt that significant quantities of unfrozen water will be present in the frozen clay at temperatures as warm as -1 to -2°C. On the basis of phenomenological relationships developed by Anderson and Tice (1972),

---

[1,2] Pawluk, S. 1972. Personal communications.

[3] Quigley, R. 1973. Personal communication.

the unfrozen water content for this soil has been estimated at approximately 20% by weight of dry soil for a temperature of -1°C. Therefore, a substantial portion of the water retained in the blocks of soil which occupy positions between ice lenses probably exists in the liquid state. This unfrozen water is one possible source for the ice which appears to accumulate along shear planes formed in frozen soils.

It was apparent that performing similar shear tests on specimens carved from undisturbed permafrost core would provide a better opportunity to document any ice structure that was present prior to shear. An adequate assessment could be obtained by examining the lenses of segregated ice exposed on the sample's exterior. Triaxial shear strength data had been obtained for silty clay from Zone 4 at the Fort Simpson landslide headscarp (see Chapter VI): therefore, this material was adopted for additional research on the frictional behaviour of fine-grained frozen soils. Results obtained from tests using this material constitute one of the few instances where the strength of an undisturbed permafrost soil has been documented, particularly for warm temperature conditions and very slow rates of strain.

Figures 3.5, 3.6 and 3.7 show strength envelopes obtained by shearing the Zone 4 soil at three different rates of rigid displacement. An attempt was made to keep the specimen temperatures constant between -1.4°C and -1.5°C during shear. Data points plotted on these figures correspond to the peak shear stresses measured during the first cycle of each test, with exceptions as noted. In two different tests, shear displacement was halted when the midpoint was reached in the second shear cycle. The normal stress was then increased and some time passed before the tests were resumed. The open circles on Figures 3.5 and 3.7 indicate the peak strengths measured during the second half of those shear cycles. Changes in normal stress have been noted on the stress-deformation curves for these tests (see Appendix C).

The peak strength envelope in Figure 3.5 indicates a friction angle of about 23° for the tests conducted at the slowest of the three strain rates used. This agrees with the effective friction angle of 23 to 24° that was obtained for this soil when thawed (see Section 6.5). The failure envelope defined by the triaxial testing was nonlinear, so the effective friction angle quoted above corresponds to the portion where effective stresses exceed 200 kN/m^2 (30 psi). Other direct shear tests on frozen soil were performed at faster displacement rates. Failure envelopes for these tests indicate some frictional response, but Figures 3.5 and 3.6 suggest that the friction angles decrease as the strain rate is increased.

Figure 3.8 shows apparent cohesive intercepts plotted against time to failure for the Fort Simpson silty clay and for 20-30 mesh Ottawa sand (from Sayles, 1973). This form of data presentation is a modification of the method used by Vialov (1962) to describe the time-dependent uniaxial strength of frozen soils. Test results from both sources show the geometric cohesive intercept decreasing with increasing time to failure. This relationship implies that with sufficiently slow strain rates or long time to failure, an increasing fraction of the total shear strength can be attributed to frictional mechanisms. Behaviour observed in this study is consistent with Vialov's (1962) and Vialov and Susherina's (1964) findings which were discussed in Section 2.4 and substantiates predictions made by Ladanyi (1975). These authors have attributed the cohesive component of shear strength in frozen soils entirely to the time-dependent strength of the ice matrix. It follows that the dependence of cohesion on strain rate (time) and temperature is directly related to resistance offered by the ice phase during shear and deformation of frozen soils.

Most of the differences between the apparent cohesion for sand and clay in Figure 3.8 can be explained by differences in test temperature. Different soil porosities may also be responsible for some portion of the gap between these two lines. Also, the Fort Simpson silty clay almost certainly contained a significant amount of unfrozen water and each sample had several through-going veins of segregated ice.

For a time to failure of 90 to 100 hours, the cohesive intercept from the Mountain River clay, Series B tests (Figure 3.4) falls slightly below the value determined for Fort Simpson silty clay under similar testing conditions. This lower cohesion is probably the result of a remoulded soil structure and slightly warmer test temperatures associated with Series B. It appears that for longer times to failure, the apparent cohesive intercept tends to zero, regardless of soil type. As this occurs, effects associated with differences in soil texture, density, structure and temperature apparently diminish.

Shear-induced fabric

In the preceding, reference was made to certain structural features which had apparently developed during shear. These fabric changes were accentuated by the thin ice lenses which accumulated along the various shear planes. Inspecting interior longitudinal sections obtained at the end of shear revealed distinct ice segregations and sketches were made of each specimen. Post-shear ice structure was then compared to the sketches of segregated ice structure which had been exposed in the exterior faces prior to testing.

Figure 3.9 shows cross-sections of all of the specimens of silty clay from the Fort Simpson landslide headscarp which were sheared in this study. Most of the specimens exhibit a nearly continuous ice lens occupying what appears to be the principal shear plane. Numerous other lenses were visible along lesser shear structures which tended to be concentrated in and adjacent to the shear zone. The orientations of these fine lenses suggested shear features that were similar to those which are known to develop in conventional direct shear tests (Morgenstern and Tchalenko, 1967a, 1967b, Tchalenko, 1968). Riedel shear zones were observed in most of the samples and some thrust features extended well away from the principal shear zone. These thrust shear zones seemed to have developed best in specimens subjected to large cumulative horizontal displacement (e.g. FS-08 and FS-16).

The degree to which accumulation of ice lenses enhanced shear structures appeared to be intensified by having distinct ice lenses present prior to shear. Naturally occurring ice lenses functioned as a source for at least part of the water that eventually made its way into the shear zone. Examples of specimens which are thought to have developed thicker or more numerous ice lenses in their shear zones because of ice present at the outset are FS-04, FS-07, and FS-09. In particular, the latter developed an ice-rich zone at the point where the principal shear plane intersected a natural ice lens.

Examination of the soil surfaces adjacent to the ice-enriched shear zones revealed that slickensides had developed in every sample. These polished surfaces were observed along both the principal shear planes and many of the thrust shear zones which extended into the relatively intact soil. After drying, it could be seen that high spots on the principal shear planes had become noticeably glossy. Selected examples of shear plane surfaces were viewed at high magnification in a scanning electron microscope. A thin layer of highly oriented particles had formed along the shear plane. Within just a few microns of that surface, however, the undisturbed soil fabric had been preserved intact. Therefore, it appeared that the oriented fabric developed by shearing action in these frozen soils was restricted to a thin layer immediately adjacent to the shear plane. It was not possible to determine whether the particle orientation had been produced by mineral contacts during the early stages of shear, or whether the polishing was caused by differential movement between the ice and soil as horizontal displacements accumulated.

The cross-sections in Figure 3.9 suggest that increased water contents might be expected in the immediate vicinity of the shear zone. After each sample had been sectioned longitudinally, the shear zones were cut away to compare their water contents with those obtained for the remaining soil. Water content profiles obtained this way are summarized in Figure 3.10. A band saw was used to section the samples, and some specimens were cut into as many as five separate layers. The majority were sawed into three sections, simply separating the shear zone from the top and bottom of the specimen. Deviations from the average water content are shown in Figure 3.10. Water contents were usually higher in the vicinity of the shear plane, and this increase apparently occurred at the expense of the rest of the sample. Since light paraffin oil was used to flood the specimens during shear, there were no external sources for providing this 'extra' water. It should also be noted that the material extruded along the shear plane consisted mainly of ice and was not included in the shear zone water content determinations.

At the relatively warm test temperatures used, the migration of unfrozen soil water could be responsible for the changed conditions observed. Intact soil peds situated within the network of ice lenses were actually quite dense and may have exhibited dilatant behaviour when subjected to shear. It is well known that negative pore pressures can develop in a dilating soil and such a phenomenon may have been responsible for attracting water to the shear zone. The process of water migration toward shear zones in frozen soils has important engineering implications. On the basis of features observed during this study, extrapolation to field conditions suggests that sustained shear movements along a well-developed rupture surface could produce an accumulation of ice and contribute to a progressive deterioration of the available shear strength. This would probably be accompanied by displacement rates approaching those observed for pure ice.

Components of strength

Experimental results described in the preceding sections are in general agreement with shear strength concepts for frozen soils which were described in Chapter II. Test data reported there demonstrated that shear strength of frozen sand exhibited identifiable frictional and cohesive components. The experiments performed in connection with this study were designed to explore the strength characteristics of frozen, fine-grained soils at temperatures and strain rates approximating those encountered in the geotechnical analysis of slopes or loaded foundations.

Figures 3.3 to 3.7 show that if frozen clays are sufficiently dense so that most of the shearing occurs through intact soil rather than ice, then the frictional component of strength will depend directly upon the normal stress or confining pressure. The friction angle determined from samples sheared at the slowest rate was the same as that obtained from triaxial tests on the same soil after thawing. Increases in strain rate were accompanied by an overall increase in strength, but the friction angles tended to decrease.

Previous studies (e.g. Neuber and Wolters, 1970) had invariably concluded that frozen clays exhibited a negligible frictional response to changes in confining pressure. The strength envelopes shown in Figures 3.3 through 3.7 clearly indicate that the opposite is true. However, it appears that very slow strain rates must be employed before a definite frictional response can be identified. Ladanyi (1974) has suggested that a finite interval of time must follow the application of stress before a frozen soil's behaviour can be resolved in terms of effective stress concepts. He also states that stresses initially carried by the ice matrix must be dissipated by creep before the soil skeleton can fully assume the hydrostatic and shearing stresses applied. This transfer of stress must be a time-dependent process since it is governed by creep. Therefore, mobilization of friction at the soil particle contacts can occur only if strain rates are sufficiently slow for creep deformation in the ice matrix to permit the soil skeleton to assume most of the applied stress. Even if each soil grain is completely coated with ice, stresses at the contact points will be large enough that, with the passage of time, creep and regelation may displace the ice and give way to a solid contact between mineral particles.

At lower mean stresses, the shear strength of frozen clays will depend mainly on the cohesive nature of the ice matrix, particularly if rates of shear are fast. As stress levels are increased, the cohesive component may constitute a decreasing fraction of the total strength. Alkire and Andersland (1973) have observed that ice occupying pore spaces in frozen sand inhibits the development of frictional resistance, so that friction angles measured may actually be smaller than those obtained for the same soil in an unfrozen state. They have argued that the combined effects of high confining pressure and particles being restrained by the ice matrix tend to retard any tendency for volume change. A decrease in the component of strength normally associated with dilatancy thus tends to reduce the measured friction angle. That similar behaviour was not observed in the shear tests on frozen clay reported here, was probably the result of smaller pore sizes and the presence of unfrozen water in the soil. Results suggest that at the slowest rate of strain, shearing resistance offered by the ice matrix was so small that it was possible for the full effective friction angle to be mobilized.

Figures 3.6 and 3.7 show that at faster strain rates, apparent friction angles were less than the effective friction angle for the thawed soil. Figure 3.5 demonstrates that this same friction angle can be duplicated under frozen conditions by conducting shear at sufficiently slow rates of strain. Sayles (1973), on the basis of tests on Ottawa sand, concludes that long-term strength is a function of the effective angle of internal friction which can be determined by performing simple, standard tests on the unfrozen sands.

An indication of volume change was obtained by measuring the vertical movement of the load cap. Some portion of the volumetric strain can be attributed to sample extrusion and phase change associated with temperature fluctuation. However, the vertical movements do provide a crude indication of volumetric straining occurring due to shear. Review of the test results shown in Appendix C, Table C.-, permits the following general observations:

1) During the first cycle of shear, volume changes were small and usually positive.

2) With sustained shearing, volume changes became negative as the result of extrusion.

3) Immediately following each reversal, small volumetric increases were usually superimposed on a typically decreasing trend.

Since the volumetric strains were small, it follows that the contribution of dilatancy to strength will also be small.

The accumulation of ice in the shear zone suggests that some dilation may be the result of redistribution of water on a micro scale. It may be possible to apply some of the concepts which Boulton (1975) has used in describing basal shear in glaciers, to ice structures observed in the test specimen shear zones. He has attempted to show that voids located downstream of protuberances on an undulating shear surface may become sites for the accumulation of ice by the process of regelation.

Figure 3.11 illustrates an ice lens observed in a section of core that was removed from the headscarp of the Fort Simpson landslide. The features noted within this core show several similarities to fabric developed along shear zones in the laboratory study. It is not possible to determine the origin of an apparent displacement discontinuity in this core. In this instance, a through-going ice lens appears to have been rigidly displaced (post-contemporaneously) along either side of a thin ice lens which has tentatively been identified as an in situ shear plane. Slickensides were observed where the soil surfaces had contacted the foliated ice.

On a larger scale, an unusual accumulation of ground ice and evidence of intense shearing have been observed in several undisturbed permafrost cores obtained from a borehole located on the valley wall of the Great Bear River near Fort Norman, N.W.T.[1]. The elevation of this sampling interval corresponds exactly with a zone where inclinometer measurements indicated that sustained shear movement has been occurring for more than a year.

---

[1] Savigny, K.W. 1976. Personal communication.

On the basis of these two examples, it appears that ice structures and slickensides observed in laboratory test specimens compare well with in situ shear zones encountered in fine-grained permafrost soils.

Figure 3.8 suggests that geometric cohesive intercepts from strength envelopes obtained at different rates of strain can be described with an expression of the form proposed by Vyalov (1962). This relationship (which appears in this thesis as Equation 2.12) may not be rigorous, but the data do seem to fit it reasonably well.

Some of the literature discussed in Chapter II has suggested that it may be possible to relate the geometric cohesive intercept directly to the flow behaviour of polycrystalline ice. Figure 3.12 illustrates an idealized cross-section of a direct shear specimen. If a distinct shear zone can be identified, it can be assumed that distortion within that portion of the specimen can be approximated by a condition of simple shear. Shear strain rates can then be computed from the rigid displacement rates imposed in each test. The shear box configuration must be resolved in terms of effective stresses and strain rates (Nye, 1953) before any relationship between the cohesive intercept and strain rate can be assessed in terms of the constitutive relationship that is summarized in Figure 2.1.

The sketches shown in Figure 3.9 indicate that a well-defined shear zone can be identified in each of the direct shear specimens. The approximation proposed in Figure 3.12 therefore seems quite reasonable.

To permit comparison with the behaviour of ice, measured displacement rates and cohesive intercepts were converted to effective strain rates and stresses. These strain rates were subsequently used to extract a corresponding effective shear stress from the flow law for ice given in Figure 2.1. Stresses thus determined could presumably be equated to those required to produce an identical rigid displacement rate if pure ice were being tested in the shear box. Prior to shear, ice along the shear plane was largely restricted to pore spaces. Therefore, shear stresses predicted from the flow law required some adjustment to account for actual distribution of ice. It was assumed that the pore ice carried the same shear load on a reduced shear plane area, so a correction was made by multiplying the flow law shear stress times the average soil porosity to estimate the cohesive intercept. Clearly, this approach was approximate at best, and only served to obtain a crude estimate of the magnitude of shear stress carried by the ice matrix. Continuous ice lenses on the shear plane were not considered since it was felt that some time and displacement were required to develop these features.

The average water content of the 16 specimens tested was 30%. Assuming complete saturation, this corresponds to an average porosity of about 0.45. Table 3.2 has summarized these calculations and presents a comparison of the measured and 'predicted' cohesive intercepts. Agreement was good at the two slowest strain rates, but the calculated intercept for the fastest rate exceeded the experimental value considerably. Differences between the predicted and measured cohesive intercepts were expected since several assumptions and simplifications had been made. Even with the discrepancy at the fastest strain rate, it appears that reasonable estimates of shearing strength can be made if the conditions of stress, temperature, and strain rate are adequately defined.

3.4 ISOTHERMAL CONFINED CREEP TESTS ON FROZEN SOILS

An entirely different experimental program formed the second portion of this study of the geotechnical properties of frozen fine-grained soils. Laboratory testing consisted of observing the creep behaviour of undisturbed specimens which had been subjected to a long-term application of constant stress under isothermal conditons. The soil specimens used in this study were trimmed from core segments of the same silty clay used in the direct shear program.

Laboratory apparatus

A specialized apparatus was constructed that was capable of applying a constant stress, maintaining it over long periods of time, measuring axial deformations, and controlling fluctuations in sample temperature within acceptable limits. A sectional view of the modified triaxial cell used for these isothermal creep tests is shown in Figure 3.13. Modifications to suit the specific requirements of this study included the installation of friction-reducing surfaces on the load platens, heat exchanger coils to provide temperature control, and a thermistor probe to monitor temperatures during the test.

Axial loads were applied with a Bellofram air cylinder actuated by a pressure-regulated air supply. Various Bellofram sizes were used to obtain the magnitude of axial load required in a particular test. The air cylinder connecting rod applied axial stresses via a steel ball resting in a recess at the end of the creep cell load ram. Thompson linear bushings were used to guide the load ram and minimize shaft friction.

Initial attempts to use conventional natural rubber membranes with aqueous solutions of methyl alcohol or ethylene glycol were not successful. While these fluids satisfied the necessary freezing point depression criterion, they invariably caused chemical damage to the membrane. The cracking, blistering and crazing often resulted in small amounts of leakage which were sufficient to damage the sample. Direct leakage and diffusion occurring through the rubber produced significant amounts of ice corrosion and sample deterioration over the lengthy test durations required in this study.

To decrease the risk of aborting a test in its terminal stages, light paraffin oil was used to apply confining pressures within the creep cell. Although the oil was messy to work with, it caused no visible adverse effects. Laboratory trials were conducted to assess the potential for intrusion into the soil during prolonged tests. As part of this preliminary study, cell pressures were elevated well beyond the range intended for use in the creep tests. No intrusion was observed during these trials so the paraffin method of applying confining pressure was adopted. As an added precaution, a spray bottle was used to apply a thin coat of ice to all of the test specimens before placing them in contact with the oil. A technical note published by Iverson and Moum (1974) later confirmed the decision to use oil as a confining fluid. Their work demonstrated that rubber membranes need not be used in triaxial testing if:

1) The cell fluid is immiscible with the soil pore fluid; and,
2) The interface between these fluids is stable under the prevailing conditions of pore geometry and applied cell pressure.

A physical assessment of the pressures required to cause oil to flow into the soil pores indicated, that for clays, the oil-water interface could conceivably sustain pressures as great as 10 atmospheres before intrusion would occur. Therefore, a frozen clay with ice in its pores should be capable of withstanding similar pressures without the risk of intrusion. Cell pressures were controlled by regulating air pressures applied to an oil-filled reservoir outside the cold room.

The creep cells were located inside a controlled environment laboratory where ambient air temperatures could be maintained between -1 and -2°C. To decrease fluctuations in sample temperature, an aqueous solution of ethylene glycol was circulated from a constant temperature bath through a set of heat exchanger coils mounted inside the cell. Figure 3.14 shows a schematic layout of the apparatus used in the creep testing program. To diminish the effects of air temperature fluctuations occurring in the cold room, a closely fitted, insulated cabinet was constructed which completely enclosed the loading frame and creep cells. The exterior of the creep cell was also covered with a layer of Styrofoam insulation. An Atkins Type-3 thermistor cemented inside a piece of stainless steel tubing was inserted through a Swagelok fitting and monitored cell fluid temperatures adjacent to the test specimen. It was felt that a good approximation of the actual soil temperature could be obtained by measuring fluid temperature at the sample mid-height.

Axial stresses were determined indirectly with an electric pressure transducer by measuring the air pressure acting in the Bellofram. Each of the Bellofram was calibrated with a load cell to establish relationships between air supply pressures and the resulting piston force. Valving was arranged so that both cell pressures and axial loads could be measured with the same transducer. The resolution of this instrument, when combined with the air pressure regulation, permitted determination and control of the axial stress to within 0.1%. A Hewlett-Packard 24DCDT linearly variable displacement transducer (LVDT) clamped to the axial load ram was capable of measuring deformations to an accuracy exceeding 7.5×10^{-4} cm (3×10^{-4} in). Output signals from the pressure transducer, LVDT's and thermistors were monitored and recorded at specified time intervals with a data acquisition system. Information thus obtained included a record of axial deformation as a function of time, and permitted a review of the temperature control, axial loads, and cell pressures throughout each test. Temperatures were checked manually on a regular basis and when slight deviations were detected, the refrigerated bath was adjusted accordingly. This procedure made it possible to maintain nearly isothermal conditions throughout each test.

Materials and sample preparation

Samples used in the creep studies were trimmed from core which had been extracted from Zones 3 and 4 of the Fort Simpson landslide headscarp (refer to Appendix A, Figure A.6). Specimens containing typical, randomly oriented, reticulate ice structure were selected for the tests. The index properties of this soil are given in Table 3.1

To ensure a relatively uniform ice structure within each sample, a maximum lehgth of about 12 to 13 cm was adopted since longer specimens usually contained single thick ice lenses. The core was trimmed to a testing diameter of 10 cm (4 in) with a small soil lathe. An overhead milling machine was then used to trim the sample ends parallel to each other. Each specimen was sprayed with a fine mist of water to completely cover it with a thin coat of ice. Apart from functioning as an oil-proof membrane during the creep testing, encapsulating the samples in ice also retarded desiccation which might have otherwise been caused by sublimation during storage. Specimens stored for any length of time between preparation and testing were wrapped carefully and sealed in double polyethylene bags.

Since specimen lengths were less than the normally adopted minimum of twice the diameter, it was felt that lubricated load platens should be used to reduce end friction during the tests. Previous research has shown that using friction reducers at either end of short soil specimens is an effective means of duplicating strength results obtained in tests with conventional sample lengths (Rowe and Barden, 1964; Duncan and Dunlop, 1968). Lubricating the load cap and base pedestal required the use of centering pins to restrain the specimen from lateral movement following the application of axial load. Shallow holes drilled in either end of the creep specimens accepted pins which had been fixed at the center of each load platen. Specimen weights, dimensions and externally visible ice features were all recorded prior to set-up. As water contents determined from pieces trimmed from the ends were seldom representative, bulk density was adopted as the basis for comparing specimens.

Creep testing procedure

Setting up the isothermal confined creep tests was performed entirely within the confines of the cold room. Once the equipment had been cooled to subfreezing temperatures, the load platen surfaces were prepared with surface lubricants. Figure 3.15 shows a sectional view of the base pedestal with details of the friction reducing precautions. The contact surfaces of the pedestal and load cap had been covered with a thin sheet of Teflon. This was coated with an even film of Dow-Corning high vacuum grease. A second film of lubricant containing molybdenum disulphide was then applied. Finally, a thin sheet of neoprene rubber was placed on top of each lubricated surface to separate the sample from the grease. Neoprene membranes were used in preliminary testing, but adopting oil as a confining fluid eliminated the necessity to jacket the specimens so their use was discontinued.

Once the load platens had been lubricated, creep specimens were located on the pins and set up with the load cap in place. The upper half of the creep cell was then lowered and clamped onto the base to make a seal. Circulation of refrigerated fluid through the heat exchangers was commenced while the cell was being filled with paraffin oil. It should be noted that prior to each test, the thermistor probe calibration was checked against an ice bath at 0°C. The temperature sensor was then lowered into position through a Swagelok bulkhead adaptor and, as a last step, the exterior of the cell was enclosed in Styrofoam insulation.

A small axial stress was applied to seat the load platens against the test specimen. Valves were then closed off inside the cold room so the cell pressure and axial stress could be adjusted externally without applying any load to the sample. The air pressure regulators used to control these stresses were located on a control panel outside the cold room. This arrangement avoided problems which were encountered with the condensate freezing and interfering with normal operation when the regulators had been located in a sub-freezing environment. Once the air pressures had been set at appropriate values, cell pressure and axial load were controlled by opening valves on lines located inside the cold room. Cell pressures were applied a minimum of three days prior to increasing the deviatoric stress and initiating of creep. This provided some time for adjusting the test temperatures and allowing the sample to reach thermal equilibrium.

The creep tests were usually run with two cells set up side by side in the same load frame and enclosed within a single insulated cabinet. Once the load platens had been seated, LVDT's were clamped to the load rams on each cell. Following adjustments to the LVDT output voltage, the insulated cabinet was closed and sealed. When conditions were considered stable, initial readings were taken and the valve controlling the Bellofram was opened which resulted in the sudden application of axial load. Air pressure in the Bellofram built up to the desired level within a matter of a few seconds. During each creep test, cell pressures and axial loads were checked for constancy at intervals of one to two days. The axial load was adjusted periodically to account for changes in the cross-sectional area that was calculated from axial strains by assuming that the sample volume did not change. Deformations occurring over time intervals of several days were normally quite small, so a constant axial stress (± 0.5%) could be maintained quite easily.

Records of the test data were subsequently reduced with a simple Fortran program. Small temperature fluctuations seemed to cause irregularities in the time-deformation curves. To avoid the difficulties which these would cause in computing strain rates, a five-point moving average was employed to smooth the data. Figure 3.16 shows how effectively this technique removed the irregularities induced by temperature. Strain rates were determined continuously in the data reduction process by numerically differentiating axial strain with respect to time. Standard relationships were employed which used strains measured at three successive points in time and calculated the rate at the center point for each increment of time. Interpretation of the data was facilitated by using graphical displays of various combinations of the reduced data which were produced by a computer-controlled Calcomp bed plotter.

3.5 CREEP BEHAVIOUR FROM LABORATORY TESTS

The literature discussed in Chapter II indicates that both strength and deformation characteristics of ice and frozen soils are highly dependent upon the duration of load. Certain aspects of this behaviour are amenable to study in laboratory tests, and this section describes the results of a series of constant axial stress, isothermal creep experiments which were performed with different confining pressures.

Typical test results

Sayles (1973) has reported that even though care was exercised to eliminate or at least minimize experimental inconsistencies related to specimen composition, preparation procedure, and testing conditions, there were still notable variations in his results. Since undisturbed, fine-grained permafrost soils were used in this study, it seemed probable that the results might prove difficult to interpret.

Effects primarily caused by fluctuations in test temperature have been mentioned in the preceeding section. Temperatures were usually controlled to within ± 0.1 C° of the desired value, but sudden, small increases often initiated a temporary acceleration in the observed axial creep rate. Figure 3.16 illustrates this behaviour reasonably well since most of the perturbations in the strain-time curve appear to be preceded by an increase in specimen temperature. Employing a five point moving average has smoothed the experimental curve effectively by distributing the brief, temperature-related disturbances over longer intervals of time. This technique probably provides a reasonable approximation of the average creep response to axial load which would be observed if temperature could be held perfectly constant. A portion of this incremental creep behaviour may also be the product of random stabilization of minute shear displacements occurring along various planes of weakness within the specimen.

Stage loading was employed in most of the tests. This was accomplished by allowing the specimen to attain what appeared to be steady state creep conditions before applying one or more additional increases in axial stress. The results from a typically stage-loaded creep test are shown in Figure 3.17. These curves illustrate the classical transition from primary or transient creep into secondary steady state creep. By plotting both strain and strain rate as a function of time, it is possible to determine whether the specimen has actually exhibited true steady-state creep.

Conventionally, a straight line has been fitted tangent to the axial strain versus time curve. The slope of this line has then been used to estimate the secondary creep rate. Since strain rates for these tests had been evaluated continuously by numerically differentiating the normal creep curve, a plot of axial strain rate versus time could also be drawn. An alternate and more reliable means of determining the steady state creep rate consisted of taking the value which the strain rate curve approached asymptotically at large times. For the particular test illustrated in Figure 3.17, it can be seen that secondary creep rates estimated by using these two different methods are in reasonable agreement with each other. Similar curves were obtained for each of the tests and all are included in Appendix C.

In certain tests, the axial stress was held constant while the confining pressure was either increased or decreased. Other tests were initiated with considerably different confining pressures but identical axial stresses. Data obtained using these different combinations were inconsistent. However, the results did indicate that increasing the confining pressure tended to prolong transient creep and slightly reduced the ultimate steady state creep rate obtained with a specific axial stress. This observation is consistent with the frictional effects discussed in Chapter II in that a higher ice content would tend to decrease the number of soil particle contacts in a given specimen.

An inspection of the various creep curves obtained in this study indicates that in the early portion of most tests, strain rate continues to decrease with time. This behaviour suggests an empirical power law relationship between creep strain rate and time. Figure 3.18 shows logarithmic plots of strain rate versus time for the first loading stage of four different tests conducted with axial stresses ranging from 35 kN/m^2 to 227 kN/m^2 (5 psi to 33 psi). Although significant fluctuations in strain rate occurred, a considerable portion of this could be attributed to small changes in test temperature and computational limitations inherent to the numerical differentiation technique which was used in their determination. Even with these departures from ideal behaviour, the experiments have yielded curves with shapes that closely resemble the general form shown in Figure 2.3. This transition from attenuating primary creep to a constant secondary creep rate can be phenomenologically described with a power law taking the form given by Equation 2.9.

$$\frac{d\varepsilon}{dt} = \dot{\varepsilon} = At^a + B \qquad (2.9)$$

By determining the constants in this equation experimentally, it should be possible to define strain rate as a function of time for an arbitrary material, temperature, and applied stress.

Rigorously, data plots like the ones shown in Figure 3.18 should be used to establish appropriate constants in the primary creep equation. Strains produced by these transient processes could then be subtracted from the total measured strain to obtain a residual displacement. This would presumably be the sole product of steady state or secondary, non-attenuating creep processes. A linear equation (obtained by linear regression analyses or some other suitable technique) relating residual strains to time could then be derived, and its slope would define the secondary creep rate. If this secondary strain rate were quite small, the influence exerted by steady state processes on the primary portion of the logarithmic plot of strain rate versus time would be insignificant. Separating the primary and secondary creep strains with the procedure described above would probably not be necessary in most cases. At small times, strains due to secondary creep would be small and at longer times, primary creep processes will have diminished to a rate that is considerably less than the secondary strain rate. Transient creep will dominate at early times and steady state processes will begin to control the strain rate as time passes.

In the data reported in this study, there was no attempt made to separate the transient and steady state components of creep. Rather, it was assumed that the parameter B in Equation 2.9 equalled zero at the outset and that primary creep ceased entirely at large times. This simplistic approach was thought to be warranted in view of the marginal quality of most of this data. However, data which might be obtained from other tests conducted at colder temperatures with improved thermal control and larger deviatoric stresses might justify using a more comprehensive analysis. Only that data obtained during the first load stage of multi-stage tests has been used to determine constants describing primary creep behaviour. Hult (1966) has outlined a method to reconstruct primary creep curves for cases where deviatoric stress has been abruptly increased at some arbitrary point in time. The construction assumes a strain-hardening creep law, and Hult (1966) comments that in experiments where metals have experienced this sort of stress history, measured results compare reasonably well with theoretical predictions. Unfortunately, numerous irregularities in the data collected for this study precluded the analytical construction of true primary creep curves for second and subsequent loading stages.

A summary of the results obtained from creep tests performed on undisturbed samples of the Fort Simpson silty clay appears in Table 3.3. Additional details pertaining to the source and techniques used to prepare these samples are contained in Appendices A and B. The laboratory creep curves can be found in Appendix C.

Transient creep

Other experiments discussed in Chapter II have shown that subsequent to immediate elastic deformations, the instantaneous slopes of the strain-time curves (i.e. creep rate) obtained for ice and frozen soils decrease with time and eventually assume a constant value. Methods outlined in the preceding sections and in Chapter II have been used to analyze transient creep behaviour observed during the first load stage of each test conducted in this study.

Figure 3.18 illustrates the typical linearity obtained at small times on the logarithmic plots of strain rate against time. The transient creep rate term in Equation 2.9 consists of a constant (A), and a time exponent (a) for any given deviatoric stress and temperature. Tabulated data indicate that A exhibits only slight variability, while the exponent a (slope of the line) increases from -1 and approaches zero when the applied stress becomes large. Figure 3.19 shows a possible means of expressing this nonlinear relationship between the applied stress and its associated primary creep exponent.

Ladanyi and Johnston (1973) have reported contradictory behaviour in their logarithmic plots of volumetric strain versus time which had been derived from a multi-stage pressuremeter creep test performed in a frozen, varved silt-clay. Their interpretation of the data had apparently been based on an extrapolation of lines drawn tangent to the creep curves at an arbitrary time of 15 minutes. An alternative interpretation can be obtained by fitting straight lines to the creep curves. At a time of one minute, the ordinate intercepts of these lines converge on a relatively narrow range of volumetric strains. These intercept values have been derived in a manner similar to that used to obtain the constant A in this thesis. Also, the creep exponent derived from these curves varies from approximately -0.6 at the lowest stress used, and approaches zero as the pressuremeter's internal stresses are increased.

Using simple relationships like Equation 2.9 to describe creep behaviour phenomenologically constitutes a gross over-simplification of more rigorous physical relationships. Formulating a general expression to cover a wide range of stresses and temperatures for even a single material type would require an enormous amount of experimental work to define the necessary parameters. Similar efforts would be required to describe the simultaneous process of steady state creep.

A logarithmic plot of the transient creep exponent versus applied stress is shown in Figure 3.19. This graph indicates that a power law relationship may exist between these two variables. The flow law for ice described in Chapter II was also a power law, relating steady state creep rates to stress. Figure 3.20 shows a semi-logarithmic plot of primary creep exponents versus the steady state creep rates eventually obtained in those same tests. Although these results cannot be considered conclusive, they do suggest an interesting topic for future research. If a relationship like this can be shown to be tenable, the need to conduct long-term tests to define steady state conditions might be relaxed. Some control testing would still be required, but results from relatively short term pressuremeter testing might eventually be used more confidently to predict both transient and steady state creep behaviour.

From Figure 2.1, it can be seen that small applied stresses produce very slow steady state creep rates. Under these circumstances, transient creep processes could conceivably dominate total deformations some time after the initial application on load. This might be especially true at temperatures close to 0°C where steady state behaviour has not yet been well-defined. Data presented by both Vialov (1962) and Sayles (1973) indicate that large times are required before creep behaviour makes the transition from deformation dominated by non-attenuating processes to a condition of steady state.

Steady state creep

Although the slopes of tangents drawn to creep curves have been used to estimate steady state creep rates, the reanalysis of Mellor and Testa's (1969b) data discussed in Chapter II demonstrates that this technique has not always been reliable. It appears that a more acceptable method of determining steady state creep rates might involve the use of a logarithmic plot of strain rate against time. Presenting data in this manner provides a clear definition of the point at which the instantaneous creep rate becomes constant with time. Typical data shown in Figure 3.17 suggest that steady state creep rates estimated from strain-time curves are in reasonable agreement with the strain rate approached assymptotically at large times. Logarithmic plots of strain rate _versus_ time like those shown in Figure 3.18 were used to determine steady state creep rates (B or $\dot{\epsilon}_s$) which are listed in Table 3.3.

Experimentally-derived steady state strain rates were poorly defined in those tests conducted at the lower stress levels. However questionable they may be, strain rates were determined as accurately as possible, and a logarithmic plot of axial stress against axial strain rate including data from all of the tests appears as Figure 3.21. It can be seen that considerable scatter exists for test data obtained at axial stresses of less than 100 kN/m^2 (15 psi). An examination of the creep curves for these particular tests (see Appendix C) indicates that steady state creep rates were extremely difficult to estimate. Also shown are data points derived from tests reported by Sayles and Haines (1974) which were conducted on a similar material (Suffield clay) at a slightly cooler temperature of -1.7°C. The durations of these tests ranged from 30 to 50 days.

The heavy curve shown in Figure 3.21 represents an experimentally derived flow relationship for the Fort Simpson silty clay and has a bilinear shape. A power law fitting the straight line portion at stresses above 100 kN/m^2 (15 psi) has an exponent of approximately 2.75. This value is consistent with the flow law exponent reported for polycrystalline ice in Chapter II. If this line is extended through the Suffield clay data points, a single straight line defines the flow law for these soils. Until better tests can be conducted at low stresses and warm temperatures on both frozen soil and ice, it seems premature to recognize any sort of bilinear flow law. After having fitted a straight line through the data for Suffield clay and results from tests at higher stresses on the Fort Simpson silty clay, the steady state creep rates are one to two orders of magnitude faster than those indicated for ice under similar conditions of stress and temperature. This difference in creep rates may be the result of one or more of the following factors:

1) The presence of significant quantities of unfrozen water in fine-grained soils at temperatures close to 0°C.
2) Shear movements occurring along soil-ice interfaces at contacts between discrete ice lenses and intact soil.
3) Acceleration of creep in the ice lenses caused by softening and crystal boundary thickening caused by chemical impurities which were excluded from the soil water during freezing.

Closer correspondence to the behaviour observed for ice would be anticipated at colder temperatures or in highly ice-rich soils.

Table 3.3 shows that when specimens were subjected to the same axial stress, higher confining pressures appeared to result in slightly slower secondary creep rates. The most probable explanation for this behaviour is that confining pressures increase the stress carried by the soil skeleton so that greater frictional strength must be overcome to produce shear movement and creep. It follows that creep rates could be attenuated by elevating the confining pressure if some form of 'drainage' in the frozen soil results in the soil skeleton carrying an increased mean stress. Decreased creep rates under high confining pressures have also been reported for frozen sands (Alkire and Andersland, 1973; Sayles, 1973).

One exception to this trend was observed in Tests 5 and 6 where the confining pressure was suddenly reduced from 552 kN/m^2 (80 psi) to zero with the axial stress being held constant. It was expected that the secondary creep rates would increase, but instead, they appeared to decrease by as much as a factor of 5. These results are questionable since the procedure employed did not provide any time for the specimen to equilibrate after adjusting the confining stress.

The data also indicate some effects which are related to the characteristics of individual specimens. All other factors being the same, behavioural differences associated with physical characteristics seemed to be more strongly affected by internal ground ice structure than frozen bulk density. The presence of features such as through-going ice lenses inclined at favourable angles had very noticeable effects. Samples were thus selected to eliminate nonuniformities which might have made the interpretation of test data more difficult. Cores used for the tests reported here were prepared so that each specimen contained a similar, evenly-distributed network of thin reticulate ice lenses.

It was anticipated that warmer temperatures would result in faster creep rates. Tests run with temperatures closest to 0°C displayed greater sensitivity to fluctuations in temperature control. This response was almost certainly related to the increasing rate of change in the unfrozen water content as 0°C was approached.

The creep specimens were all examined in detail once the tests had concluded. Most of them appeared to have strained uniformly and showed no indication of bulging or distinct shear planes. In a very few instances, small amounts of movement appeared to have occurred along ice lenses, but in general, the assumption of volume constancy appeared to have been a reasonable one.

3.6 DISCUSSION OF RESULTS

The data presented in this chapter are unique for two reasons:

1) A majority of these tests were performed at near-thawing temperatures on natural and relatively undisturbed fine-grained permafrost soils.
2) The tests were performed at slow strain rates with low stresses and very long test durations.

The slow strain rates used in the direct shear testing meant that several experiments lasted for more than 30 days. Fortunately, the results obtained appear to have justified the experimental difficulties which were encountered. Similarly, the creep study required long testing times before steady state conditions could be identified with confidence. The challenge of conducting these long-term tests was compounded by the necessity for extremely effective temperature control when working within 2°C of the melting point.

This study of the strength and deformation behaviour of natural permafrost soils has shown that a mechanistic description of the interaction between shear and creep given in Chapter II was reasonably accurate. The applicability of this conceptual model had been demonstrated for frozen sands, but much of the literature pertaining to the properties and behaviour of frozen, fine-grained soils seemed quite ambiguous. The results of these experiments have shown that Ladanyi's (1974, 1975) basic model for frozen soil behaviour can be used with reasonable confidence in making predictions of creep settlements and time-dependent bearing capacities for foundations on frozen soils. These same concepts may also find application in estimating and interpreting time-settlement relationships for piles in permafrost, as well as in establishing the conditions of limiting equilibrium when analyzing the stability of slopes which are affected by permafrost conditions.

The direct shear testing has demonstrated that frozen fine-grained soils exhibited a definite frictional response. If imposed strain rates are sufficiently slow, the friction angle mobilized can equal the effective angle of shearing resistance obtained for the same soil in an unfrozen state. Higher geometric cohesive intercepts were observed with increasing rates of strain, the magnitude apparently being controlled mainly by the strain rate and soil temperature. The magnitudes of these cohesion intercepts were estimated by using the flow law for ice (Figure 2.1) to compute a shear stress corresponding to the strain rate imposed during the test. The cross-sectional area of the specimen was then corrected to the average amount of ice actually present in the shear plane (i.e. proportional to the soil's porosity). It was also found that the available shear strength decreased as the horizontal deformations accumulated. The observed reduction in strength can be at least partially attributed to the formation and accumulation of a thin layer of segregated ice along the shear plane. Slickensides were noted on the soil surfaces which had been in contact with shear-induced ice lenses. Samples of Fort Simpson silty clay used in these tests were quite dense so it seems probable that these polished surfaces formed during the early stages of shear. Indications of dilatant behaviour during the first and some subsequent cycles of shear suggest that unfrozen water and ice may be attracted to the shear zone, ultimately producing the accumulation of ice observed there.

This particular observation has serious implications with respect to the long-term behaviour of footings, piles, and slopes involving permafrost soils. Since sustained shear movements can apparently cause increases in ice content within shear zones, imposing stresses which exceed a soil's long-term shear strength could conceivably lead to a condition of deteriorating stability. With an underestimated load, deformation rates might increase, as the ultimate strength and creep rate of an ice-rich shear zone would be governed by the properties of ice. These structures were observed in all of the direct shear specimens, but it was not determined whether similar lensing could be produced during transient and steady state creep. Sheared samples examined were characterized by a well-developed shear zone that was crisscrossed with numerous compounded shear planes. Decreasing friction angles observed were in good agreement with Ladanyi's (1974) prediction that faster strain rates would inhibit the full mobilization of frictional resistance in the soil. The direct shear testing also demonstrated that changing the normal stress acting on a shear plane had little or no effect on strength mobilized once an ice lens had formed there.

The most important finding was that, contrary to previous suggestions that frozen, fine-grained soils exhibit no frictional response, these tests have shown that the soil's effective angle of internal friction can be mobilized if strain rates are sufficiently slow. Under low normal stresses and at faster strain rates, the frozen strength is dominated by the cohesive component. This quantity is largely controlled by the strength of ice and is therefore dependent upon strain rate, temperature, and ice content.

The creep testing program demonstrated that the deformation behaviour of undisturbed, fine-grained permafrost soils is amenable to rational analysis. Both transient (attentuating) and steady state processes were clearly identified. Of considerable interest was the observation that steady state creep rates determined in this study were in general agreement with those which could be estimated using the flow relationship summarized in Figure 2.1. It would seem that at warm temperatures, fine-grained soils actually creep at rates which are only slightly faster than those exhibited by ice. Although increasing the confining pressure seemed to have an attentuating effect, the resultant changes in creep rate were not large.

Limited data suggest that since the exponent describing transient creep response is a function of the applied deviatoric stress, it can also be correlated to the steady state creep rate which is ultimately obtained. Further research in this area could result in the development of a procedure for estimating steady state creep rates directly from transient creep behaviour observed in realtively short-term tests. Methods for separating transient and steady state creep processes have been discussed. It seems reasonable to conclude that utilization of these techniques in analyzing laboratory data, the results of pile load tests, *etc.*, would almost certainly improve the level of confidence in the interpretation and engineering application of results obtained.

It was generally felt that the creep data obtained in this study were subject to some criticism, as a result of testing difficulties associated with temperature control. Even so, a crude flow law was constructed, and the exponent of 2.75 relating stress to strain rate corresponds closely to the value of 3 which was determined for polycrystalline ice in Chapter II. Additional experimental work will be required before the magnitude of creep deformations occurring in frozen soils can be estimated with confidence.

This laboratory study has shown that transient creep can contribute significantly to total deformation, particularly at low stress levels. Numerous carefully instrumented and monitored long-term field and laboratory tests will be required before a comprehensive model can be developed to describe and predict the creep behaviour of frozen soils accurately. By employing analytical techniques which are physically sound, solutions to specific problems can be obtained through the sensible interpretation of several tests which have simulated design loading conditions.

TABLE 3.1 SUMMARY OF SOIL INDEX PROPERTIES

SOIL	PERCENT CLAY (less than 2μ)	PERCENT SILT	LIQUID LIMIT	PLASTIC LIMIT	PLASTICITY INDEX
Mountain River Clay[1]	50-65 (55)[2]	35-50 (45)	40-52 (48)	20-22 (21)	27
Fort Simpson Clay[1,3]	50-85 (60)	15-50 (40)	45	20	25

[1] X-ray diffraction analyses performed on the clay-sized fraction of both soils indicated that illite and kaolinite were the major identifiable minerals. Chlorite and montmorillonite were also present in trace amounts.

[2] Numbers shown in brackets are average values.

[3] Samples tested were obtained from Zone 4. See Chapter V and Appendix A for details regarding stratigraphic position.

TABLE 3.2 COMPARISON OF MEASURED AND PREDICTED COHESION INTERCEPTS

TEST SERIES	RIGID DISPLACEMENT RATE ($cm\ s^{-1}$)	STRAIN RATE (s^{-1})	EFFECTIVE SHEAR STRAIN RATE (s^{-1})	EFFECTIVE SHEAR STRESS[1] ($kN\ m^{-2}$)	COHESION INTERCEPT PREDICTED[2] ($kN\ m^{-2}$)	COHESION INTERCEPT MEASURED ($kN\ m^{-2}$)
1	1.10×10^{-6}	8.00×10^{-7}	4.00×10^{-7}	420	190	180
2	3.51×10^{-6}	3.43×10^{-6}	1.72×10^{-6}	610	275	240
3	2.16×10^{-5}	2.27×10^{-5}	1.13×10^{-5}	~1200	540	290

[1] Effective shear stress (Nye, 1953) determined by estimating the stress required to produce that strain rate from the flow law shown in Figure 2.1.

[2] Predicted cohesion intercept obtained by multiplying the shear stress by the soil's average porosity to correct for the actual volume of ice present.

TABLE 3.3 SUMMARY OF LABORATORY DATA FROM CONSTANT STRESS CONFINED, ISOTHERMAL CREEP TESTS

TEST	FROZEN BULK DENSITY γ_f (Mg m^{-3})	AVERAGE TEMPERATURE (°C)	DEVIATORIC STRESS $\sigma_1 - \sigma_3$ (kN m^{-2})[2]	CONFINING STRESS σ_3 (kN m^{-2})	PRIMARY CREEP COEFFICIENTS A (% min^{-1})	PRIMARY CREEP COEFFICIENTS a	SECONDARY CREEP RATE B or $\dot{\varepsilon}_s$ (% min^{-1})	REMARKS
1-A	1.77	-0.75	20.7	69	4.7×10^{-2}	-0.97	4.2×10^{-5}	
1-B		-0.75	48.3	69			2.2×10^{-5}(?)	Poor Temperature control
1-C		-0.75	82.7	69			3.7×10^{-5}(?)	
2-A	1.68	-0.75	20.7	69	4.7×10^{-2}	-0.97	4.6×10^{-5}	
2-B		-0.80	48.3	69			2.6×10^{-5}(?)	Poor Temperature control
2-C		-0.80	82.7	69			3.4×10^{-5}(?)	
3-A	1.84	-0.95	34.5	345	2.8×10^{-2}	-0.97	6.1×10^{-6}	
3-B		-0.95	69.0	345			3.0×10^{-5}	
4-A	1.65	-0.90	34.5	345	4.7×10^{-2}	-0.97	2.2×10^{-5}	
4-B		-1.00	69.0	345			2.5×10^{-5}	
5-A	1.84	-0.95	34.5	552	1.0×10^{-1}	-1.05	8.2×10^{-6}	
5-B		-0.90	82.7	552			2.5×10^{-5}	
5-C		-0.90	82.7	0			1.0×10^{-5}	
6-A	1.91	-0.85	34.5	552	4.7×10^{-2}	-1.00	8.7×10^{-6}	
6-B		-0.85	82.7	552			2.7×10^{-5}	
6-C		-0.80	82.7	0			5.1×10^{-6}	
7-A	1.61	-1.40	172	207	1.2×10^{-1}	-0.73	3.9×10^{-5}	Too Cold, Poor Data
7-B		-0.90	329	207			6.1×10^{-4}	
8-A	1.81	-1.25	172	207	1.8×10^{-2}	-0.78	4.3×10^{-5}	Too Cold, Poor Data
8-B		-1.10	331	207			4.7×10^{-5}	
9-A	1.75	-0.80	241	621	2.2×10^{-2}	-0.40	2.1×10^{-4}	
9-B		-0.80	379	621			6.3×10^{-4}	
10-A	1.66	-0.80	227	621	2.9×10^{-2}	-0.46	1.1×10^{-4}	
10-B		-0.75	386	621			8.4×10^{-4}	

---

[1] Coefficients to fit equation 2.9, $\dot{\varepsilon} = AT^a + B$ (Compatible units)

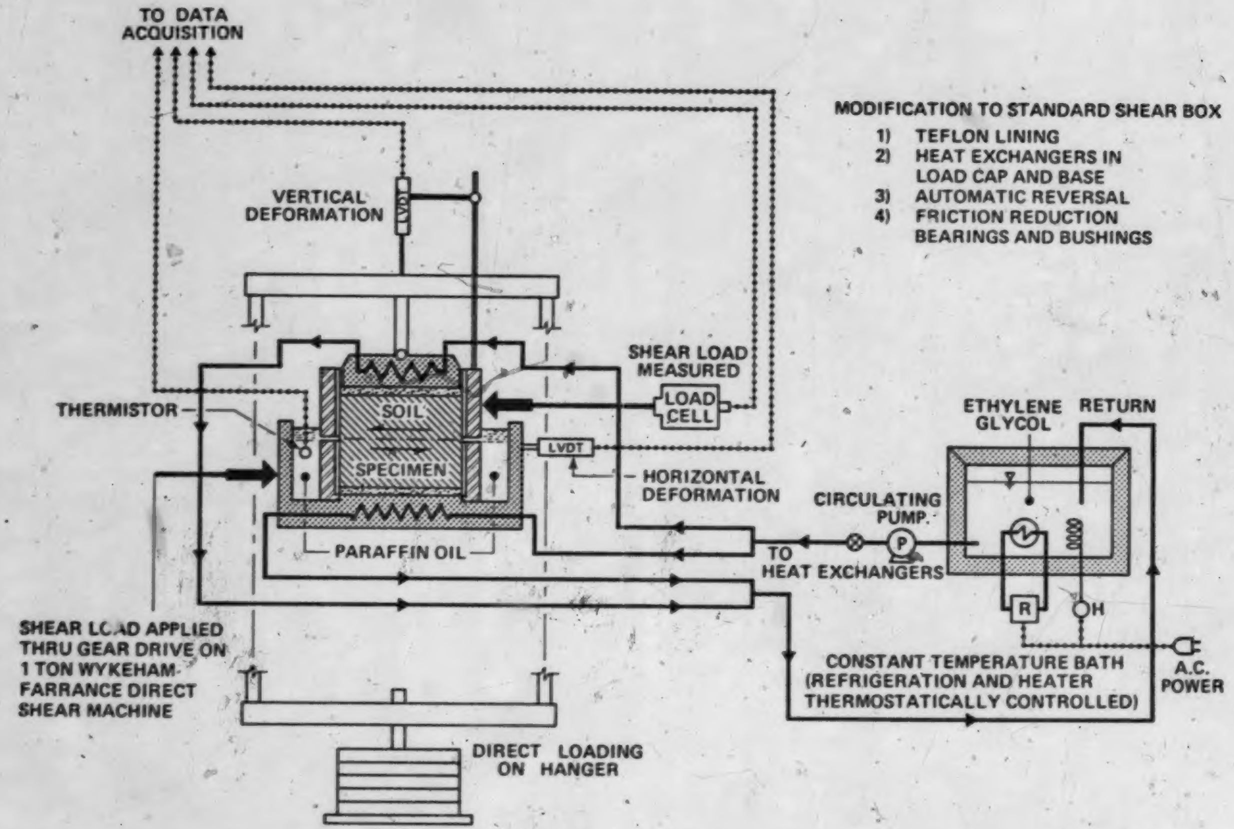
TO DATA ACQUISITION
MODIFICATION TO STANDARD SHEAR BOX
1) TEFLON LINING
2) HEAT EXCHANGERS IN LOAD CAP AND BASE
3) AUTOMATIC REVERSAL
4) FRICTION REDUCTION BEARINGS AND BUSHINGS
VERTICAL DEFORMATION
LVDT
SHEAR LOAD MEASURED
LOAD CELL
THERMISTOR
SOIL
SPECIMEN
LVDT
HORIZONTAL DEFORMATION
ETHYLENE GLYCOL
RETURN
CIRCULATING PUMP
P
PARAFFIN OIL
TO HEAT EXCHANGERS
R
H
SHEAR LOAD APPLIED THRU GEAR DRIVE ON 1 TON WYKEHAM-FARRANCE DIRECT SHEAR MACHINE
CONSTANT TEMPERATURE BATH (REFRIGERATION AND HEATER THERMOSTATICALLY CONTROLLED)
A.C. POWER
DIRECT LOADING ON HANGER

Figure 3.1 Schematic layout of shear box and associated equipment used in direct shear tests on frozen soils

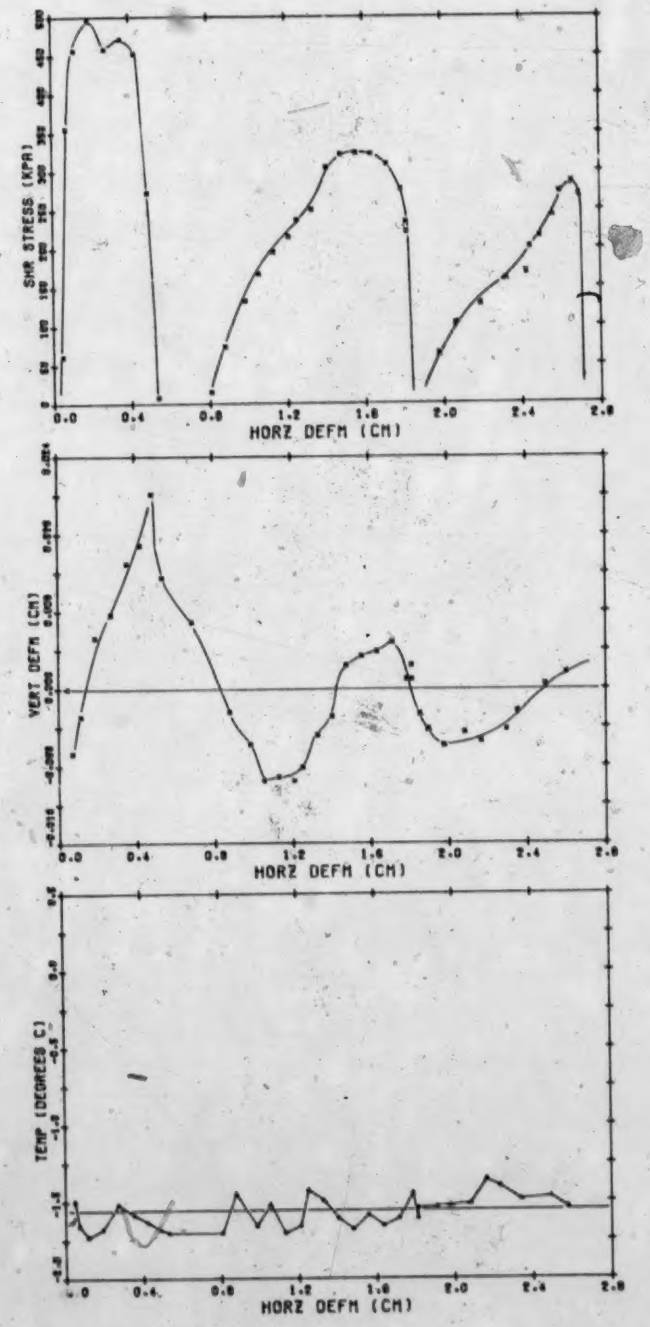

Figure 3.2 Typical results from a direct shear test conducted on frozen soil (Test FS-11) $\sigma_n = 370$ kN/m^2, $\gamma_f = 1.93$ Mg/m^3, and sheared at 1.9 cm/day

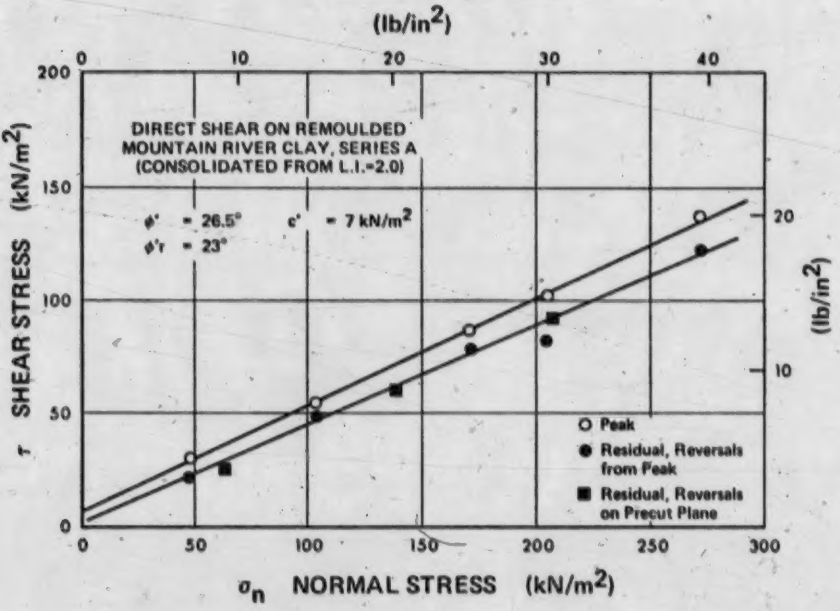

Figure 3.3 Direct shear envelopes for reconstituted Mountain River clay, Series A (unfrozen)

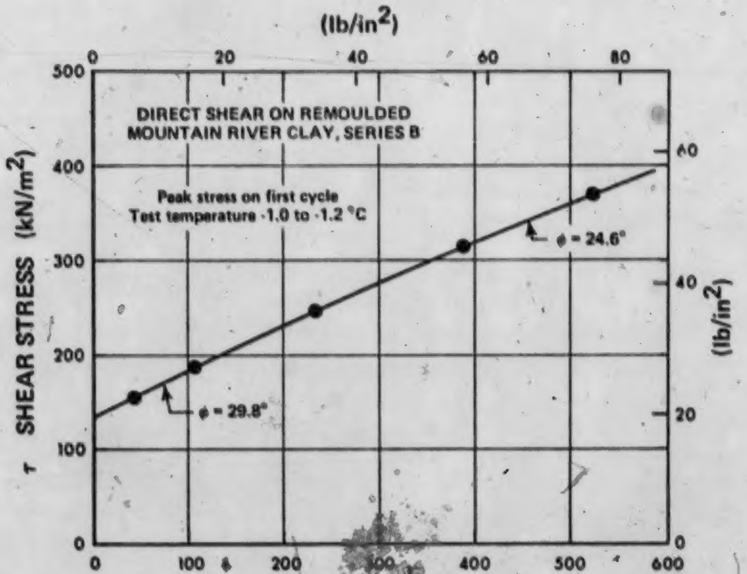

Figure 3.4 Direct shear envelope for reconstructed Mountain River clay, Series B (frozen)

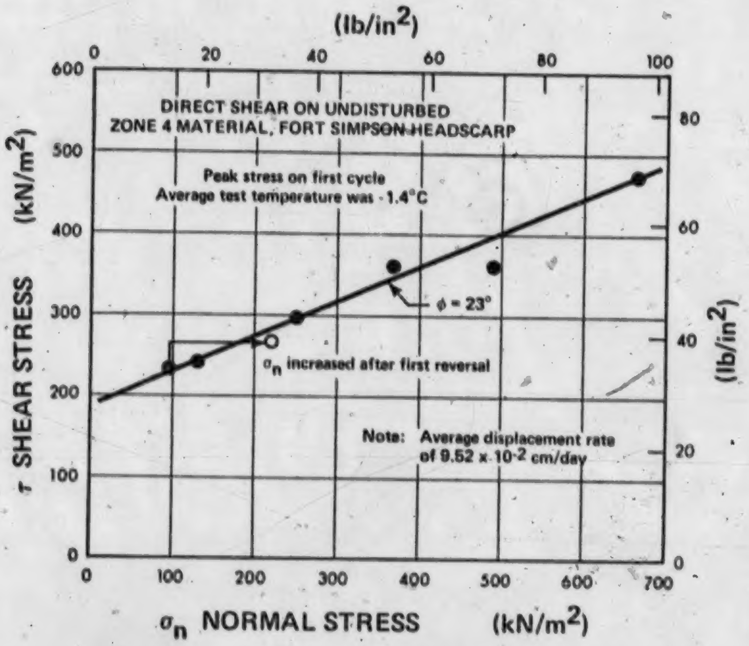

Figure 3.5 Direct shear envelope for Fort Simpson silty clay (Rate 1)

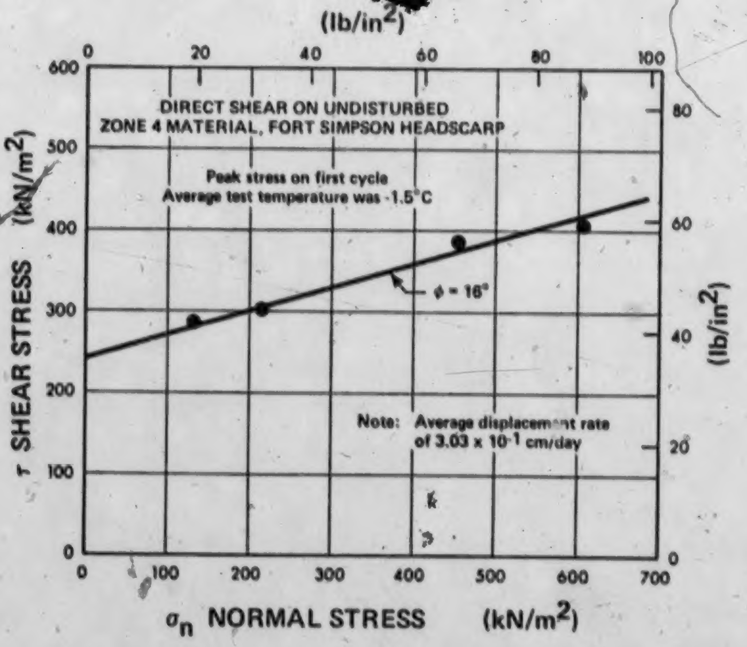

Figure 3.6 Direct shear envelope for Fort Simpson silty clay (Rate 2)

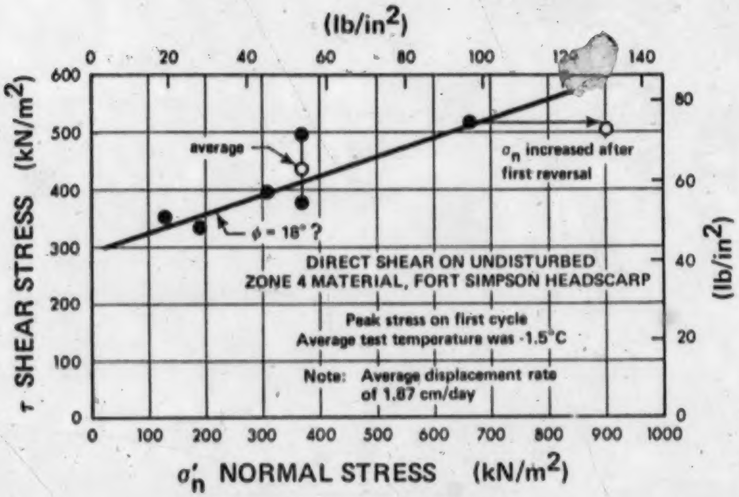

Figure 3.7 Direct shear envelope for Fort Simpson silty clay (Rate 3)

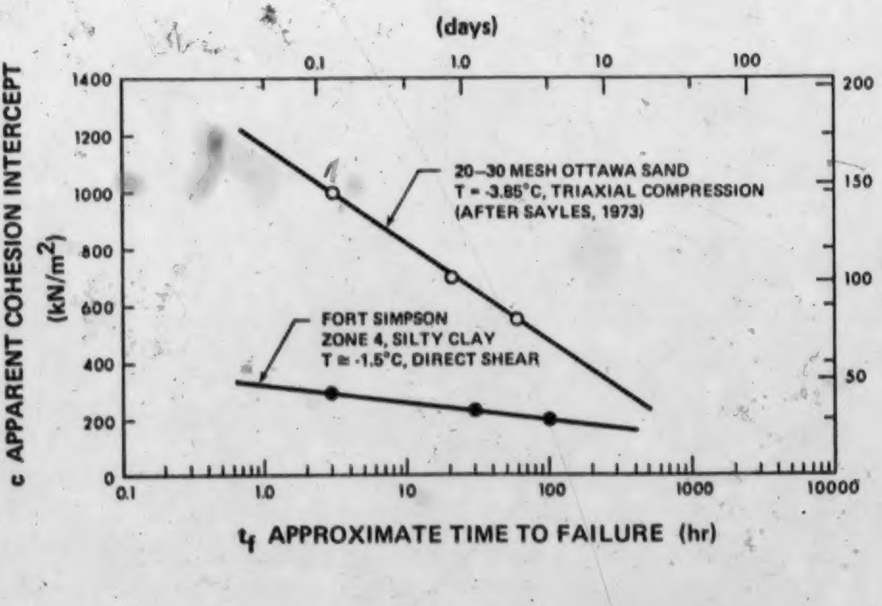

Figure 3.8 Apparent cohesion intercept as a function of time to failure

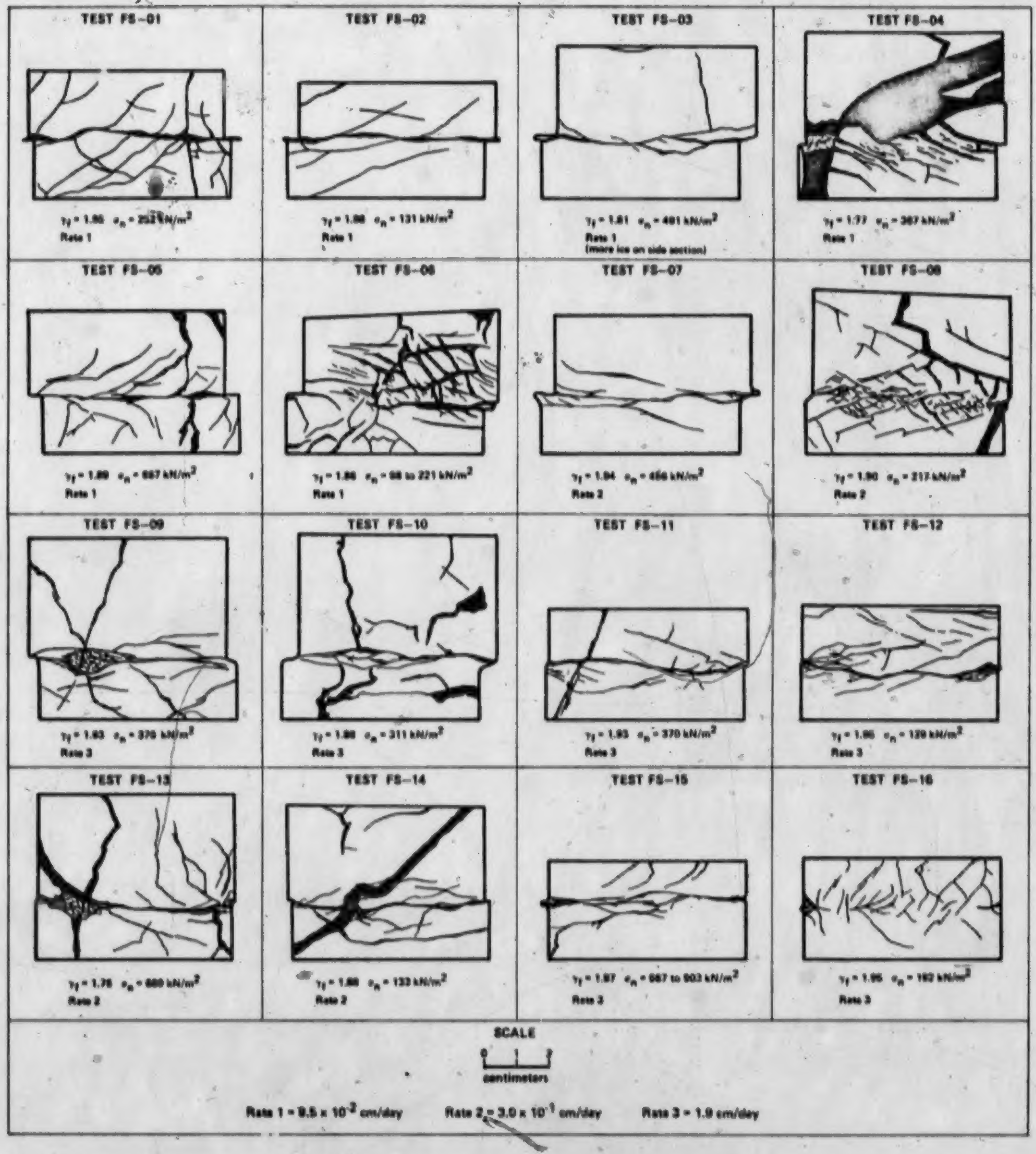
TEST FS-01
$\gamma_f = 1.85$ $\sigma_n = 252$ kN/m^2
Rate 1
TEST FS-02
$\gamma_f = 1.88$ $\sigma_n = 131$ kN/m^2
Rate 1
TEST FS-03
$\gamma_f = 1.81$ $\sigma_n = 401$ kN/m^2
Rate 1
(more ice on side section)
TEST FS-04
$\gamma_f = 1.77$ $\sigma_n = 387$ kN/m^2
Rate 1
TEST FS-05
$\gamma_f = 1.89$ $\sigma_n = 687$ kN/m^2
Rate 1
TEST FS-06
$\gamma_f = 1.86$ $\sigma_n = 98$ to 221 kN/m^2
Rate 1
TEST FS-07
$\gamma_f = 1.94$ $\sigma_n = 456$ kN/m^2
Rate 2
TEST FS-08
$\gamma_f = 1.90$ $\sigma_n = 217$ kN/m^2
Rate 2
TEST FS-09
$\gamma_f = 1.83$ $\sigma_n = 370$ kN/m^2
Rate 3
TEST FS-10
$\gamma_f = 1.88$ $\sigma_n = 311$ kN/m^2
Rate 3
TEST FS-11
$\gamma_f = 1.93$ $\sigma_n = 370$ kN/m^2
Rate 3
TEST FS-12
$\gamma_f = 1.86$ $\sigma_n = 129$ kN/m^2
Rate 3
TEST FS-13
$\gamma_f = 1.76$ $\sigma_n = 680$ kN/m^2
Rate 2
TEST FS-14
$\gamma_f = 1.88$ $\sigma_n = 133$ kN/m^2
Rate 2
TEST FS-15
$\gamma_f = 1.87$ $\sigma_n = 687$ to 903 kN/m^2
Rate 3
TEST FS-16
$\gamma_f = 1.95$ $\sigma_n = 182$ kN/m^2
Rate 3
SCALE
0 1 2
centimeters
Rate 1 = 9.5×10^{-2} cm/day
Rate 2 = 3.0×10^{-1} cm/day
Rate 3 = 1.9 cm/day

Figures 3.9 Sketches of ice structure in sheared specimens of Fort Simpson silty clay

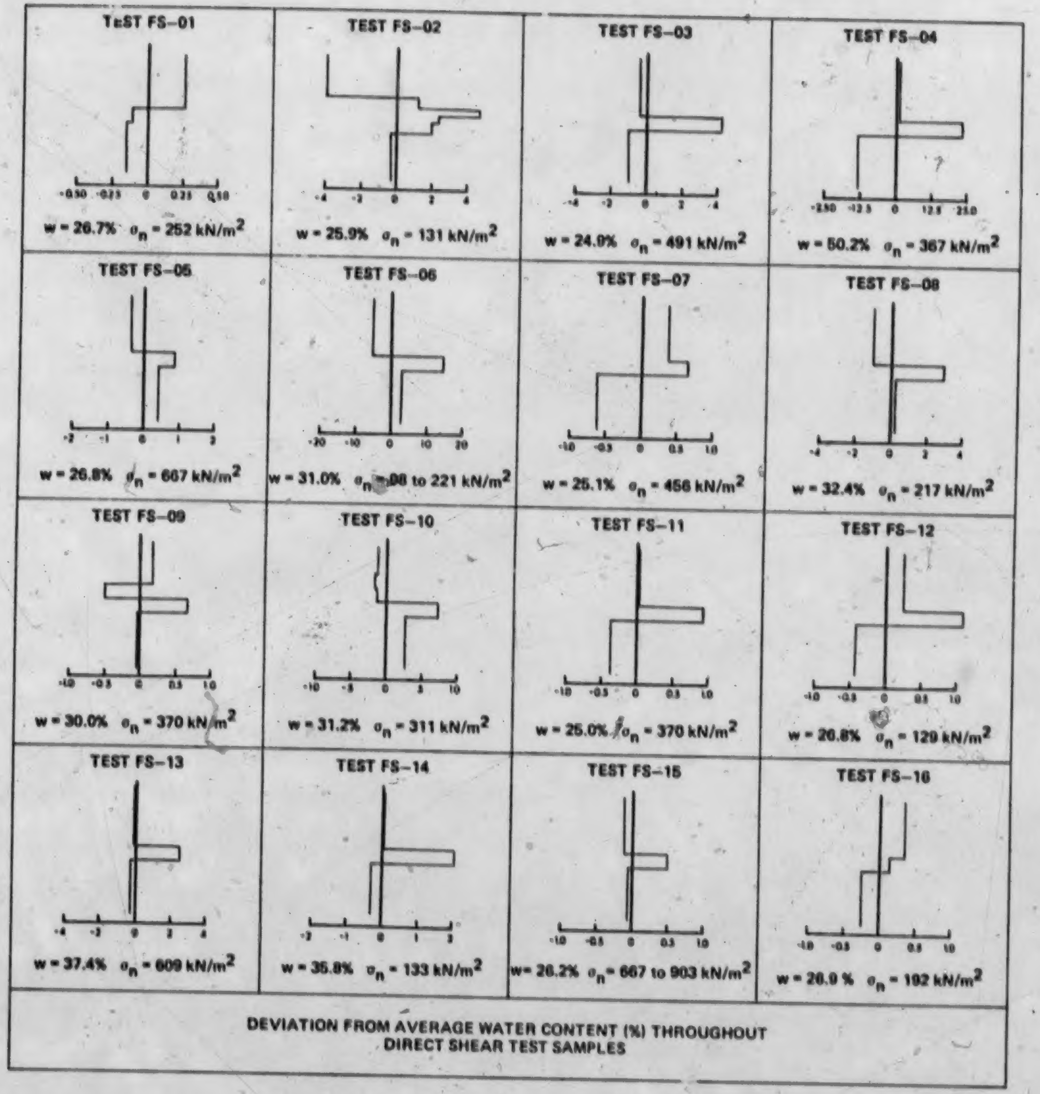

Figure 3.10 Water content profiles in sheared specimens of Fort Simpson silty clay

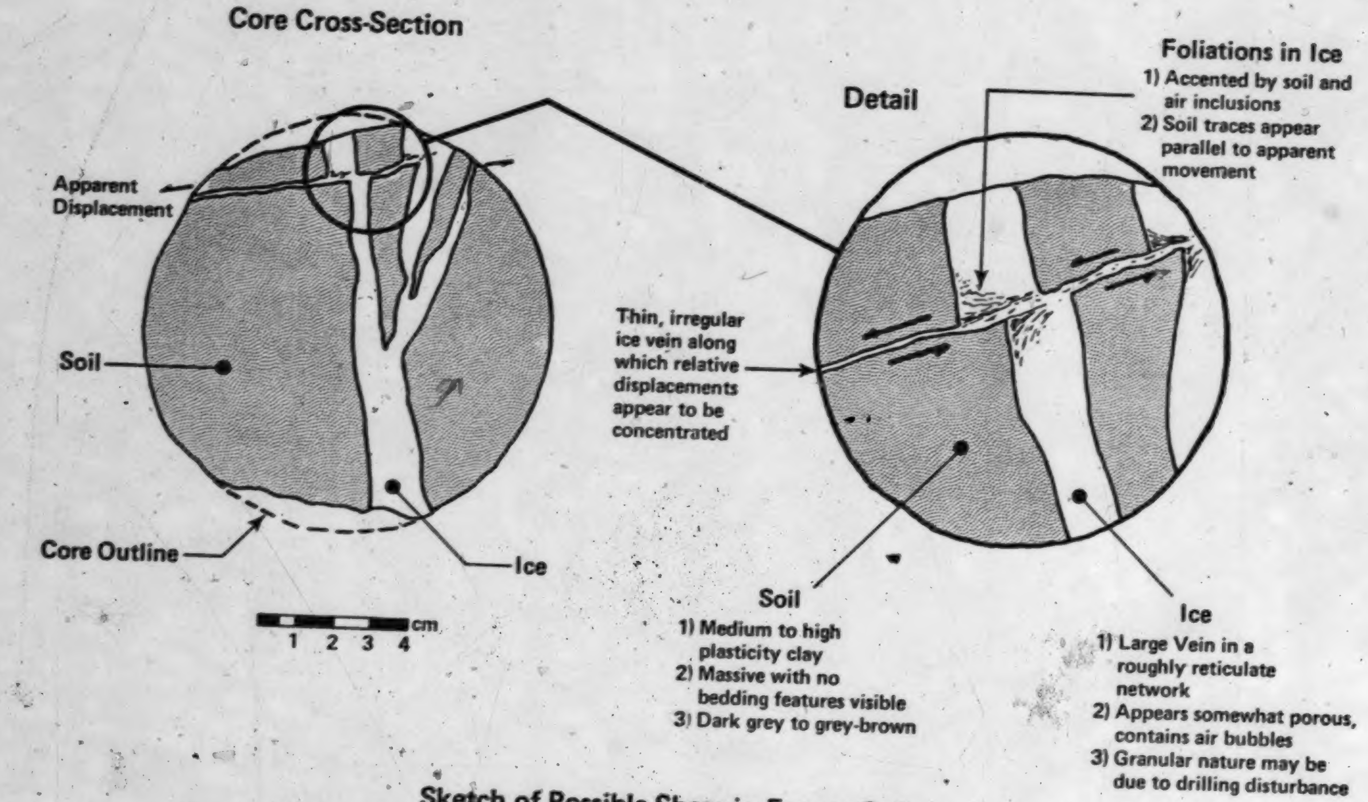
Core Cross-Section
Detail
Foliations in Ice
1) Accented by soil and air inclusions
2) Soil traces appear parallel to apparent movement
Apparent Displacement
Soil
Thin, irregular ice vein along which relative displacements appear to be concentrated
Core Outline
Ice
1 2 3 4 cm
Soil
1) Medium to high plasticity clay
2) Massive with no bedding features visible
3) Dark grey to grey-brown
Ice
1) Large Vein in a roughly reticulate network
2) Appears somewhat porous, contains air bubbles
3) Granular nature may be due to drilling disturbance

Sketch of Possible Shear in Frozen Soil
Observed in a Horizontally Oriented Core — Fort Simpson Landslide Headscarp

Base of Zone 3, Sampled October, 1973

Figure 3.11 Sketch of possible shear-induced fabric observed in a core taken from the Fort Simpson landslide

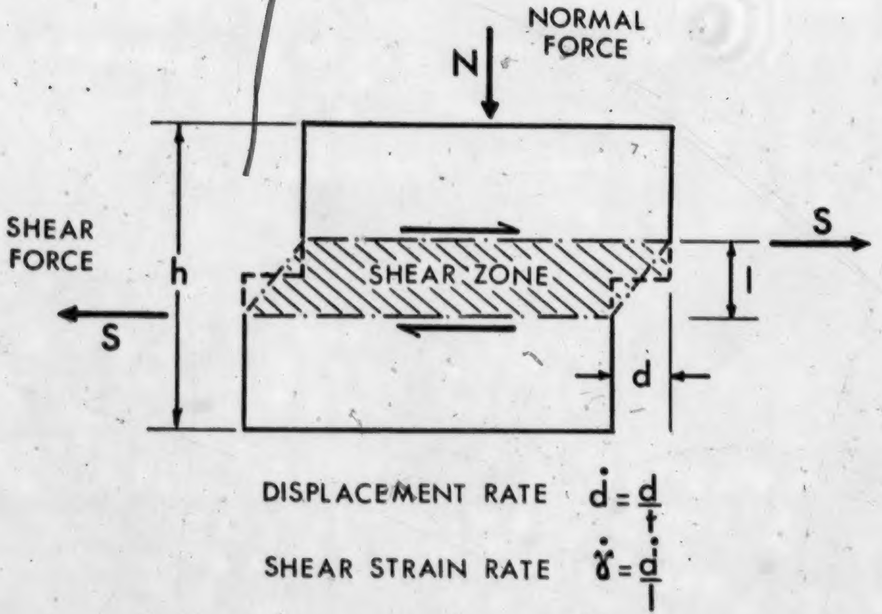
NORMAL FORCE
N
SHEAR FORCE
S
h
SHEAR ZONE
S
l
d
DISPLACEMENT RATE $\dot{d} = \frac{d}{t}$
SHEAR STRAIN RATE $\dot{\gamma} = \frac{\dot{d}}{l}$

Figure 3.12 Idealization of direct shear test to estimate strain rates from an assumed condition of simple shear

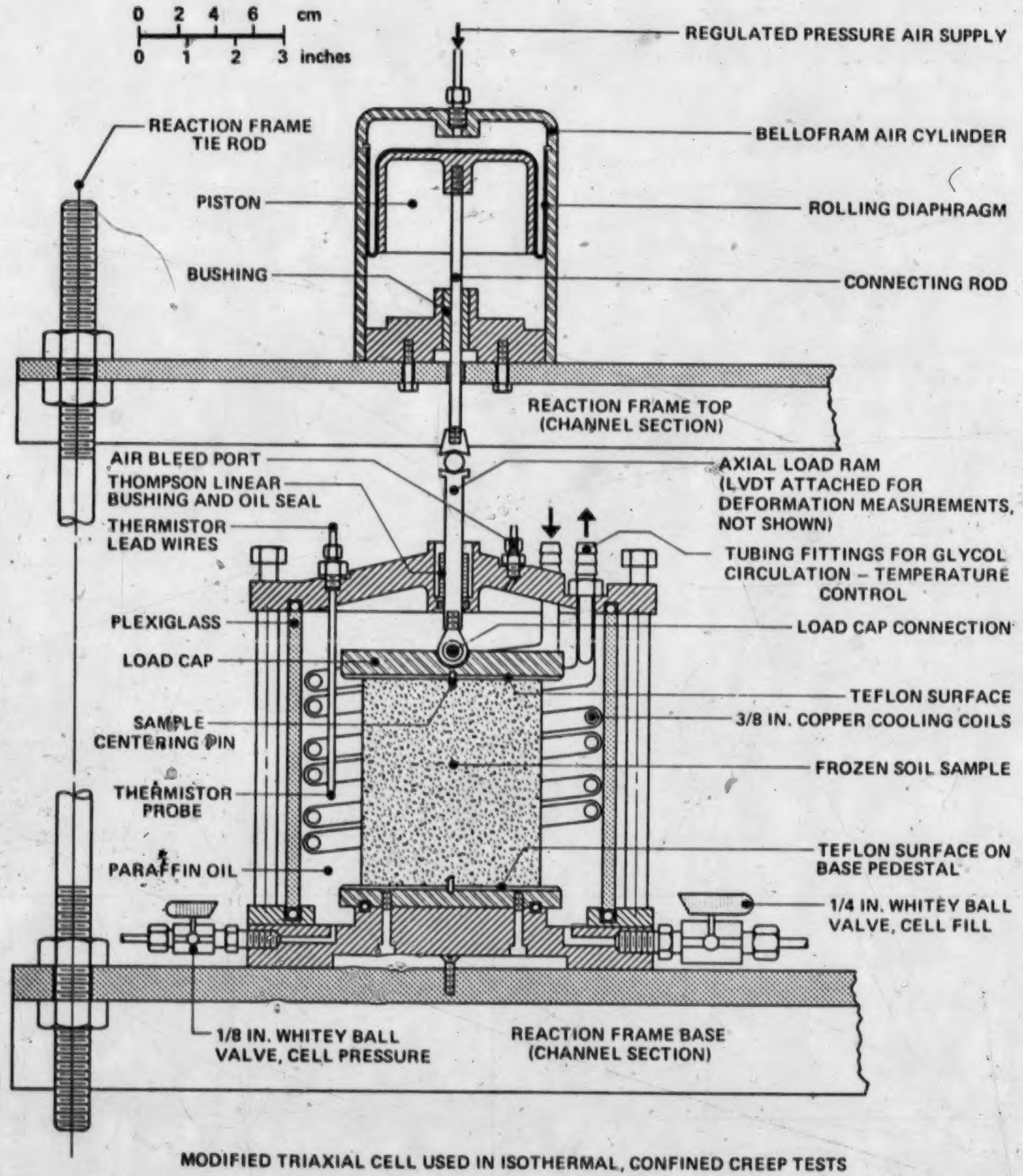
0 2 4 6 cm
0 1 2 3 inches
REGULATED PRESSURE AIR SUPPLY
REACTION FRAME TIE ROD
BELLOFRAM AIR CYLINDER
PISTON
ROLLING DIAPHRAGM
BUSHING
CONNECTING ROD
REACTION FRAME TOP (CHANNEL SECTION)
AIR BLEED PORT
THOMPSON LINEAR BUSHING AND OIL SEAL
AXIAL LOAD RAM (LVDT ATTACHED FOR DEFORMATION MEASUREMENTS, NOT SHOWN)
THERMISTOR LEAD WIRES
TUBING FITTINGS FOR GLYCOL CIRCULATION – TEMPERATURE CONTROL
PLEXIGLASS
LOAD CAP CONNECTION
LOAD CAP
TEFLON SURFACE
SAMPLE CENTERING PIN
3/8 IN. COPPER COOLING COILS
FROZEN SOIL SAMPLE
THERMISTOR PROBE
PARAFFIN OIL
TEFLON SURFACE ON BASE PEDESTAL
1/4 IN. WHITEY BALL VALVE, CELL FILL
1/8 IN. WHITEY BALL VALVE, CELL PRESSURE
REACTION FRAME BASE (CHANNEL SECTION)

MODIFIED TRIAXIAL CELL USED IN ISOTHERMAL, CONFINED CREEP TESTS

Figure 3.13 Elevation sectional view of apparatus used in isothermal, confined creep tests

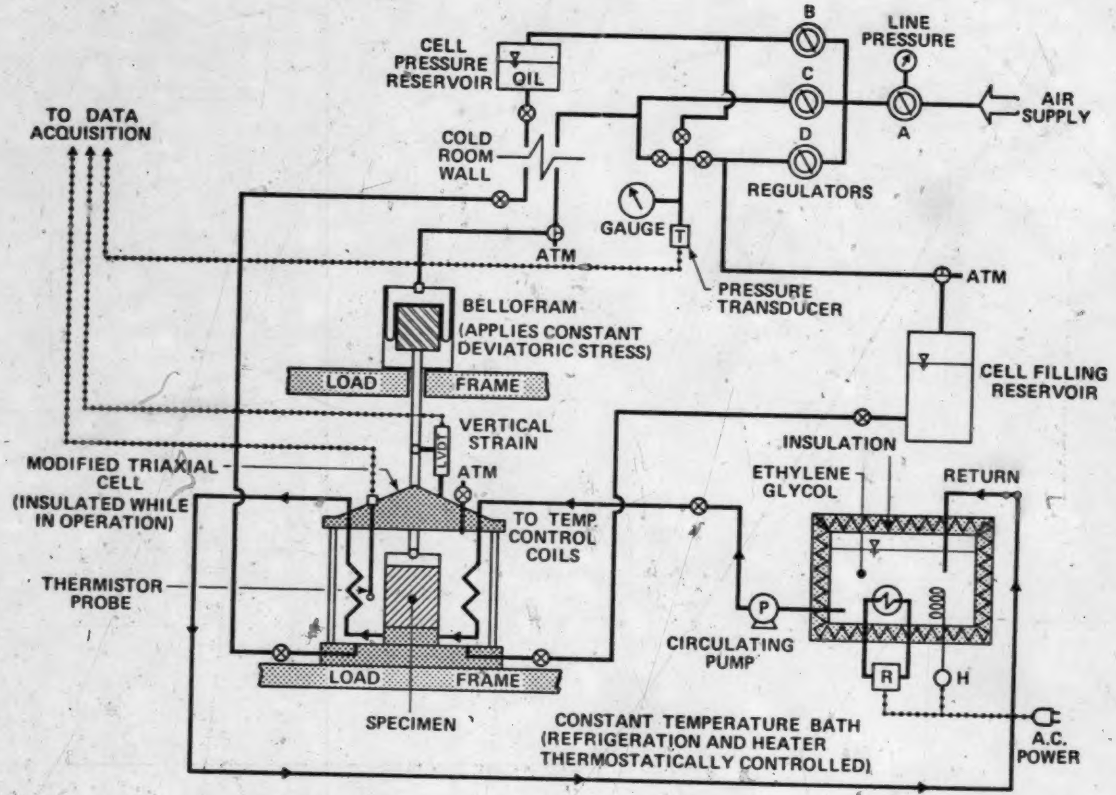
CELL PRESSURE RESERVOIR
OIL
B
C
D
A
LINE PRESSURE
AIR SUPPLY
REGULATORS
TO DATA ACQUISITION
COLD ROOM WALL
GAUGE
T
ATM
PRESSURE TRANSDUCER
ATM
BELLOFRAM (APPLIES CONSTANT DEVIATORIC STRESS)
LOAD
FRAME
CELL FILLING RESERVOIR
VERTICAL STRAIN
LVDT
ATM
INSULATION
ETHYLENE GLYCOL
RETURN
MODIFIED TRIAXIAL CELL (INSULATED WHILE IN OPERATION)
TO TEMP CONTROL COILS
THERMISTOR PROBE
P
CIRCULATING PUMP
R
H
LOAD
FRAME
SPECIMEN
CONSTANT TEMPERATURE BATH (REFRIGERATION AND HEATER THERMOSTATICALLY CONTROLLED)
A.C. POWER

Figure 3.14 Schematic layout of creep cell and associated equipment used in isothermal, confined creep tests on frozen soils

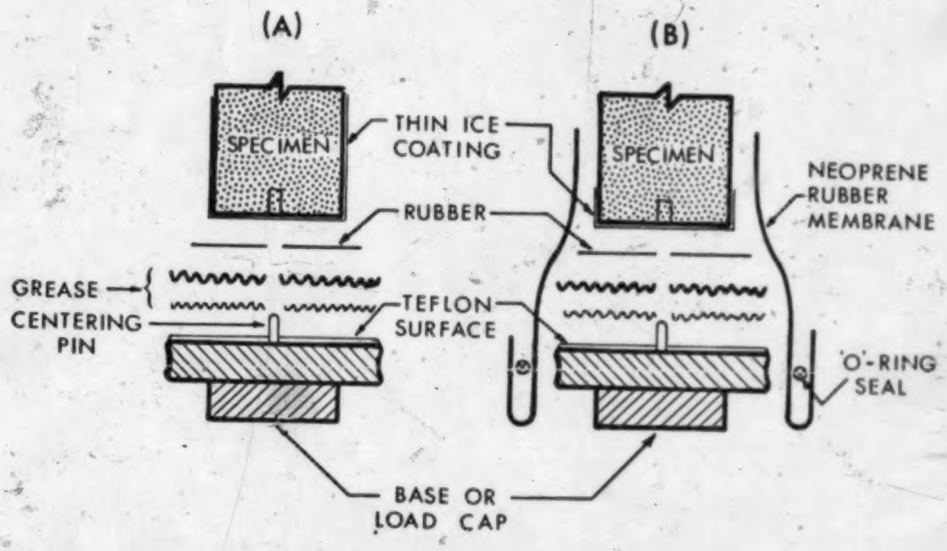
(A)
(B)
SPECIMEN
SPECIMEN
THIN ICE COATING
NEOPRENE RUBBER MEMBRANE
RUBBER
GREASE
CENTERING PIN
TEFLON SURFACE
'O'-RING SEAL
BASE OR LOAD CAP

Grease consists of a coat of Dow - Corning high vacuum, covered by a molybdenum disulphide lubricant preparation.

Figure 3.15 Detail of alternate methods of end-lubrication employed in creep tests

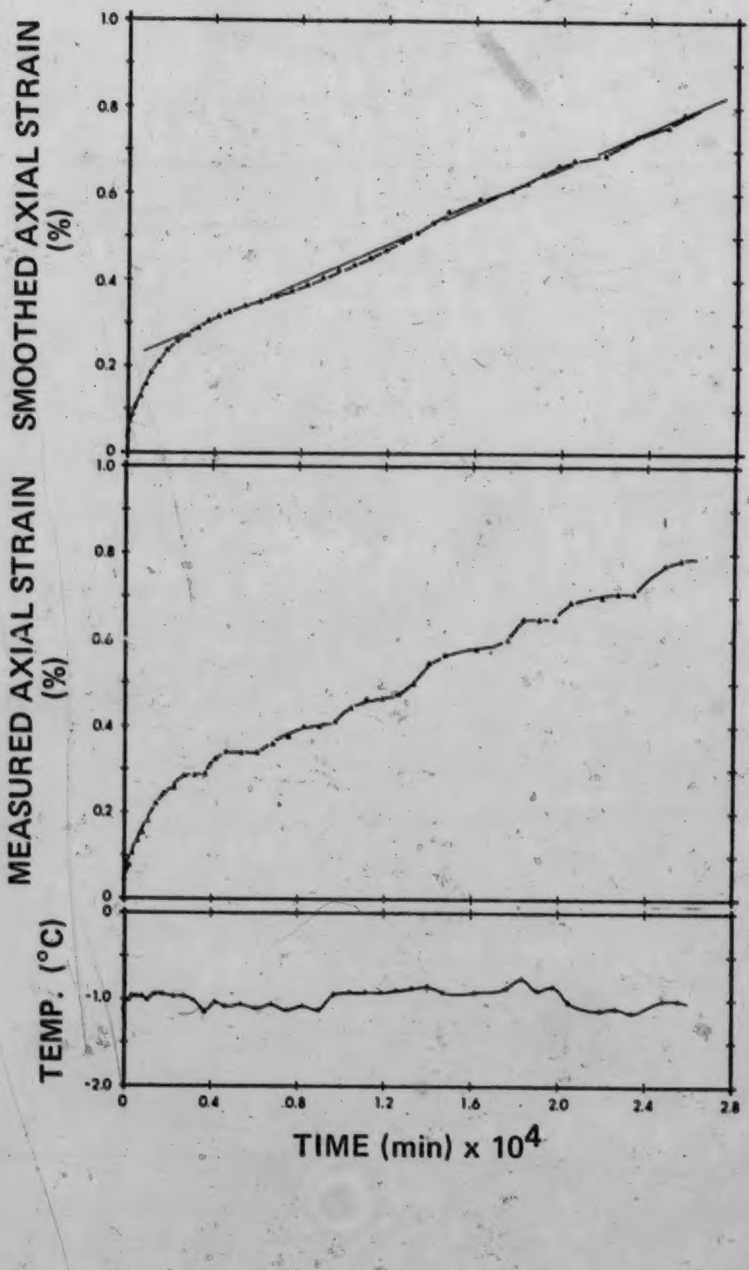

Figure 3.16 Results from a typical creep test illustrating the use of a five point moving average to smooth the ε - t curve (Test 3-B)

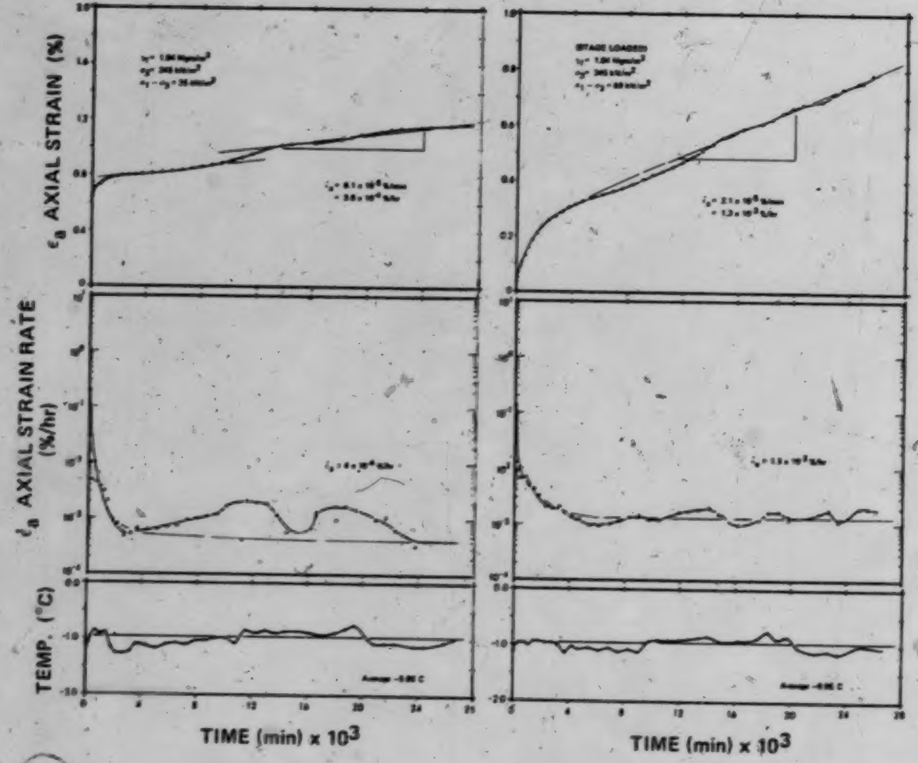

Figure 3.17 Complete results for a typical, multi-stage creep test (Tests 3-A and 3-B)

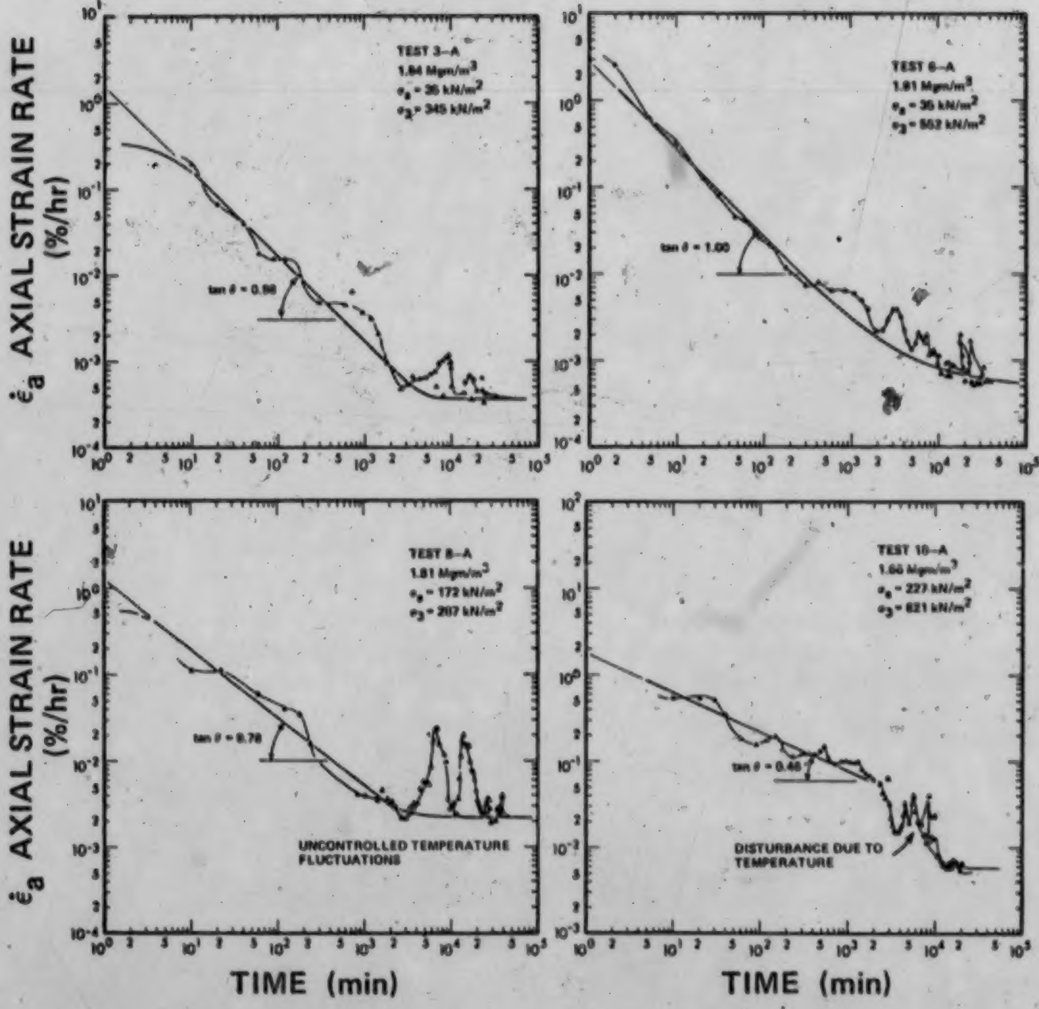

Figure 3.18 Logarithmic plots of strain rate versus time for first-stage loading

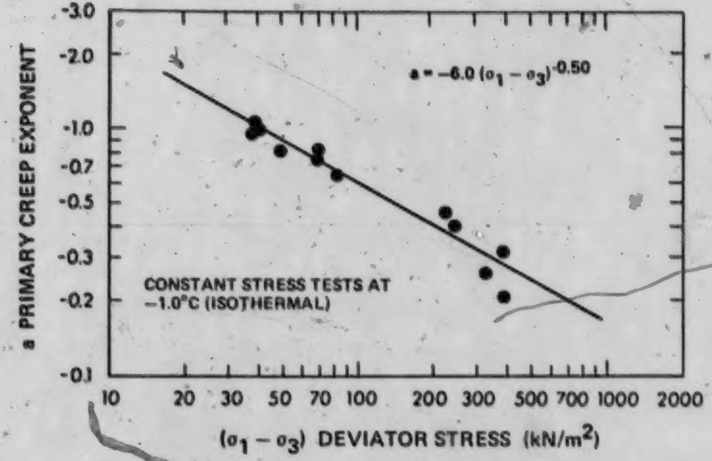

Figure 3.19 Relationship between primary creep exponent and applied deviatoric stress (includes some multi-stage data at higher stresses)

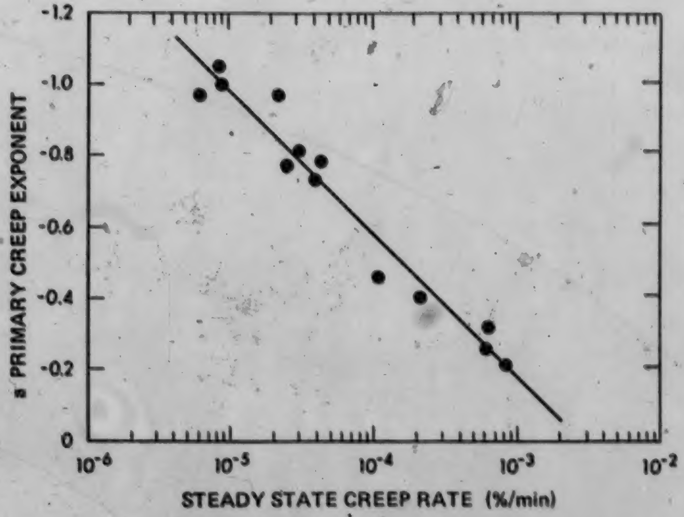

Figure 3.20 Tentative relationship between primary creep exponent and steady stage creep rate (includes data from some multi-stage tests obtained at higher stresses)

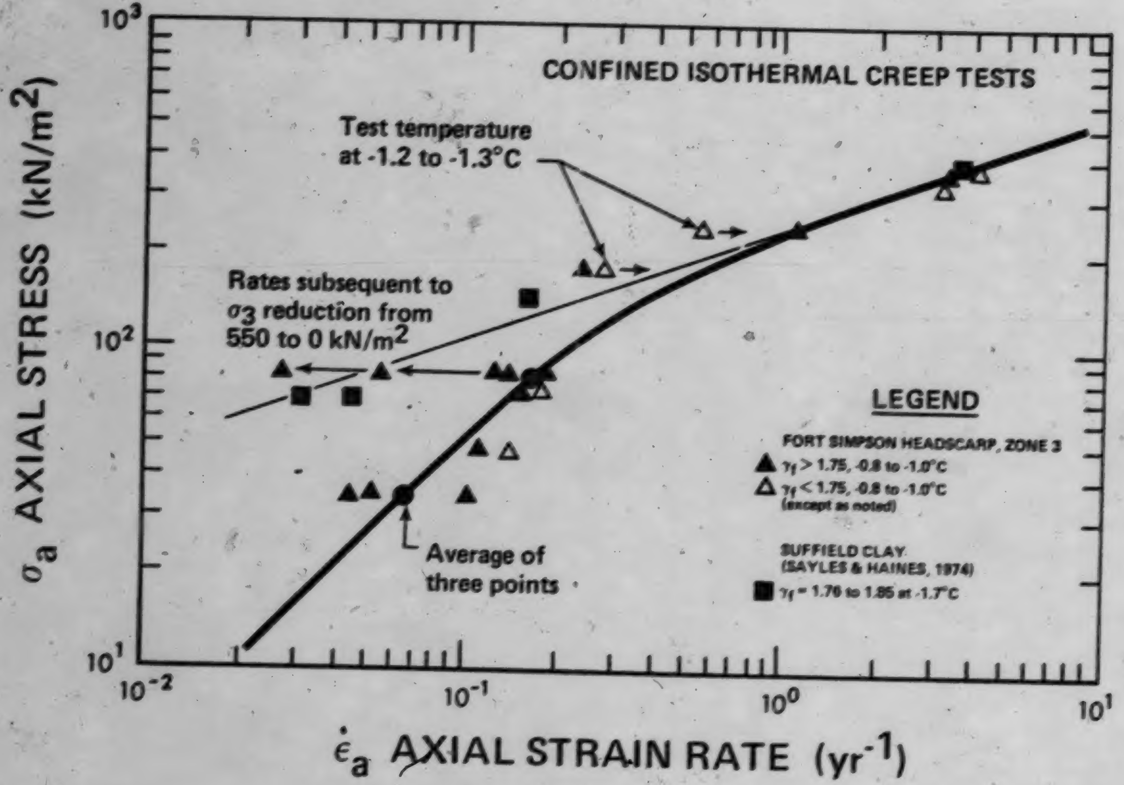

Figure 3.21 Tentative flow relationship established from creep tests conducted on fine-grained frozen soils

CHAPTER IV

REVIEW OF GEOTECHNICAL PROPERTIES OF THAWING SOILS

4.1 PROBLEMS ASSOCIATED WITH THAW

Introduction

Development of petroleum, natural gas and other natural resources in arctic regions has necessitated certain engineering innovations to deal with problems peculiar to this environment, not the least of which are the difficulties associated with thawing soils. It is obvious that many projects will involve thaw since the maintenance of frozen conditions under all circumstances is neither technically or economically feasible. It has been widely recognized that soil properties deteriorate due to thaw but there have been few examples where available analytic capabilities have been applied to predict these changes. The following provides a review of current (1976) practice and reflects that influence which an appreciation of soil behaviour during thaw has had on design and construction.

Soviet practice

Construction in connection with heavy industrial development has been underway in the arctic and subarctic regions of the U.S.S.R. since the early 1940's. These activities have included open pit and underground mines, hydroelectric developments, surface transportation networks, pipelines, and cities with multistoried buildings. In his synthesis of experience gained from these various activities, Tsytovich (1973) has emphasized the need to include design provision for settlements occurring with the thawing of permafrost soils. He comments that the majority of construction failures recorded in the north can be attributed directly to the omission from design of foundation settlements and decreases in shear strength that accompany thaw. These concerns are especially important when dealing with ice-rich soils. Soviet practice recognizes the importance of determining the properties of frozen and thawing soils, and indicates that incorporating these features in design procedures will ensure the safety and adequate performance of most structures.

Tsytovich (1973) states that in moist soils, the freezing process causes development of distinct cryogenic structures, the specific forms of which are determined by material type, moisture availability and ground thermal conditions. In their study of the effects of freezing, Soviet researchers have found that soil structure and texture have a considerable influence on the consolidation and shear strength of thawed soils. If thawed void ratios exceed those prior to freezing, increases in compressibility and reductions in shear strength are generally observed. The presence of relatively dense aggregates of soil particles (with moisture contents approaching the plastic limit) has an important influence on soil behaviour. In summary, Tsytovich (1973) cites the following properties pertaining exclusively to thawing soils, which he feels are most important:

1) Under load, void ratio changes experienced by thawing soils may exceed those for similar unfrozen soils.
2) Water permeability after thawing may be increased by one or two orders of magnitude over values for the same unfrozen soil, decreasing with time (due to swelling) and consolidation stress.
3) Pore water pressures generated during the thaw of ice-rich soils may result in conditions of low effective stress.
4) Denser soils produce relatively small pore water pressures during thaw and consequently exhibit measurable strengths.

Qualitative and quantitative descriptions of the behaviour and properties of thawing soils have been the topic of a considerable volume of Soviet literature. It is regrettable that only recently have portions of this work (largely completed prior to 1965) become available to the North American engineering community.

North American practice

Sanger (1969) has reviewed North American experience with the design and construction of foundations in permafrost areas. He suggests that continued thaw-consolidation associated with thermal degradation initiated during or subsequent to construction introduces risk since estimates of settlement (and especially differential settlement) are highly uncertain. Discussion of more recent engineering work in the Arctic is given in Linell and Johnston (1973). Aside from limited investigations conducted under the auspices of United States military agencies, methods for including the effects of thawing permafrost in design were virtually non-existent prior to the late 1960's. Exceptions to this are the development of hydroelectric facilities along the Nelson River (MacDonald, 1963; Johnston, 1969; Brown and Johnston, 1970; MacPherson et al., 1970) and some undocumented highway construction in Alaska and the Canadian north. Until recently, structures with low tolerance for movements have been either relocated to thaw-stable sites or, more often, founded in permafrost with precautions taken to maintain the ground in a frozen condition. With the recent enactment of restrictive arctic land-use regulations in both Canada and the U.S.A., attention has tended to center on environmental damage produced by thaw.

Current concerns

In the late 1960's, discovery of marketable reserves of petroleum and natural gas on the Alaskan North Slope initiated a sudden increase in engineering activity in the Arctic. It was eventually concluded that transportation of oil from the Arctic coast to an ice-free port could best be accomplished with a 48 inch (122 cm) diameter pipeline that would be buried along a significant portion of its route. Maintaining oil temperatures at approximately 70°C would result in thawing of the surrounding permafrost wherever the pipe was buried. Among problems considered in connection with this project were the stability (Woodward-Clyde and Associates, 1970) and differential settlements (Palmer, 1972) of the plug of thawed soil surrounding the pipe. Lachenbruch (1970) studied potential problems created by the presence of a hot-oil pipeline in permafrost. Although the conclusions of his study reflected a limited understanding of the mechanical properties of thawed soils, they did serve to focus attention on the geotechnical aspects of such a project.

The possibility also exists that casing in production wells which penetrate permafrost could be subjected to significant axial stresses if downdrag were exerted by the settlement of adjacent thawing soils (Koch, 1971). This problem of soil-structure interaction has been treated in more analytical detail by Palmer (1973). McRoberts and Morgenstern (1974) have identified two types of mass movement common to thawing soils and have developed an analysis that permits preliminary evaluation of slope stability. Other studies (Smith and Berg, 1973; Pufahl _et al._, 1974) have examined the construction and subsequent performance of roadway cuts excavated in permafrost.

Planning for the construction of various transportation facilities including a highway, a chilled gas pipeline and a hot oil pipeline (all in the Mackenzie River Valley), has served to focus Canadian attention on a group of concerns which are similar to those described above. Foremost among these is the potential for environmental damage if melting is induced by disturbance of the thermal equilibrium of the permafrost. The post-thaw behavioural characteristics of high compressibility and low shear strength for ice-rich fine-grained soils have been recognized, but it is clear that if theoretical analyses are to be applied to engineering problems with any confidence, realistic parameters must be determined to describe soil behaviour. The establishment of a rational basis for coping with thawing soils can best be achieved by an examination of the following items:

1) Evaluation of the progress of the thaw front with time.
2) Evaluation of total thaw settlements.
3) Evaluation of excess pore pressures associated with consolidation during thaw.
4) Evaluation of available shear strength.

4.2 THAWING OF FROZEN SOILS

Analysis of thaw

Several techniques of thermal analysis are currently available which permit the evaluation of thaw depths with time. Solution methods range from modification of the simple Neumann problem to complex numerical methods. Nixon and McRoberts (1973) have presented some useful solutions to one-dimensional problems with simple boundary conditions. The dominant variables in thaw problems have been isolated for the general case of a step temperature applied to the surface of a homogeneous mass of frozen soil. The subsequent movement of the thaw interface with time is given by:

$$X = \alpha\sqrt{t} \qquad (4.1)$$

where X is the depth of thaw
t is time, and
α is a constant, determined analytically as the root of a transcendental equation.

In practice, α is simply a parameter which describes the rate of thaw. Nixon and McRoberts (1973) indicate that since a specific thermal solution is seldom an end in itself, a one-dimensional approach may be entirely adequate for application to many field problems.

Analyses of problems including the effects of nonhomogeneity, complex two-dimensional geometry, space and time dependent properties, and mixed boundary conditions are possible only through the utilization of a digital computer. Various finite element and finite difference schemes are available for suitable modelling of these more complex circumstances (Hwang _et al_., 1973; Sykes _et al_., 1974a; Sykes _et al_., 1974b).

Thermal analysis

In their examination of factors affecting the thawing of frozen soils, Nixon and McRoberts (1973) have assessed the relative effects of thermal properties in determining the rate of thaw. Their study indicates that evaluation of the temperature dependence of less important parameters such as thermal conductivity is totally unwarranted. By making use of estimated thermal properties, thaw can apparently be described with accuracy sufficient for geotechnical purposes. In conclusion, they state that, "continuing research into the thermal properties of soils is considered, at our present state of understanding, to be subordinate to the requirement for a more exact knowledge of the geotechnical properties of thawing soils." The suggestion that thermal properties can be either calculated or estimated with reasonable accuracy from published data (_e.g._, Kersten, 1949) has been supported by several recent studies.

Comparing predicted and observed thaw rates for laboratory tests on reconstituted soils, Morgenstern and Smith (1973) found that measured values fall approximately 15% below computed rates. The presence of unfrozen water was not accounted for in these estimates, and had its effect been included, a better correspondence might have emerged. Nixon and Morgenstern (1974) tested undisturbed samples in a similar manner, and by taking account of the unfrozen water, obtained α values averaging 7% greater than predicted.

A comparison of measured and calculated thaw rates has been made by McRoberts (1975) for several cases of field thawing. He has concluded that although extensions to the simple Neumann thaw model are sometimes necessary, agreement between observed and computed α values is good. In addition, he has demonstrated that the magnitude and range of thaw rates encountered in nature is not large. Penner et al. (1975), after testing compacted fine-grained soils from the Mackenzie Highway, have reported good agreement between their measured thermal conductivity values and those reported by Kersten (1949). They conclude that this correspondence has enhanced the reliability of previously published data for use in general thermal calculations. A comparison of field and laboratory values of thermal conductivity would, however, still be of value. Laboratory thermal conductivities have been evaluated for undisturbed, ice-rich permafrost soils by Slusarchuk and Watson (1975). Thermal conductivities were again found to be in good agreement with published values for similar soils at corresponding unit weights and water contents. This study draws attention to the fact that the thermal conductivities of high ice-content soils do not approach the value for pure ice as might have been expected. The lower values observed are attributed to the thermal resistance of tiny air bubbles and discontinuities occurring naturally in undisturbed ice-rich permafrost.

4.3 CONSOLIDATION OF THAWING SOILS

Thaw-consolidation theory

Central to any effort to describe the behaviour of thawing permafrost is an evaluation of the effective stress in the soil. It is this quantity that uniquely controls both volume change and shear strength.

Tsytovich et al. (1965) have predicted that if a soil is subjected to a sudden step temperature, settlement will proceed linearly with the square root of time. Unfortunately, their attempt to establish the boundary conditions at the thaw line was incomplete. Zaretskii (1969) was probably the first to recognize that settlements due to thaw could be separated into three components, namely:

1) Settlement brought about by volume reduction associated with change of phase of ice in the soil pores and gas compression.
2) Consolidation settlement occurring during the period of thaw.
3) Consolidation settlement occurring subsequent to the completion of thaw.

Although the original translation is somewhat confusing, a more recent description of this work appearing in Tsytovich (1973) makes it clear that Zaretskii's original assumption about the boundary condition at the thaw line was essentially identical to that later given by Morgenstern and Nixon (1971). Figure 4.1 shows the one-dimensional configuration for thaw-consolidation assumed in the following derivations. The key statement in their solution of the thaw-consolidation problem is that "for a saturated soil ... any flow from the thaw line is accommodated by a change in volume of the soil". The equation derived to describe this condition was:

$$P_o + \gamma' X - u(X,t) = c_v \frac{\frac{\partial u(X,t)}{\partial x}}{\frac{dx}{dt}} \qquad (4.2)$$

$$\text{at } x = X(t), \quad t > 0$$

where P_o denotes the stress applied to the soil surface,

γ' denotes the submerged density of the soil,

$u(X,t)$ denotes the excess pore water pressure at the thaw front,

c_v denotes the coefficient of consolidation,

X denotes the distance to the thaw plane from the soil surface (see equation 4.1),

x denotes depth from the ground surface, and

t denotes time.

Zaretskii (1969) has derived a slightly different equation, but both analyses assume the following expression for the solution of the problem:

$$u(X,t) = A \operatorname{erf} \frac{x}{2\sqrt{c_v t}} + Bx \qquad (4.3)$$

where A and B are constants found from the boundary conditions, and erf denotes the error function.

Although Zaretskii's solution takes the same general form as that obtained by Morgenstern and Nixon (1971) it contains an inexplicable dependence on the average dry density of the thawing soil. Other things being equal, this relationship predicts that the degree of consolidation at the end of thaw will be reduced by decreasing the soil's dry density. Comparing this to the Morgenstern and Nixon's linear thaw-consolidation solution, it can be seen that Zaretskii consistently predicts an end-of-thaw degree of consolidation that is as much as 7% higher, thus tending away from conservatism.

Both treatments conclude that excess pore pressures and the degree of consolidation in thawing soils are dependent upon the thaw consolidation ratio R, a term emerging from the analytical solutions and defined by:

$$R = \frac{\alpha}{2\sqrt{c_v}} \qquad (4.4)$$

This ratio describes the relative rate at which water is generated and dissipated at the thaw front. Morgenstern and Nixon (1971) have assumed that if no volume change were permitted after thaw, the initial effective stress in the soil would be equal to zero. This seems reasonable for extremely ice-rich soils, and they observe that should this term become substantial, its effect would be to diminish pore pressures generated by melting and thus reduce the severity of problems arising during the thawing of frozen soils.

Although this simple model is somewhat idealized, the basic theory can be modified to include a variety of thermal and loading conditions of practical interest (Nixon and Morgenstern, 1973a). The one-dimensional theory of consolidation of thawing soils has been extended to consider separately:

1) Description of the movement of the thaw front by a more general power law.
2) A non-linear stress-strain relationship for the soil skeleton.

Sykes et al. (1974b) have attempted the formulation of a two-dimensional finite element model for thaw-consolidation which would enable the assessment of effects associated with complex geometry and nonhomogeneity.

Laboratory studies - artificially prepared permafrost

In the preliminary stages of research in a new area, it is customary to undertake laboratory studies on remoulded soils. Relative homogeneity is assured by controlling variables like the stress history, texture and thermal history, thus eliminating or significantly reducing variations which would be unavoidable with undisturbed samples. Smith (1972) and Smith and Morgenstern (1973) have described the development of a permafrost oedometer (permode) suitable for the experimental study of remoulded soils. Their research was designed to assess the validity of the one-dimensional thaw-consolidation theory previously formulated by Morgenstern and Nixon (1971). Within the permode configuration, settlements during thaw were observed to proceed proportionally with the square root of time. In Figure 4.2, the dependence of both the degree of consolidation and maximum excess pore pressures upon the thaw consolidation ratio (R) is shown to be good agreement with the theoretical relationship. For these tests, the assumption was made that the initial effective stress was zero. The authors draw attention to the difficulties associated with the evaluation of in situ permeability and compressibility characteristics, and speculate that determination of field permeabilities will be essential for an accurate estimate of R.

In connection with the same study, Smith (1972) observed that for a given average void ratio, soils subjected to a freeze-thaw cycle exhibit an increase in permeability of one to two orders of magnitude in the range of low applied stresses. This behaviour was attributed to the formation of small channels in positions occupied by segregated ice prior to thaw. He has also demonstrated that successive freeze-thaw cycles performed under constant stress can produce significant reductions in void ratio. Smith has suggested that local overconsolidation was caused by negative pore pressures generated during freezing, so that upon thaw, the sample would swell. If permitted to drain, however, the soil would not return to its original void ratio.

Recognizing the importance of the effective stress remnant in a soil skeleton thawed in an undrained condition, Nixon and Morgenstern (1973b) undertook an experimental examination of this quantity (hereafter referred to as the 'residual stress'). Experimental evidence (Smith, 1972) suggested that the thermal and stress histories prior to and associated with permafrost formation could be effective in reducing void ratios and result in a significant residual stress upon soil thawing. The thaw-consolidation theory developed for soils exhibiting nonlinear compressibility (Nixon and Morgenstern, 1973a) indicates that the magnitude of pore pressures produced by thaw will depend very much upon the ratio of the final effective stress to the residual stress.

Residual stress

Since a physical appreciation of the role of residual stress in the behaviour of thawing soils is essential to understanding much of the experimental data presented in subsequent chapters of this thesis, the following recapitulation extracted from Nixon and Morgenstern (1973b) should serve to familiarize the reader with this concept. Referring to Figure 4.3, a sediment with a known stress history is shown, having been normally consolidated to an effective stress P_o at a point A. With freezing in the absence of drainage, a small increase in average void ratio from point A to B accommodates the volume change associated with phase change as most of the water in the pores turns to ice. Thawing the soil without drainage returns the void ratio to e_o, which often produces an increase in pore water pressure. If the void ratio is sufficiently high, observed pore pressures can approach or even equal the total stress acting on the sample. Thus, it follows that effective stresses are reduced subsequent to thaw, and in extreme cases, may for all practical purposes equal zero. By permitting drainage, a reduction in void ratio brings the soil into effective stress equilibrium at point C. Externally, the freeze-thaw cycle under constant external stress has brought about a net decrease in volume, represented by AC.

At lower stress levels in fine-grained soils, the tendency for development of negative pore water pressures during freezing has been recognized. Small lenses and other discrete bodies of ice are routinely observed to form in the soil, even under conditions of closed-system freezing. If the total quantity of moisture in the sample remains unchanged, any redistribution of water must have the effect of over-consolidating (and possibly desaturating) certain soil elements with respect to the external load. This suggests that soil lying between segments of discrete ice has probably been subjected to an effective stress exceeding P_o.

Upon thawing, overconsolidated elements of soil may retain effective stresses greater than P_o. As thaw progresses, excess water is made available in the macropore system previously occupied by ice, and the adjacent soil swells to absorb available free water. The stress path followed by the soil during this process is shown by the dashed line ADE in Figure 4.3.

During swelling, all soil elements do not necessarily achieve the same effective stress and void ratio. The material nearest to the macropores may swell a great deal, coming to equilibrium at an effective stress somewhat less than P_o. Soil further from the pores could then retain relatively high effective stresses for some time after thaw by virtue of its overconsolidated state.

If the soil is capable of absorbing all of the water freed by ice melting, then the remaining effective stress is the residual stress, σ_o'. Alternately, if the soil swells to a state where the effective stress is negligible and some excess pore fluid still remains, then the residual stress will be zero. Following thaw, free drainage will permit the soil to consolidate (or swell) under the action of an external load to some effective stress, P_o. During reloading along the line EC, stress-strain behaviour will be typical of an overconsolidated soil. The net strain from the frozen to the fully thawed state (line BC) has been termed the thaw strain.

From the foregoing, it should be obvious that the behaviour of thawing permafrost is strongly influenced by its stress and thermal histories. The residual stress will affect pore pressures, settlements associated with thaw, and the undrained strength of the thawed soil mass. In their experimental study, Nixon and Morgenstern (1973b) utilized a modified permode to measure residual stresses in two different reconstituted silty clays. The tests revealed an excellent linear correlation between soil void ratio and logarithm of the effective stress. Figure 4.4 shows that by following entirely different stress paths in two separate test series, essentially identical relationships were obtained between e and σ_o'.

Laboratory studies - undisturbed permafrost

In addition to testing reconstituted materials, Nixon and Morgenstern (1973b) also measured residual stresses in a number of undisturbed samples of silt obtained from a site near Norman Wells, N.W.T. A similar linear relationship was observed between void ratio and the logarithm of residual stress. Scatter in the data at higher stress levels was attributed to difficulty in measuring pore pressures as the soil became relatively incompressible. A trend indicating an increase in residual stress with depth was demonstrated for this site. Less sophisticated tests conducted on undisturbed permafrost have attempted to characterize the magnitude of thaw strains associated with different soil types. Woodward-Clyde Associates (1970) has documented the results of an extensive testing program conducted in connection with the Alyeska Pipeline. The results of this study were subsequently presented in an abbreviated form (Luscher and Afifi, 1973). By correlating axial thaw strain to frozen dry density, relationships have been developed that facilitate estimates of thaw settlements for silts and granular soils directly from index properties (excluding effects due to the thawing of ice lenses or massive ice). Thaw strain data is presented as a function of the applied consolidation stress, and consequently, the thawed soil's compressibility also enters the analysis.

Another group of uncontrolled thaw-settlement tests have been reported by Speer et al. (1973) who show that a relationship can be developed between frozen bulk density and total settlement. Their study indicates that a useful correlation may exist between frozen bulk density and thaw strain for a given mineral soil type, thus permitting estimates of settlement magnitudes and variability within specific geologic units. Combining data from several sites, a least squares curve was fitted to obtain the equation,

$$A = 73.6 - 101.8 \ln \gamma_f \qquad (4.5)$$

where A is the thaw strain (percent), and

γ_f is the frozen bulk density (Mg/m^3).

A study reported by Keil _et al_. (1973) led to a similar correlation for varved lacustrine soils with the generally larger thaw strains reported probably being due to differences in the soil and ground ice types encountered. Watson _et al_. (1973b) have provided additional data for the density-settlement correlation. They also note that permeabilities for undisturbed samples of clayey soils thawed under low stresses are relatively high (1×10^{-5} to 1×10^{-4} cm/s). Small increases in overburden pressure brought about a rapid decrease in permeability of two to three orders of magnitude.

Field studies of thaw

To date, only one field test has been conducted that is sufficiently well documented to be amenable to analysis. Watson _et al_. (1973a) have presented data collected during Mackenzie Valley Pipe Line Research Limited's (MVPL) brief operation of a hot-oil pipeline test section at Inuvik, N.W.T. Information recorded at the site included ground temperatures, pore water pressures and settlements. Details of the instrumentation used at that site have been described elsewhere by Slusarchuk _et al_. (1973). Morgenstern and Nixon (1975) have analyzed the MVPL test site data, making use of their (1971) linear thaw-consolidation theory. The general agreement demonstrated between predicted and observed rates of thaw, pore pressures, and settlements improves confidence in estimates of _in situ_ performance based upon existing theories and making use of results determined in standard laboratory tests.

McRoberts and Morgenstern (1973, 1974) have examined the stability of thawing slopes within the framework of thaw-consolidation theory and suggest that thaw-generated pore water pressures have been an important factor in a number of cases of instability observed in the Mackenzie River Valley. Excess pore water pressures measured at the thaw front in several mudflows constitute an indirect confirmation of correspondence between field and laboratory behaviour.

4.4 SHEAR STRENGTH OF THAWING SOILS

The well-known dependence of shearing resistance upon effective stress remains valid for thawing soils. By using thaw-consolidation theory to establish pore water pressures, it should be possible to determine shear strength if the effective friction angle and pore pressure parameters are known for the soil in question. In the preceeding section, it was shown that the freezing process has a considerable influence on the consolidation properties of thawing soils. Investigation of their behaviour during shear would verify the application of thaw-consolidation theory to problems pertaining to instability and deformation.

Laboratory studies

Broms and Yao (1965) have documented the effects of freezing and subsequent thaw on the shear strength of a compacted silty clay. They observe that changes in mechanical properties can be attributed to one or more of the following:

1) Internal redistribution of water.
2) Volume and density changes due to soil water freezing.
3) An overall increase in water content during open system freezing.

In their study, a variety of freezing conditions were simulated by varying freezing rates, surcharge pressures and drainage conditions during sample preparation.

Unconsolidated undrained tests showed that slow freezing rates (in conjunction with water inflow being allowed during open-system freezing) could result in shear strengths of less than 10% of the values obtained for the control specimens. This loss in strength was attributed to the presence of 'layers of water' occupying the locations of former ice lenses. These were thought to permit development of high pore pressures during thaw and shear under undrained conditions. Furthermore, compacted soils subjected to several freeze-thaw cycles approached full saturation when frozen at slow rates under open-system conditions.

Stress paths followed in these tests demonstrated the effect of the apparent overconsolidation caused by the negative pore water pressures generated during freezing. These preconsolidation effects were most noticeable on samples frozen at fast rates without drainage. The effective angle of shearing resistance remained unaffected by freezing, but increased moisture contents did cause a reduction in the cohesion intercept. The influences of effective stress changes experienced during freezing were more apparent in the shapes of the stress vectors during shear, which were typical of those normally associated with overconsolidated clays. This behaviour may be related to the fact that compaction was used to prepare the soil specimens prior to freezing. Kaplar (1965) pointed out that bringing the soil to maximum Proctor density is equivalent to heavy preloading. This could provide an alternate reason for the similarity of stress paths followed by soils subjected to either overconsolidation or a freeze-thaw cycle.

Thomson and Lobacz (1973) employed direct shear tests to determine strengths along a frozen-thawed interface in a remoulded silty soil. Their procedure ensured that fully drained conditions existed during shear, and they measured an effective angle of shearing resistance not significantly different from that of the unfrozen soil. It is of interest to note that results from triaxial tests on samples which had been frozen then thawed could be interpreted as exhibiting a nonlinear envelope, even though the authors have chosen to approximate the failure relationship with a straight line.

Watson _et al_. (1973) report, but do not comment on, results from several consolidated undrained triaxial tests performed on undisturbed samples.

Soviet research

Very little of the Soviet research dealing with the shear strength of thawing soils appears in the translated literature, but several interesting reports are available. Tsytovich _et al_. (1957) have indicated that strength reductions experienced by soils subjected to a freeze-thaw cycle are a consequence of structural changes, moisture redistribution, and water concentration in ice lenses. Maximum reductions in shear strength have been observed in soils possessing a stratified or cellular (reticulate) structure. Cryogenic fissures retained after thaw apparently produce significant increases in permeability and compressibility at low effective stress levels. At higher consolidation pressures, the magnitudes of these variables tend to conform with values observed for the unfrozen soil. Increases in the coefficient of consolidation at low stress levels have also been attributed to fabric changes produced by the freezing process (Vodolazkii, 1962). His observations indicate that under field conditions, the cryogenic structure is retained for some time after thaw, but eventually disappears after two to three months.

Shusherina and Tsytovich (1967) have presented undrained shear strengths for clay soils that demonstrate consistent strength reductions for samples which had been subjected to a freeze-thaw cycle. The experimentally determined unfrozen and thawed shear strengths emerge as linear functions of bulk density, with the ratio of these two strengths remaining essentially constant throughout the documented density range. Water segregated as ice during freezing is released upon thaw but is not immediately reabsorbed. They suggest that this condition is a major factor contributing to the strength reduction process in thawing soils. This response has even been noted for clays frozen under closed-system conditions with moisture contents as low as the plastic limit.

A number of in situ vane shear tests performed in a thawing earth fill also gave a linear correlation between shearing strength and density. Although subsequent data exhibits considerably more scatter, increases in strength that were reported over the three month period following thaw are probably related to the dissipation of excess pore pressures in the fill. Other vane tests in soil beneath an excavation showed very low strengths near the thaw plane, again implying the presence of excess pore water pressures.

4.5 ROLE OF MACROSTRUCTURE IN THAWED SOIL BEHAVIOUR

Ground ice origins

Hughes (1974) has indicated that, aside from the obvious thermal conditions necessary for the formation of permafrost, the distribution and form of ground ice normally encountered is the product of several interrelated conditions summarized in the following:

1) The physical properties of sediments within a geologic unit.
2) Origin and postdepositional history of the geologic unit.
3) Spatial relationships between geologic units.
4) Hydrogeologic conditions from the onset of permafrost aggradation.

Figure 4.5 shows a genetic classification scheme proposed by Mackay (1972a) that demonstrates some of these associations on the basis of water origin, dominant transfer processes and resultant ground ice types. A wide variety of forms can be found within the range of geologic materials typically encountered.

Occurrences of ground ice documented in connection with engineering investigations have been reported primarily in unconsolidated sediments of Pleistocene age. Pore ice is not a particularly distinguishing feature since ice will necessarily be present in the voids of any sediment that was moist prior to permafrost invasion. More visibly obvious, and of greater concern, is ice in excess of that required to occupy the porosity of apparently intact soil. This segregated ice constitutes the majority of ground ice encountered in permafrost areas and ranges from thin veins, barely visible to the naked eye, to thick tabular bodies of the sort described by Mackay (1971).

Till plains, which consist of a relatively thin veneer of lodgement till overlying bedrock, make up roughly 50% of the land area in the vicinity of the Mackenzie River Valley (Hughes, 1974). The compact nature of these materials, combined with their relatively low permeability, almost totally restricts the formation of segregated ice. Next in areal extent are the clays, silts, and sands that were deposited in glacial lakes impounded along the valley during deglaciation.

Ice in glaciolacustrine sediments

Particular interest has been focused on ground ice formed within fine-grained glaciolacustrine sediments. These materials are the most potentially troublesome to geotechnical engineers due to the typically high water contents that render them unstable when thawed. A survey of naturally occurring instability in the vicinity of the Mackenzie River Valley reported by McRoberts and Morgenstern (1973) has indicated that mass movements are most frequently associated with the frozen clays, silts, and sands found in glacial lake basins. They also note the invariable occurrence of segregated ice in sediments exposed at the headscarps of these landslides and flows visited in the course of their study.

It seems probable that the construction of highway backslopes in these same deposits would be accompanied by the considerable risk of precipitating similarly unstable conditions (Pufahl et al., 1974).

Concern has also been expressed regarding the effects which local ground ice variability could have on the total and differential settlements sustained by a warm-oil pipeline founded in permafrost (Speer et al., 1973). Bedded silts and clays which had been deposited in glacial lakes were identified as a problematic terrain unit and an extensive laboratory testing program subsequently demonstrated that design concerns were well founded. Additionally, ground ice structure apparently plays a significant role in sustaining slope retreat at the ablating headscarps of bimodal flows in these same silty clays (Pufahl, 1976).

Although more detail regarding the field identification and description of ground ice could be given, it is instructive to review the three most common structures developed when ground ice forms in soils. Without reference to origin or subsequent developmental processes, Tsytovich (1973) has described three easily distinguished structures shown schematically in Figure 4.6.

Soils with massive structure contain a uniform distribution of pore ice, and occasionally some fine, random, discontinuous veins. These soils are characteristically quite dense. They generally exhibit negligible to moderate thaw strains and satisfactory thawed strengths, with almost none of the structure associated with freezing being retained after thaw. The thawed behaviour of these soils is, then, not markedly different from similar material that has not experienced a freeze-thaw cycle. The same generalization is certainly not true of soils with either stratified or reticulate structures, both of which exhibit reduced shear strengths and larger strains upon thaw. Since these are apparently the most common ice structures found in glaciolacustrine sediments, the following provides a brief review of ice formation processes for each case.

Taber (1929) concluded that conditions of high initial water content and easy water access during freezing were favourable to the formation of alternating soil and ice layers with an essentially horizontal attitude. A more quantitative description of the physical processes leading to the formation of rhythmic ice bands has been given by Martin (1959). Both authors have indicated that stratified structure is most frequently observed in relatively silty soils and can generally be attributed to the transport of water to the freezing front which results in moisture contents that exceed the soil's pre-freezing equilibrium moisture content. Experience has shown that large thaw strains and very low shear strengths are commonly associated with soils containing a stratified ice structure.

Taber (1929) also conducted freezing tests on clay soils and observed that the low permeability limited water supply so that ice segregation caused shrinkage cracks to form. As freezing advanced, these cracks gradually filled with clear ice and enlarged themselves, extending downward and combining with horizontal veins to form a cellular or reticulate structure. In several instances, vertical or steeply inclined planes of weakness developed and intersected ice veins which had previously formed in essentially horizontal attitudes. Subsequent differential growth of the horizontal lenses apparently caused local contemporaneous 'faulting' along these high-angle flaws. The partitioning walls of clear ice were gradually thickened with water derived from the clay blocks contained within. Beskow (1935) has documented a similar process where water for ice veins growing well behind the freezing front was removed from the adjacent clay.

More recently, Mackay (1974) has reviewed the literature concerning reticulate ice vein networks and, on the basis of his field observations, has discussed theories of origin and growth. He indicates that soils exhibiting reticulate structure yield little excess water when they thaw, lending support to the suggestion that ice veins have grown in shrinkage cracks and consist of water derived locally. The most favorable conditions for producing this sort of structure would then be where steep temperature gradients occur in massive soils with low permeabilities. This observation is in close agreement with the sequence of events proposed by Hughes (1974), depicting the exposure and subsequent freezing of a stratigraphic cross-section thought to be typical of conditions prevalent in the glaciolacustrine basins of the Mackenzie River Valley. Although segregated ice in clay typically appears as a reticulate network, thick horizontal bands of relatively clear ice, and even downward grading into massive segregated ice have also been reported (Hughes, 1973[1]; Mackay, 1975; Pufahl, 1976).

Since the reticulate structure is three-dimensional, it is especially important to recognize this macrostructure in the examination of ice and soil in small diameter core samples.

---

[1] Hughes, O.L. 1973. Personal communication.

Effects of thawed fabric

Fissures present in soils possessing either stratified or reticulate structure will probably produce significant increases in permeability at the low stress which normally correspond to field thaw conditions.

Watson et al. (1973) found that undisturbed samples obtained at the MVPL Inuvik test site and thawed under low overburden pressures had relatively high coefficients of permeability. However, small increases in pressure caused a large decrease in permeability. This behaviour is also supported by the results of in situ permeability tests reported by Rowley et al. (1973). Thawed soil permeabilities of 10^{-4} cm/s considerably exceeded the values which might have been anticipated on the basis of the soil's grain size curve. In their analysis of performance data for a hot-oil pipeline test section at the same site, Morgenstern and Nixon (1975) chose to use laboratory permeabilities for the appro³ priate stress range. They have suggested that the measured field values were too high and cite several reasons to support this view.

High permeabilities have been reported for low plasticity clays from the Copper River Basin in Alsaka (Woodward-Clyde Associates, 1970) The results of falling head permeability tests performed on 2.5 in. (6.4 cm) and 7.7 in. (19.6 cm) diameter samples are shown in Figure 4.7. All specimens tested were recovered from the same geologic unit. These data demonstrate the importance of relating sample size to soil structural features. The larger diameter cores clearly contained a more representative sample of in situ fabric, specifically the fissuring associated with ground ice. On this basis, it was concluded that the macrostructure was responsible for a permeability increase of at least two orders of magnitude in the low stress range.

The development of a well-defined secondary structure has also been described in highway subgrade soils frozen under essentially closed-system conditions (Bergan, 1973; Bergan and Fredlund, 1973; Fredlund _et al._, 1975). Laboratory measurements on remoulded and undisturbed clay samples have demonstrated that a freeze-thaw cycle produces a significant reduction in matric suction. These changes in the subgrade soil parameters apparently influence the soil's response to dynamic loading, and hence contribute to the fatigue damage of overlying asphaltic concrete pavements. The explanation offered for the suction decrease is an accumulation of water in the secondary structure that results from the melting out of segregated ice. On thawing, the relatively higher moisture contents in the macrostructure control suction values measured in the laboratory. The action of external stresses and internal suction gradients can, over the course of time, restore uniform soil moisture distributions and lead to an increase in observed suctions.

Experience with structured soils

It is clear that discontinuities produced by melting ice lenses are the dominant features in post-thaw fabric. On the basis of structural similarities, a number of parallels can be drawn from geotechnical experience gained with similar materials which are more familiar in terms of conventional practice. Rowe (1972) has authored an excellent treatise on the role of soil fabric in geotechnical engineering practice. He emphasizes the need to firstly, recognize features of fabric during sampling operations, and secondly, take proper account of the effect that fabric details have on the interpretation of site geology as well as soil strength and consolidation properties.

The consolidation behaviour of fissured clays suggests that secondary structure provides additional drainage capacity, particularly at low stress levels (Kazi and Knill, 1969; McGown and Radwan, 1975). Test results indicate the importance of sample size and macrofabric for testing under stresses which lie at or below the in situ overburden pressure. As effective stresses increase, fissures close and the scatter in permeability data observed between otherwise similar samples decreases (see Figure 4.8). Permeabilities tend toward uniform values that are characteristic of the homogeneous intact clay.

Marsland (1972) has described the role played by extensive fissuring in producing a nonlinear failure envelope for London clay. At low normal stresses, the soil behaves like a slightly dilatant granular material with the clay lumps remaining relatively intact during shear. The effects of large overconsolidation stresses are apparent only within the hard lumps. As the normal stress is increased, however, larger portions of the shear plane pass through the intact material and a definite peak strength is produced. The stress-strain curves obtained from this series of fully drained triaxial tests are shown in Figure 4.9. Marsland also emphasizes the absolute necessity of testing representative soil elements (in the laboratory or field) with specific attention being paid to recognized relationships between sample dimensions and the spacing of discontinuities. It seems reasonable to conclude that permafrost soils exhibiting a stratified or reticulate structure in the thawed state should behave similarly to fissured clays.

Research objectives

At present, there is a paucity of well-documented field case histories describing thaw-induced settlements or instability. This suggests that laboratory or in situ testing to evaluate properties of undisturbed fine-grained permafrost soils would provide information of considerable value. A primary objective in any preliminary study should then be an attempt to define the role of cryogenic structure in the geotechnical behaviour of thawing soils.

Reference to Figure 4.10 provides a summary of the various processes thought to be occurring during the thaw of a fine-grained soil possessing reticulate structure. The frozen clay shown contains through-going sedimentary and cryogenic features. As thaw proceeds, water released from the melting ice network will soften the adjacent soil and flow along the secondary structure in response to any existing hydraulic gradient. Water will also make its way into bedding features such as silt lenses.

Availability of water permits the soil blocks or 'peds' to eventually swell to a moisture content in equilibrium with the in situ effective stresses. At the completion of thawing, it is probable that the secondary structure will be fully saturated and possess a moisture content somewhat higher than average. Lumps retained within the softened matrix will have lower water contents and may not be fully saturated. If external stresses are high, water will continue to drain preferentially along the fissures until effective stresses become sufficiently high to cause closure of the structure. Under these circumstances, water migration would continue within the soil blocks. With lower external stresses, it seems less likely that drainage and local moisture redistribution would occur. Suctions within the lumps would then constitute the only potential driving water from the secondary structure into the intact soil. This model suggests several behavioural features that have a great deal in common with other soils possessing a definite secondary structure such as the more familiar fissured clays.

The physics of thawing soils are understood reasonably well, and analytic solutions are now available for application to a wide variety of engineering problems. However, very little detailed information exists describing the geotechnical behaviour of thawing soils. With numerous important problems confronting the geotechnical engineer in the Arctic, it is probable that those situations involving the thawing of frozen soil will be the most common and potentially serious from both structural and economic points of view. Fine-grained permafrost soils, particularly glaciolacustrine clays, have been singled out for attention in this thesis. The subsequent chapters present a detailed laboratory examination of their geotechncial behaviour when thawed.

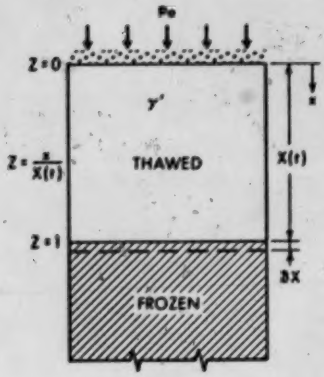
Pe
Z=0
z
γ'
Z = $\frac{x}{X(t)}$
THAWED
X(t)
Z=1
δX
FROZEN

Figure 4.1 One-dimensional thaw-consolidation (after Morgenstern and Nixon, 1971)

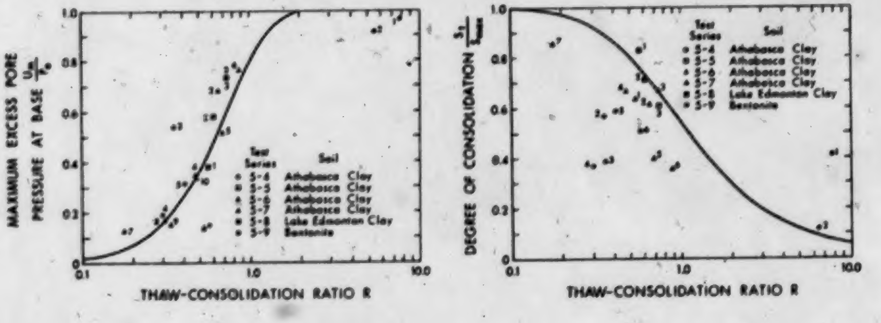

Figure 4.2 Maximum base pore pressures and degree of consolidation: a comparison of theory and experiment (after Morgenstern and Smith, 1973)

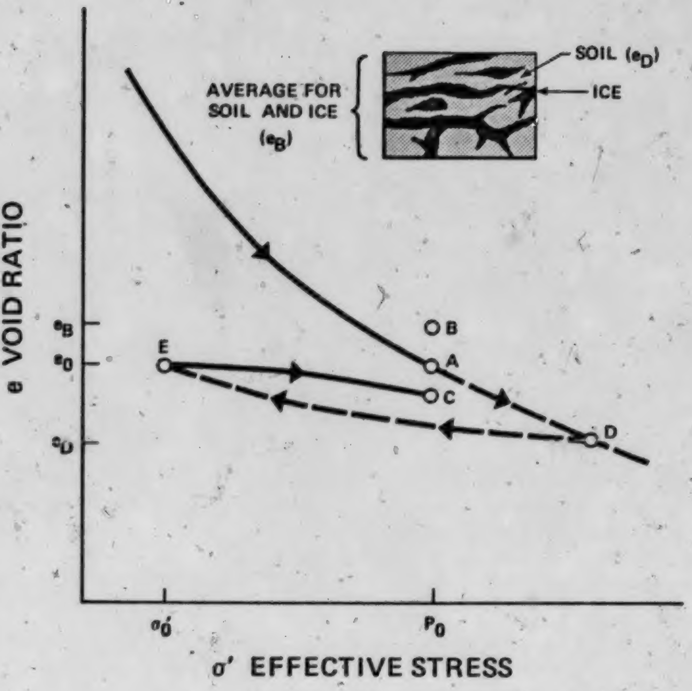

Figure 4.3 Stress path for a soil during a closed system freeze-thaw cycle (after Nixon and Morgenstern, 1973b)

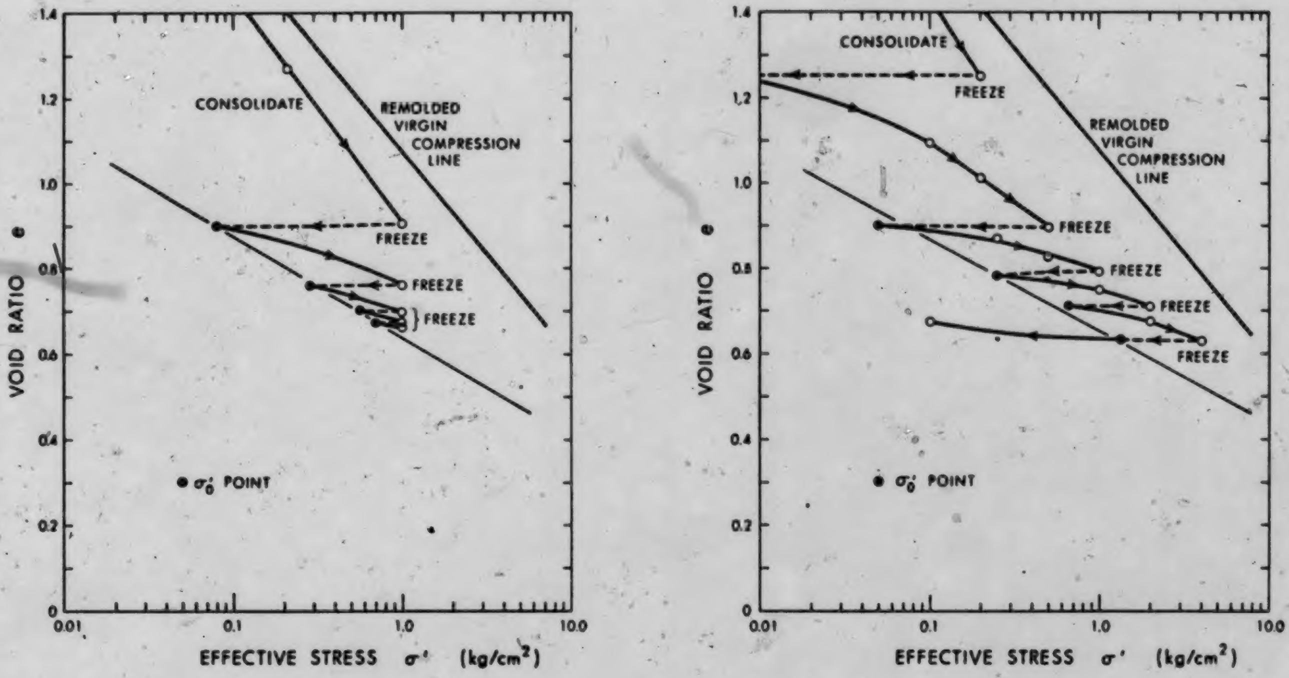

Figure 4.4 Different stress paths followed during the measurement of residual stress for reconstituted Athabasca clay (after Nixon and Morgenstern, 1973b)

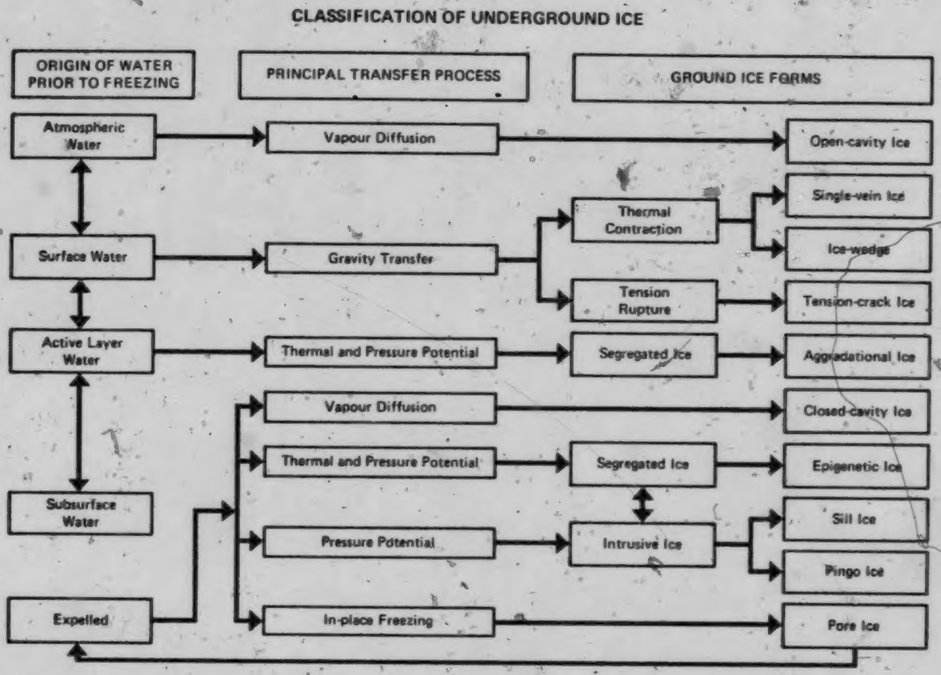
CLASSIFICATION OF UNDERGROUND ICE
ORIGIN OF WATER PRIOR TO FREEZING
PRINCIPAL TRANSFER PROCESS
GROUND ICE FORMS
Atmospheric Water
Surface Water
Active Layer Water
Subsurface Water
Expelled
Vapour Diffusion
Gravity Transfer
Thermal and Pressure Potential
Vapour Diffusion
Thermal and Pressure Potential
Pressure Potential
In-place Freezing
Thermal Contraction
Tension Rupture
Segregated Ice
Segregated Ice
Intrusive Ice
Open-cavity Ice
Single-vein Ice
Ice-wedge
Tension-crack Ice
Aggradational Ice
Closed-cavity Ice
Epigenetic Ice
Sill Ice
Pingo Ice
Pore Ice

Figure 4.5 Classification of underground ice (after Mackay, 1972a)

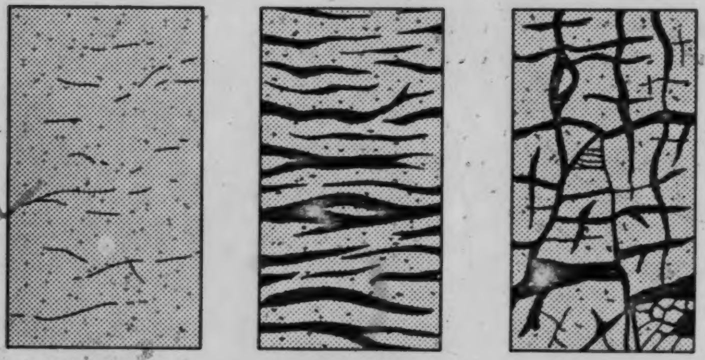
MASSIVE (pore ice)

STRATIFIED (segregated ice)

RETICULATE (segregated ice)

Figure 4.6 Structure of frozen soils and associated ground ice forms (after Tsytovich, 1973)

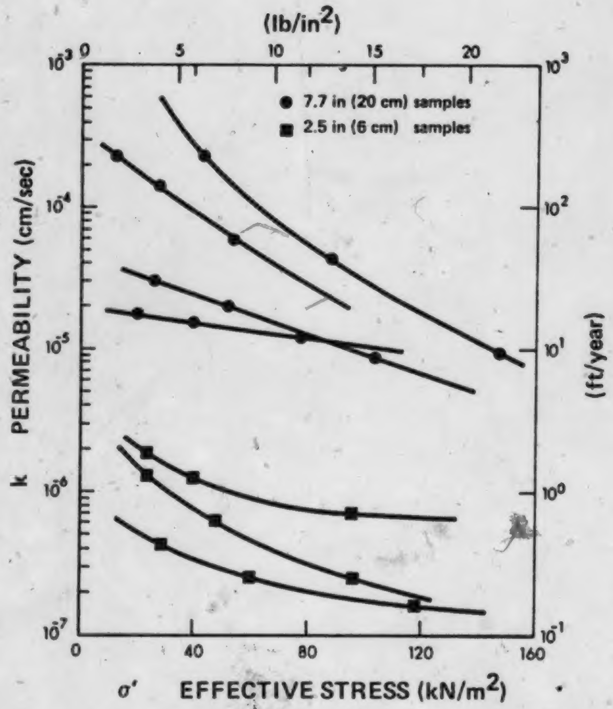

Note: 1) Permeability measured in oedometer with falling head test
2) ML-CL, all samples taken from same geologic unit, Copper River Basin, Alaska

Figure 4.7 Permeability test results for low plasticity clays, Copper River Basin, Alaska (after Woodward-Clyde Associates, 1970)

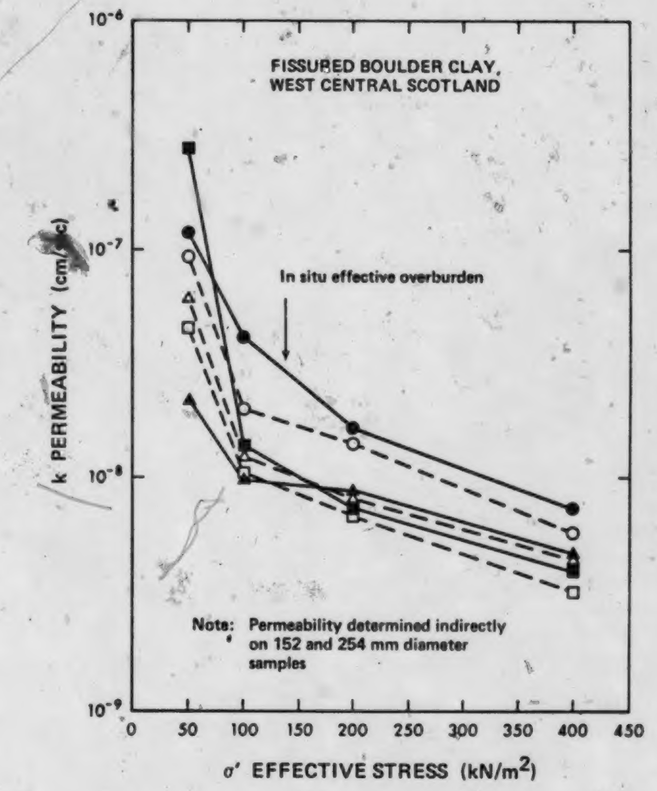

Note: Permeability determined indirectly on 152 and 254 mm diameter samples

Figure 4.8 Permeability as a function of stress for fissured boulder clay (after McGown and Radwan, 1975)

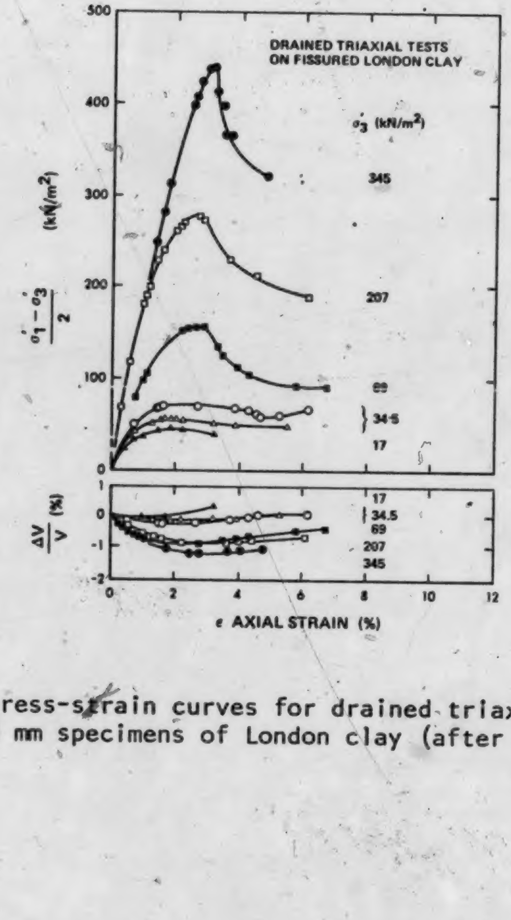

Figure 4.9 Stress-strain curves for drained triaxial tests on 98 mm specimens of London clay (after Marsland, 1972)

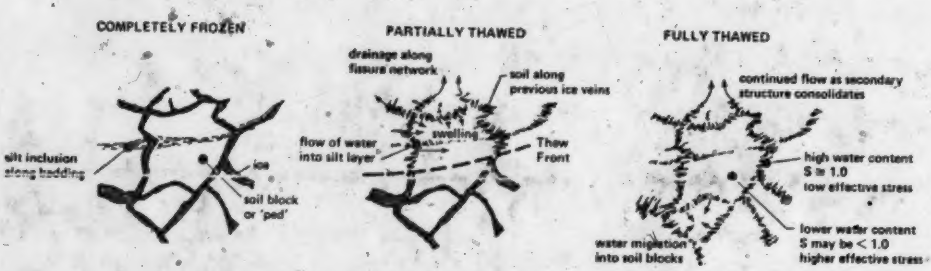
COMPLETELY FROZEN
silt inclusion along bedding
ice
soil block or 'ped'
PARTIALLY THAWED
drainage along fissure network
soil along previous ice veins
swelling
flow of water into silt layer
Thaw Front
FULLY THAWED
continued flow as secondary structure consolidates
high water content
S ≅ 1.0
low effective stress
lower water content
S may be < 1.0
higher effective stress
water migration into soil blocks

Figure 4.10 Thawing in a soil with reticulate structure

CHAPTER V

LABORATORY STUDIES OF CONSOLIDATION IN THAWING SOILS

5.1 INTRODUCTION

A mathematical model to describe the process of consolidation and experimental results to substantiate the theoretical work have been discussed in Chapter IV. As a next step, it is important to more accurately determine the soil properties used in the theory, with particular reference to natural materials. Subsequent sections describe laboratory tests on 10 cm (4 in.) diameter undisturbed samples of fine-grained permafrost soil obtained from three different sites in the Mackenzie River Valley. Discussions concentrate on the measurement of residual stress and consolidation properties, and an attempt is made to relate them to the depositional and thermal history of the sediments.

5.2 FACTORS AFFECTING CONSOLIDATION AND SETTLEMENT

The analysis of consolidation and settlement in thawing soils begins with a determination of the effective stresses acting in the soil. At the thaw front, the effective stress is described by:

$$\sigma'(X,t) = P_o + \gamma' X - u(X,t) + \sigma'_o \tag{5.1}$$

with symbols as defined in Chapter IV. The surface surcharge (P_o) and the thawed soils' submerged density (γ') can be evaluated. With the application of a step temperature at the soil surface, the depth of thaw (X) is related to the square root of time by the constant α. The dependence of the excess pore pressure (u (X,t)) on the thaw-consolidation ratio has been discussed in Section 4.3. Since the thaw-consolidation ratio contains both thermal and geotechnical properties, the precision with which pressures can be predicted will depend upon the accuracy with which α and c_v can be determined. The residual stress (σ_o') is apparently best determined by laboratory measurement.

Nixon and McRoberts (1973) have shown that in thaw problems, the dominant variables are ground surface temperature, the thermal conductivity of the thawed soil, and the quantity of water involved in phase change. Field and laboratory studies described in Section 4.2 provide reasonable assurance of the general applicability of Kersten's (1949) data in thermal calculations. Thermal variables entering the thaw-consolidation ratio are reasonably well-defined, whereas knowledge of the equally important geotechnical variables is less complete.

The coefficient of consolidation is the parameter which describes the rate of dissipation of excess pore water pressures and is related to soil permability and compressibility by the following:

$$c_v = \frac{k}{m_v \gamma_w} \tag{5.2}$$

where k denotes the coefficient of permeability of the soil, and

m_v denotes the coefficient of volume compressibility.

Mineralogy, texture, and stress history all influence compressibility, whereas permeability is, in addition to these factors, affected by fabric.

Rowe (1970) has suggested that m_v can be adequately determined from oedometer tests. Permeability, however, should be obtained either from in situ measurements or laboratory tests on large diameter samples which include representative fabric. Even the results of in situ permeability tests are subject to error since effects due to stress dependence are difficult to assess. Al Dahir et al. (1970) have demonstrated the importance of scale and stress level in applying laboratory results to the interpretation of field data. They showed that consolidation coefficients calculated from field records of pore pressure dissipation could be as much as an order of magnitude higher than laboratory values. The tendency for these differences to decrease at higher effective stresses was attributed to the diminished role of secondary structure under field conditions.

The difficulties involved in estimating either k or m_v for in situ conditions are well known. No attempt has yet been made to account for the stress dependence of consolidation properties in the development of thaw-consolidation theory. Extensions do, however, include a nonlinear e-σ' relationship with c_v assumed constant. To include property variations in the theory is not yet practically justified, but a realistic value for c_v is essential to obtaining an accurate prediction of pore pressure. For problems involving thawing permafrost, in situ permeability tests are not feasible and will seldom be practicable since the soil would normally be frozen at the time of the site investigation. This limitation increases the importance of obtaining and testing undisturbed samples which are representative of the in situ fabric.

The magnitude of the residual stress term in equation 5.1 has a significant influence on excess pore pressures predicted by the non-linear theory. A semi-logarithmic correlation has been found between thawed, undrained void ratio and residual stress, but additional testing of natural permafrost is required before this parameter can be routinely and confidently included in analysis and design (Nixon and Morgenstern, 1973b). Nevertheless, features such as cryogenic structure will influence the experimental measurement of residual stresses.

The expression giving total settlement for thawing, non-homogeneous soils consists of two terms and takes the form:

$$S = \int_{o}^{H} A(z)dz + \int_{o}^{H} m_v(z)\Delta\sigma' \, dz \qquad (5.3)$$

where $A(z)$ denotes the thaw settlement parameter at depth z,

$m_v(z)$ denotes the coefficient of volume compressibility at depth z,

$\Delta\sigma'$ denotes the effective stress change, and

H denotes the thickness of thawed soil.

The shape of the assumed thaw settlement curve in Figure 5.1 has been substantiated by thaw strain data reported by Watson et al. (1973). The thaw settlement parameter has been equated to the apparent relative settlement of a permafrost sample thawed under a no-load condition. A standard procedure to evaluate this quantity has not yet been established. Correlations between thaw strain and frozen bulk density have only been used to estimate settlements, so refinement of the test method is probably not justified. Thaw strain includes the large initial compression that occurs at low stresses as well as volume change associated with the ice-water transformation. The second term in equation 5.3 is settlement due to consolidation with m_v assumed constant. For soils exhibiting large thaw strains, this term will be small when compared to the total settlement. If the prediction of time-dependent settlement is required, more involved formulations are available (Morgenstern and Nixon, 1971; Nixon, 1973). Transient settlement behaviour is related to the dissipation of excess pore pressures and therefore depends upon the thaw consolidation ratio R.

Much larger variations can be anticipated in the geotechnical than in the thermal parameters for soils. Knowing index properties and water contents, the rate of thaw in a frozen soil can be predicted from published relationships with accuracy sufficient for most geotechnical purposes. The uncertainty in obtaining a value for α is considerably less than the uncertainty in estimating or measuring c_v.

In situ testing to assess thawed properties is precluded by practical considerations. With laboratory testing as the only alternative, care must be exercised to obtain truly representative results. Site investigation requirements should include the determination of accurate stratigraphic, water content, and density profiles as well as obtaining undisturbed core suitable for laboratory testing. Tests on representative samples should be performed over a stress range that approximates field loading conditions.

5.3 MODEL FOR CLOSURE OF THE SECONDARY STRUCTURE

In the process of thaw-consolidation, c_v is the most important geotechnical parameter and its magnitude is strongly influenced by the permeability of the thawed soil. Recognizing permeability's stress dependence, Nixon (1973) has emphasized the importance of performing tests at the correct stress level to estimate in situ permeability. Research cited in Chapter IV has shown that fissured soils exhibit a variation in permeability related to changes in effective stress. In most instances, a reduction in permeability has been found with increasing stress, and these initial decreases become less pronounced at higher stresses. Stress increases reduce porosity, which in turn, diminishes permeability. The much larger reductions in permeability displayed by undisturbed soils have generally been attributed to closure of structural discontinuities such as cracks, fissures, and root holes.

The influence of cracks on the permeability of rock has been reviewed by Morgenstern and Guther (1972) who draw attention to effects related to pressure changes. The aspect ratio of a crack is much higher than that of a pore, and since cracks are more prone to closure, stress changes have a significant effect on the permeability of a fractured porous medium. The use of Darcy's law to describe flow through a fissured or fractured media has been justified by Snow (1967). Water can then be assumed to flow everywhere in the medium and not just along joints and fissures. The equivalent permeability of such a material is given by:

$$k = k_f + k_s \tag{5.4}$$

where k_f denotes the permeability of the fissure system (strongly stress dependent), and

k_s denotes the intrinsic permeability of the soil (weakly stress dependent).

The intrinsic permeability will remain essentially constant because compression of the soil skeleton will be negligible over the relatively narrow range of stresses anticipated for most thawing situations. At low stresses, the permeability of a joint or fissure system will significantly exceed the intrinsic permeability of the soil. Although the overall permeability will be a function of average effective stress, it is also possible that fissure closure could be induced by changes in shear stress.

Terzaghi (1960) has explained the permeability of a jointed rock mass by proposing a model consisting of three similar sets of mutually perpendicular joints. He assumed that plane laminar flow occurred through two sets of joints and at right angles to the third. Figure 5.2 shows such an idealized soil mass with a set of intersecting discontinuities with a width of b and spacing D. The average velocity for laminar flow between two plates is given by:

$$V = \frac{1}{12\mu} \left(\frac{\partial P}{\partial x}\right) b^2 \tag{5.5}$$

where b denotes the spacing of the plates (joint width),

μ denotes the dynamic viscosity of water,

$\frac{\partial P}{\partial x}$ denotes the pressure gradient, $\gamma_w i$, in which

i denotes the hydraulic gradient.

Discharge is then determined by the product of flow velocity and area (x^2). For the soil element in Figure 5.2, a unit area is seen to contain a fissure area of $2x^2b/D$. By making the appropriate substitutions into Darcy's law, the following is obtained:

$$k_f = \frac{\gamma_w b^3}{6\mu D} \qquad (5.6)$$

Equation 5.6 suggests that small changes in b will produce large changes in k_f. Fissure closure will be determined by effective stress. By neglecting swelling effects, a functional relationship can be found between permeability, effective stress, and the geometry of the macrostructure of the soil. To describe experimental data typically obtained for fractured rock, Guther (1972) has suggested the function:

$$k = \frac{A}{(\sigma_a + T)^N} \qquad (5.7)$$

where σ_a denotes average effective stress, and
A, T, and N are empirical constants.

Equation 5.7 will plot as a straight line of log k against log $(\sigma_a' + T)$.

Since the stress dependence of permeability is directly related to fissure width, a similar relationship can be developed by expressing fissure width as a function of effective stress:

$$b = \frac{b_o}{(\sigma_a' + T)^n} \qquad (5.9)$$

where b_o denotes initial fissure width, and
n is an empirical constant.

The fissure width for any effective stress is then substituted into Equation 5.6 to obtain the equivalent permeability of the fissure system. Adding this value to the intrinsic permeability (Equation 5.4) yields the apparent permeability as a function of stress.

Figure 5.3 is a log-log plot of stress against permeability. The behaviour of these thawed samples appears to be described adequately by a relationship with the same form as equation 5.7. The initial average fissure width and spacing can be estimated from the ice network visible on frozen soil samples. Since this method of describing fissure system geometry is an arbitrary process, it cannot be used to estimate in situ permeabilities with any degree of confidence. Adopting this approach to model the interaction between macrostructure and effective stress is useful in explaining the large changes in permeability which are observed in thawing soils.

Combining equations 5.4, 5.6 and 5.8 yields the following expression:

$$k = k_s + \frac{\gamma_w}{6\mu D} \frac{b_o^3}{(\sigma_a{}' + T)^{3n}} \tag{5.10}$$

which can be reduced to the same form as equation 5.7 if:

$$A = \frac{\gamma_w b_o^3}{6\mu D} \quad \text{and } N = 3n$$

An apparent value for n can be determined from the type of data shown in Figure 5.3. With the inclusion of the appropriate values for the other parameters, predicted and observed relationships between σ' and k can be compared.

Sample NW3-5A displayed a reticulate ice network that closely resembled the assumed configuration. Measurements of average geometry were made and the exponent was evaluated from Figure 5.3. Figure 5.4 shows that the predicted σ'-k curve agrees well with experimental results. Duplication of experimental data in this case was possible only because the exponent 'n' was evaluated from results that were to be predicted. The curves in Figure 5.4 demonstrate that the fissure closure model provides an explanation for stress-dependent consolidation properties in thawing soils. By developing a semi-empirical equation to describe the decrease in permeability with increasing stress, it is possible to obtain a better understanding of the contributions made by the different elements of soil fabric in determining the soil's overall permeability.

5.4 TESTING EQUIPMENT AND PROCEDURES

Laboratory equipment

Laboratory equipment has been developed to permit the detailed study of thawing soils. The most sophisticated and versatile item has been the permafrost oedometer or permode (Smith, 1972) used to perform thaw-consolidation tests on remoulded clays. The original apparatus and instrumentation are described in detail by Morgenstern and Smith (1973). Later, a number of design improvements were incorporated which permitted both the testing of undisturbed permafrost samples 2.5 in. (6.4 cm) in diameter, and the measurement of residual stress.

The objectives of this research program required that testing be done on a large number of 10 cm diameter samples. To facilitate sample preparation and test setup procedures, two larger diameter permodes were designed and constructed. The following equipment improvements were made:

1) The pore pressure measurement system was redesigned to minimize its volume, eliminate air bubble entrapment, and permit transducer recalibration at any time.
2) Modifications to the valving were included which permitted measurement of pore water pressures at either the top or base of the sample.
3) Zero volume change valves were added to give complete control of drainage as well as to permit flushing of the top and bottom porous stones during and after test assembly.
4) Base pedestal height was increased to reduce difficulty previously encountered in placing the lower 'o' ring seal.
5) A double 'o' ring seal on the load cap minimized the possibility of leakage.
6) Since there was no need to maintain controlled thaw with relaxed requirements for temperature control, thermo-electric modules were replaced by fluid being circulated through heat exchangers in the base and load cap.

A diagram of the apparatus used for consolidation, permeability, residual stress and thaw-consolidation tests is shown in Figure 5.5. The permode is basically a fixed-ring, low friction oedometer providing complete control of sample drainage and measurement of pore water pressures. The split barrel design developed by Nixon and Morgenstern (1973b) was retained to facilitate the testing of undisturbed samples. Because of its low thermal conductivity, the barrel exterior and bottom section of the base were made from polyvinyl chloride (PVC). Following earlier designs, the load ram was threaded into the load cap to minimize any tendency for tilting. Ram alignment was maintained by a Teflon bushing set into an aluminum guide bar. The barrel was lined internally with a Teflon insert which, together with a greased rubber membrane, virtually eliminated friction on the sample sides.

Sintered stainless steel porous stones replaced the usual carborundum stones which deteriorated and frequently cracked when subjected to freeze-thaw action. The lower porous stone was connected to the pressure transducer by a 1/16 in. (0.16 cm) inside diameter bore. During the manufacture of valve assemblies, care was taken to minimize the internal volume of the pressure measuring system. A small, threaded bleeder valve was built into the transducer block so the transducer could be zeroed to atmospheric pressure with no flow of water occurring either into or out of the sample. Undersized neoprene 'o' rings were used to seal the rubber membrane to the load cap and base pedestal. In addition, the clamping action of the barrel on the lower 'o' ring assisted in producing a completely watertight seal. Each of the 1/8 in. drainage tubes leading from the load cap were connected to valves which permitted the control of flow from top end of the sample. All valves used were 1/8 in. Teflon seated Whitey ball valves (zero volume change) and all tubing connections were made with Swagelok fittings.

By clamping a linearly variable displacement transducer (LVDT) solidly to the load guide bar at the top of the sample barrel, settlement was measured directly to an accuracy of better than 0.0002 cm (0.0001 in.). An electrical resistance strain-gauged diaphragm pressure transducer with a resolution of approximately 0.15 KN/m^2 (0.02 psi) was used to measure sample pore water pressures and hydraulic gradients applied in the constant head permeability tests. Provision was not made for the routine use of thermistors or thermocouples since adopting uncontrolled thaw had eliminated the necessity for temperature measurement in most of the testing. However in thaw consolidation tests, both base and load cap temperatures were monitored by using precision thermometers to measure temperatures in the circulator baths. The accuracy obtained by determining the step temperature in this manner was checked by inserting a thermistor between the load cap and sample. By using pumps to circulate either refrigerated or heated fluid it was possible to minimize differences observed between the bath and heat exchanger temperatures. Shielded cables transmitted LVDT and transducer output signals to a data acquisition system which provided continual monitoring of pore pressures and settlements.

Testing procedure

Prior to each test, the permode and test specimen were placed in the sample preparation room for two to three hours to bring them to a uniform temperature in the -5 to -8°C range. Test specimens were turned on a small lathe to a diameter that corresponded to a close internal fit in the permode. Specimen lengths were usually in the 5 to 6 cm range but several as long as 8 and 9 cm were tested. An overhead milling machine was used to face the ends plane to each other and perpendicular to the core axis. Complete details regarding procedures and equipment for sample preparation and storage are given in Appendix B.

To prevent freezing of the fluid in the pore pressure measuring system, earlier studies had made use of automotive antifreeze in a 50%

or stronger aqueous solution. Sample deterioration was not reported, but from the writer's experience, it is certain that these high antifreeze concentrations caused significant erosion. To diminish this effect, an aqueous solution of reagent ethylene glycol was prepared at as low a concentration as possible while only marginally preventing fluid freezing at ambient cold room temperatures. By reducing the concentration of the freezing point depressant, sample erosion and chemical attack on the latex membrane were minimized. The deaired porous stones were cooled after being boiled in a 20% solution of ethylene glycol.

Alternating between warm and cold environments produces condensation which is known to cause deterioration of strain gauge bonding. To avoid changes in calibration and zero shift, the pressure transducer was replaced with a solid plug during assembly to avoid unnecessarily subjecting the instrument to large temperature changes. A pre-cooled, pressurized source of deaired ethylene glycol solution was used to flush and deair the pore pressure measurement and drainage assembly.

The process of placing a piece of frozen core into the permode was begun by rolling a rubber membrane onto the sample. The three 'o' ring seals were then slipped over the sample, outside the membrane. Before moving the lower porous stone into place, the recess in the base pedestal was flooded. With the stone in place, a wet filter paper was slid onto the fluid meniscus, taking care to eliminate all air bubbles trapped underneath. Excess fluid was wiped away and the sample in its rubber jacket was set directly on the filter paper. By rolling the membrane down and snapping the lower 'o' ring into its groove, the base seal was established. It was not always possible to remove trapped air when this process was repeated for the load cap. Once the specimen was enclosed and sealed, the split barrel halves were positioned and bolted together. The Teflon liner and all 'o' ring grooves were routinely cleaned and coated with Dow-Corning silicone grease prior to each assembly. With the barrel and guide bar clamped into place on the base assembly, the ram was threaded into the load cap. Application of an axial stress of 30 to 50 kN/m^2 (4 to 7 psi) made it possible to flush fluid through the lines and porous stones to remove any air trapped during setup, thus ensuring that the entire system was deaired. After closing all valves, the permode and sample were placed in a loading frame and prepared for testing in a warmer laboratory. This sequence was used to mount permafrost specimens prior to any one of the several different tests that could be conducted using the permode assembly.

The layout of the complete system used in conjunction with the permode for thaw-consolidation, residual stress, consolidation, and permeability testing is shown in Figure 5.5. With the permode and sample in place in the loading frame, components were properly seated by applying a nominal stress of 75 to 100 kN/m^2 (10 to 15 psi). Valves to both the load cap and base were opened to permit drainage and dissipation of any pore pressures that remained in the measuring system. Following removal of the plug, the pressure transducer was torqued into its receptacle and deaired. Axial stress on the frozen sample was adjusted to the test value and heat exchanger lines were connected to their appropriate baths and pumps. Permode drainage lines were deaired prior to connection with volume change indicators or burettes. The pressure transducer was zeroed to atmospheric pressure and the LVDT was initialized prior to starting the test.

5.5 DESCRIPTION OF SOILS TESTED

The undisturbed permafrost samples used in this testing program were obtained from the following sites:

1) A landslide headscarp on the left bank of the Mackenzie River, located approximately 35 km (22 mi) downstream (west) of Fort Simpson, N.W.T.
2) Borings on the MVPL ice variability study site, 1.6 km (1 mi) northeast from the townsite of Norman Wells, N.W.T.
3) Borings in the Noell Lake vicinity, some 27 km (16 mi) north of Inuvik, N.W.T.

It was anticipated that the fine-grained ice-rich soils present at these sites would provide marginal or unsatisfactory foundation conditions for projects such as a buried hot oil pipeline. Higher construction costs associated with rerouting or implementing some form of above-ground support prompted and justified a detailed assessment of geotechnical properties for these materials. The geographic locations of these sampling sites have been indicated on Figure 1.1.

Frozen core samples were obtained with a modified CRREL-type shell-auger core barrel, one meter in length. The 11 cm (4.25 in) internal diameter produced slightly oversized core which could then be trimmed during sample preparation to remove disturbed or desiccated material from its exterior. Sampling sites were restricted to locations where previous investigations had indicated recovery of fine-grained ice-rich permafrost soils. Limited research funds meant that site selection was restricted to those locations which were accessible from commercially serviced air strips. Descriptions of sampling equipment and procedures, site maps, borehole logs and soil classification test data appear in Appendix A.

Fort Simpson landslide site

In the vicinity of the landslide at Mile 226 (see Figure A.3), the Mackenzie River has cut its valley through the sediments of a proglacial lake. Intact slopes adjacent to the slide area are vegetated with mature white spruce interspersed with occasional birch. The inspection of soil exposures and a limited amount of test drilling indicate that the occurrence of ground ice in glaciolacustrine silts and clays is common in this region (McRoberts and Morgenstern, 1973; Rutter *et al.*, 1973). In the valley west of Fort Simpson, the fine-grained sediments lie in a wedge-shaped body which thins away from the river. The thickness of silt and clay in the immediate vicinity of the sampling site appears to be in the order of 40 to 50 meters (130 to 160 ft).

The headscarp section exposed in October, 1973, was composed of a uniform deposit of silt and clay with minor amounts of sand. A slight decrease in grain size was observed with depth and this was accompanied by increased plasticity. In Appendix A, a plasticity chart and typical grain size curves are given which summarize the textural properties of the soils at this site. Distinctions between the four zones identified on the stratigraphic log of the headscarp were based on the soil and ice structures that characterized each unit in the exposure. The lateral variability apparent in the exposure suggested that there was little to be gained from measuring the depth at which each core was taken. Therefore, only the source zone and core orientation were recorded. Samples from this site were used to conduct an experimental study of the effects which various types of ground ice structure would have on geotechnical behaviour. Laboratory testing was limited to samples extracted from the three lower zones.

McRoberts (1973) and Pufahl (1976) have commented on the evolution of the soil profile at this site. For the purposes of this study, Zone 2 has been called a fossil active layer but it may also be flow debris that has been refrozen. Dendrochronological studies incidate that this site was subjected to an intense forest fire some 130 to 140 years ago (Pufahl, 1976). Thermal disturbance associated with this event could account for the marked structural differences between Zones 2 and 3. At the same liquid limit, material from Zone 2 invariably exhibited lower plasticity indices than the underlying soil from Zone 3. This may reflect textural coarsening due to the mixing-in of silt and sand derived from the mantle of deltaic or alluvial sand outcropping further upslope. In the exposure examined, materials that make up Zones 3 and 4 appear to have remained undisturbed from the time of their deposition.

When the same headscarp was visited a year later (after some 12 m of ablation retreat), the headscarp was considerably different, with new materials exposed consisting of a channel infilled by sand containing silty clay inclusions. Several inactive ice wedges were present at the upper surface of the sand. At this time, the sand was still overlain by material that resembled the Zone 2 mapped the previous year. Its presence suggests that Zone 2 was probably formed some time after glaciolacustrine sediment deposition had ceased and permafrost aggradation had begun. The depth and age of the permafrost at this site are not known but its relatively warm temperature (-1.5°C to -0.5°C) indicates a condition of delicate equilibrium with prevailing climatic conditions.

Core samples were taken from Zones 2, 3 and 4 in vertical, horizontal, and intermediate orientations. Figure A.6 shows a typical section and the following is a summary of the principal characteristics of each of the zones in the exposure:

1) Brown sandy silt, thawed active layer.
2) Grey-brown silty clay, highly disturbed with predominantly horizontal segregated ice.
3) Grey silty clay, coarse reticulate segregated ice structure.
4) Dark grey silty clay, fine reticulate segregated ice intersected by thick, subhorizontal ice veins or layers.

Variations in structure, density, and orientation permitted comparisons between significantly different samples that otherwise exhibited identical external features.

Norman Wells site

A previous study of the effects of ground ice variability on resulting thaw settlements at the site near Norman Wells provided a considerable volume of preliminary data (Speer _et al_., 1973). The insert in the location plan (Figure A.4) shows the array of boreholes initially drilled during the MVPL study (as well as the three subsequent borings made for this study, designated NW2, NW3, and NW4). Local relief is flat and several small, shallow lakes dot the area. Vegetation consists of a moderately dense stand of black spruce. A muskeg with scattered larch lies directly to the northeast.

The site is in a shallow, poorly drained channel that lies at the foot of a long slope rising to the nearby Norman Range. It is underlain by massive or thickly bedded silty clays that are a minimum of 12 m in thickness. These lacustrine sediments were deposited in an extensive glacial lake that was impounded along the Mackenzie valley during deglaciation (Hughes et al., 1973). An upward textural gradation from clay through silt to sand is typical of deposits that would normally be expected in the central portion of a former lake basin. The profile contains variable quantities of ice in the form of randomly oriented veins up to 5 cm in thickness. Organic specks and discrete layers of sticks and leaves can be found as deep as 8 m. Below this depth, increases in density and plasticity are accompanied by a reduction in the quantity of segregated ice. Borings for this study were placed within a 2 m radius to minimize the effects of lateral variability. A profile derived from the composite borehole log (Figure A.10) showed the following strata:

1) Mechanically and thermally reworked silts and sands (0 to 2 m).
2) Silty clay with peat, low to medium plasticity (2 to 9.5 m).
3) Clay, medium to high plasticity (9.5 to 12.5+ m).

Noell Lake site

Examination of pipeline exploration boreholes drilled northeast of Noell Lake had indicated a clay with low to medium plasticity. Rampton (1972, 1974) has described the general area as subdued, hummocky and rolling moraine composed of a dark, sticky clay with variable stone content. These sediments are certainly not glaciolacustrine and this final drilling site was selected to obtain samples of a material that was texturally similar to the previous locations, but that differed significantly in its depositional history.

There are several thermokarst lakes in the immediate vicinity and local soils have probably been modified to some extent by thermokarst action. The morainic stony clay is thought to overlie a complex of texturally variable marine and fluvial sediments with relief being largely controlled by the presence or absence of massive ice or ice-rich beds at depth. Rampton (1974) has indicated that this ice is commonly found at the contact between the stony clay (till or till-derived colluvium) and the underlying coarser deposits. Excess ice appearing as discrete veins is also found within the stony clay.

The drilling site was located at the margin of a slight linear depression that conducts surface runoff toward Noell Lake. Raised-center polygons or earth hummocks cover the area and produce a local relief of approximately 0.5 m. The sampling site lies at a lower elevation than the surrounding tundra and probably occupies the drained terminus of a migrating thermokarst depression. Active mudflows were observed along the margins of nearby lakes.

The upper 1.5 to 2 meters have been subjected to severe cryoturbation in the active layer. Material below this is the ubiquitous stony clay which, at this site, has a highly disturbed appearance. The type and quantity of ground ice encountered with depth was extremely erratic, but a general increase in density with depth was indicated. A simplification of the profile (Figure A.15) consists of:

1) Reworked sandy silt, high ice content, present-day or fossil active layer (0 to 2 m).

2) Dark grey silty clay with stones, low to medium plasticity, highly disturbed, ice content extremely variable (2 to 8m).
3) Grey silt and fine sand, low plasticity, contorted bedding, high ice content (8 to 10.5 m).
4) Stony clay as above (10.5 to 12+ m).

The generally fine-grained texture of the soils sampled and used in this study is summarized for the three different sites in Figure 5.7.

5.6 RESIDUAL STRESS MEASUREMENTS

Testing procedure

With the sample prepared and mounted in the permode as described in Section 5.4, uncontrolled thawing was initiated by circulating warm water through both the load cap and base heat exchangers. The usual procedure was to start this portion of the test with an applied vertical stress equal to approximately half the estimated *in situ* effective overburden stress. Thaw typically took from 30 to 60 minutes, depending on sample height and ice content. Base pore water pressures were monitored continually and if sub-atmospheric values were observed, load increments were applied to keep pore pressures slightly positive and thus avoid damage to the pressure transducer. At the completion of thawing, the sample and permode were brought into thermal equilibrium with the laboratory room temperature.

Nixon and Morgenstern (1973b) have described two methods for the determination of residual stress in *saturated* soils. The technique adopted in this study was a modification of their 'null method' which

which maintained pore water pressures close to zero during the thawing portion of the test by manipulating the applied total stress. The possibility that permafrost soils might not always be fully saturated was confirmed by test data that is discussed in Chapter VI of this thesis. At the end of thaw, observations of pore pressure response to additional load increments ensured that neither side friction nor small-scale non-homogeneity influenced the measured value of residual stress. Results from tests on typical soils in the Norman Wells and Noell Lake profiles are given in Figures 5.8 and 5.9. If leakage was observed past any seal, or the pore pressures measured at the base continued to decay under constant total stress, it was apparent that the sample was not being maintained in an undrained condition. These conditions constituted justification for the rejection of data from the residual stress portion of that particular test.

The pore pressure reaction curves obtained suggest that residual stress can be determined by extrapolating the response line to a vertical stress that corresponds to a condition of zero pore pressure. The slope of the line also provides some indication of the overall pore pressure response of the soil. Assuming that the maximum stress acts vertically, the relationship given by Skempton (1954) can be written as:

$$\bar{B} = \frac{\Delta u}{\Delta \sigma_1} = \frac{\Delta u}{\Delta \sigma_v} \qquad (5.11)$$

where $\bar{B}$ denotes the overall pore pressure coefficient,

Δu denotes the increase in pore pressure, and

$\Delta\sigma_1 = \Delta\sigma_v$ denotes the increase in the major total principal stress (vertical).

Determination of the overall pore pressure coefficient is important in the estimation of pore pressures at the thawing front, since a $\bar{B}$ of less than unity will have the effect of reducing predicted magnitudes of pore pressure. The decrease observed in $\bar{B}$ with increasing density and residual stress is consistent with the overconsolidation and possible desaturation known to accompany closed-system freezing. Further discussion of pore pressure response to total stress changes is given in Chapter VI.

At the completion of each test, the total stress was decreased to an intensity equal to approximately twice the residual stress. Undrained thaw strain was determined by noting the total compression that had occurred during thaw and pore pressure reaction testing. Figure 5.10 shows values of this parameter measured on selected samples from the Norman Wells site. Disregarding the two samples which contained significant quantities of peat, undrained thaw strains are in close agreement with the solid line representing the computed contraction associated with phase change.

Consolidation was initiated by opening the top and bottom drainage valves. Measurement of expelled water volumes permitted calculation of moisture content and void ratio changes with each stress increment. The LVDT monitored vertical strain and its signal was recorded at specific time intervals by the data acquisition system. Permeability, compressibility, and consolidation coefficients were determined in the usual manner from each successive application of load. Constant head permeability tests were routinely performed at the end of each consolidation stage and a detailed discussion of test procedure and results appears in the next section. Data from the residual stress, consolidation, and permeability tests are summarized in tabular form in Appendix C.

At the completion of testing, all drainage valves were closed and external loads were removed from the sample. The cores were removed for water content determination which, in turn, permitted calculation of the void ratio for any point in the test. It should be noted that volume changes from settlement observations on some of the denser samples often exceeded the volume of water expelled during consolidation. In addition to the reasons given by Nixon and Morgenstern (1973b), the greater variability of residual stresses measured for undisturbed samples refrozen at higher stresses may have been caused by desaturation effects.

Residual stresses were also measured in a triaxial cell and close agreement was found with results obtained in the permode. Initial tests on silty clay from the Fort Simpson site frequently indicated negligible residual stresses. These samples had been thawed under very low cell pressures and it was suspected that the absence of a pressure gradient during thaw allowed most of the water produced by the melting of discrete ice to remain in the cryogenic fissure system. Measured pore pressures then reflected the response of the high water content soil occupying and adjacent to the secondary structure. Testing consistently yielded very low residual stresses, regardless of sample density. The tendency to measure the response of the secondary structure instead of the whole sample was overcome by thawing triaxial specimens under a moderate cell pressure. This procedure seemed to assist and accelerate the process of moisture redistribution prior to conducting the residual stress test proper. Cell pressure increments were applied in a manner similar to that adopted in the permode test procedure. Pore pressure response observed in these tests allowed evaluation of the pore pressure parameter B. Samples used in triaxial shear strength tests were routinely subjected to the same procedure.

Laboratory test results

The existence of a linear relationship between the thawed, undrained void ratio (e_t) and the logarithm of residual stress (σ_o') has been demonstrated for both reconstituted and undisturbed permafrost soils (Nixon and Morgenstern, 1973b). The results reported in this thesis provide a convincing confirmation of this relationship. An attempt to correlate residual stress with frozen bulk density proved unsuccessful.

Figure 5.11 presents both permode and triaxial cell determinations of residual stress for material from zones 3 and 4 of the Fort Simpson landslide headscarp. The data is confined to a relatively narrow band and agreement between results obtained with the two different types of testing equipment is encouraging. Similar relationships are given in Figures 5.12 and 5.13 which summarize residual stress data from the Norman Wells and Noell Lake sites.

Several patterns emerge from the data. Firstly, it would appear that the slope of the e_t - log σ_o' relationship is related to plasticity since the highly plastic clays from Norman Wells were found to have the steepest e_t - σ_o' line. Lower plasticity indices for the siltier clays from the Fort Simpson and Noell Lake sites give reduced slopes, with the flattest one corresponding to the clayey silt found near the surface at the Normal Wells site. This behaviour is consistent with the conceptual model presented in Section 4.3 to explain the development of residual stresses in thawing soil. Higher plasticity is usually associated with an increased clay content, which in turn, causes greater compressibility and a potential for larger negative pore pressures during freezing. The combination of these two features produces a steeper curve for the residual stress-void ratio relationship.

Secondly, there is a tendency for a reduction in scatter of the data with increasing residual stress for all soils except the medium to highly plastic silty clay at Norman Wells. The different behaviour exhibited by this material is probably related to the frequent presence of peat layers in the test specimens. Uncertainty in the computation of void ratios is increased by the presence of organic material. The presence of peat also increases the difficulties associated with pore pressure measurement since it decreases the system stiffness. If problems with compliance or side friction were not encountered at higher stress levels, the uniformity of measured residual stresses would increase as effects related to secondary structure were diminished by its closure. At lower stresses, however, differences in residual stress might be anticipated between two similar samples at a given void ratio, due entirely to differences in the macrostructural response.

In addition to providing properties such as permeability and the coefficient of consolidation, compression following residual stress measurement also provides an e-log σ' relationship for each soil tested. Nixon and Morgenstern (1973a, 1974) have indicated that to predict pore pressures during thaw, σ_o' must be determined when a nonlinear function is used to describe the deformation of the soil skeleton. To evaluate residual stress indirectly for ice-rich soils, they suggested a graphical construction which extrapolates the e-log σ' line back to the thawed, undrained void ratio as shown in Figure 5.14. The absolute accuracy of the residual stress obtained in this manner was shown to be of secondary importance. Since it was not possible to perform a thaw consolidation test and measure the residual stress on the same sample, they assumed that for ice-rich soils, the value of σ_o' was so small that the extrapolation procedure approximated the first portion of the e-log σ' curve with sufficient accuracy.

For a number of samples, residual stress determination was followed by consolidation to define the e-log σ' relationship. Figures 5.15, 5.16 and 5.17 show data of this sort for boreholes at the Norman Wells and Noell Lake sites with depths as indicated. It should be re-emphasized that each void ratio calculation is subject to some error if organic material is present, or if the soil is not fully saturated. Using the best available data for specific gravity of soil solids and assuming full saturation, it can be seen that the measured residual stress points (open circles) consistently fall on the extrapolated e-log σ' line. This provides a convincing demonstration of the general applicability of the procedure described for the graphical construction of σ_o' from post-thaw consolidation data.

Further inspection of Figures 5.15 and 5.16 reveals the remarkable uniformity of the compression index (slope of the e-log σ' line) over the full soil profile at the Norman Wells site. Disregarding absolute values of void ratio, this consistent compression behaviour attests to the similarity of the depositional history and soil constituents throughout the depth interval sampled. These similarities become more apparent when the microfabric of the undisturbed soil is examined with the aid of a scanning electron microscope (Appendix B). Although the percentage of silt sizes determined by hydrometer analysis was variable, fabric inspection showed that identifiable silt grains were almost totally absent. Instead, silt-sized particles appeared to be aggregates of kaolinite and illite clay sizes. This general uniformity at the microstructural level provides some insight into the uniformity of the compression index where textural changes would normally suggest significant behavioural differences.

A similar trend did not emerge for samples from the Noell Lake site. The variability in compression behaviour found for these soils reflects the highly erratic and disturbed nature of the soils encountered in this profile. Linearity of the e-log σ' relationships remains a consistent feature.

Differences in void ratio at the same stress level exhibited by soils which appear to be similar can be attributed to inaccuracies in the determination of the specific gravity of soil solids (G_s) and the degree of saturation (S) used in void ratio calculations. G_s tests were invariably performed on samples from which organic material had intentionally been separated. This procedure, although aiding in the characterization of soil minerals, tends to artificially elevate void ratios computed for soils which do contain significant quantities of organic material. Skemptor and Petley (1970) have shown that a correlation can be developed between ignition loss and G_s for organic and peaty soils. The highly variable nature of peat inclusions in the upper 8 m of the Norman Wells soil profile precluded the application of such a correlation to void ratio calculations since ignition loss determinations would have been required for each sample tested.

For nearly all of the tests shown in Figures 5.15, 5.16, and 5.17, the residual stress point plotted at the thawed, undrained void ratio lies on or slightly below the extrapolated e-log σ' line. Points along the consolidation compression curve are back-calculated from the final water content and measurements of water volumes expelled during each loading stage. The assumption of full saturation is probably reasonable at higher consolidation stresses but many samples tested in this study were almost certainly unsaturated at the time of thaw. Direct evaluation of the degree of saturation was hampered by uncertainty in the accuracy of G_s for each particular sample. It is clear that by using values of S of less than unity in calculating void ratios, residual stress points would be moved closer to or even above the extrapolated e-log σ' lines. The occurrence of peat inclusions was confined to samples from the Norman Wells site since soils from other locations were essentially free of organic material.

Summary of results

All of the available results from experimental determinations of residual stress for both undisturbed and reconstituted soils are assembled in Figure 5.18. Here, the thawed, undrained void ratio (e_t) is plotted against measured residual stress (σ_o') using a logarithmic scale for stress. Water content and void ratio have been related by assuming full saturation and an average soil grain density of 2.7. In many respects, these data are similar to the sedimentation compression curves given by Skempton (1970). At a given void ratio, residual stress is apparently dependent upon the amount of clay mineral present as indicated by the liquid limit. The fact that more plastic soils exhibit higher residual stresses for any given water content has been discussed previously. The various materials summarized in this figure have similar clay mineralogies and consequently, effects related to this variable could not be determined. Figure 5.18 suggests that typical Mackenzie Valley soils with bulk moisture contents of 35% or less might be expected to exhibit a significant residual stress. Geophysical methods (e.g. surface resistivity) may prove to be a feasible means of delineating this characteristic moisture content in situ.

If the data appearing in Figure 5.18 are replotted in terms of liquidity index instead of void ratio, the points for clay soils are seen to occupy a distinct band as shown in Figure 5.19. It is interesting to note that the slope of this band is essentially identical to that for the sedimentation compression of clays reported by Skempton (1970). However, at any particular liquidity index, residual stresses fall significantly below corresponding effective overburden pressures (P_o) for normal consolidation. The similarity of the band slopes may explain the tendency observed for residual stress distributions with depth to fall parallel to the in situ effective stress line.

The discrepancy between σ_o' and the effective overburden pressure at the same liquidity index is related to the stress path followed to reach each condition. In Figure 4.4, we have seen freeze-thaw action bring about a large decrease in void ratio under conditions of constant applied stress. To obtain the same void ratio (or liquidity index) along the virgin compression line would require much larger effective stresses. Effective overburden pressures during normal consolidation are defined by the virgin branch of the e-logσ' curve, while in a closed system, residual stresses are determined by swelling to the pre-freezing void ratio. The differences in e-logσ' behaviour between virgin compression and swelling are well known. The flat line followed during swelling subsequent to thaw means that small increases in void ratio will produce large reductions in effective stress. Thus, considering the stress path followed during a closed system freeze-thaw cycle, it is reasonable to expect that the LI-logσ_o' line should fall well to the left of the LI-log P_o line. Experimental results are in agreement with anticipated behaviour.

The line for silts in Figure 5.19, although parallel to the clay band, lies some distance to its right. A plausible explanation for this deviation is that liquid and plastic limits used in the LI calculations may be in error. The composition of the sandy silt unit (8 to 10.5 m) at the Noell Lake site was irregular and it is quite possible that Atterberg limits determined in that interval were not representative of the material included in the residual stress samples. Limits given by Nixon and Morgenstern (1973b) were used to compute liquidity indices for the various undisturbed Norman Wells silt samples. A summary of site conditions at the Gas Arctic test facility (Pemcan Services, 1972) indicates that a more plastic soil is present below the 2.5 m depth. Using these alternate liquid and plastic limits to recompute LI values moves the silt line much closer to the other data.

Several correlations can be derived for residual stresses, but for the purposes of design work, expressing the data in the form e_t-log σ_o' curves for each geologic unit (as shown in Figures 5.11, 5.12, 5.13 and 5.19) is probably most satisfactory. This form of presentation describes the laboratory results for a particular soil in a straightforward manner and defines the relationship between residual stress and the thawed undrained void ratio.

In situ profiles

Nixon and Morgenstern (1973b) found an approximately linear increase in residual stress with depth for another site at Normal Wells (CAGSL test site, formerly operated by Gas Arctic; site plan in Figure A.4 shows the location). With laboratory results obtained in the course of research for this thesis, it was possible to obtain a similar correlation to depths of 12 m at both the Norman Wells and Noell Lake sites.

Residual stress profiles are given for boreholes NW2 and NW3 (Norman Wells site) in Figures 5.20 and 5.21 respecitvely. A trend for increasing residual stress with depth is clearly demonstrated in each case. The solid lines shown are probably a reasonable approximation of the actual in situ relationship. Open circles on the density profile indicate the γ_f of samples for which residual stresses were determined.

The two boreholes were drilled within 2 m of each other, and consequently, the density profiles are similar. The solid line indicating the relationship between density and depth is a curve drawn through density averages for sampling intervals of 0.5 m. It can be seen that σ_o' for samples with higher than average densities plot to the right of the apparent σ_o'-depth relationship. The opposite is true for samples with below-average density. A change in residual stress behaviour is seen at the transition from low to high plasticity clay near the 5 m depth. Below this depth, σ_o' is related to density deviations produced by peaty layers, local desaturation, and local accumulation of ground ice. This natural variability is, in turn, related to temporal and spatial fluctuations of processes that governed formation of the sediment profile. A more detailed discussion of the transport and depositional agencies responsible for the accumulation of materials encountered in this glaciolacustrine sequence appears in Appendix A.

In Figure 5.22, a similar presentation of data is given for borehole NL2 at the Noell Lake site. Quantities of ground ice encountered between the depths of 1 and 8 m were extremely variable, and are reflected in both the density and residual stress profiles. This site is located among active thermokarst lakes and the majority of the section sampled may have been reworked by thermokarst migration at some time in the past. Even with this disturbance, a general trend emerges which indicates an increase in residual stress with depth. The sandy silt between 8 and 10.5 m was very ice-rich, exhibiting low density and zero residual stress. Directly below this, a sharp increase in density produced a corresponding response in the residual stress. The low plasticity silty clay at the bottom of the borehole appeared to be much less disturbed than the texturally similar material sampled nearer the surface. The extraordinarily high σ_o' values in Figure 5.22 came from samples which were almost certainly unsaturated. Difficulties and uncertainties involved with the measurement of pore pressures in unsaturated soils raise questions regarding the credibility of residual stresses determined in these few tests. By contrast, other samples in close proximity had high ice contents and consequently, zero residual stress. A more detailed description of local and regional geologic features pertinent to this profile are given in Appendix A.

An increase in residual stress with depth has been shown for both the Norman Wells and Noell Lake sites. Specific geotechnical data has been related to a sequence of geologic events that seem reasonable for each locality. Even so, a number of criticisms can be applied to this data, the most obvious being that in many instances, densities of samples tested did not correspond to the average _in situ_ density. Again, this point raises the controversial question of representative sampling and testing discussed in Section 4.5. Until test results from large samples are used to corroborate field test observations or performance data, little more can be done to advance existing confidence in the measurement and prediction of residual stresses _in situ_. It is encouraging to note that theoretical concepts developed earlier appear to be consistent with the behaviour of natural soils. Furthermore, the fact that samples containing segregated ice can exhibit substantial residual stresses and small thaw strains suggests that many of the behavioural inferences made on the basis of currently accepted ground ice logging procedures should be subject to careful review.

5.7 PERMEABILITY MEASUREMENTS

Testing procedure

At the completion of each residual stress test, samples were subjected to one or more load increments to determine consolidation characteristics. Permeability coefficients could be calculated indirectly from the consolidation data for each stress increase, but it was recognized that these values would be influenced by the accuracy with which the soil's compressibility and coefficient of consolidation had been evaluated. Since the permode enabled complete control of drainage, it was a simple matter to obtain more reliable data by conducting constant head permeability tests at the end of each consolidation stage. Figure 5.6 details the plumbing which allowed water to be conducted under pressure through the transducer valve assembly to the sample base. This procedure permitted accurate measurement of the applied head at any time during the test.

The water supply was maintained at constant pressure in a reservoir mounted approximately one meter above the permode. Pressures applied were kept well below those transmitted to the specimen by hanger loads. At low consolidation stresses, the pressure reservoir was opened to the atmosphere so that only a small gravity head was applied to conduct the permeability test. As hanger loads were increased, regulated air pressure was incremented in the reservoir to increase the applied head. The imposed hydraulic gradient could then be computed by evaluating the current length of the sample. Venting the reservoir to atmosphere also provided a convenient check on the transducer's calibration factor.

Drainage from the top of the sample was measured in a burette attached to a moveable mount. During tests with small applied heads, gradient fluctuations were minimized by adjusting the position of the burette to keep the outflow water level at a constant elevation. Permeabilities were computed from the record of outflow volume against time. Use of the falling head method was confined to samples from the Fort Simpson landslide headscarp which were tested in a 10 cm oedometer rather than the permode.

Permeabilities obtained by the three different methods described above were in good agreement for samples which were fully saturated. Differences between the indirect results and permeabilities measured by direct methods were usually noted whenever soils were unsaturated or contained discrete organic layers. To conduct direct permeability tests on these materials, water was flushed through the sample for a reasonable length of time before flow measurements were commenced. It was hoped that this procedure would serve to fill the voids along the principal flow paths. Correspondence between volumes of inflow and outflow measured in several such tests confirmed the applicability of this technique.

Laboratory test results

Core was taken from the Fort Simpson landslide headscarp in a variety of orientations, and samples contained both stratified (Zone 2) and reticulate (Zones 3 and 4) ground ice structures. Permeability test results for samples from Zone 2 are shown in Figure 5.23. The development of ground ice has produced a system of horizontal structural discontinuties which might be expected to produce anisotropic permeability. The experimental data confirms this impression since the stratified structure apparently contributes significantly to the bulk permeability. This observation does require some qualification, however, since closure of the horizontal structure was probably inhibited by the inability of the permode to model in situ stress conditions and still measure directional permeability. A permeability ratio ranging from 5 to 10 in the low stress range (less than 50 kN/m^2) is probably representative of field behaviour. These curves illustrate the extremely non-linear relationship between permeability and effective stress and confirm that relatively large permeabilities are encountered in the low to moderate stress range.

In Figures 5.24 and 5.25, similar data are shown for material with reticulate structure obtained from Zones 3 and 4. No attempt was made to distinguish between the behaviour of these two soils since the structure for each was quite similar, even though Zone 4 samples tended to be slightly denser. Having recgonized the difficulties associated with interpreting oedometer data from tests on horizontal core, no attempt was made to explore anisotropic effects with the reticulate structure. Here again, a permeability decrease of approximately two orders of magnitude was produced by increasing the effective stress to approximately 50 kN/m^2. The reticulate structure apparently exhibits much larger differences in behaviour between samples under the same pressure, which indicates a greater variability in the structural sensitivity to stress.

Figure 5.25 shows an expanded section of some of the curves given in Figure 5.24. A general trend for lower permeability with higher density is apparent, but the sample with the lowest density (1.65 Mg/m^3) also exhibited the most rapid decrease in permeability as the effective stress were increased. This core contained a thick, sub-horizontal ice lens which decreased sample density but contributed little to the fabric enhancement of permeability. Deviations such as this only serve to emphasize the need to select test specimens carefully when attempting to obtain an accurate representation of in situ structure. When working with core obtained from a borehole, the assessment of structure can prove to be a difficult task. It was fortunate that the landslide headscarp exposure provided an excellent opportunity to obtain an accurate impression of the bulk structure, one which could not have been gained from examination of core.

Data from the Zone 3 and 4 material exhibited considerably more scatter between samples than did the vertical permeabilities measured for soil from Zone 2. Closure of the stratified structure in the latter was a direct result of the vertical stress applied, whereas the reticulate structure's response was also influenced by changes in horizontal stress. This feature, in combination with a wider range of frozen bulk densities, accounts for the greater amount of data scatter exhibited under low stresses by material from Zones 3 and 4. Terminal or intrinsic permeabilities of 1 x 10^{-7} cm/s were lower than the 4 x 10^{-7}cm/s determined for Zone 2 soils which reflects slight textural differences between the units. Although no experimental data is available for larger samples, inspection of the discontinuity spacings in these specimens indicates that the 10 cm permode was probably large enough to eliminate most of the scale effects relating to secondary structure in these particular soils.

Selected permeability data for samples from the Norman Wells test site are given in Figure 5.26. Once again, the large decrease in permeability associated with structural closure at low stresses is a dominant feature. Intrinsic permeabilities measured at higher stress levels are consistently lower for soils with higher clay contents or plasticity. A wide range in permeability is apparent, even at high stresses, because materials encountered at this site range from silts to highly plastic clays. Even so, as would be predicted by the fissure closure model discussed in Section 5.3, macrostructure dominates permeability behaviour in the low stress range.

Similar results obtained for samples from Noell Lake are summarized in Figure 5.27. The ice-rich and highly structured near-surface material underwent a permeability decrease of nearly three orders of magnitude before approaching a constant value under higher stresses. Sandy silt in the 8 to 10.5 m depth interval showed almost no structural influence, even though distinct reticulate features were visible in the frozen core. Permeability differences between samples in this unit could usually be attributed to textural differences. The stony clay in this profile gave permeability results which were highly variable. The apparent disturbance and erratic ice contents probably contributed significantly to this nonuniform permeability behaviour. Flattening of the k-σ' relationship for this soil appeared to occur at a stress of 80 kN/m^2, slightly higher than the 50 kN/m^2 value that was found to be typical for the other two sampling sites.

Permeabilities in profile

Figures 5.28 and 5.29 show permeability variations in profile for the Norman Wells and Noell Lake sites, respectively. These permeabilities have been interpolated from k-σ' curves at the appropriate calculated _in situ_ overburden pressure. At Norman Wells, the decrease in permeability with depth is consistent with increasing plasticity and closure of the macrostructure in response to higher stresses. The regularity of this trend reflects the overall uniformity of sediments encountered at this site. The deviation indicated at the 7.5 m depth is due to several layers of peaty material which tended to increase soil permeabilities.

Combined variations in soil texture and ground ice produced a much less regular relationship between permeability and depth at the Noell Lake site, but a sensible relationship did emerge when the erratic stratigraphy was taken into account.

Summary of results

In Figures 5.30 and 5.31, permeabilities are plotted as a function of void ratio for materials from the Fort Simpson site. The data plot as a straight line on semi-logarithmic axes. Figure 5.30 shows that horizontal samples from Zone 2 displayed permeabilities that were slightly higher than those obtained from vertically oriented samples with similar void ratios. Reasons for this behaviour have been discussed above. Several data points lie below the line, and it seems quite probable that by correcting for the degree of saturation, a closer correspondence might be obtained. The average void ratio of soils containing stratified structure apparently describes most of the fabric dependent properties since a single e-log k relationship fits the observed behaviour reasonably well.

Figure 5.31 shows that this is not necessarily true for the reticulate structure sampled from Zones 3 and 4. Here, small void ratio decreases produce large changes in permeability, and data from all of the tests converge on a single line for permeabilities of less than 10^{-6}

cm/s. In this instance, void ratio cannot, by itself, account for effects related to the macrostructure's response to stress. Several different networks of discontinuities, each with different spacings and widths, could conceivably be described by the same average void ratio.

Samples from the Norman Wells and Noell Lake sites both showed similar sorts of behaviour. High ice content samples often showed no definite structural influence, while those with a well-developed reticulate structure displayed a rapid decrease in permeability with the small void ratio changes occurring during the early stages of loading. In many instances, samples with similar bulk densities exhibited markedly different e-log k relationships.

The object of several tests performed was to assess the reproducibility of data. Figure 5.32 shows consolidation and permeability test results for two apparently identical samples which had been trimmed from the same piece of core. For stresses exceeding 10 kN/m^2, results obtained from the two different tests were essentially identical. In another case, a short specimen was tested in the permode and compared to a much larger specimen tested in a triaxial cell. Again, permeability coefficients were identical at the same stress level.

5.8 COEFFICIENT OF CONSOLIDATION MEASUREMENTS

The previous section has shown that large reductions in permeability are produced by increases in effective stress as consolidation proceeds. It remains to examine the effect which this has on the coefficient of consolidation (c_v). Nixon (1973) obtained very little c_v

data for undisturbed permafrost but he has suggested that the determination of correct in situ permeabilities is an essential prerequisite to the application of thaw consolidation theory to practical problems.

A sketch of a typical but somewhat 'idealized' permafrost sample appears as an inset in Figure 5.33. A well-developed cryogenic structure is apparent and the sample contains no organic inclusions. Test results shown for this section of core are typical and demonstrate some important features. Although permeability decreases by approximately two orders of magnitude as the stress increases from 0 to 200 kN/m^2, c_v varies by no more than a factor of 5. It can be seen that at very low stresses, reductions in permeability are not completely compensated by compressibility, so that the coefficient of consolidation actually decreases slightly. Once the fissures close, permeability changes occur more gradually. Since the thawed soil has been somewhat overconsolidated by the freezing process, compressibility continues to decrease with increasing stress. Interaction between these two properties causes the coefficient of consolidation to increase slightly or remain relatively constant throughout the stress interval.

In Figure 5.34, c_v data is given for Zone 2 material from the Fort Simpson site. There are very few indications of anisotropy; thus, it appears that the larger horizontal permeabilities have been compensated by the soil being more compressible in that direction. At stresses below 40 to 50 KN/m^2, measured values of c_v are relatively high for low to medium plastic silty clays and tend toward a constant value of 1 x 10^{-3} cm^2/s ($\pm$). The wide range in permeability indicated for this material in the 0 to 50 kN/m^2 stress range is almost certainly related to structural differences between samples. Testing specimens of larger diameter might serve to reduce this scatter, but it seems probable that the geotechnical engineer would still be faced with difficulties when deciding on an appropriate relationship to represent in situ behaviour.

Similar test results for the Norman Wells and Noell Lake sites are summarized in Figures 5.36 and 5.37, respectively. Comments concerning the permeability data from these sites can be applied equally well to the explanation of similar trends in consolidation behaviour. It should be noted that considerably lower c_v values have been measured for samples of the highly plastic clay found below the 10 m depth at Norman Wells, and for some of the stony clay from the Noell Lake site. With respect to pore pressure generation, it is geotechnically fortunate that large residual stresses were measured. Otherwise, concerns about the thaw-stability of these soils would have been well-founded.

Estimates of c_v at the in situ effective overburden pressure for these two sites have been plotted in profile in Figures 5.38 and 5.39. The upper 6 to 8 meters at the Norman Wells site appear to be free-draining with less desireable materials being encountered at depths below 10 meters. A trend showing the coefficient of consolidation decreasing with depth reflects finer particle sizes and increasing plasticity. Figure 5.39 shows that although surficially reworked material and the sandy silt at the 8 to 10.5 meter depth have relatively high c_v values, the stony clay is not at all free-draining. The Noell Lake profile suggests that if the upper clay unit were to impede drainage from the underlying and extremely wet sandy silt, the potential for instability is high, especially for conditions involving seismic loads.

To assess the effects that testing in the permode configuration might have had on c_v measurements, results were compared with data obtained from the triaxial consolidation of samples with similar densities that had been taken from the same approximate depth or zone. The general agreement indicated in Figure 5.40 confirms an earlier suggestion that side friction in the permode was minimal. All of the specimens set up in the triaxial cell were fitted with side drains to facilitate the dissipation of pore pressures during subsequent shear. Since the permeabilities of these thawed soils were large at low stress levels, low efficiencies for the side drains would virtually eliminate the possibility for radial flow during consolidation in the triaxial cell (Bishop and Gibson, 1963). As stresses were increased and soil permeabilities decreased, side drain effectiveness would tend to increase. By accounting for this, a correction for the appropriate amount of radial drainage would place the c_v values well below those computed from triaxial consolidation, if it were assumed that drainage occurred only from the sample ends. Since the values plotted for c_v (triaxial) were based upon the assumption that side drains were totally ineffective (i.e. one-dimensional drainage in the triaxial cell), any tendency to the contrary would move the data points closer to the dashed line.

5.9 THAW-CONSOLIDATION TESTS

A limited number of thaw-consolidation tests were run on samples from the Fort Simpson and Norman Wells sites. Since residual stress and consolidation behaviour had been defined for these soils, it seemed worthwhile to supplement the comparison between measured and predicted pore pressures for undisturbed permafrost. Base temperatures were controlled by circulating fluid from a refrigerated bath, while heated water imposed the step temperature required to initiate and sustain thaw. Pore pressure and settlement curves, and a tabluar summary of the data are given in Appendix C.

Figure 5.41 demonstrates the good agreement obtained between measured pore pressures and estimated values based on nonlinear thaw-consolidation theory (Nixon and Morgenstern, 1973a). Residual stresses used in the calculations were obtained from Figures 5.11 and 5.12. These were checked using the σ_o' construction method discussed in Section 5.6 (see Figure 5.14), and were found to agree well with measured values for most of the samples tested. Pore pressure measurements defined the effective stress at the thaw front, so an appropriate consolidation coefficient could then be used in the calculations. If the applied loads produced effective stresses at the thaw front in excess of 50 kN/m^2 (7 psi), post-thaw c_v's seemed to be adequate. Bars joining points in Figure 5.41 indicate pore pressures calculated after assuming a reasonable range of c_v for cases where accurate values had not been determined.

In certain instances, measured pore pressures were significantly less than those predicted from theory. It is probable that if unsaturated soils were encountered, measured pore pressure response would be some fraction of that anticipated for a fully saturated system. Using a correlation developed between the pore pressure coefficient $\bar{B}$ and the frozen bulk density, predicted pore pressures were adjusted accordingly with the equation that follows:

$$u = B\left(\frac{u}{P_o - \sigma_o'}\right)_{theory} \tag{5.12}$$

High frozen bulk densities for several samples tested necessitated corrections for reduced pore pressure response. Appropriate $\bar{B}$ values were used in Equation 5.12 to obtain revised values for predicted pore water pressures. By accounting for effects which desaturation had imposed upon response, Figure 5.41 indicates that good agreement can still be obtained between theory and experiment. It should be noted that measured pore pressures did not exceed predicted values in any of the samples tested.

Thaw strains measured in the permode have been plotted as a function of frozen bulk density in Figures 5.42 and 5.43. It can be seen that these data points fall reasonable close to the correlation given by Speer et al. (1973) and Watson et al. (1973). In each case, outliers were samples with high organic content, having either been sampled from the active layer or the peaty zones encountered at depth.

5.10 INTERPRETATION OF LABORATORY TEST RESULTS

The laboratory tests described by Morgenstern and Smith (1973) and Nixon and Morgenstern (1973b, 1974) have revealed much about the fundamental properties of fine-grained permafrost soils during thaw-consolidation. High void ratio soils exhibit markedly nonlinear stress-strain behaviour since the soil skeleton must expel large quantities of water to gain small increases in effective stress. The behaviour of these soils has been successfully described with a nonlinear thaw-consolidation theory (Nixon and Morgenstern, 1973a). However, to accomplish this, an exact determination of the residual stress is necessary for estimating excess pore pressures at the thaw front.

A study of natural soils from three different sites has shown that a correlation can be developed between void ratio and logσ_o' for each soil type. For the purposes of design, a similar relationship could be established between residual stress and water content. Data suggest that for silty clays from the Mackenzie Valley, significant residual stresses can be anticipated wherever in situ water contents fall below approximately 35%. The permode was used to measure residual stresses in this study, but Figures 5.15, 5.16 and 5.17 indicate that elaborate equipment and procedures may not be necessary. Using the graphical construction technique described by Nixon and Morgenstern (1974), it appears that residual stress can be estimated with sufficient accuracy by extrapolating post-thaw consolidation data to the thawed, undrained void ratio. Its inherent versatility still makes the permode an attractive apparatus for this sort of laboratory work. Testing to determine values for σ_o' and c_v is currently within the capability of most well-equipped geotechnical laboratories. Once the e-log σ_o' relationship has been established for each characteristic soil type, the most important requirement becomes obtaining accurate stratigraphy, water contents, and in situ densities. This might best be accomplished by augmenting sampling operations with information from a selected group of downhole and surface geophysical tools.

The consolidation efficiency of which the freezing process is capable has been demonstrated in Figure 5.19 where effective (or residual) stresses are associated with smaller liquidity indices than might be anticipated for a normally consolidated soil. Residual stresses are a response to swelling following thaw. Locally variable overconsolidation occurs during freezing as water is drawn out of the soil and into inclusions of segregated ice. Irreversible strains take place in the soil skeleton so that the same average void ratio before and after thaw is associated with quite different effective stresses. The difference in slope between the compression and swelling curves accounts for the decrease in effective stress that occurs during an undrained freeze-thaw cycle under constant external stress.

In situ, the occurrence of a residual stress reduces the magnitude of consolidation settlement and increases the soil's undrained shear strength. A decrease in the liquidity index or void ratio with depth should normally be indicative of increasing residual stresses in the thawed soil. Although the variability encountered with natural deposits causes some scatter, a trend for increasing residual stress with depth is apparent from the data for both the Norman Wells and Noell Lake sites.

Some explanation of the sensitivity of permeability to changes in effective stress has been given by the suggested model for closure of the cryogenic macrostructure. Increases in permeability related to structure indicate the importance of obtaining and testing samples which are representative of _in situ_ conditions. Even though permeability decreases sharply by as much as two orders of magnitude in response to small increases in effective stress, the coefficient of consolidation is much less sensitive to these same changes. Permeability decreases are apparently accompanied by similar reductions in compressibility, with the net effect being only small variations in c_v over sensible ranges of stress. In soils containing reticulate ground ice structure, the coefficient of consolidation reaches a minimum value at a stress corresponding to closure of the structure, and remains essentially constant thereafter. The success obtained herein by using post-thaw c_v data for pore pressure predictions can be attributed to the fact that for stresses above 30 to 50 kN/m^2, changes in the coefficient of consolidation are small.

The possibility exists that by using the lower c_v values obtained at higher effective stress levels, pore pressure predictions for thaw-consolidation at lower stresses would exceed actual values. This is a conservative error. The permeability of thawing soils is nonlinear, so that under certain conditions, impeded drainage could contribute to increasing the pore water pressures in the vicinity of the thaw front. A moderate surface load such as a gravel pad could produce effective stress increases in the underlying soils that would, in turn, diminish permeabilities and hinder drainage from the thawing soils at depth.

Thaw consolidation tests on undisturbed permafrost soils have demonstrated good agreement between measured and predicted pore water pressures when the appropriate σ_o' and c_v were used in the nonlinear theory. The complex consolidation behaviour observed for cryogenically-structured soils presents considerable problems to the engineer faced with the task of choosing parameters for use in design. Furthermore, many soils are not fully saturated and exhibit a diminished pore pressure response to the application of changes in stress. Empirical correlations developed between $\bar{B}$ and frozen bulk density, as described in Section 6.2, can be used to correct pore pressure predictions made on the basis of assumed full saturation. A vast majority of the undisturbed soils tested in this study exhibited a linear e-log σ' consolidation curve which suggests that the nonlinear thaw-consolidation theory should be adopted as a matter of course when dealing with natural soils.

Difficulties encountered with establishing specific gravities and hence, void ratios and degrees of saturation, could be avoided if ignition losses were determined for selected samples. The peat and other organic material present in the Norman Wells soils complicated interpretation of some of the data. Gases produced by decomposition processes have probably been another factor diminishing the pore pressure response characteristics of these materials.

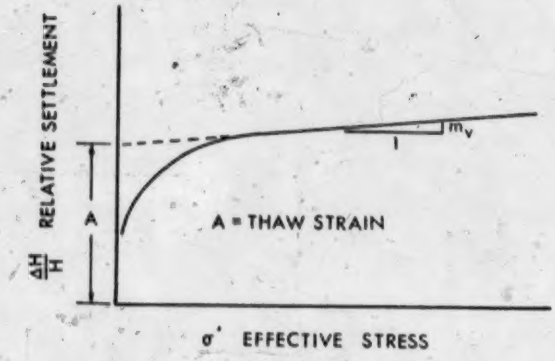

Figure 5.1 Generalized thaw settlement curve

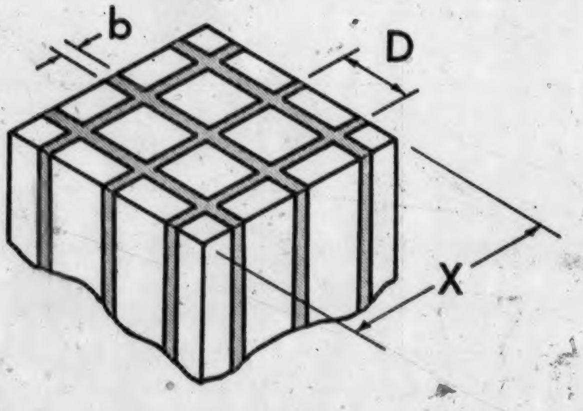

Figure 5.2 Model to investigate the effect of fissuring on permeability

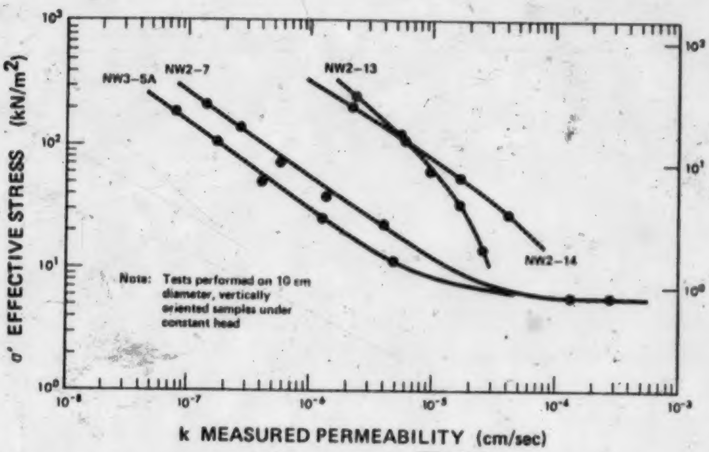

Figure 5.3 Typical results from permeability tests on thawed soil

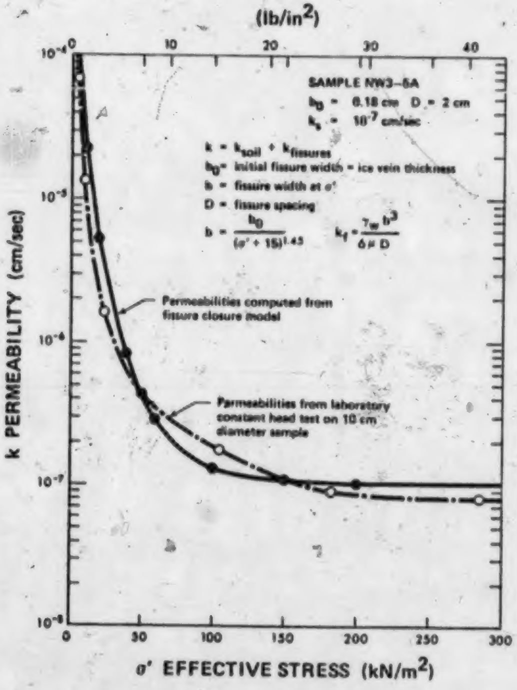

Figure 5.4 Comparison of predicted and observed permeabilities for thawed soil

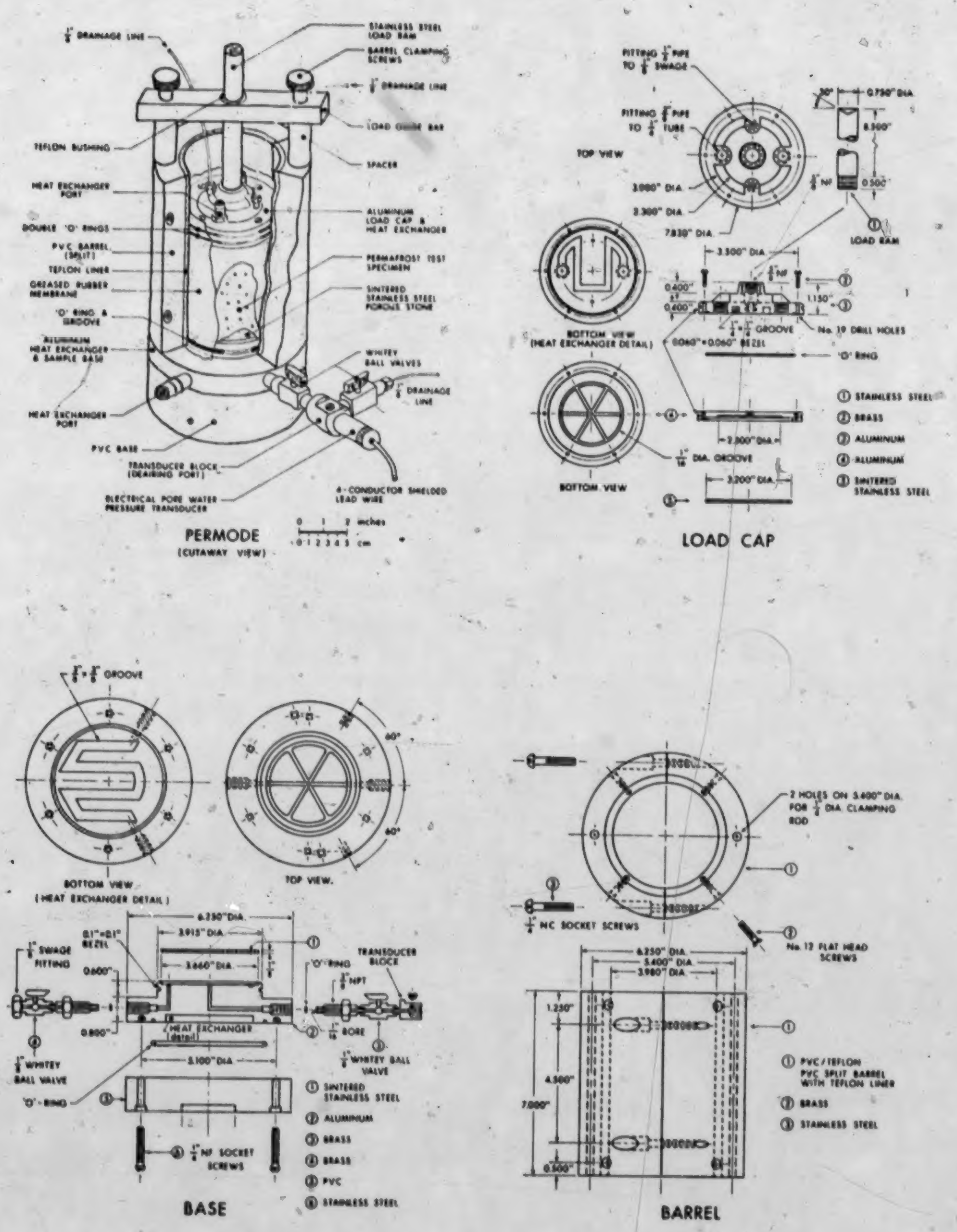
1/8" DRAINAGE LINE
STAINLESS STEEL LOAD RAM
BARREL CLAMPING SCREWS
1/8" DRAINAGE LINE
LOAD GUIDE BAR
TEFLON BUSHING
SPACER
HEAT EXCHANGER PORT
ALUMINUM LOAD CAP & HEAT EXCHANGER
DOUBLE 'O' RINGS
PVC BARREL (SPLIT)
TEFLON LINER
PERMAFROST TEST SPECIMEN
GREASED RUBBER MEMBRANE
SINTERED STAINLESS STEEL POROUS STONE
'O' RING & GROOVE
ALUMINUM HEAT EXCHANGER & SAMPLE BASE
WHITEY BALL VALVES
1/8" DRAINAGE LINE
HEAT EXCHANGER PORT
PVC BASE
TRANSDUCER BLOCK (DEAIRING PORT)
ELECTRICAL PORE WATER PRESSURE TRANSDUCER
4-CONDUCTOR SHIELDED LEAD WIRE
0 1 2 inches
0 1 2 3 4 5 cm
PERMODE
(CUTAWAY VIEW)
FITTING 1/8" PIPE TO 1/8" SWAGE
FITTING 1/8" PIPE TO 1/8" TUBE
TOP VIEW
3.000" DIA.
3.300" DIA.
7.830" DIA.
30°
0.750" DIA.
8.500"
3/8" NF
0.500"
① LOAD RAM
3.300" DIA.
3/8" NF
0.400"
0.400"
1.150"
BOTTOM VIEW (HEAT EXCHANGER DETAIL)
1/4" × 1/4" GROOVE
No. 19 DRILL HOLES
0.060" × 0.060" BEZEL
'O' RING
④
2.300" DIA.
1/16" DIA. GROOVE
BOTTOM VIEW
3.200" DIA.
⑤
① STAINLESS STEEL
② BRASS
③ ALUMINUM
④ ALUMINUM
⑤ SINTERED STAINLESS STEEL
LOAD CAP
3/8" × 3/8" GROOVE
60°
60°
BOTTOM VIEW (HEAT EXCHANGER DETAIL)
TOP VIEW.
6.250" DIA.
3.915" DIA.
0.1" × 0.1" BEZEL
3.660" DIA.
1/8" SWAGE FITTING
0.600"
0.800"
'O' RING
TRANSDUCER BLOCK
1/8" NPT
HEAT EXCHANGER (detail)
1/16" BORE
④ 1/8" WHITEY BALL VALVE
1/8" WHITEY BALL VALVE
5.100" DIA.
'O'-RING
⑥ 1/4" NF SOCKET SCREWS
① SINTERED STAINLESS STEEL
② ALUMINUM
③ BRASS
④ BRASS
⑤ PVC
⑥ STAINLESS STEEL
BASE
2 HOLES ON 5.400" DIA. FOR 1/4 DIA. CLAMPING ROD
1/4" NC SOCKET SCREWS
No. 12 FLAT HEAD SCREWS
6.250" DIA.
5.400" DIA.
3.980" DIA.
1.250"
4.500"
7.000"
0.500"
① PVC/TEFLON PVC SPLIT BARREL WITH TEFLON LINER
② BRASS
③ STAINLESS STEEL
BARREL

Figure 5.5 10 cm diameter permode with sectional views of its major components

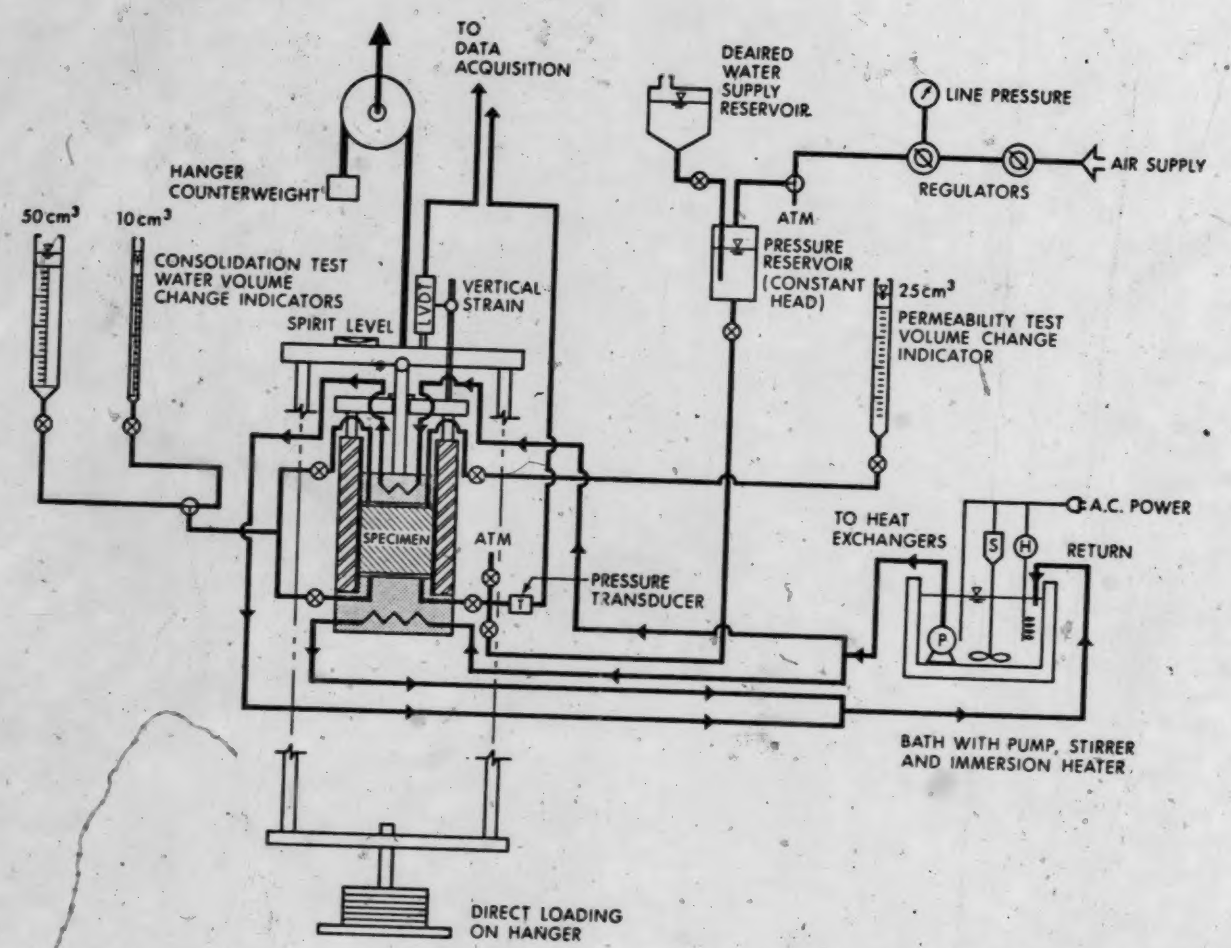
TO DATA ACQUISITION
HANGER COUNTERWEIGHT
50 cm³
10 cm³
CONSOLIDATION TEST WATER VOLUME CHANGE INDICATORS
SPIRIT LEVEL
LVDT
VERTICAL STRAIN
SPECIMEN
ATM
PRESSURE TRANSDUCER
T
DEAIRED WATER SUPPLY RESERVOIR
ATM
PRESSURE RESERVOIR (CONSTANT HEAD)
LINE PRESSURE
REGULATORS
AIR SUPPLY
25cm³
PERMEABILITY TEST VOLUME CHANGE INDICATOR
TO HEAT EXCHANGERS
A.C. POWER
S
H
P
RETURN
BATH WITH PUMP, STIRRER AND IMMERSION HEATER
DIRECT LOADING ON HANGER

Figure 5.6 Schematic layout of permode and associated apparatus used in residual stress, thaw-consolidation and coventional consolidation tests

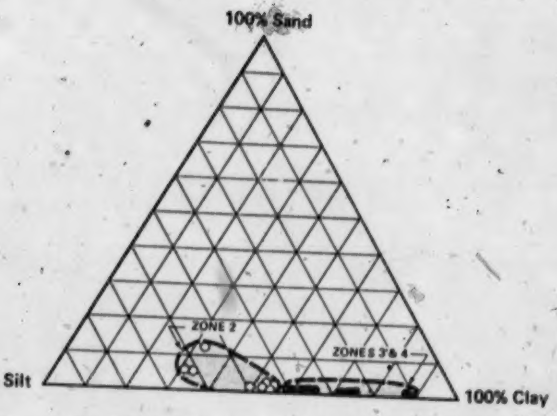

FORT SIMPSON LANDSLIDE HEADSCARP

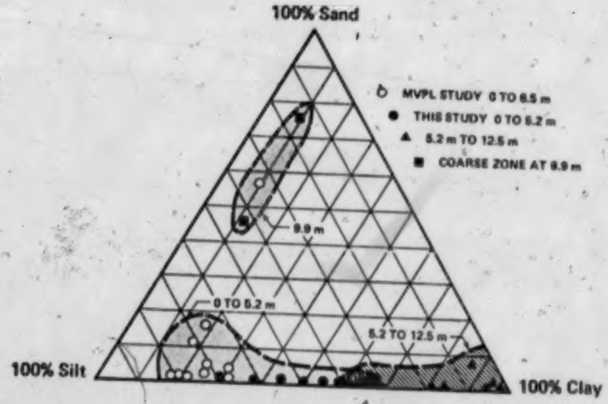

MVPL ICE VARIABILITY SITE, NORMAN WELLS

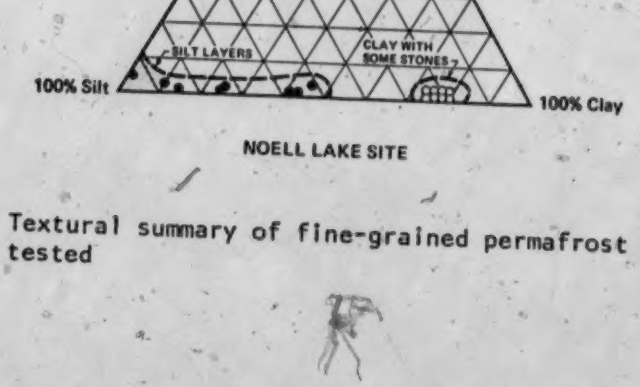

NOELL LAKE SITE

Figure 5.7 Textural summary of fine-grained permafrost soils tested

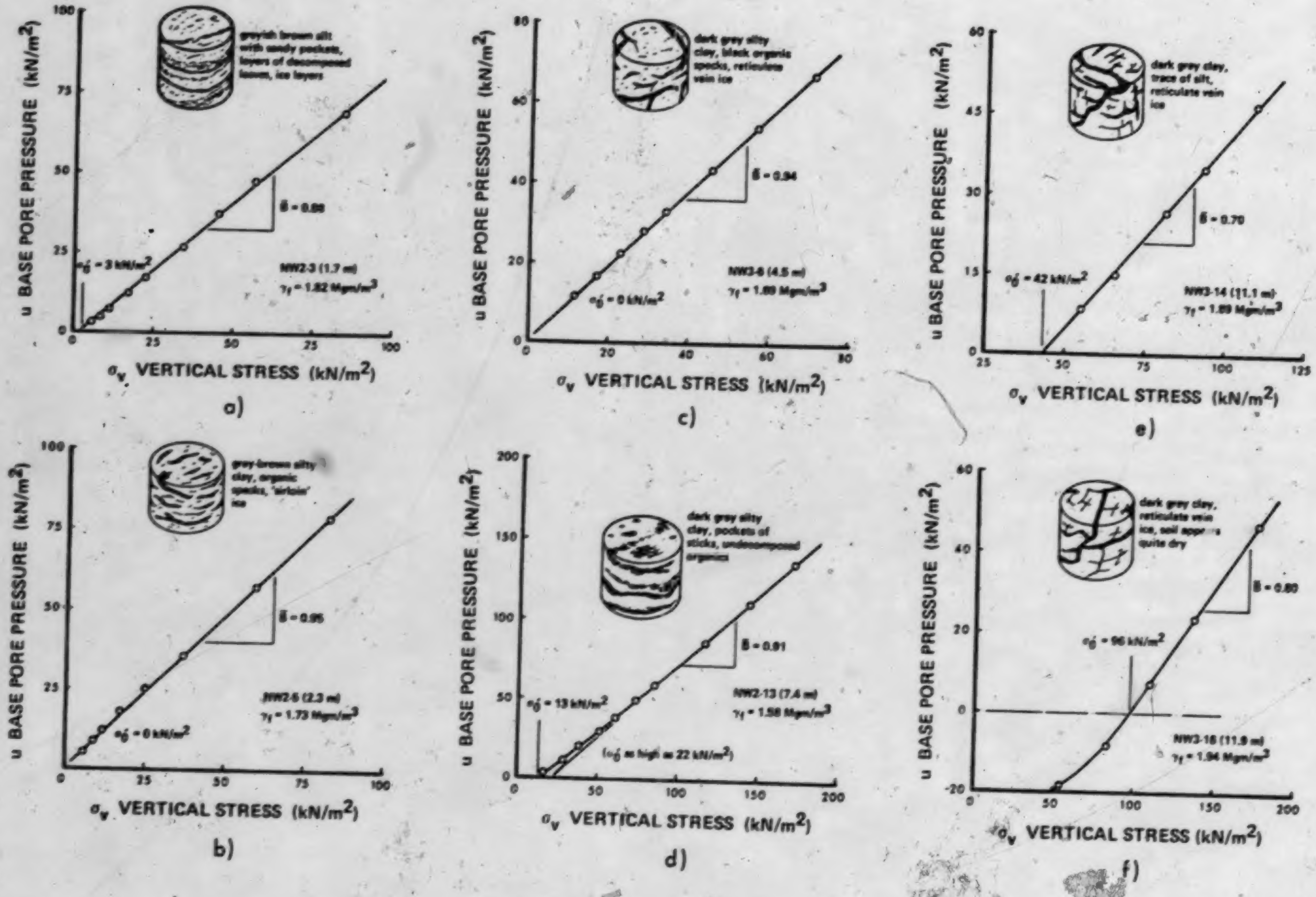

Figure 5.8 Typical residual stress test results, MVPL ice variability site, Norman Wells

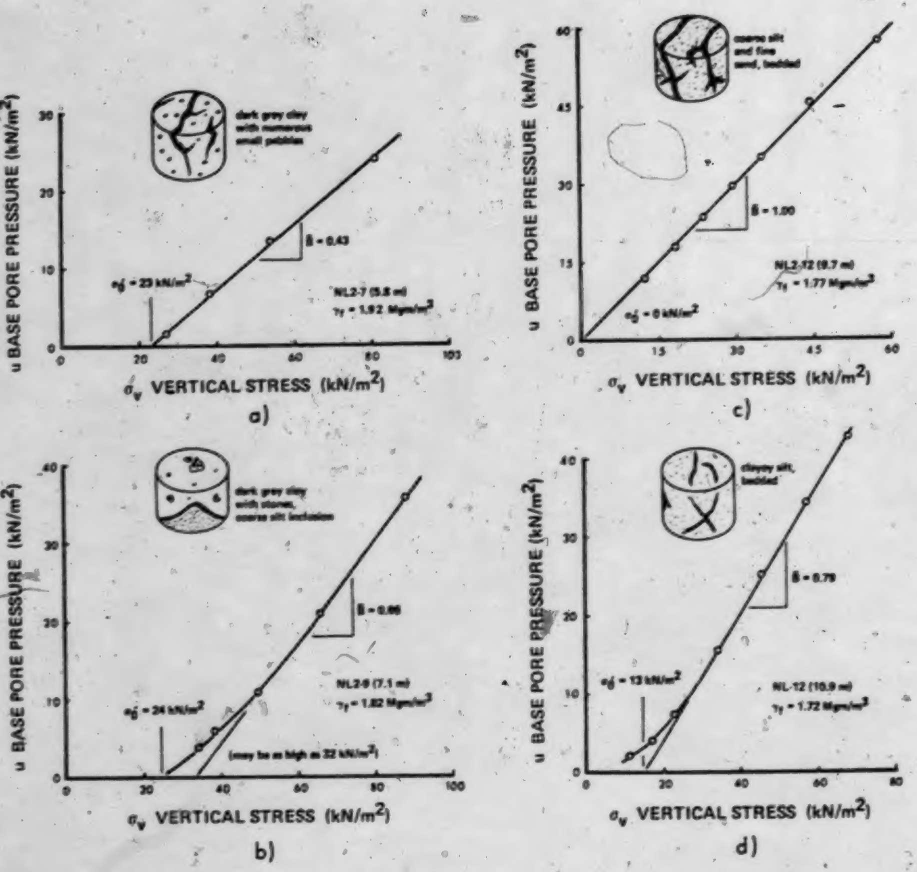

Figure 5.9 Typical residual stress test results, Noell Lake site

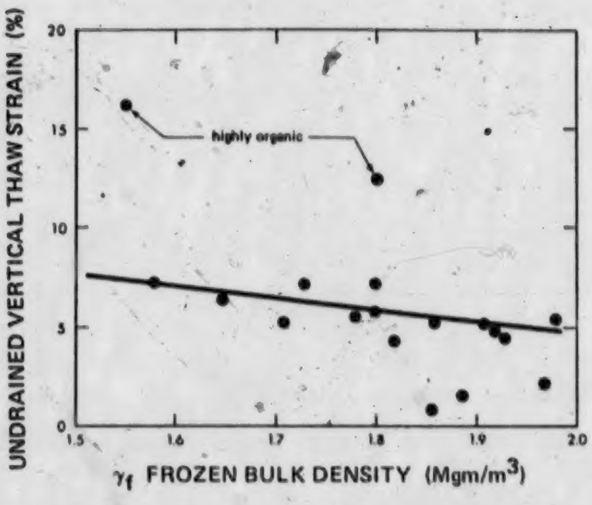

Figure 5.10 Vertical thaw strain without drainage, samples from Norman Wells site

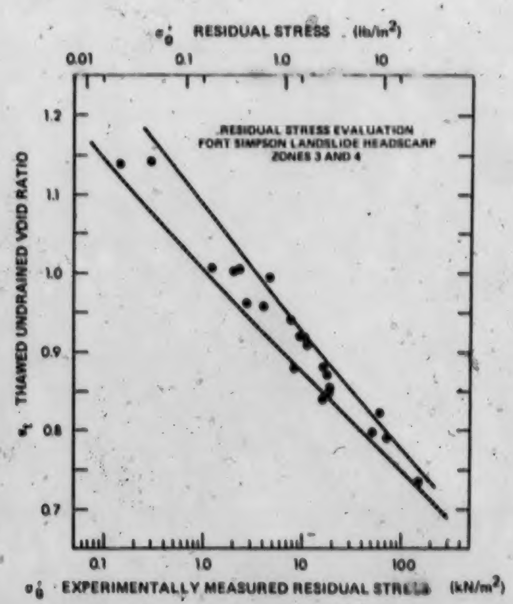

Figure 5.11 Summary of residual stress tests, Fort Simpson landslide headscarp site

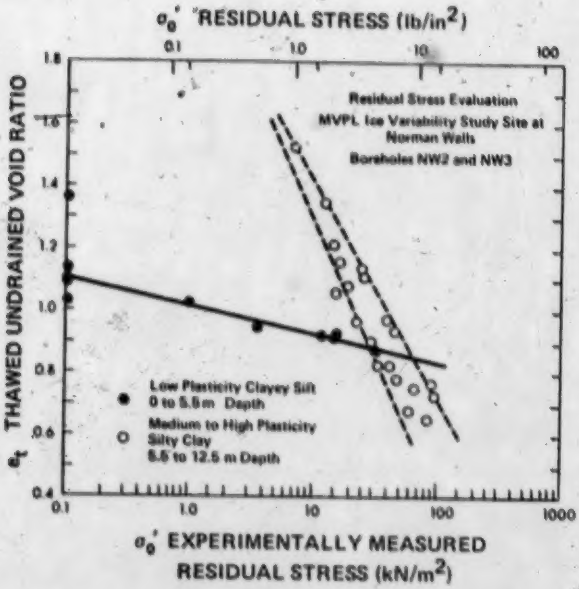

Figure 5.12 Summary of residual stress tests, MVPL ice variability site, Norman Wells

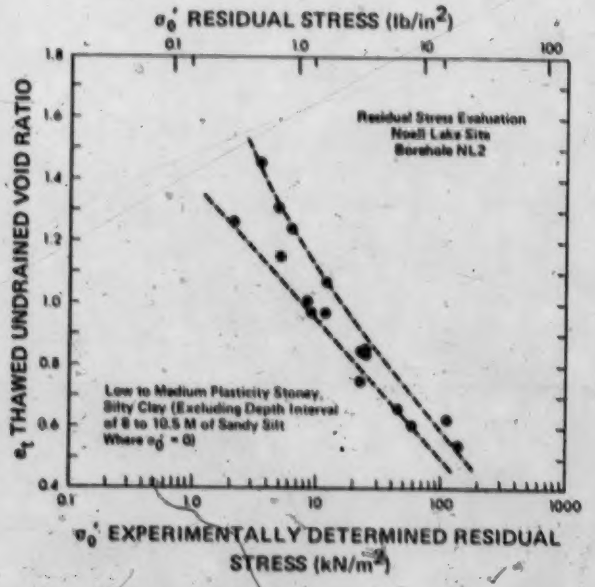

Figure 5.13 Summary of residual stress tests, Noell Lake site

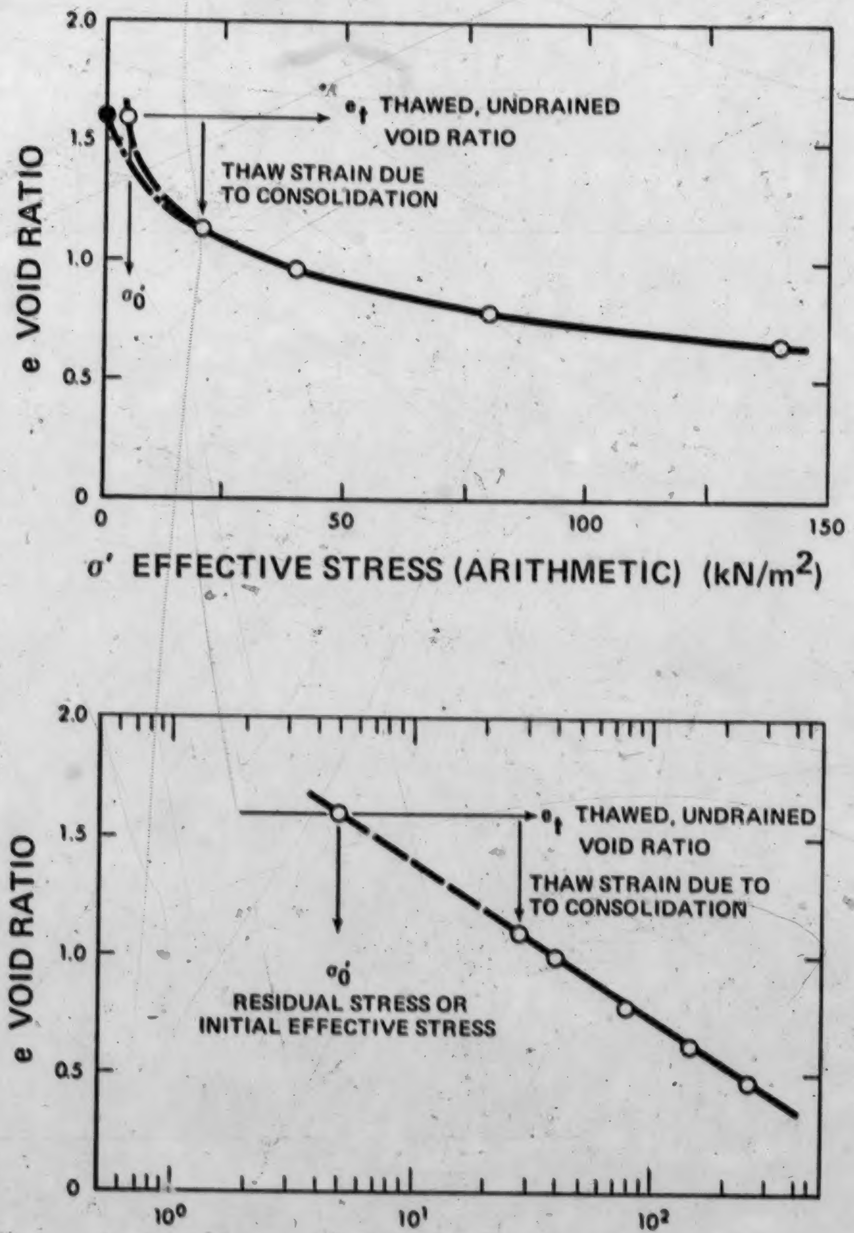

Figure 5.14 e - σ' relationships on arithmetic and logarithmic scales showing σ'_o construction

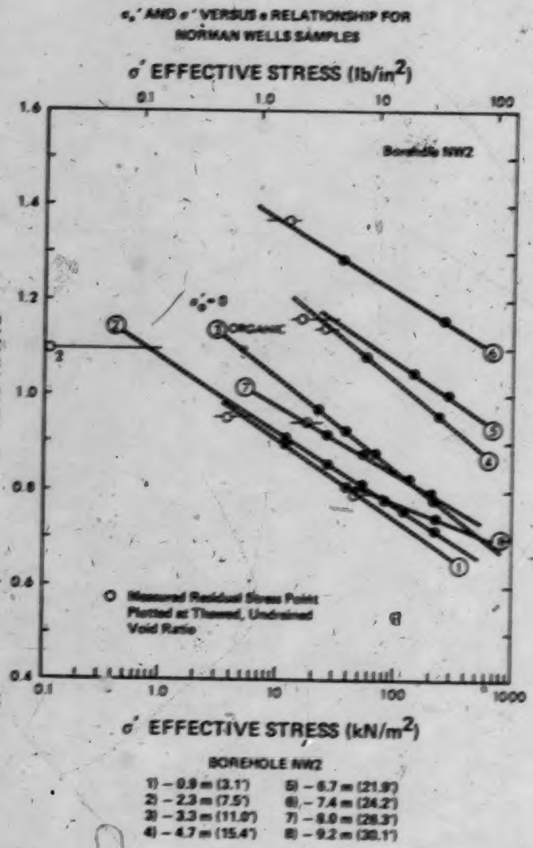

Figure 5.15 e - log σ' curves for residual stress test specimens, Borehole NW2

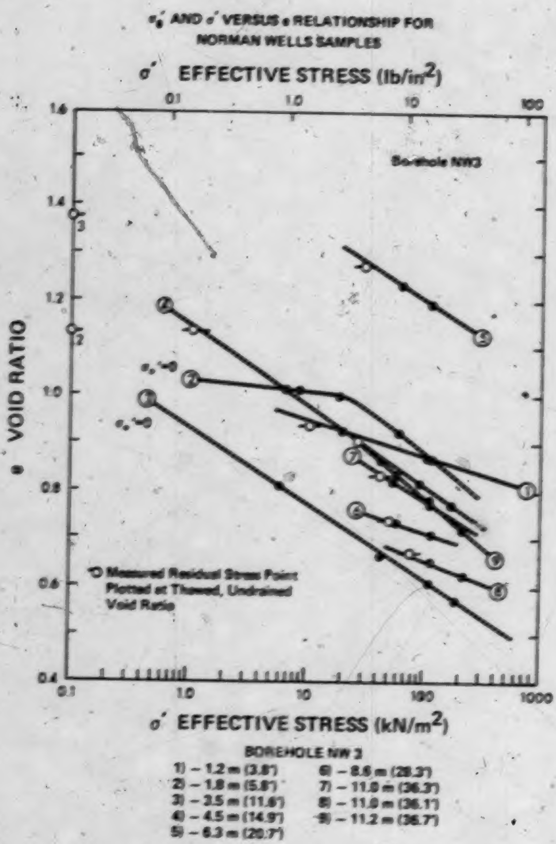

Figure 5.16 e - log σ' curves for residual stress test specimens, Borehole NW3

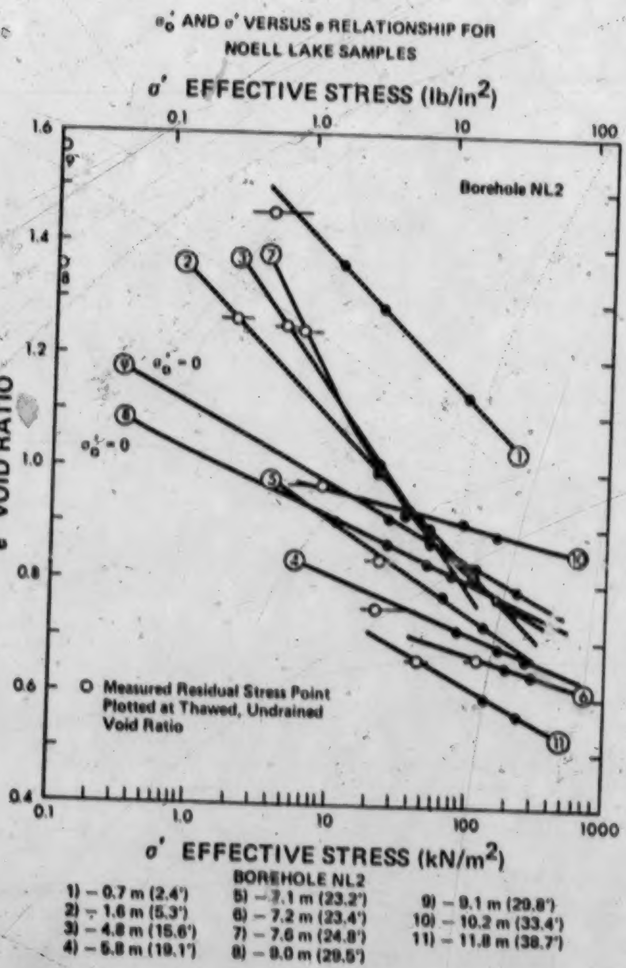

Figure 5.17 e - log σ' curves for residual stress test specimens, Borehole NL2

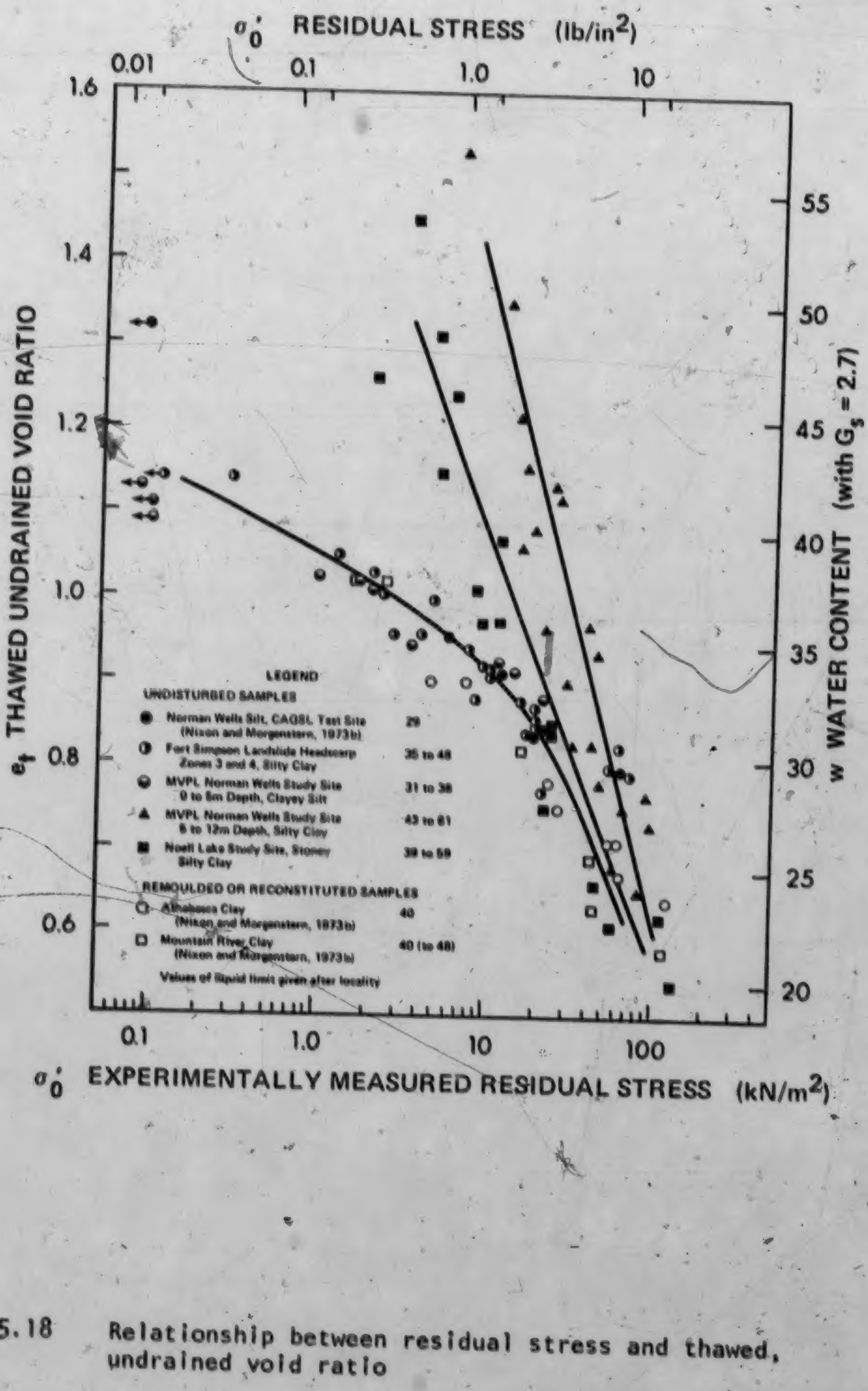

Figure 5.18 Relationship between residual stress and thawed, undrained void ratio

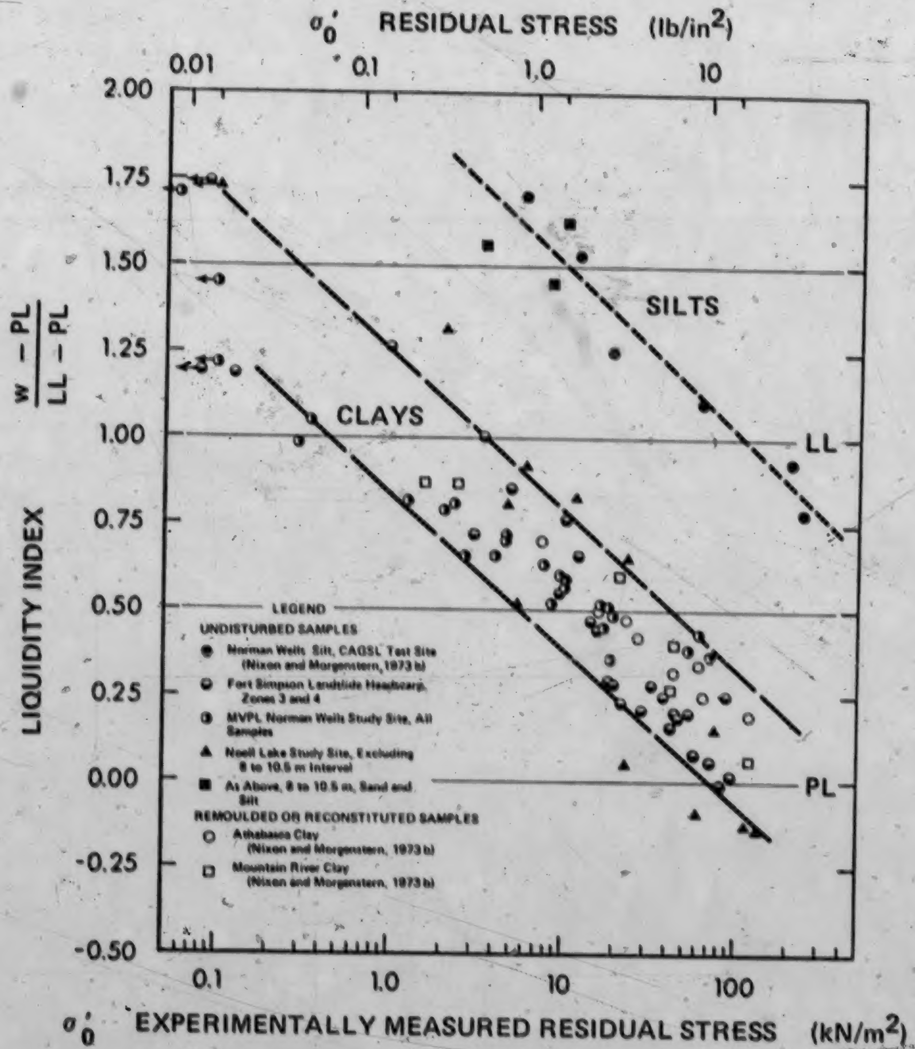

Figure 5.19 Relationship between liquidity index and residual stress

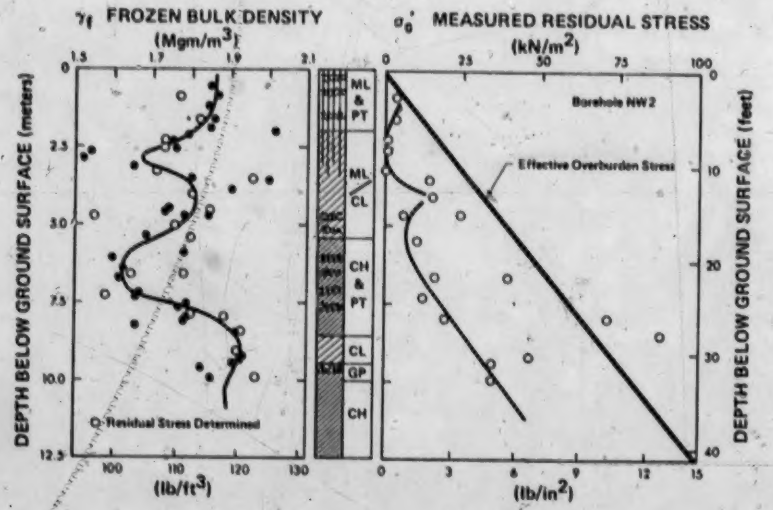

Figure 5.20 Residual stress profile, Borehole NW2

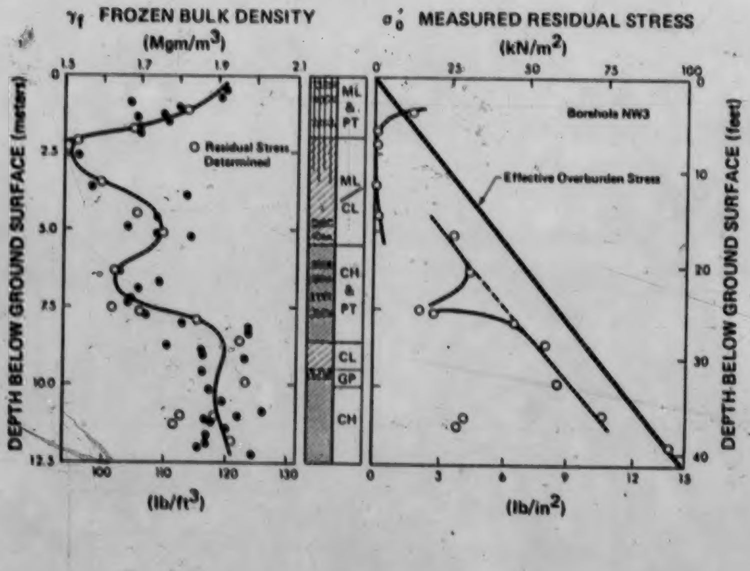

Figure 5.21 Residual stress profile, Borehole NW3

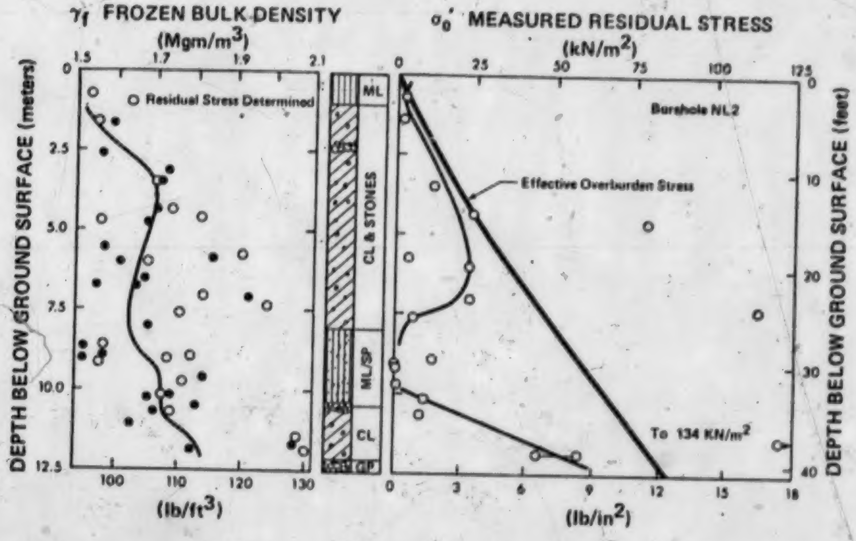

Figure 5.22 Residual stress profile, Borehole NL2

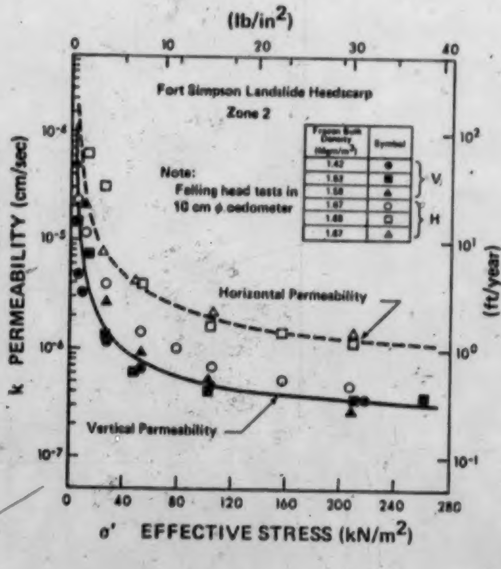

Figure 5.23 Summary of permeability test results, Zone 2, Fort Simpson landslide headscarp

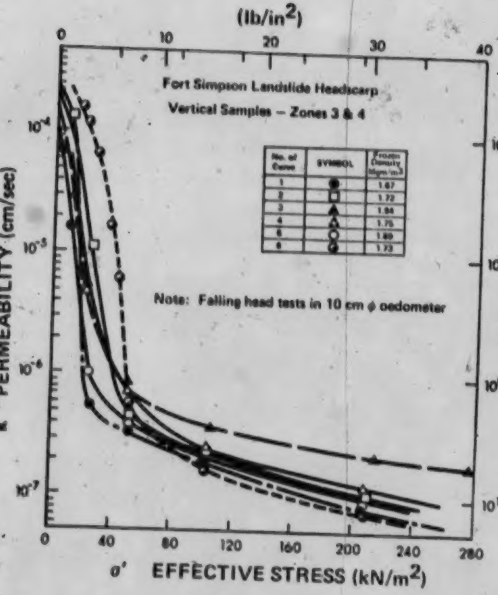

Figure 5.24 Summary of permeability test results, Zones 3 and 4, Fort Simpson landslide headscarp

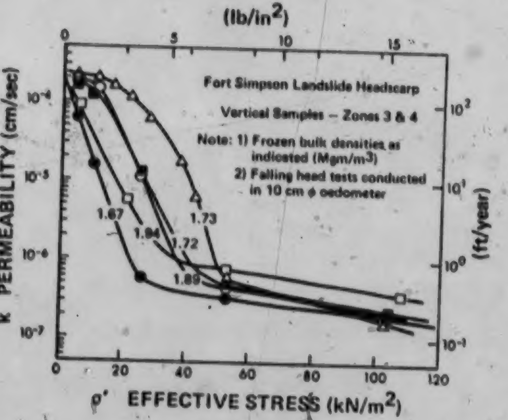

Figure 5.25 Data from Figure 5.24 replotted to show low stress portion in more detail

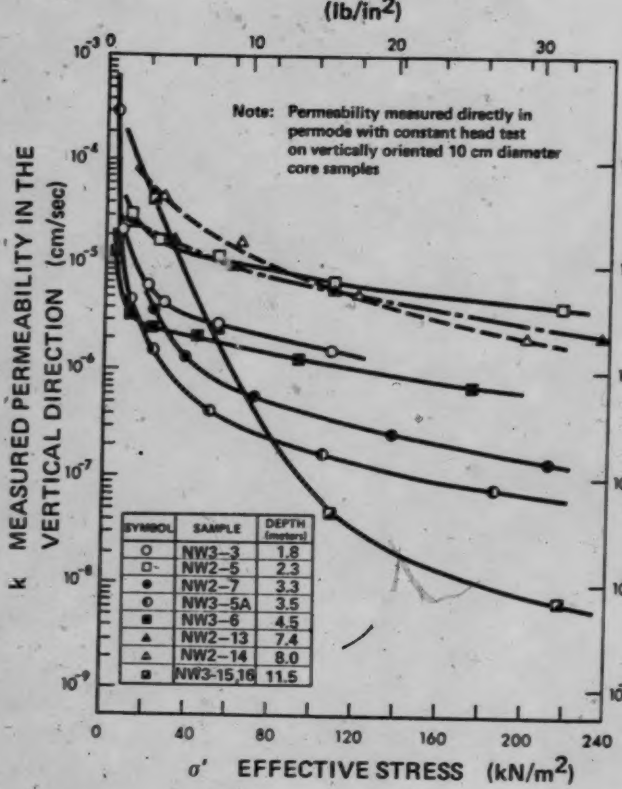

Note: Permeability measured directly in permode with constant head test on vertically oriented 10 cm diameter core samples

Figure 5.26 Summary of permeability test results, MVPL ice variability site, Norman Wells

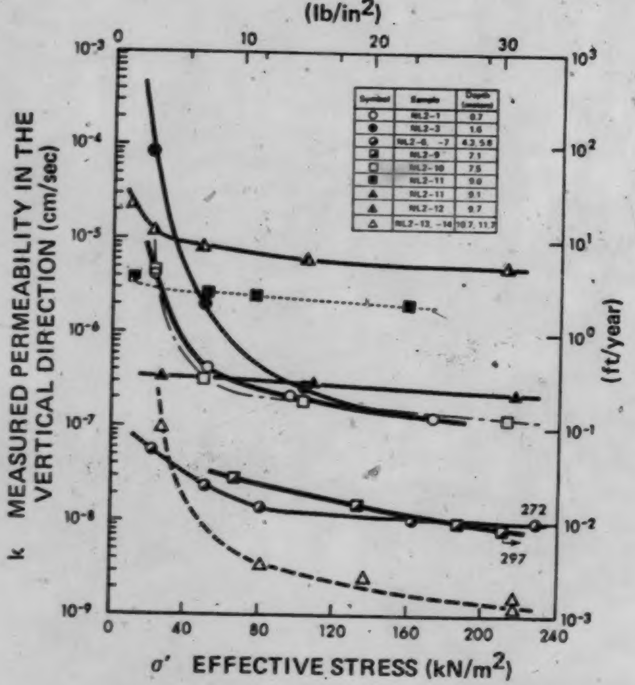

Note: Permeability measured directly in permode with constant head test on vertically oriented 10 cm diameter core samples.

Figure 5.27 Summary of permeability test results, Noell Lake site

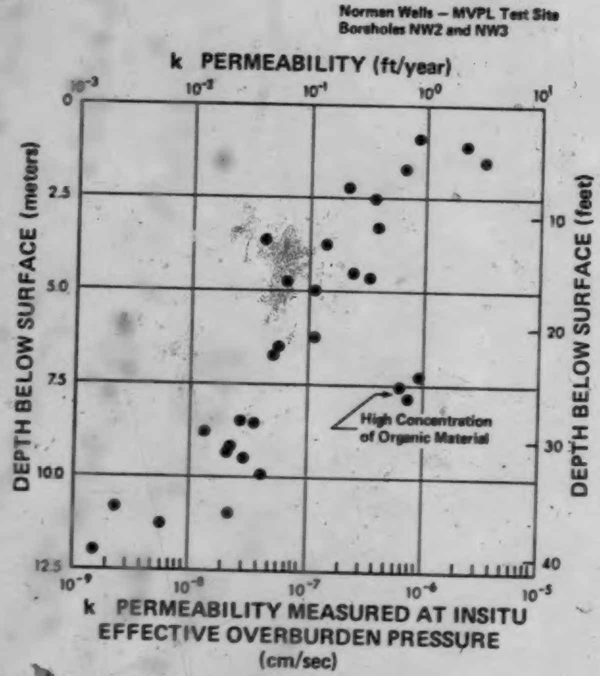

Note: Direct permeability measured by constant head test on 10 cm diameter samples consolidated to a stress equal to the insitu effective overburden pressure

Figure 5.28 Profile of permeabilities at in situ effective overburden pressure, Norman Wells site

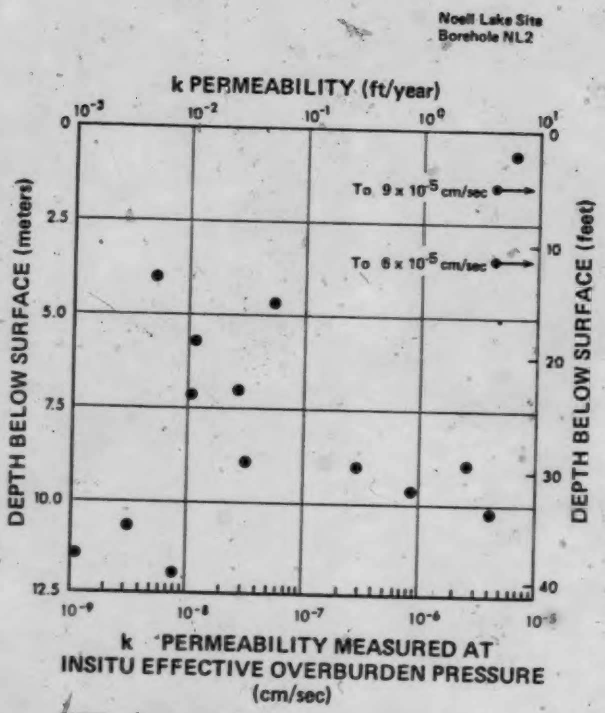

NOTE: Direct permeability measured by constant head test on 10 cm diameter samples consolidated to a stress equal to the insitu effective overburden pressure

Figure 5.29 Profile of permeabilities at in situ effective overburden pressure, Noell Lake site

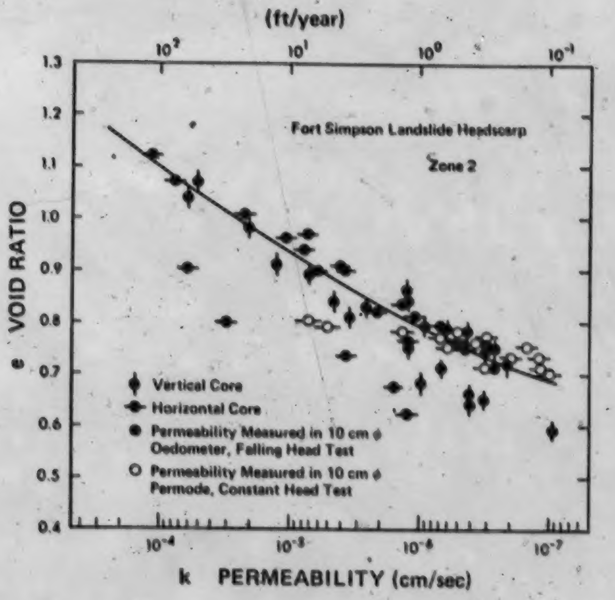

Figure 5.30 Void ratio - permeability relationship, stratified structure

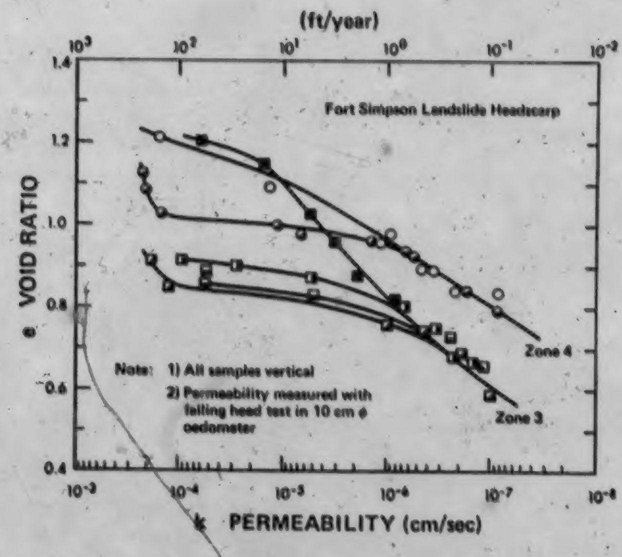

Figure 5.31 Void ratio - permeability relationship, reticulate structure

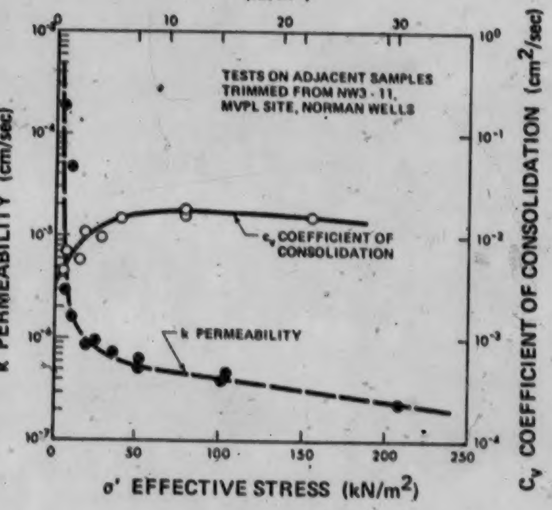

Figure 5.32 Reproducibility of test results

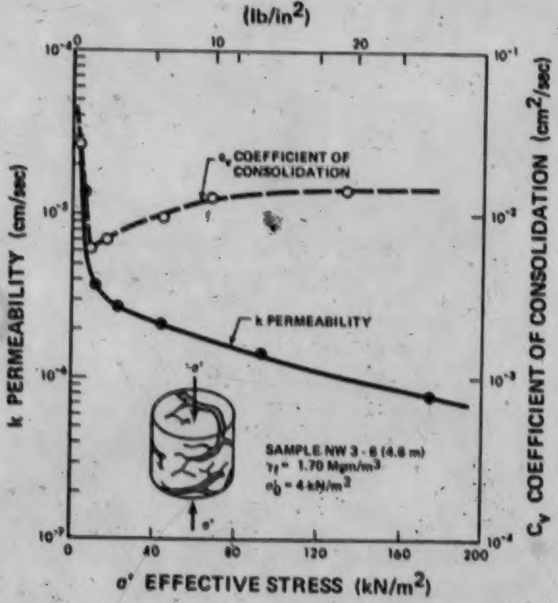

Figure 5.33 Typical relationship between consolidation coefficient and permeability

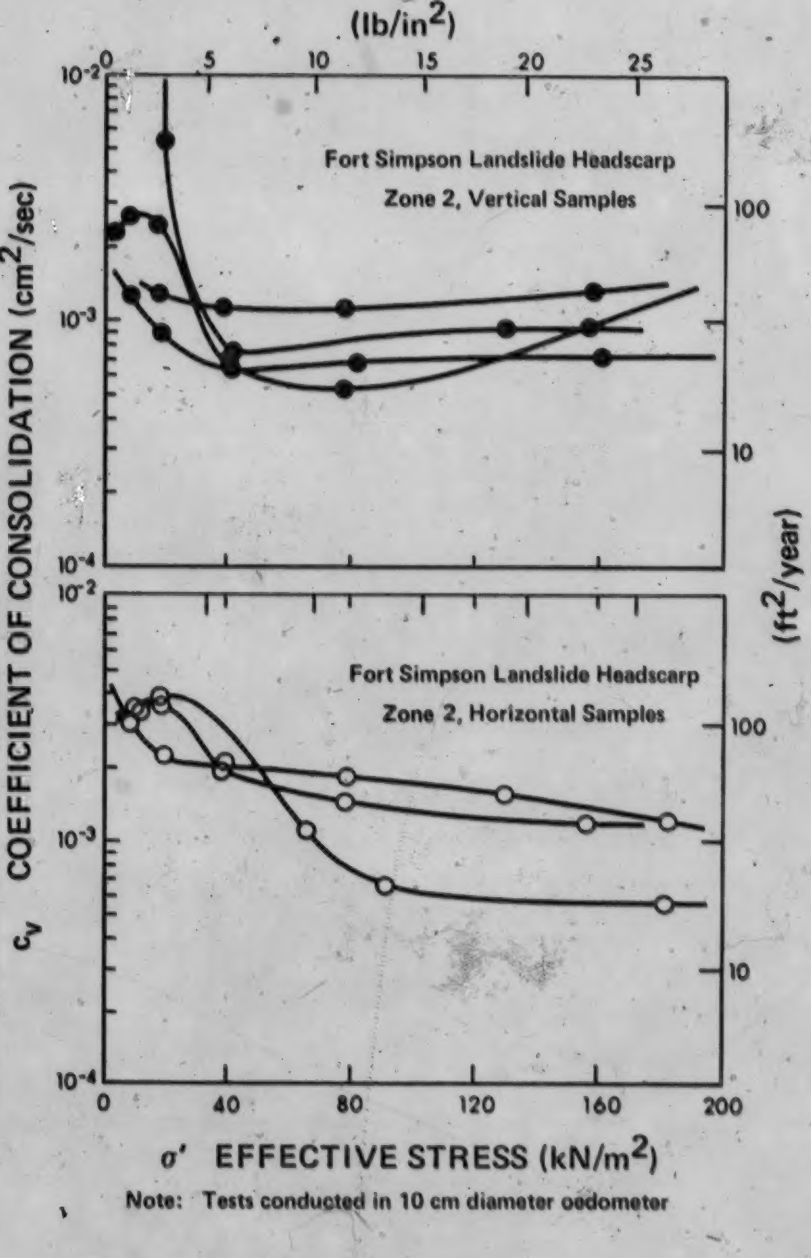

Figure 5.34 c_v versus σ', stratified structure, Zone 2, Fort Simpson landslide headscarp

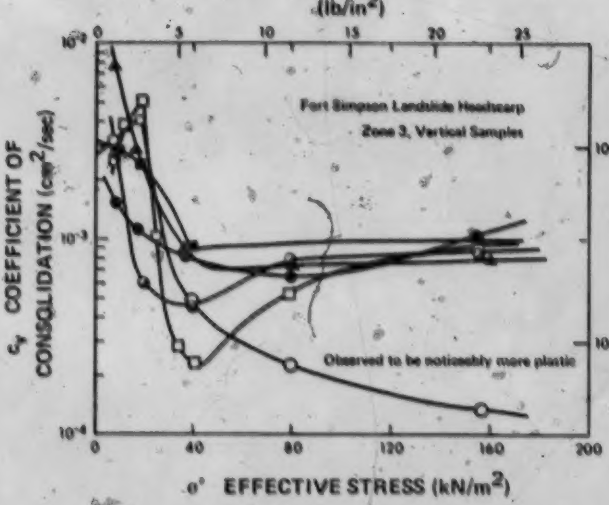

Figure 5.35 c_v versus σ', reticulate structure, Zone 3, Fort Simpson landslide headscarp

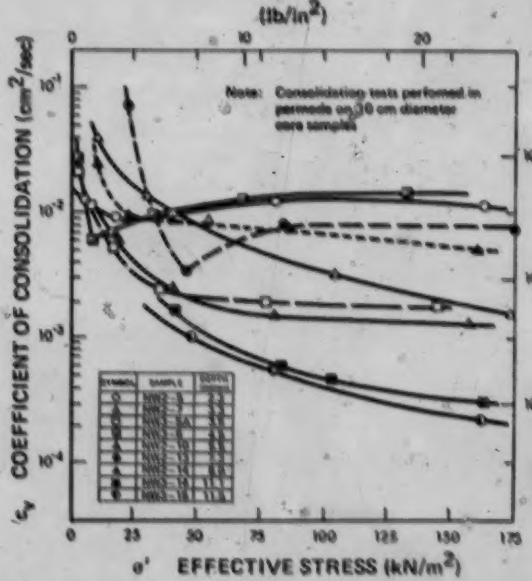

Figure 5.36 c_v versus σ', Norman Wells site

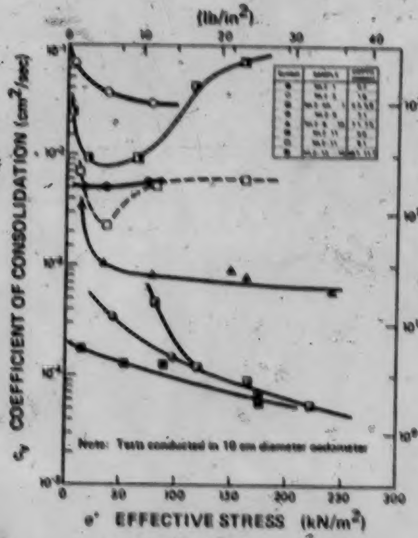

Figure 5.37 c_v versus σ', Noell Lake site

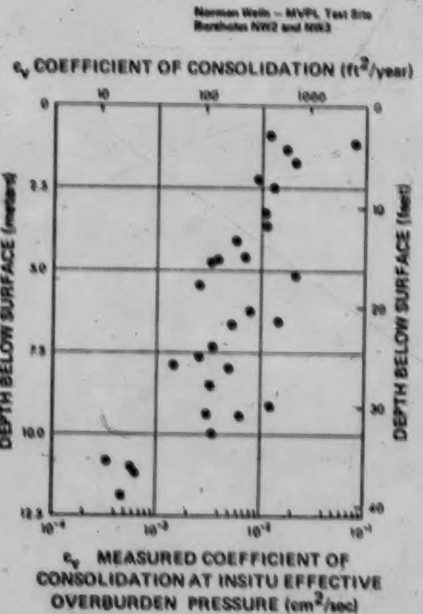

Figure 5.38 Profile of c_v at *in situ* effective overburden pressure, Norman Wells site

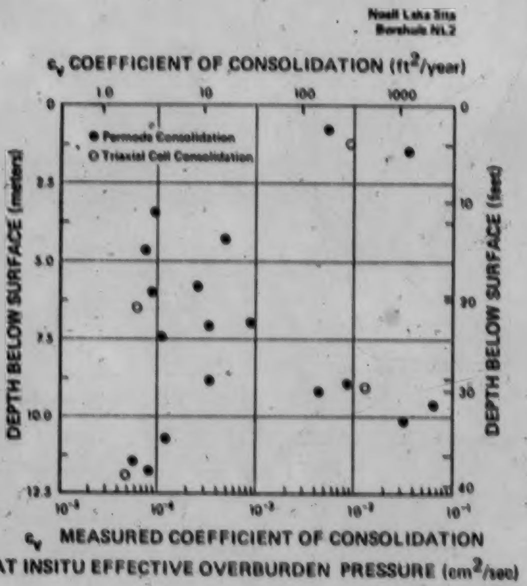

Figure 5.39 Profile of c_v at in situ effective overburden pressure, Noell Lake site

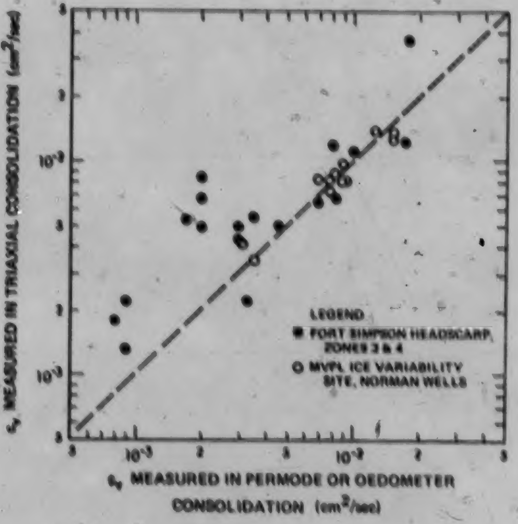

Figure 5.40 Comparison of c_v determined in permode and triaxial cell

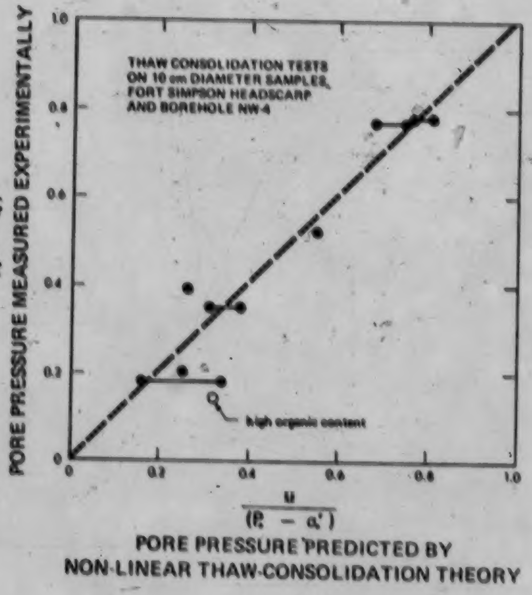

Figure 5.41 Thaw-consolidation test results for undisturbed permafrost samples

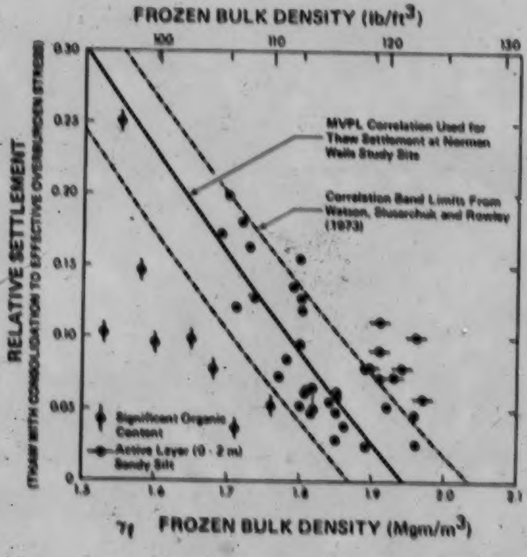

Figure 5.42 Thaw strains for undisturbed permafrost, Norman Wells site

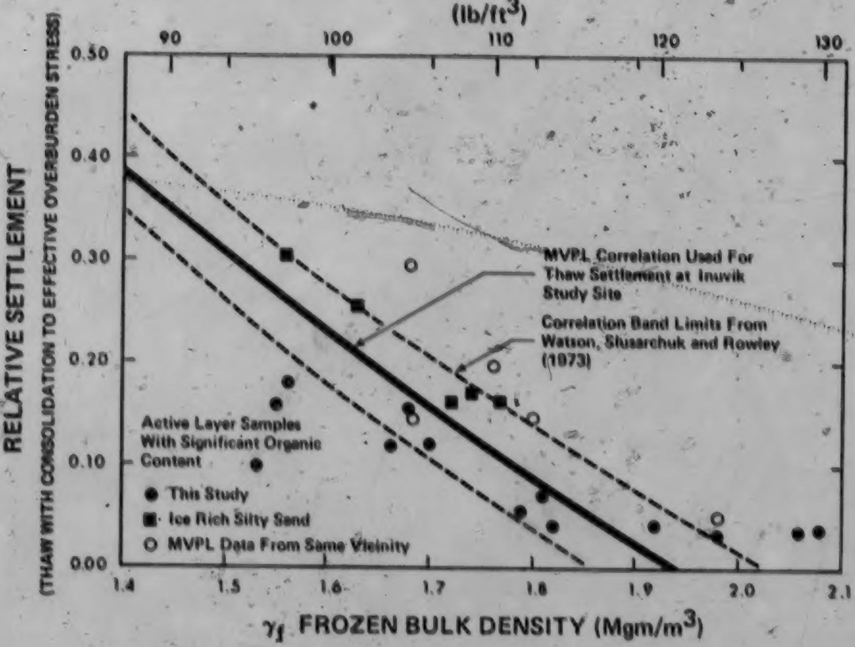

Figure 5.43 Thaw strains for undisturbed permafrost, Noell Lake site

CHAPTER VI

LABORATORY STUDIES OF SHEAR STRENGTH IN THAWING SOILS

6.1 INTRODUCTION

Research pertaining to the geotechnical properties of undisturbed permafrost upon thaw has primarily concerned itself with the determination of index properties, thaw strain behaviour, and undrained strength.[1] The few tests conducted to obtain strength data in terms of effective stress have not been reported in sufficient detail to be of fundamental value (Watson *et al.*, 1973). Since the stability of thawing soils is a current concern, gaining a clearer understanding of their shear strength behaviour would certainly be an asset. Undisturbed frozen core obtained in connection with the laboratory studies described in Chapter V provided an opportunity to investigate selected aspects of the strength-effective stress relationships for thawed permafrost soils.

Properties such as shear strength, compressibility, permeability, and the coefficient of earth pressure at rest are likely to be modified by soil freezing and thawing. The magnitude of these modifications will depend to a great extent upon the changes in soil structure effected by freeze-thaw cycling. The objectives of the study described in this chapter were:

---

[1] Most of these data consist of one-time proprietary reports compiled in the course of oil and gas pipeline feasibility studies carried out in both Canada and Alaska.

1) To examine the effect of macrostructural cryogenic features on strength in terms of effective stress in thawed, undisturbed fine-grained permafrost soils; and,

2) To evaluate the pore pressure parameters required to describe the behaviour of these same soils in undrained shear.

The principle of effective stress is fundamental to all discussions of shearing resistance in soils. The preceding chapters have referred to analyses developed for the estimation of pore pressures generated during consolidation in thawing soils. Use of the appropriate consolidation parameters permits evaluation of in situ effective stresses and hence, the maximum shearing resistance. To supplement laboratory studies of consolidation properties, isotropically consolidated undrained triaxial compression tests were carried out on numerous 10 cm (4 in) diameter specimens obtained from the Fort Simpson and Norman Wells sampling sites. Extreme textural variability encountered in the soil profile at the Noell Lake site made it apparent that analyzing shear test results from these samples might prove difficult. Since strength data specific to a particular site would contribute little or nothing to a fundamental study, detailed testing was restricted to samples from the two other sites where meaningful comparisons could be made between tests.

6.2 DESCRIPTION OF SOILS TESTED

Soil characteristics

It was necessary that frozen samples 22 to 24 cm (9 to 9.5 in) long be used to ensure a length to diameter ratio of two after thaw (and possible consolidation). Drilling in ice-rich soils invariably results in core breakage along thicker ice veins, so obtaining completely intact sections long enough for triaxial testing limited the number of suitable samples available. A hand-held motorized auger was used to drill core at the Fort Simpson site. A large quantity of core was obtained and the mechanical breakage caused by the core barrel was kept to a minimum. The headscarp was divided into four zones, largely on the basis of ground ice structure. These have been described in Section 5.5 and a more detailed account of the stratigraphy is given in Appendix A. The material from Zone 2 typically exhibited large thaw strains, so to keep testing procedure simple, shear strength studies were restricted to core from Zones 3 and 4. The drilling equipment used at the Norman Wells site caused considerably more sample breakage, but enough intact core was obtained to permit an adequate shear testing program for each of the different soil types identified. A more detailed description of sampling equipment and procedures employed is given in Appendix A.

Core taken from Zones 3 and 4 at the Fort Simpson site consisted of an essentially homogeneous dark grey silty clay that contained a regular, reticulate ice structure. The soils at the Norman Wells site were similar but more variable. The profile was made up of thickly bedded silt and clay which typically contained organic specks and peaty layers. The sediments at both sites had been deposited in glacial lakes impounded along the Mackenzie River Valley during the retreat of the last Wisconsin ice sheet. Clay contents of 40 to 70% were found with illite and kaolinite being identified as the major clay mineral species present. These soils were all classified as inactive (Skempton, 1953). A scanning electron microscope examination of microfabric revealed a closely packed turbostratic structure (Collins and McGown, 1974) with predominantly horizontal orientation of the clay between larger, silt-sized particles. The clay particles also occur as aggregates of various types, and very few discrete silt grains were observed. Most of the silt-sized particles examined actually consisted of aggregates of clay minerals. Borehole logs and a complete summary of index and classification testing data for these soils appear in Appendix A.

Representative sampling

The influence which macrostructure exerts on both the field and laboratory shear strength of fissured clays has been the subject of a considerable volume of literature (see for example: Marsland, 1972; Bishop et al., 1965). When a frozen soil containing reticulate ice lenses thaws, the structural discontinuities remaining are not unlike a system of fissures. Thawing and fissured soils possess similar secondary structures and might therefore be expected to behave in a like manner during shear. Data given in Chapter V have confirmed this hypothesis of similitude for consolidation behaviour, but the complex nature and variability of undisturbed soils make these generalizations difficult to substantiate under many circumstances.

It is difficult to obtain consistently representative samples of fissured clays, and coring ice-rich fine-grained soils is subject to the same uncertainties. A bias toward lower moisture contents and higher densities for intact core is inherent since icier sections are more susceptible to mechanical disturbance during drilling. Core segments used in the triaxial testing program had frozen bulk densities ranging from 1.8 to 2.0 Mgm/m^3 with corresponding water contents of 30 to 40%. Peaty inclusions in the Norman Wells samples introduced additional variability, making density data from that site more difficult to correlate with other properties. Visible organic material was totally absent in core obtained from Zones 3 and 4 at the Fort Simpson site.

Both the soil and ground ice structure for each of the Zones in the Fort Simpson landslide headscarp appeared to be quite uniform. This exposed section afforded an opportunity to assess the intrinsic heterogeneity of typical permafrost soils by performing frequency analyses of measured frozen bulk densities (γ_f) and water contents (w). In natural soils like these, density and water content in situ should have been controlled by essentially random processes. Variability may be large or small depending upon the relative influences of steady and transient effects during sediment deposition and subsequent permafrost aggradation. Even so, it can be reasonably supposed that the core sampled randomly from the headscarp constitutes a normal population. The basis for dividing the headscarp into four zones was described in Section 5.5. It has also been assumed that samples taken from each of the zones can be treated as independent populations. Although the zonation boundaries were transitional rather than being sharp contacts, both w and γ_f should still be expected to exhibit normal distributions about their means within each Zone.

For the purposes of statistical analysis, data for samples from Zones 3 and 4 were grouped together since the cores could not be distinguished from each other once the thick, icy layers had been removed from the latter. Figure 6.1 shows the frequency distributions of γ_f and w and the results of the analyses are summarized in Table 6.1. The 72 pieces of core included in this study had volumes of 300 to 2300 cm^3 and masses which ranged from 500 to 3700 gm. The distributions are Gaussian, and it is apparent that both the density and water content relationships are skewed-normal. This asymmetry reflects sampling bias associated with firstly, ice exclusion by mechanical damage to thick lenses and icy sections during drilling; and secondly, the removal of larger ice bodies from samples being prepared for testing. This practice has little or no bearing on the shear strength test results, but it does tend to indicate higher densities and lower water contents than are probably representative of _in situ_ conditions. Thicker ice lenses were usually trimmed out prior to shear or consolidation testing, since their presence during thaw would only make the tests more difficult to perform. Ice lenses were spaced more closely in the stratified structure typically found in Zone 2, but a frequency analysis of data from those samples yielded similarly skewed distributions. It would seem that without exercising a great deal of care, conventional sampling techniques are probably seldom capable of obtaining continuous and accurate profiles of γ_f and w _in situ_. A detailed description of the potential use of specialized downhole logging tools to obtain continuous profiles and assist in overcoming this difficulty appears in Appendix A.

Macrofabric

It is unlikely that the clays at either sampling site had been previously subjected to an overburden pressure much greater than that existing at the time of sampling. However, effective stress changes occurring during freezing are known to produce behaviour similar to that which is considered characteristic for overconsolidated soils. A detailed discussion of the stress path followed by a soil during a freeze-thaw cycle has been given in Section 4.3. It was shown that primary soil fabric can be mechanically disturbed by the formation of fissures associated with ice lenses and the subsequent remoulding of adjacent soil as excess water becomes available from the melting of nearby segregated ice. When fine-grained soils with reticulate ice veins thaw, the clay blocks usually remain intact. If sufficient quantities of water are present as discrete ice lenses, thaw produces a fabric consisting of stiff lumps in a matrix of softer clay. The remoulded appearance of the soil adjacent to secondary structural features is similar to the weathering produced by seasonal water content changes in fissured clays described by Brewer (1964). Chandler (1972) has described a similar macrostructure in the Lias clay consisting of small 'stratified' lumps or lithorelicts which have been rotated so that intact bedding features contained therein assume various attitudes in a softer matrix. He suggests that since this disturbance extends to considerable depths, the formation and melting of ground ice lenses may have produced this fabric at the time that permafrost conditions prevailed during the Pleistocene. Moisture content differences of as much as 10 percent were observed between the matrix and blocks of soil from Zone 3 specimens thawed undrained under low stresses.

Density - water content relationships

If it can be assumed that all of the water present in a frozen soil is in the form of ice, the relationship between bulk density (γ_f) and water content (w) in a saturated soil is given by:

$$\gamma_f = \frac{G_s\gamma_w\ (1 + 1.09w)}{(1 + 1.09G_s w)} \tag{6.1}$$

Similarly, if the soil is unsaturated:

$$\gamma_f = \frac{G_s\gamma_w\ (1 + \frac{1.09}{S}\,w)}{(1 + \frac{1.09G}{S}\,w)} \tag{6.2}$$

where S denotes the degree of saturation.

Equations 6.1 and 6.2 ignore the fact that some water commonly exists in the liquid phase in the fine-grained soils at temperatures as cold as several degrees below 0°C (Anderson and Tice, 1972). Furthermore, these equations assume that freezing or thawing is accompanied by an increase or decrease in overall volume which corresponds to that produced by the phase change of water in the soil. If the pores remain filled with either ice or water in the saturated case, the presence of unfrozen water instead of ice will have the effect of increasing the bulk density measured for the frozen soil.

If the soil skeleton is sufficiently rigid, water movement toward discrete ice lenses may not be fully accommodated by volumetric strain. This local moisture depletion is not necessarily accompanied by an equal pore volume decrease, so that the net result can be desaturation. Ice formation drives air out of solution, and in addition to gases produced by the in situ decomposition of organic material, this causes the gas bubbles which are often observed in ice lenses. The rotation and vibration of core barrels during sampling can initiate cracking or bulking within the lenses, effectively reducing the unit weight of the ice. Even on carefully machined cores, volumetric determination from the measurement of external dimensions can lead to errors which usually result in calculated densities which are slightly less than actual values. Total immersion or fluid displacement techniques would have been preferred for volumetric measurements, but were purposely not adopted in this study so that sample contamination could be avoided. The possibility of small dimensioning errors was also recognized, but no attempt was made to apply corrections to the measured densities.

The factors indicated above all tend to artificially diminish the frozen bulk density that would be observed for a given soil water content. In Figure 6.2, densities and water contents are plotted for 72 samples from Zones 3 and 4 at the Fort Simpson site. Lines based on equations 6.1 and 6.2 have been superimposed to show the effects which variations in the degree of saturation and G_s have on computed densities. Most of the data points fall within a saturation limit of 90 to 100% and specific gravities of 2.72 ±0.02. These curves suggest that many of the samples tested were unsaturated in the frozen state. Moisture-density data for soils from all the sampling sites have been presented in a similar manner in Appendix A.

6.3 TESTING EQUIPMENT AND PROCEDURE

Description of the apparatus

The four standard triaxial cells used in this study were capable of accommodating 10 cm (4 in) diameter samples (see Bishop and Henkel, 1962, for mechanical details of cell construction). Several modifications were required to render the cells suitable for use in the sub-freezing environment that was required for test setup. For example, the cold can cause the brass bushings to shrink tightly onto the load ram. This immobility would then result in considerable difficulty in the setup procedure. To remedy this specific problem, the honed brass bushings were replaced with Thomson linear ball-bushings and an oil seal. It was then necessary to replace the standard ram with case-hardened steel to prevent scoring which would have otherwise been caused by the balls in the Thomson bushing. Valves and connections were converted to 0.3 cm (1/8 in.) Whitey zero volume change ball-valves (Teflon seats) with Swagelok fittings. The pore water pressure transducer block used was similar to the one shown on the permode base in Figure 5.5. An auxiliary drainage line was added so that the porous stone beneath the load cap could be flushed.

The layout of a typical triaxial cell and associated equipment used in the strength tests is shown in Figure 6.3. Constant cell pressures and backpressures were maintained by regulating air pressure over water in reservoirs. These pressures were monitored and coarsely adjusted by observing the Bourdon gauge; a pressure transducer was used to make more accurate measurements. Water expelled during consolidation was measured with a 100 cm^3 volume change indicator. Plumbing was designed to permit a flow reversal so that volume changes exceeding the basic burette capacity could still be monitored. Occasionally, extremely large volume changes occurred during initial consolidation stages, and these were measured by simply directing the draining fluid into a graduated cylinder. Whitey ball-valves and Swagelok fittings were used exclusively throughout the plumbing system. Compressive loads were applied to the sample with a 100 kN (10 T) capacity, constant displacement rate, gear-driven Wykeham-Farrance press.

A linearly variable displacement transducer (LVDT) was clamped to the load ram to measure axial deformations. These displacement measurements were accurate to better than 0.001 cm (0.0005 in). A 10 kN (2000 lbf) capacity shear web load cell (resistance strain gauged) with a resolution of approximately 5N (1 lbf) was used to measure axial compressive loads. The load cell was attached directly to the reaction frame, although placement within the triaxial cell would have been preferred. Electrical strain-gauged diaphragm pressure transducers were used to measure cell pressures, backpressures, and soil pore water pressures. Ranges of 0 to 700 kN/m^2 (0-100 psi) and 0 to 200 kN/m^2 (0-30 psi) were used with resolutions of 0.25 kN/m^2 (0.04 psi) and 0.15 kN/m^2 (0.02 psi) respectively. LVDT, load cell, and pressure transducer signals were conveyed to a data acquisition system where displacements, loads and pore pressures were recorded at predetermined time intervals.

Sample preparation and setup

All of the tests described were conducted on undisturbed samples which had been obtained with a CRREL-type auger core barrel. Either a circular-bladed rock saw or a power band saw were used to cut the intact core into appropriate lengths. Sample diameters were turned to 10 cm (4 in.) on a small soil lathe. While the sample was still held in the lathe, a slotted filter drain (Watman 54 paper) was attached by applying water to the outside of the core with an atomizer. Cold ambient air temperatures froze the fine spray immediately and ice held the side drain in place. The external dimensions and mass of the specimen were measured and recorded prior to commencing the test setup.

The triaxial cell and saturated porous stones were allowed to cool in the sample preparation room for one to two hours. The setup procedure was begun by forcing fluid (ethylene glycol 20% aqueous solution) through the various cell base valves to deair the drainage and pore pressure measurement systems. With a porous stone in place on the pedestal, more fluid was permitted to flow in and form a meniscus. A saturated filter paper was then laid on the stone, and after excess fluid had been wiped away, the soil sample was set in place. This procedure was duplicated during placement of the load cap, upper porous stone, and filter paper. Care was taken to ensure that the ends of the side drains contacted both porous stones. A special stretching cylinder was used to place a latex rubber membrane (0.03 cm thick) around the sample. If a lengthy test duration or several consolidation stages were anticipated, a second membrane was added as a precautionary measure. The membrane was stroked against the core in an upward direction to remove any air that had been trapped. Neoprene 'o' rings were then rolled off of the membrane stretcher, first onto the pedestal and then onto the load cap. Two rings were used at each end to ensure a watertight seal. The top drainage lines were flushed to deair them before final connections were made to the load cap.

Once the necessary internal connections were completed, the upper cell section was lowered into position and clamped down with tie bolts. A nominal air pressure of approximately 100 kN/m^2 (15 psi) was applied inside the cell so that fluid could be circulated through the porous stones and drainage lines. This completely deaired the assembled test and also provided an opportunity to detect leaks while corrective measures were still possible. Excess fluid was drained away before closing the valves and venting off the cell air pressure. The load ram was then lowered into contact with the load cap so its protruding height could be measured and recorded. This would later enable evaluation of sample length changes occurring during thaw and subsequent consolidation stages. With setup complete, the sample and triaxial cell were ready to be moved into a warmer room for thaw, consolidation, and compression. For reasons explained in Section 5.4, a plug was used in lieu of the pressure transducer while the cell was in the cold room.

Testing procedure

Triaxial specimens were thawed under an all-around pressure by filling the cell with water. The apparatus was usually left until the following day to ensure that equilibrium conditions had been obtained. By applying the cell pressure through a burette, it was possible to measure undrained volume changes during thaw. At this point in the test, the pore pressure transducer was installed in the cell base and deaired by flushing water through the cavity. A pore pressure reaction test was then performed by measuring response to the application of increments of cell pressure. This permitted simultaneous determination of the residual stress and the pore pressure parameter B (Skempton, 1954). The same method was employed for residual stress tests on short samples as a triaxial alternate to the procedure normally employed with the permode. Residual stress was defined in this test by extrapolating the pore pressure response curve to a cell pressure corresponding to zero pore pressure. Prior to commencing either unconsolidated undrained (UU) shear or isotropic consolidation, the confining stress was set at some value exceeding the measured residual stress.

Drainage was not permitted during the UU-test so axial compression determined the undrained shear strength. Cell pressures exceeding σ_o' were applied to induce positive pore pressures prior to commencing shear. This resulted in a stress axis translation so that reductions in pore pressure occurring during shear could be measured without having to determine negative values. Pore pressures were monitored for some time prior to shear to be sure that equilibrium conditions had been established.

The load cell output was initialized for zero deviatoric stress with the cell pressure holding the load ram up against it. Contact with the sample was made by turning the load platen up by hand. Initial LVDT readings were taken before engaging the gear drive, then axial compression was commenced at a predetermined displacement rate. At set time intervals throughout the test, simultaneous measurements of axial strain, compressive load and pore pressure were recorded by a Hewlett-Packard data acquisition system.

To obtain shear strengths at effective stresses exceeding the residual stress, samples were stage-consolidated isotropically. Quantities of water expelled during thaw were measured in a graduated cylinder. For subsequent consolidation stages with smaller volume changes, a more precise burette indicator was used. Once the desired effective stress had been obtained, any air bubbles which had become entrapped were eliminated by flushing water through the drainage and pore pressure measurement systems. The transducer was zeroed to atmospheric pressure, then residual pore water pressures remaining after consolidation were determined. A confining pressure increment was applied to check the value of the B parameter prior to shear and to induce positive pore pressures in the sample for reasons which were explained previously. This increase in pore pressure also served to dissolve some of the gas remaining in the sample while approximating conditions of stress increase that might be encountered under field loading conditions. From this point onward, the procedure adopted for conducting an isotropically consolidated undrained shear test was identical to that described for the UU-test.

Strain rates used in each test were determined from the consolidation properties of the particular soil being tested. Interpretation of consolidation data from tests employing side drains requires special consideration of the relative permeabilities of the drains and soil (Bishop and Gibson, 1963). Head losses in the filter strips can cause errors which will be negligible only for clays with very low permeabilities. Further complications are related to the lack of continuity of slotted side drains, but in any case, their presence certainly accelerates the equalization of excess pore pressures during undrained shear. In Section 5.7, it was shown that the Fort Simpson and Norman Wells soils exhibited large permeabilities at stresses less than about 50 kN/m^2 (7 psi). Even after the effective stress had been increased, values of less than 10^{-7} cm/s were seldom encountered. Many soil permeabilities were as high as values published for the filter strips used as side drains (Bishop and Gibson, 1963), so it was apparent that in these cases, the drains would be completely ineffective. Consolidation coefficients were computed by assuming that drainage occurred only toward the ends of the sample. Figure 5.40 indicates that c_v's determined in this manner were in general agreement with those obtained from consolidation tests conducted in the permode. Decreases in soil permeability produce an increase in the effectiveness of the side drains. If it were possible to include a correction for the effect of side drains, computed c_v values would tend to be lower than those which were computed assuming no radial drainage. The general agreement between consolidation coefficients obtained in the permode and the triaxial cell indicates that in triaxial consolidation with side drains, soil permeability was sufficiently high that almost all of the sample drainage occurred one-dimensionally toward the ends.

To avoid potential ambiguity in determining appropriate times to failure (Bishop and Henkel, 1962), c_v's used in the calculations were obtained from permode tests on similar material at the appropriate effective stress level. Axial deformation rates of 8×10^{-4} cm/min (3×10^{-4} in./min) were adopted to shear all of the Fort Simpson samples and the more plastic soils from the Norman Wells site. Faster rates were used to test the siltier, near-surface soils from the latter site. These strain rates were sufficiently slow to ensure that at least 95% equalization of the pore pressures or suctions developed during shear had been obtained. Requirements for fully drained testing were satisfied so that, even if assumed c_v values were in error, it is highly probable that pore pressures measured in the undrained tests were correct.

Several tests performed at low confining pressures were stopped at an axial strain of approximately 10%. The sample was then consolidated to a higher effective stress prior to resuming shear. This technique was adopted to increase the amount of strength data obtained for the Norman Wells site since there was a limited number of useable samples.

At the completion of shearing, all valves were closed before reducing the confining pressure and draining the cell. The apparatus was dismantled and a bulk moisture content obtained by removing a full length slice, 2 to 3 cm (1 in.) thick, from the center of the sample. Wherever possible, a moisture content was also determined for material trimmed from the shear plane.

Test results were tabulated and reduced with a simple Fortran program that was also capable of producing graphical presentations of the test data on a computer-controlled Calcomp bed plotter. Calculated deviatoric stresses were based on the average cross-sectional area obtained from measurements of axial strain and sample volume changes prior to shear. In some instances, failure involved the relative displacement of several separate lumps, resulting in an irregular cross-section. No suitable means was found to evaluate deviatoric stress in these cases, so the usual method of area correction was retained. Failure criteria based on both the maximum deviatoric stress and the maximum principal effective stress ratio were considered.

6.4 ROLE OF PORE WATER PRESSURES

Pore pressure response

In describing the role of the principle of effective stress in soil mechanics, Terzaghi (1936) stated that:

> "all the measureable effects of a change in stress such as compression, distortion and a change of shearing resistance are exclusively due to changes in the effective stresses".

Pore water pressures must be known to define effective stresses accurately, and hence, soil behaviour in general. Skempton (1954) has described the undrained pore pressure change (Δu) occurring due to changes in the principal stresses $\Delta\sigma_1$ and $\Delta\sigma_3$, with the equation:

$$\Delta u = B[\Delta\sigma_3 + A(\Delta\sigma_1 - \Delta\sigma_3)] \qquad (6.3)$$

where A and B are pore pressure coefficients.

B defines the ratio of pore pressure changes in response to an increment in the all-around stress, $\Delta\sigma_3$. The changes in pore pressure resulting from application of deviator stress are similarly given by the parameter A. It has been suggested (Skempton, 1954) that the pore pressure ratio $\bar{B}$ can be used to estimate pore pressure changes generated by an increase in the major principal stress, especially where this stress can be approximated by the overburden pressure. Equation 6.3 is rearranged to give:

$$\bar{B} = \frac{\Delta u}{\Delta\sigma_1} = B\left[1 - (1-A)\left(1 - \frac{\Delta\sigma_3}{\Delta\sigma_1}\right)\right] \qquad (6.4)$$

Bishop (1954) has rewritten Equation 6.4 as:

$$\bar{B} = B\left[\frac{1 - (1-A)\;(1-K)}{1 - B(1-A)\,(1-K)}\right] \qquad (6.5)$$

where K is the ratio of principal effective stresses $\Delta\sigma_3' / \Delta\sigma_1'$. This indicates that $\bar{B}$ will be a function of the principal effective stress ratio and additional complexity is introduced by the dependence of the A parameter on the same ratio.

Under normal conditions, B will equal one if the soil is fully saturated. In this case, Equation 6.5 indicates that B and $\bar{B}$ should be equal, regardless of values for A or K. Theoretical and experimental studies (Lee _et al_., 1969; Wissa, 1969) have shown that B values of less than one can be obtained under certain circumstances, even though the soil is fully saturated. It is improbable that the stiff structure necessary for this sort of response might be encountered in thawing permafrost soils. Differences would normally be anticipated between B values measured in a triaxial cell and $\bar{B}$ values measured in a permode if the soil were not fully saturated.

B and $\bar{B}$ parameters

In Figures 6.4 and 6.5, values for B and $\bar{B}$ are plotted agiast frozen bulk density for samples from the Norman Wells and Noell Lake sites. These pore pressure reaction tests were performed on thawed samples either during the evaluation of residual stress, or prior to triaxial testing. Aside from a few samples containing large amounts of organic material, the rest follow a clear trend. For the Norman Wells site (Figure 6.4), samples with frozen bulk densities of less than 1.8 Mg/m^3 consistently exhibit responses in the range of 0.9 to 1.0, indicating nearly full saturation. As densities increase, however, a great deal of scatter develops with responses on some samples dropping as low as 0.4. A similar relationship is illustrated in Figure 6.5 for the Noell Lake samples, although the behavioural transition occurs at a slightly lower density.

Specific measured values in each case are of less interest than the trends. In Figure 6.4, several B values (triaxial) fall as low as 0.5 so it would seem that the lower $\bar{B}$ values (permode) cannot be entirely attributed to pore pressure response being diminished by side friction. The wide scatter in the data is probably related to structural differences between samples which have similar densities. Even though their average degree of saturation may be less than one, samples with thicker ice lenses will often have higher values of B and $\bar{B}$, since pore pressure response will be dominated by softened soil in the cryogenic structure. In more massive samples, measured response will reflect the lower average degrees of saturation which apparently accompany higher densities.

Figure 6.6 shows the results of pore pressure reaction tests in profile for the Norman Wells site. There is not much scatter at depths of less than 5 m, but as peaty layers become more numerous in the 5 to 8 m interval, large variations in the measured values of B and $\bar{B}$ are observed. Below the 8 m depth, there are apparently no organic inclusions and high densities are typical. Reticulate structure in these dense soils is responsible for the variability indicated in pore pressure response characteristics. Under these circumstances, it is difficult to anticipate in situ response from the extrapolation of laboratory results to field scale. The importance of recognizing these limitations in practice can only be assessed by observing pore pressures under controlled circumstances in the field.

The considerable influence which cryogenic structure has on pore pressure response during thaw is illustrated in Figure 6.7. The B parameter was determined for each of these samples immediately following undrained thaw. Each was then allowed to drain and consolidate by increments to successively higher effective stresses. A pore pressure reaction test was performed at the end of each consolidation stage and the results obtained confirm the behaviour anticipated for thawed soils possessing a distinct cryogenic macrostructure. At low effective stresses, the high pore pressure response measured is due to the presence of soft, saturated soil along the ice-lens fissures. As effective stresses are increased, this softened soil consolidates and measured pore pressure response decreases to approach that of the overconsolidated and usually desaturated lumps which the fissures surround. The two samples tested in this case had similar frozen bulk densities and displayed B values which diminished from greater than 0.9 to less than 0.7 as the consolidation stresses were increased to 250 kN/m^2 (35 psi). These results confirm the suggestion that some of the data scatter which is apparent in the three previous figures can be attributed to inherent differences in structure existing between particular samples. Obvious difficulties remain in selecting representative samples for testing when the results will be used to predict in situ behaviour.

A parameter

Consolidation and swelling occur simultaneously in soil samples during undrained thaw. Specimens thawed in a triaxial cell under an equal all-round pressure will follow a different stress path than those thawed in a permode under conditions of zero lateral yield, even though no drainage is permitted in either case. Departures in the pore pressure response characteristics of otherwise similar samples are a consequence of the different stress paths followed during thaw. The applied stress ratio (K) is different in each case and aside from its direct effect on $\bar{B}$, the A parameter will also reflect differences in consolidation stress conditions (Simons, 1960; Henkel and Sowa, 1963).

In Figures 6.8 and 6.9, the pore pressure parameter A shows a dependence upon effective stress, and hence, upon the response of the secondary structure to the application of deviatoric stress. Under small stresses, shear results in a strong tendency for dilatancy as sliding along the boundaries of intact lumps of soil leads to failure along pre-existing discontinuities. Dilation occurring in an undrained test generates a reduction in pore water pressure. These suctions are reflected in the low or negative values found for A at effective confining pressures of 50 kN/m^2 (7 psi) or less. Permeability data discussed in Section 5.7 suggest that this corresponds approximately to the stress required to produce closure of the secondary structure. By increasing average effective stresses, the lumps become more tightly interlocked and resist any tendency to dilate during shear. At elevated stresses, failure planes develop primarily through intact soil. As effective stresses are increased, the A parameter falls between 0.2 to 0.4 and is in good agreement with typical magnitudes reported for lightly overconsolidated clays (Skempton and Bjerrum, 1957).

The values given for the A parameter in Figures 6.8 and 6.9 should not be construed as an accurate representation of pore pressure response to the application of shearing stresses _in situ_. These data are subject to the same criticisms that have been directed toward the application in practice of A values obtained from conventional (σ_3 = constant) displacement-controlled triaxial shear tests on isotropically consolidated samples. However, the variation in A indicated in these tests does serve to demonstrate the role played by cryogenic structure in pore pressure response to shear for thawing soils.

6.5 TRIAXIAL SHEAR STRENGTH TESTS ON UNDISTURBED PERMAFROST

Typical test results

Undrained tests with measurements of pore pressure have been carried out on thawed, isotropically consolidated samples of undisturbed fine-grained permafrost soils. To minimize ambiguity in interpreting the results, only samples with B values exceeding 0.95 were deemed acceptable for interpreting effective shear strength parameters. Appendix C contains a complete summary of the results obtained with tests on soils from the Fort Simpson, Norman Wells, and Noell Lake sites. These strengths have been determined on the basis of both the maximum deviatoric stress and maximum principal effective stress ratio failure criteria.

Typical relationships between deviatoric stress, obliquity, pore water pressure (as inferred by the A parameter), and strain, are illustrated in Figure 6.10. These particular results were obtained from consolidated undrained tests performed on samples taken from Zones 3 and 4 at the Fort Simpson landslide headscarp. At low effective stresses, it can be seen that the deviatoric stress climbed slowly to a value that remained nearly constant, even after peak strength had been reached.

Obliquity is seen to peak early in each test, but larger strains are apparently required to mobilize maximum deviatoric stresses. This stress-strain behaviour is typical of shear through the soft matrix which surrounds the harder, intact lumps of clay.

At medium and high stress levels, the lumps tend to become more tightly interlocked and the deviatoric stress peaks at a much lower strain. A distinct peak is suggested in Figure 6.10(d), characteristic of behaviour usually associated with overconsolidated clays. The peak stress ratios consistently occur early in each test at axial strains of 2 or 3%. Deviatoric stress maxima are obtained at axial strains that decrease with increasing effective confining pressure. In these undrained tests, pore pressures initially increased then decreased rapidly to approach an essentially constant value at larger strains. In many cases, these pore pressures were still decreasing slightly when maximum deviator stress was reached.

A single major shear plane was observed in most of the samples but smaller shears were also common. Slickensides were frequently found well away from the main shear plane. These usually occupied discontinuities associated with ice lenses, suggesting that shear features may be produced during thaw and consolidation by relative movement occurring between lumps.

Stress paths in consolidated-undrained tests

Figure 6.11 gives some typical stress paths showing the relationship between $(\sigma_1' - \sigma_3')/2$ and $(\sigma_1' + \sigma_3')/2$ during undrained shear. In the low stress range, stress paths rise from the isotropic consolidation pressure to meet the failure envelope at a point corresponding to the maximum effective stress ratio (open circles), then follow along the envelope until failure is reached at peak deviatoric stress (closed circles). At higher consolidation pressures, the stress paths assume a shape characteristic of soils which have been subjected to some preload or overconsolidation. These stress paths invariably depart from the failure envelope once peak deviator stress has been reached. Numbers appearing beside each of the curves identify the corresponding Fort Simpson test series numbers.

An interesting example of the influence which secondary structure may exert during compression is illustrated in Figure 6.12. Shear movement initially occurred along a discontinuity that had previously been occupied by a 4 to 6 mm (1/4 in.) thick ice lens. The stress path rose to the failure envelope as slip proceeded along this primary shear plane. Once the stress ratio had peaked, the stress path fell away slightly, and with continued axial strain, a second shear plane formed to intersect the first almost orthogonally. Although portions of the second shear plane followed cryogenic fissures, most of it passed through intact soil. Once again, the stress path rose to touch the envelope then fell away rapidly. Since each of the points along the curve represents approximately one percent of axial strain, it can be seen that small deformations produce large increases in stress in the early portions of these undrained compression tests. The slow deformation rates employed ensured that pore pressures measured at the base of the sample accurately reflected those acting in the shear zone.

Shear strength envelopes

Maxima for either the deviatoric stress or the principal effective stress ratio are usually adopted as failure criteria in triaxial testing. In undrained shear, these criteria are rarely coincident. Figures 6.13 and 6.14 show shear strength envelopes for the Fort Simpson Zone 3 and 4 material obtained by adopting, respectively, each of the failure criteria mentioned above. The most significant feature of these envelopes is their change in slope as the mean stress is increased. The curves are quite similar although the $(\sigma_1' - \sigma_3')$ peak failure criterion does yield a slightly lower ultimate ϕ' value. For all practical purposes, the curved failure envelopes pass through the origin and suggest a geometric cohesive intercept (c') equal to zero.

The same data is shown again in Figure 6.15 where the sample source and core orientation have been indicated. The curves in this figure are based on failure at peak deviatoric stress. For small normal effective stresses, ϕ' equals 28° to 32° and decreases to 23° or 24° at effective stresses of 300 kN/m^2 (40 psi). This same sort of failure envelope curvature has been reported for other clayey soils possessing blocky structure (Bishop et al., 1965; Marsland, 1972; Mitchell, 1975). In the pressure range examined, there appear to be no marked differences between the effective strength parameters obtained for vertical and horizontal samples. The scatter in the data was sufficient to obscure any clear indication of anisotropy.

Tests conducted on core from the Norman Wells site yielded similar results. Strength envelopes for each characteristic soil type are given in Figure 6.16. At larger stresses, the highly plastic clay from below 10 m displayed the lowest ultimate friction angle. Each of the envelopes is curved and has a zero cohesive intercept similar to that found for the Fort Simpson soils. In Figure 6.17, a wider range of stress is shown for material from the 0 to 2 m interval, indicating that envelope curvature persists under effective stresses well beyond those likely to be encountered in most field problems.

A portion of the curvature observed may be related to the breakdown of silt-sized aggregates of clay minerals, but most of the nonlinearity can be attributed to the stress-dependent response of the blocky secondary structure. In this study, similar proportions of illite and kaolinite were found in soils tested from each of the three different sampling sites. In the low stress range, envelope shape was influenced more by soil macrostructure than the intrinsic frictional characteristics of the intact soil. At higher effective stresses, ϕ' values of 23° to 25° were found, even though there were considerable textural differences between the soils. It may be significant that the 26° peak and 23° residual angles obtained for reconstituted Mountain River Clay (Figure 3.2) bracket the peak effective friction angles found for similar, but undisturbed soils from the Fort Simpson and Norman Wells sites.

An insufficient number of satisfactory samples were available to adequately define strength properties for soils from the Noell Lake site.

6.6 UNDRAINED SHEAR STRENGTH

Residual stress

When a sample of frozen soil is removed from the ground, its residual stress defines the effective stress acting when that soil is thawed in an undrained state. Aside from constituting the starting point for estimating excess pore pressures and settlements during thaw, this effective stress will also govern available shearing strength. A relationship can be derived to relate the undrained strength of normally consolidated saturated clays to their effective overburden pressure (Skempton and Bishop, 1954). Nixon and Morgenstern (1974) have suggested that this same expression might be used to relate the undrained strength of a purely fictional thawed soil to its residual stress (σ_o'). This equation is written as:

$$\frac{c_u}{\sigma_o'} = \frac{[K + A(1 - K)] \sin \phi'}{1 + (2A - 1) \sin \phi'} \tag{6.6}$$

where c_u is the undrained strength of the thawed soil,

K is the ratio of horizontal to vertical effective stress with no lateral yield,

A is the pore pressure coefficient at maximum deviatoric stress, and

ϕ' is the effective angle of shearing resistance of the soil.

A plot of undrained shear strength with depth might then be expected to reflect the in situ profile of residual stress. Figure 6.18 shows the undrained strengths found with depth at the Norman Wells site. Moisture contents found for these samples gave liquidity indices which were slightly below average values indicated for the corresponding depth. This was probably due to the exclusion of ice which occurred during sampling and specimen preparation. The undrained strengths varied considerably with depth, as might have been anticipated from the residual stress profiles (Figures 5.20 and 5.21).

Equation 6.6 was originally intended to describe the relationship between undrained strength and vertical effective stress in situ for soils with a much different stress history than that experienced by thawing permafrost. In ideal, normally consolidated clays, K is often approximated by $1 - \sin\phi'$. Making that assumption, Figure 6.19 shows the range of c_u/p or c_u/σ_o' ratios computed from Equation 6.6 using the range of effective friction angles and A parameters found to be typical for soils tested in this study. In the low effective stress range, where A values were zero or negative, and friction angles were at their highest, predicted values for c_u/σ_o' ratios are significantly greater than the c_u/p ratios usually given for normally consolidated clays. However, if the coefficient of earth pressure at rest approaches the active case, the Equation 6.6 reduces to:

$$\frac{c_u}{\sigma_o'} = \frac{\sin\phi'}{1+\sin\phi'} \qquad (6.7)$$

This relationship, plotted as a dashed line in Figure 6.20, is independent of A and only weakly affected by ϕ'. To be able to predict undrained strengths (given the in situ effective stress and appropriate strength parameters), it is necessary that both A and K be known with confidence for the thawing ground in question.

Measured undrained strengths

Effective strength envelopes and pore pressure parameters have been determined for soils from the Fort Simpson and Norman Wells sites. Samples tested were thawed, and in many instances, consolidated under an equal all-round pressure. In each test series, selected specimens that exhibited a finite residual stress were sheared undrained. Results from these tests are summarized in Figures 6.21 and 6.22. The Fort Simpson data covers a residual stress range that is broad enough for the nonlinearity of the c_u/σ_o' ratio to become apparent. Curvature of this sort would be anticipated if ϕ' decreased and A increased with increasing σ_o', as is the case. Data for the Norman Wells site falls in a narrower σ_o' range and defines what appears to be a simple, linear c_u/σ_o' relationship.

The ratio between vertical and horizontal stresses (K) is necessarily equal to one when these soils are thawed in a triaxial cell under an isotropic stress. Hence, consolidation or swelling processes occurring during undrained thaw will be in response to that same isotropic stress. Table 6.2 compares experimentally measured c_u/σ_o' ratios to those computed by substituting measured values of A and ϕ' into Equation 6.6. A values used were the averages of those measured in the tests reported. Reasonable agreement was observed between computed and measured undrained strengths.

At present, virtually nothing is known about the coefficient of earth pressure at rest in thawing ground, since these soils follow a stress path that is quite different from those encountered in conventional soil mechanics. It is also known that the value of the A parameter measured in compression is quite sensitive to sample disturbance and the pre-shear consolidation stress path (Bishop and Bjerrum, 1960; Simons, 1960; Skempton and Sowa, 1963). Anisotropy, strain rate, and the rotation of principal stresses are all factors which deserve consideration in assessing the undrained strength of thawing ground.

Lastly, it was observed that water contents in the shear zone invariably fell within one percent of the sample's bulk water content. Agreement of this sort is remarkable when the complex fabric of the samples sheared is considered, and indicates that negligible redistribution of moisture has occurred during shear.

6.7 INTERPRETATION OF LABORATORY RESULTS

Marsland (1972) has described a dilative failure mode at low confining pressures for stiff, fissured London clay. Mechanical and mathematical model have been developed by Ladanyi and Archambeault (1969) to explain a similar mechanism of dilative failure in a jointed rock mass. They have proposed a general shear strength equation to describe curved failure envelopes, and Ladanyi (1970) has subsequently suggested that this same approach might be used to describe two simulataneous failure modes in a jointed clay mass. The simultaneous shear along softened joint planes and through intact material produces a curved failure envelope with strength at low stresses being influenced more by the clays' macrostructure than its intact stregnth. While the equation may well be conceptually correct, several parameters are involved which would prove difficult to determine experimentally, and for this reason, it seems improbable that this approach could be used for routine purposes.

The strength envelopes determined for the soils described in this study all showed obvious curvature. This can be attributed directly to dilative failure in the blocky structure that remains when reticulate ice melts out. The structure produced by freezing and ice segregation permits easy access to water upon thaw. The mechanical disturbance resulting from differential volume changes during freezing accelerates post-thaw softening of soil adjacent to these ice lens fissures. Although intact soil blocks apparently retain their original lacustrine clay fabric, the softened soil within the fissured network becomes progressively remoulded. Chandler (1969, 1972) has described similar features and behaviour in soil profiles thought to have been subjected to permafrost conditions during the Pleistocene. The presence of these fissures lowers soil strength at low stresses by eliminating cohesion.

Although no cohesion intercept was found for the materials tested in this study, it is conceivable that a finite cohesion might be observed with unsaturated samples. When the envelope extends into the low pressure range, caution is indicated in applying a cohesion intercept extrapolated back from tests performed at conventional pressures (e.g. 200 to 400 kN/m^2). Adopting a c' and ϕ' obtained at these stresses will predict significantly higher strengths than the values which could ultimately be mobilized. The possibility of envelope curvature has been anticipated in the slope stability design assumptions described by Canadian Arctic Gas Pipeline Limited (1974).

In the past, concern has been expressed regarding the size of the element of soil tested in relation to the spacing, geometry, and nature of discontinuities such as fissures (Marsland and Butler, 1967; Skempton and Petley, 1967; Morgenstern, 1967; Lo, 1970; Marsland, 1972). In this study of thawed permafrost soils, it was possible to maintain ratios of specimen diameter to average ice lens spacing greater than two in most cases. At Norman Wells, however, the nature of the core precluded an adequate assessment of the ground ice structure in situ. Although it appeared that the size criterion was usually satisfied, some of the samples used may not have been large enough to completely eliminate effects related to the presence of discontinuities.

For a particular sediment, the accuracy with which laboratory strengths can represent field behaviour will depend considerably upon the spacing and geometry of cryogenic discontinuities. The length of time a soil mass remains under a particular stress will also affect its strength if softening remains a possibility. Of course, tests on small specimens that do not contain representative structure will simply reflect the shear strength properties of the intact clay.

Extreme variations would normally be anticipated with undrained strengths measured in the laboratory, since the clays all exhibit a very flat swelling curve. Small changes in water content during thaw will produce large differences in effective stress, and therefore, in strength.

Local diversity in the freezing and stress histories, ground ice structure, and basic textural properties, will then be responsible for the spatial differences in undrained strength.

Nixon and Morgenstern (1974) have suggested that Equation 6.6 can be applied to the prediction of undrained strengths from measured values of residual stress. This approach requires other input parameters including ϕ', A, and K (assuming full saturation). Effective strength parameters can be determined with accuracy sufficient for engineering purposes by following any convenient stress path to failure. The first stage in the usual procedure is isotropic consolidation ($K = 1$). _In situ_, both K and A will be different from values determined in this sort of triaxial test. The coefficient of earth pressure at rest will certainly be less than one in an ice-rich thawing soil, and this suggests that consolidation should be conducted anisotropically, even during undrained thaw. Pore water suctions during soil freezing undoubtedly cause some isotropic volume change. This is evidenced indirectly by the formation of shrinkage cracks which eventually fill with ice to become the familiar reticulate ice networks. Upon thaw, some portion of this strain must be irreversible, so it could be argued that K during thaw might even be less than $K \approx 1 - \sin \phi'$ which was probably the case prior to freezing. As K approaches the active condition, c_u/σ_o' becomes much less sensitive to both ϕ' and A. If this condition is assumed as a lower bound, c_u/σ_o' falls in the 0.3 to 0.4 range and will provide a conservative estimate of undrained strength in terms of residual stress.

The experimentally measured undrained strengths compare well with c_u/σ_o' values computed by substituting appropriate values for ϕ', A, and

K into Equation 6.6. It should be appreciated, however, that this A parameter is strongly influenced by the stress ratio. Experimental studies have shown that, with overconsolidated soils, anisotropic consolidation results in a higher value for A than does isotropic consolidation (Simons, 1960; Blight, 1965). This suggests that, by virtue of lower A values and a higher K, undrained strengths reported herein may be considerably higher than those which could be mobilized _in situ_. A small or negative A value in combination with a K = 1 explains the unrealistically high c_u/σ_o' values that were obtained in these undrained tests. The circumstances surrounding thawed soil behaviour lead to the conclusion that reasonable undrained strengths can only be obtained if the sample is thawed under an anisotropic stress field to simulate _in situ_ conditions. Subsequent consolidation and shear will yield values of A and K that would be more appropriate for application to field problems.

Furthermore, residual stresses obtained under isotropic stress conditions in the triaxial cell might be expected to differ from those found under conditions of zero lateral yield in the permode. There is probably a pore pressure response to the deviatoric stress applied in the permode so that, unless A were by chance equal to zero, permode and triaxial σ_o' values would not be expected to equal each other. In Section 5.6 it was indicated that, by using two different test procedures, similar residual stresses were obtained for the homogeneous soils at the Fort Simpson site. This indicates that either K must have been equal to approximately one _in situ_ (unlikely) or the appropriate value of the A parameter was close to zero. Residual stresses determined in the triaxial cell for materials from the Norman Wells site could not be correlated with permode results. They were erratic and probably reflected local variations in both K and A. Considering the constraints in each test, it seems reasonable to expect that residual stresses determined in the permode would probably be more representative of in situ conditions. Caution must be exercised in the use of relationships such as Equation 6.6 unless a better appreciation of in situ values for A and K can be obtained. Vane shear tests and anisotropically consolidated undrained tests present a possible means of exploring these unknowns. It should be noted that testing thawed soils after isotropic consolidation, while defining appropriate values for c' and ϕ', cannot hope to yield meaningful values for the A parameter. For this reason, undrained strengths determined in the conventional manner will necessarily be unconservative. Furthermore, sampling disturbance usually imparts some conservatism to measured strengths, but, since frozen core is a nearly perfectly undisturbed sample, this effect cannot be assumed in an assessment of thawed soil behaviour.

From the preceeding, it should be clear that application of this sort of strength data to problems like evaluating the stability of slopes requires a careful examination of the parameters involved as well as the testing techniques which have been employed to obtain them. Mitchell (1975) has suggested that the conventional (σ_3 = constant) displacement-controlled triaxial test is not well suited to defining strength envelopes for soils exhibiting dilative failure. The stress paths shown in Figure 6.11 lend support to his contention, since before peak deviatoric stress is reached, soils tested at low confining pressures attain $(\sigma_1' + \sigma_3')/2$ values well beyond the range of normal stresses encountered in most slope stability problems. This observation is especially applicable to the case of active layer detachment slides, flows, and other shallow mass movements. These circumstances suggest that careful appraisal of the stress path selected to produce failure is a necessary prerequisite to serious analysis and design. A modification of the hydraulic triaxial cell described by Bishop and Wesley (1975) might be considered for use in future studies of the undrained strength of thawing soils.

TABLE 6.1 FREQUENCY ANALYSES OF w AND γ_f FOR ZONES 3 AND 4

ITEM	MEAN	STANDARD DEVIATION
Density	1.78	0.12
Density[1] (Mg/m^3)	1.80	0.12
Water Content	40	11
Water Content[1] (%)	39	10

[1] Weighted with respect to sample volume

TABLE 6.2 COMPARISON OF COMPUTED AND MEASURED c_u/σ_o' RATIOS

SITE	EFFECTIVE STRESS RANGE (kN/m^2)	ϕ' (degrees)	A_f	c_u/σ_o' Computed	c_u/σ_o' Measured
Fort Simpson	0 - 5	28	0.05	0.81	0.79
	150 - 200	24	0.20	0.53	0.46
Norman Wells	0 - 40	31	-0.05	1.21	1.26

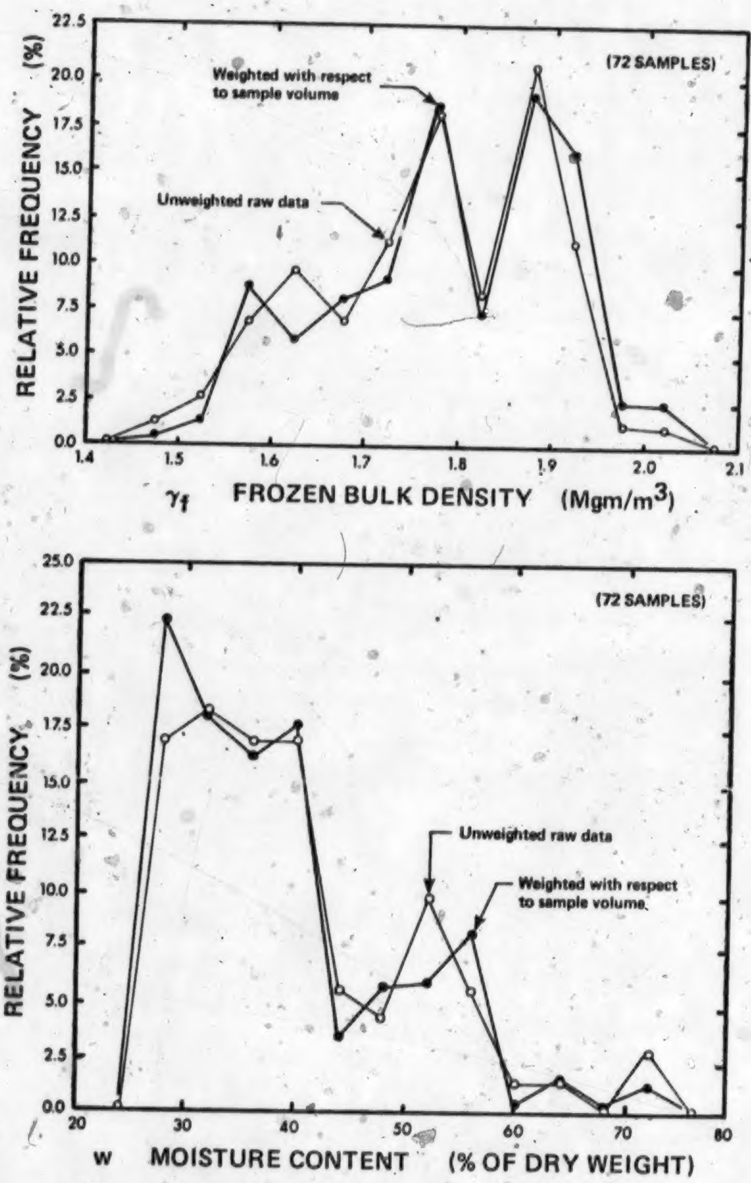

Figure 6.1 Frequency distributions of frozen bulk density and water content for samples from Zones 3 and 4, Fort Simpson landslide headscarp

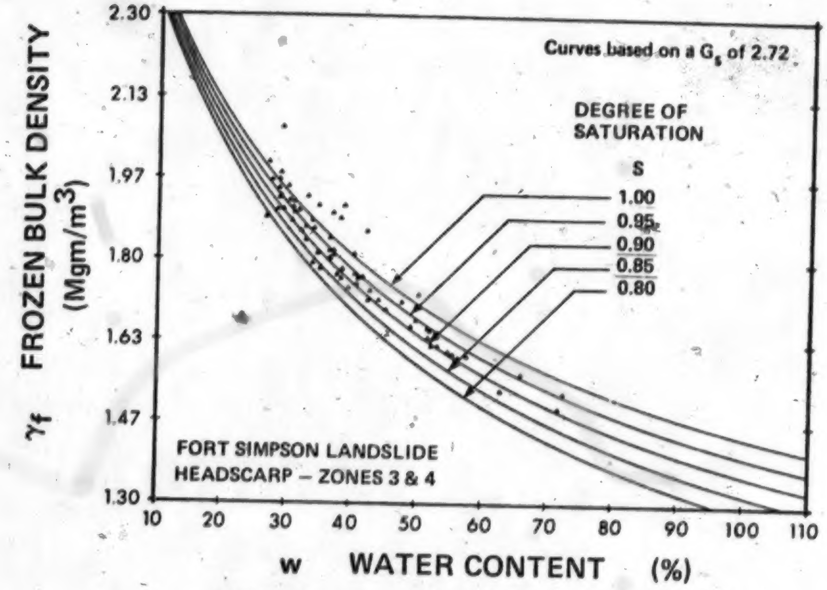

EFFECT OF VARIATION OF DEGREE OF SATURATION

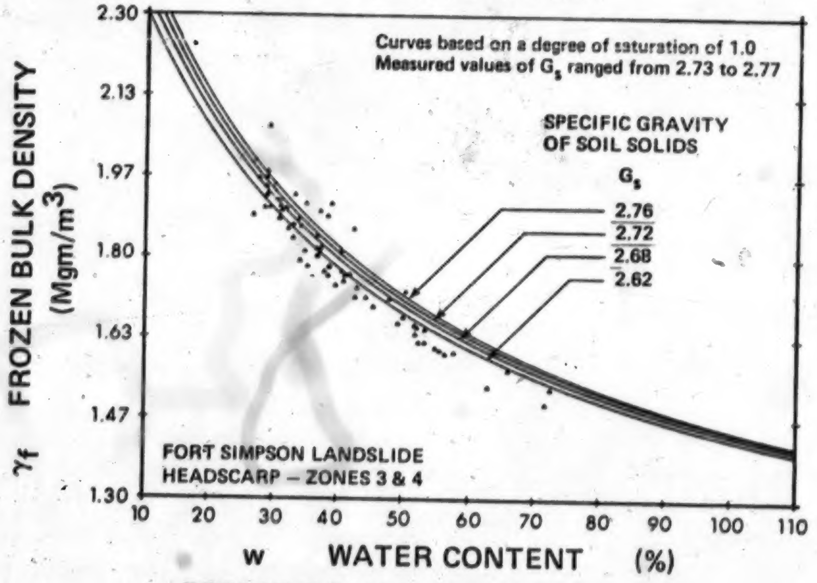

EFFECT OF VARIATION OF SPECIFIC GRAVITY OF SOIL SOLIDS

Figure 6.2 Frozen bulk density - water content relationships for samples from Zones 3 and 4, Fort Simpson landslide headscarp

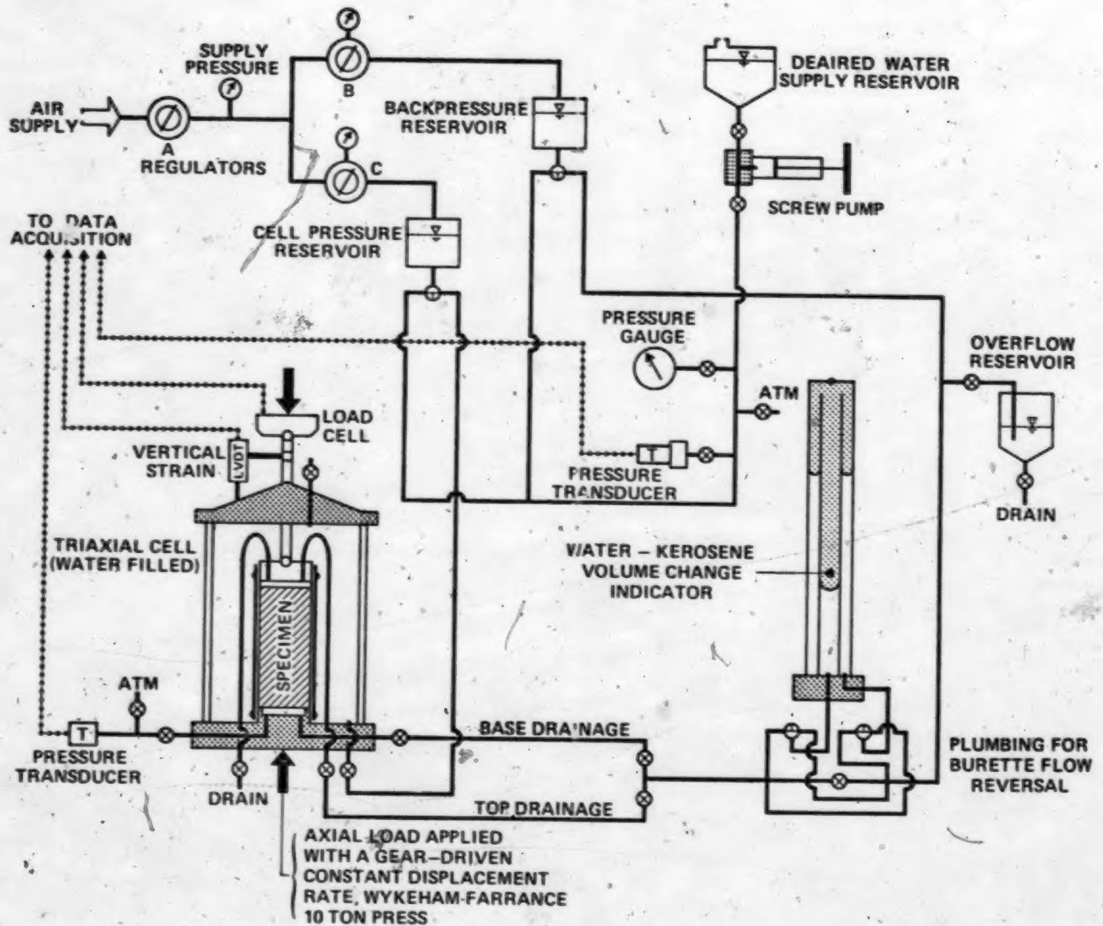
SUPPLY PRESSURE
AIR SUPPLY
A
REGULATORS
B
C
BACKPRESSURE RESERVOIR
CELL PRESSURE RESERVOIR
DEAIRED WATER SUPPLY RESERVOIR
SCREW PUMP
TO DATA ACQUISITION
PRESSURE GAUGE
ATM
OVERFLOW RESERVOIR
DRAIN
LOAD CELL
VERTICAL STRAIN
LVDT
PRESSURE TRANSDUCER
TRIAXIAL CELL (WATER FILLED)
WATER – KEROSENE VOLUME CHANGE INDICATOR
SPECIMEN
ATM
T
PRESSURE TRANSDUCER
DRAIN
BASE DRAINAGE
TOP DRAINAGE
PLUMBING FOR BURETTE FLOW REVERSAL
AXIAL LOAD APPLIED WITH A GEAR–DRIVEN CONSTANT DISPLACEMENT RATE, WYKEHAM-FARRANCE 10 TON PRESS

Figure 6.3. Schematic layout of triaxial cell and associated equipment used in strength tests

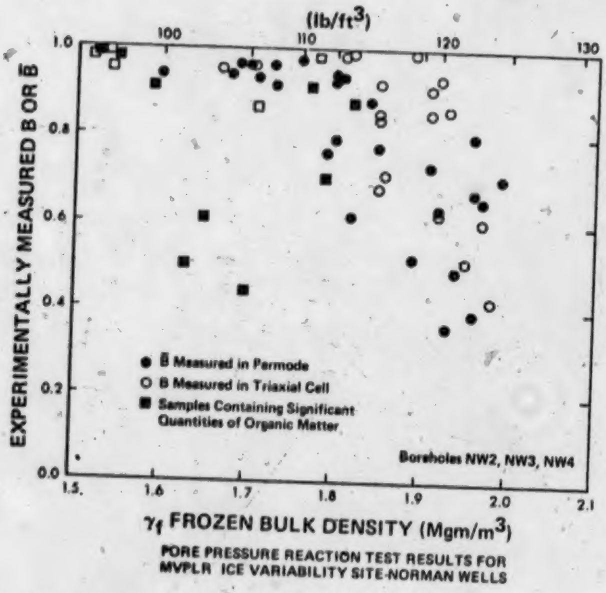

Figure 6.4 Pore pressure reaction test results for thawed soils, Norman Wells site

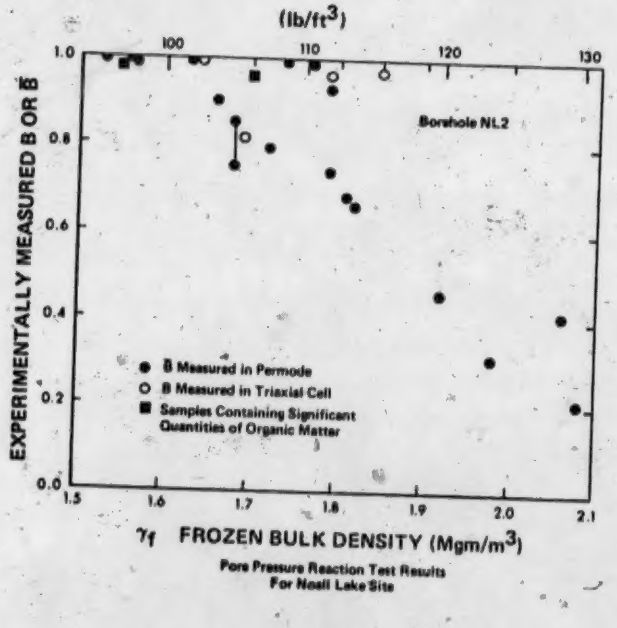

Figure 6.5 Pore pressure reaction test results for thawed soils, Noell Lake site

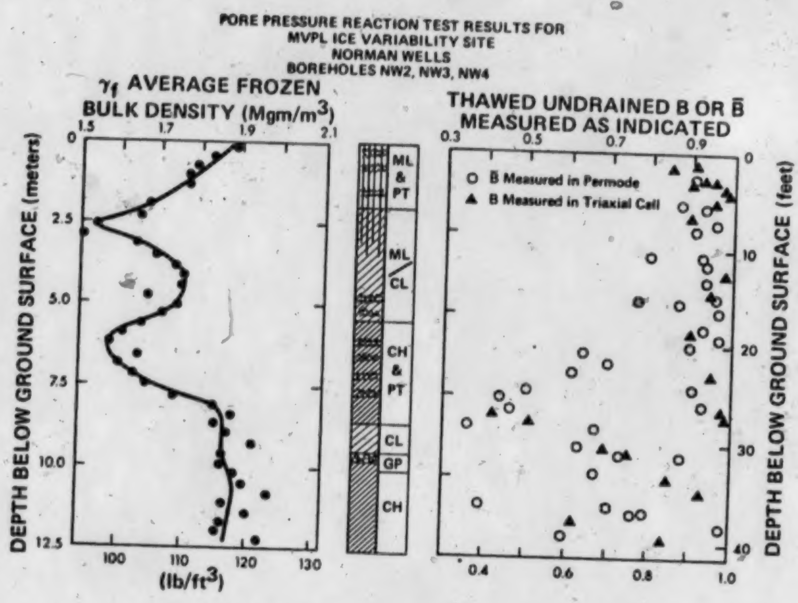

Figure 6.6 Pore pressure reaction test results related to stratigraphy, Norman Wells site

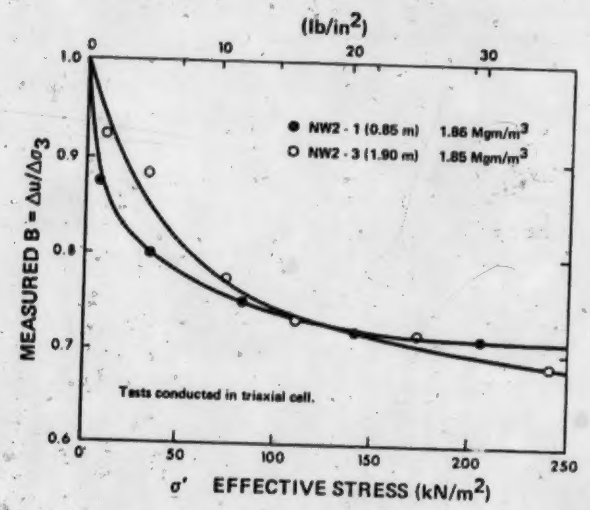

Figure 6.7 Pore pressure parameter B measured with increasing consolidation stress

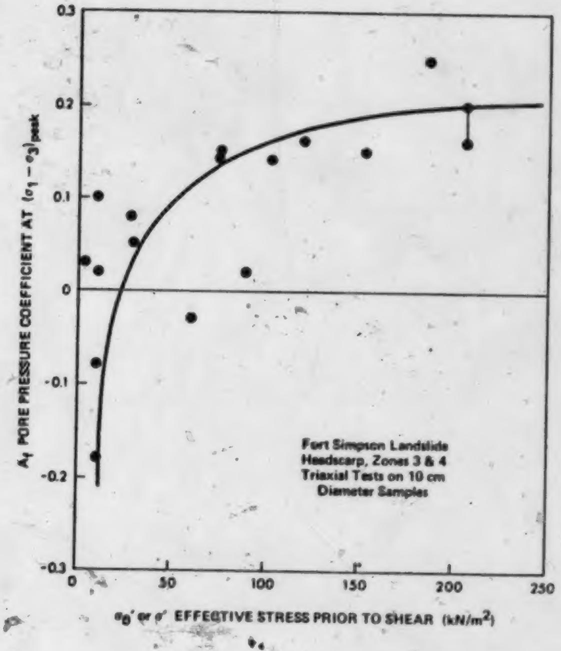

Figure 6.8 Pore pressure parameter A measured at failure in triaxial compression, Fort Simpson samples

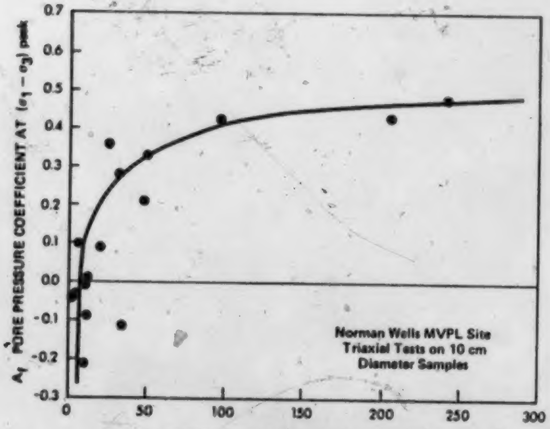

Figure 6.9 Pore pressure parameter A measured at failure in triaxial compression, Norman Wells samples

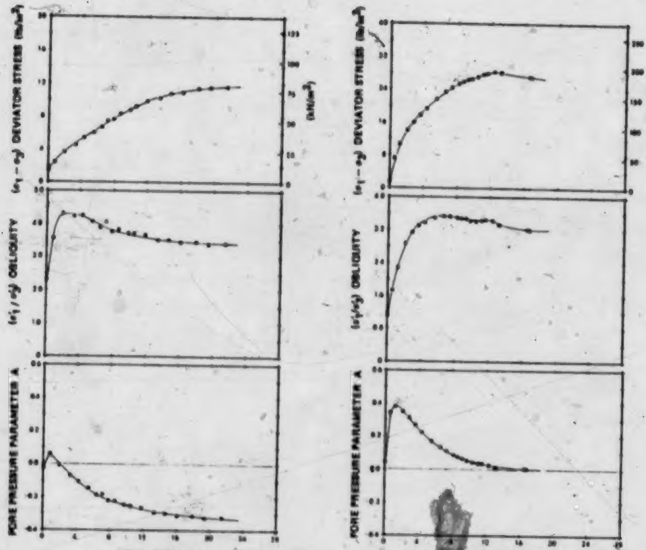

a) TEST FS-T-16 γ_t = 1.88 Mgm/m³
σ'_3 = 11 kN/m² (Residual stress)

b) TEST FS-T-11 γ_t = 1.90 Mgm/m³
Consolidated to σ'_3 = 65 kN/m²

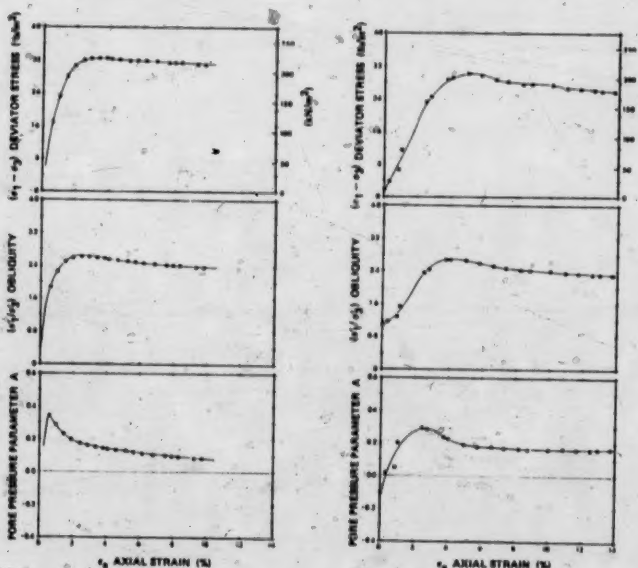

c) TEST FS-T-04 γ_t = 2.04 Mgm/m³
σ'_3 = 155 kN/m² (Residual stress)

d) TEST FS-T-02 γ_t = 1.89 Mgm/m³
Consolidated to σ'_3 = 295 kN/m²

Figure 6.10 Typical consolidated, undrained triaxial compression test results, Zones 3 and 4, Fort Simpson landslide headscarp

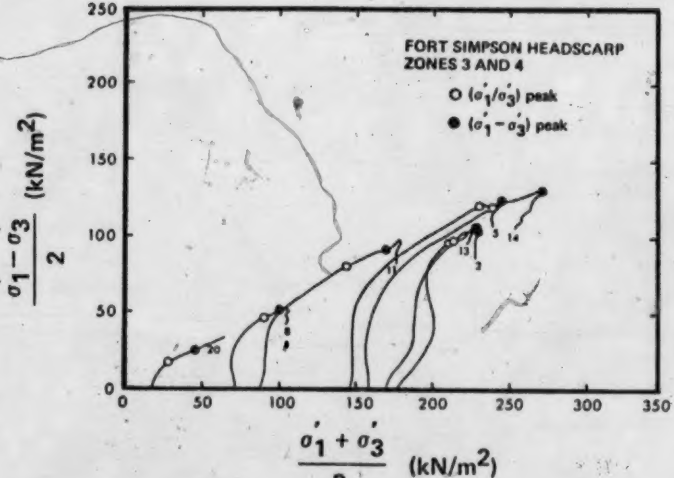

Figure 6.11 Stress paths during triaxial compression with σ_1'/σ_3' and $(\sigma_1 - \sigma_3)$ peaks indicated

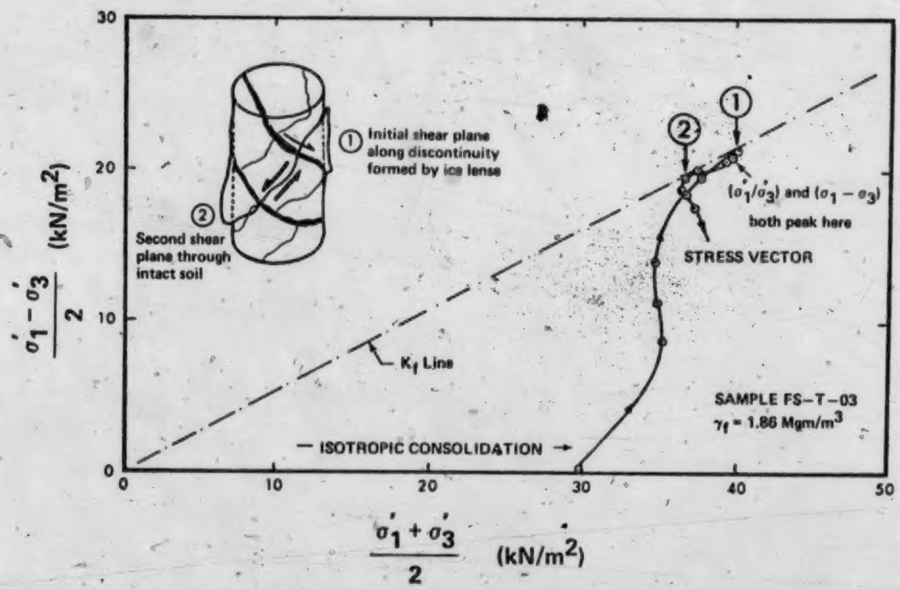

Figure 6.12 Effects which secondary structure may have on stress path shape during shear

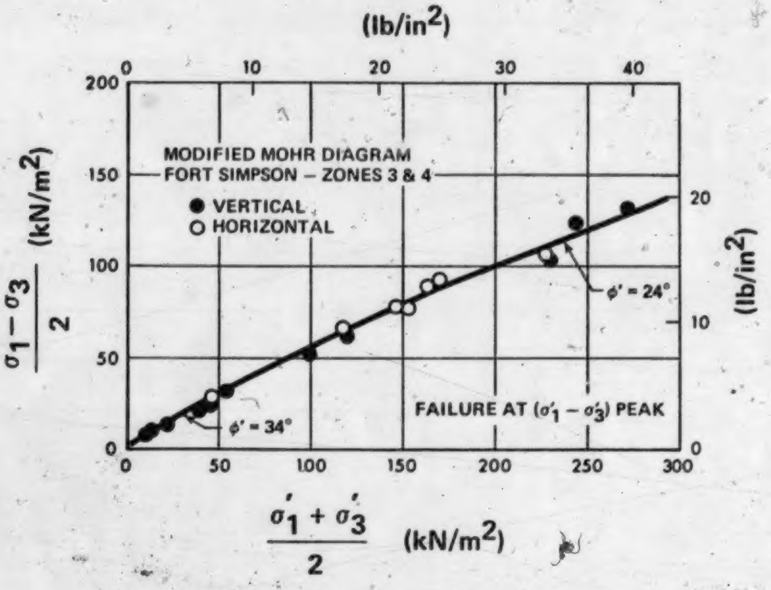

Figure 6.13 Shear strength envelope using a maximum deviatoric stress failure criterion

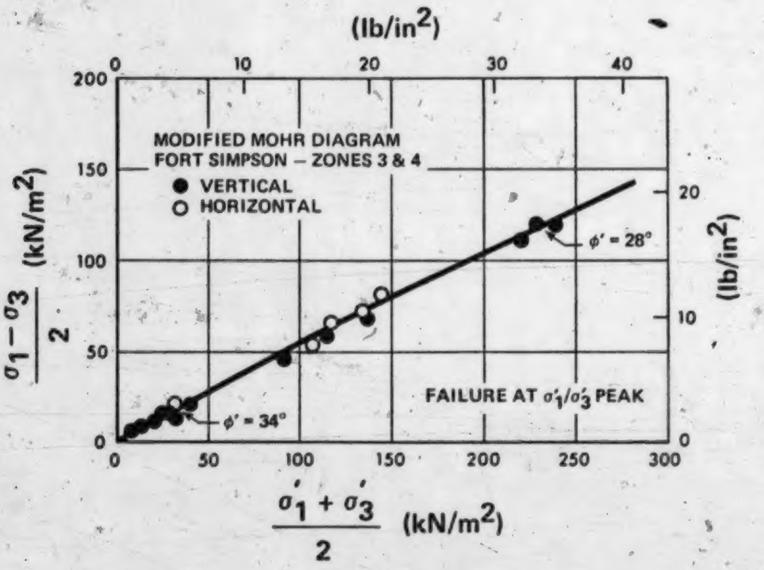

Figure 6.14 Shear strength envelope using a maximum obliquity failure criterion

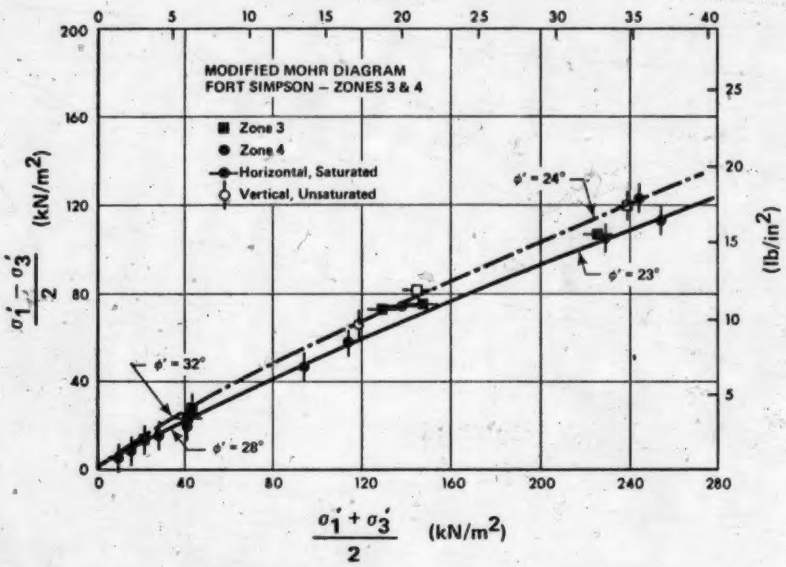

Figure 6.15 Strength envelope for soils from Zones 3 and 4, Fort Simpson landslide headscarp

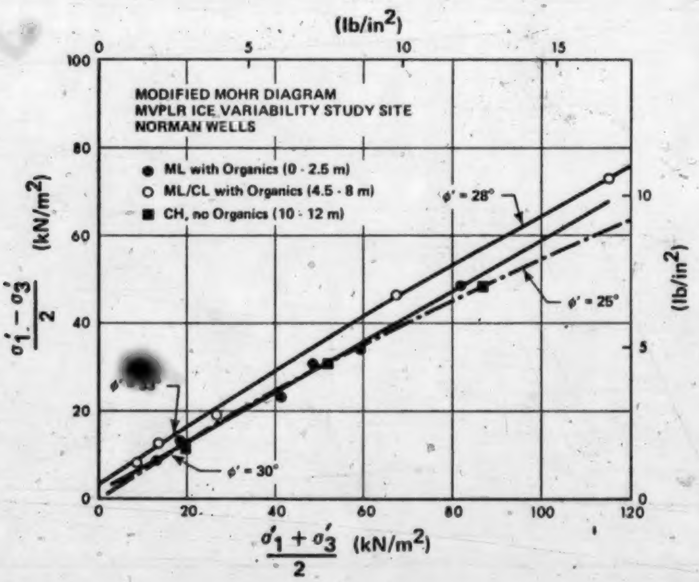

Figure 6.16 Strength envelope for soils from Norman Wells site

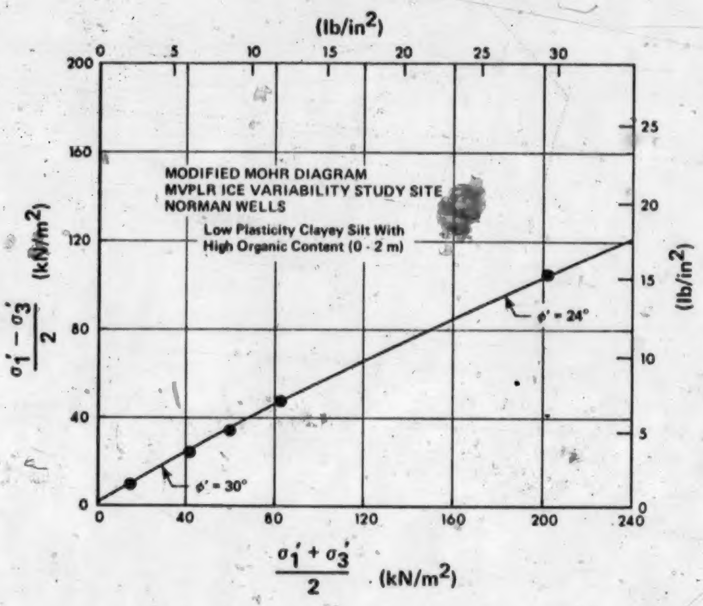

Figure 6.17 Nonlinearity of strength envelope over a wide stress range

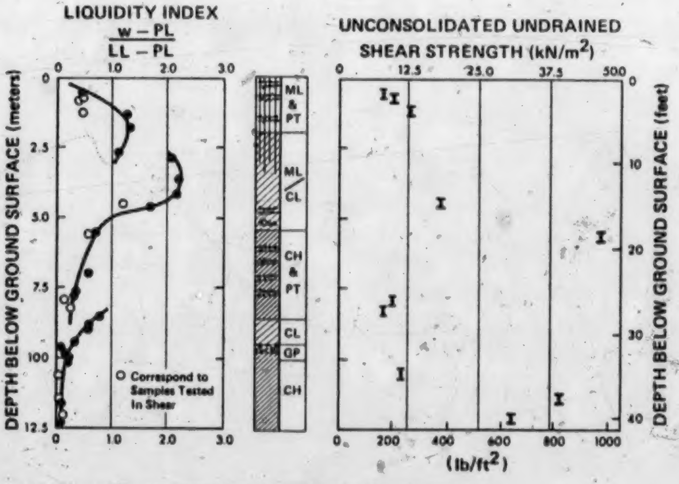

NOTE: Tests were conducted on 10 cm diameter samples that were thawed and sheared undrained

Figure 6.18 Undrained strength test results in profile, Norman Wells site

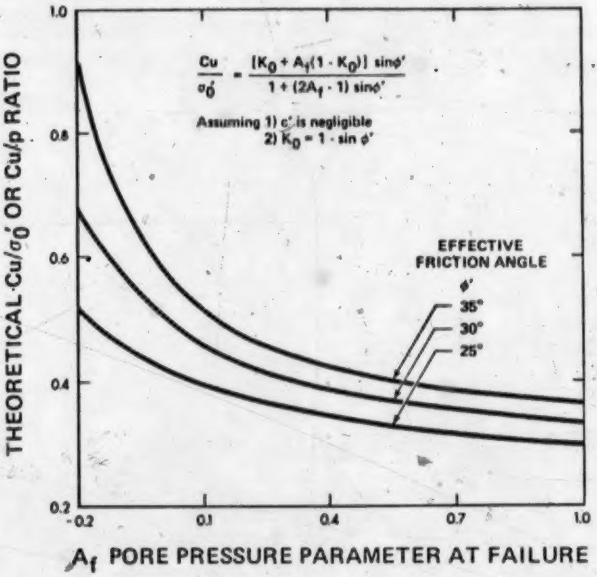

Figure 6.19 Sensitivity of c_u/p ratio to A parameter for a typical range of friction angles

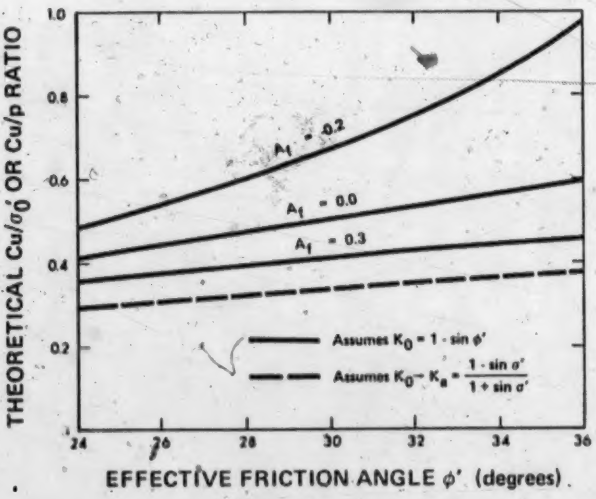

Figure 6.20 Sensitivity of c_u/p ratio to friction angle for a typical range of A parameter values

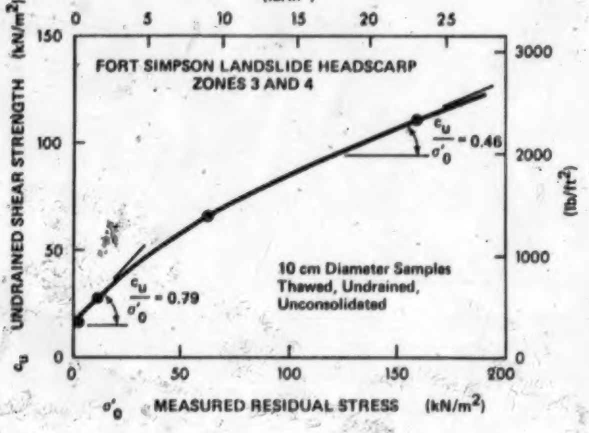

Figure 6.21 Undrained strength as a function of residual stress, Fort Simpson site

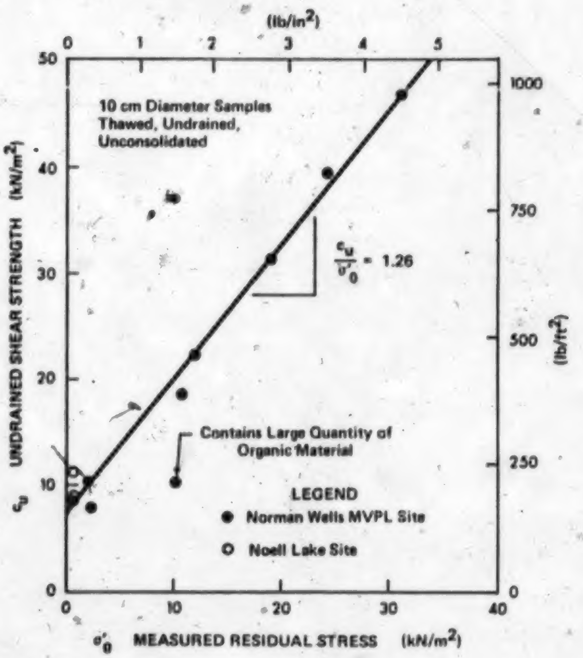

Figure 6.22 Undrained strength as a function of residual stress, Normal Wells site

CHAPTER VII

CONCLUDING REMARKS

7.1 SITE INVESTIGATION PRACTICE

The design and construction of civil engineering works is normally preceeded by a site investigation that is intended to provide some definition of subsurface conditions. This investigation establishes the feasibility and economics of a project, and furnishes some or all of the information required for associated geotechnical analyses and design. However, obtaining access to conduct site investigations in Canada's arctic and subarctic regions is invariably a difficult and expensive undertaking. Such work is normally conducted distant from laboratory facilities so that drilling and sampling operations are usually completed some time before any core can be examined or tested in a laboratory environment. To adequately prepare for unforseen circumstances, planning for these site investigations should depart from routine practice by:

1) Increasing the depth of boreholes.
2) Decreasing the spacing between boreholes.
3) Increasing the number of undisturbed samples taken and returned to laboratory facilities.

In most cases, the additional expense associated with a more thorough initial program on site constitutes only a small fraction of the cost involved in mobilizing drilling equipment and personnel to conduct a supplementary field program.

Where permafrost conditions prevail, the soil fabric is invariably dominated by structural features associated with ground ice. In this thesis, laboratory results have indicated that fabric has a significant influence on the geotechnical behaviour of both frozen and thawing soils. Therefore, primary fabric formed during sedimentation and secondary fabric which has developed thereafter should be described in considerable detail. This implies a comprehensive account of ground ice features which can only be obtained from the examination of undisturbed core. A detailed description of stratigraphy and structure is essential since soil classification on the basis of index tests and textural analyses can seldom be used to indicate the more complex geotechnical characteristics exhibited by natural deposits in situ. Techniques available for sampling permafrost provide core diameters which rarely exceed 10 cm (4 in.), and borehole logs are commonly prepared from an examination of this sort of sample. Viewing the same or similar material in section at an exposed face certainly facilitates a more realistic visualization of bulk fabric than do ground ice features included in small diameter cores.

When disturbed samples are taken instead of intact core, logs detailing materials encountered are restricted to textural descriptions. Without some prior knowledge of the site, it is difficult or impossible to infer genetic origin, stratigraphy, macrofabric, and other geological details. In both frozen and thawed soils, discontinuities produced by freeze-thaw processes or the presence of discrete ice lenses are important factors affecting soil behaviour. Practical limitations on sample quality complicate obtaining accurate descriptions of quantities and types of ground ice, especially when it is present in thick streaks which are either badly shattered or washed away during coring. Difficulties such as these emphasize the need to select sampling equipment carefully, so that core obtained will have dimensions sufficiently large to contain representative and identifiable ground ice structure.

Although the NRC-CRREL system (Pihlainen and Johnston, 1963) system for field description of permafrost soils has received wide use in practice, it is only modestly capable of providing an adequate log of ground ice conditions. Volumetric percentages of segregated ice are based on visual estimates and little attention is usually paid to accuracy. Direct measurements of cumulative ice lens thickness over core lengths of 20 to 50 cm (8 to 20 in.) are seldom made, so ice contents reported on routine borehole logs are often more qualitative than quantitative. The NRC-CRREL system is most deficient in soils which contain a reticulate ice structure or are extremely ice-rich. Therefore, the development of a more comprehensive scheme for the field identification, classification and description of ground ice is urgently required. This system would concentrate on primary features such as the amount and distribution of ice in the soil, the geometry of its occurrence, and the nature of the soil included between discrete ice lenses. Secondary features pertaining to ice petrology, genetic origin, hydrogeological conditions at the time of permafrost aggradation, and the soil's geothermal history could become important if a more detailed understanding of the relationship between the ice and its host sediments was sought. However, obtaining data pertaining to secondary features is not usually practical, especially in the field. Once primary features have been logged, superimposing the ground ice description on a detailed stratigraphic log provides a sound basis for interpreting the genetic origin of each ice type encountered in the borehole.

Results presented in this thesis suggest that in addition to index and textural properties, representative values of water content and frozen bulk density in profile are important in the assessment of geotechnical behaviour for frozen or thawing soils. These properties can also be used to obtain a clearer understanding of the geological and freezing histories which the soils have experienced. Obtaining representative water content and density data requires considerable effort in selecting appropriate equipment and conducting the subsequent sampling operation. To stress this point, a study worthy of note is one reported by Lau and Lawrence (1976) which analyzed a large volume of drilling results obtained in the Mackenzie River Valley. Their data indicate that under similar terrain conditions, the frequency and amount of ground ice reported when conducting disturbed sampling was invariably less than when continuous undisturbed samples were taken. After recognizing the practical limitations which normally control accuracy obtained in logging ground ice quantities from intact core, it is apparent that continuous undisturbed sampling methods should be given preference where permafrost conditions are anticipated. Large diameter samples certainly provide a better opportunity to log ground ice conditions correctly. This sort of sampling should be specified whenever possible so that fabric contained in specimens selected for more sophisticated laboratory testing will be representative of conditions _in situ_.

Considering the high costs associated with drilling and sampling activities in the Canadian North, it is clear that the introduction of new methods for supplementing data obtained from boreholes would certainly be welcomed. Downhole geophysical tools offer some promise in this regard, particularly when a need to correlate stratigraphy or specific soil properties exists. Continuing research and development to refine sampling equipment and procedures is required before the quality of core obtained can be improved, especially in the case of soils which contain significant quantities of segregated ice. Minimizing or eliminating mechanical disturbance to ice inclusions will result in improved accuracy in logging ground ice conditions, and in determining profiles of water content and frozen bulk density which are representative of conditions _in situ_. Concern with sample quality must also be continued throughout their transport and storage. The judicious use of field laboratory facilities can minimize risks which would otherwise be necessary if large quantities of core had to be shipped from remote sites to established geotechnical laboratories. At the same time, a field laboratory permits obtaining a greater amount of data per borehole than might otherwise be collected.

7.2 ENGINEERING BEHAVIOUR OF PERMAFROST SOILS

Frozen soils

A review of published results obtained from tests on polycrystalline ice and various frozen soils has suggested that shear strength and creep behaviour are intimately related. An approximate flow relationship has been developed for ice and consists of a power law which relates strain rate to stress with an exponent that is approximately equal to 3. Temperature effects in this relationship are included in a creep modulus which appears to be amenable to analysis within the framework of rate process theory.

Laboratory testing conducted as part of the research reported in this thesis substantiates the concept that shear strength in ice-poor frozen soils depends upon normal stress. The friction angle mobilized in these tests was essentially identical to that which could have been determined from conventional drained tests on the same soil in a thawed state. The results of previous laboratory studies have documented this sort of behaviour for sands, but other limited testing reported in the literature had indicated that frozen fine-grained soils did not behave in a frictional manner. By conducting shear tests at sufficiently slow rates of strain, results reported herein confirm that ice-poor frozen silty clays do exhibit frictional strength. Rate and temperature dependence are included in a cohesive intercept which becomes small or negligible when strain rates are very slow. The strength and deformation characteristics of ice-rich soils probably correspond more closely to behaviour observed for ice, although effects which soil inclusions may have on these properties require further study.

Inspecting samples which had been subjected to direct shear revealed that some redistribution of moisture had occurred within the shear zones. This was evidenced by the formation of semi-continuous ice lenses along both principal and secondary shear planes and resulted in a net increase in soil water content within the shear zone. Accumulation of segregated ice along failure planes implies that sustained shear movement could lead to an acceleration in displacement rates if the applied stress were to remain constant. The amount of unfrozen water present and its mobility are factors which are certainly important to obtaining an understanding of this process.

The creep behaviour of frozen soils is less well-defined. Additional testing under both laboratory and field conditions is required before design work governed by deformation criteria can be undertaken with any degree of confidence. In particular, the effects which thermal conditions have on the creep behaviour of fine-grained soils are accentuated by changes in unfrozen water content: these tend to be most dramatic at temperatures within 2 or 3°C of the melting point. Data presented here indicate that at near-thawing temperatures, fine-grained soils may creep at rates which are faster than those given for ice. However, several questions have been raised regarding temperature control, measurement and uniformity of strain, and methods employed to interpret the test results. A critical examination of analytical methods used to evaluate laboratory creep data in the past has revealed that considerable errors have occasionally been introduced in the determination of creep rates. In such cases, interpretation may be confused to the point that certain basic behavioural characteristics are overlooked. Methods described here for reducing creep data eliminate some of the interpretive problems by utilizing continuous differentiation of the time-strain curves to establish strain rates. These same analytical procedures have been successful in identifying both attenuating and steady state creep processes in a series of tests performed on undisturbed, fine-grained permafrost soil.

Thawed and thawing soils

The results of various tests reported in this thesis have consistently shown that macrostructural features associated with segregated ice have a significant effect on the strength, permeability, and consolidation properties of thawed soils. These findings emphasize the great importance of obtaining and testing specimens which contain fabric that is representative of *in situ* conditions. Geology and conditions prevailing during permafrost aggradation are reflected in a soil's behaviour upon thaw. Obtaining a better appreciation of geotechnical properties in profile has been a definite aid in interpreting geological histories for sections logged at both the Norman Wells and Noell Lake sampling sites. Data collected there indicate that simple index properties like density, water content, texture, and liquidity index can reveal a great deal about the deposition of sediments and the subsequent invasion of permafrost conditions.

Consolidation testing has revealed that a vast majority of these undisturbed samples exhibit a linear relationship between void ratio and the logarithm of effective stress. Consolidation coefficients measured during some tests hanged by more than an order of magnitude, and usually decreased as stresses were increased. A review of complementary permeability data has demonstrated that at low effective stresses, open structural discontinuities are capable of conducting significant amounts of water. However, as effective stresses are increased, structural closure effects a marked decrease in permeability. Consolidation coefficients determined from post-thaw settlement data may be quite conservative when used to predict pore pressures generated by thaw. Limited data contained in this thesis suggest that the nonlinear thaw-consolidation theory (Nixon and Morgenstern, 1973a) should be adopted for most cases of thaw involving natural soils. Appropriate values for the residual stress and c_v would be required to obtain a meaningful theoretical prediction of pore pressures.

An extensive investigation of residual stresses in undisturbed permafrost soils has shown that for a specific soil type, this quantity is uniquely related to the thawed, undrained void ratio. It can also be correlated with plasticity characteristics and liquidity indices. Redistribution of soil water, and irreversible strains occurring due to local increases in effective stress during freezing, control the residual stress (σ_o') measured when the soil is thawed under undrained conditions. Finding that e-log σ_o' curves were typically linear made it possible to obtain σ_o' values by extrapolating post-thaw consolidation data back to the thawed, undrained void ratio. Estimates of σ_o' made in this way agreed well with values measured directly in the tests. For each soil type tested, linear correlations have been developed between the thawed, undrained void ratio and the logarithms of experimentally measured values of residual stress. Similar relationships can probably be developed for any other soil type.

The permode used to perform these tests proved to be quite versatile and demonstrated its utility as a basic apparatus for conducting laboratory tests on thawing soils. This detailed study of residual stresses and the consolidation of natural soils has shown that relatively unsophisticated testing methods can provide sufficient geotechnical data to permit the application of existing thaw-consolidation in analysis and design. Further experimental work on the consolidation and related properties of thawing permafrost will probably result in diminished returns unless site-specific data are required. Other research topics which might yield useful results are a controlled investigation of structural scale effects and the prototype development of a suitable piece of in situ testing equipment like the modified compressometer described by Janbu and Senneset (1973). At this point in time, better confirmation of existing theories and laboratory data should remain as a priority item. Carefully planned and executed field thaw tests are the only means available to increase engineering confidence in our ability to understand and predict the behaviour of thawing soils.

Consolidated undrained triaxial tests with pore pressure measurement were performed on several different soil types, and the results consistently showed a nonlinear failure envelope. This is a reflection of the way in which a dilatant macrostructure dominates strength behaviour at low effective stresses. At those low stresses, peak friction angles were significantly higher than might have otherwise been anticipated on the basis of soil texture and plasticity. This nonlinear behaviour will have the greatest bearing on cases like active layer detachments or flows, where conditions of low effective stress will certainly be common.

Secondary structure also has an effect on the pore pressure response to changes in both the all-round and deviatoric stresses. Softened soil, situated adjacent to discontinuities which were formerly occupied by ice lenses, initially exhibits a high pore pressure response to changes in confining pressure. This pore pressure increase gradually dissipates as water either drains away or is absorbed by the soil peds as they swell. Data obtained indicate that as samples are consolidated to higher confining stresses, the pore pressure coefficient B decreases. This behaviour suggests that in the long term, response may be mainly governed by the peds. In fine-grained soils, moisture content data indicate that these peds have usually been desaturated by suctions generated during freezing. The measured A_f parameters were negative in tests conducted at low effective stresses, which indicates that the peds were behaving as intact units by dilating, with failure planes tending to follow existing structural discontinuities. At higher stresses, shear planes also formed through the peds, and higher values were observed for A_f.

Undrained strengths appeared to be related directly to the residual stress. By using the measured σ_o' as an initial effective stress and including appropriate values for A, K, and ϕ', close agreement was obtained between theoretically predicted and measured values of undrained strength. A detailed review of the data led to the conclusion that providing for anisotropic consolidation during thaw was probably essential to the measurement of realistic undrained strengths and pore pressures during shear. Testing procedures used in the course of this research may have obtained undrained strengths which were too high, and it is certainly questionable whether they are at all representative of shear strengths which could be mobilized *in situ*. This means that testing procedures may also affect the measurement of residual stress, since pore pressures generated by the application of a deviator stress are strongly influenced by conditions of lateral restraint. In the analysis of cases such as active layer detachments where low effective stresses certainly prevail, pore pressures generated in a dilatant macrostructure may warrant the additional experimental difficulty of adhering to a more appropriate stress path during thaw and shear.

7.3 FURTHER RESEARCH

In a field which has only received serious geotechnical attention during the last decade, many topics remain which require further research. The study described in this thesis involved several different laboratory programs, and of all the experimental problems encountered, obtaining adequate temperature control in tests performed on frozen soil proved to be the most difficult.

Although there is probably not much more basic laboratory work on thawed soils required, the following are noted as being topics deserving of attention:

1) Determining the effects which conditions of applied stress have on the measurement of residual stresses.
2) Determining pore water pressures generated during shear when realistic stress paths are followed.
3) Comparing shearing behaviour and pore pressure response under conditions of isotropic, anisotropic, and K_o consolidation.

Although using undisturbed materials in these studies provides additional detail on other natural soils, the interpretation of experimental results will almost always be complicated due to their inherent variability.

Of greater significance is the need to conduct more tests on frozen soils at stress levels and temperatures which correspond to typical field conditions. Continued research in this area is particularly important in light of the fact that creep behaviour in frozen soils is still rather poorly understood. Although some of the work reported in this study has resulted in the development of more rational methods for analyzing experimental creep data, additional tests on natural permafrost soils are still required before field behaviour can be thoroughly understood or predicted. A definitive study of consolidation processes in frozen soil to explore mechanisms and processes controlling moisture migration would also be of considerable interest.

Very little practical experience with the design or performance of foundations in arctic regions has been documented. Theories have been developed which provide analytical solutions to several key problems, but before these can be used in routine design practice, determination of appropriate, and often complex, material properties is required. Some degree of confidence in the general applicability of these theoretical treatments must also be gained. With this virtual absence of well-documented case histories, detailed performance records from any structure founded on frozen or thawing soils will constitute welcome data. To obtain optimum benefit from information of this sort, it is essential that the results be analyzed and interpreted in a rational manner.

Almost any activity which enhances the geotechnical engineer's ability to understand and predict the behaviour of frozen or thawing soils is costly. At the same time, the expense involved with instrumentation, performance monitoring, or conducting large-scale field tests may be warranted if the costs defrayed by reducing the necessity for conservatism in design are sufficient. The most fruitful areas for future research in permafrost engineering probably relate to developing methods and equipment which are capable of improving both the quality and quantity of information collected during site investigations. Although less glamorous than developing elegant theoretical treatments, activities which are currently hindered by deficiency include drilling, sampling and logging procedures, downhole and surface geophysical methods, and in situ tests.

REFERENCES CITED

Akili, W. 1966. Stress effect on creep rates of a frozen clay soil from the standpoint of rate process theory. Unpubl. Ph.D. Thesis, Michigan State Univ., East Lansing, Michigan. 108 p. (University Microfilms 66-843)

Akili, W. 1970. On the stress-creep relationship for a frozen soil. Mat. Res. and Standards, 10(1), pp. 16-22.

Akili, W. 1971. Stress-strain behaviour of frozen fine-grained soils. Highway Res. Rec., No. 360, pp. 1-8.

Al-Dhahir, Z., Kennard, M.F., and Morgenstern, N.R. 1970. Observations on pore pressures beneath the ash lagoon embankments at Fiddler's Ferry power station. In Situ Investigations in Soils and Rocks, British Geotechnical Society, London, pp. 265-276.

Alkire, B.D. 1972. Mechanical properties of sand-ice materials. Unpubl. Ph.D. Thesis, Michigan State Univ., East Lansing, Michigan. 197 p. (University Microfilms 73-12, 656)

Alkire, B.D., and Andersland, O.B. 1973. The effect of confining pressure on the mechanical properties of sand-ice materials. J. Glaciol., 12(66), pp. 469-481.

Andersland, O.B., and Akili, W. 1967. Stress effect on creep rates in a frozen clay soil. Géotechnique, 17(1), pp. 27-3[illegible]

Andersland, O.B., and AlNouri, I. 1970. Time-dependent strength behaviour of frozen soils. Proc. ASCE, 96(SM4), pp. 1249-1265.

Anderson, D.M., Tice, A.R., and McKim, H.L. 1973. The unfrozen water and apparent specific heat capacity of frozen soils. In Permafrost: The North American Contribution to the 2nd International Conference, Yakutsk, pp. 289-295.

Anderson, D.M. 1967. The interface between ice and silicate surfaces. J. Colloid Interface Sci., Vol. 25, pp. 174-191.

Anderson, D.M., and Hoekstra, P. 1965. Migration of inter-lamellar water during freezing and thawing of Wyoming bentonite. Soil Sci. Soc. Am. Proc., Vol. 29, pp. 498-504.

Anderson, D.M., and Morgenstern, N.R. 1973. Physics, chemistry and mechanics of frozen ground: a review. In Permafrost: The North American Contribution to the 2nd International Conference, Yakutsk, pp. 257-288.

Anderson, D.M., and Tice, A.R. 1971. Low-temperature phases of interfacial water in clay-water systems. Soil Sci. Soc. Am. Proc., 35(1), pp. 47-54.

Anderson, D.M., and Tice, A.R. 1972. Predicting unfrozen water contents in frozen soils from surface area measurements. Highway Res. Rec., No. 393, pp. 12-18.

Anderson, D.M., and Tice, A.R. 1973. The unfrozen interfacial phase in frozen soil water systems. Ecological Studies, Vol. 4, pp. 107-124.

Baker, T.H.W. 1976. Transportation, preparation and storage of frozen soil samples for laboratory testing. In ASTM Spec. Tech. Publ. No. 599, pp. 88-112.

Baker, T.H.W., Frederking, R.M.W., and Hoffman, D.R. 1976. Performance characteristics of the geotechnical cold rooms. Building Research Note, NRC Canada, No. 109. 19 p.

Banin, A., and Anderson, D.M. 1974. Effects of salt concentration changes during freezing on the unfrozen water content of porous materials. Water Resour. Res., 10(1), pp. 124-128.

Barnes, P., and Tabor, D. 1966. Plastic flow and pressure melting in the deformation of ice. Nature, Vol. 210, No. 5039, pp. 878-882.

Barnes, P., Tabor, D., and Walker, J.C.F. 1971. The friction and creep of polycrystalline ice. Proc. Roy. Soc. London, Vol. 324A, pp. 127-155.

Bender, J.A. 1967. Deformation of excavations in a high polar névé. In Physics of Snow and Ice, H. Oura (Editor), Institute of Low Temp. Sci., Hokkaido Univ., Sapporo, Japan, Vol. 1, Part 2, pp. 973-982.

Bergan, A.T. 1972. Some considerations in the design of asphalt concrete pavements for cold regions. Unpubl. Ph.D. Thesis, University of California, Berkley. 333 p.

Bergan, A.T., and Fredlund, D.G. 1973. Characterization of freeze-thaw effects on subgrade soils. Presented to the Symposium on Frost Action on Roads, Organization for Economic Cooperation and Development, Oslo, Norway. (Research Report RP-4, Dept. Civil Eng., U. of Sask., Saskatoon).

Beskow, G. 1935. Soil freezing and frost heaving with special application to roads and railroads, Swed. Geol. Series C, 26th Yearbook, No. 3. (Translated from the original Swedish by J.O. Osterberg, Northwestern Univ., Evanston, Ill. 1947).

Bishop, A.W. 1954. The use of pore pressure coefficients in practice. Géotechnique, 4(4), pp. 148-152.

Bishop, A.W., and Bjerrum, L. 1960. The relevance of the triaxial test to the solution of stability problems. In Proc. ASCE Research Conf. on Shear Strength of Cohesive Soils, Boulder, Colorado, pp. 437-501.

Bishop, A.W., and Gibson, R.E. 1963. The influence of the provisions for boundary drainage on strength and consolidation characteristics of soils measured in the triaxial apparatus. In Laboratory Shear Testing of Soils, ASTM Spec. Tech. Publ. No. 361, pp. 435-451.

Bishop, A.W., and Green, G.E. 1965. Influence of end restraint on the compression strength of a cohesionless soil. Géotechnique, 15(3), pp. 243-265.

Bishop, A.W., and Henkel, D.J. 1962. The measurement of soil properties in the triaxial test (2nd Edition). Edward Arnold, London. 228 p.

Bishop, A.W., Webb, D.L., and Lewis, P.I. 1965. Undisturbed samples of London clay from the Ashford Common Shaft: strength-effective stress relationships. Géotechnique, 15(1), pp. 1-31.

Bishop, A.W., and Wesley, L.D. 1975. A hydraulic triaxial apparatus for controlled stress path testing. Géotechnique, 25(4), pp. 657-670.

Black, R.F. 1969. Thaw depressions and thaw lakes - a review. Biul. Peryglac., No. 19, pp. 131-150.

Blight, G.E. 1965. Shear stress and pore pressure in triaxial testing. Proc. ASCE, 91 (SM6), pp. 25-39.

Boulton, G.S. 1975. Processes and patterns of subglacial sedimentation: a theoretical review. In Ice Ages: Ancient and Modern, A.E. Wright and F. Mosely (Editors), Seel House Press, Liverpool, pp. 7-42.

Brewer, R. 1964. Fabric and mineral analysis of soils. John Wiley and Sons, New York. 470 p.

Brodskaia, A.G. 1962. Compressibility of frozen ground. Moscow, Izd-Vo Acad. Nauk SSR, pp. 2-83. (translated from the original Russian in 1970, U.S. Dept. Commerce, NTIS No. AD 715087)

Broms, B.B., and Yao, Y.C. 1964. Shear strength of a soil after freezing and thawing. Proc. ASCE, 90(SM4), pp. 1-25.

Brown, R.J.E. 1970. Permafrost in Canada. Univ. of Toronto Press, Toronto. 234 p.

Brown, W.G., and Johnston, G.H. 1970. Dykes on permafrost: predicting thaw and settlement. Can. Geotech. J., 7(4), pp. 365-371.

Budd, W.F. 1969. The dynamics of ice masses. Australian National Antarctic Research Expeditions Scientific Reports, Series A(IV), Glaciology Publ. No. 108. 216 p.

Burt, T.P., and Williams, P.J. 1976. Hydraulic conductivity in frozen soils. Earth Surface Processes, Vol. 1, pp. 349-360.

Butkovich, T.R., and Landauer, J.K. 1959. The flow law for ice. SIPRE Res. Rept. No. 56. 7 p.

Butkovich, T.R., and Landauer , J.K. 1960. Creep of ice at low stresses. SIPRE Res. Rept. No. 72. 6 p.

Canadian Arctic Gas Pipelines Limited. 1974. Responses to Pipeline Assessment Group requests for supplementary information, Toronto.

Chamberlain, E. 1969. Some triaxial shear strength tests on frozen soil and ice. U.S. Army CRREL, Draft Interim Technical Report. 32 p.

Chamberlain, E., Groves, C., and Perham, R. 1962. The mechanical behaviour of frozen earth materials under high pressure triaxial test conditions. Géotechnique, 22(3), pp. 469-483.

Chandler, R.J. 1969. The effect of weathering on the shear strength properties of Keuper Marl. Géotechnique, 19(3), pp. 321-334.

Chandler, R.J. 1972. Lias clay: weathering processes and their effect on shear strength. Géotechnique, 22(3), pp. 403-431.

Colbeck, S.C. 1970. The flow law for temperate glacier ice. Unpub. Ph.D. Thesis, Univ. of Washington, Seattle, Washington. 149 p. (University Microfilms 71-16,934)

Colbeck, S.C., and Evans, R.F. 1973. A flow law for temperate glacier ice. J. Glaciol., 12(64), pp. 71-86.

Collins, K., and McGown, A. 1974. The form and function of microfabric features in a variety of natural soils. Géotechnique, 24(2), pp. 223-254.

Conway, J.B. 1967. Numerical methods for creep and rupture analyses. Gordon and Breach Science Publishers, New York. 204 p.

Dillon, H.B., and Andersland, O.B. 1967. Deformation rates of polycrystalline ice. In Physics of Snow and Ice, H. Oura (Editor), Institute of Low Temp. Sci., Hokkaido Univ., Sapporo, Japan, Vol. 1, Part 1, pp. 313-328.

Drost-Hansen, W. 1967. The water-ice interface as seen from the liquid side. J. Colloid Interface Sci. Vol. 25, pp. 131-160.

Duncan, J.M., and Dunlop, P. 1968. The significance of cap and base restraint. Proc. ASCE, 94 (SM1), pp. 271-290.

Emery, J.J., and Nguyen, T.Q. 1974. Simulation of ice flow problems. In Applications of Solid Mechanics, 2nd Symposium (CSME-CSCE-ASME) McMaster University, Vol. 1, pp. 30-45.

Farrar, D.M., and Coleman, J.D. 1967. The correlation of surface area with other properties of nineteen British clay soils. J. Soil Sci., 18(1), pp. 118-124.

Fredlund, D.G., Bergan, A.J., and Sauer, E.K. 1975. Deformation characterization of subgrade soils for highways and runways in northern environments. Can. Geotech. J., 12(2), pp. 213-223.

Fukuo, Y. 1966. On the rheological behaviour of frozen soil (Part 1). Bull. Dis. Prev. Res. Inst. (Kyoto U.), 15(3), pp. 1-7.

Gerrard, J.A.F., Perutz, M.F., and Roch, A. 1952. Measurement of the velocity distribution along a vertical line through a glacier, Proc. Roy. Soc. London, Vol. 213A, pp. 546-558.

Glen, J.W. 1952. Experiments on the deformation of ice. J. Glaciol., 2(12), pp. 111-114.

Glen, J.W. 1955. The creep of polycrystalline ice. Proc. Roy. Sci. London, Vol. 228A, pp. 519-538.

Goughnour, R.R., and Andersland, O.B. 1968. Mechanical properties of a sand-ice system. Proc. ASCE, 94(SM4), pp. 923-950.

Guther, H. 1972. Some problems in non-homogenous seepage. Unpubl. M.Sc. Thesis, Univ. of Alberta, Edmonton, Alberta.

Heiner, A. 1972. Strength and compaction properties of frozen soil. National Swedish Building Research Document D11.1972. 116 p.

Henkel, D.J., and Sowa, V.A. 1963. The influence of stress history on stress paths in undrained triaxial tests on clay. In Laboratory Shear Testing of Soils, ASTM Spec. Tech. Publ. No. 361, pp. 280-291.

Hobbs, P.V. 1974. Ice Physics, Clarendon Press, Oxford. 837 p.

Hoekstra, P. 1969. The physics and chemistry of frozen soils. Highway Res. Board Spec. Rept. No. 103, pp. 78-90.

Hooke, R.L., Dahlin, B.B., and Kauper, M.T. 1972. Creep of ice containing fine sand. J. Glaciol., 11(63), pp. 327-336.

Hughes, O.L. 1974. Geology and permafrost in relation to hydrology and geophysics. In Permafrost Hydrology, Proceedings of a Workshop Seminar, Can. Nat. Comm. Int. Hydrological Decade, Environment Canada, pp. 21-28.

Hughes, O.L., Veillette, J.J., Pilion, J., and Hanley, P.T. 1973. Terrain evaluation with respect to pipeline construction, Mackenzie Transportation Corridor, Central Part, Lat. 64° to 68° N. Environmental-Social Committee, Northern Pipelines, Task Force on Northern Oil Development, Report No. 73-37. 74 p.

Hult, J.A.H. 1966. Creep in engineering structures. Blaisdell Publ. Co., Waltham, Massachusets, 115 p.

Hunter, J.A., and Veillette, J. 1976. Borehole density logging in permafrost, Tuktoyaktuk, District of Mackenzie. GSC Paper 76-1A, Report of Activities, p. 417.

Hwang, C.T., Murray, D.W., and Brooker, E.W. 1972. A thermal analysis for structures on permafrost, Can. Geotech. J., 9(1), pp. 33-46.

Iverson, K, and Moum, J. 1974. The paraffin method - triaxial testing without a rubber membrane. Géotechnique, 24(4), pp. 665-670.

Janbu, N., and Senneset, K. 1973. Field compressometer - principles and applications. Proc. 8th Int. Conf. Soil Mech. Found. Eng., Moscow, Vol. 1-1, pp. 191-198.

Jellinek, H.H.G. 1967. Liquid-like (transition) layer on ice. J. Colloid Interface Sci., Vol. 25, pp. 192-205.

Johnston, G.H. 1969. Dykes on permafrost, Kelsey Generating Station, Manitoba, Can. Geotech. J., 6(2), pp. 139-157.

Kaplar, C.W. 1965. Discussion of 'Shear strength of a soil after freezing and thawing' by B.B. Broms and Y.C. Yao. Proc. ASCE, 91(SM2), pp. 91-97.

Kazi, A., and Knill, J.L. 1969. The sedimentation and geotechnical properties of the Cromer Till between Happisburgh and Cromer, Norfolk. Quart. J. Eng. Geol., Vol. 2, pp. 63-86.

Keil, L.D., Neilsen, N.M., and Gupta, R.C. 1973. Thaw-consolidation of permafrost dyke foundations at the Long Spruce Generating Station. Preprints, 26th Can. Geotech. Conf., Toronto, pp. 134-141.

Kent, D.D. 1974. State variables for partly frozen soil. Unpubl. M.Sc. Thesis, Univ. of Sask., Saskatoon, Sask.. 161 p.

Kent, D.D., Fredlund, D.G., and Watt, W.G. 1975. Variables controlling behaviour of a partly frozen saturated soil. In Proc. Conf. on Soil Water Problems in Cold Regions, Calgary, Alberta. Special Task Force, Div. Hydrology, Am. Geophys. Union, pp. 70-88.

Kersten, M.S. 1949. Thermal properties of soils. Univ. of Minnesota, Eng. Exp. Station Bull. No. 28. 227 p.

Keys, W.S. 1968. Geophysical logging of permafrost, Fairbanks, Alaska - a feasibility study. USGS Tech. Mem. No. 24. 5p.

Keys, W.S., and MacCary, L.M. 1971. Application of borehole geophysics to water-resources investigations. Chapter E1, Book 2, Collection of Environmental Data, Techniques of Water-Resources Investigations of the USGS. 126 p.

Koch, R.D. 1971. The design of Alaskan North Slope production wells. Proc. Inst. Mech. Eng. (London), Vol. 185, pp. 989-1001.

Lachenbruch, A.H. 1970. Some estimates of the thermal effects of a heated pipeline in permafrost. U.S.G.S. Circular 632. 23 p.

Ladanyi, B. 1970. The mechanics of landslides in Leda clay: Discussion. Can. Geotech. J., 7(4), pp. 506-507.

Ladanyi, B. 1972. An engineering theory of creep of frozen soils. Can. Geotech. J., 9(1), pp. 63-80.

Ladanyi, B. 1974. Bearing capacity of frozen soils. Preprints, 27th Can. Geotech. Conf., Edmonton, pp. 97-107.

Ladanyi, B. 1975. Bearing capacity of strip footings in frozen soils. Can. Geotech. J., 12(3), pp. 393-407.

Ladanyi, B. and Archambeault, G. 1969. Simulation of shear behaviour of a jointed rock mass. 11th Symp. Rock Mech. at Berkley, Ca., Soc. Mining Eng., AIME, New York, pp. 105-125.

Ladanyi, B. and Johnston, G.H. 1973. Evaluation of in situ creep properties of frozen soils with the pressuremeter. In Permafrost: The North American Contribution to the 2nd International Conference, Yakutsk, pp. 310-319.

Ladanyi, B. and Johnston, G.H. 1974. Behaviour of circular footings and plate anchors in permafrost. Can. Geotech. J., 11(4), pp. 531-553.

Lambe, T.W., and Whitman, R.V. 1969. Soil Mechanics. John Wiley and Sons, New York. 553 p.

Langdon, T.G. 1973. Creep mechanisms in ice. In Proc. Symp. Phys. and Chem. of Ice, E. Whalley, S.J. Jones, and L.W. Gold (Editors), Roy. Soc. Can., Ottawa. pp. 356-361.

Lau, J.S.O., and Lawrence, D.W. 1976. Winter ground-ice distribution for selected map areas, Mackenzie Valley. In Report of Activities, Geological Survey of Canada, Paper 76-1B, pp. 161-168.

Lee, K.L., Morrison, R.A., and Haley, S.C. 1969. A note on the pore pressure parameter B. 7th Int. Conf. Soil Mech. Found. Eng., Mexico City, Vol. 1, pp. 231-238.

Linell, K.A., and Johnston, G.H. 1973. Engineering design and construction in permafrost regions: a review. In Permafrost: The North American Contribution to the 2nd International Conference, Yakutsk, pp. 553-576.

Litvinov, A. Ya. 1966. Field determination of the overall moisture content of frozen ground with thick streaks of ice. Soil Mech. Found. Eng., No. 3 (May-June), pp. 184-185.

Lo, K.Y. 1970. The operational strength of fissured clays. Géotechnique, 20(1), pp. 57-74.

MacDonald, D.H. 1963. Design of Kelsey dikes. In Permafrost: Proceedings of an International Conference, National Academy of Sciences, Washington, D.C., pp. 492-496.

MacKay, J.R. 1963. The Mackenzie Delta area, N.W.T. Can. Dept. Mines Tech. Surv., Geog. Br., Mem. 8. 202 p. (republished as Geological Survey of Canada Misc. Report 23, 1974)

MacKay, J.R. 1971. The origin of massive icy beds in permafrost, Western Arctic Coast, Canada. Can. J. Earth Sci., 8(4), pp. 397-422.

MacKay, J.R. 1972a. The world of underground ice. Ann. Assoc. Am. Geogr., 62(1), pp. 1-22.

Mackay, J.R. 1972b. Offshore permafrost and ground ice, Southern Beaufort Sea, Canada. Can. J. Earth Sci., 9(11), pp. 1550-1561.

MacKay, J.R. 1974. Reticulate ice veins in permafrost, Northern Canada. Can. Geotech. J., 11(2), pp. 230-237.

MacKay, J.R. 1975. Reticulate ice veins in permafrost, Northern Canada: Reply. Can. Geotech. J., 12(1), pp. 163-165.

MacKay, J.R., and Matthews, W.H. 1973. Geomorphology and Quaternary history of the Mackenzie valley near Fort Good Hope, N.W.T., Canada. Can. J. Earth Sci., 10(1), pp. 26-41.

MacPherson, J.G., Watson, G.H. and Koropatnick, A. 1970. Dykes on permafrost foundations in northern Manitoba. Can. Geotech. J., 7(4), pp. 356-364.

Marsland, A. 1972. The shear strength of stiff fissured clays. In Stress Strain Behaviour of Soils, R. Parry (Editor), G.T. Foulis Ltd., Henley-on-Thames, pp. 56-68.

Marsland, A., and Butler, M.E. 1967. Strength measurements on stiff Barton clay from Fawley, Hampshire. Proc. Geot. Conf., Oslo, Vol. 1, pp. 139-146.

Martin, R.T. 1959. Rhythmic ice banding in soils. Highway Res. Board Bull. 218, pp. 11-23.

Martin, R.T. 1962. Adsorbed water on clay: a review. Proc. 9th Conf. Clays and Clay Minerals, Pergamon Press, New York, pp. 28-70.

McGown, A., and Radwan, A.M. 1975. The presence and influence of fissures in the boulder clays of West Central Scotland. Can. Geotech. J., 12(1), pp. 84-97.

McKay, A.S., and O'Connel, L.P. 1976. The permafrost density logger. J. Can. Petrol. Tech., 15(1), pp. 69-74.

McRoberts, E.C. 1973. Stability of slopes in permafrost. Unpubl. Ph.D. Thesis, Univ. Alberta, Edmonton. 370 p.

McRoberts, E.C. 1975. Some aspects of a simple secondary creep model for deformations in permafrost slopes. Can. Geotech. J., 12(1), pp. 98-105.

McRoberts, E.C. 1975. Field observations of thawing in soils. Can. Geotech. J., 12(1), pp. 126-130.

McRoberts, E.C., and Morgenstern, N.R. 1973. A study of landslides in the vicinity of the Mackenzie River, Mile 205 to 660. Environmental-Social Committee, Northern Pipelines, Task Force on Northern Oil Development, Report No. 73-35. 96 p.

McRoberts, E.C., and Morgenstern, N.R. 1974a. The stability of thawing slopes. Can. Geotech. J., 11(4), pp. 447-469.

McRoberts, E.C., and Morgenstern, N.R. 1974b. Stability of slopes in frozen soil, Mackenzie Valley, N.W.T. Can. Geotech. J., 11(4), pp. 554-573.

Meier, M.F. 1960. Mode of flow of the Saskatchewan glacier, Alberta, Canada. U.S.G.S. Paper 351. 70 p.

Mellor, M. 1969. The stress dependence of the secondary creep rate at low stresses: reply to Prof. J. Weertman's letter. J. Glaciol., 8(54), p. 495 (Letter).

Mellor, M., and Smith, J.B. 1967. Creep of snow and ice. In Physics of Snow and Ice, H. Oura (Editor), Institute of Low Temp. Sci., Hokkaido Univ., Sapporo, Japan, Vol. 1, Part 2, pp. 843-855.

Mellor, M., and Testa, R. 1969a. Effect of temperature on the creep of ice. J. Glaciol., 8(52), pp. 131-145.

Mellor, M., and Testa, R. 1969b. Creep of ice under low stress. J. Glaciol., 8(52), pp. 147-152.

Mitchell, J.K. 1976. Fundamentals of Soil Behaviour. John Wiley and Sons, New York. 422 p.

Mitchell, J.K., Campanella, R.G., and Singh, A. 1968. Soil creep as a rate process. Proc. ASCE, 94(SM1), pp. 231-253.

Mitchell, R.J. 1975. Strength parameters for permafrost slopes in Champlain Sea clays. Can. Geotech. J., 12(4), pp. 447-455.

Morgenstern, N.R. 1967. Shear strength of stiff clay. Proc. Geot. Conf., Oslo, Vol. 2, pp. 59-72.

Morgenstern, N.R. 1969. Specialty session on 'Structural and Physico-chemical Effects on the Properties of Clays'. 7th Int. Conf. Soil Mech. Found. Eng., Mexico City, Vol. 3, pp. 445-471.

Morgenstern, N.R., and Guther, H. 1972. Seepage into an excavation possessing stress-dependent permeability. Proc. Symp. on Percolation Through Fissured Rocks, Karlsruhe, T2-C, 15 p.

Morgenstern, N.R., and Nixon, J.F. 1971. One-dimensional consolidation of thawing soils. Can. Geotech. J., 8(4), pp. 558-565.

Morgenstern, N.R., and Nixon, J.F. 1975. An analysis of the performance of a warm-oil pipeline in permafrost, Inuvik, N.W.T. Can. Geotech. J., 12(2), pp. 199-208.

Morgenstern, N.R., and Smith, L.B. 1973. Thaw-consolidation tests on remoulded clays. Can. Geotech. J., 10(1), pp. 25-40.

Morgenstern, N.R., and Tchalenko, J.S. 1967a. Microscopic structures in kaolin subjected to direct shear. Géotechnique, 17(4), pp. 309-328.

Morgenstern, N.R., and Tchalenko, J.S. 1967b. Micro-structural observations in shear zones from slips in natural clays. Proc. Geot. Conf., Oslo, Vol. 1, pp. 147-152.

Nersesova, Z.A., and Tsytovich, N.A. 1963. Unfrozen water in frozen soils. In Permafrost: Proceedings of an International Conference, National Academy of Sciences, Washington, D.C., pp. 230-234.

Neuber, H., and Wolters, R. 1970. Mechanical behaviour of frozen soils under triaxial compression. (In German). Fortsch. Geol. Rheinld u. Westf., Krefeld, Germany, No. 17, pp. 499-536.

Nixon, J.F. 1973. The consolidation of thawing soils. Unpubl. Ph.D. Thesis, Univ. Alberta, Edmonton, Alberta. 300 p.

Nixon, J.F., and McRoberts, E.C. 1973. A study of some factors affecting the thawing of frozen soils. Can. Geotech. J., 10(3), pp. 439-452.

Nixon, J.F., and McRoberts, E.C. 1976. A design approach for pile foundations in permafrost. Can. Geotech. J., 13(1), pp. 40-57.

Nixon, J.F., and Morgenstern, N.R. 1973a. Practical extensions to a theory of consolidation for thawing soils. In Permafrost: The North American Contribution to the 2nd International Conference, Yakutsk, pp. 367-377.

Nixon, J.F., and Morgenstern, N.R. 1974. Thaw-consolidation tests on undisturbed fine-grained permafrost. Can. Geotech. J., 11(1), pp. 202-214.

Nye, J.F. 1953. The flow law of ice from measurements in glacier tunnels, laboratory experiments and the Junfraufirn borehole experiments. Proc. Roy. Soc. London, Vol. 219A, pp. 477-489.

Nye, J.F. 1957. The distribution of stress and velocity in glaciers and ice sheets. Proc. Roy. Soc. London, Vol. 239A, pp. 113-133.

Nye, J.F. 1965. The flow of a glacier in a channel of rectangular, elliptic or parabolic cross section. J. Glaciol., 5(41), pp. 661-690.

Odquist, F.K.G. 1966. Mathematical theory of creep and creep rupture. Oxford Mathematical Monograph, Clarendon Press, Oxford. 168 p.

Osterkamp, T.E. 1975. Structure and properties of ice lenses in frozen ground. In Proc. Conf. on Soil Water Problems in Cold Regions, Calgary, Alberta, Canada. Special Task Force, Div. Hydrology, Am. Geophys. Union, pp. 89-111.

Palmer, A.C. 1972. Settlement of a pipeline on thawing permafrost. Proc. ASCE, 98(TE3), pp. 477-491.

Palmer, A.C. 1973. Thawing and differential settlement close to oil wells through permafrost. In Principles of the control of cryogenic processes during the development of permafrost regions, Yakutsk Book Press, Yakutsk, Russia, pp. 161-170.

Paterson, W.S.B., and Savage, J.C. 1963. Measurements of the Athabasca Glacier relating to the flow law of ice. J. Geophys. Res., 68(15), pp. 4537-4543.

Penner, E. 1961. Ice-grain structure and crystal orientation in an ice lens from Leda clay. Bull. Geol. Soc. Am., Vol. 72, pp. 1575-1578.

Penner, E., Johnston, G.H., and Goodrich. L.E. 1975. Thermal conductivity laboratory studies of some Mackenzie Highway soils. Can. Geotech. J., 12(3), pp. 271-288.

Pemcan Services. 1972. Norman Wells Natural Gas Pipeline Research Facility - Subsurface Conditions. Report to Gas Arctic Systems Study Group.

Perkins, T.K., and Ruedrich, R.A. 1973. The mechanical behaviour of synthetic permafrost. Soc. Petroleum Engineers Journal (AIME), 13(8), pp. 211-220.

Pihlainen, J.A., and Johnston, G.H. 1963. Guide to a field description of permafrost for engineering purposes. Tech. Mem. 79, NRC 7576, Assoc. Com. on Soil and Snow Mechanics, Nat. Res. Council Canada.

Pufahl, D.E. 1976. The behaviour of thawing slopes in permafrost. Unpubl. Ph.D. Thesis, University of Alberta, Edmonton, Alberta. 323 p.

Pufahl, D.E., Morgenstern, N.R., and Roggensack, W.D. 1974. Observations on recent highway cuts in permafrost. Environmental-Social Committee, Northern Pipelines, Task Force on Northern Oil Development, Report No. 74-32. 53 p.

Rampton, V.N. 1972. Surficial geology and landforms of Aklavik (107B-E1/2). G.S.C. Open File Map 119.

Rampton, V.N. 1974. Terrain evaluation with respect to pipeline construction, Mackenzie Transportation Corridor, Northern Part, Lat. 68°N to Coast. Environmental-Social Committee, Northern Pipelines, Task Force on Northern Oil Development, Report No. 73-47. 44 p.

Rampton, V.N. 1974. The influence of ground ice and thermokarst upon the geomorphology of the Macknezie-Beaufort Region. In Third Guelph Symposium on Geomorphology, Arctic and Alpine Processes, pp. 43-59.

Raymond, C.F. 1973. Inversion of flow measurements for stress and rheological parameters in a valley glacier. J. Glaciol., 12(64), pp. 19-44.

Roggensack, W.D. 1975. Large scale laboratory direct shear tests on ice. Can. Geotech. J., 12(2), pp. 169-178.

Rosenquist, I.Th. 1959. Mechanical properties of soil-water systems. Proc. ASCE, 85(SM2), pp. 41-53.

Rowe, P.W. 1970. Representative sampling in location, quality and size. Sampling Soil and Rock, ASTM Spec. Tech. Publ. No. 483, pp. 77-106.

Rowe, P.W. 1972. The relevance of soil fabric to site investigation practice. Geotechnique, 22(2), pp. 195-300.

Rowe, P.W., and Barden, L. 1964. Importance of free ends in triaxial testing. Proc. ASCE, 90(SM4), pp. 1-27.

Rowley, R.K., Watson, G.H., Wilson, T.M., and Auld, R.G. 1973. Performance of a 48-in. warm-oil pipeline supported on permafrost. Can. Geotech. J., 10(2), pp. 282-303.

Ruedrich, R.A., and Perkins, T.K. 1973. A study of factors which influence the mechanical properties of deep permafrost. Paper No. SPE-4587, Presented at 48th Ann. Fall Meeting Soc. Pet. Eng. of AIME, Las Vegas, Nevada. 15 p.

Rutter, N.W., Boydell, A.N., Savigny, K.W., and Everdingen, R.O. 1973. Terrain evaluation with respect to pipeline construction, Mackenzie Transportation Corridor, Southern Part, Lat. 60° to 64°N. Environmental-Social Committee, Northern Pipelines, Task Force on Northern Oil Development, Report No. 73-36. 135 p.

Sanger, F.J. 1969. Foundations of structures in cold regions. Cold Regions Science and Engineering Monograph III-C4, U.S. Army CRREL. 91 p. (Presently under revision)

Sanger, F.J., and Kaplar, C.W. 1963. Plastic deformation of frozen soils. In Permafrost: Proceedings of an International Conference, National Academy of Sciences, Washington, D.C., pp. 305-314.

Sayles, F.H. 1968. Creep of frozen sands. U.S. Army CRREL Tech. Rept. 190. 54 p.

Sayles, F.H. 1973. Triaxial and creep tests on frozen Ottawa sand. In Permafrost: The North American Contribution to the 2nd International Conference, Yakutsk, pp. 384-391.

Sayles, F.H., and Haines, D. 1974. Creep of frozen silt and clay, U.S. Army CRREL Tech. Rept. 252. 50 p.

Scott. R.F. 1969. The freezing process and mechanics of frozen ground. Cold Regions Science and Engineering Monograph II-D1, U.S. Army CRREL. 65 p.

Schreve, R.L., and Sharp, R.P. 1970. Internal deformation and thermal anomalies in lower Blue Glacier, Mount Olympus, Washington, D.C., J. Glaciol., 9(55), pp. 65-86.

Simons, N.E. 1960. The effect of overconsolidation on the shear strength characteristics of an undisturbed Oslo clay. Proc. ASCE Research Conf. on Shear Strength of Cohesive Soils, Boulder, Colorado, pp. 747-763.

Skempton, A.W. 1953. The colloidal 'activity' of clays. Proc. 3rd Int. Conf. Soil Mech. Found. Eng., Zurich, Vol. 1, pp. 57-61.

Skempton, A.W. 1954. The pore-pressure coefficients A and B. Géotechnique, 4(4), pp. 143-147.

Skempton, A.W. 1970. The consolidation of clays by gravitational compaction. Q. Jl. Geol. Soc. London, Vol. 125, pp. 373-411.

Skempton, A.W., and Bishop, A.W. 1954. Soils. In Building Materials, Their Elasticity and Inelasticity. Ed. by M. Reiner with the assistance of A.G. Ward, Amsterdam, North-Holland Publishing Co., Chapter X, pp. 417-482.

Skempton, A.W., and Bjerrum, L. 1957. A contribution to settlement analysis of foundations on clay. Géotechnique, 7(4), pp. 168-178.

Skempton, A.W., and Pettey, D.J. 1967. The strength along structural discontinuities in stiff clays. Proc. Geot. Conf., Oslo, Vol. 2, pp. 29-46.

Skempton, A.W., and Pettey, D.J. 1970. Ignition loss and other properties of peats and clays from Avonmouth, King's Lynn, and Cranberry Moss. Géotechnique, 20(4), pp. 343-356.

Skempton, A.W. and Sowa, V.A. 1963. The behaviour of saturated clays during sampling and testing. Géotechnique, 13(4), pp. 269-290.

Slusarchuk, W.A., and Watson, G.H. 1975. Thermal conductivity of some ice-rich permafrost soils. Can. Geotech. J., 12(3), pp. 413-424.

Slusarchuk, W.A., Watson, G.H., and Speer, T.L. 1973. Instrumentation around a warm oil pipeline buried in permafrost. Can. Geotech. J., 10(2), pp. 227-245.

Smith, N., and Berg, R. 1973. Encountering massive ground ice during road construction in Central Alaska. In Permafrost: The North American Contribution to the 2nd International Conference, Yakutsk, pp. 730-736.

Snow, D.T. 1967. Anisotropic permeability of fractured rocks. In Hydrology and Flow through Porous Media (Muskat Volume). R.J.M. DeWiest (Editor), Academic Press, New York.

Speer, T.L., Watson, G.H., and Rowley, R.K. 1973. Effects of ground-ice variability and resulting thaw settlements on buried oil pipelines. In Permafrost: The North American Contribution to the 2nd International Conference, Yakutsk, pp. 746-752.

Smith, L.B. 1972. Thaw consolidation tests on remoulded clays. Unpubl. M.Sc. Thesis, Univ. of Alberta, Edmonton, Alberta. 157 p.

Steinemann, S. 1958. Experimentelle Untersuchunger zur Plastizitat von Eis. Beitrage zur Geologie de Schweiz, Geotechnische Serie Hydrologie, Nr. 10.

Susherina, Ye P., and Tsytovich, N.A. 1967. Experiments on the effects of freezing and subsequent thawing on clay strength. U.S. Army CRREL Draft Translation 285. 14 p. (Translated from original Russian in 1971)

Swinzow, G.K. 1962. Investigation of shear zones in the ice sheet margin, Thule area, Greenland. J. Glaciol., 4(32), pp. 215-229.

Sykes, J.F., Lennox, W.C., and Charlwood, R.G. 1974. Finite element permafrost thaw settlement model. Proc. ASCE, 100 (GT11), pp. 1185-1201.

Sykes, J.F., Lennox, W.C., and Unny, T.E. 1974. Two-dimensional heated pipeline in permafrost. Proc. ASCE, 100(GT11), pp. 1203-1214.

Taber, S. 1929. Frost heaving. J. Geol., Vol. 37, pp. 428-461.

Tabor, D., and Walker, J.C.F. 1970. Creep and friction of ice. Nature, Vol. 228, pp. 137-139.

Tchalenko, J.S. 1968. The evolution of kink-bands and the development of compression textures in sheared clays. Tectonophysics, Vol. 16, pp. 159-174.

Terzaghi, K. 1936. The shearing resistance of saturated soil and the angle between planes of shear. Proc. 1st Int. Conf. Soil Mech. Found. Eng., Harvard, Vol. 1, pp. 54-56.

Terzaghi, K. 1960. Discussion of 'Rockfill dams, Wishon and Courtright concrete face dams' by J.B. Cooke. Proc. ASCE, 86(PO1), pp. 89-92.

Thomas, R.H. 1971. Flow law for Antarctic ice shelves. Nature (Phys. Sci.), Vol. 232, pp. 85-87.

Thomas, R.H. 1973a. The creep of ice shelves: theory. J. Glaciol., 12(64) pp. 45-53.

Thomas, R.H. 1973b. The creep of ice shelves: interpretation of observed behaviour. J. Glaciol., 12(64), pp. 55-70.

Thompson, E.G., and Sayles, F.H. 1972. In situ creep analysis of room in frozen soil. Proc. ASCE, 98(SM9), pp. 899-915.

Thomson, S., and Lobacz, E.F. 1973. Shear strength at a thaw interface. In Permafrost: The North American Contribution to the 2nd International Conference, Yakutsk, pp. 419-426.

Tice, A.R., Anderson, D.M., and Banin, A. 1973. The prediction of unfrozen water contents in frozen soils from liquid limit determinations. Symposium on Frost Action in Roads, Oslo, Organization for Economic Cooperation and Development, Vol. 1, pp. 329-344, and Vol. 3, pp. 63-65.

Tsytovich, N.A. 1973. Mechanics of frozen soil. Vysshaya Shkda Press, Moscow. 427 p. (Russian translated and published under the title 'The Mechanics of Frozen Ground' (1975), McGraw-Hill, New York)

Tsytovich, N.A., Vyalov, S.S., Martynov, G.A., and Susherina, Ye.P. 1957. Changes in soil properties on freezing and thawing. U.S. Army CRREL Draft Translation No. 329. 31 p. (Translated from the original Russian in 1971).

Tsytovich, N.A., Zaretsky, Yu.K., Grigoryeva, U.G., and Ter-Martirosyan, Z.G. 1965. Consolidation of thawing soils. Proc. 6th Int. Conf. Soil Mech. and Found. Eng., Toronto, Vol. 1, pp. 390-394.

Ueda, H., Sellman, P., and Gunars, A. 1975. USA CRREL snow and ice testing equipment. CRREL Spec. Rept. 146. 14p.

Vialov, S.S. (Ed.) 1959. Rheological properties and bearing capacity of frozen soils. U.S. Army CRREL Tran. No. 74. 219 p. (Translated from the original Russian in 1965)

Vialov, S.S. (Ed.) 1962. The strength and creep of frozen soils and calculations for ice-soil retaining structures. U.S. Army CRREL Tran. No. 76. 301 p. (Translated from the original Russian in 1965)

Vialov, S.S., and Susherina, Ye. P. 1964. Resistance of frozen soils to triaxial compression. Merzlotnye Issledovaniya, No. 4, pp. 340-375. (Translated from the original Russian in 1970 by the U.S. Army Foreign Science and Technology Center, NTIS No. AD 713981)

Vodolazkii, U.M. 1962. Strength characteristics of thawed clayey ground at various stages of consolidation. U.S. Army CRREL Draft Translation No. 267. 10 p. (Translated from the original Russian in 1971)

Voitkovski, K.F. 1960. The mechanical properties of ice. Moscow Izd. Akademii Navk, S.S.R. 100 p. (Translated from the original Russian by the Am. Meteor. Soc., Boston)

Watson, G.H., Rowley, R.K., and Slusarchuk, W.A. 1973a. Performance of a warm oil pipeline buried in permafrost. In Permafrost: The North American Contribution to the 2nd International Conference, Yakutsk, pp. 759-766.

Watson, G.H., Slusarchuk, W.A., and Rowley, R.K. 1973b. Determination of some frozen and thawed properties of permafrost soils. Can. Geotech. J., 10(4), pp. 592-606.

Weertman, J. 1969. The stress dependence of the secondary creep rate at low stresses. J. Glaciol., 8(54), pp. 494-495 (Letter).

Weertman, J. 1973. Creep of ice. In Proc. Symp. Phys. and Chem. of Ice. E. Whalley, S.J. Jones, and L.W. Gold (Editors). Roy. Soc. Can. Ottawa, pp. 320-337.

Williams, P.J. 1963. Specific heats and unfrozen water content of frozen soils. Proc. 1st Can. Conf. on Permafrost, NRC Tech. Mem. 76, pp. 109-126.

Williams, P.J. 1964. Experimental determination of apparent specific heats of frozen soils. Géotechnique, 14(2), pp. 133-142.

Williams, P.J., and Burt, T.P. 1974. Measurement of hydraulic conductivity of frozen soils. Can. Geotech. J., 11(4), pp. 647-650.

Wilson, S.D. 1959. Report on the 1958 Tuto ramp slope indicator measurements. Report prepared by Shannon and Wilson for U.S. Army Corps of Engineers.

Wissa, A.E.Z. 1969. Pore pressure measurement in saturated soils. Proc. ASCE, 90(SM4), pp. 1063-1073.

Woodward-Clyde and Associates. 1970. Thaw plug stability in the Copper River Basin, Report prepared for Aleyeska Pipeline Service Co. Ltd., Houston, Texas.

Wu, T.H. 1966. Soil mechanics. Allyn and Bacon, Inc., Boston. 431 p.

Yong, R.N., and Warkentin, 1966. Introduction to Soil Behaviour. The MacMillan Company, New York. 451 p.

Zaretskii, Yu.K. 1968. Calculations of the settlement of thawing soil. Soil Mechanics and Foundation Engineering, No. 3 (May-June), pp. 151-155.

APPENDICES

APPENDIX A
FIELD WORK

A.1 SAMPLING EQUIPMENT AND PROCEDURES

Each of the permafrost cores tested in this study was obtained with a shell auger core barrel. Sampling devices used in the field work were manufactured in the Department of Civil Engineering Machine Shop, University of Alberta, and were patterned after the USA-CRREL ice auger. Over the past 15 years, the CRREL ice auger has been used throughout the cold regions of the world for sampling in snow, ice, and frozen organic and fine-grained mineral soils (Ueda, 1975). Figure A.1 presents a sketch of the double helical auger core barrel and summarizes its basic features (also see Plate A.24). The core barrels used to obtain samples for the laboratory program described in the body of this thesis were all constructed to provide a 10 cm (4 inch) inside diameter. Modifications to models which had been used previously included:

1) Eliminating the outside drive collar at the top of the barrel, thus promoting the movement of the cuttings up the flites to where they could be reservoired.
2) Redesigning the cutting teeth and using case-hardened steel instead of attaching tungsten carbide inserts to the leading edge.
3) Providing a convenient bayonet drive connection on barrels used in hand sampling operations.
4) Constructing the core barrels from stainless steel tubing.
5) Thickening, and thereby strengthening the core barrel at its top by providing an inside collar where the drive head is attached.

To promote rapid core barrel penetration in fine-grained permafrost soils, the angle between the front surface of the cutting edge and surface being cut was set at 55°. A positive back clearance angle of between 30° and 35° was adopted. With this configuration, cutting was most effective when a back clearance of approximately 0.5 cm (0.2 inches) was maintained. A small inside clearance of up to 0.03 cm (0.01 inches) was provided by setting the cutting teeth to overlap the inside surface of the core barrel. These teeth were made from case-hardened Keewatin tool steel and exhibited good wear characteristics when cutting fine-grained frozen soils. In sandier materials, it remained necessary to use tungsten carbide inserts soldered onto the cutting face, but a great deal of breakage was experienced when stones were encountered. More recent experience with seismic grade inserts has indicated that their greater durability renders them satisfactory for this particular application. Some of the hardened teeth were field-sharpened with a grinder when the cutting edge became dull. They proved to be quite durable in cutting through soil which contained a few pebbles, and suffered less breakage than the earlier carbide inserts had. A core catcher was not provided since cuttings normally jammed into the gap between the core and the inside of the barrel. Inside friction built up until the core broke off, and also held it in the barrel during extraction from the borehole. Whenever a mechanical break did not occur during the coring run, the cores were separated at the cutting face by jarring the core barrel or pushing a wedge into the annulus to snap the core with a cantilivering action. The core barrel was then run down the borehole to extract the loose piece of core.

At the Fort Simpson landslide headscarp sampling site, core barrels were turned with a gasoline-driven post-augering unit that could be handled by two men (see Plate A.22). The auger frame was 1.2 m (4 feet) wide, so the maximum torque produced by the engine could be resisted without causing excessive strain to the operators. This technique proved to be quite successful since it was possible to maintain a good feel for conditions at the cutting face. Force applied to the cutting surface could be varied accordingly, and several unbroken cores as long as 0.8 metres (2.5 feet) were obtained. Both horizontal and vertical holes were drilled to depths of more than 2.0 metres (6.2 feet) into the headscarp. Scaffolding was used to provide footing and access to various levels of the near-vertical slope (see Plates A.2 and A.3). Some difficulty was encountered with cuttings which packed tightly near the cutting shoe and prevented material from travelling the full length of the flites to be cleared at the top of the core barrel. This problem was remedied by spreading a thin film of oil along the outside of the barrel before each coring run. Binding occasionally occurred which necessitated freeing the core barrel with a jack. In one extreme case, the core barrel became frozen in, so commercial antifreeze was poured into the borehole where it was allowed to stand for several hours. This eventually eroded and softened the frozen soil to the extent that the core barrel could be extracted with ease. Cuttings reservoired above the top of the core barrel occasionally froze to the wall of the borehole and impeded extracting the sampler from the ground. Chipping, jacking, and antifreeze were used to remedy this condition.

Normally, core length was limited by the storage capacity for cuttings which collected along the flitings and in the reservoir space above the barrel. In hand drilling operations, the coring process seemed most effective if the barrel was retrieved after each 0.3 to 0.5 m (1 to 1.6 feet) of penetration so the flites could be cleared. This procedure also seemed to reduce the amount of mechanical breakage experienced by the core. Obtaining long sections of intact core with the hand augering equipment was possible since the operators were able to 'hear' or 'feel' whether ice or soil was being cut. When thick ice lenses were being penetrated, the relatively steep leading angle on the cutting face resulted in fracturing and spalling unless downhole pressures were reduced. A reduction gearbox placed between the engine and the core barrel resulted in maximum rates of rotation of approximately 120 rpm. Slower rates in the range of 30 to 50 rpm resulted in coring penetration rates of 0.3 to 0.4 m (1 to 1.2 feet) per minute. It was noted that breakage was usually restricted to through-going ice lenses, and probably resulted from cracking brought about by the action of the cutting teeth.

A heliportable 'Ranger' drill rig was used to advance the boreholes at both the Norman Wells (MVPL) and Noell Lake sampling sites. This drill rig employed a 40 horsepower gasoline engine and hydraulic pump, turning the augers and the core barrel with a variable-speed, reversible, hydrostatic drive. This permitted backing the core barrel up whenever it became jammed or frozen in. Substantial pullout force was also available since the drive head was attached to a hydraulic ram with a 1.5 m (5 foot) stroke. Considerably more core breakage occurred with the 'Ranger' rig since the driller was less able to match torque and downhole pressure to the characteristics of the material being cut by the core barrel. At Norman Wells, the drill rig was mounted on a flatbed truck, but the remoteness of the Noell Lake site necessitated using lighter skid gear that would be moved with a helicopter. This second configuration reduced the downhole weight available and made it more difficult to drill to a depth of 12 m (40 feet) there.

Core logging in the field consisted of detailed observations of sedimentary structure, ice content and structure, soil texture, and plasticity. Depth intervals for each coring run were established by measuring the borehole depth once the core barrel had been retrieved. Material packed between the core and inside of the barrel usually necessitated mechanical assistance to extrude the core. A propane torch was also employed to heat the core barrel slightly and decrease internal adhesion. Each core was caught in a tray where visual logging was performed before it was placed in a plastic sleeve and sealed. Details noted on each core sleeve included borehole number, depth interval, top end, and sampling date.

The following summarizes sampling equipment and logistics details pertaining to each of the sampling sites.

Fort Simpson Landslide Headscarp

Sampled: May, 1973; October, 1973; October 1974

Ambient Air Temperature: 15° to 18°C; -8° to -1°C;
-4°C; respectively

Equipment: 10 cm CRREL core barrel driven by a gasoline-powered post-auger unit

Access: Equipment and cores transported to and from Fort Simpson with an Alouette II helicopter. Personnel were either flown in or walked approximately 2.5 km (1.6 miles) from the Mackenzie Highway along a cutline.

Norman Wells (MVPL) Sampling Site

Sampled: Late February, 1974

Ambient Air Temperature: -35° to -45°C

Equipment: 10 cm CRREL core barrel driven a 'Ranger' drill (truck mounted)

Access: A four-wheel-drive truck driven from Norman Wells along seismic lines which had been cleared by a bulldozer

Noell Lake Sampling Site

Sampled: Early March, 1974

Ambient Air Temperature: -40° to -45°C

Equipment: 10 cm CRREL core barrel driven by a 'Ranger' drill on helicopter-portable skid gear

Access: Equipment, personnel, and core transported from Inuvik with Bell 205A-1 and Bell 206B helicopters

Several insulated core boxes were constructed to store core on site and ensure its safe transport back to laboratory facilities in Edmonton. The main features of these core boxes are summarized in Figure A.2. The sampling operations described in connection with this study were generally conducted when ambient air temperatures were below 0°C in the field, so very few problems were encountered with handling or storing core there. The only potential difficulty arose when samples were consigned for shipment on commercial air freight carriers. The boxes were painted bright yellow with outside markings clearly indicating the perishable nature of their contents. The key to successful core transport using insulated boxes lay in ensuring that an airtight seal was provided for the sample compartment. This was accomplished by using an RTV silicone rubber caulking compound along the insulation joints and around the perimeter of the lid. The cores were jacketed and sealed in 10 mil thickness polyethyene tubing. Snow was packed in the boxes prior to sealing them for shipment so that sublimation would be kept to a minimum. This also permitted storing the core in a cold room for extended periods before opening the boxes to commence laboratory work.

A.2 DESCRIPTION OF THE SAMPLING SITES

General geographic locations for the three sampling sites used in this study have been presented in Figure 1.1. Detailed location plans for the Fort Simpson, Norman Wells, and Noell Lake sampling sites are shown in Figures A.3, A.4 and A.5 respectively. The following presents detailed stratigraphy and a summary of soil properties for materials encountered at these three sampling sites.

Fort Simpson Landslide Headscarp Sampling Site (Mile 226)

A section exposed at the headscarp of a large landslide located on the left bank of the Mackenzie River approximately 32 kilometres (18 miles) downstream from Fort Simpson, N.W.T. was measured and sampled intensively. The landslide and features of the headscarp are illustrated on Plates A.1, A.2, and A.3. McRoberts (1973) and Pufahl (1976) have described this landslide and summarized pertinent regional geological features. Lacustrine sediments have filled this portion of the Mackenzie Valley and essentially form a wedge, thinning away from the river to discontinuous patches. The texture of these lacustrine sediments invariably consists of clay, silt, and sand sizes with a general tendency for decreasing mean grain size with depth. At the time the site was sampled, the headscarp had exposed a surficial layer of sand that generally increased in thickness with distance from the river. A silty clay or clayey silt layer with sand pockets containing finer-grained rip-off clasts was present beneath the sand. The lacustrine silty clay became finer-grained with depth, and bedding features were difficult to distinguish. A stratigraphic section for the headscarp exposed in October, 1973, is shown in Figure A.6. The zones indicated have been described in Chapter V and were differentiated on the basis of distinctly different amounts and types of ground ice exposed. Plasticity characteristics for these soils are summarized in Figure A.7. The data points parallel the A-line and it can be seen that these soils exhibit low to intermediate plasticity. Data points determined for material from Zone 2 lie closer to the A-line as a result of their slightly coarser texture. Moisture contents and frozen bulk density data determined from core obtained at this site are plotted in Figure A.8. Solid lines shown on these graphs have been calculated from theoretical relationships presented as Equations 6.1 and 6.2. It can be seen that for reasonable ranges of G_s, many data points plot below the line which indicates that most of these soils were not saturated. This characteristic is especially noticeable with material from Zone 2. Textural characteristics of the headscarp soils are summarized in Figure A.9. Samples from Zone 2 contained some sand and coarse silt, while samples from Zones 3 and 4 consisted predominantly of clay with lesser quantities of silt. Properties for the material from Zone 2 indicate that this relict active layer has been subjected to numerous freeze-thaw cycles which probably desaturated the soil and mixed in some of the coarser, near-surface sand as a result of extensive cryoturbation. Typical ground ice structures encountered in each of the different zones are shown on Plates A.4 through A.7.

Norman Wells (MVPL) Sampling Site

During or subsequent to glaciation of the Mackenzie River Valley, ice dams situated somewhere to the north of Sans Sault Rapids caused a large proglacial lake to be impounded along the valley. At its maximum, this lake may have extended as far south as the vicinity of Fort Norman. Differential crustal rebound makes establishing maximum lake levels somewhat difficult, but it is probable that at its maximum, this body of water reached an elevation of at least 150 m (500 feet) above sea level. Major sources of detrital material were tributatires which roughly correspond to channels occupied by the present-day Mountain, Carcajou, Great Bear, and Keel Rivers. Mackay and Matthews (1973) have suggested that with the retreat of the ice lobe that occupied the Mackenzie plain in late Wisconsin time, the Mackenzie began to flow along the lowlands to the west of the Franklin Mountains. The lake developed along these lowlands, and its early stages, was dammed to an altitude of approximately 240 m (800 feet) above sea level by ice still present on the north and northwest. The basin gradually filled, and with the disappearance of the ice dam, ponded at an elevation of approximately 95 m (310 feet) above sea level behind a bedrock ridge situated southwest of Fort Good Hope. This stage has been dated at approximately 11,000 to 11,500 C_{14} years before present. A series of spillways developed across the ridge and led to the eventual downcutting of the Ramparts and complete drainage of the lake impounded above that point by approximately 6100 C_{14} years before present. In the intervening time, further downcutting has resulted in the Mackenzie River becoming incised in former lake and river sediments.

The MVPL ice variability study site at Norman Wells is located approximately 3 km (1.5 miles) back from the right bank of the Mackenzie River. Surface elevations at the site indicate that this portion of the valley would have been submerged by water impounded during both the ice and bedrock dammed glacial lake stages. The sequence of sediments encountered in the boreholes drilled as part of this study are summarized in the stratigraphic profile presented as Figure A.10. C_{14} dates[1] determined from peat layers indicate reasonable agreement with the regional sequence of events outlined by Mackay and Matthews (1973). Sediments in the first 2 m probably consist of alluvial material deposited by the active Mackenzie River during downcutting. Stratified silts and clays beneath this were probably deposited in the glacial lake impounded behind the Ramparts bedrock high. The deepest occurrence of discrete organic material at a depth of 7.5 m gave an age of 9300 C_{14} years before present. Below that, a pebble lag was encountered at a depth of approximately 9.5 metres, and this was underlain by highly plastic, thinly bedded clay. The liquidity index profile suggests that three distinct sedimentation sequences have occurred in this depth interval. The absence of organic material, and the fine-grained, highly plastic nature of soil samples recovered from below a depth of 10 metres suggest that this portion of the profile was probably deposited in a deep water, distal environment. These sediments probably date back to the ice dammed glacial lake phase. Examination of organic inclusions in the soils between the depths of 3 and 9 m suggest a gradual transition from a shallow, nearshore environment to shoreline or backwater sedimentation. Again, this sequence of events corresponds to the post-Wisconsin geomorphic development that Mackay and Matthews (1973) have described.

Textural properties of the soils encountered in this profile have been summarized in Figure A.11. Once again, the data points tend to parallel the A-line. These soils exhibited low to high plasticity, and several samples had a plasticity index which had been reduced the presence of organic material. Figure A.12 summarizes moisture content and frozen bulk density data that was determined from samples obtained with a CRREL core barrel (this study). As was noted for the Fort Simpson Site, the results plotted here indicate that many of the samples were probably not fully saturated. However, interpretation of this data is complicated by the fact that organic material present in many samples made it difficult to establish meaningful values for G_s. In Figure A.13, data extracted from the

---

[1] Personal Communication. Dr. W. Blake Jr., 1975.

MVPL studies demonstrate the mechanical disturbance which resulted from sampling with a vibratory core barrel. There is considerably more scatter in this data, and points generally plot at lower frozen bulk densities for a given water content. Grain size curves and a summary of textural data for soils from the Norman Wells sampling site are presented in Figure A.14.

Photographs of typical cores taken from this profile are included as Plates A.8 through A.15. These illustrate typical ice structures which were encountered as well as some of the organic inclusions and sedimentary structures. Of particular note are the stratified ice lenses on Plate A.8 which are characteristic of soils from the active layer. Plate A.9 shows a core which includes numerous charred sticks and roots that were probably a shoreline deposit of charred wood washed in from burned areas on the slopes surrounding the lake. Plates A.13 and A.15 both illustrate a well-developed reticulate ice structure.

Noell Lake Sampling Site

Rampton (1973) has indicated that surficial materials in the vicinity of Noell Lake consist of till and till-derived deposits which have usually been described as stony clay. The till is a black, sticky clay containing stones up to boulder sizes, and the matrix material has presumably been derived from Cretaceous shale to the south. The area is dotted with thermokarst lakes which are common within the terrain unit and probably result from the melting of large bodies of massive ice and icy sediments at depth. The topography is gently rolling, but glacial landforms which might provide a key to the depositional environment for these sediments are indistinct and difficult to identify or delineate. The ground surface at this sampling site was covered with bare-centred hummocks which had diameters ranging from 2 to 4 m (6 to 12 feet). Micro-relief was in the order of 0.4 m (1.5 feet). The stratigraphic profile determined from drilling and sampling at this site is summarized in Figure A.15.

Soils at the site consisted of 1 m (3 feet) of sandy silt which exhibited well-developed cryoturbation features. The layer of gravel encountered in a depth of 1.5 m probably corresponds approximately to the maximum active layer penetration which has occurred since deglaciation. Between the depths of 1.5 and 8 m, a dark grey silty clay containing some gravel sizes was encountered. This material included several thick ice layers, and very high ice contents were logged in the 6 and 8 m depth interval. Between 8 and 10.5 m, sampling revealed an ice-rich stratified sand which contained sedimentary structures indicative of slumping. Below 10.5 m, a stony clay similar to that logged between 1.5 and 8 m was encountered. The borehole was terminated at a depth of 12.5 m when the core barrel met refusal on a cobble. Pertinent geotechnical and classification index properties have been summarized on the borehole log. Figure A.16 presents plasticity characteristics for the soils encountered at this site. Once again, the data points parallel the A-line, with the exception of those which contained organic material. Moisture content and frozen bulk density data presented in Figure A.17 follow the same trends exhibited by core taken from the Fort Simpson and Norman Wells sampling sites. Once again, there is strong indication that many fine-grained permafrost soils exist _in situ_ in an unsaturated state. Textural characteristics for these soils are summarized with several grain size curves that are presented in Figure A.18. Photographs of typical sections of core from this profile are included as Plates A.16 through A.21. The highly disturbed structure observed on these cores and generally high liquidity indices suggest that much of this profile may consist of soils which have been reworked by thermokarst processes. Permafrost aggradation into sediments which have slumped at the perimeter of a migratory thermokarst lake may explain the unusually high liquidity indices encountered in this borehole.

X-ray diffraction analyses were performed on representative samples from all of the sampling sites described in this thesis and the results are summarized in Table A.1. These data document an essentially uniform mineralogy for glaciolacustrine sediments sampled along the valley.

A.3 IMPROVING SITE INVESTIGATION TECHNIQUES

In summary, the sampling techniques which were employed to obtain core used in these laboratory studies consistently involved use of the CRREL core barrel. Plate A.22 shows a hand-operated, motorized coring arrangement. Although two men were required to use the unit, it was capable of obtaining a large quantity of undisturbed core characterized by only slight mechanical breakage. This was accomplished at a relatively low cost. By way of comparison, core obtained with the heliportable 'Ranger' drill shown in Plate A.23 suffered considerably greater mechanical breakage, and resulted in costs which ranged from 5 to 7 times those incurred with the post-augering unit. A more detailed view of the modified CRREL core barrel, cutting teeth, and helical fliting is shown on Plate A.24. Upon completing the sampling, it was recognized that coring with equipment of this sort resulted in significant but unavoidable amounts of mechanical breakage of core. This had the effect of biasing moisture content and frozen bulk density data by destroying some of the thicker ice lenses. Deficiencies in this regard have been discussed in Chapters VI and VII.

Of the various techniques available to determine the distribution of ice in frozen ground, soil sampling with the subsequent laboratory analysis of core has been the most common method used for engineering purposes. This process is time consuming, costly, and often yields data which are not representative. If experience gained in other geosciences can be applied to overcome some of the deficiencies encountered in logging permafrost, it seems reasonable to speculate that correctly interpreted geophysical logs might find beneficial application in many field programs. They could be used to reduce future drilling costs by guiding the location of boreholes and enabling vertical and horizontal extrapolation of data derived from undisturbed samples.

Geophysical logs can be interpreted to determine lithology, bulk density, and moisture content. Keys and MacCary (1971) have presented a detailed summary and objective appraisal of the application of borehole geophysics to the applied earth sciences. Specifically, a feasibility study described by Keys (1968) demonstrated that valid geophysical logs can be made in boreholes drilled in permafrost. He has suggested that properly made logs can be interpreted in terms of bulk density, organic content, moisture content, and the location of ice segregations. Numerous recommendations were made, including one that logging should be done with enclosed research equipment to permit wider climatic latitude for operation, thus reducing the drift caused by environmental temperature fluctuations and their effects on both the instrumentation and subsurface probes. A stable power generator is required for quantitative work. McKay and O'Connell (1976) have described field techniques and results obtained using logging instruments specifically designed to measure density _in situ_, in lieu of determining core densities in the laboratory. They conclude that the response characteristics of a scattered gamma ray logging tool are well suited to the measurement of relatively low permafrost densities and ice contents _in situ_. Their results demonstrate that nuclear density logging is an accurate and economical method of obtaining continuous density profiles in permafrost soils. Records from boreholes drilled on the MVPL test site near Inuvik in 1971 indicate that geophysical logs of density and ice volume were in reasonable agreement with data obtained from the analysis of core in a laboratory. Another study of borehole density logging and permafrost has been reported by Hunter and Viellette (1976). They performed shallow, dry-hole drilling on the GSC geophysical control site near Tuktoyaktuk. Six holes were logged to a depth of 9.5 metres and gamma-gamma measurements conducted at intervals of 0.15 metres (0.5 feet) up hole resulted in good correlations between the count rate and ice content. A stratigraphic resolution of better than 0.5 metres (1.5 feet) was obtained.

Some boreholes on the Norman Wells (MVPL) ice variability site were logged with nuclear equipment. Figure A.19 shows a comparison between density profiles obtained from direct measurements on permafrost core, and a continuous density profile obtained using geophysical borehole logging techniques. It can be seen that reasonable agreement was obtained. In Figure A.20, a comparison is shown between density profiles obtained with the MVPL nuclear logger and undisturbed core obtained from a borehole drilled nearby (this study). Although there is considerably more scatter in this data, trends for density change indicated by the nuclear log follow the same trends exhibited by laboratory core densities. These particular nuclear logs were obtained with small and portable equipment, and are therefore affected by deficiencies normally associated therewith.

Figure A.21 shows a more complete suite of logs obtained from a borehole drilled near Fairbanks, Alaska. Here the gamma-gamma log clearly shows interstratification between silt and thick layers of segregated ice. The resistivity log shows similar characteristics. It could be argued that even if the borehole logging results could not be used quantitatively, they do provide an extremely valuable means of assessing the relative amounts of soil and ice encountered in profile. There is little doubt that this technique could be advantageously used to extrapolate data across a site where numerous boreholes were being drilled. Having some core densities to check the downhole logging results provides an opportunity to use the geophysical logs in a quantitative sense. The results of the studies cited above indicate that a single point resistance log could probably be run to check stratigraphy and give a preliminary indication of the locations of excessively ice-rich zones. Supplementing this qualitative information with water content and density logs determined using neutron-neutron and gamma-gamma probes respectively, in situ profiles of bulk density and water content could then be obtained to complement the preliminary stratigraphy. High degrees of accuracy are obtainable if certain conditions can be met, a particular one being that hole diameters should not vary. Dry auger holes produced by a CRREL core barrel are thus ideally suited for borehole geophysical tools. One drawback to this sort of system is that to obtain large sampling volumes requires the use of high energy radiation sources.

In obtaining representative moisture contents in the laboratory, very few difficulties are usually encountered with soils which contain thin stratified cryogenic structure. However, if the soil contains thick irregular ice lenses or reticulate structure, it becomes necessary to take numerous specimens or large volumes to obtain accurate and representative water contents. Litvinov (1966) has given several recommendations for the overall moisture content of frozen ground containing thick ice lenses or reticulate cryogenic structure. Relationships derived by him make it possible to relate volumetric ice contents logged in the field to moisture contents determined in the laboratory. Thus, when field ice content logs are in question, laboratory moisture content data can be used to check them. The opposite is also true if there is some uncertainty whether the samples selected for moisture content determination in the laboratory were truly representative of the bulk material encountered in situ. Comparative checks of this sort are recommended so that some confidence can be developed in the accuracy of volumetric ice content logs obtained under field conditions. There is little question that more detailed core logging procedures and geophysical tools developed specifically for site investigations in permafrost are both required. However, a detailed treatment of the entire topic is beyond the scope of this thesis.

TABLE A.1 SUMMARY OF X-RAY DIFFRACTION ANALYSES[1] CONDUCTED ON CLAY FRACTION (< 2μ)

SOURCE LOCATION	DEPTH OR ZONE	MINERAL IDENTIFIED[3]					
		ILLITE	KAOLINITE	CHLORITE	MONTMOR-ILLONITE	QUARTZ	CALCITE
MOUNTAIN RIVER	RIVER BANK	S (S)	M (W)	A (T)	T (M)	A	A
FORT SIMPSON LAND-SLIDE SITE	Z2	S	W	T	T	P	A
	Z2	S	W	T	T	P	A
	Z3	S	W	A	A	P	A
	Z3	S	W	T	T	P	A
	Z4	S	W	T	T	P	P
	Z4	S	W-M	T	T	P	P
NORMAN WELLS SITE	1.8m	S	M	W	A	P	A
	2.9m	S	W-M	T	A	P	A
	6.1m	S	M	T	T	P	A
	8.7m	S	S	T	A	P	A
	9.9m	S	M	T	T	P	A
	12.3m	S	S	W	A	P	A
NOELL LAKE SITE	1.8m	S	M	A	T	P	A
	5.0m	S	M	T	T	P	A
	7.1m	S	M	T	W	P	A
	10.7m	S	M	T	T	P	A

---

[1] Analyses performed by Alberta Research Council

[2] Amount of mineral present indicated by the relative intensity of peaks on the trace, includes both width and height of peak

A - Absent, background only
P - Present
T - Trace, mineral distinguished
W - Weak, peak small in width or height but clearly distinguished
M - Medium, well-defined peak
S - Strong, dominant peak

[3] Other analyses performed on the same material by Dr. S. Pawluk indicated a larger quantity expandable mineral present as interstratified hydrous mica - montmorillonite. Alternate results are shown in brackets.

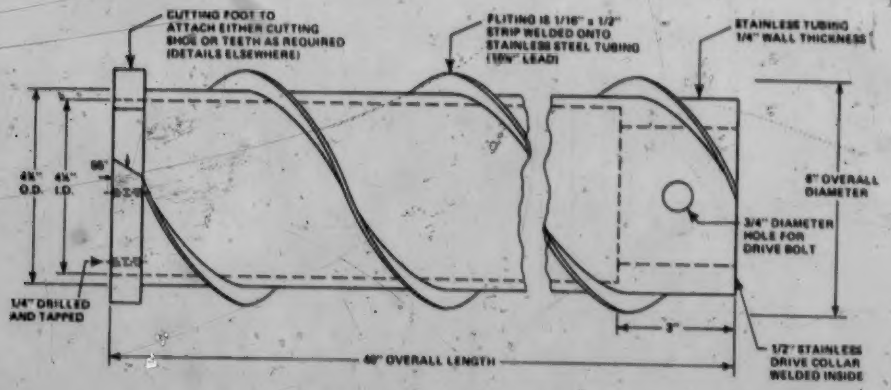
CUTTING FOOT TO ATTACH EITHER CUTTING SHOE OR TEETH AS REQUIRED (DETAILS ELSEWHERE)
FLITING IS 1/16" x 1/2" STRIP WELDED ONTO STAINLESS STEEL TUBING (10¾" LEAD)
STAINLESS TUBING 1/4" WALL THICKNESS
4¾" O.D.
4¼" I.D.
90°
8" OVERALL DIAMETER
3/4" DIAMETER HOLE FOR DRIVE BOLT
1/4" DRILLED AND TAPPED
3"
40" OVERALL LENGTH
1/2" STAINLESS DRIVE COLLAR WELDED INSIDE

Figure A.1 Sketch of modified CRREL auger core barrel used in sampling operations

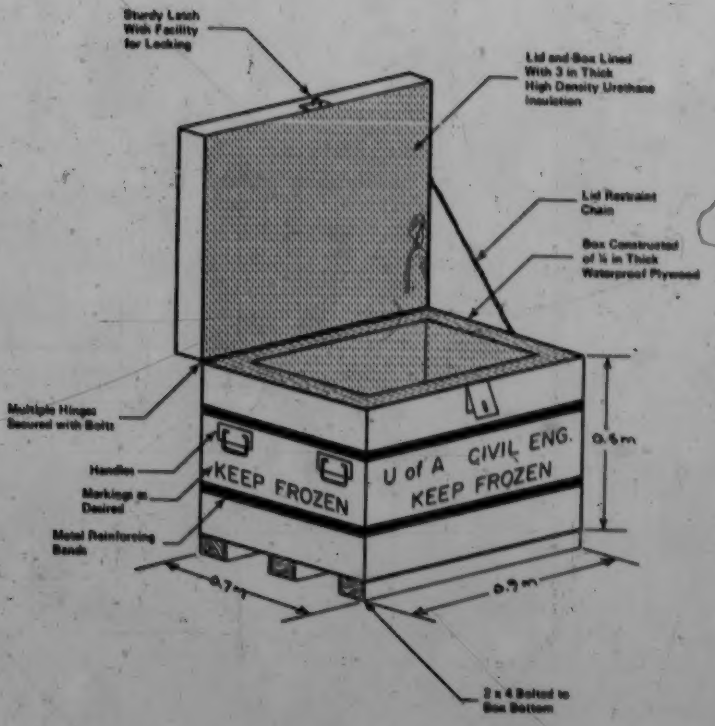
Sturdy Latch With Facility for Locking
Lid and Box Lined With 3 in Thick High Density Urethane Insulation
Lid Restraint Chain
Box Constructed of ½ in Thick Waterproof Plywood
Multiple Hinges Secured with Bolts
Handles
Markings as Desired
Metal Reinforcing Bands
KEEP FROZEN
U of A CIVIL ENG.
KEEP FROZEN
0.5m
0.7m
0.9m
2 x 4 Bolted to Box Bottom

Figure A.2 Insulated core box used for field storage and transport of permafrost samples

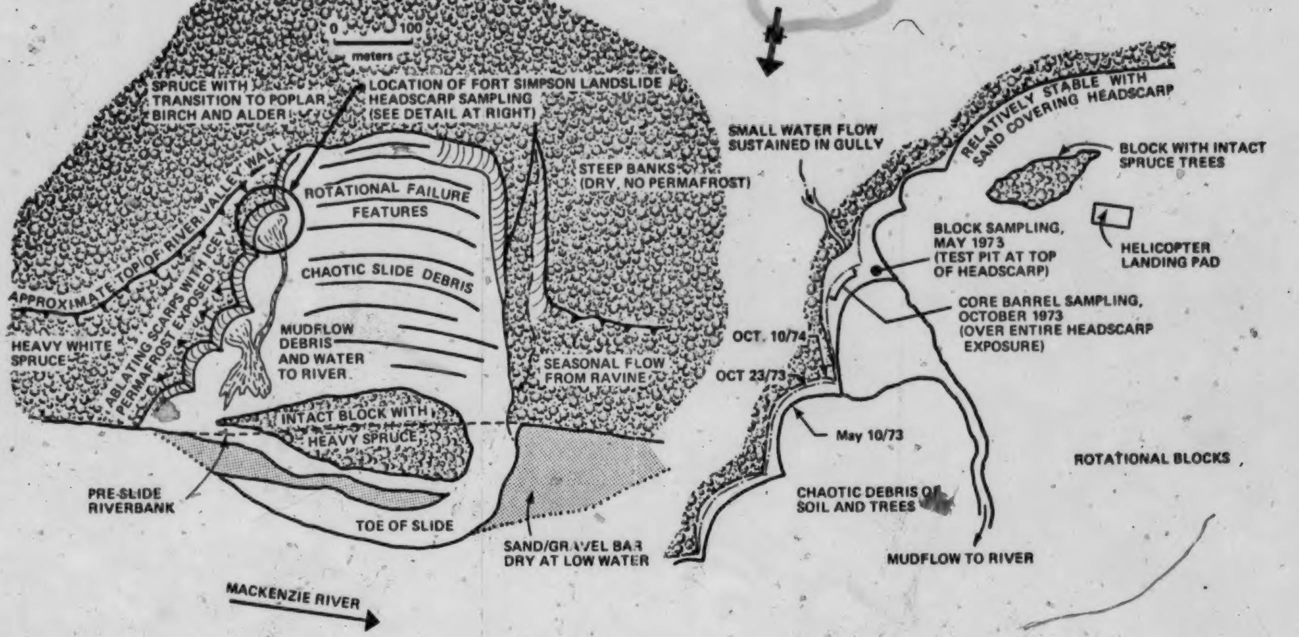
0 100
meters
SPRUCE WITH TRANSITION TO POPLAR BIRCH AND ALDER
LOCATION OF FORT SIMPSON LANDSLIDE HEADSCARP SAMPLING (SEE DETAIL AT RIGHT)
APPROXIMATE TOP OF RIVER VALLEY WALL
ABLATING SCARPS WITH ICEY PERMAFROST EXPOSED
HEAVY WHITE SPRUCE
ROTATIONAL FAILURE FEATURES
CHAOTIC SLIDE DEBRIS
MUDFLOW DEBRIS AND WATER TO RIVER
STEEP BANKS (DRY, NO PERMAFROST)
SEASONAL FLOW FROM RAVINE
INTACT BLOCK WITH HEAVY SPRUCE
PRE-SLIDE RIVERBANK
TOE OF SLIDE
SAND/GRAVEL BAR DRY AT LOW WATER
MACKENZIE RIVER
SMALL WATER FLOW SUSTAINED IN GULLY
RELATIVELY STABLE WITH SAND COVERING HEADSCARP
BLOCK WITH INTACT SPRUCE TREES
BLOCK SAMPLING, MAY 1973 (TEST PIT AT TOP OF HEADSCARP)
HELICOPTER LANDING PAD
CORE BARREL SAMPLING, OCTOBER 1973 (OVER ENTIRE HEADSCARP EXPOSURE)
OCT. 10/74
OCT 23/73
May 10/73
ROTATIONAL BLOCKS
CHAOTIC DEBRIS OF SOIL AND TREES
MUDFLOW TO RIVER

Figure A.3 Location plan for Fort Simpson landslide headscarp sampling site (Mile 226)

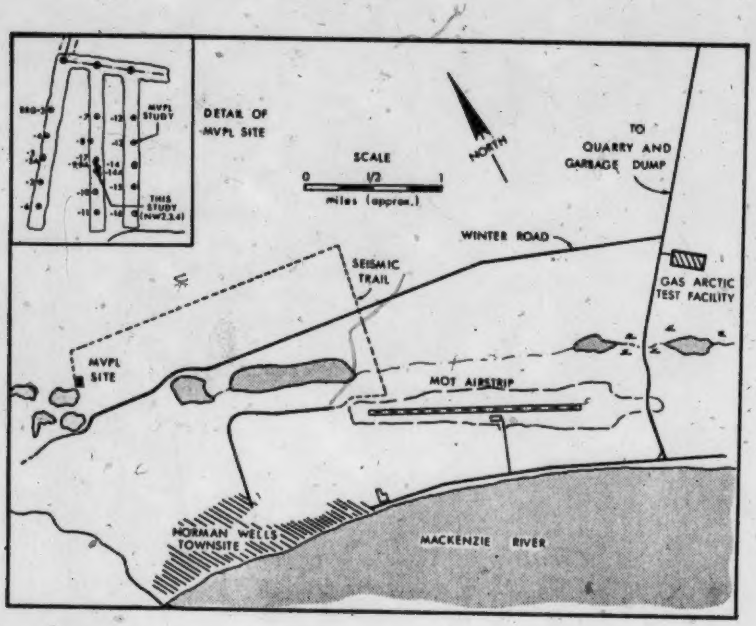
DETAIL OF
MVPL SITE
MVPL STUDY
THIS STUDY (NW2,3,4)
-7
-12
-14
-14A
-15
-16
-17
SCALE
0
1/2
1
miles (approx.)
NORTH
TO QUARRY AND GARBAGE DUMP
WINTER ROAD
SEISMIC TRAIL
GAS ARCTIC TEST FACILITY
MVPL SITE
MOT AIRSTRIP
NORMAN WELLS TOWNSITE
MACKENZIE RIVER

Figure A.4 Location plan for Norman Wells (MVPL) sampling site

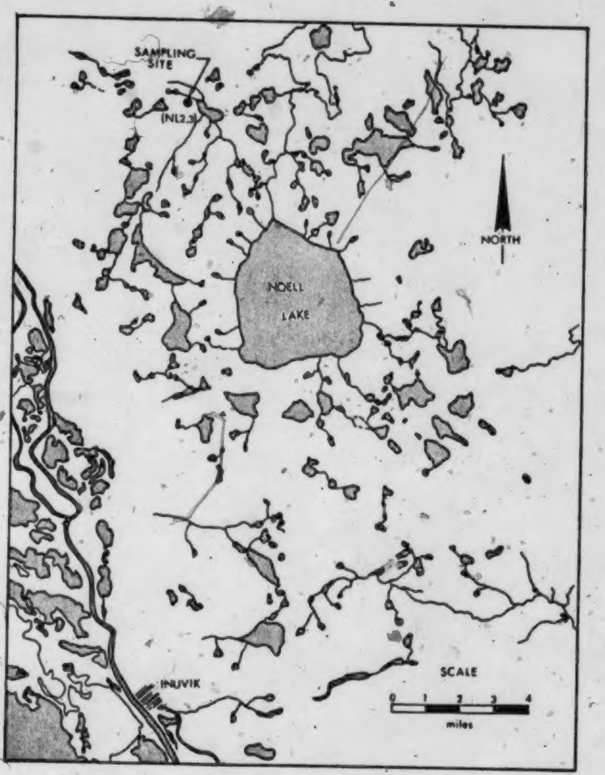
SAMPLING SITE
(NL2,3)
NOELL LAKE
NORTH
INUVIK
SCALE
0
1
2
3
4
miles

Figure A.5 Location plan for Noell Lake sampling site

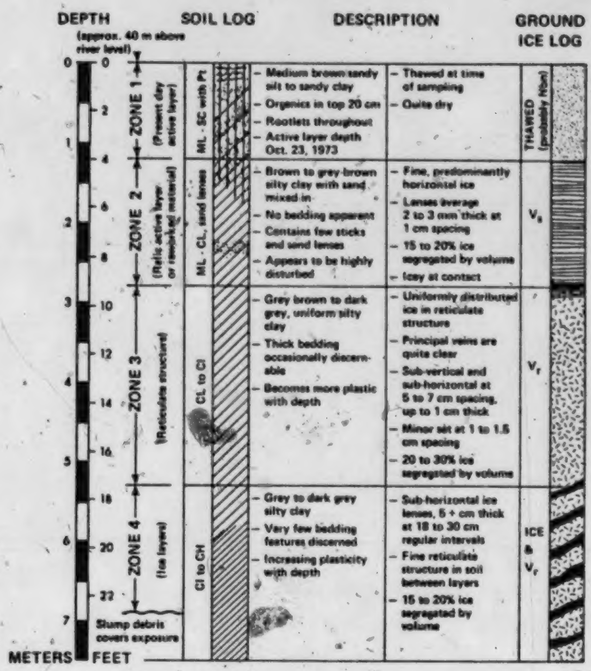
DEPTH
(approx. 40 m above river level)
SOIL LOG
DESCRIPTION
GROUND ICE LOG
0
1
2
3
4
5
6
7
METERS
0
2
4
6
8
10
12
14
16
18
20
22
FEET
ZONE 1
(Present day active layer)
ZONE 2
(Relic active layer or reworked material)
ZONE 3
(Reticulate structure)
ZONE 4
(Ice layers)
Slump debris covers exposure
ML - SC with Pt
ML - CL, sand lenses
CL to CI
CI to CH
– Medium brown sandy silt to sandy clay
– Organics in top 20 cm
– Rootlets throughout
– Active layer depth Oct. 23, 1973
– Brown to grey-brown silty clay with sand mixed in
– No bedding apparent
– Contains few sticks and sand lenses
– Appears to be highly disturbed
– Grey brown to dark grey, uniform silty clay
– Thick bedding occasionally discernable
– Becomes more plastic with depth
– Grey to dark grey silty clay
– Very few bedding features discerned
– Increasing plasticity with depth
– Thawed at time of sampling
– Quite dry
– Fine, predominantly horizontal ice
– Lenses average 2 to 3 mm thick at 1 cm spacing
– 15 to 20% ice segregated by volume
– Icey at contact
– Uniformly distributed ice in reticulate structure
– Principal veins are quite clear
– Sub-vertical and sub-horizontal at 5 to 7 cm spacing, up to 1 cm thick
– Minor set at 1 to 1.5 cm spacing
– 20 to 30% ice segregated by volume
– Sub-horizontal ice lenses, 5 + cm thick at 18 to 30 cm regular intervals
– Fine reticulate structure in soil between layers
– 15 to 20% ice segregated by volume
THAWED (probably Nbn)
V_s
V_r
ICE & V_r

Figure A.6   Log of typical headscarp section exposed at the Fort Simpson landslide (October, 1973)

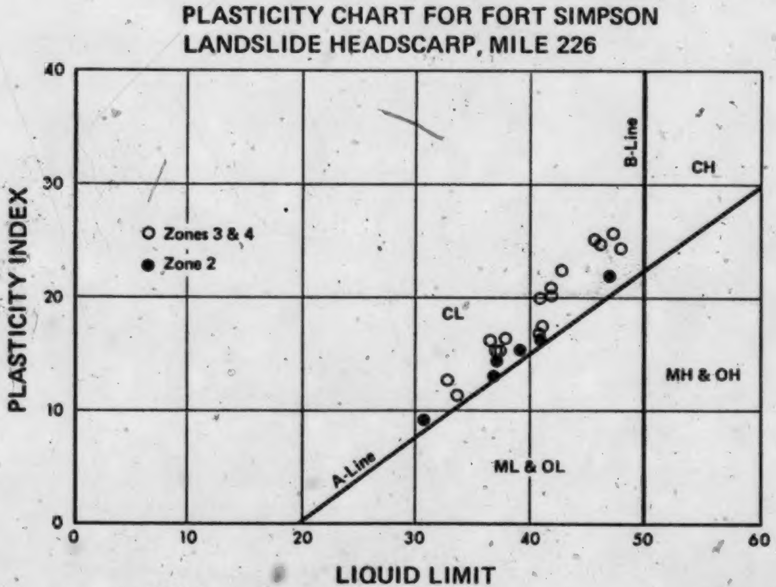

Figure A.7   Plasticity chart for soils from the Fort Simpson landslide headscarp sampling site

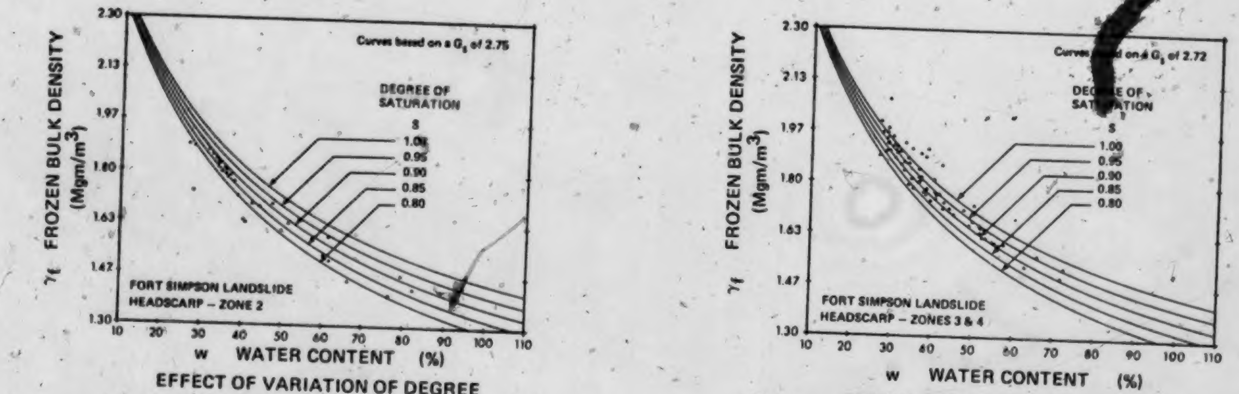

EFFECT OF VARIATION OF DEGREE OF SATURATION

EFFECT OF VARIATION OF DEGREE OF SATURATION

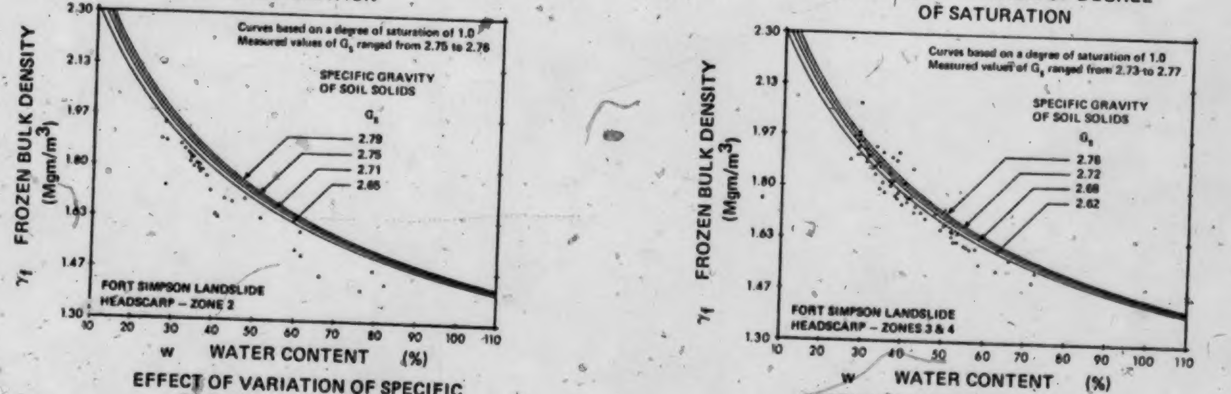

EFFECT OF VARIATION OF SPECIFIC GRAVITY OF SOIL SOLIDS

EFFECT OF VARIATION OF SPECIFIC GRAVITY OF SOIL SOLIDS

Figure A.8 Moisture content and frozen bulk density data for soils from the Fort Simpson landslide headscarp sampling site

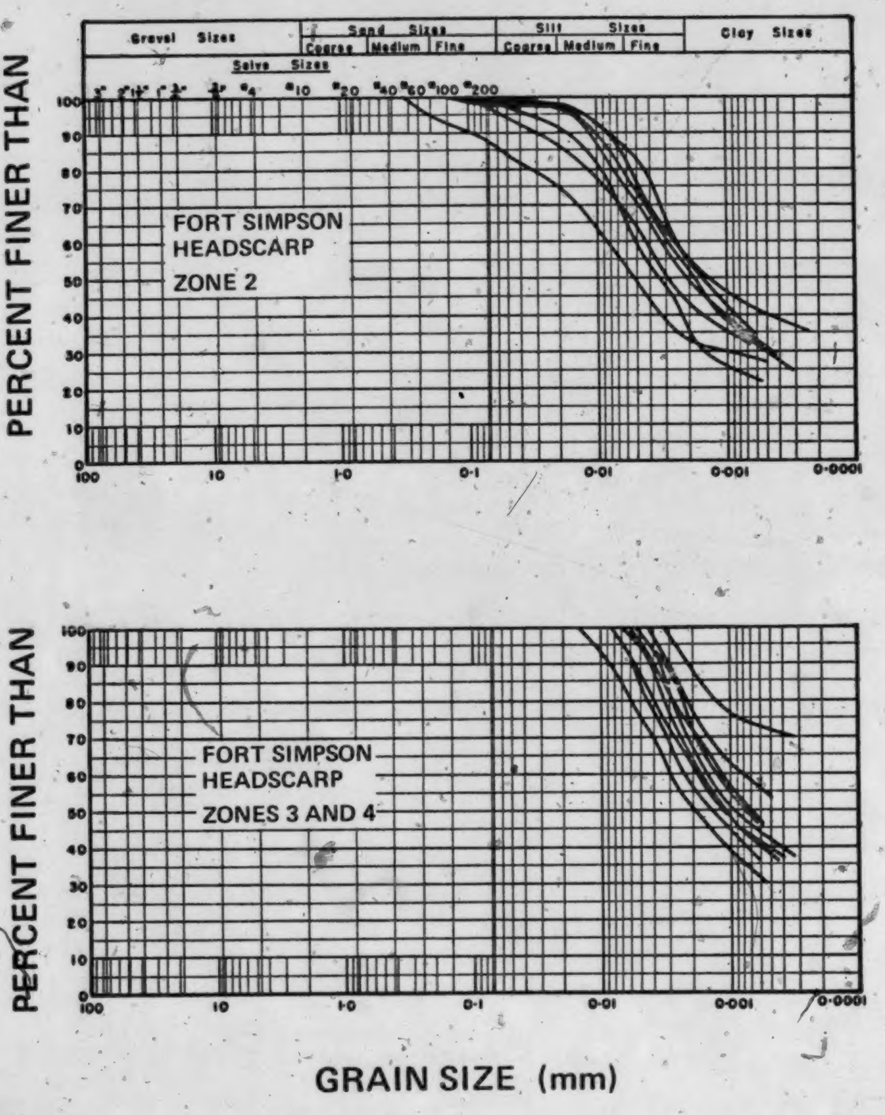

Figure A.9 Grain size curves for soils from the Fort Simpson landslide headscarp sampling site (MIT scale)

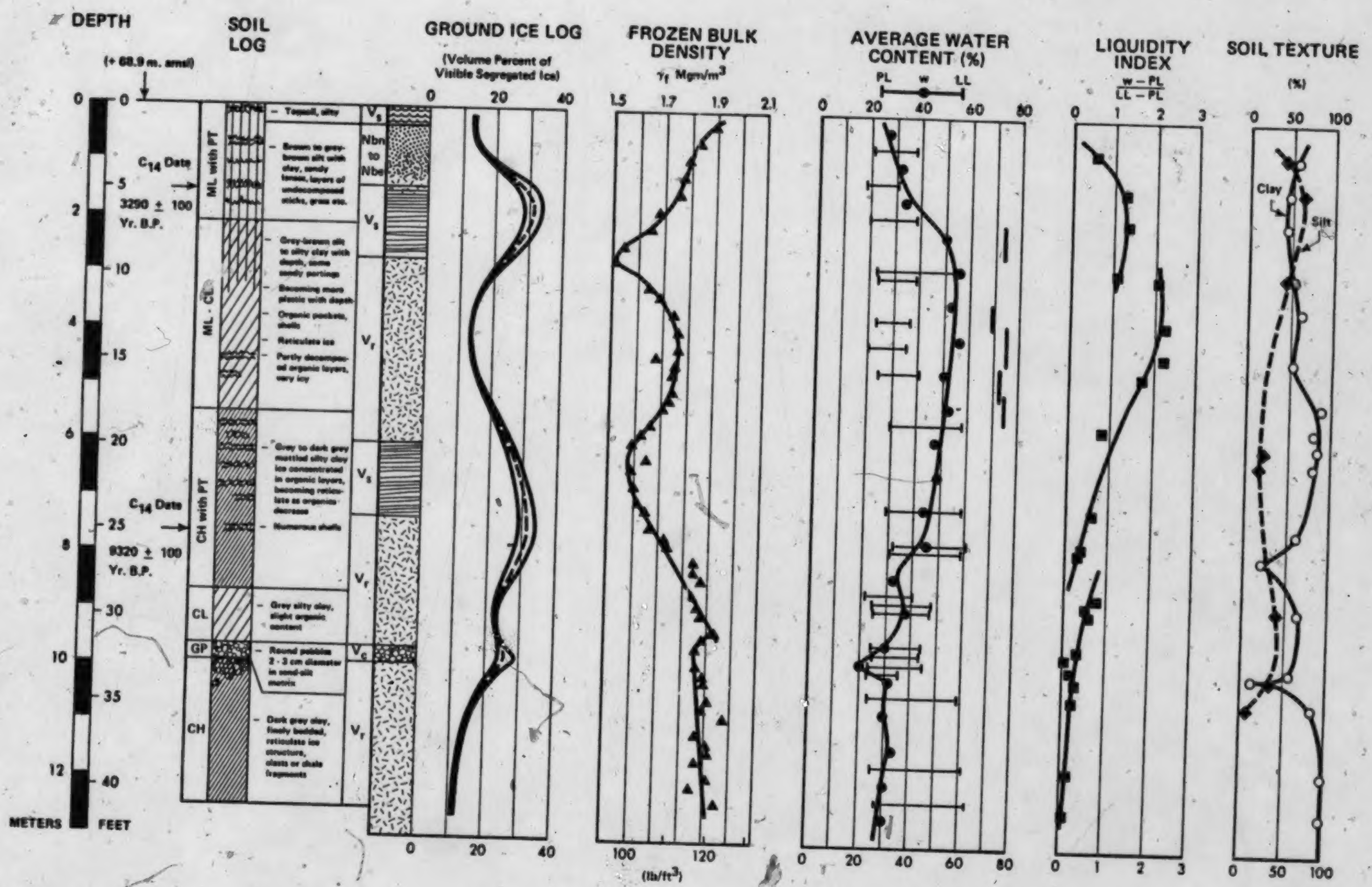

Figure A.10 Borehole log for Norman Wells sampling site

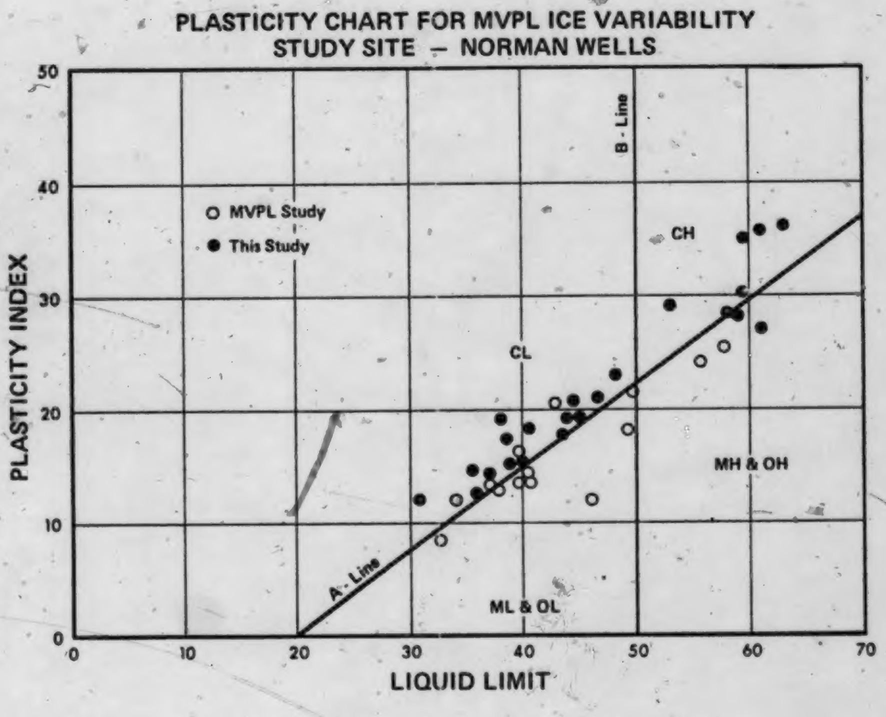

Figure A.11 Plasticity chart for soils from the Norman Wells sampling site

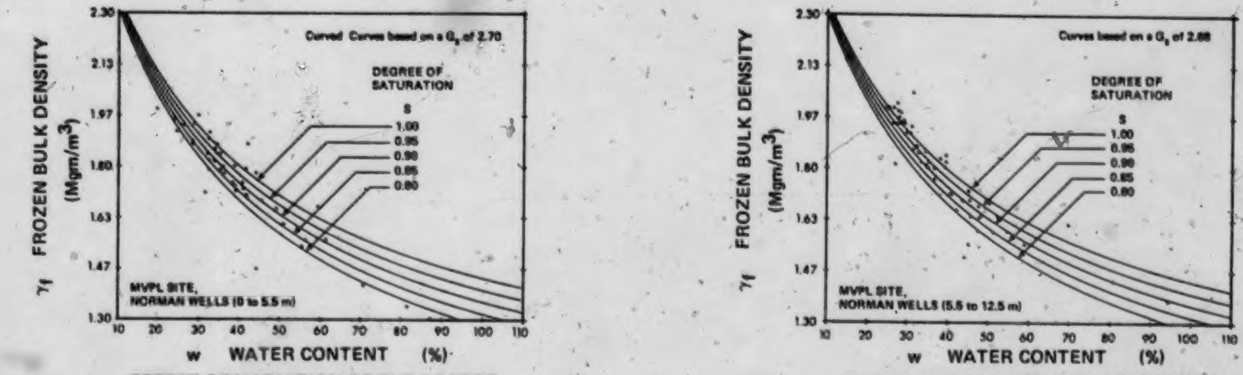

EFFECT OF VARIATION OF THE DEGREE OF SATURATION

EFFECT OF VARIATION OF THE DEGREE OF SATURATION

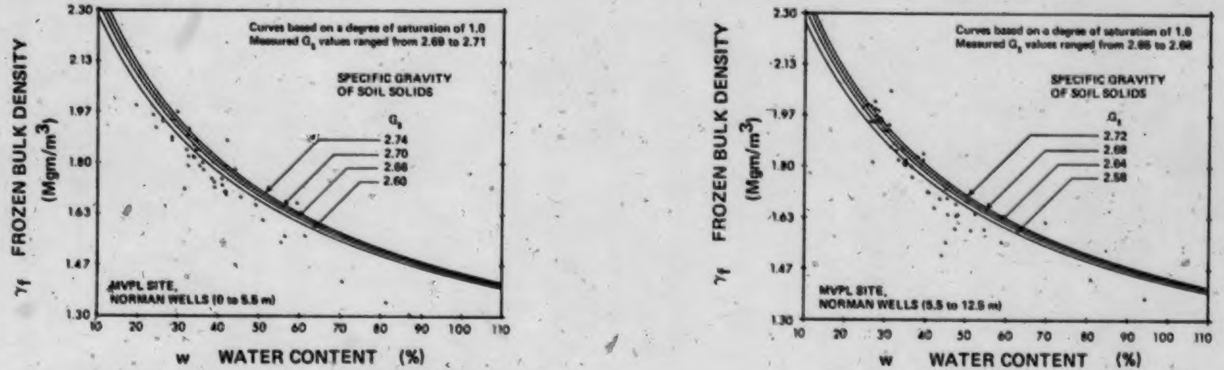

EFFECT OF VARIATION OF THE SPECIFIC GRAVITY OF SOIL SOLIDS

EFFECT OF VARIATION OF THE SPECIFIC GRAVITY OF SOIL SOLIDS

Figure A.12 Moisture content and frozen bulk density data for soils from the Norman Wells sampling site (this study)

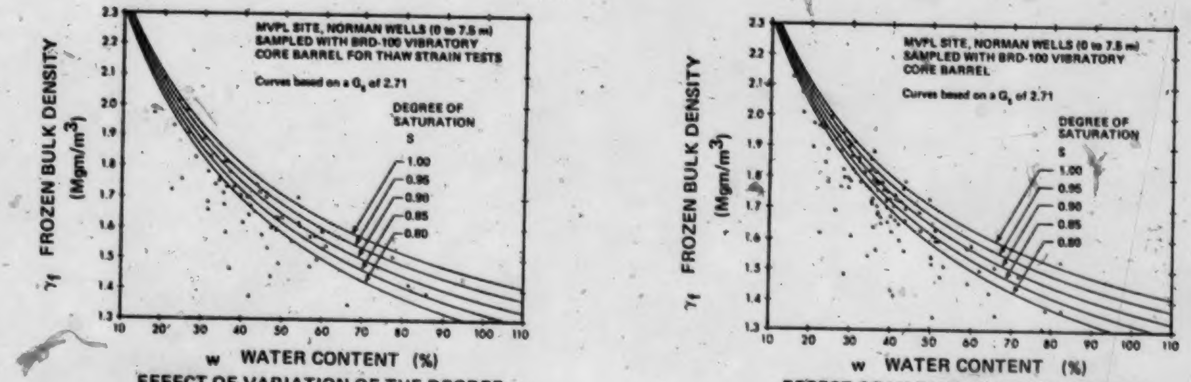

EFFECT OF VARIATION OF THE DEGREE OF SATURATION

EFFECT OF VARIATION OF THE DEGREE OF SATURATION

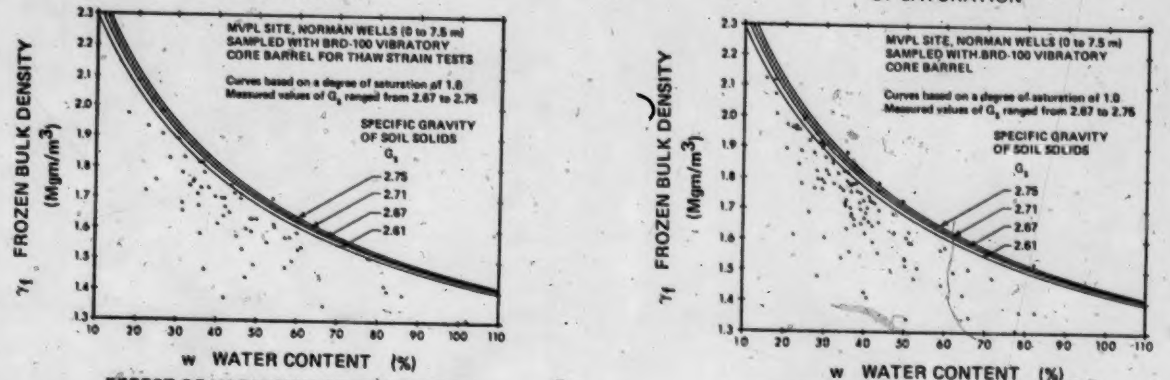

EFFECT OF VARIATION OF THE SPECIFIC GRAVITY OF SOIL SOLIDS

EFFECT OF VARIATION OF THE SPECIFIC GRAVITY OF SOIL SOLIDS

Figure A.13 Moisture content and frozen bulk density data for soils from the Norman Wells sampling site (data from MVPL)

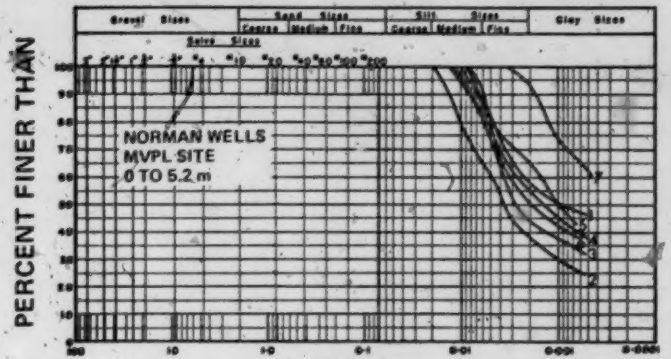

No.	1	2	3	4	5	6	7
Depth (meters)	0.4	1.3	1.8	2.8	3.4	4.2	5.1

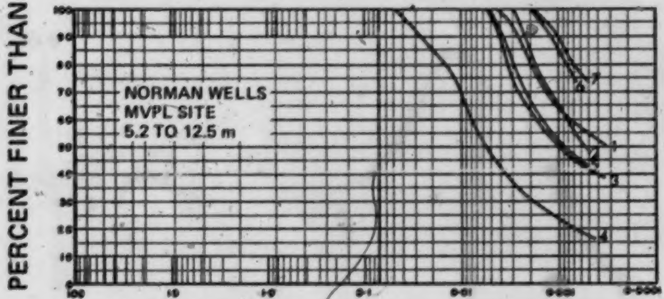

No.	1	2	3	4	5	6	7
Depth (meters)	5.6	6.1	7.3	7.7	8.7	11.5	12.3

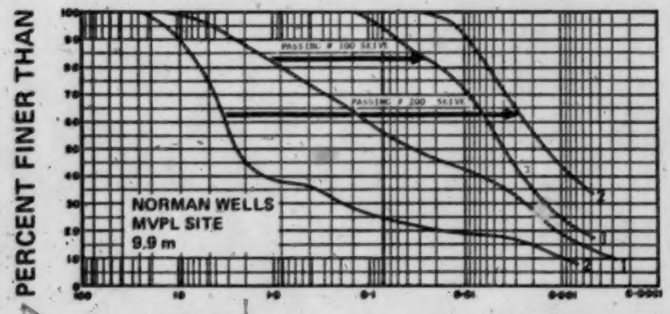

GRAIN SIZE (mm)

Figure A.14 Grain size curves for soils from the Norman Wells (MVPL) sampling site

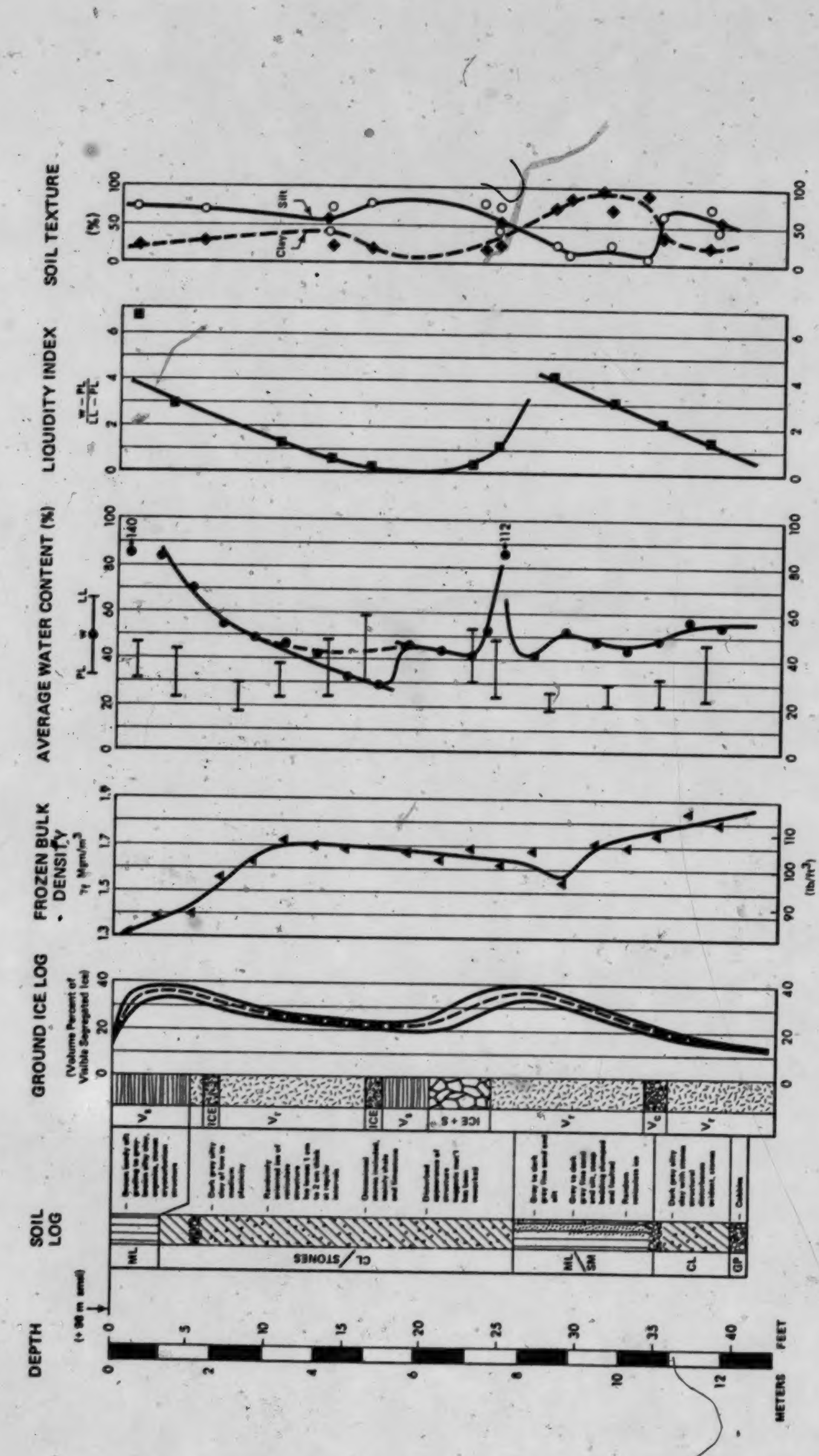

Figure A.15 Borehole log for Noell Lake sampling site

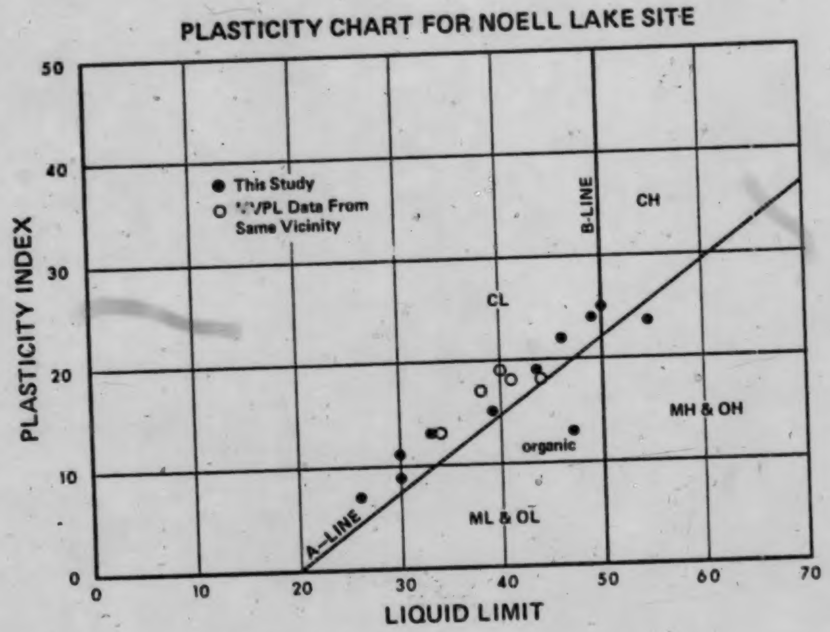

Figure A.16 Plasticity chart for soils from the Noell Lake sampling site

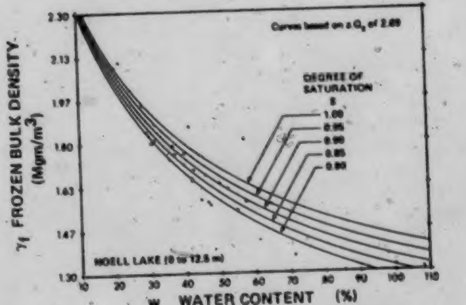

EFFECT OF VARIATION OF DEGREE OF SATURATION

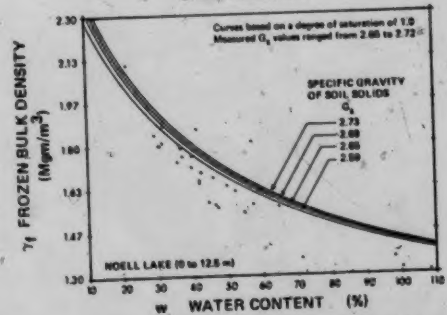

EFFECT OF VARIATION OF THE SPECIFIC GRAVITY OF SOIL SOLIDS

Figure A.17 Moisture content and frozen bulk density data for soils from the Noell Lake sampling site

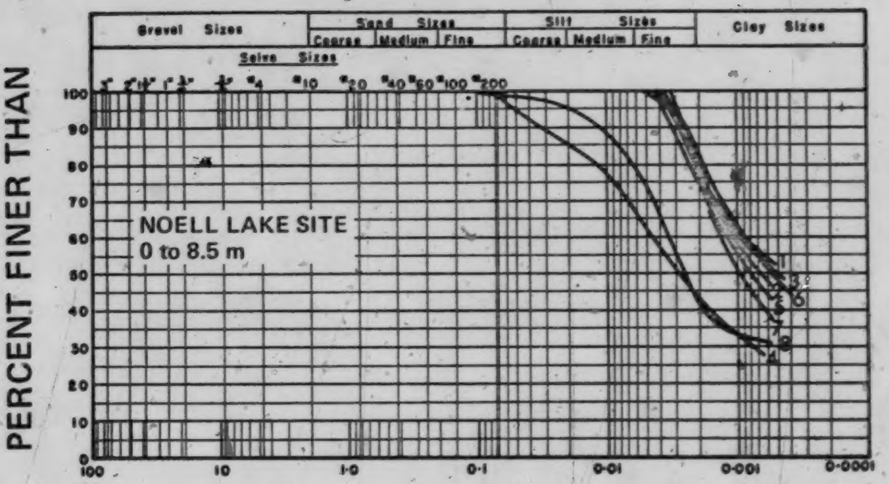

No.	1	2	3	4	5	6	7	8
Depth (meters)	0.4	1.8	4.2	4.4	5.0	7.1	7.5	8.1

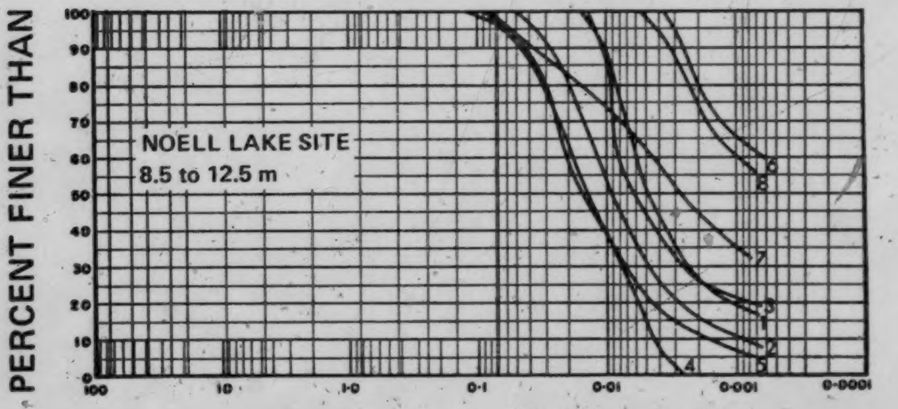

No.	1	2	3	4	5	6	7	8
Depth (meters)	8.6	8.8	9.7	9.8	10.6	10.7	11.6	12.1

Figure A.18 Grain size curves (excluding pebbles) for soils from the Noell Lake sampling site

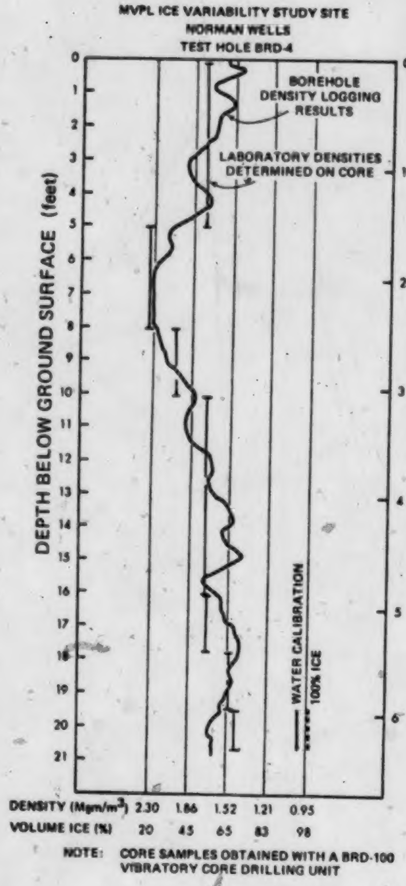

Figure A.19 Comparison between density profiles obtained from laboratory measurements on core and downhole nuclear log (MVPL data)

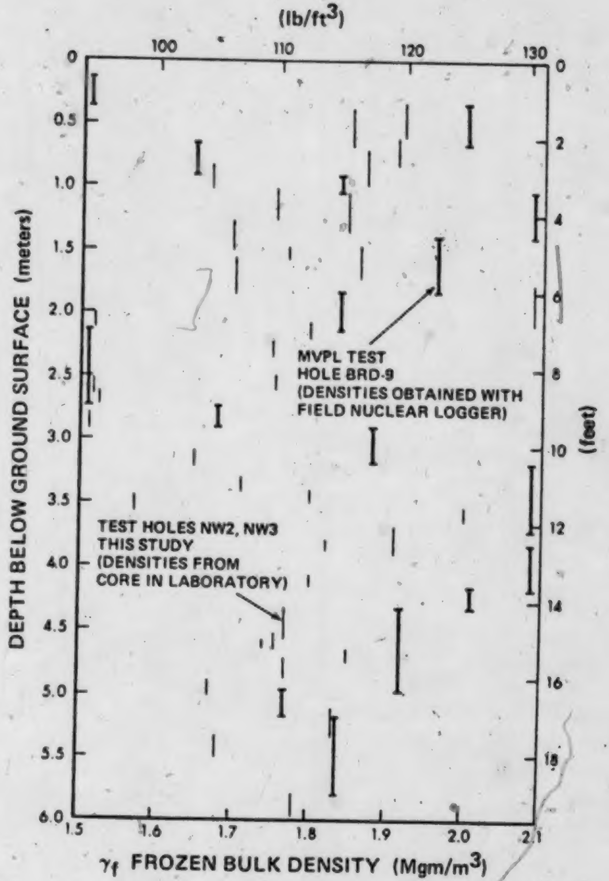

Figure A.20 Comparison between density profiles obtained from MVPL nuclear log and laboratory measurements on core from this study.

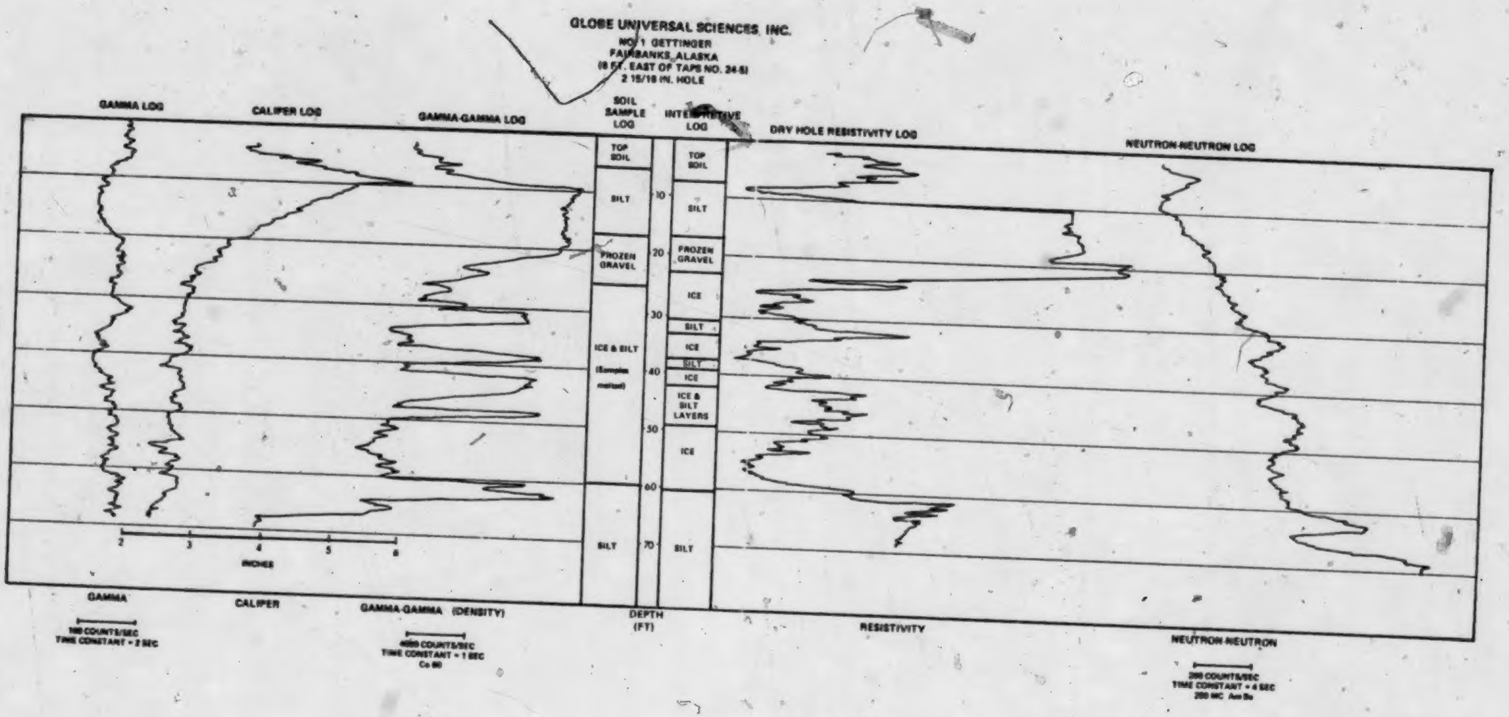

Figure A.21 Complete suite of logs for a borehole drilled in permafrost (courtesy of Well Reconnaissance Inc., Dallas, Texas)

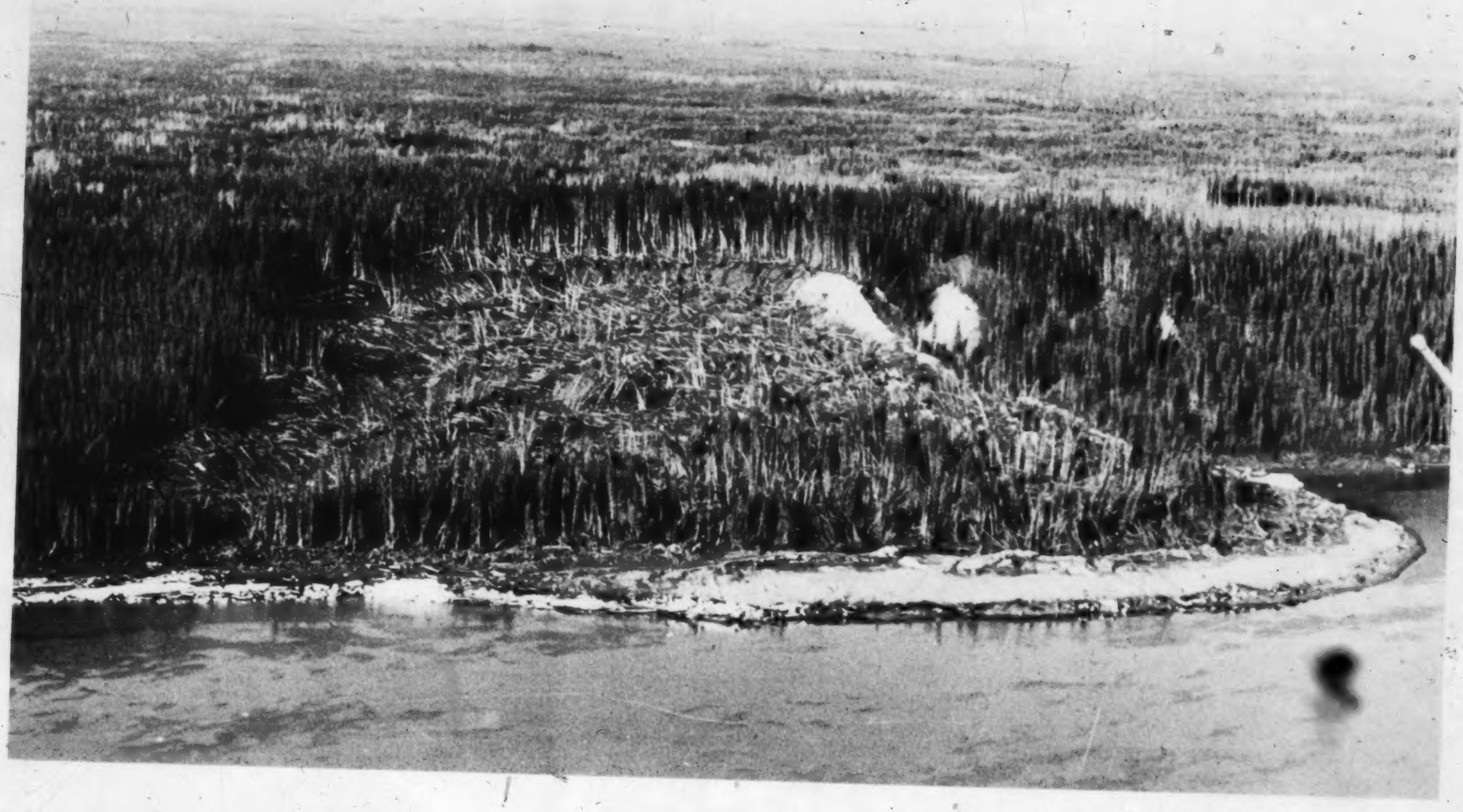

Plate A.1 Aerial view of Fort Simpson landslide sampling site, Mile 226, Mackenzie River (May, 1973)

Plate A.2 Headscarp sampling site, Fort Simpson landslide (October, 1973)

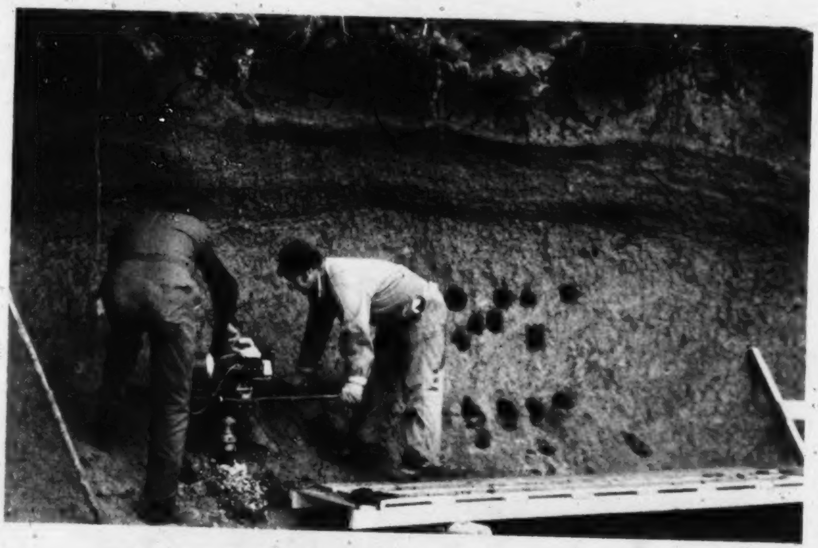

Plate A.3 Headscarp sampling site showing contact between Zones 2 and 3 (October, 1973)

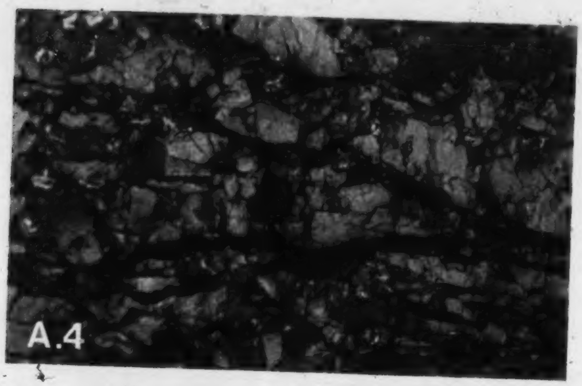
A.4

A.5

A.6

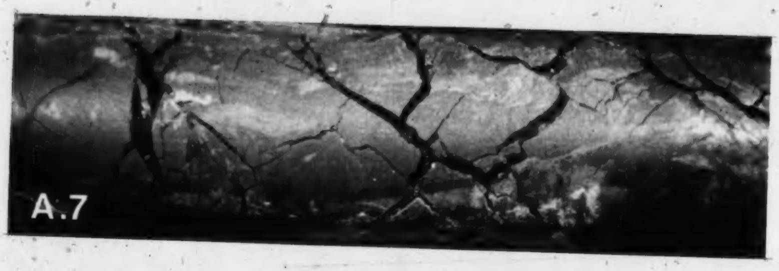
A.7

Plate A.4	Zone 3 structure exposed in vertical section, lens cap for scale (October, 1973)
Plate A.5	Zone 2, horizontal core (10 cm diameter)
Plate A.6	Zone 3, horizontal core (10 cm diameter)
Plate A.7	Zone 4, horizontal core (10 cm diameter)

A.8

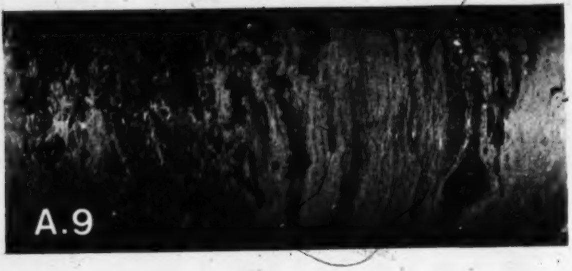

A.9

A.10

A.11

Plate A.8	Borehole NW2, 1.03 to 1.34 m (10 cm diameter)
Plate A.9	Borehole NW2, 1.83 to 2.07 m (10 cm diameter)
Plate A.10	Borehole NW2, 3.66 to 3.90 m (10 cm diameter)
Plate A.11	Borehole NW4, 5.82 to 6.00 m (10 cm diameter)

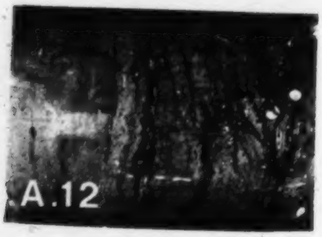

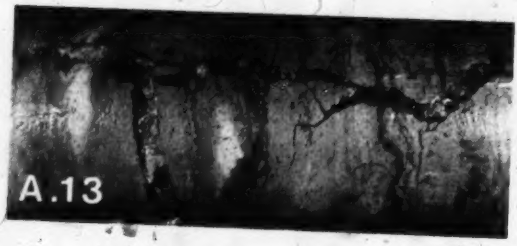

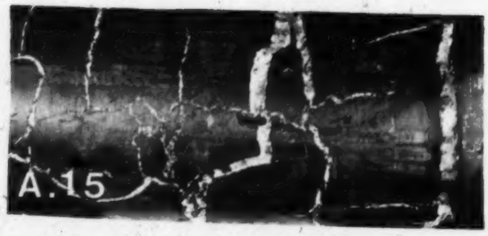

Plate A.12	Borehole NW2, 7.92 to 8.12 m (10 cm diameter)
Plate A.13	Borehole NW2, 8.17 to 8.38 m (10 cm diameter)
Plate A.14	Borehole NW3, 10.45 to 10.67 m (10 cm diameter)
Plate A.15	Borehole NW3, 11.89 to 12.13 m (10 cm diameter)

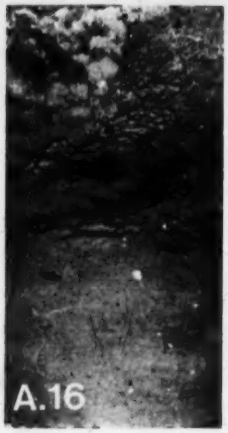

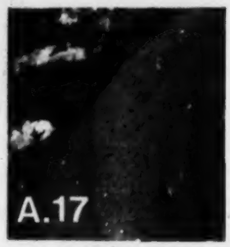

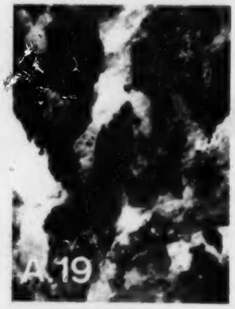

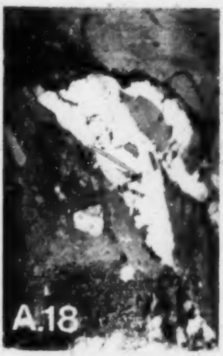

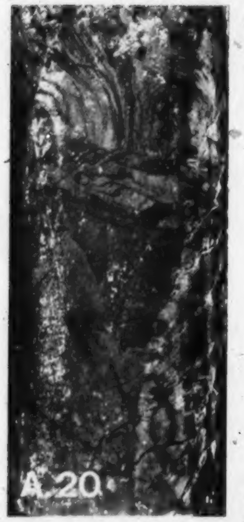

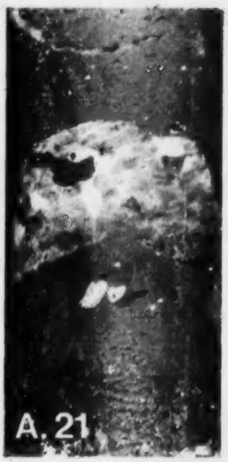

Plate A.16	Borehole NL2, 0.64 to 0.92 m (10 cm diameter)
Plate A.17	Borehole NL2, 4.26 to 4.39 m (10 cm diameter)
Plate A.18	Borehole NL2, 6.55 to 6.71 m (10 cm diameter)
Plate A.19	Borehole NL2, 7.50 to 7.62 m (10 cm diameter)
Plate A.20	Borehole NL2, 9.45 to 9.69 m (10 cm diameter)
Plate A.21	Borehole NL2, 10.97 to 11.21 m (10 cm diameter)

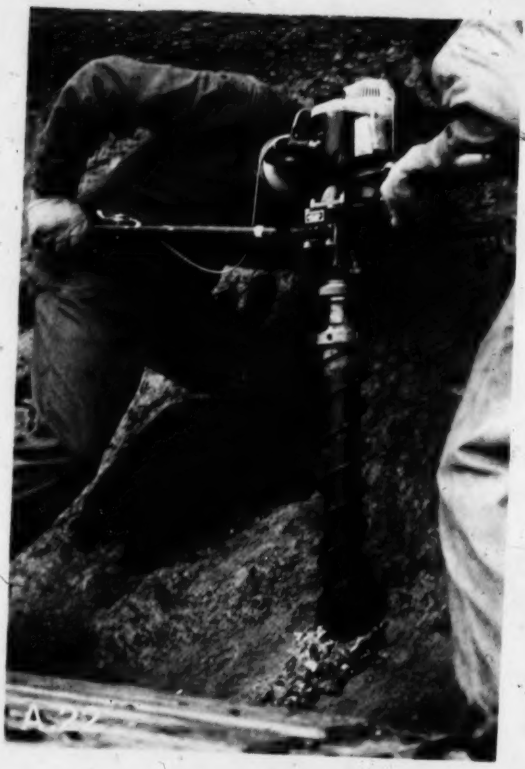
A.22

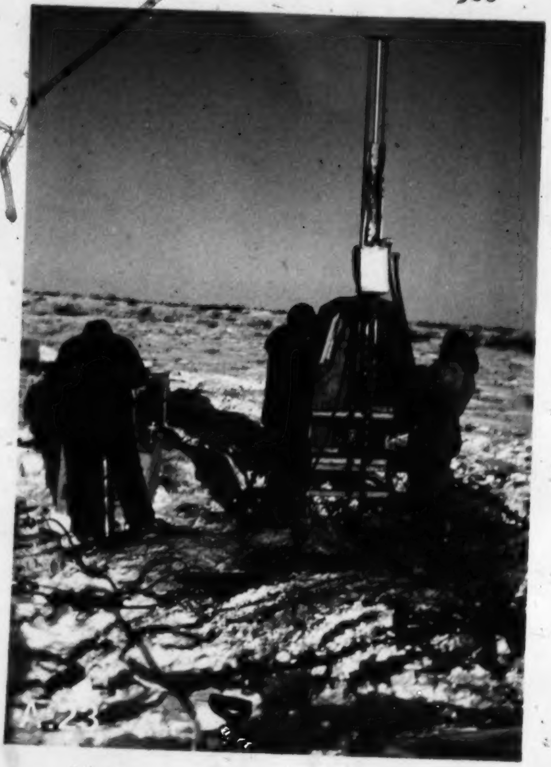
A.23

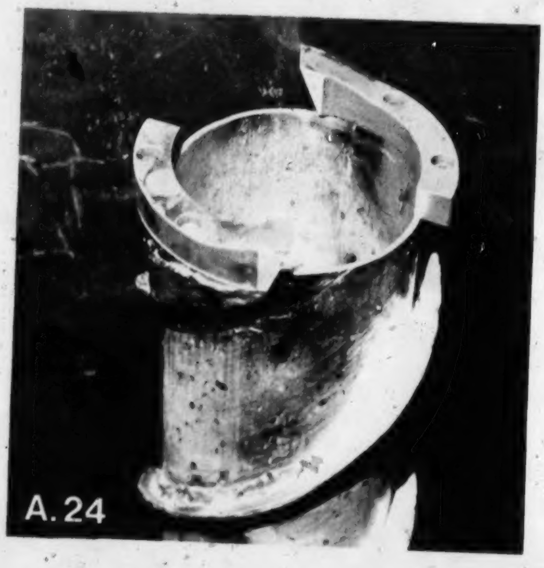
A.24

Plate A.22 Modified CRREL core barrel driven by gasoline-powered post-augering unit

Plate A.23 Heliportable "Ranger" drill equipped with hydrostatic drive (Mobile Augers and Research Ltd., Edmonton, Alberta)

Plate A.24 Closeup view of modified CRREL core barrel and cutting teeth

APPENDIX B

LABORATORY EQUIPMENT AND PROCEDURES

B.1 SAMPLE STORAGE AND PREPARATION

Sealed core boxes which contained samples returned from the field were stored for extended periods of time in cold room facilities without noticeable sample deterioration occurring. The successful storage over long periods was probably due in part to the fact that these samples had been packed with snow prior to sealing the lid. Some cores were stored for periods as long as six months before testing was commenced, and when opened, showed no discernable signs of desiccation. Untrimmed core stored in domestic deep freezes was packed in a similar manner with ice chips and snow. By making sure that the plastic sleeves fitted tightly and that each sample was packed in snow or crushed ice, it appeared that sublimation could be totally prevented.

When preparing samples for testing, it was essential to handle them with gloves to prevent damage that would otherwise be caused by localized thawing. It was found that room temperatures ranging from -5 to -8°C were best suited for maintaining workability and personal comfort while machining the specimens. The cores were rough-cut with a band saw, and a rotary diamond saw with a table guide was usually used to trim the ends. Cutting plastic soils with this device was difficult since cuttings built up on the saw blade and sometimes generated enough friction to stall the motor. The diamond saw was extremely effective in coarse-grained or pebbly soils, and also cut through highly ice-rich material quite well. In these soils, cutting proceeded rapidly, and it appeared that friction actually caused the diamond blade to melt, rather than cut its way through the core.

After being rough-cut to the required dimensions, cores were usually prepared for testing by turning them down on a small soil lathe which was designed specifically for that purpose. Plate B.1

illustrates the equipment used to trim permafrost core in this study. The lathe was fitted with a tungsten carbide cutter that was shaped to have a minimum 45° back clearance. A rounded cutting face appeared to give the best results. Rotational speed on the lathe was adjusted by trial and error to accommodate the specific characteristics of the material being worked. Ice-rich samples would only tolerate thin cuts being taken on each pass, since deeper cuts caused the ice to shatter or spall. In dense, plastic soils, cuts of up to 0.25 centimetres (0.1 inch) could be made without adverse effects. Once the designated diameter had been obtained, the sample was rotated slowly by hand and sprayed with a fine mist of water to build up a thin, even coating of ice. This film of ice retarded sublimation during storage and could easily be removed prior to testing. Between preparation and testing, the samples were stored in sealed, evacuated, double plastic bags. The bagged samples were then immersed in snow or ice crystals and placed in a commercial deep freezer operating at a temperature of approximately -10°C. Observations on samples stored for periods exceeding one year indicate that the methods described above held sublimation within tolerable limits. Several passes with an overhead milling machine were taken to face the ends off square. A four-point cutter with tungsten carbide inserts was turned at approximately 400 rpm, and successfully cut through all of the specimens, even including those which contained pebbles. This same machine was used to prepare samples for the direct shear tests and is shown on Plate B.2. Baker (1976) has described other methods for transporting, storing, and preparing permafrost samples for laboratory testing. He has also presented a more detailed discussion of the process of sublimation.

B.2 LABORATORY EQUIPMENT, PLANT AND INSTRUMENTATION

Several plates have been included here to illustrate the pieces of laboratory apparatus employed in the research work described in the body of this thesis. Plate B.3 shows the direct shear apparatus that was used to study shear strength in the frozen soils. The hanger assembly applying normal load, an LVOT measuring vertical deformation, and coolant lines running to and from the shear box are all clearly visible. The isothermal confined creep apparatus is shown on Plate B.4. The load frame and Bellofram air cylinders are seen applying axial load to the sample through a steel ball and load ram. Cooling coils and coolant lines can also be seen. At the extreme right of the photograph are segments of insulation which were normally fitted around the creep cells. The insulated cabinet which surrounded the cells throughout each test is viewed in this photograph with its front removed. Plate B.5 illustrates the permode with a residual stress test in progress. This photograph shows the lines circulating warm water through the load cap and base, a hanger applying vertical load, an LDVT measuring vertical deformation, and a pressure transducer measuring pore water pressures at the sample base. Drainage lines are connected to a burette, and wires from the LDVT and pressure transducer lead away to the data acquisition system. Plate B.6 shows a triaxial test in progress on a thawed permafrost core. Instrumentation consisting of an LDVT, load cell, and pore pressure transducer are all visible. The control board with its air pressure regulators, volume change indicators, and valving for the various cell pressure and drainage lines can be seen on the left side of the photograph.

Throughout the course of each testing program, frequent calibrations were performed on each piece of instrumentation that was used. Pressure transducers were checked by measuring precisely determined water heads which were maintained in the laboratory. LVDT's and load cells were calibrated at temperatures corresponding to those which would prevail as ambients during the testing. Whenever instruments were moved from cold to warm environments, they were sealed inside a plastic bag which then protected them from adverse effects which might have otherwise resulted from condensation. Power supply voltages in the data acquisition system were also checked at regular intervals. Moving pressure transducers in and out of a cold environment was avoided in all cases since it was recognized that this sort of abuse would accelerate the deterioration of strain gauge bonding on the transducer diaphragm. Therefore, a small plug was inserted in the transducer block during test set ups in the cold room. This plug was later removed and replaced with a pressure transducer once the apparatus had been warmed up to room temperature.

Figure B.1 presents a 7 day record of temperatures measured at 4 different points in the isothermal creep apparatus. A thermistor placed in the temperature-controlled refrigerated bath indicated a maximum fluctuation of 0.05 C°. Room air temperatures fluctuated by nearly 2 C° and were significantly affected by the brief cold room defrost cycles which occurred twice daily. A third thermistor was placed inside the insulated test chamber, but outside the creep cell. It indicated a damped temperature record that followed room temperature fluctuations quite closely. The combined effects of fluid circulated from the bath and additional insulation placed around the creep cell were able to keep temperature fluctuations measured adjacent to the test sample within approximately ±0.1C°. Although the room was lighted with florescent lamps, it can be seen that leaving the lights on for an extended period of time had a noticeable effect on the room temperature. This temperature record provides some indication of the problems associated with achieving acceptable temperature control in long term tests. Results obtained in this study suggest that the technique of placing thermally sensitive tests within an insulated test chamber, and using forced circulation of temperature-controlled fluids is capable of maintaining nearly isothermal conditions over extended time periods. Providing for high capacity flow from the refrigerated baths and including large heat exchanger coils are important elements of this procedure. It is also essential to include maximum amounts of insulation and ensure that metallic components in the apparatus are thermally isolated from parts of the testing frame which extend outside the isolation chamber. It may also be avantageous to operate the refrigerated bath within a cold room where better overall temperature control can be obtained. The fact that several occasions of mechanical failure of the refrigeration plant were encountered during the course of this research stresses the importance of providing a temperature alarm system for each cold room. An investment of this sort is easily justified when the costs associated with obtaining undisturbed permafrost core are determined, especially when the difficulty associated with replacing it is taken into consideration. Similar steps are probably also warranted with individual long term tests. Baker et al. (1976) have discussed various aspects of geotechnical cold room operation and design in considerably more detail.

Since thermistors have the property of being ultrasensitive resistors, their resistance-temperature characteristics are extremely nonlinear. This nonlinearity necessitated the use of a buffering circuit (shown in Figure B.2) to linearize the output obtained from Atkins type 3 thermistors which were excited with a constant voltage power supply. The thermistors used in this study were linearized over a narrow temperature range that was of particular interest in the laboratory programs. The Atkins type 3 thermistor has a resistance of approximately 5870 ohms at +20°C and 51800 ohms at -20°C. Resistors used in the circuit shown in Figure B.2 are summarized as follows:

R1 = 6000 ohms
R2 = 9760 ohms
R3 = 9760 ohms
R4 = 50000 ohms
R5 = adjustable, 2000 ohms maximum
R6 = 3000 ohms
R7 = 48000 ohms
R8 = adjustable, 5000 ohms maximum

A power supply was used to provide a constant six volt excitation to the bridge. Output was measured with a digital voltmeter. It can be seen that resistances 5 and 6 must be adjusted to equal the resistance of the thermistor at +20°C. Resistances 7 and 8 are then adjusted to equal the resistance of the thermistor at -20°C. All of the thermistors used in the study were combined with a linearizing circuit that was adjusted in this manner, and each was calibrated against a digital quartz thermometer. Closely matched results were obtained which permitted using a spline function interpolation routine to generate a universal thermistor calibration curve. This curve was then tabled with the computer and could be called upon during data reduction to convert recorded voltages to temperatures. The linearization circuit also had a built in calibration test so that small changes in electronic conditioning could be compensated by adjusting the 1000 ohm variable resistance located at the extreme left of the circuit.

B.3 SCANNING ELECTRON MICROSCOPE STUDY OF MICROSTRUCTURE

A Cambridge scanning electron microscope (SEM) was used to conduct a brief microfabric study of some of the different soil types encountered in the laboratory program reported in the body of this thesis. Several plates have been included which illustrate some of the typical features observed in the course of the SEM study. Specimens were prepared for viewing by first freeze-drying them. Fractured surfaces were conditioned by coating them with epoxy and peeling the face once the specimen had been mounted on a stud. Specimens containing shear planes were handled carefully to minimize disturbance to any oriented fabric which might be present along structures which had been induced during testing.

Plate B.7 is a vertical view of a shear plane that was removed from one of the direct shear specimens described in Chapter III. The scale on this and all of the other scanning electron micrographs has been indicated in the upper left hand corner of each plate. A high degree of orientation is apparent, and the clay mineral species of illite and kaolinite can be identified. Photographs taken in vertical sections through this and other shear planes revealed that the zone of highly oriented and compressed fabric was restricted to a thickness of 10 to 20 microns below the surface viewed here. Photographs with a lower magnification revealed well-defined striations and slickensides on the shear plane.

Plate B.8 shows fabric exposed on a typical vertical section in glaciolacustrine silty clay from the Fort Simpson landslide headscarp. This particular sample was taken from Zone 4. Vertical runs from the upper right to the lower left hand corner of the photograph. This plate shows a strongly dispersed structure characterized by a particularly high degree of plate parallelism which approaches completely preferred orientation. Some textural stratification can be discerned on a larger scale. Fabric in this material ranged from being strongly dispersed as shown here, to turbostratic with particle orientation generally paralleling the bedding planes. Most of the mineral particles on this plate are viewed edge-on.

On plate B.9, several silt-sized units can be seen, and it is apparent that these consist of compact aggregates of discrete and identifiable clay mineral particles. This condition is consistent with the fact that these sediments were glacially eroded from Cretaceous shales in the Fort Simpson vicinity, and were subsequently deposited in a glaciolacustrine environment after being transported over a relatively short distance. Distinct silt-sized particles were discerned only in material that was sampled from Zone 2. All other silt sizes consisted of aggregates of clay particles.

Plate B.10 shows typical fabric from the stratified silty clay sampled at the Norman Wells site. Structure visible here is quite similar to that observed with the Fort Simpson material and tends to be mainly turbostratic. Once again, very few discrete silt grains were identified. On this sample, vertical runs from the upper right to the lower left corner of the photograph. Plate B.11 shows similar material, but includes a piece of organic material. The diagonal linear feature is probably part of a piece of grass or a root filament.

Plate B.12, shows very compact fabric which was observed in a dense piece of till extracted from the Noell Lake profile. The photograph orientation is approximately correct, and it can be seen that the particles exhibit a strong preferred orientation. The dominant factor in producing this structure has probably been the extreme degree of compression produced by overburden stresses during glaciation. Small pebbles included in the till were also examined and exhibited mineralogy that was similar to the matrix soil. As in all of the previous plates, distinct silt sizes were seldom observed.

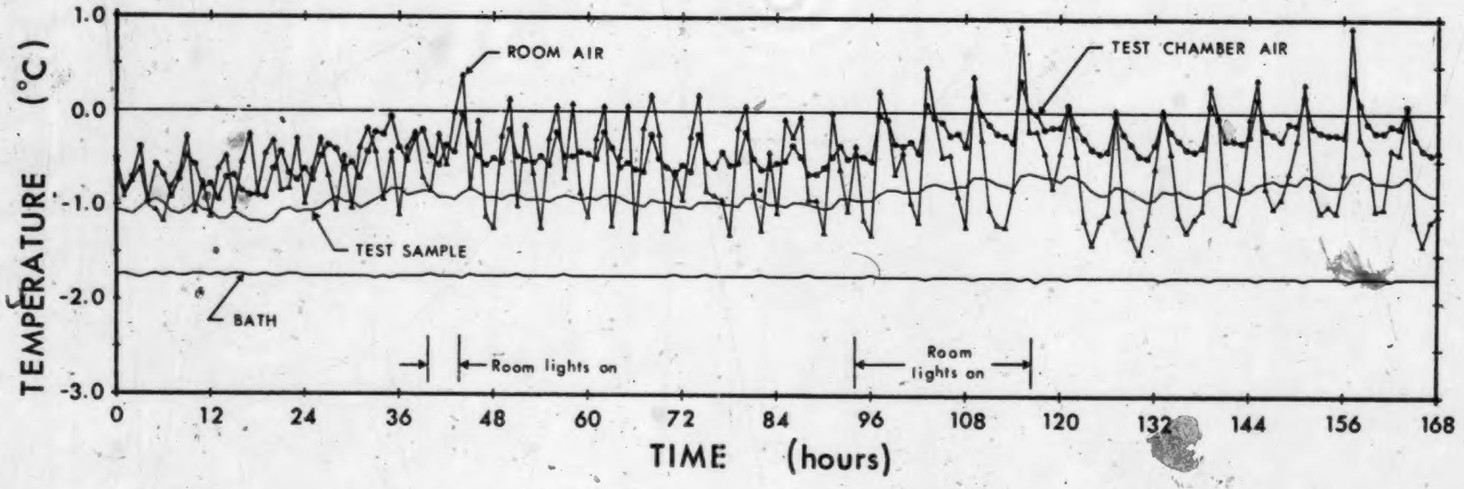

Figure B.1 Temperature record for an isothermal confined creep test

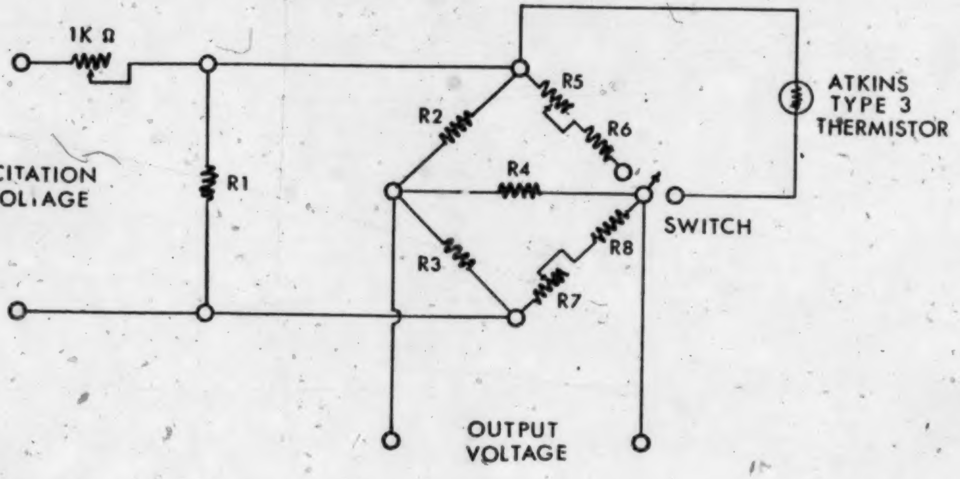
1K Ω
EXCITATION VOLTAGE
R1
R2
R3
R4
R5
R6
R7
R8
ATKINS TYPE 3 THERMISTOR
SWITCH
OUTPUT VOLTAGE

Figure B.2 Circuit for linearizing output signal from thermistor

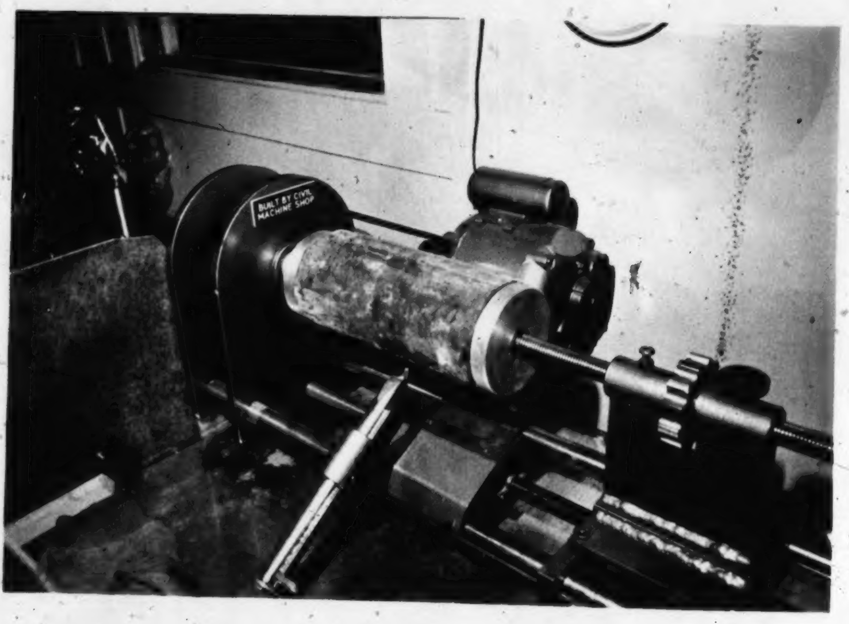
BUILT BY CIVIL
MACHINE SHOP

Plate B.1 Soil lathe used to trim permafrost core

Plate B.2 Overhead milling machine with carbide cutter, used to trim permafrost core

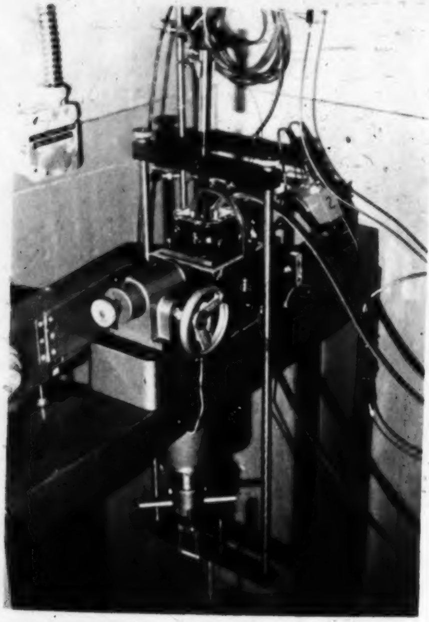

Plate B.3 Direct shear apparatus

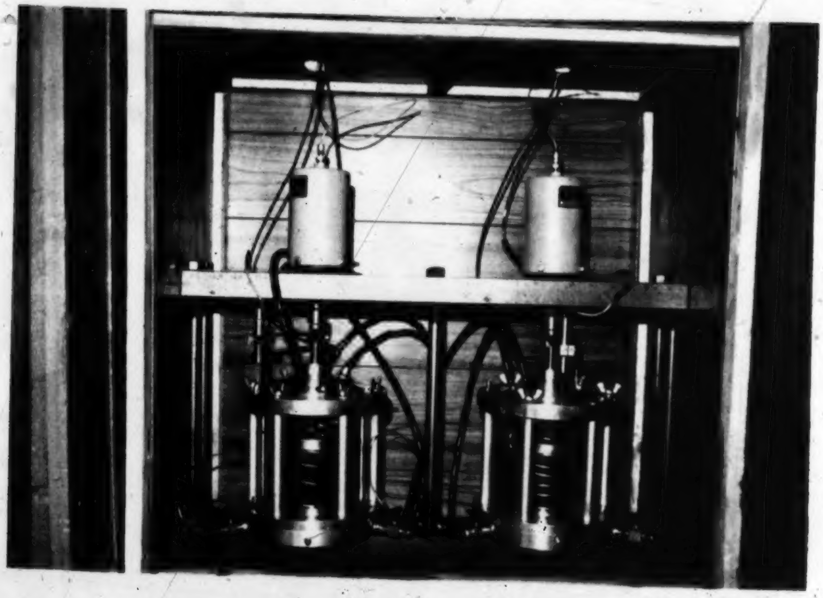

Plate B.4 Isothermal confined creep apparatus

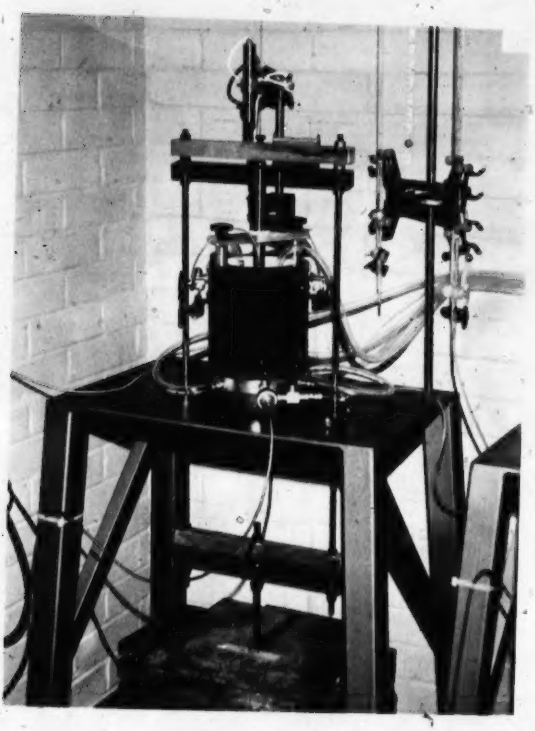

Plate B.5 Residual stress test in progress showing permode and associated apparatus

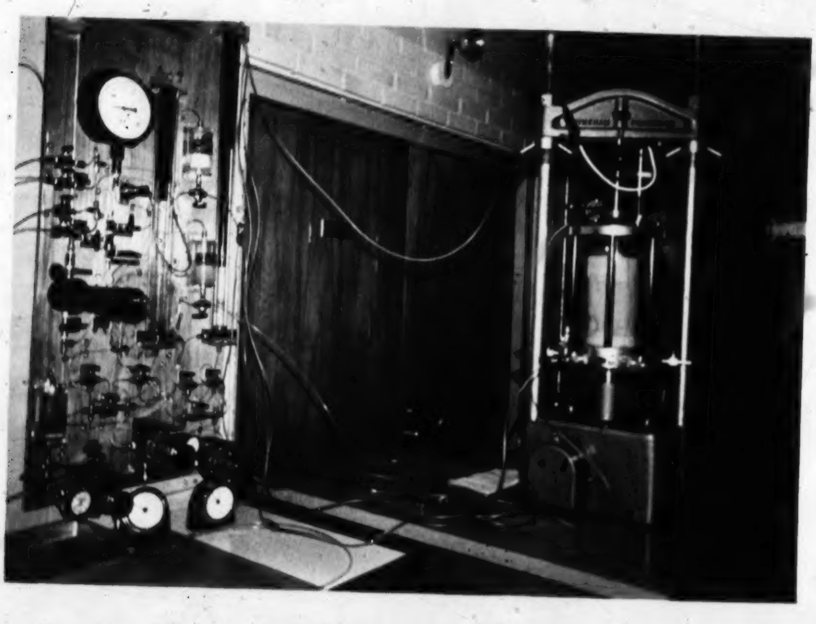

Plate B.6 Triaxial test in progress showing cell and associated apparatus

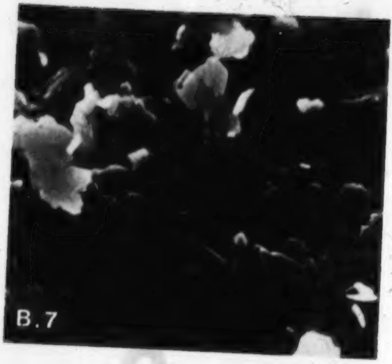

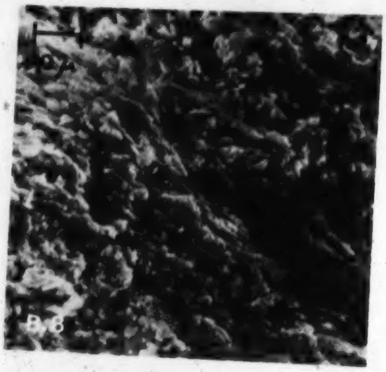

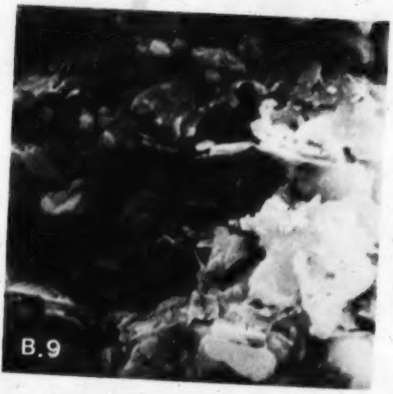

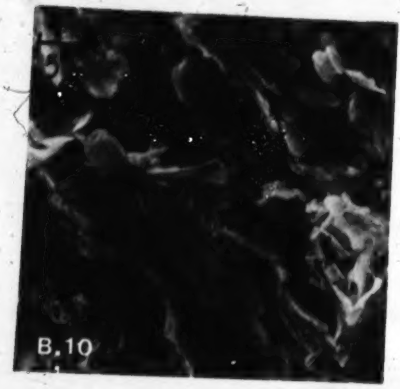

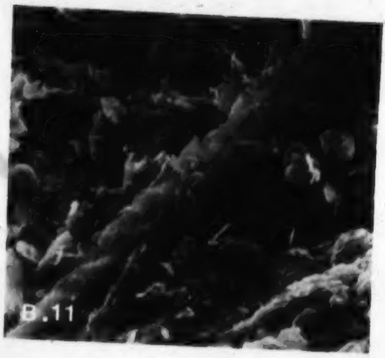

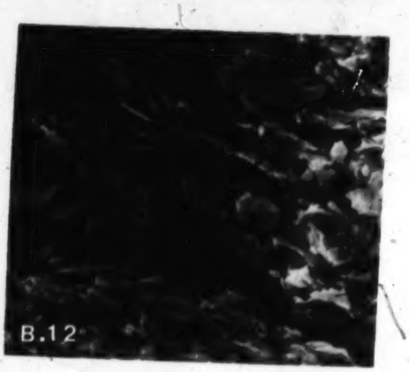

Plate B.7	Vertical view of shear plane in frozen soil
Plate B.8	Stratification and typical fabric, Zone 4, Fort Simpson sampling site
Plate B.9	Aggregates of recognizable clay minerals making up silt-sized grains
Plate B.10	Typical fabric in laminated silty clay, Norman Wells (MVPL) sampling site
Plate B.11	Organic inclusion in silty clay, Norman Wells (MVPL) sampling site
Plate B.12	Compact fabric in dense silty clay, Noell Lake sampling site

APPENDIX C

SUMMARY OF LABORATORY TEST DATA

C.1 DIRECT SHEAR TESTS

TABLE C.1 SUMMARY OF DATA FROM DIRECT SHEAR TESTS, FORT SIMPSON LANDSLIDE HEADSCARP SAMPLING SITE (ZONE 4)

TEST	FROZEN BULK DENSITY (Mg/m^3)	WATER CONTENT (%)	NORMAL STRESS (kN/m^2)	PEAK SHEAR STRESS (kN/m^2)	DILATANCY AT PEAK (%)	SHEAR ZONE THICKNESS[1] (cm)	DISPLACEMENT RATE (cm/day)	AVERAGE TEMPERATURE (°C)	REMARKS
FS-01	1.95	26.7	252	296 308[2]	1.10	1.8	8.3×10^{-2}	-1.40	Single vertical lens, 0.2 cm thick
FS-02	1.98	25.9	131	240 165	0.20	1.2	9.2×10^{-2}	-1.40	No segregated ice
FS-03	1.81	24.9	491	361 301	0.20	1.0	9.9×10^{-2}	-1.40	Very thin, randomly oriented lenses
FS-04	1.77	50.2	367	374 313	0.0	1.3	9.6×10^{-2}	-1.45	Oblique diagonal lens, 1.5 to 2 cm thick, soil inclusions
FS-05	1.89	26.8	667	471 370	0.30	1.7	10.4×10^{-2}	-1.40	0.9 cm vertical lens intersecting corner; otherwise, thin random lensing
FS-06	1.86	31.0	98 (221)[3]	274 265	0.20	1.6	9.8×10^{-2}	-1.40	Very thin, randomly oriented lenses
FS-07	1.95	25.1	456	396 319 245	-0.10	1.1	2.9×10^{-1} 1.0	-1.60	Hairline lenses, oblique; 0.6 cm lens intercepting corner
FS-08	1.90	32.4	218	261 246 261 219	0.30	1.0	2.9×10^{-1} 1.8	-1.45	Continuous 0.3 cm vertical lens running diagonally, soil inclusions
FS-09	1.93	30.0	370	376 268 232	0.0	1.1	1.8	-1.60	Thin, randomly oriented lenses, reticulate structure
FS-10	1.88	21.2	311	394 233 200 163 184 148	0.55	0.8	1.9	-1.45	Adjacent to FS-09, vertical 0.2 cm lens and other thinner ones randomly oriented
FS-11	1.93	25.0	370	495 324	0.15	0.9	2.0	-1.60	Very thin, subvertical lenses concentrated on one side
FS-12	1.95	26.8	129	359 195 149 104	1.10	1.0	1.9	-1.45	Single oblique lens, 0.1 cm thick
FS-13	1.76	37.4	609	408 319 229	-0.05	0.9	3.0×10^{-1}	-1.50	Sub-vertical lense running from corner to corner, thickens to 0.8 cm near the top, soil inclusions
FS-14	1.88	35.8	133	286 240	-0.05	1.1	3.3×10^{-1}	-1.45	Oblique diagonal lens, 0.3 cm thick
FS-15	1.97	26.2	667 (903)	517 505 386 368 334	0.35	1.0	1.9	-1.40	Massive, no segregated ice visible
FS-16	1.95	26.8	192	333 291 267 289 277 289 271 290	2.0	1.0	1.8	-1.30	As above

---

[1] Shear zone thickness estimated from shear structures visible on longitudinal, vertical section of specimen examined after the test had been completed.

[2] Indicates peak shear stress mobilized in second and subsequent cycles of shear.

[3] Normal stress increased at the midpoint on the second cycle of shear (after first shear box reversal).

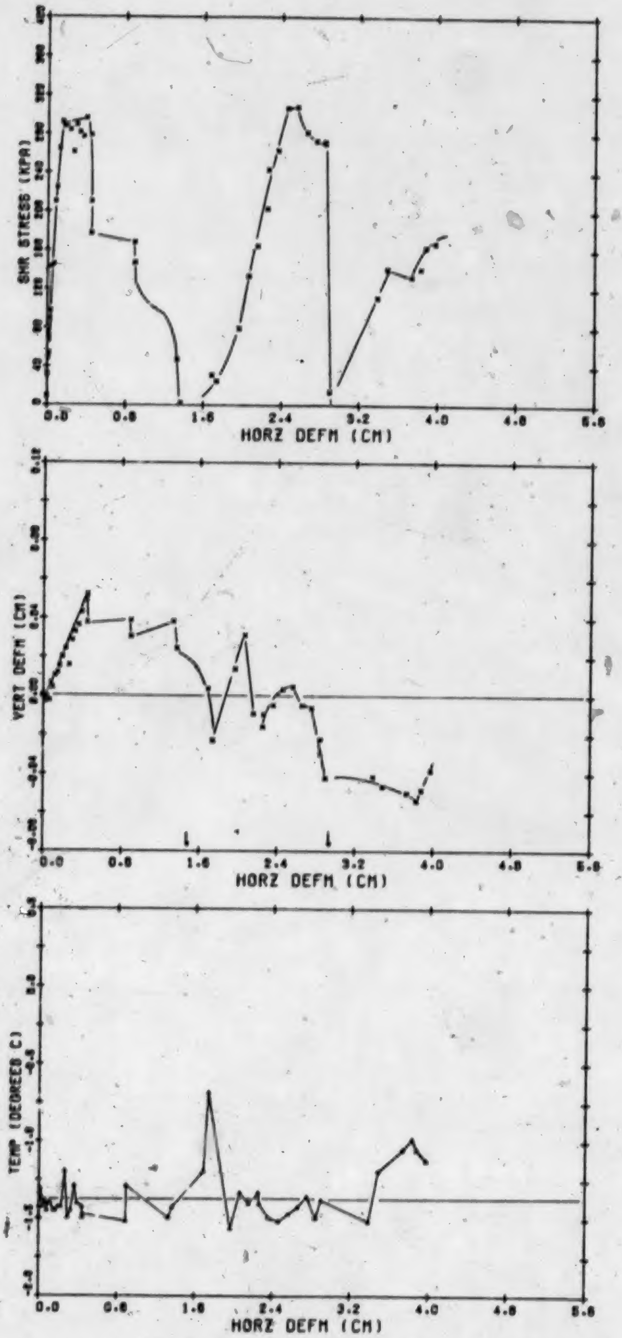

Figure C.1 Direct shear test FS-01

σ_n = 252 kN/m^2 γ_f = 1.95 Mg/m^3

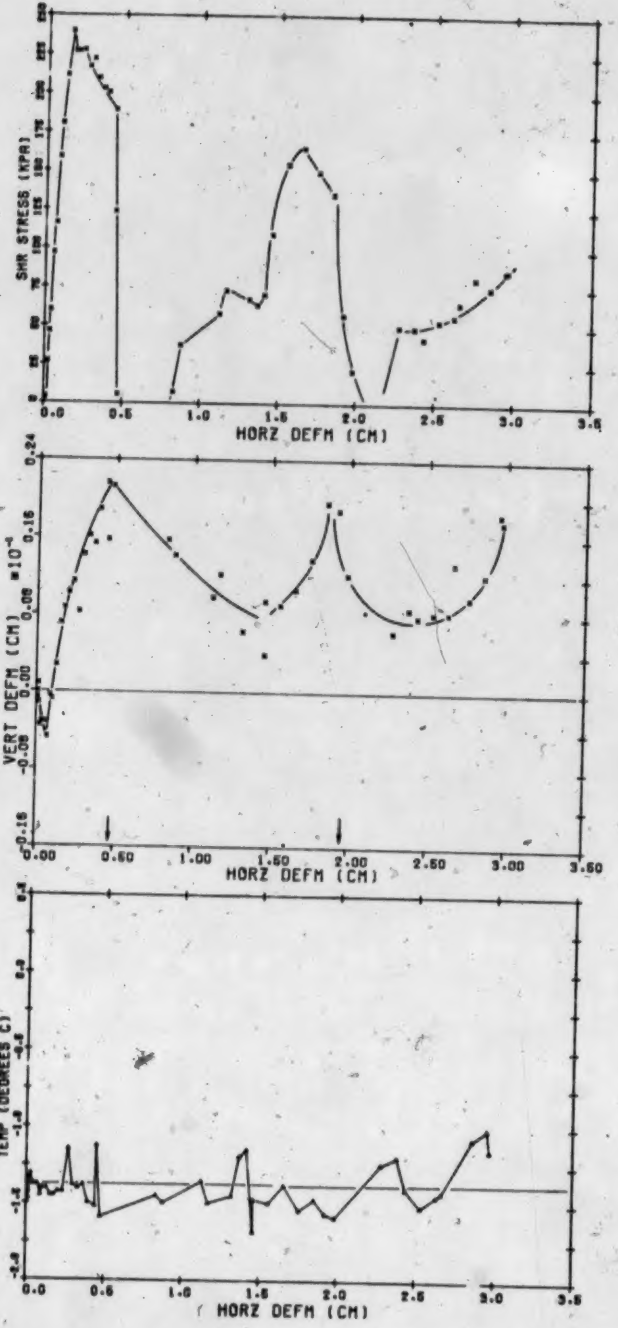

Figure C.2 Direct shear test FS-02

$\sigma_n = 131\ \text{kN/m}^2 \quad \gamma_f = 1.98\ \text{Mg/m}^3$

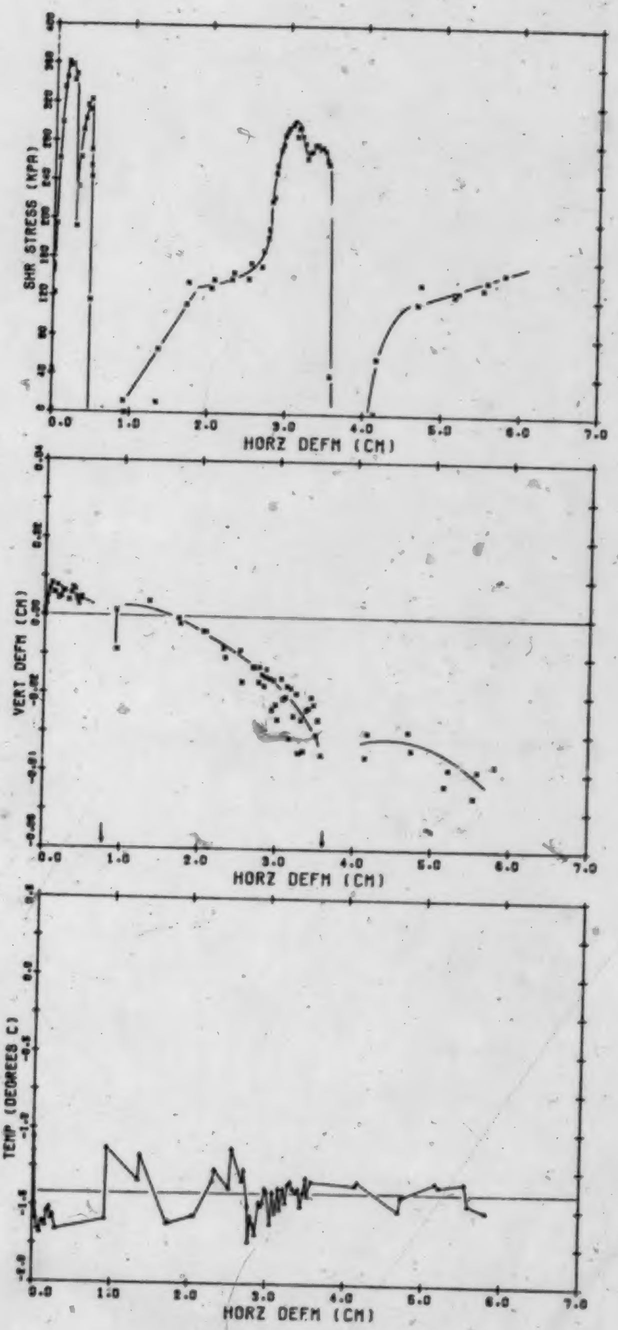

Figure C.3 Direct shear test FS-03

$\sigma_n = 491\ \mathrm{kN/m^2} \quad \gamma_f = 1.81\ \mathrm{Mg/m^3}$

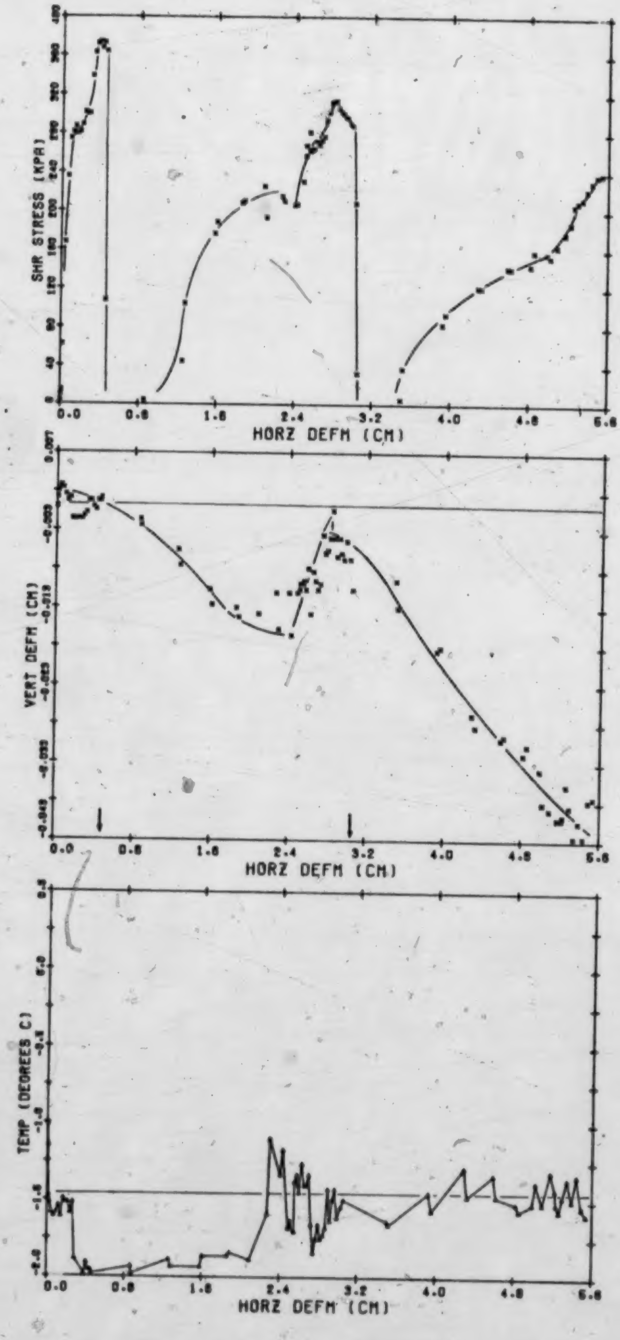

Figure C.4 Direct shear test FS-04

$\sigma_n = 369\ kN/m^2 \quad \gamma_f = 1.77\ Mg/m^3$

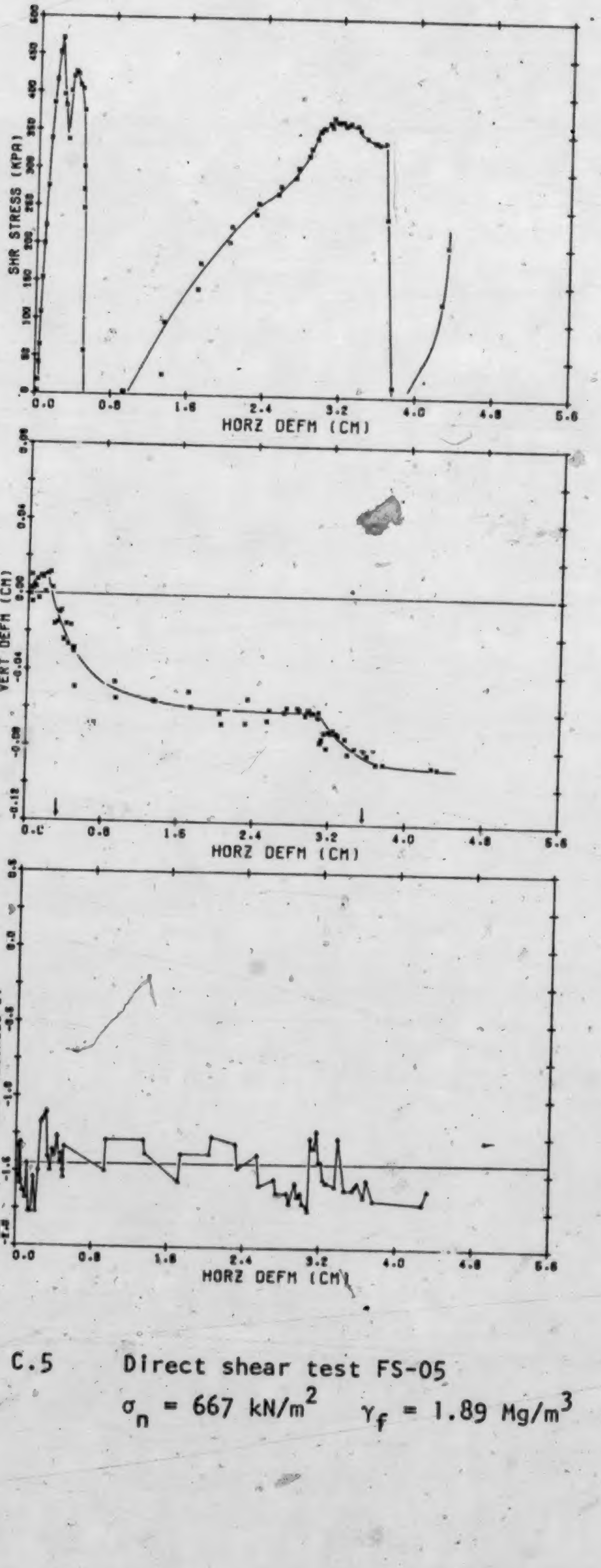

Figure C.5 Direct shear test FS-05

$\sigma_n = 667$ kN/m^2 $\gamma_f = 1.89$ Mg/m^3

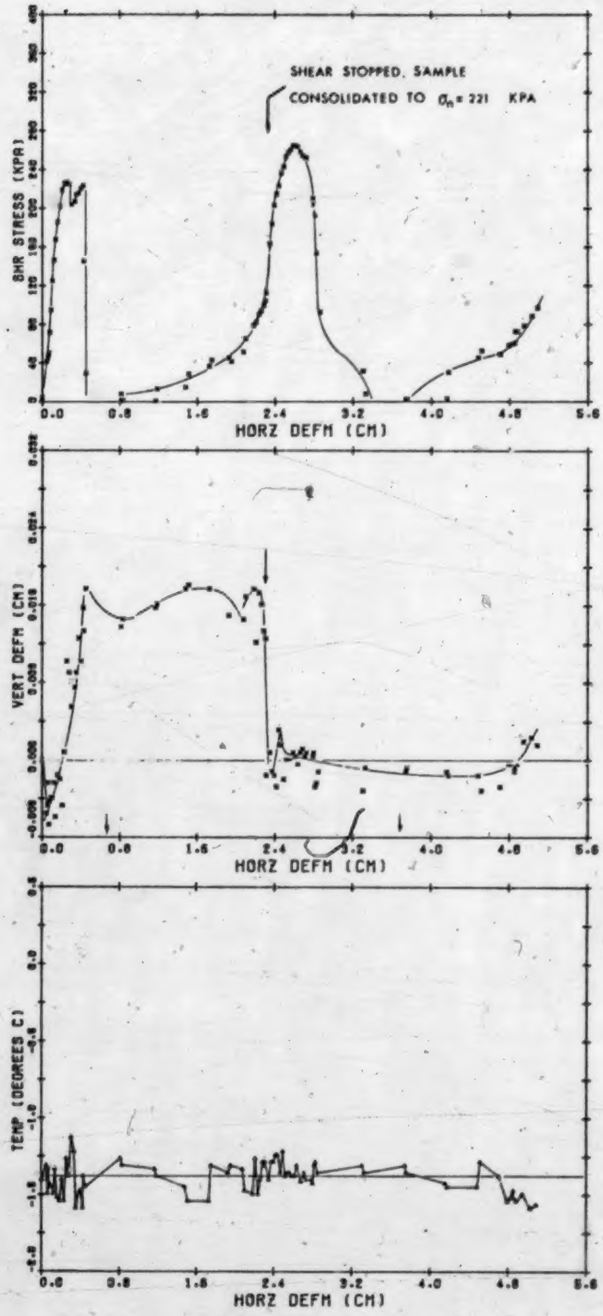

Figure C.6 Direct shear test FS-06

σ_n = 98 kN/m^2 γ_f = 1.86 Mg/m^3

221 kN/m^2

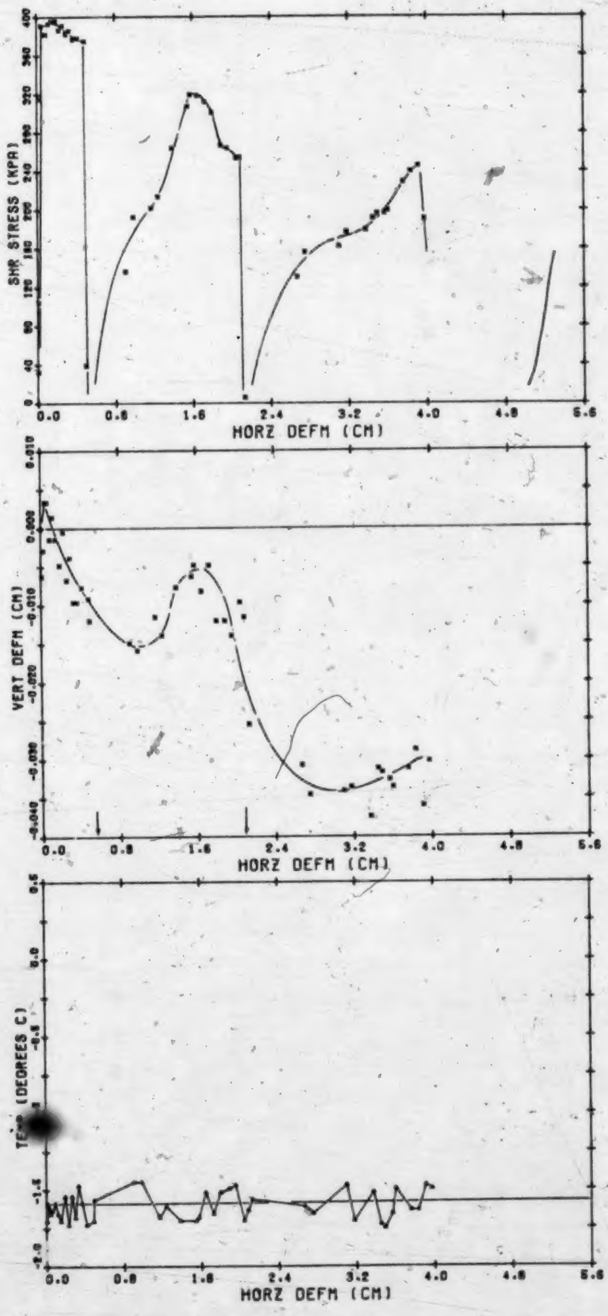

Figure C.7 Direct shear test FS-07

$\sigma_n = 456\ \mathrm{kN/m^2} \quad \gamma_f = 1.94\ \mathrm{Mg/m^3}$

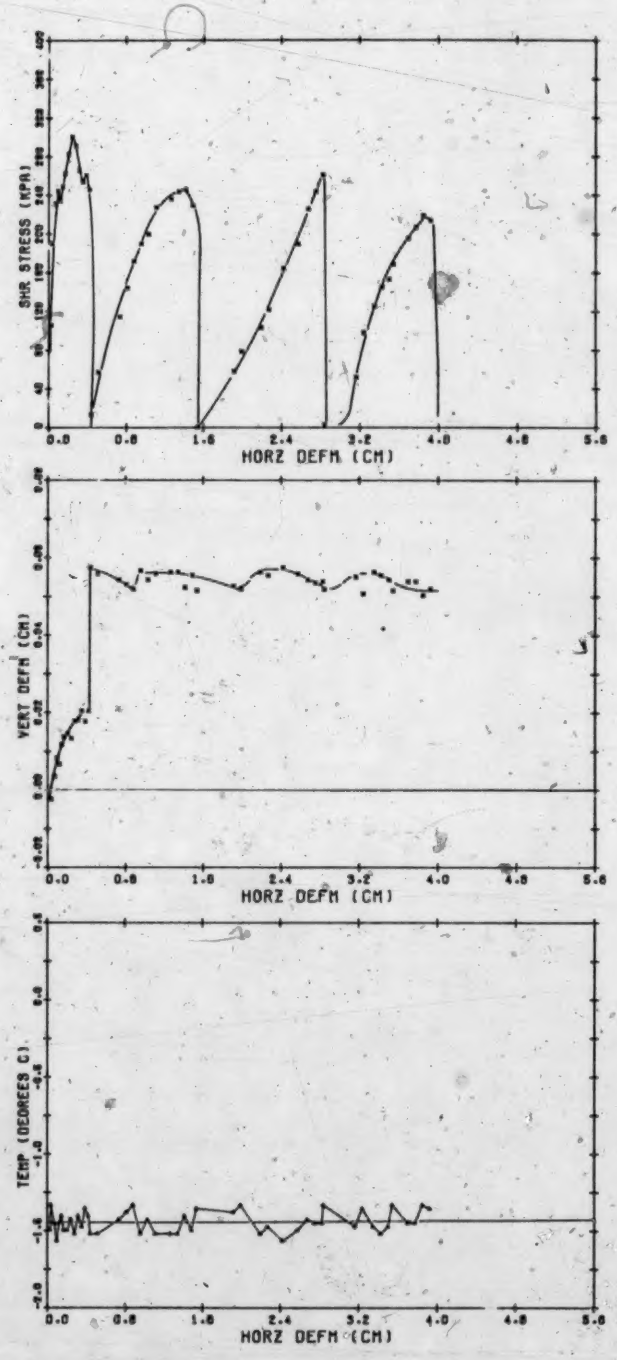

Figure C.8 Direct shear test FS-08

$\sigma_n = 217\ \text{kN/m}^2 \quad \gamma_f = 1.90\ \text{Mg/m}^3$

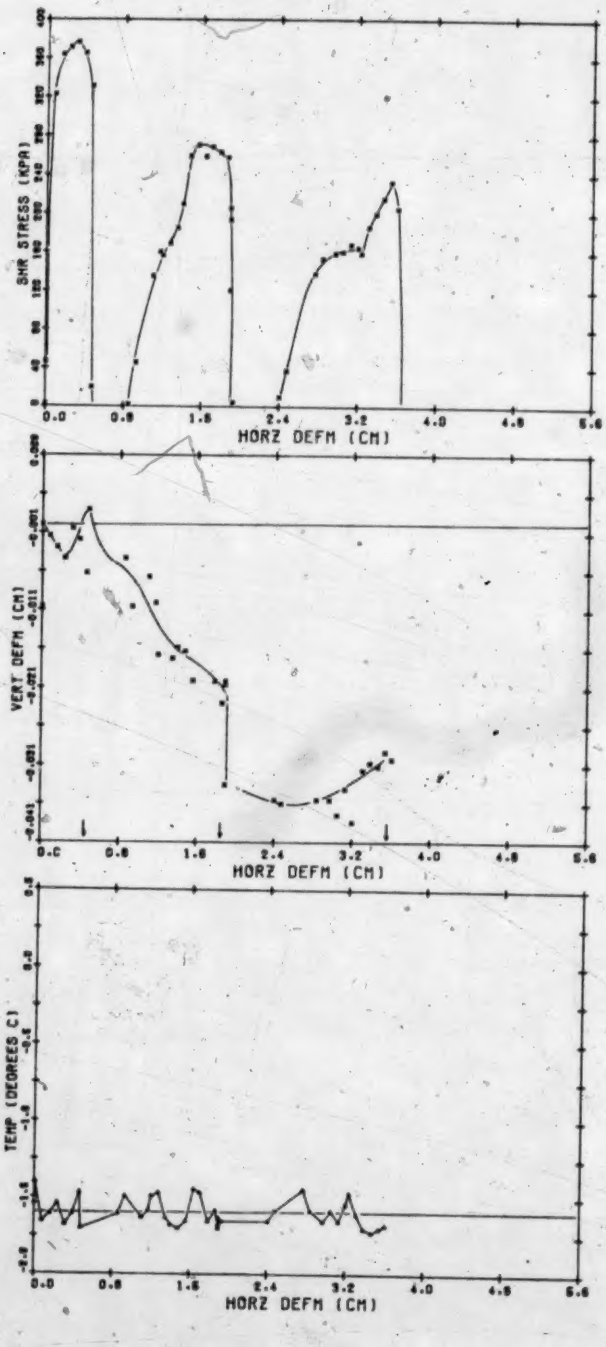

Figure C.9 Direct shear test FS-09

$\sigma_n = 370$ kN/m^2 $\gamma_f = 1.93$ Mg/m^3

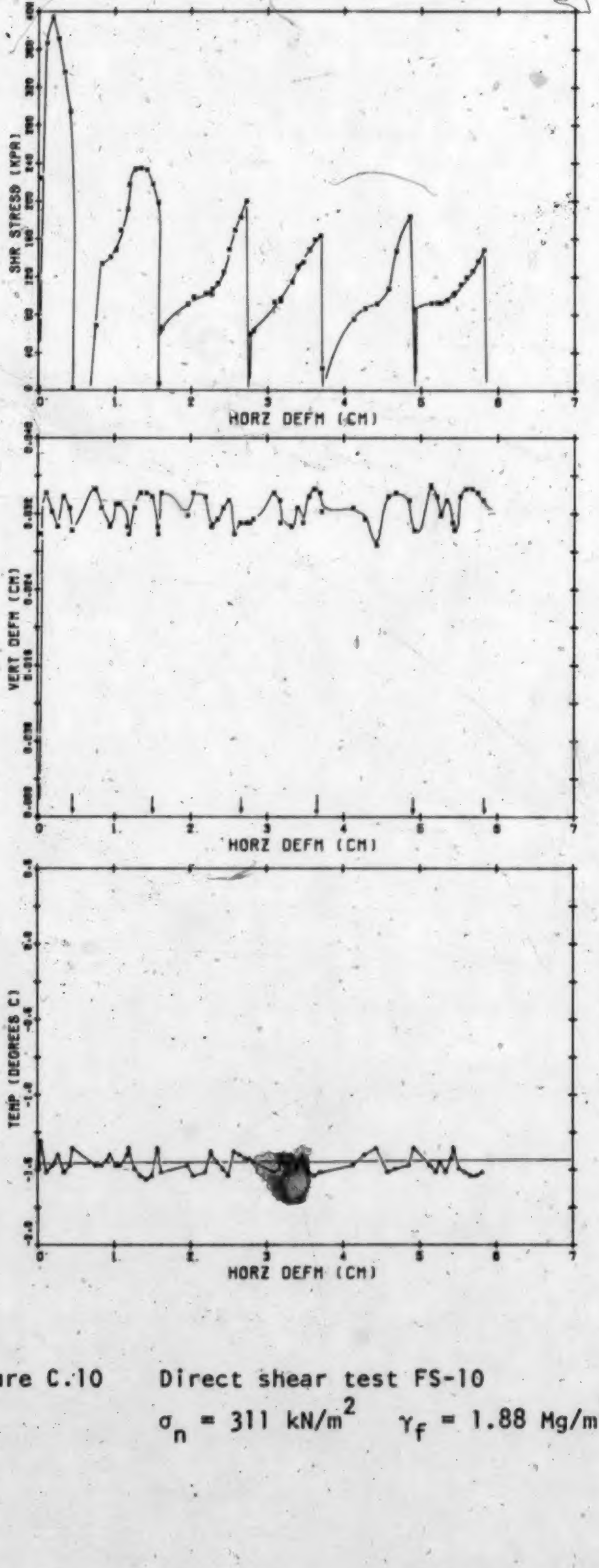

Figure C.10 Direct shear test FS-10

$\sigma_n = 311$ kN/m^2 $\gamma_f = 1.88$ Mg/m^3

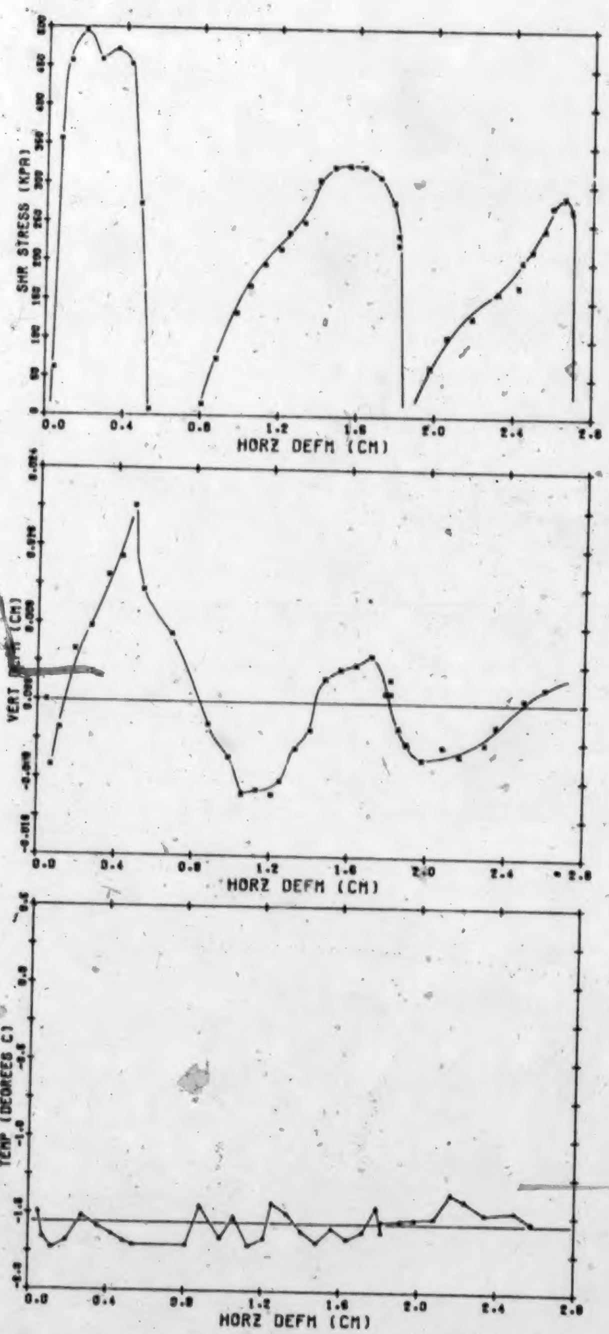

Figure C.11 Direct shear test FS-11

$\sigma_n = 370\ \text{kN/m}^2 \quad \gamma_f = 1.93\ \text{Mg/m}^3$

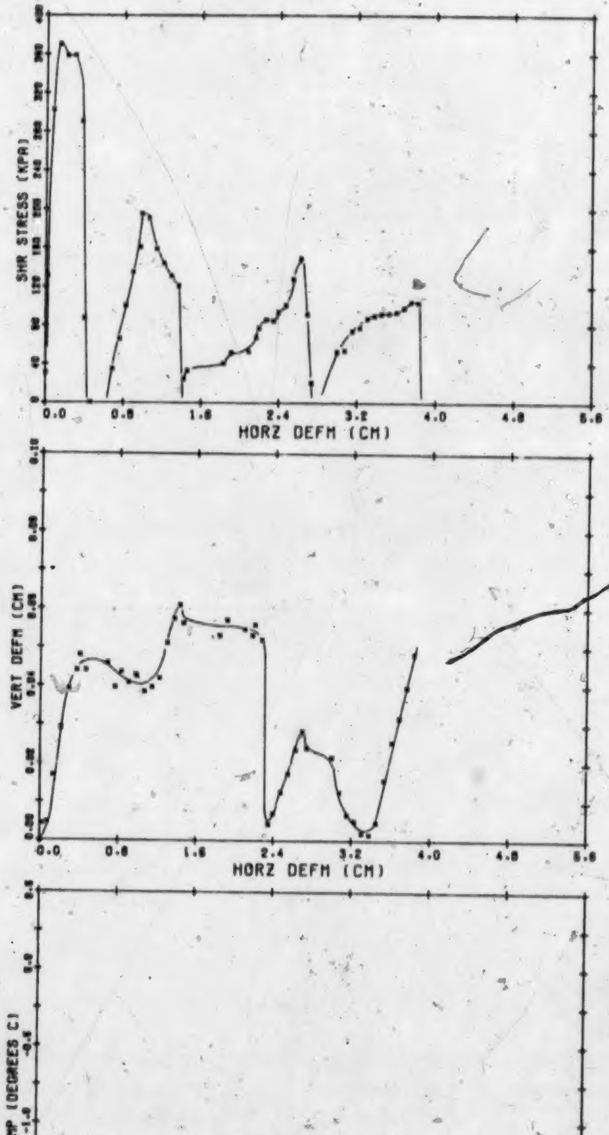

Figure C.12 Direct shear test FS-12
$\sigma_n = 129\ \text{kN/m}^2 \quad \gamma_f = 1.95\ \text{Mg/m}^3$

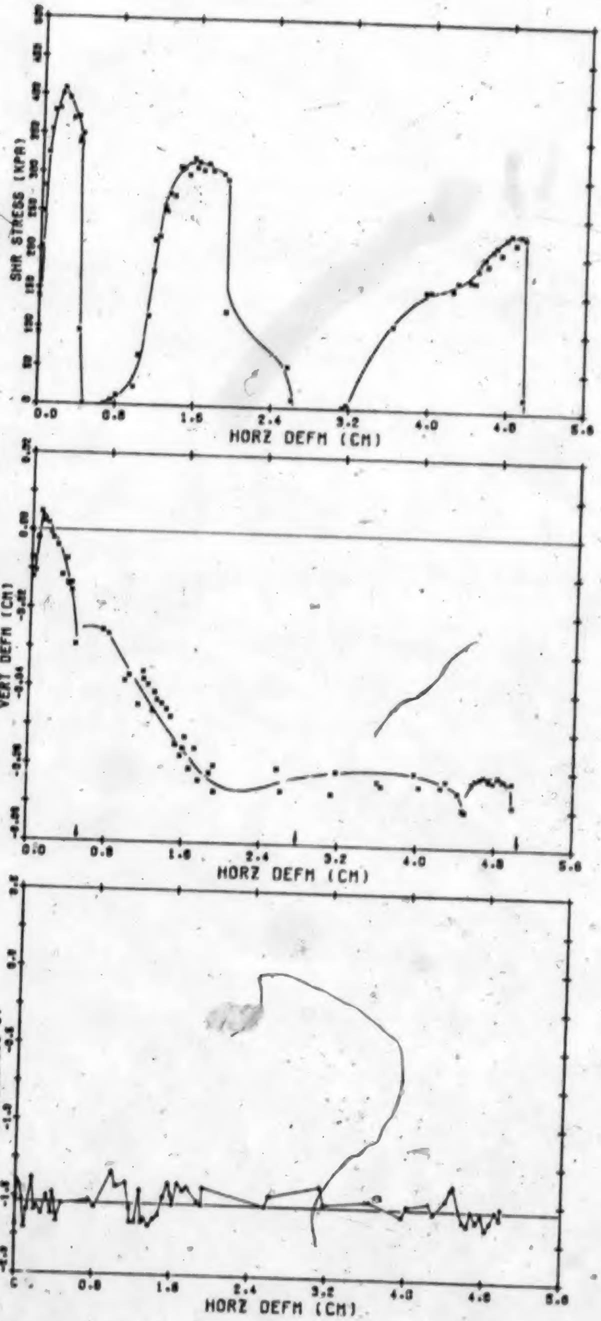

Figure C.13 Direct shear test FS-13
$\sigma_n = 609$ kN/m^2 $\gamma_f = 1.76$ Mg/m^3

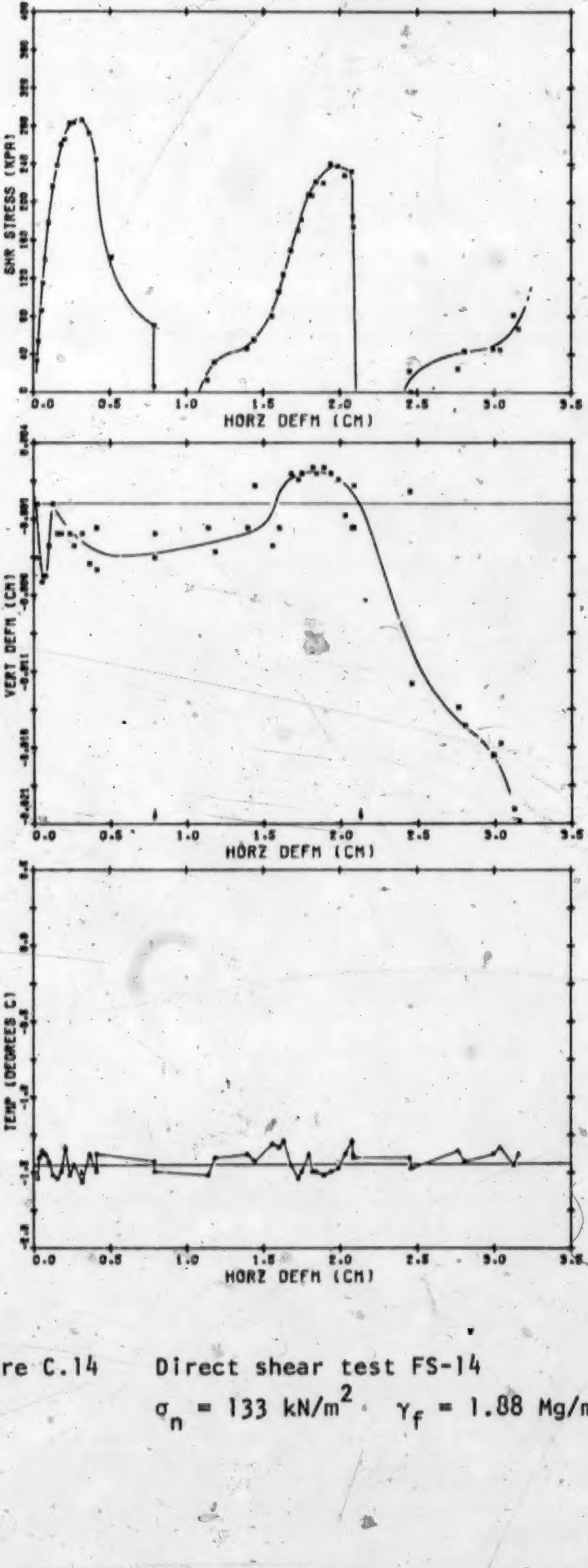

Figure C.14 Direct shear test FS-14
σ_n = 133 kN/m^2 γ_f = 1.88 Mg/m^3

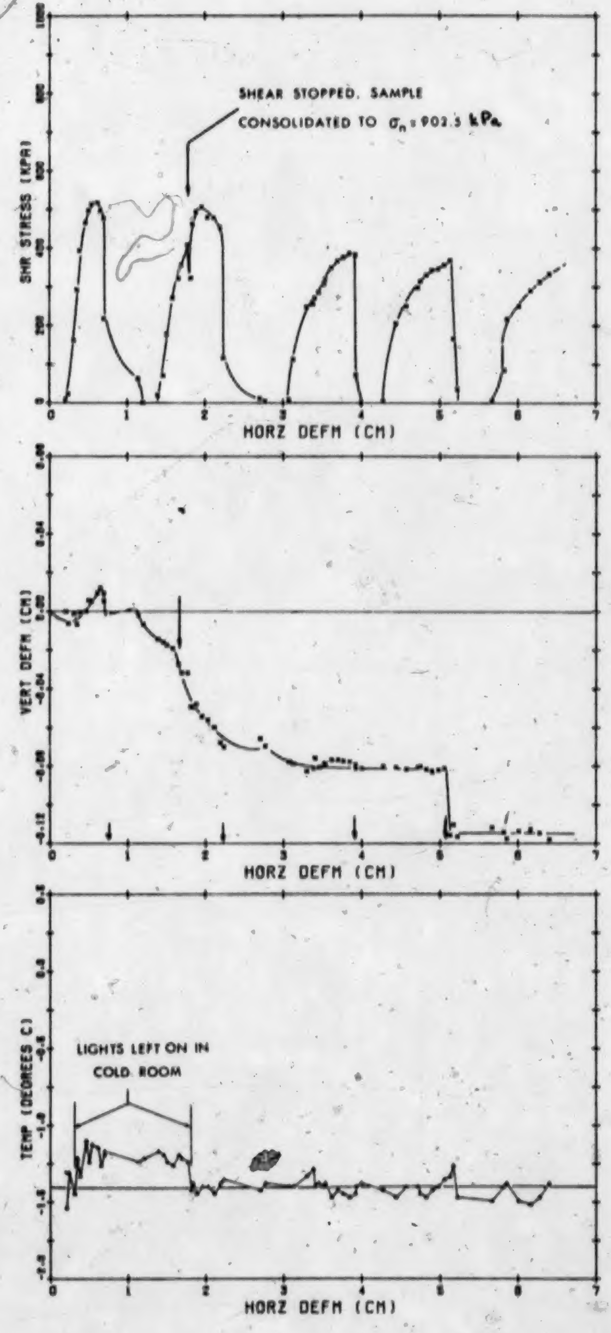

Figure C.15 Direct shear test FS-15

σ_n = 667 kN/m^2 γ_f = 1.97 Mg/m^3
903 kN/m^2

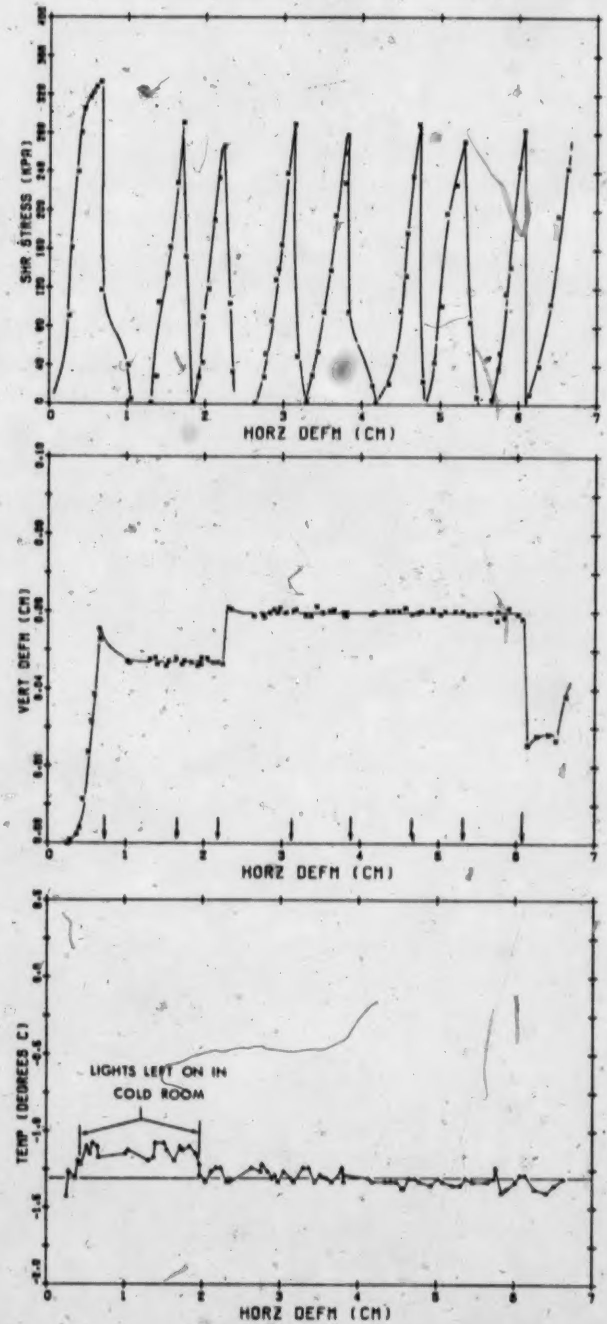

Figure C.16 Direct shear test FS-16

σ_n = 192 kN/m^2 γ_f = 1.95 Mg/m^3

C.2 ISOTHERMAL CONFINED CREEP TESTS

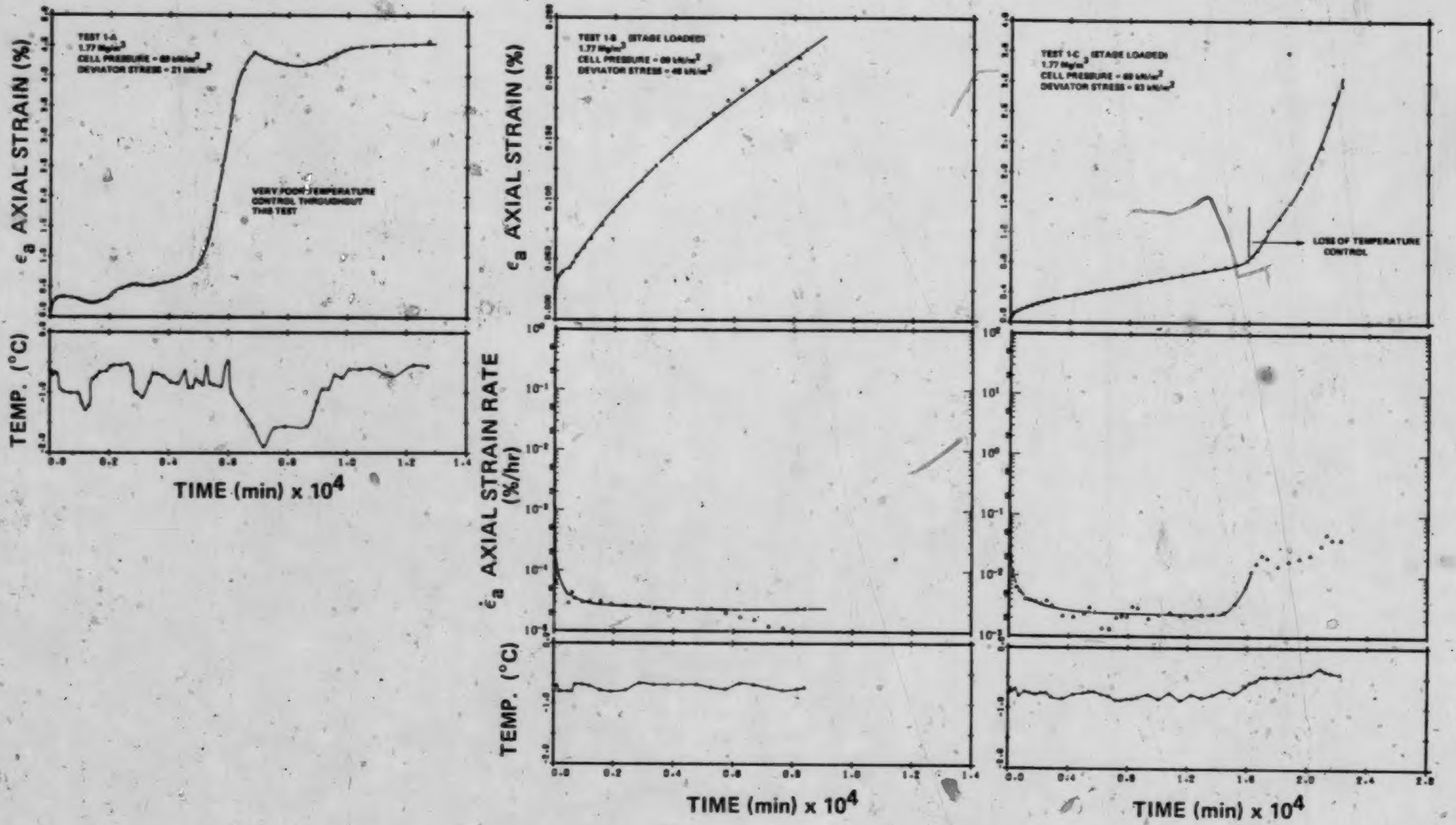

Figure C.17 Creep tests 1-A,B,C (stage loaded)

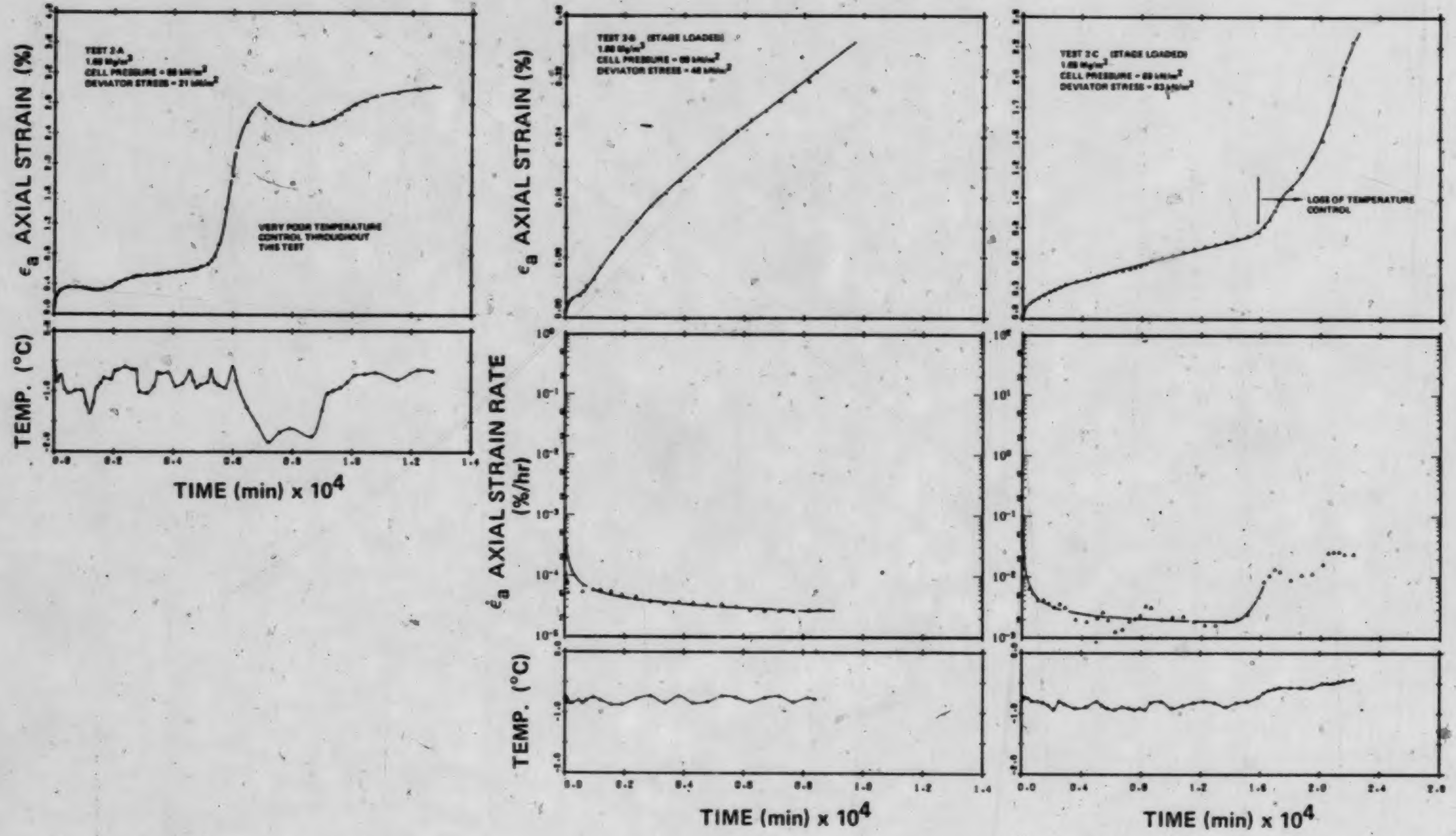

Figure C.18 Creep tests 2-A,B,C (stage loaded)

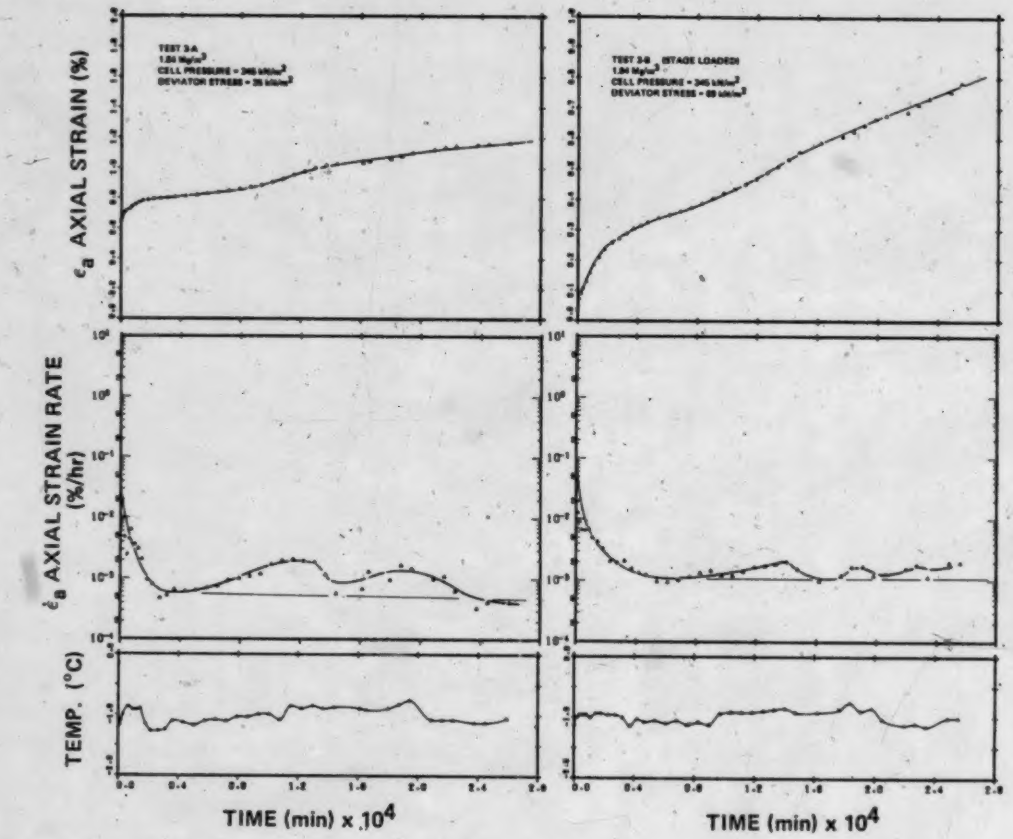

Figure C.19 Creep tests 3-A,B (stage loaded)

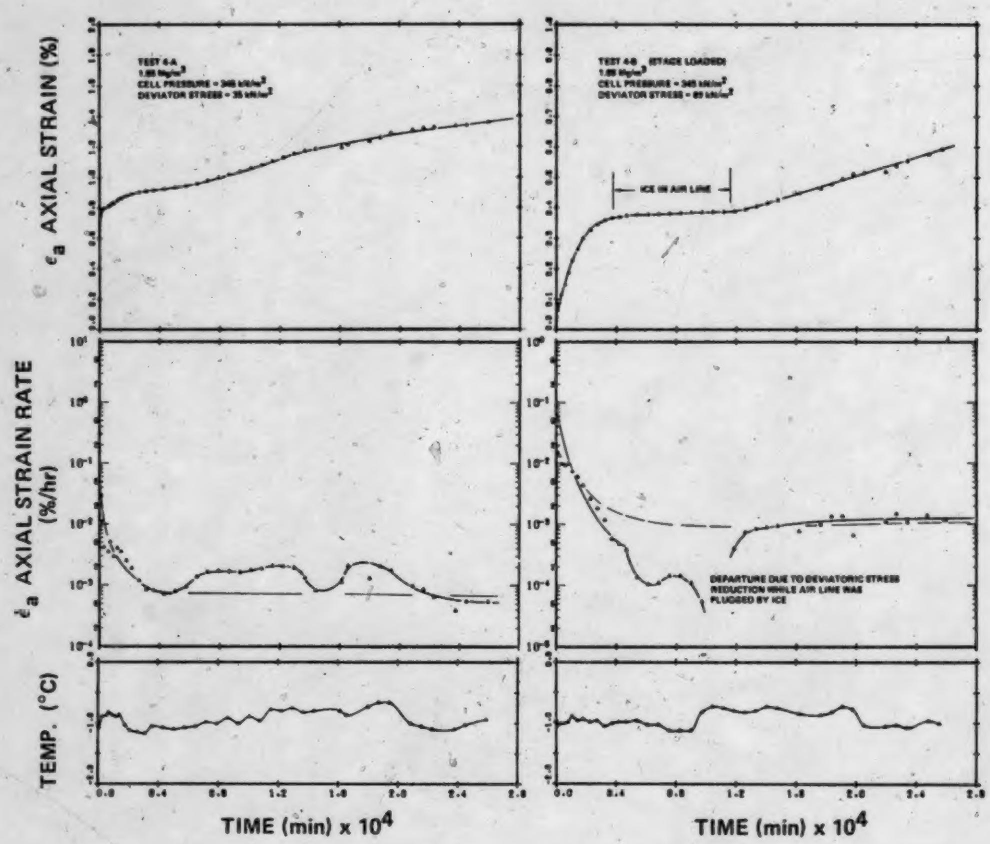

Figure C.20 Creep tests 4-A,B (stage loaded)

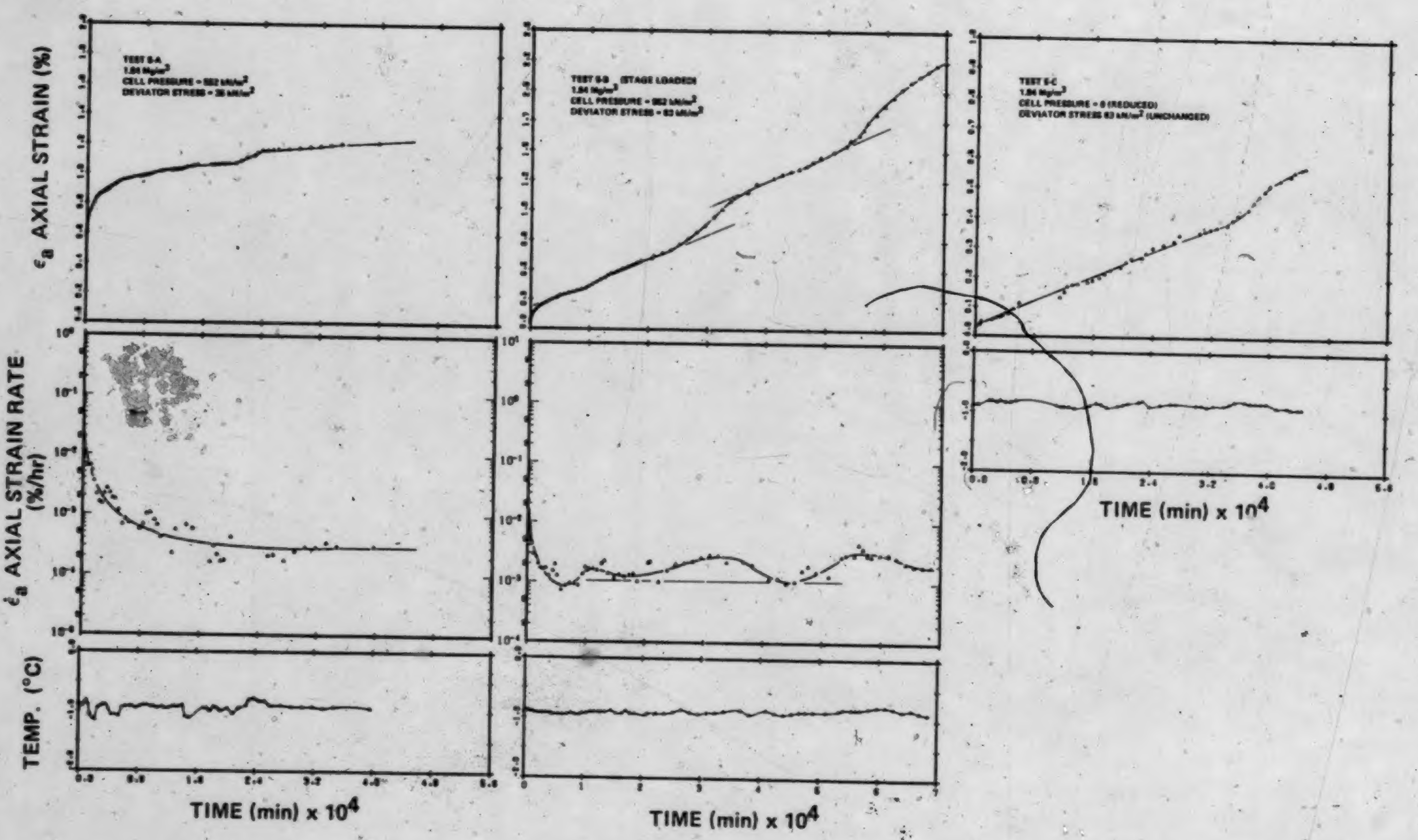

Figure C.21 Creep tests 5-A,B,C, (stage loaded)

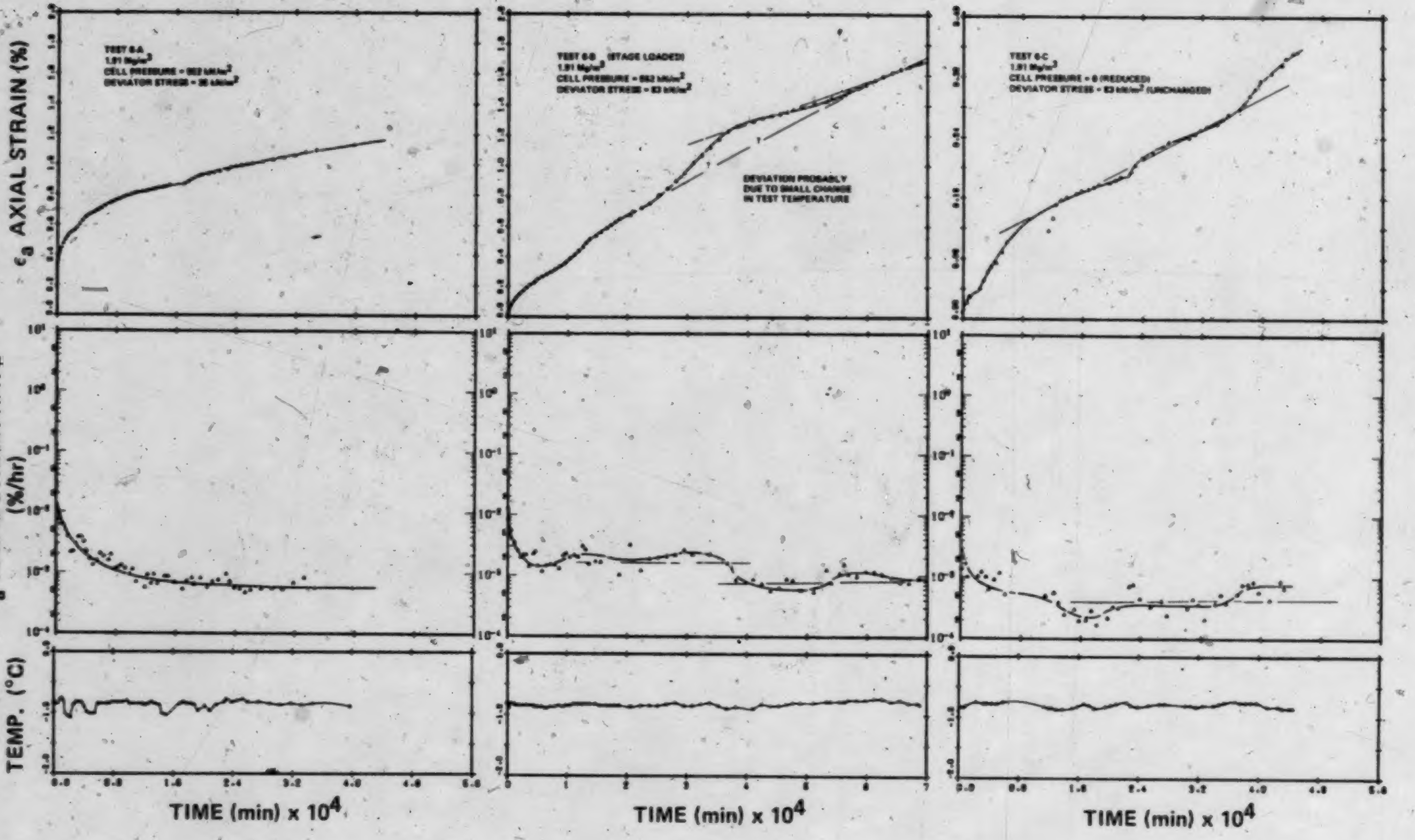

Figure C.22 Creep tests 6-A,B,C, (stage loaded)

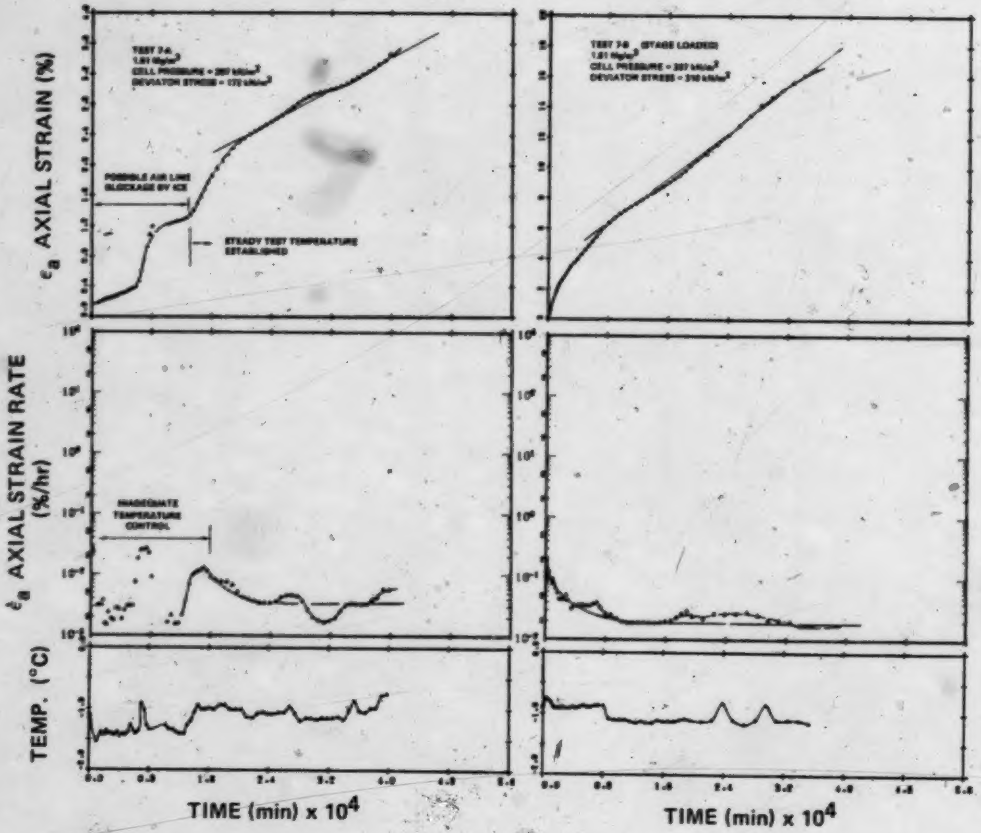

Figure C.23 Creep tests 7-A,B (stage loaded)

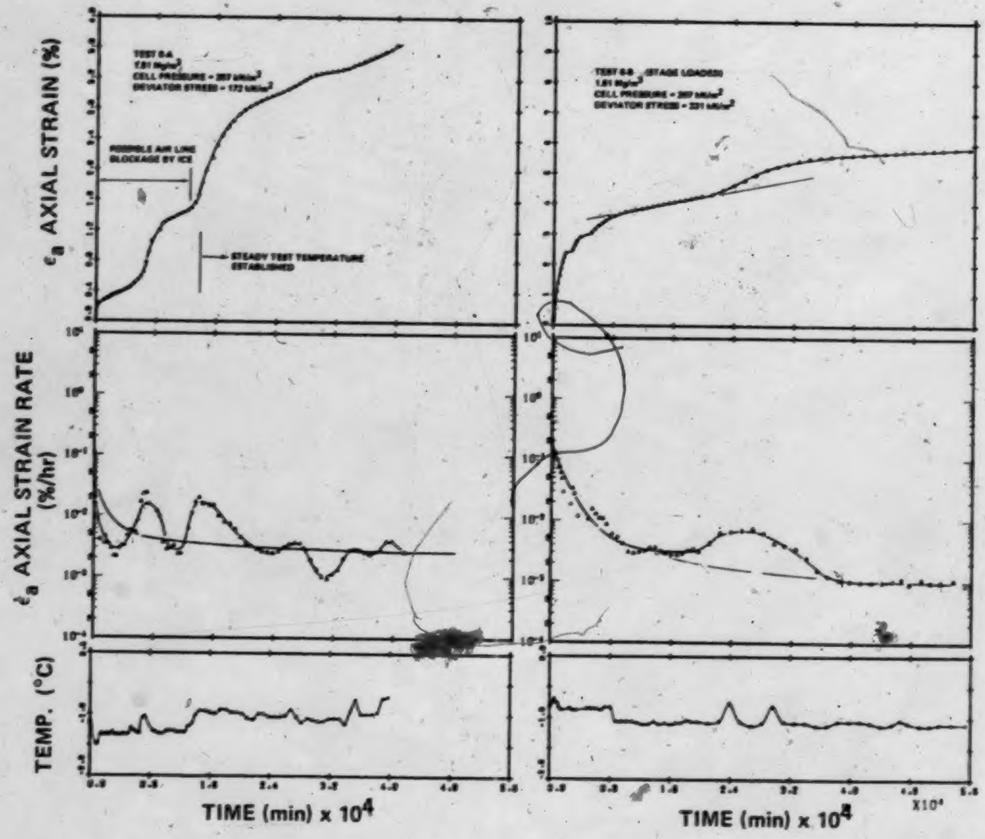

Figure C.24 Creep tests 8-A,B (stage loaded)

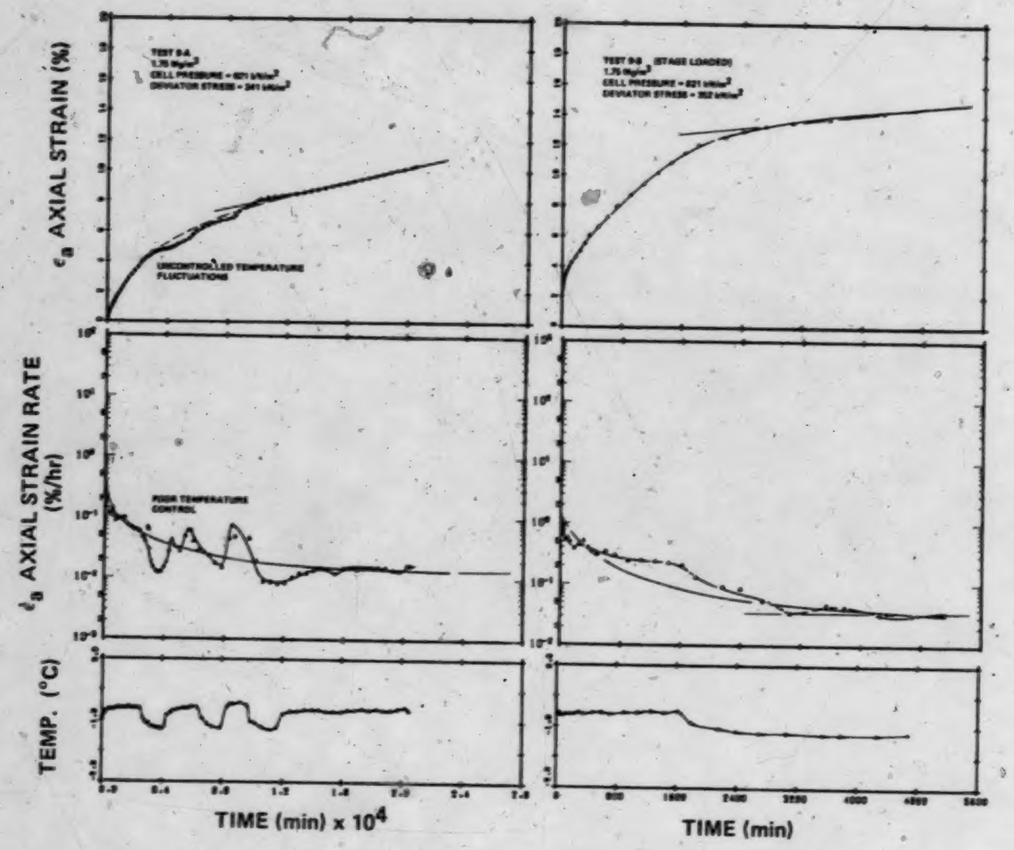

Figure C.25 Creep tests 9-A,B (stage loaded)

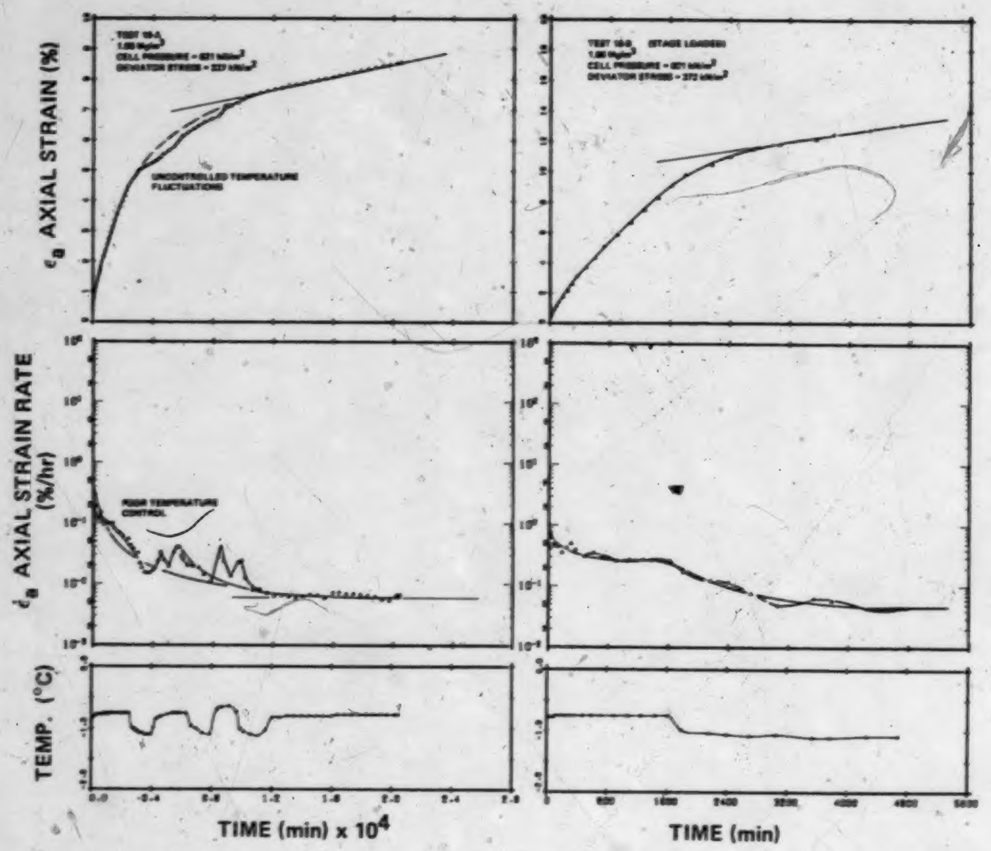

Figure C.26 Creep tests 10-A,B (strage loaded)

C.3 RESIDUAL STRESS TESTS

TABLE C.2 SUMMARY OF RESIDUAL STRESS AND CONSOLIDATION DATA OBTAINED IN THE PERMODE, FORT SIMPSON LANDSLIDE HEADSCARP SAMPLING SITE

CORE	ZONE ATTITUDE	FROZEN BULK DENSITY (Mg/m^3)	WATER CONTENT initial/ (final) (%)	UNDRAINED VOLUMETRIC STRAIN (%)	VERTICAL THAW STRAIN (%)	RESIDUAL STRESS (kN/m^2)	EFFECTIVE STRESS (kN/m^2)	COEFFICIENT OF CONSOLIDATION (cm^2/s)	PERMEABILITY (cm/s)	$\overline{S}$	GROUND ICE DESCRIPTION
24B	3-H	1.94	28.6 (26.0)	3.3	5.4	19	19			0.83	Reticulate structure with lenses to 0.2 cm
							66	6.8×10^{-3}	6.1×10^{-7}		
							148	8.1×10^{-3}	3.2×10^{-7}		
24C	3-H	1.84	33.3 (30.4)	9.9	11.8	10	10				As above
							45		1.9×10^{-7}		
24C	3-H	1.92	35.0 (28.5)		7.0						As above
							81	3.0×10^{-3}	7.2×10^{-6}		
							162	3.4×10^{-3}	1.5×10^{-7}		
24E	3-H	1.90	33.0 (26.7)	1.6	5.3	10	10			0.81	Very little visible ice
							27		5.3×10^{-6}		
							54	4.6×10^{-3}	7.0×10^{-7}		
							108	3.9×10^{-3}	1.6×10^{-7}		
							190	3.3×10^{-3}	1.3×10^{-7}		
24E	3-H	1.88	31.7 (25.8)	4.3	6.1	19	19			0.83	Two thin lenses running vertically, part way through the sample
							45	3.9×10^{-3}	3.2×10^{-7}		
							99	3.2×10^{-3}	2.8×10^{-7}		
							154	3.3×10^{-3}	1.3×10^{-7}		
							234	3.4×10^{-3}	1.0×10^{-7}		
21B	4-V	1.52	62.8 (34.5)	4.8	34.9	3	3			0.93	Ice lens 0.8 cm thick running obliquely across sample
							23	2.3×10^{-2}	9.2×10^{-7}		
							50	7.1×10^{-4}	3.6×10^{-7}		
							104	8.6×10^{-4}	8.5×10^{-7}		
21B A	4-V	1.90	30.2 (27.8)		10.9						As above, adjacent on core but with only fine reticulate ice
							54	6.9×10^{-3}	5.2×10^{-7}		
							108	4.6×10^{-3}	3.6×10^{-7}		

TABLE C.3 SUMMARY OF RESIDUAL STRESS DATA OBTAINED IN THE PERMODE, NORMAN WELLS (MVPL) SAMPLING SITE

BOREHOLE	DEPTH INTERVAL (m)	FROZEN ρBULK (Mg/m^3)	WATER CONTENT Initial/(Final) (%)	UNDRAINED VERTICAL STRAIN (%)	VERTICAL THAW STRAIN (%)	RESIDUAL STRESS (kN/m^2)	$\overline{B}$	EFFECTIVE STRESS (kN/m^2)	VOID RATIO[1] (THAWED)	DIRECT PERMEABILITY (cm/s)	COEFFICIENT OF CONSOLIDATION (cm^2/s)	MUNSELL COLOR (FROZEN)	FABRIC DESCRIPTION AND COMMENTS
NW2	0.91-0.99	1.77	35.2 (27.8)	4.8	7.3	3	0.91		0.95				
								11	0.90	8.7×10^{-6}	1.3×10^{-2}	10YR 6/6	Stratified segregated ice; generally less than 0.2 cm thick; horizontal; 10% excess
								38	0.80	2.8×10^{-6}	1.7×10^{-2}		
								92	0.74	1.4×10^{-6}	1.5×10^{-2}		
NW3	1.13-1.20	1.82	34.3 (32.3)	5.0	5.0+	13	0.61		0.93				
								23	0.92	1.4×10^{-5}	7.8×10^{-2}	10YR 5/6	Massive with very little segregated ice; roots and some black specks
								50	0.91	1.4×10^{-5}	1.3×10^{-1}		
								105	0.87	1.4×10^{-5}	8.8×10^{-2}		
NW2	1.62-1.74	1.82	32.5 (30.5)	4.3	4.8	3	0.88		0.88				
								11	0.87	3.4×10^{-5}	1.8×10^{-2}	10YR 4/3	Stratified silt and sand; thin horizontal ice lenses along bands of undecomposed leaves, etc.
								28	0.83	2.8×10^{-5}	1.3×10^{-2}		
NW3	1.74-1.83	1.68	41.8 (33.1)	5.2	7.8	0	0.94		1.13				
								8	1.07	2.1×10^{-5}	2.2×10^{-2}	10YR 3/1	Stratified silt with sand dustings along bedding planes; root fragments; mottled
								20	1.01	5.5×10^{-6}	2.1×10^{-2}		
								27	0.98	4.3×10^{-6}	1.3×10^{-2}		
								54	0.93	2.9×10^{-6}	9.8×10^{-3}		
								109	0.87	1.6×10^{-6}	1.2×10^{-2}		
NW2	2.23-2.35	1.73	40.7 (26.5)	5.0	16.4	0	0.96		1.10				
								11	0.91	3.0×10^{-6}	1.3×10^{-2}	10YR 4/1	Brown, massive silt with grey mottling; stratified ice; approx. 20% excess; black organic specks
								26	0.85	1.7×10^{-6}	9.2×10^{-3}		
								54	0.81	1.2×10^{-6}	9.6×10^{-3}		
								109	0.76	7.3×10^{-7}	1.3×10^{-2}		
								218	0.72	4.2×10^{-7}	1.1×10^{-2}		

TABLE C.3 CONTINUED

BOREHOLE	DEPTH INTERVAL (m)	FROZEN BULK (Mg/m^3)	WATER CONTENT Initial/ (Final) (%)	UNDRAINED VERTICAL STRAIN (%)	VERTICAL THAW STRAIN (%)	RESIDUAL STRESS (kN/m^2)	$\overline{B}$	EFFECTIVE STRESS (kN/m^2)	VOID RATIO[1] (THAWED)	DIRECT PERMEABILITY (cm/s)	COEFFICIENT OF CONSOLIDATION (cm^2/s)	MUNSELL COLOR (FROZEN)	FABRIC DESCRIPTION AND COMMENTS
MW2	3.29-3.38	1.71	40.8 (29.0)	5.2	12.3	0	0.93		1.12		4.0×10^{-2}	10YR 4/1	Layers of undecomposed organics with ice; also some subhorizontal ice lenses to 0.8 cm thick intersecting these
								23	0.97	4.0×10^{-6}	1.3×10^{-2}		
								38	0.92	1.4×10^{-6}	8.7×10^{-3}		
								71	0.88	5.8×10^{-7}	3.4×10^{-3}		
								137	0.82	2.7×10^{-7}	1.6×10^{-3}		
								214	0.78	1.4×10^{-7}			
MW3	3.47-3.57	1.60	50.9	3.9	9.6	0	0.94		1.37		2.1×10^{-2}	10YR 4/1	Subvertical and subhorizontal ice lenses 0.8 cm thick intersecting each other; mottled; fine rootlets and some black specks
								6	0.82	2.9×10^{-4}	1.1×10^{-2}		
								11	0.75	4.9×10^{-6}	5.3×10^{-3}		
								23	0.70	1.5×10^{-6}	2.4×10^{-3}		
								50	0.66	4.2×10^{-7}	1.9×10^{-3}		
								105	0.61	1.7×10^{-7}	1.8×10^{-3}		
								136	0.57	3.0×10^{-8}			
MW2	3.54-3.63	1.96	19.5	10.1	10.1	15(?)	0.80		0.92			10YR 4/1	Reticulate structure with ice lenses averaging 0.15 cm thick; mottled; rootlets and black specks (Permeability data questionable, sample probably unsaturated)
								27		4.1×10^{-7}	1.2×10^{-2}		
								54		6.2×10^{-7}	5.3×10^{-3}		
								108		2.1×10^{-7}	4.7×10^{-3}		
								190	0.61	1.3×10^{-7}			
MW3	4.51-4.57	1.69	41.8	4.3	17.3	1	0.96		1.13		2.7×10^{-2}	5YR 5/2	Reticulate structure continuous from end to end. mottled; some roots and sticks
								6	1.01	1.4×10^{-5}	6.0×10^{-3}		
								11	0.95	3.4×10^{-6}	7.0×10^{-3}		
								23	0.89	2.8×10^{-6}	9.7×10^{-3}		
								44	0.86	2.1×10^{-6}	1.3×10^{-2}		
								93	0.83	1.4×10^{-6}	1.4×10^{-2}		
								174	0.78	7.8×10^{-7}			

TABLE C.3 CONTINUED

BOREHOLE	DEPTH INTERVAL (m)	FROZEN BULK (Mg/m^3)	WATER CONTENT Initial/(final) (%)	UNDRAINED VERTICAL STRAIN (%)	VERTICAL THAW STRAIN (%)	RESIDUAL STRESS (kN/m^2)	$\overline{B}$	EFFECTIVE STRESS (kN/m^2)	VOID RATIO[1] (THAWED)	DIRECT PERMEABILITY (cm/s)	COEFFICIENT OF CONSOLIDATION (cm^2/s)	MUNSELL COLOR (FROZEN)	FABRIC DESCRIPTION AND COMMENTS
NW3	4.51-4.57	1.69	41.8 (28.6)	4.3	17.3	1	0.96		1.13			5Y 5/2	Reticulate structure continuous from end to end; mottled; some roots and sticks
								6	1.01	1.4×10^{-5}	2.7×10^{-2}		
								11	0.95	3.4×10^{-6}	6.0×10^{-3}		
								23	0.89	2.8×10^{-6}	7.0×10^{-3}		
								44	0.86	2.1×10^{-6}	9.7×10^{-3}		
								93	0.83	1.4×10^{-6}	1.3×10^{-2}		
								174	0.78	7.8×10^{-7}	1.4×10^{-2}		
NW2	4.63-4.69	1.85	42.0 (35.2)	5.7	5.9	25	0.77		1.14			5Y 5/2	Small amount of stratified ice along bedding; mottled; thinly bedded with organic-rich layers; black specks and fibres
								54	1.08	2.0×10^{-5}	4.0×10^{-3}		
								108	1.05	3.7×10^{-6}			
								216	0.95	$\approx 5.0 \times 10^{-7}$			
NW2	4.08-4.15	1.80	32.4 (28.1)	9.5	—	15	0.93		0.88(?)				Mottled, silty clay interlaminated with decomposed organic layers; thin stratified ice along bedding
								63		—	5.8×10^{-3}		
								118	0.76	—	5.8×10^{-3}		
NW3	5.00-5.09	1.76	44.0 (42.5)	4.1	5.2	19 to 25	0.97	77	1.14	1.1×10^{-6}	2.0×10^{-2}	5Y 5/2	Massive; fine subvertical ice lenses
NW2	5.49-5.64	1.80	39.4 (27.5)	5.4	15.5	10	0.93		1.06			5Y 5/1	Reticulate structure with 5 to 10% excess ice; laminations inclined, roots and pockets of partially decomposed organics; dry ripoff clasts in silty clay matrix (leak at top seal)
								27		—	5.9×10^{-3}		
								54		—	2.5×10^{-3}		
								108		—	1.5×10^{-3}		
								218	0.74	—	1.3×10^{-3}		

TABLE C.3 CONTINUED

BOREHOLE	DEPTH INTERVAL (m)	FROZEN BULK (Mg/m^3)	WATER CONTENT Initial/ (frozen) (%)	UNDRAINED VERTICAL STRAIN (%)	VERTICAL THAW STRAIN (%)	RESIDUAL STRESS (kN/m^2)	$\overline{B}$	EFFECTIVE STRESS (kN/m^2)	VOID RATIO[1] (THAWED)	DIRECT PERMEABILITY (cm/s)	COEFFICIENT OF CONSOLIDATION (cm^2/s)	MUNSELL COLOR (FROZEN)	FABRIC DESCRIPTION AND COMMENTS
NW2	6.58-6.65	1.78	36.4 (32.9)	5.6	8.5	39 (to 50?)	0.70		0.98		—	5Y 2.5/1	Stratified ice lenses along layers of undecomposed sticks, grass, etc.; 0.6 to 0.8 cm thick
								50	0.92	5.5×10^{-7}			
								81	0.91	4.9×10^{-7}	1.5×10^{-2}		
								135	0.88	3.8×10^{-7}	—		
NW2	6.66-6.74	1.65	42.1	6.2	9.9	16	0.61		1.12		—	5Y 2.5/1	As above, organics mixed with clay and consist of grass and sedges which were still green
								109		—			
								163	1.05	3.5×10^{-7}	3.5×10^{-3}		
								272	1.00	1.1 x 10-7	1.1×10^{-3}		
NW2	7.32-7.44	1.58	51.2 (41.8)	7.2	14.7	12	0.91		1.37		—	5Y 3/1	As above, recurrent layers of organic material; horizontal ice lenses from 0.9 to 1.2 cm thick
								14		2.5×10^{-5}			
								33		1.7×10^{-5}	7.1×10^{-2}		
								60		9.8×10^{-6}	3.4×10^{-3}		
								109		6.1×10^{-6}	8.0×10^{-3}		
								243	1.12	2.2×10^{-7}	7.3×10^{-3}		
NW3	7.65-7.80	1.70	40.4 (39.3)	5.0	—	19	0.44		1.08(?)		—	5Y 4/1	Minor reticulate ice; single layer of leaves, grass, etc. 1 cm thick
								27		4.3×10^{-4}			
								54	1.00(?)	6.2×10^{-6}	2.5×10^{-2}		
NW2	7.92-8.08 (A)	1.80	35.1 (29.4)	6.1	12.7	19	0.93		0.94			5Y 5/1 & 5Y 4/2	Laminated silty clay with organic inclusions; reticulate structure with major horizontal lenses; intact organic debris at regular 5 cm intervals
								27	0.91	4.2×10^{-5}	9.4×10^{-3}		
								54	0.88	1.7×10^{-5}	8.9×10^{-3}		
								120	0.82	5.5×10^{-6}	7.7×10^{-3}		
								202	0.79	2.2×10^{-6}	5.1×10^{-3}		

TABLE C.3 CONTINUED

BOREHOLE	DEPTH INTERVAL (m)	FROZEN BULK (Mg/m^3)	WATER CONTENT Initial/(Frozen) (%)	UNDRAINED VERTICAL STRAIN (%)	VERTICAL THAW STRAIN (%)	RESIDUAL STRESS (kN/M^2)	$\overline{B}$	EFFECTIVE STRESS (kN/m^2)	VOID RATIO (THAWED)	DIRECT PERMEABILITY (cm/s)	COEFFICIENT OF CONSOLIDATION (cm^2/s)	MUNSELL COLOR (FROZEN)	FABRIC DESCRIPTION AND COMMENTS
NW2	7.92-8.08 (B)	1.89	29.6 (29.6)	4.6	—	72	0.46	252	0.79	2.6×10^{-6}	1.4×10^{-3}	5Y 4/2	Organic inclusions; relatively free of visible ice
NW2	8.47-8.56	1.93	28.9 (27.9)	4.5	—	89	0.36	93	0.77	3.0×10^{-7}	—	5Y 5/1	Massive with very little segregated ice
NW3	8.58-8.67	1.96	27.5 (26.5)	2.9	4.7	55	0.67	57	0.74	1.2×10^{-7}	—	5Y 5/1	Oblique reticulate ice lense; shell fragments and several thin organic bands
								111	0.71	9.4×10^{-8}	3.1×10^{-3}		
NW2	9.14-9.24	1.92	29.2 (27.7)	5.0	5.2	47	0.63	81	0.79 0.78	3.2×10^{-7}	1.4×10^{-2}	5Y 5/1	No visible ice; small shells and black organic specks
								136	0.77	2.9×10^{-7}	1.9×10^{-2}		
								218	0.74	2.3×10^{-7}	1.3×10^{-2}		
NW2	9.37-9.42	1.91	30.9 (29.7)	5.1	7.2	33	0.73	54	0.83 0.82	3.1×10^{-7}	—	5Y 4/1	Fine mottling; no visible segregated ice; few small gravel sizes
								93	0.81	2.7×10^{-7}	6.2×10^{-3}		
								147	0.80	2.2×10^{-7}	5.3×10^{-3}		
NW2	9.91-10.03	1.97	25.3 (23.5)	2.2	5.8	34 to 59	0.65	82	0.69	4.5×10^{-7}	—	5Y 5/1 to 5Y 2.5/1	Severely contorted bedding; subhorizontal ice lenses; sandy seams and gravel sizes
								136	0.64	3.3×10^{-7}	2.3×10^{-2}		
NW3	10.94-11.02	1.96	24.5 (23.0)	2.7	2.9	74 to 84	0.39	109	0.67	2.0×10^{-8}	—	5Y 3/1	Fine reticulate structure; ice appears as hairline cracks; soil quite dry
								218	0.63	4.0×10^{-9}	3.0×10^{-4}		

TABLE C.3 CONTINUED

BOREHOLE	DEPTH INTERVAL (m)	FROZEN BULK (Mg/m^3)	WATER CONTENT initial/ (frozen) (%)	UNDRAINED VERTICAL STRAIN (%)	VERTICAL THAW STRAIN (%)	RESIDUAL STRESS (kN/m^2)	$\overline{B}$	EFFECTIVE STRESS (kN/m^2)	VOID RATIO (THAWED)	DIRECT PERMEABILITY (cm/s)	COEFFICIENT OF CONSOLIDATION (cm^2/s)	MUNSELL COLOR (FROZEN)	FABRIC DESCRIPTION AND COMMENTS
NW3	11.02-11.11	1.89	30.6 (28.2)	2.5		42	0.70		0.83		1.0×10^{-3}	5Y 3/1	Fine reticulate structure; no organic material; some fine gravel sizes
								54	0.82	3.1×10^{-7}	—		
								109	0.77	2.0×10^{-7}			
NW3	11.13-11.28 (A)	1.80	33.2 (26.4)	5.2	11.9	29	0.79		0.90		1.6×10^{-3}	5Y 3/1	Fine reticulate structure with horizontal lenses predominant
								55	0.84	2.6×10^{-6}	6.0×10^{-4}		
								109	0.78	4.8×10^{-8}	2.2×10^{-4}		
								217	0.72	6.9×10^{-9}			
NW3	11.13-11.28 (B)	1.79	34.5 (30.6)	7.0	13.5	22	0.76		0.97		—	5Y 3/1	Reticulate structure with fine lenses every 2 to 3 cm; some fine gravel sizes
								23	0.83	3.0×10^{-5}			
NW3	11.31-11.89	1.94	27.8 (26.8)	4.0	7.9	96	0.59		0.76		4.6×10^{-4}	5Y 3/1 to 5Y 2.5/1	Numerous fine reticulate ice lenses; soil appears quite dry
								109	0.73	4.7×10^{-9}			

[1] Void ratios have been computed assuming a) an appropriate G_s
b) full saturation

Due to the second assumption, some void ratios indicated may be lower than actual values.

TABLE C.4 SUMMARY OF RESIDUAL STRESS DATA OBTAINED IN THE PERMODE, NOELL LAKE SAMPLING SITE

BOREHOLE	DEPTH INTERVAL (m)	FROZEN BULK DENSITY (Mg/m^3)	WATER CONTENT Initial/ (Final) (%)	UNDRAINED VERTICAL STRAIN (%)	VERTICAL THAW STRAIN (%)	RESIDUAL STRESS (kN/m^2)	$\bar{B}$	EFFECTIVE STRESS (kN/m^2)	VOID RATIO^1 (THAWED)	DIRECT PERMEABILITY (cm/s)	COEFFICIENT OF CONSOLIDATION (cm^2/s)	MUNSELL COLOR (FROZEN)	FABRIC DESCRIPTION AND COMMENTS
NL2	0.64-0.82	1.53	54.9 (42.8)	5.7	9.8	3(?)	1.00		1.46			10YR 4/2 to 10YR 3/1	Stratified ice, 30% excess; cryoturbation features; fine gravel sizes
								11	1.36				
								23	1.28	4.2×10^{-6}	5.2×10^{-3}		
								50	1.20	4.0×10^{-7}	5.1×10^{-3}		
								96	1.13	2.2×10^{-7}	5.7×10^{-3}		
NL2	1.52-1.71	1.55	47.3 (30.6)	6.3	15.4	2	0.98		1.26			10YR 4/1	Predominantly reticulate structure with lenses to 0.4 cm; some undecomposed sticks, twigs
								8					
								23	1.00	8.2×10^{-5}	7.6×10^{-2}		
								50	0.91	2.0×10^{-5}	3.7×10^{-2}		
								104	0.82	2.6×10^{-5}	3.0×10^{-2}		
NL2	3.44-3.57	1.70	39.8 (34.6)	4.7	11.7	12	0.96		1.07		1.0×10^{-4}	10YR 3/1	Single vertical ice lense; one side hard clay, the other silty sand
								27	0.88	6.2×10^{-5}			
NL2	4.27-4.39	1.74	30.4 (24.6)	5.1		25 to 80?	0.68		0.82		Swelling	10YR 3/1 to 5Y 2.5/1	Silt with pebbles in abrupt contact with dense plastic clay; minor reticulate ice
								55		3.5×10^{-9}	4.8×10^{-4}		
								109	0.79	5.0×10^{-9}	8.9×10^{-5}		
								219	0.66	3.0×10^{-9}			
NL2	4.69-4.82	1.56	46.6 (33.3)	6.5	17.8	5	0.99		1.34			10YR 3/1 to 5Y 2.5/1	Blocky; reticulate structure with ice lenses to 0.6 cm thick
								23	1.03	5.6×10^{-9}	7.2×10^{-5}		
								150	0.90	2.4×10^{-8}			
NL2	5.76-5.91	1.92	27.9 (24.6)	2.7	4.3	23	0.46		0.75		2.7×10^{-4}	10YR 3/1	Reticulate structure with some ice lenses 1 to 1.5 cm thick; dense clay with occasional pebbles
								81	0.72	1.4×10^{-8}	1.2×10^{-4}		
								161	0.68	1.2×10^{-8}	5.1×10^{-5}		
								273	0.66	9.4×10^{-9}			
NL2	5.94-6.04	1.68	42.6 (32.3)	4.7	15.4	5	0.75 to 0.85				1.1×10^{-4}	10YR 3/1	Highly disturbed, reticulate ice to 0.5 cm in thickness dominating (top seal leaking)
								23			5.0×10^{-5}		
								49					
NL2	7.01-7.13 (A)	1.82	29.3 (26.9)	3.2	4.2	23	0.66		0.84		3.3×10^{-4}	10YR 3/1	Dense silty clay in oblique contact with silt containing gravel; reticulate structure; lenses to 0.8 cm thick
								66	0.78	2.8×10^{-8}	1.5×10^{-4}		
								134	0.73	1.5×10^{-8}			
NL2	7.01-7.13 (B)	1.98	24.6 (23.4)	3.4	3.5	114	0.31		0.66		8.9×10^{-4}	10YR 3/1	As above
								187	0.65	9.7×10^{-9}	5.9×10^{-4}		
								297	0.63	8.6×10^{-9}			
NL2	7.48-7.62	1.66	46.0 (28.1)	4.6	11.7	6	0.90		1.24		3.6×10^{-3}	10YR 3/1 to 5Y 2.5/1	Very fine silty sand with reticulate structure; some horizontal lenses to 3 cm thick
								23	1.09	4.8×10^{-6}	1.0×10^{-3}		
								50	0.89	3.0×10^{-7}	8.2×10^{-4}		
								104	0.81	2.0×10^{-7}	7.6×10^{-4}		
								213	0.76	1.3×10^{-7}			
NL2	8.87-8.96	1.79	31.5 (26.0)	3.5	5.5	24	0.74 to 0.93		0.85		3.4×10^{-4}	10YR 3/1	Thin sandy laminations in silty clay; reticulate structure; some gravel
								109	0.71	3.3×10^{-8}			
NL2	8.96-9.05	1.63	49.8 (28.5)	5.0	25.6	0	1.00		1.36		2.5×10^{-2}	10YR 3/1	Fine silty sand with clay lump inclusions, stratified; reticulate structure with ice lenses to 0.6 cm thick
								11	0.90	3.8×10^{-6}	8.9×10^{-3}		
								26	0.87	2.9×10^{-6}	8.5×10^{-3}		
								50	0.83	2.7×10^{-6}	9.1×10^{-3}		
								77	0.81	2.5×10^{-6}	4.1×10^{-3}		
								158	0.78	2.0×10^{-6}			

TABLE C.4 CONTINUED

BOREHOLE	DEPTH INTERVAL (m)	FROZEN BULK DENSITY (Mg/m^3)	WATER CONTENT Initial/ (Final) (%)	UNDRAINED VERTICAL STRAIN (%)	VERTICAL THAW STRAIN (%)	RESIDUAL STRESS (kN/m^2)	$\bar{B}$	EFFECTIVE STRESS (kN/m^2)	VOID RATIO[1] (THAWED) -	DIRECT PERMEABILITY (cm/s)	COEFFICIENT OF CONSOLIDATION (cm^2/s)	MUNSELL COLOR (FROZEN)	FABRIC DESCRIPTION AND COMMENTS
NL2	9.05-9.11	1.56	57.4 (29.0)	5.1	30.9	0	1.00		1.56				
								27	0.92	3.2×10^{-7}	6.9×10^{-3}	10YR 3/1	As Above
								54	0.87	3.0×10^{-7}	2.2×10^{-3}		
								108	0.83	2.9×10^{-7}	5.6×10^{-3}		
								217	0.79	2.1×10^{-7}	6.0×10^{-3}		
NL2	9.69-9.75	1.77	36.7 (28.2)	4.8	16.2	0	0.99		1.05				
								11	1.00	2.4×10^{-5}	9.0×10^{-2}	10YR 4/1 to 10YR 2.5/1	Fine silty sand, stratified; bedding features contorted; reticulate structure with ice lenses from 0.3 to 0.6 cm thick
								23	0.88	1.1×10^{-5}	1.6×10^{-1}		
								50	0.83	8.7×10^{-6}	6.6×10^{-2}		
								104	0.80	6.4×10^{-6}	1.5×10^{-1}		
								213	0.77	5.1×10^{-6}	7.0×10^{-2}		
NL2	10.2-10.2[illegible]	1.72	35.8 (32.5)		16.3	10	0.79		0.97				
								34	0.93	4.7×10^{-5}	6.0×10^{-3}	10YR 4/1 to 10YR 2.5/1	Stratified silty sand with clay lump inclusions, contorted; reticulate structure with ice lenses to 0.3 cm thick
								88	0.91	4.0×10^{-5}	3.1×10^{-2}		
								155	0.88	3.1×10^{-5}	2.3×10^{-2}		
NL2	10.67-10.76	1.74	37.2 (26.5)	4.6	16.9	7(?)	1.00		1.00				
								27	0.81	1.0×10^{-7}	1.7×10^{-4}	10YR 3/1	Blocky, stiff clay with some shale fragments; subhorizontal ice lenses to 1.2 cm thick
								81	0.72	3.1×10^{-9}	1.2×10^{-4}		
NL2	11.40-11.52	2.06	20.4 (19.9)	2.5	3.7	135	0.41		0.55				
								218	0.54	8.7×10^{-10}	5.8×10^{-5}		Massive silty clay with some stones; no visible segregated ice (probably not saturated)
NL2	11.70-11.83	2.08	21.7 (19.4)	3.5	3.9	45 to 57	0.75		0.66				
								136	0.59	2.4×10^{-9}	1.6×10^{-4}	10YR 3/1	Silty clay with stratification features and pebbles; reticulate structure with 10 to 15% segregated ice
								217	0.57	1.5×10^{-9}	6.8×10^{-6}		

---

[1] Void ratios have been computed assuming a) an appropriate G_s
b) full saturation
Due to the second assumption, some void ratios indicated may be lower than actual values

TABLE C:5 SUMMARY OF RESIDUAL STRESS AND CONSOLIDATION DATA OBTAINED IN THE TRIAXIAL CELL, FORT SIMPSON LANDSLIDE HEADSCARP SAMPLING SITE

TEST	ZONE-ATTITUDE	FROZEN BULK DENSITY (Mg/m^3)	WATER CONTENT Initial/ (Final) (%)	UNDRAINED VOLUMETRIC STRAIN (%)	VERTICAL THAW STRAIN (%)	RESIDUAL STRESS (kN/m^2)	EFFECTIVE STRESS (kN/m^2)	COEFFICIENT OF CONSOLIDATION (cm^2/s)	GROUND ICE DESCRIPTION	SOIL FABRIC DESCRIPTION
FS-01	4-V	1.66	40.8 (31.2)			0	0		Three subhorizontal lenses 0.5 to 0.7 cm thick	Massive, taken from between thick icy layers
							48	7.5 × 10^{-4}		
							103	1.3 × 10^{-3}		
FS-02	4-V	1.89	34.7 (28.3)	4.0	6.0	4	4		As above, same core	As above
							103	5.0 × 10^{-3}		
							207	6.5 × 10^{-3}		
FS-03	4-V	1.86	38.1 (32.8)	3.6	7.5	3	3		Icy section near one end	Massive, from immediately below a 10 cm thick layer of ice
							17	7.6 × 10^{-4}		
					9.2		34	8.0 × 10^{-4}		
FS-04	4-V	1.97	26.9 (25.3)		-0.1	100(?)			Thin reticulate ice lenses	From below a thick ice lense, some desiccation
FS-05	4-V	2.06	23.1 (22.0)		0.1	56	56		Sparse reticulate ice, lenses thin	Massive, from below a 6.5 cm ice lense
							138	6.4 × 10^{-3}		
FS-06	3-H	1.61	53.1 (32.8)	10.6	15.9	0	7		Predominantly reticulate ice, 20% excess in veins 0.5 cm + thick	Indistinct stratification
							21	7.2 × 10^{-3}		
					16.9		41	4.3 × 10^{-3}		
FS-07	4-V	1.92	39.0 (30.0)		1.0	63			Fine reticulate ice	From between 2 thick ice lenses, massive
FS-08	4-V	1.82	36.5 (33.8)			2	2		Fine reticulate ice, subvertical lenses as thick as 1 to 1.5 cm	As above
							17	5.5 × 10^{-3}		
							34	5.3 × 10^{-3}		
					9.6		83	6.0 × 10^{-3}		
FS-09	3-H	1.90	28.6 (26.3)	—	6.1	0	0		Several discrete subhorizontal ice lenses averaging 0.5 cm in 0.5 cm in thickness	Gradational stratification, sandy silt to silty clay
							14	1.3 × 10^{-2}		
					7.3		28	1.2 × 10^{-2}		
FS-10	3-H	1.89	31.0 (25.7)	8.3	—	5	5		Reticulate ice with several thicker horizontal layers	Silty, vague stratification
							41	3.4 × 10^{-3}		
							83	7.9 × 10^{-3}		
FS-11	3-H	1.90	28.8 (27.6)	6.9	8.7	10	10		Fine reticulate structure	Silty
							66	9.5 × 10^{-3}		
FS-12	4-H	1.88	38.8 (36.2)	—	—	2	2		Coarse reticulate structure, lenses 0.5 cm thick	High plastic clay, sample collapsed during thaw
							45	8.3 × 10^{-4}		
							90	5.6 × 10^{-4}		
FS-13	3-H	1.70	47.6 (28.8)	—	—	0	0		Fine reticulate structure	From base of zone 3, just above thick ice layer
							41	8.6 × 10^{-3}		
							90	6.3 × 10^{-3}		
							186	7.0 × 10^{-3}		
FS-14	3-V	1.95	28.8 (28.8)	—	0.7	70(?)			Fine reticulate structure, thick horizontal lens near top	Silty clay with thin sandy seams @ 4 to 6 cm spacings
FS-15	3-H	1.75	41.5 (28.7)	3.3	—	0	0		Fine reticulate structure	From base of Zone 3
							31	2.7 × 10^{-2}		
							62	8.6 × 10^{-3}		
					15.5		131	1.2 × 10^{-2}		
FS-16	3-V	1.88	29.2 (29.2)		3.2	10			Reticulate, several thicker lenses	Silty clay, some sandy seams
FS-17	3-V	1.84	32.0 (32.0)	4.9	8.2	3			As above	As above
FS-18	4-V	1.79	40.2 (36.0)	—	—	2	2		Reticulate ice, some lenses as thick as 0.6 to 0.8 cm	Between thick ice layers
					16.1	11		1.3 × 10^{-2}		
FS-19	4-V	1.74	38.2 (32.2)	4.8		2	2		Fine reticulate structure, more closely spaced	Massive silty clay
					18.1		11	3.7 × 10^{-2}		
FS-20	4-V	1.77	33.8 (29.4)	4.7		0	0		As above	As above
					14.6		11	6.2 × 10^{-2}		

TABLE C.6 SUMMARY OF RESIDUAL STRESS AND CONSOLIDATION DATA OBTAINED IN THE TRIAXIAL CELL, NORMAN WELLS (MVPL) SAMPLING SITE

BOREHOLE	DEPTH INTERVAL (m)	FROZEN BULK DENSITY (Mg/m^3)	WATER CONTENT Initial/ (Final) (%)	UNDRAINED VOLUMETRIC STRAIN (%)	VERTICAL THAW STRAIN (%)	RESIDUAL STRESS (kN/m^2)	EFFECTIVE STRESS (kN/m^2)	COEFFICIENT OF CONSOLIDATION (cm^2/s)	B	FABRIC DESCRIPTION AND COMMENTS
MW2	0.4-0.7	1.85	28.4 (25.4)	3.2	6.1	0	10			Fine vertical and sub-vertical lenses; peaty layers
								7.5×10^{-3}		
							40		0.85	
MW2	0.7-1.0	1.86	24.8 (19.9)	2.9	3.8	2.1	10		0.96	Fine ice lenses, roughly reticulate; sand partings
								5.0×10^{-3}		
							33			
								1.4×10^{-2}		
							80			
								1.4×10^{-2}		
							138			
								1.3×10^{-2}		
							206		0.71	
MW2	1.0-1.3	1.85	24.4 (21.9)	7.2	7.9	3.8			1.00	Predominantly horizontal lenses; 20% at one end; thicker layers of peat and sticks
MW2	1.5-1.7	1.85	34.4 (30.3)	3.5	4.8	2.8	11			Some ice along organic layers; otherwise - thin stratified; peat layers; some shale chips
								4.2×10^{-1}		
							33			
								1.4×10^{-2}		
							72			
							110			
								2.5×10^{-2}		
							174			
							241		0.89	
MW2	1.8-2.1	1.53	55.4		10.3	2.1	2		1.00	No segregated ice; thin bedded sandy silt; numerous charred sticks
								8.0×10^{-3}		
							11			
								7.3×10^{-2}		
							36		1.00	
MW2	4.3-4.6	1.72	38.8 (34.0)		18.0	2.5	3			Recticulate ice lenses to 1 cm thick; blocky; thinly bedded; organic specks
								1.6×10^{-2}		
							18		0.93	
MW2	3.2-3.4	1.82	39.4	3.0	6.2	3.1	2			Recticulate ice lenses to 1 cm thick, vertical and horizontal; thinly bedded; peat layers
								9.7×10^{-3}		
							34		1.00	
MW3	0.6-0.8	1.93	23.7		7.3	10			0.92	Fine ice lenses, predominantly horizontal; mottled; organic specks; some stick and roots
MW3	1.0-1.2	1.91	26.1		11.1	12			0.91	As above
MW3	7.9-8.1	1.81	38.0		6.3	1.7			0.98	Fine ice lenses, usually along peat layers; contorted bedding
MW3	10.4-10.6	1.92	26.2		7.1	11			0.93	Fine ice lenses; icey layers with soil inclusions; dark and light grey-brown mottling; contorted bedding; some stone
MW3	11.3-11.5	1.92	27.5		1.0	17			0.62	As above
MW3	11.9-12.1	1.85	32.0		2.8	15			0.84	Reticulate structure, lenses 0.5 to 0.7 cm thick; very thinly laminated
MW4	5.3-5.8	1.71	45.0		3.7	31			0.74	Few horizontal lenses; stratified with numerous peaty layers; sticks and roots
ADDITIONAL TESTS ON SMALLER SPECIMENS										
MW2	1.0-1.2	1.85	34.0			0			0.98	
MW2	3.7-3.9	1.91	28.7			0				Peaty layers; sticks
								1.3×10^{-3}		
							11			

TABLE C.6 CONTINUED

BOREHOLE	DEPTH INTERVAL (m)	FROZEN BULK DENSITY (Mg/m³)	WATER CONTENT Initial/ (Final) (%)	UNDRAINED VOLUMETRIC STRAIN (%)	VERTICAL THAW STRAIN (%)	RESIDUAL STRESS (kN/m²)	EFFECTIVE STRESS (kN/m²)	COEFFICIENT OF CONSOLIDATION (cm²/s)	B	FABRIC DESCRIPTION AND COMMENTS
MV2	7.2-7.3	1.67	50.1 (38.2)			36	36 177 354	3.7×10^{-2} 8.8×10^{-3}	0.95	
MV2	93.-9.4	1.93	38.0			~51			0.86	
MV3	1.5-1.7	1.70	39.0			1.5			0.96	
MV3	2.5-2.6	1.41	70.5	7.5		0			0.97	
MV3	5.2-5.3	1.84	33.8	3.1					1.00	
MV3	8.1-8.3	1.98	28.4	3.4		43	55 110	3.3×10^{-2}	0.48	
MV3	8.3-8.4	1.95	28.3 (26.5)	3.6		17	17 27 117	8.7×10^{-3} 4.8×10^{-3}	0.51	
MV3	9.1-9.2	1.97	26.5	3.0		16			0.70	
MV3	10.1-10.2	1.97	22.4	1.6			76	7.4×10^{-3}		
MV3	10.8-10.9	2.02	31.3	3.6					0.98(?)	
MV3	11.7-11.8	1.83	29.7	3.1			28 55	2.0×10^{-4}	0.98	
MV4	4.4-4.7	1.35	41.3	6.5					1.00	

C.4 THAW-CONSOLIDATION TESTS

TABLE C.7 SUMMARY OF RESULTS FROM THAW-CONSOLIDATION TESTS

SAMPLE	DEPTH (m)	FROZEN BULK DENSITY (Mg/m^3)	WATER CONTENT (%)	c_v (ASSUMED)[1] (cm^2/s)	c_v (POST-THAW) (cm^2/s)	R	$\frac{u}{P_o - \sigma'_o}$ THEORY[2]	$\frac{u}{P_o - \sigma'_o}$ MEASURED	$\frac{\bar{B}\,u}{P_o - \sigma'_o}$[3]	COMMENTS
MWA-2	4.25	1.78	42	3.0×10^{-2}		0.22	0.16	0.18		
					7.4×10^{-3}	0.45	0.46	0.18	0.34	
MWA-3	4.69	1.77	42	5.0×10^{-3}		0.57	0.61	0.77		
					3.4×10^{-3}	0.69	0.75	0.77	0.68	
MWA-4	5.30	1.94	30	8.0×10^{-3}	8.0×10^{-3}	0.51	0.43	0.20	~ 0.25	Upper portion of sample unsaturated
MWA-5A	5.67	1.54	89	2.0×10^{-2}		0.29	0.47	0.14		High organic content
					8.5×10^{-3}	0.45	0.67	0.14	0.32	
MWA-5B	5.91	1.37	94	8.0×10^{-3} to 2.0×10^{-2}						Extremely large volume change
					1.0×10^{-2}	0.31	0.37	0.37		
MWA-7	7.12	1.68	45	8.0×10^{-3}		0.45	0.43	0.26		Possilbe leakage at base of permode
					4.1×10^{-3}	0.63	0.63	0.26	0.39	
MWA-7	7.66	1.54	45		5.2×10^{-3}	0.66	0.81	0.78	0.77	
FS-23	—	1.92	35	5.0×10^{-3}		0.73	0.70	0.35	0.31	Possible leakage at base of permode
					3.0×10^{-3}	0.95	0.36	0.35	0.38	
FS-24	—	1.90	30		6.9×10^{-3}	0.61	0.66	0.52	0.55	

[1] c_v assumed on the basis of experimentally determined values to correspond with the effective stress conditions at the thawing front

[2] Nixon and Morgenstern (1973) nonlinear theory

[3] $\bar{B}$ estimated on the basis of correlations obtained with frozen bulk density in other tests

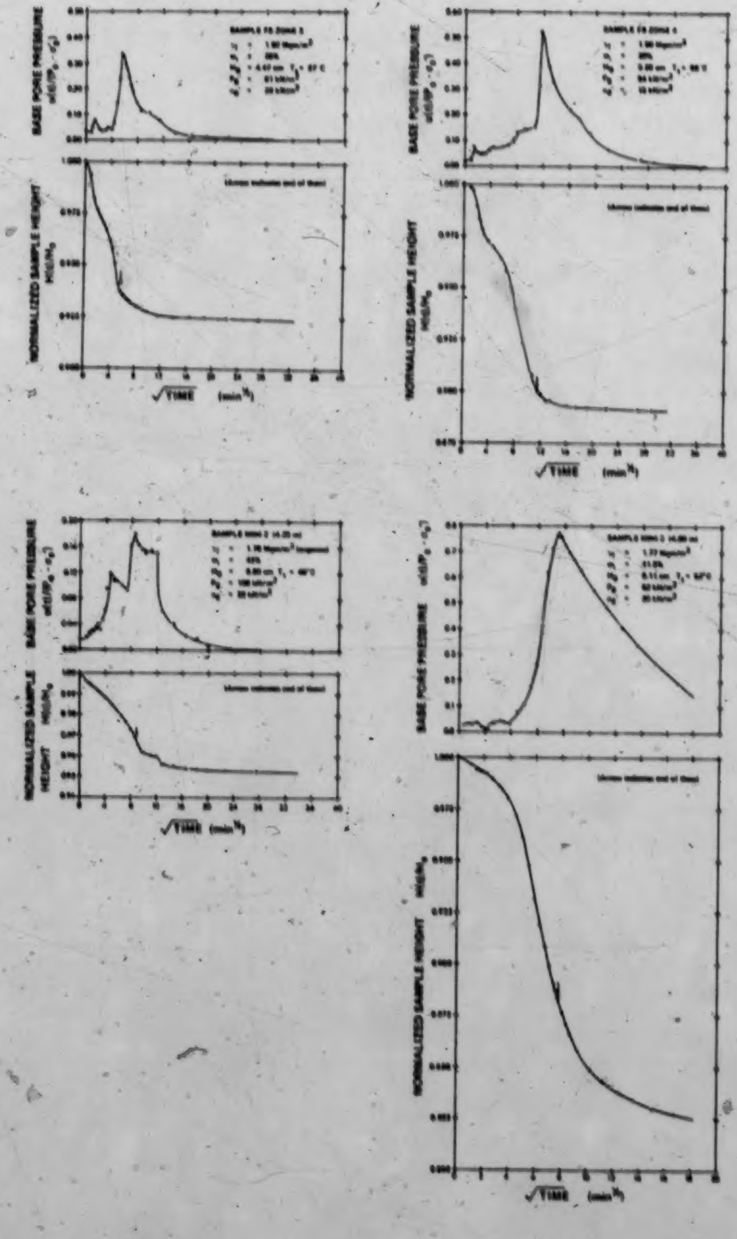

Figure C.27a Thaw-consolidation test data

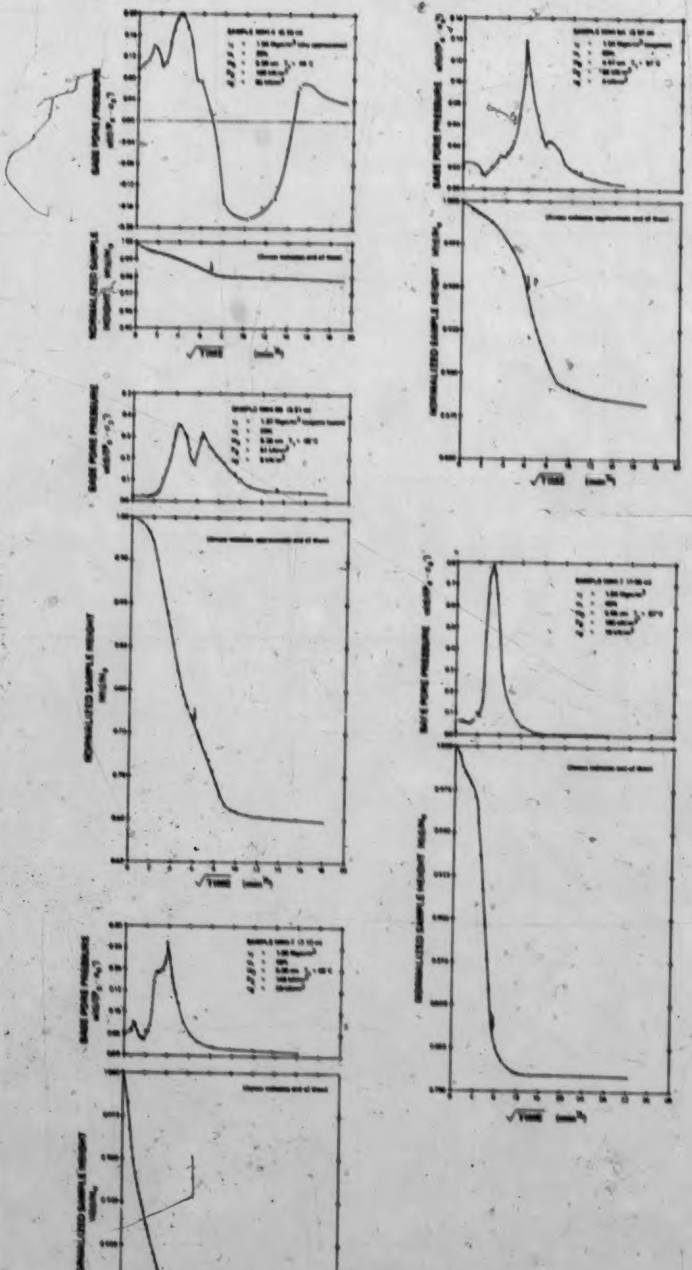

Figure C.27b Thaw-consolidation test data (continued)

C.5 TRIAXIAL STRENGTH TESTS

TABLE C.8 SUMMARY OF RESULTS FROM CONSOLIDATED UNDRAINED TRIAXIAL TESTS, FORT SIMPSON LANDSLIDE HEADSCARP SAMPLING SITE

TEST	ZONE - ATTITUDE	FROZEN BULK DENSITY (Mg/m^3)	σ' (INITIAL) (kN/m^2)	$\sigma_1 - \sigma_3$ (PEAK) (kN/m^2)	ϵ_f (%)	σ_1 / σ_3 (PEAK)	A_f	B	w (%)	REMARKS
FS-01	4-V	1.66	103	109	8.9	3.1	0.14	1.00	31	Ice layers included
FS-02	4-V	1.89	207	208	4.0	2.7	0.18	1.00	31	Between 2 thick ice lenses
FS-03	4-V	1.86	30	42	4.8	3.2	0.05	1.00	28	Below ice lens 10 cm thick
FS-04	4-V	1.97	172	223	3.8	2.6	0.15	0.94	33	Below thick ice lens, backpressure saturation
FS-05	4-V	2.04	138	247	5.7	3.2	0.12	0.95	28	Pore pressures decreasing during shear
FS-06	3-H	1.61	41	—	—	—	—	1.00	33	Leakage developed
FS-07	4-V	1.92	43	131	8.3	3.5	0.03	0.99	30	Between 2 thick ice lenses, backpressure saturation
FS-08	4-V	1.92	64	93	5.3	3.1	0.16	1.00	30	Between 2 thick ice lenses
FS-09	3-H	1.90	27	55	5.7	4.7	0.08	0.98	27	Silty, not much segregated ice
FS-10	3-H	1.89	83	145	5.7	3.7	-0.03	0.96	26	Silty, fine reticulate ice
FS-11	3-H	1.90	66	161	6.6	3.5	0.10	0.82	28	Silty, fine reticulate ice
FS-12	4-H	1.88	89	149	6.9	3.3	0.20	0.95	26	Icey section near base of specimen
FS-13	3-H	1.70	186	212	8.1	2.7	0.25	1.00	29	Near contact with Zone 4
FS-14	3-V	1.95	72	260	7.1	3.0	0.15(?)	0.7-0.8	29	Tested without consolidating specimen, relatively free of ice
FS-15	3-H	1.75	121	149	7.6	3.1	0.16	1.00	29	Near contact with Zone 4
FS-16	3-V	1.88	11	51	7.1	4.1	-0.18	0.92	29	Thin reticulate ice structure, tested without consolidating specimen
FS-17	3-V	1.84	2	24	9.4	3.5	0.03	0.98	32	As above
FS-18	4-V	1.77	11	17	11.5	4.8	-0.16	0.94	32	Regular reticulate structure
FS-19	4-V	1.74	11	18	6.1	4.4	0.20(?)	0.95	32	As above } From the
FS-20	4-V	1.77	11	32	3.8	3.8	0.02	~1.00	29	As above } same core

TABLE C.9 SUMMARY OF RESULTS FROM CONSOLIDATED UNDRAINED TRIAXIAL TESTS, NORMAN WELLS (MVPL) SAMPLING SITE

TEST	BOREHOLE	DEPTH INTERVAL (m)	FROZEN BULK DENSITY (Mg/m³)	σ'_c (INITIAL) (kN/m²)	$\sigma_1 - \sigma_3$ (PEAK) (kN/m²)	ε_f (%)	σ_1'/σ_3'	A_f	B	w (%)	REMARKS
NW-01	NW2	0.4-0.7	1.85	10	17	5.6	5.0	0.01	0.85	35	Stratified silty sand, relict active layer, tested without consolidating specimen
NW-02	NW2	0.4-0.7	1.85	48	64	3.2	3.3	0.21	0.92	23	Stratified silty sand
NW-03	NW2	0.7-1.0	1.86	206	211	10.4	3.2	0.43	0.71	20	Silty, organic layers, reticulate ice
NW-04	NW2	1.0-1.3	1.89	4	27	4.4	6.2(?)	-0.33	1.00	24	Thinly bedded silty clay, tested without consolidating specimen
NW-05	NW2	1.0-1.3	1.82	48	93	6.5	4.0	0.33	1.00		From same core as above
NW-06	NW2	1.5-1.7	1.85	241	189	6.6	3.8	0.48	0.78	30	Contact between sand, silt with shale chips and silty clay with peat layers
NW-07	NW2	1.8-2.1	1.53	11	44	6.9	—	—	1.00	53	Thinly bedded silty clay, peat layers, sticks and roots, p.w.p. erratic
NW-08	NW2	1.8-2.1	1.54	36	63	7.0	4.9	0.44(?)	0.95	48	From same core as above
NW-09	NW2	4.3-4.6	1.72	10	37	6.2	5.7	-0.01	0.98	34	Reticulate ice, blocky structure, peat layers
NW-10	NW2	8.2-8.4	1.82	2	15	8.0	—	0.10	1.00	39	Reticulate ice, organic specks, sandy partings, tested without consolidating specimen
NW-11	NW2	8.2-8.4	1.83	34	59	6.2	3.2	-0.11	1.00	28	From same core as above
NW-12	NW3	0.6-0.8	1.93	10	20	6.0	—	-0.21	0.92	24	Tested without consolidating specimen, problems with pore pressure measurement
NW-13	NW3	1.0-1.3	1.91	12	44	3.6	3.6	-0.09	0.91	26	Massive, fine reticulate ice structure
NW-14	NW3	7.9-8.1	1.81	6	20	3.8	—	-0.03	0.93	30	Reticulate ice, tested without consolidating
NW-15	NW3	10.4-10.6	1.92	11	23	7.3	3.8	-0.10	0.93	26	Reticulate ice, soil appeared quite dry,tested without consolidating specimen
NW-16	NW3	10.4-10.5	1.92	24	78	5.4	2.4	0.35	0.92	30	Reticulate ice, sandy partings, tested without consolidating specimen
NW-17	NW3	11.9-12.1	1.85	19	62	4.9	4.1	0.09	0.84	32	Reticulate ice, tested without consolidating specimen
NW-18	NW4	5.5-5.8	1.71	31	93	4.8	5.5	0.38	0.78	45	Contact plastic clay and highly organic silt, failed along boundary
NW-19	NW4	5.5-5.8	1.71	97	145	4.0	4.4	0.43	0.86	40	From same core as above, mostly silty clay interbedded with peat